5th INTERNATIONAL ENGINEERING SYMPOSIUM – IES2016

Faculty of Engineering (Building No.2)
Kumamoto University

March 2-4, 2016

Kumamoto University

Conveners
Shuichi TORII
Professor, Department of Mechanical System Engineering
Kumamoto University, Japan
&
Katta VENKATARAMANA
Professor, Department of Civil Engineering
NITK, Surathkal, India

Organized by
Graduate School of Science & Technology
Kumamoto University, Japan

In association with
National Institute of Technology Karnataka, India

PROCEEDINGS OF

5th INTERNATIONAL ENGINEERING SYMPOSIUM – IES2016

Venue

Faculty of Engineering (Building No.2)
Kumamoto University

Date

March 2-4, 2016

Conveners

Shuichi TORII
Professor, Department of Mechanical System Engineering
Kumamoto University, Japan
&
Katta VENKATARAMANA
Professor, Department of Civil Engineering
NITK, Surathkal, India

Organized by

Graduate School of Science & Technology
Kumamoto University
Kumamoto City, Japan

In association with

National Institute of Technology Karnataka
Surathkal, Mangalore, India

PREFACE

The 1st International Engineering Symposium (IES2011), the 2nd International Engineering Symposium (IES2012), the 3rd International Engineering Symposium (IES2013) and the 4th International Engineering Symposium (IES2015) were organized very successfully at Kumamoto University with more than 100 participants from India, Japan, Indonesia, Thailand, Taiwan, Vietnam and other countries. With the objective of continuing the interaction between the researchers during these symposia, the 5th International Engineering Symposium (IES2016) has been organized in the month of March, 2016. This symposium provides a common platform for bringing together researchers for expanding academic collaboration. It is expected that the emerging technologies and scientific advancements in these themes will be disseminated during the Symposium. Presentations will also feature new and innovative technologies in the relevant fields.

As part of this symposium, the researchers and the students from abroad have been invited to visit Kumamoto University and get exposed to its educational and research activities. The event focuses on the current R&D of the participating institutions on topics of mutual interest, with a special emphasis on "Science & Technology". The emerging technology and scientific advancements are discussed during the symposium. Presentations feature new and innovative technologies in the relevant fields.

This proceedings volume contains the technical papers presented at the symposium. The topics include a wide spectrum of themes covering major disciplines of science and engineering. The effort put in by the faculty, the staff and the students of Kumamoto University in organizing this event are greatly appreciated.

We sincerely hope that you will find the contents of this proceedings volume useful and productive. We look forward to more intense academic collaborations and research interactions in the coming days, to achieve the common goal of technological advancement for global peace and prosperity.

Shuichi Torii
Katta Venkataramana
Conveners

IES2016 Program Schedule

Venue: Faculty of Engineering, Building No.2

March 2, 2016 (Wednesday)

10:00 –10:30	Registration
10:30 – 11:00	***Opening Address & Introduction of GSST***
11:00 – 11:50	**Keynote Lecture** *(K1)*
11:50 – 12:20	Tea Break
12:20 – 13:00	**Keynote Lectures** *(K2)*
13:00 – 14:00	Lunch
14:00 – 17:00	**Campus Tour & Laboratory Visits**
17:00 – 17:30	Free Time
17:30 – 19:00	Welcome Reception

March 3, 2016 (Thursday)

10:00 – 11:30	**Technical Sessions** *(C1,C4, C7)*
11:30 – 11:45	Tea Break
11:45 – 13:00	**Technical Sessions** *(M1,C2,C5,E1)*
13:00 – 14:00	Lunch
14:00 – 15:30	**Technical Sessions** *(M2,C3,C6,E2)*
15:30 – 16:00	Tea Break
16:00 – 17:30	Free Time
17:30 – 19:00	Symposium Dinner

March 4, 2016 (Friday) ***Lunch & Dinner Venue - FORICO Cafeteria***

9:00 – 18:00	**Field visits**

Notations:

K Keynote Lectures
M Technical Sessions (Mechanical Engineering & Related Fields)
C Technical Sessions (Civil Engineering & Related Fields)
E Technical Sessions (Electrical, Electronics, Computer Engineering & Related Fields)

Contents

Keynote Lectures

Civil Engineering & Related Fields

Mechanical Engineering & Related Fields

Electrical, Electronics, Computer Engineering & Related Fields

KEYNOTE LECTURES

5th International Engineering Symposium - IES 2016
March 2-4, 2016, Kumamoto University, Japan

Soft-Tribology: Practical Applications for Human Activity and Environmentally Sustainable Technology

Yoshitaka Nakanishi

Professor, Graduate School of Science & Technology, Kumamoto University, Japan
Email: y-naka@mech.kumamoto-u.ac.jp

ABSTRACT: According to the glossary of the OECD, Tribology is defined as "the science and technology of interacting surfaces in relative motion and of related subjects and practices." Controlling friction and wear to improve maintenance and reliability, saving energy and resources, as well as protecting the environment are all important roles of tribology.

A new term, Soft-Tribology, has been proposed which focuses on the physical and chemical interface and interaction between soft and hard materials. The wide range of interface science included within this term has begun to stimulate scientific discussion about the industrial applications for engineering products in sustainable technology and in biomedical engineering from tissue to molecular levels, with practical applications related to improving the quality of life.

This talk will give a clear exposition of Soft-Tribology from a practical application perspective.

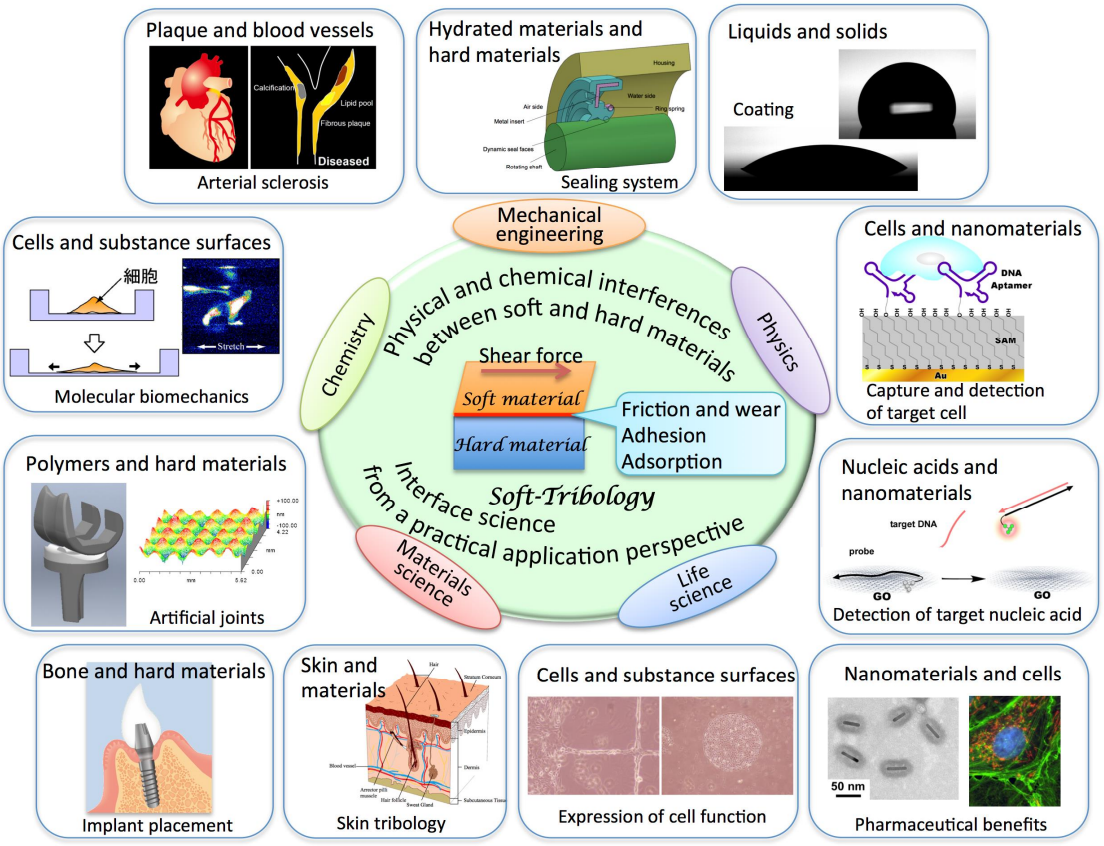

5th International Engineering Symposium - IES 2016
March 2-4, 2016, Kumamoto University, Japan

Seismic Retrofitting of Historic Structures

Madhura Harisangam and Katta Venkataramana

Department of Civil Engineering, National Institute of Technology Karnataka, Surathkal, Mangalore 575025, India. email: mharisangam@gmail.com

ABSTRACT: Preserving historic buildings not only benefits a culture and identity but also businesses and local economy. Unfortunately, most of the ancient buildings have suffered from damages caused by seismic activities. Therefore they need to be strengthened. However it may also possible that changes made for strengthening lead to destruction of their historic identity and valuable components. Therefore for retrofitting of historic buildings innovative approach is also considered worldwide along with conventional methods. The following report considers three case studies involving retrofitting techniques used in Peru, Italy, India and USA.

***Keywords**: Historic structures, Seismic retrofit, adobe building, GFRP*

INTRODUCTION

There are a lot of historic buildings around the world which must be preserved for future generations for their cultural, architectural, symbolic, social or historic aspects. Apart from this it also boosts local business. Unfortunately, most of the ancient buildings are precarious to deterioration because of various natural and manmade actions. Majority of old heritage buildings are fragile to earthquakes and therefore they need retrofitting. However if only technical aspects of restoration are considered without giving attention to historical and cultural values of the buildings; it will lead to destruction of its historic identity and valuable components. Therefore modern building codes that are basically devised for new structures cannot suitably be applied in such buildings. Therefore different techniques and materials are being used nowadays for retrofitting of such structures.

The principles that govern the retrofit

- Avoid intervention to maximum extent possible.
- Retrofitting measures should be harmonious to the heritage character and principles of conservation.
- New elements must be non-intrusive and compatible with existing materials.
- New elements should not be a cause of further damage
- Easy implementation.
- Supplementary system should also be designed to be reversible

Behaviour of masonry buildings

Most of the historic structures are masonry structures composed of stone, bricks, adobe and mortar. These are mainly designed to take gravity loads. They lack detailing to transfer seismic forces from structure to the foundation. Such structures have high resistance and stiffness but low ductility. Moreover damages are accumulated for years. Structural drawings are also not available for many structures.

GENERAL METHODOLOGY AND TECHNIQUES

1. Historical and experimental documentation
2. Material characteristics
3. Structural model
4. Actions
5. Analysis
6. Failure criterion and assessment
7. Repairing and/or strengthening decisions and reanalysis
8. Execution of retrofit work

CASE STUDIES

1. Restoration of adobe church in Piura, Peru

Historic older adobe buildings, based on the nature of their construction, are susceptible to severe damage during earthquakes. This church is a nearly 100-year-old adobe structure (Figure 1). Nine triangular wood trusses supported the original roof (Figure 2). The trusses rested directly on the lateral adobe walls. No wooden beam tying the trusses to the wall was used. Under the roof trusses, a false ceiling was built attached to the trusses. In addition to vertical cracks at the corners of the walls, there were major horizontal cracks across the back wall due to moisture seepage.

Structural Reinforcement Measures
The original trusses were dismantled and rebuilt as they had a very low factor of safety for carrying the weight of the roof. Their original shape width dimensions, and position of the elements were kept same as the original ones (Figure 3). Wooden beam on top of the adobe wall with steel plates connected the roof trusses to the lateral walls. Strips of galvanized welded–wire fabric having 19-mm square openings between the wires were placed over the adobe walls (Figure 4).

2. Seismic upgrade of masonry Bell Tower in Naples, Italy.

Located in Naples, Italy the Bell Tower of Santa Maria del Carmine is a 17th century structure (Figure 5). The tower has six levels and above 56m a peared shaped dome makes the structure 68m tall. Previous attempts of retrofitting include use of steel ties and reinforced injections. Due to detrimental effects of corrosion on the steel ties, need for realizing new ties made of materials having high durability and chemical inertia was established.

Retrofitting measures
It was planned to remove the existing damaged ties and replaced with new ties arranged according to the same position and using the same existing holes. The new material used is GFRP (glass fiber reinforced polymer). It is composite material made of polymer matrix reinforced with glass fibers. GFRP materials have superior mechanical and chemical properties. Due to light weight, transportation as well as installation operations are easier. A specific system of ties and end anchorage was designed accordingly (Figure 6).

3. Mani Mandir Complex Morbi, Gujarat India

Built in the 1930s, this complex comprises of a very ornate masonry building in yellow sandstone in the traditional Indo-Saracenic style of architecture. The extensive damage suffered during 2001 Bhuj earthquake has left the building unfit for occupation leaving some parts of the building in inevitable danger of collapse.

Some portions of the roof slab suffered collapse (Figure 7). Heavy cracking of the arches with the dislodged keystones was observed (Figure 8). Deformation of the arches was also seen. Many decorative galleries and some walls were pushed out and away from the building. Extensive crack formation was observed in many walls. Numerous walls opened out at corners.

Methods of retrofitting
Introduction of diagonal bracing elements on the underside of the first floor was proposed to develop diaphragm action. The perpendicular walls were to be connected to each other by cross-pinning with stainless steel rods of 8mm and 10mm diameters at every 600 mm along

the height. Introducing horizontal reinforced bands to existing masonry walls was considered. A stainless steel tie with a turnbuckle is proposed where there is movement of support. Grouting the cracks in the wall with a low-strength grout compatible with the stone was suggested.

4. Congregation Sherith Israel, California

Congregation Sherith Israel (Figure 9) is a pioneer synagogue of the American West that was founded in 1849. The structure has ornate sandstone cladding. The interior walls are famous for the murals. Although it survived 1906 and 1989 earthquakes with some relatively minor damages, it was threatened with closure due to its non compliance with safety majors required in the event of major earthquake.

Structural retrofitting measures

Early attempts of retrofitting include addition of steel bands to suture the cracks (Figure 10). Previous design proposals would have caused major changes in the appearance of the building which is against the basic philosophy behind retrofitting of such structure. Therefore it was decided to drill through the stone and brick walls and insert steel rods and grouting. This method is also known as center coring (Figure 11). Additionally localized composite wraps were also used. The doors were refinished to match original standard while upgrading to meet current code. (Figure 12)

CONCLUDING REMARKS

- Historic buildings are of significant importance due to various cultural and economical aspects.
- Historic buildings are prone to damages caused by earthquakes due to their age, lack of detailing to transfer earthquake loads safely to ground and poor maintenance. Therefore these structures require retrofitting.
- In retrofitting of historic structures apart from structural strength consideration proper attention must be given to preserve their historic value.
- Various conventional and non conventional methods are being used all over the world for retrofitting.
- In India after 2001 Bhuj earthquake the need of retrofitting of the historic structures is highlighted.
- Retrofitting methods and strict maintenance regime can help to protect these structures longer.

REFERENCES

[1] Branco, M et al (2011), Seismic Rehabilitation Of Historical Masonry Buildings, Engineering Structures 33 (2011) 1626–1634

[2] Ceroni, F et al (2009), Case Study: Seismic Upgrade of a Masonry Bell Tower Using Glass Fiber-Reinforced Polymer Ties, DOI: 10.1061/_ASCE_CC.1943-5614.0000001

[3] Forouzandeh, A et al (2014), The Evaluation of Structural Strengthening of Historic Building on the Basis of Architectural and Restoration Consideration, Journal of Civil Engineering and Architecture Research, Vol. 1, No. 3, 2014, pp. 157-178

[4] Paret, T F et al (2008), Using traditional and innovative approaches in the seismic evaluation and strengthening of a historic unreinforced masonry synagogue, Engineering Structures 30 (2008) 2114–2126

[5] Petrozzi, G R et al(2014), Restoration of a Historic Adobe Church, American Society of Civil Engineers DOI: 10.1061/(ASCE)SC.1943-5576.0000226

[6] Shethi, A. et al (2004), Seismic Retrofitting of Mani Mandir Complex at Morbi, Gujarat, India,13th World Conference on Earthquake Engineering Vancouver, B.C., Canada August 1-6, 2004 Paper No. 2430

Fig.1 Santísima Cruz del Norte Church (Petrozzi G R et al, 2014)

Fig.2 Original roof and ceiling frame (Petrozzi G R et al, 2014)

Fig.3 Reconstructed trusses (Petrozzi G R et al, 2014)

Fig. 5. Bell Tower of Santa Maria del Carmine (Ceroni F et al, 2009)

Fig.4 Steel wire mesh and tie against the adobe walls (Petrozzi, G R et al, 2014)

Fig.6 Installation of GFRP ties (Ceroni F et al, 2009)

Fig.7 Separation of joist flanges and failure of stone slab (Shethi A et al 2004)

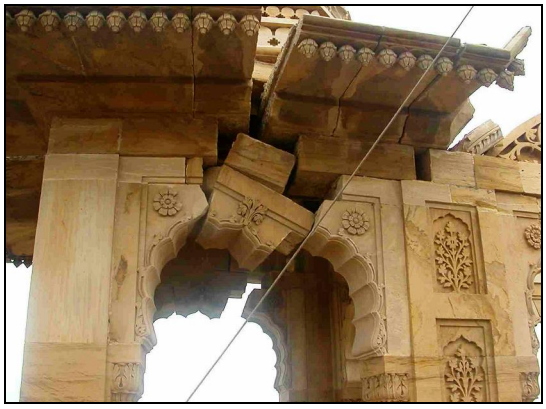

Fig.8 Destruction of Arches (Shethi, A. et al 2004)

Fig.9 Exterior of the Sherith Israel (Paret T F et al, 2008)

Fig.10 Steel angles to suture the walls (Paret T F et al, 2008)

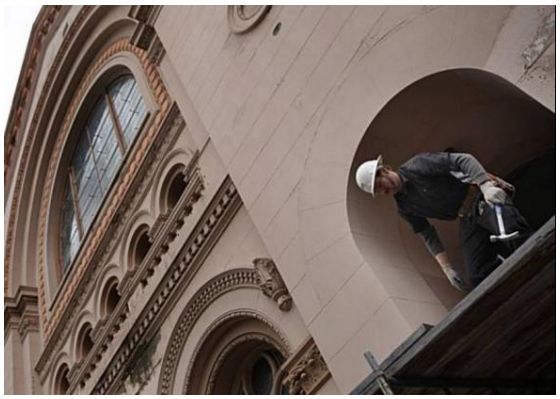

Fig.11 Erecting scaffolding for Retrofication (Lee Suzuki, 2010)

Fig.12 Restored wooden doors- (elsarch.com, 2012)

5thInternational Engineering Symposium - IES 2016
March 2-4, 2016, Kumamoto University, Japan

SOLIDS DRYING STUDIES IN A MULTIPLE DRAFT TUBE SPOUTED BED DRYER

D V R Murthy[1*], Rajashekhara S[1], Kevin Varghese Abraham[1]

1. *Department of Chemical Engineering, National Institute of Technology Karnataka, Surathkal, 575025, India. Email: dvrmvzm@gmail.com*

ABSTRACT: A rectangular column (225mm × 75mm) having three spout cells has been used as dryer in this study. Each cell is provided with a draft tube (26mm ID, 2mm holes), an inverted frustum (apex angle = 60^0) as base and a fluid inlet (21mm diameter) located at the base. Ragi seeds (spherical, diameter = 1.35mm, bulk density = 827kg/m^3) are used as solid material for drying studies with hot air as the drying medium. Batch experiments are conducted using grains having initial moisture contents of 15%, 20%, 25%, 30% and 35% on dry basis, inlet air temperatures of 35^0 , 40^0, 45^0, 50^0 and 55^0C, air flow rates of 30, 33 and 36m^3/h and bed weights of 2.0, 2.5 and 3.0kg. In each experiment batch drying time needed to obtain a final moisture content of 10% has been found. The results are presented in this paper.

Keywords: *Multiple spouted bed, porous draft tube, grain drying, drying rate, Ragi (Eleusinecoracana)*

INTRODUCTION

Solids drying is a unit operation where simultaneous transfer of heat and mass occurs from solids to air. It is an important step for maintaining quality of solid materials during safe storage and packing.

The spouted bed technique was developed by Mathur&Gishler(1955)for wheat drying. Whenagricultural grains, which are coarse granular solids,are to be kept in a continuously agitated state for removal of moisture the spouted bed seemed to be very efficient. However the conventional spouted bed (CSB) has the following limitations.

1. A large scale operation requires gas supply at a correspondingly high pressure.
2. The contact times between gas and solids can be higher in large deep beds, which may be undesirable in certain operations like drying of heat sensitive solids.
3. Existence of maximum spoutable bed depth (MSBD) beyond which proper spouting of solids is not possible.

An alternative to overcome the first two limitations is to use multiple fluid inlets within the same bed. The reported investigations related to multiple spouted beds (MSBs) are those of Peterson (1966), Foong et al (1975), Huang &Chayang (1993), Murthy & Singh (1994), Hu et al (2008), Chen et al (2013) and Dalin Chen et al (2014). However MSBs also have constraints like existence of MSBD (Murthy, 1991) and limited operational regime to maintain stable spouting (Murthy & Singh, 1996).

We can overcome the third limitation by providing an axially positioned draft tube (DT) in a CSB; also, DT helps to have a close control over particle history in the bed (Ishikura et al., 2003). Some of the reported works related to solids drying in DT CSBs are those of Ando et al. (2002), Olazar et al. (2011), and Berghel&Renstrom (2014). Ishikura et al. (2003) compared the characteristics of CSBs with and without draft tubes.

However in an operation like solids drying presence of a DT prevents lateral transport of gas from spout to annulus region thereby limiting drying to be occuring essentially within the DT. So, it is desirable to use a porous draft tube to carry out an operation like solids drying.

Based on the issues discussed above a MSB having porous draft tubes has been constructed and used in this study. It can help to achieve the following.

- Overcome the MSBD limitation so that large scale drying operations would be possible.
- Draft tubes can act as vertical baffles thereby avoiding the hydrodynamic instability of the bed at higher gas velocities.
- Better control of gas residence times as well as solids cycle times.
- A porous draft tube helps in maintaining lateral movement of hot gas through holes provided in the draft tube; this ensures better gas – solid contact in annular region also. As a result higher mean transfer rates of heat and mass in the entire bed may be achieved.

EXPERIMENTAL

The dryer is a rectangular column (225mm × 75mm) having three square cells; the cell configuration is shown in Fig.1. Each cell is provided with a draft tube as well as an inverted frustum (apex angle = 60^0) as base. A fluid inlet orifice (21mm diameter) is located at the base of each frustum. The broader sides of the column are made of transparent acrylic sheets for visual observations. The details of various draft tubes used are given in Table 1. It is to be noted here that the DT holes are provide in a rectangular configuration such that the number of holes for a given DT length are same in all the tubes used. Compressed air passing through a constant pressure regulator, main rotameter, electric heater and spout line rotameters enters each spout cell. Air supplied to the main rotameter is at 28^0C and 101.32 kPa(g). Valves are provided appropriately to adjust flow rate to each cell as well as total flow rate. Humidity and temperature sensors are located for measuring air conditions at required locations. A U – tube manometer is used for measuring bed pressure drop. A schematic line diagram of the experimental rig is shown in Fig. 2.
Ragi (*Eleusinecoracana*) seeds (spherical, diameter = 1.35 mm, bulk density = 827 kg/m^3) a widely used agricultural product in India, is used as solid material for drying studies.

Drying experiments are conducted using grains having initial moisture contents of 15, 20, 25, 30, and 35% on dry basis; air temperatures of 35^0, 40^0, $45^{0,}$ 50^0 and 55^0C and air flow rates of 30, 33 and 36 m^3/h. The bed weights reported and the corresponding static bed heights are for dry solids at ambient conditions. The flow rates, bed pressure drops and MSBD are measured at ambient conditions.

Solids of required weight and water of appropriate quantity are thoroughly mixed to obtain wet solids batch needed for a given experimental run. Air flow is adjusted to the required value and it is heated to required temperature and supplied to the empty dryer. Wet solids batch is loaded into the column after it attains steady state. Solid samples are taken from the dryer at regular time intervals and kept in desiccators and their weights are noted. These samples are kept in an oven maintained at 70^0C for sufficiently long times so that they become bone dry. Using the weight differences the moisture content of each sample at a given time is found. Moisture content versus time plots are prepared for all runs; from these plots batch drying times needed to achieve a final moisture content of 10% from given initial moisture content are obtained.

RESULTS AND DISCUSSION

Influence of operating variables on drying rate

The drying of ragi seeds has been found to be occurring under falling-rate period under all conditions used in this study. Typical rate curves are shown in Fig.3. When the solids are amorphous and

fibrous in nature, the moisture is held as an integral part of the solid structure; the moisture movement through solid structure can be very slow by diffusion. So, these solids have not exhibited any constant rate period.

The effect of operating variables like inlet air temperature (T_a), initial moisture content of solids (X_0), air flow rate (v_0) and bed weight (w_b) on drying are shown in Figures 3 – 5. The results indicate that as T_a increases the drying rate (R_d) increased; an increased T_a leads to increased driving forces for both heat & mass transfer leading to higher R_d. The total amount of moisture to be removed will be higher for solids with higher X_0 and hence an increase in X_0 leads to longer batch times to reach the given final moisture content of solids. As v_0 increases the solids circulation in the bed increases, leading to better transfer rates of heat & mass; hence moisture removal rate has been found to be higher at larger v_0. At a given v_0, the solids circulation rate will be lower when w_b is increased;this in turn leads to lower transfer rates of heat & mass, which results in lower moisture removal rate for larger bed weight.

The results have shown that a higher T_a, higher v_0, lower X_0 and lower w_b would lead to faster drying rates. However, it should be noted here that higher T_a& v_0 will increase the operating costs, lower w_b leads to more number of batches to be handled and X_0 of fresh agricultural grains is fairly fixed.

Performance comparison between nonporous and porous draft tubes

Drying experiments are carried out using 26 mm ID draft tubes with and without holes. The results are presented in Figure 6.The graph shows that presence of holes increased the rate of drying by allowing lateral transport of gas from spout to annulus region and providing better contact between gas and solids. Hence it is desirable to use a porous draft tube to carry out an operation like solids drying.

CONCLUSIONS

The following conclusions are drawn based on the results obtained in this study.

1. An increase in air inlet temperature and air flow rate, decrease in initial moisture content of solids and bed weight will lead to reduction in batch drying time.
2. The batch drying time is found to be more for MSB with non-porous draft tubes.

So, the overall performance of the proposed design seems to be good. Scale up of this design for large scale drying operations should be possible, but needs to be studied.

Note: D V R Murthy and Rajashekhara S have applied for an Indian Patent having the title "MULTIPLE POROUS DRAFT TUBES SPOUTED BED CONTACTOR". The application number is 2940/CHE/2015 and dated June 11, 2015

REFERENCES

[1] Ando, S., Maki, T., Nakagawa, Y., Namiki, N., Emi, H. and Otani, Y.(2002). "Analysis of the drying process of seed particles in a spouted bed with a draft tube."*Adv. Powder Technol.*, 13(1), 73–91.

[2] Berghel. J and Renström.R. (2014)."An Experimental Study on the Influence of Using a Draft Tube in a Continuous Spouted Bed Dryer."*Dry. Technol.*, 32(5), 519–527.

[3] Chen, C., Lim, J. and Grace, J. R.,(2013). "Stability of slot rectangular spouted beds with multiple slots." *The Can. J. Chem. Eng.,*91, 1768–1775.

[4] Dalian Chen, X. Liu, W. Zhong, Y. Shao, and B. Jin, (2014) "Interactions of Spout Jets in a Multiple Spouted Bed," vol. 92, no. June, pp. 1150–1159,.

[5] Foong, S. K., Barton, R. K., Ratcliffe, J. S.(1975). "Characteristics of multiple spouted beds" *Mech. and Chem. Eng. Trans.*Instn.Engrs. Australia. 11, 7-12.

[6] Hu, G., Gong, X., Wei, B. and Li, Y.(2008). "Flow Patterns and Transitions of a Novel Annular Spouted Bed with Multiple Air Nozzles," *Ind. Eng. Chem. Res.* 47, 9759–9766.

[7] Ishikura .T,Nagashima.H, and Ide.M,(2003) "Hydrodynamics of a spouted bed with a porous draft tube containing a small amount of finer particles," vol. 131, pp. 56–65

[8] Mathur K.B, and Gishler, P.E., (1955). "A technique for contacting gases with coarse solid particle."*A.I.Ch.E. Jour.* 1(2), 157 – 164.

[9] Murthy D.V.R.,(1991). "Hydrodynamic studies in Gas – Solid and Liquid – Solid multiple spouted beds," Ph.D Thesis, Mangalore university, Karnataka, India

[10] Murthy D.V.R, Singh, P.N., (1994). "Minimum spouting velocity in multiple spouted beds" *Can. J. Chem. Eng.,* 72, 235-239.

[11] Murthy D.V.R, Singh, P. N.,(1996). "minimum spouting velocity in multiple spouted bed" Chapter 32, Mixed – Flow Hydrodynamics; A*dvances in Engineering Fluid Mechanics Series,* edited by Nicholos P. Gulf publishing co., USA. 741-758
[12] Olazar, M., Lopez, G., Altzibar, H. and Bilbao, J. (2011)."Modelling batch drying of sand in a draft-tube conical spouted bed."*Chem. Eng. Res. Des.*, 89(10).2054–2062.
[13] W. Peterson, US 3242586 (1966), NAT. RES. COUNCIL, invs.

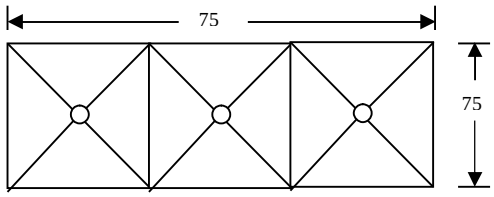

Fig.1. Spout cell configuration

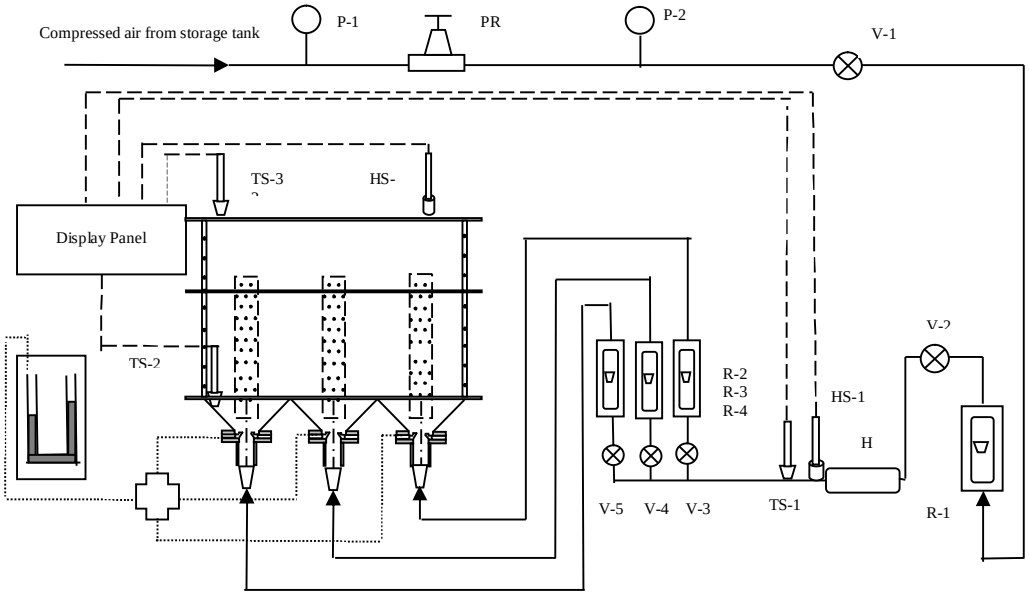

P-1,P-2 =Pressure gauge; PR=Pressure Regulator; V-1, V-2, V-3, V-4, V5, = Globe Valves; R1, R2, R3, R4, = Rotameteres; H = Heater; HS-1,HS-2 = Humidity Sensors; TS-1, TS-2, TS-3 =Temperature Sensors

Fig. 2 Schematic line diagram of the experimental rig

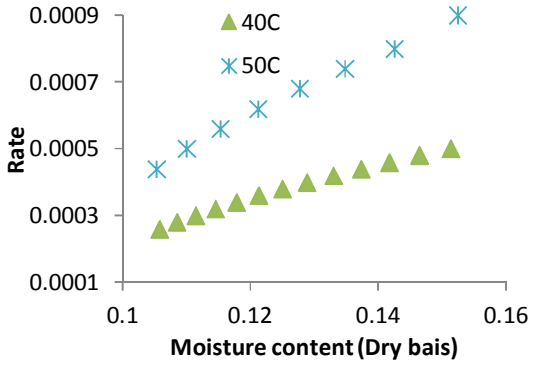

Fig. 3. Effect of inlet air temperature on rate of drying
(w_0=2.5 kg,v_0=33m^3/h,X_0=0. 15 g moisture/g dry solids)

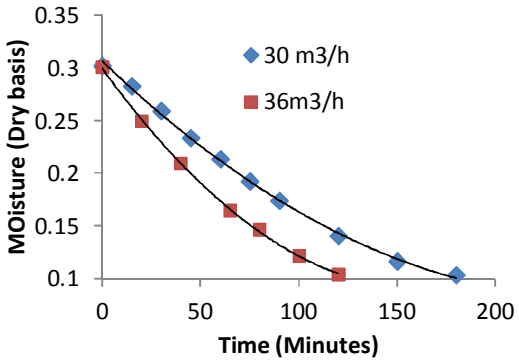

Fig. 5. Effect of air flow rate on moisture removal
(w_0=2.5 kg,T_0=55^{0}C, X_0 = 0.30 g moisture/g dry solids)

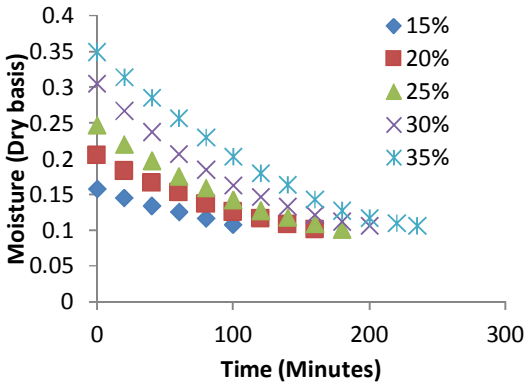

Fig.4. Effect of initial moisture content on moisture removal
(w_0 = 2.5 kg, v_0 = 30 m^3/h, Ta = 45 ^{0}C)

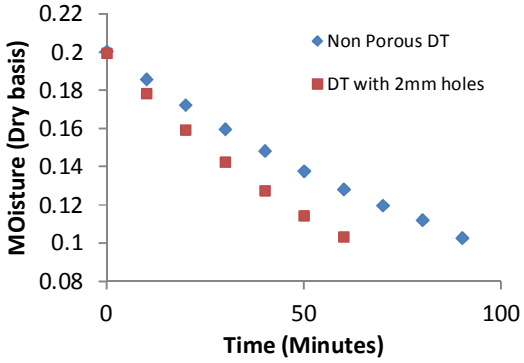

Fig.6. Effect of holes on moisture removal
(w_0=2.0 kg,T_0=55^{0}C,v_0=36m^3/h,X_0=0.2 gmoisture/g dry solids)

CIVIL ENGINEERING
&
RELATED FIELDS

5th International Engineering Symposium - IES 2016
March 2-4, 2016, Kumamoto University, Japan

Detection of Damage in Curved Plate Structures Using Lamb Waves and Geodesic Distances

G.Kausalya [1], U.Ashwin[2], Ashok kumar.S[3], S.Raja [2] and **Katta Venkataramana[3]**

1 *M.Tech student, Dept. of Civil Engineering, National Institute of Technology, Surathkal, Mangalore, India (Presenting Author) Email – kausalya.guru@gmail.com*
2 *Scientist, Structural Technologies Division, CSIR-National Aerospace Laboratories, Bangalore, India, Email - raja@nal.res.in*
3 *Senior Project Fellow, Structural Technologies Division, CSIR-National Aerospace Laboratories, Bangalore, India, Email – aeroashok06@gmail.com*
4 *Professor, Dept. of Civil Engineering, National Institute of Technology, Surathkal, Mangalore 575025, India, India Email – ven.nitk@gmail.com*

Abstract
Lamb-wave-based damage detection methods for curved plates using the geodesic based triangulation technique is investigated. This work is based on the fundamental fact that a wave takes the minimum energy path to travel between two points on a surface which reduces to the shortest distance path or geodesic. The geodesic distance between any two points on a curved surface is given by an arc of great circle. A simplified approach for computing the geodesics by unwrapping the curved plate is presented. The guided circumferential waves are generated using FE package ABAQUS EXPLICIT on curved healthy and damaged plates of different curvature. The sensor response of the monitored plate is obtained, which in the presence of damage will have reflected waves. The Time Of Flight (TOF) of the reflected waves is then measured to compute the geodesic distance. These geodesic distances are used in the ellipse algorithm for triangulation to locate the loci of possible damage location points for each actuator–sensor pair. The intersection of multiple loci from actuator sensor pairs gives the damage location.

***Keywords**: Curved plate, Circumferential Lamb waves, Geodesic distance, Triangulation*

INTRODUCTION

Monitoring the integrity of a structure is necessary in order to improve its safety, serviceability and functional life. Structural Health Monitoring (SHM) is a technique of non-destructively studying the characteristics that are related to the fitness of a system. Damage accumulation in a system can change the way the components of the system respond to applied loads. This requires both the loading and damage to be monitored continuously and predict the future operational capability of the component. Due to the fact that a structural damage causes unique scattering of the propagating waves, useful information can be obtained from the reflected waves. Therefore, wave based SHM is predominantly used for the inspection of structural components. Lamb waves refer to high frequency elastic waves in thin plates. Lamb waves are popular, mainly due to its long propagation ranges with small wavelength, making them sensitive to small damages in the structure. Most importantly, Lamb waves being sensitive to environmental conditions and structural discontinuities make them suitable for damage detection in curved panel structures.

Curved plates are used in important engineering structures such as pipelines, pressure vessels and aircrafts whose performance and safe functionality is essential. Presence of defects, such as fatigue cracks, corrosion, damage due to impact, etc. significantly affect the performance of the structure and may

result in catastrophic failure. Thus regular monitoring of safety and performance of curved panel structures is necessary. Assuming a curved plate to be a part of a hollow cylinder, the geometry of the curved plate can be described in cylindrical coordinates (r,θ,z) in which the wave propagation is as shown in the Fig.1.

Curved plates are most commonly subjected to cracks and damages that initiate and grow in the radial direction. Traditional ultrasonic techniques of non-destructive evaluation are found to be ineffective in damage detection of curved plates due to the problems associated with its geometry. This has led to the emergence of circumferential Lamb waves for locating damages in the radial direction i.e. along the circumference of the curved plate. Circumferential Lamb waves are guided waves that propagate in the circumferential direction of the curved plate.

Circumferential waves were first introduced by Viktorov (1958), as an extension of Lamb waves in a flat plate to a curved plate. The wave propagation characteristics, in both isotropic and anisotropic media have been studied in detail by, Liu and Qu (1998), Valle et al., (1999) and Towfigi et al., (2002).

As mentioned earlier, the reflected Lamb waves from the defect contains large information about the nature and location of the defect. Thus once the signals from damaged plate are extracted, it is now necessary to device new algorithms to locate, image and characterize the damage in the structure. Most algorithms are based on comparing signals with baseline signals recorded from the healthy structure. The two signals are subtracted from each other and the first arrived wave packet of the residual signal is considered to be the reflection from the defect. Valle et al., (2001) has made an attempt to locate the crack in a curved plate by operating on the backscattered signal with Digital Signal Processing (DSP) technique, and then comparing these results with the baseline signal. Tua et al., (2004) used the Hilbert–Huang transform to determine the Time of Flight (TOF) and employed the triangulation technique for the detection of linear cracks in metallic plate structure while Ng et al., (2009) used the same principle to locate damage in composite plates. Gangadharan et al., (2010) presented a new technique of damage detection in metallic and composites using triangulation method together with the concept of geodesics. Asty et al., (1978) studied the damage detection using triangulation, on a spherical surface by acoustic emission technique. Yoon et al., (1992) and Barat et al., (1993) extended the same technique onto cylindrical surfaces with the geodesic concept. Li et al., (2013) introduced the ellipse localization imaging algorithm to identify the orientation of the defect. Joel et al., (2009) investigated the suitability of time reversal technique on a cylindrical shell using guided waves from two PZT transducers. An algorithm for damage detection in an unwrapped cylindrical shell subjected to impact damage was presented by Taileh (2011).

In the present study, the geodesic concept combined with the triangulation approach is extended for identification of damage location in isotropic curved plate structures. Surface mounted piezoelectric (PZT) transducers are used to generate Lamb waves owing to the property of the PZT transducers that they can be used as both actuators and sensors. The fundamental anti-symmetric Lamb mode (A_0) is used for interrogation in the structure. Model of the curved plate and the circumferential Lamb waves is generated using a commercial FEM code, ABAQUS EXPLICIT. Numerical results for the curved isotropic plate are presented to substantiate the feasibility of the geodesic-based triangulation approach for damage detection in curved panel structures.

GEODESIC-BASED TRIANGULATION APPROACH

Damage detection using triangulation technique involves the use of time of flight (TOF) data for a wave of known velocity to construct a loci of possible damage location points for each

actuator–sensor pair and arriving at common intersections of loci of multiple actuator–sensor pairs indicating the location of the damage. Geodesic based triangulation technique involves the usage of the concept of geodesics together with triangulation technique for efficient damage detection in any kind of complex surfaces as presented by Gangadharan et al., (2010).

Geodesic approach depends on the fundamental fact that a wave takes minimum energy path to travel between two points on a surface which is nothing but the shortest distance between the two points on the surface. The geodesic distance for a planar surface between any two points is a straight line while for a curved surface is an arc of a great circle.

Barat et al., (1993) derived the expression for geodesic distance on a cylindrical surface according to which, if *ds* is an arc element on the cylindrical surface of radius *r,* in polar co-ordinates as shown in Fig.2, the length of curve between two points A and B is given by Eq.1,

$$L = \int_A^B ds \quad (1)$$

For shortest distance between A and B, the above integral will be minimum, i.e.

$$\delta L = \delta \int_A^B ds = 0$$

(2)

If the co-ordinates of A and B are (r_1, θ_1, z_1) and (r_2, θ_2, z_2) respectively, the geodesic distance is given by,

$$L = \sqrt{(r\theta_1 - r\theta_2)^2 - (z_1 - z_2)^2} \quad (3)$$

Using this concept of geodesics, a simplified approach is adopted for damage detection in curved plate with a circular sensor array shown in Fig.3 (a), by unwrapping the plate i.e., the curved plate becomes a rectangular flat plate of size $(r\theta_{total} \times h)$, where θ_{total} the angle formed by the curved plate at the center and *h* is the height of the curved plate (Fig.3 (b)).

If the co-ordinates of the sensors and damage in polar co-ordinates are assumed to be (r_1, θ_1, z_1), (r_2, θ_2, z_2), (r_3, θ_3, z_3), (r_4, θ_4, z_4) and (r_0, θ_0, z_0), respectively, after unwrapping the curved plate, the plate is now transformed into an $(r\theta, z)$ co-ordinate system, the new co-ordinates can be given now as, $(r\theta_1 \times z_1), (r\theta_2 \times z_2), (r\theta_3 \times z_3), (r\theta_4 \times z_4)$ and $(r\theta_0 \times z_0)$ respectively as shown in Fig.3 (b).The plate now being flat, the geodesic distance between any sensor and damage is a straight line given by,

$$D(S_i - d) = \sqrt{(r\theta_1 - r\theta_2)^2 - (z_1 - z_2)^2}$$

(4)

For $i = 1, 2, 3, 4$

Where $D(S_i - d)$ represents the geodesic distance between sensors and the damage. It can be observed that, irrespective of whether the plate is curved or flat, the geodesic distance between any two points is given by the same expression. Thus unwrapping a curved plate into a flat plate and transformation of co-ordinates can be seen as a simplified method of arriving at the geodesic distance.

If V_g is the group velocity of the chosen Lamb wave mode and Δt is the time taken by the wave to travel from the actuator (S_1) to the damage (*d*) and to the sensor (S_2), i.e. TOF, in the discretized structure,

$$\Delta t = \frac{D(S_1 - d)}{V_g} + \frac{D(S_2 - d)}{V_g}$$

(5)

$$\Delta t.V_g = D(S_1 - d) + D(S_2 - d)$$

(6)

Where, $D(S_1 - d)$ and $D(S_2 - d)$ are the geodesic distances computed between the sensor locations S1 and S2 and the damage *d*. The locus defined by Eq.6 is an ellipse with the actuator and the sensor being its foci. The parameters *a, b* to construct the ellipse $\frac{x^2}{a^2} + \frac{y^2}{b^2} = 1$ can be computed as, s

$$2a = D(S_1 - d) + D(S_2 - d)$$

(7)

$$b^2 = a^2 - c^2$$

(8)

Where,

$$2c = \sqrt{(r\theta_1 - r\theta_2)^2 - (z_1 - z_2)^2}$$

(9)

This implies that once the TOF and the group velocity is known, it is possible to construct an ellipse with the actuator and the sensor as its foci. With the construction of an ellipse, loci of possible damage are located for each actuator sensor pair and the intersection of multiple loci gives the location of the damage in the curved plate.

NUMERICAL STUDY ON ISOTROPIC CURVED PLATE

The geodesic based triangulation approach for the damage detection is investigated on curved Aluminum plates of different curvature, with the plate being clamped on all the sides. The plate was modelled in ABAQUS EXPLICIT FE software. Four PZT transducers (10 mm × 10 mm × 0.5 mm) placed at four corners of the plate (Fig.4 (a)) are used in the study. Combination of these transducers to form the actuator-sensor pair will give us the ellipse for triangulation.

The curved aluminum plate was modelled as three cases with different curvatures, each of them being healthy and damaged, in the form of a cut-out at the center of the plate as in Fig.4 (a). The properties of the curved plates and the transformed cylindrical co-ordinates of sensors for each plate are given in the Table 1 and 2 respectively.

A 5 cycle windowed sine pulse actuation signal with an excitation frequency of 100 kHz was used to actuate fundamental A_0 Lamb mode. Explicit dynamic analysis is carried out, the Lamb waves are generated by transducer S_1 and the responses from S_2, S_3 and S_4 were extracted (Fig.4 (b)). The group velocity obtained from dispersion curves is $C_g = 1820$ m/s.

With the obtained values of TOFs and group velocity, ellipses are constructed for each actuator sensor pair and possible location of damage is determined. The ellipses constructed for each pair are combined for a given plate and the intersection indicating the location of the damage in the curved plate is obtained using MATLAB program.

The MATLAB results of the plate with curvature of 10^o plate, for the actuator sensor pair, S_1-S_2, S_1-S_4 and S_2-S_3 is as shown in the Fig.5.

Also, the co-ordinates of damage obtained by this algorithm for all three cases is presented in the Table 3.

It can be seen that the results obtained in all three cases are in good agreement with the actual location of damage in the transformed co-ordinate system, $r\theta = 200$mm, $z = 200$mm.

CONCLUSION

In the present work, an attempt has been made to propose the triangulation approach based on the geodesic concept to locate damage in a curved isotropic plate. Three cases of curved plate were studied. A simplified approach for determining the geodesics on the curved surface is presented by unwrapping the curved plate to a flat plate. An ellipse was then constructed to ascertain the loci of the possible damage location points for each actuator–sensor pair and their intersections results indicated location of the damage in the plate. Some of the conclusions that can be drawn from the results include:

- Circumferential Lamb waves can be considered as a potential tool for damage detection in curved plates.
- Irrespective of the curvature, it was possible to locate the damage using the above presented technique.

This way, geodesic based triangulation technique of damage detection was successfully extended to curved plate structures of different curvatures and satisfactory results have been obtained. Thus, the geodesic-based triangulation method can be employed for accurate damage location in isotropic curved panel structures of any curvature.

ACKNOWLEDGEMENTS

The authors are grateful to Structural Technologies Division, NAL, Bangalore, India for providing necessary facilities required for the present study. Their appreciations extend to The Ministry of Science and Technology (DST), Government of India for their support to carry out the research (S-1-282).

REFERENCES

[1] C. Valle (1999), Guided circumferential waves in layered annular structures, Ph.D. Thesis, Georgia Institute of Technology.
[2] C. Valle, J. Qu, and L. J. Jacobs (1999), Guided circumferential waves in layered cylinders, Int. J. Eng. Sci., Vol.37, pp 1369–1387.
[3] C. Valle, J. Qu, and L. J. Jacobs (2001), Crack characterization using guided circumferential waves, J. Acoustic. Soc. Am., Vol.110, No.3. pp 1282-1290
[4] D.J. Yoon, YH.Kim, OY.Kwon (1992), New algorithm for acoustic emission source location in cylindrical structures, J. Acoustic. Emission, Vol.9, pp 237–242.
[5] G. Liu, J. Qu (1998), Guided circumferential waves in a circular annulus, J. Appl. Mech., Vol.65, pp 424-430.
[6] I.A. Viktorov (1958), Rayleigh-type waves on curved surfaces, J. Acoust. Soc. Am., Vol.4, pp 131-136.
[7] I.A. Viktorov (1967), Rayleigh and Lamb Waves, Plenum Press, New York.
[8] Joel Harley et al., (2009), Focusing of Ultrasonic Waves in Cylindrical Shells using Time Reversal, 7th International Workshop on Structural Health Monitoring.
[9] Ka Lok Jimmy Fong (2005), Ph.D. Thesis, Imperial College London, University of Lonon.
[10] M. Asty (1978), Acoustic emission source location on a spherical or plane surface, NDTE Int. Vol.11, No.5, pp 223–226.
[11] Ng C T and Veidt M (2009), A Lamb wave based technique for damage detection in composite laminates, Smart Material Structures, Vol.18 074006
[12] P. Barat, P. Kalyanasundaram, B. Raj (1993), Acoustic emission source location on a cylindrical surface, NDTEInt, Vol.26, pp 295–297
[13] R. Gangadharan, M R Bhat, C R L Murthy and S Gopalakrishnan (2010), A geodesic-based triangulation technique for damage location in metallic and composite plates, Department of Aerospace Engineering, IISc, Smart Material Structures, Vol.19 115010 (10pp)
[14] S. Towfighi, T. Kundu, M. Ehsani (2002), Elastic Wave Propagation in Circumferential Direction in Anisotropic Cylindrical Curved Plates, Journal of Applied Mechnaics, Vol.69, pp 283-291.
[15] Talieh Hajzargarbashi (2011), Ultrasonic non-destructive evaluation: impact point prediction and simulation of ultrasonic fields, Ph.D. Thesis, The University of Arizona.
[16] Tua P S, Quek S T, and Wang Q (2004), Detection of cracks in plates using piezo-actuated Lamb waves Smart Material Structures, Vol.13, pp 643–60.
[17] Xipeng Li, Chunguang Xu and Wei Dai, The segmental spherical shell thin plate Defect's detection based on transducer array (2013), 12th International Conference of the Slovenian Society for Non-Destructive Testing, Application of Contemporary Non-Destructive Testing in Engineering, pp 179-187.

Table 1 Properties of curved plate

	Radius (r mm)	Height (z mm)	Central angle (θ)
CASE 1	2291.9	400	10^o
CASE 2	381.97	400	60^o
CASE 3	208.35	400	110^o

Table 2 Transformed Co-ordinates of sensors

SENSORS	$r\theta$ mm	z mm
S1	5	5
S2	395	5
S3	5	395
S4	395	395

Table 3 Transformed Co-ordinates of damage

Co-ordinates	$r\theta$ mm	z mm
CASE 1	201.3	200
CASE 2	199.2	200
CASE 3	199.8	201

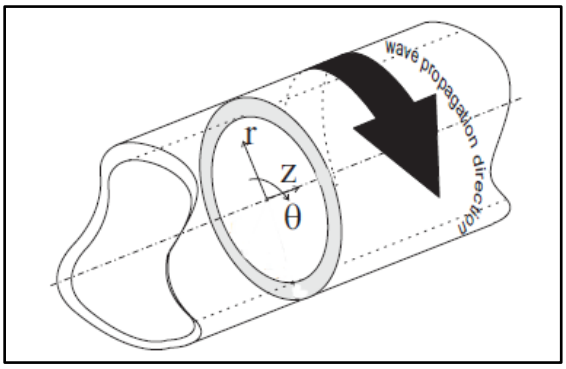

Fig.1 Wave propagation in a cylindrical curved plate [Ka Lok Jimmy Fong (2005)]

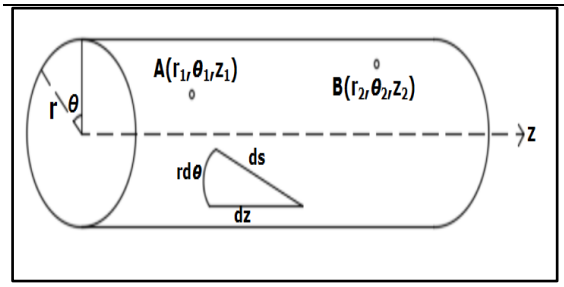

Fig.2 Co-ordinates for a cylindrical shell

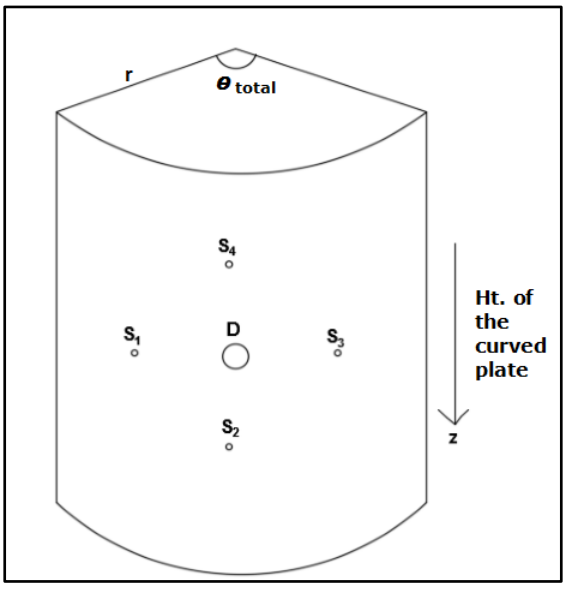

(a)

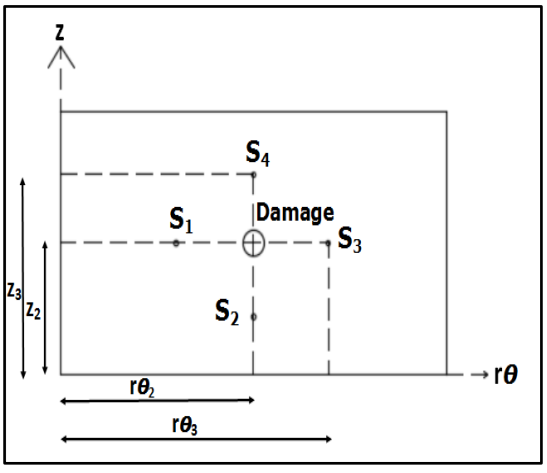

(b)

Fig.3 (a) Curved plate (b) Unwrapped curved plate with transformed co-ordinates

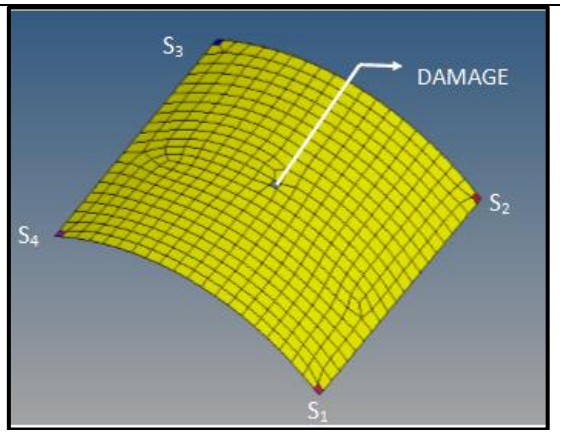

(a)

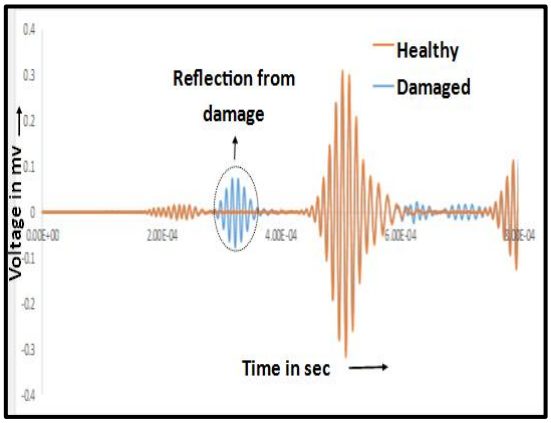

(b)

Fig.4 (a) FE model of the curved plate (b) Sensor response of actuator-sensor pair S_1-S_2 showing reflection from damage

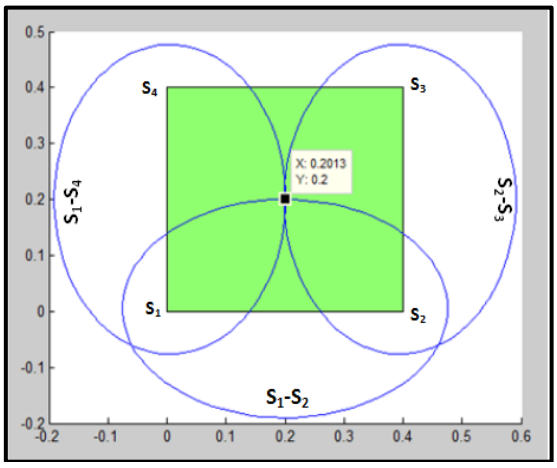

Fig.5 Triangulation of damage using ellipse

5th International Engineering Symposium - IES 2016
March 2-4, 2016, Kumamoto University, Japan

Studies on Wave Propagation in Stiffened Plate Structures

Radhika Harshini V [1], U. Ashwin[2], S. Raja [2], Katta Venkataramana[3], C.N Sathyanarayana[2]

1 M.Tech student, Dept. of Civil Engineering, National Institute of Technology, Surathkal, Mangalore, India (Presenting Author) Email – radhika6493@gmail.com
2 Scientist, Structural Technologies Division, CISR-National Aerospace Laboratories, Bangalore, India Email - raja@nal.res.in
3 Professor, Dept. of Civil Engineering, National Institute of Technology, Surathkal, Mangalore, India Email – ven.nitk@gmail.com

ABSTRACT:
Structural Health Monitoring (SHM) is a process of implementing damage detection and health characterization strategies for engineering structures. One of the popular active inspection approaches is Lamb wave based SHM, where actuation and sensing is mostly realized with surface-mounted Piezoelectric (PZT) transducers. The wave propagation behavior in stiffened plate structures is obtained using numerical simulations. In the first case, an aluminum plate with aluminum stiffeners is considered where the stiffeners are attached to the plate through equispaced rivets. As another case, a CFRP plate with adhesively bonded aluminum stiffeners is modelled. The interaction of Lamb waves with stiffeners is studied and quantified in terms of Maximum Amplitude Spectrum of the sensor responses.

***Keywords**: Structural Health Monitoring, Lamb wave, Piezoelectric transducers*

INTRODUCTION

Intensive research and development of Non-Destructive Evaluation (NDE) techniques has made it possible to identify structural damage at a very early stage. Further, the NDE has drastically improved the economic savings and service life of a structure. The service lifetime of a structure depends on the ability to detect and monitor potential development of defects, operational damages and crack initiation and propagation, among other things. Structural Health Monitoring (SHM) is a specific type of NDE technique which involves observation of a system over time using responses from an array of sensors, extraction of damage related features from these measurements, and their statistical analysis so as to determine the current state of health of the system. One of the most popular SHM techniques is Lamb-wave based damage detection in thin metallic and composite structures as observed by Zhongqing etal., (2006) and Jeong-Beom Ihn etal., (2008). Lamb waves are generated and observed using piezoelectric actuators and sensors. In these damage detection methods, information about damage (in terms of location, severity and type of damage) is carried by change in characteristics of an elastic wave due to its interaction with the damage. The primary advantage of Lamb waves is their ability to propagate over long distances, low attenuation and easy implementation using piezoelectric (Lead Zirconate Titanate, PZT) transducers. Consequently, their use allows fast and efficient inspections of industrial structures.

Stiffened panels are frequently used in aerospace, naval, and various civil engineering structures.

An aircraft structural panel of the skin-stiffener type is commonly used in aircraft construction. The panel has a skin supported by uniformly spaced stiffeners or frames. Currently, stiffened-panel aircraft structures are found in the wings and fuselage of aircraft. These panels are

typically constructed using aluminum or fiber reinforced composites. The main function of a stiffener (or stringer) is to control local buckling of a panel.

In this paper, the characteristics of the Lamb wave propagating through aluminum and CFRP panels with two longitudinal stiffeners are investigated. Wave attenuation, particularly of the A0 mode, in terms of propagation past the stiffener is studied.

Similar study was done by Liu Y (2011) and Greve etal., (2008), who investigated the propagation characteristics of Lamb waves in stiffened carbon fiber polymer matrix composite panels. Rathod etal., (2010) has presented a paper on Lamb wave based monitoring of plate stiffener debonding using a circular array of piezoelectric sensors. The group velocities of S0 and A0 modes were calculated, the attenuation of Lamb waves (particularly S0 mode, in terms of propagation distance) induced by stiffeners and delamination were evaluated, and the angular dependence of group velocity is subsequently examined.

THEORETICAL BACKGROUND ON LAMB WAVES

Guided waves in plates, also termed as Lamb waves, can be used for NDT of aircraft panels.Lamb wave theory is completely documented in a number of literatures (Viktorov (1967), Graff (1975)). Radzien etal., (2013) and Zhou etal., (2006) have studied the complications arising in the application of Lamb waves which include the existence of multiple modes and the dispersive character of the modes. An accurate calculation of dispersion curves is the first step in an adequate numerical modeling of Lamb waves. This was observed by Liang Chen etal., (2012) and Zhongqing Su etal., (2009). Furthermore, the information contained in the dispersion curves is essential in computing the distance the wave travelled.

The well-known Rayleigh-Lamb equations is given below:

$$\frac{\tan(qh)}{\tan(ph)} = -\frac{4k^2pq}{\left(k^2-q^2\right)^2} \quad (1)$$

for symmetric modes, and

$$\frac{\tan(qh)}{\tan(ph)} = -\frac{\left(k^2-q^2\right)^2}{4k^2pq} \quad (2)$$

for antisymmetric mode.

In the above equations, where *k* is wave number and *h* is the plate thickness. The variables *p* and *q* are found from the circular frequency (ω), wavenumber (*k),* and bulk longitudinal (C_L) and shear wave (C_T) velocities where *p* and *q* are computed as;

$$p^2 = \left(\frac{\omega}{C_L}\right)^2 - k^2; \qquad q^2 = \left(\frac{\omega}{C_T}\right)^2 - k^2 \quad (3)$$

Rayleigh-Lamb equations are used to determine the velocity at which a wave of a particular frequency (*f*) will propagate within the plate. These equations can only be solved numerically and is done so by trial and error method. Further from equation (1) and (2), it can be inferred that the velocity of Lamb wave is a function of frequency thickness product (*fh)*.

FINITE ELEMENT MODELING ASPECTS IN WAVE PROPAGATION

The 2D finite element (FE) models are developed to simulate Lamb wave responses of the specimens. The commercial FE package, ABAQUS® EXPLICIT which is based on central difference method, is used. The choice of element size is a very important factor in finite element modelling as the precision of the analysis depends on it. The element size for meshing the structure depends upon the wavelength of the propagating Lamb wave and is determined by the following steps.

a) Calculate phase velocity 'C_p'

$$C_p = \sqrt{\frac{E}{2\rho(1+\mu)}} \quad (4)$$

Where, *E* is the Young's modulus and ρ is the density of the material.

b) The wavelength is

$$\lambda = \frac{C_p}{f_{\max}} \quad (5)$$

where f_{max} is the maximum frequency that may be used to actuate the Lamb wave in the present model.

c) Length of the element (element size for mesh) 'L_e'

The size of the finite element, L_e, is typically derived from the smallest wavelength (λ) to be analyzed. For a good spatial resolution 10 nodes per wavelength are normally required, although some studies recommend a more stringent condition of 20 nodes per wavelength

$$L_e = \frac{\lambda}{10} \quad (6)$$

The piezoelectric actuation of the transducers is modelled as equivalent forces applied along the edges of the elements to model as the actuator. These equivalent forces are derived from the constitutive relations of piezoelectricity, as mentioned below.

The actuator equation,

$$\{\sigma\} = [C]\{\varepsilon\} + [e^T]\{E\} \quad (7)$$

The sensor equation,

$$\{D\} = [e]\{\varepsilon\} + [\kappa]\{E\} \quad (8)$$

where σ and ε are the normal stress and strain vectors, *D* is the electrical displacement vector, *e* is the piezoelectric stress constant, κ is the dielectric matrix, C is the stiffness matrix and *E* is the electric field vector.

FE SIMULATION OF LAMB WAVE PROPAGATION IN STIFFENED PANEL

In the present work we study Lamb wave propagation in aluminum and CFRP plates. Studies conducted on the interaction of Lamb wave with stiffeners show the complexities involved in using Lamb wave in stiffened plate structures.

We have considered aluminum and CFRP panels stiffened with longitudinal stiffeners as shown in *Fig.1*.In case of aluminum panel, the stiffeners are riveted to the panel, whereas in CFRP panels the stiffeners are adhesively bonded. Centrally placed two PZT actuators which are surface bonded onto top and bottom surface of the plate acts as emitters (A), generating A0 Lamb wave and 8 PZT patches (R1, R2, R3, …., R8) in a circular configuration act as sensors to sense the generated Lamb waves.

The actuation pulse is generated in a MATLAB® based program for a desired frequency and number of cycles, and these signals are windowed with standard Hanning window. A 3.5 cycle windowed sine pulse actuation signal is considered throughout. Lamb waves generated by the emitters are seen propagating in the plate structure in all directions. The responses from various sensors are collected in terms of voltage v/s time plot. *Fig.2* shows the sensor responses when a stiffened plate is excited with a wave of 60kHz frequency.

A MATLAB® program involving Hilbert Transform is used to arrive at the absolute value (amplitude in terms of volts) from the obtained sensor responses. The above procedure is repeated for different Lamb wave frequencies, varying from 10 kHz to 100 kHz, to identify the peak response and construct the maximum amplitude spectra for all the sensors.

The basis of this procedure is to generate the Maximum Amplitude Spectra (MAS) for each sensor response and monitor its variation in terms of amplitude and frequency of the propagating Lamb wave. In the present work, the MAS responses are computed both numerically and experimentally to understand the effect on MAS in the presence of stiffeners.

1. Aluminum plate

A FE model of aluminum plate is shown in *Fig.3.* The aluminium plate is 400×400×1.5 mm^3 in dimension. The L shaped stiffeners have a width of 15mm and thickness of 1mm. The dimensions of the PZT actuator and sensors are 15×15×0.5 mm^3 and 10×10×0.5 mm^3 respectively.

The material properties of the plate and PZT transducers are mentioned below.

Aluminium; *Youngs modulus= 70Gpa, Density=2820kg/m^3, Poisson's Ratio=0.33. PZT; Youngs modulus =53Gpa, Density=7500kg/m^3, Poisson's Ratio= 0.22*.

The MAS response of riveted aluminum stiffened panel estimated by numerical and experimental means are shown in *Fig.4 (a) and 4(b)* respectively.

The MAS of riveted stiffened plate indicates that the peak amplitude occurs at frequency of 30 kHz. In general, the PZT patches which are adhesively bonded on the aluminum panel shows reduced response compare to sensor response of R1 & R4 as Lamb wave propagates in the

panel. Thus riveting the stiffeners to the host structures allows the Lamb waves to propagate by marginally getting affected. The sensors R2 and R3 which are away from the stiffeners shows more reduction in the response compare to the sensors R5-R8 which are closer to the stiffener. The response curves of sensors which are at similar position coincide.

2. CFRP plate

A 400×400 mm CFRP plate of 1.8mm thickness is considered. The CFRP plate is comprised of 6 layers, each 0.3 mm thick. CFRP has the following material properties; *Young's modulus = 60 Gpa, Density = 1600 kg/m^3, Poisson's Ratio = 0.05.*

The stiffeners are adhesively bonded to the CFRP panel. MAS response, estimated by numerical and experimental means of the CFRP stiffened panel are shown in *Fig.5 (a) and 5(b)*.

For CFRP plates, the peak response frequency can be seen at a frequency of 40 KHz.It can be observed that the amplitude reduces when Lamb wave travels at an angle away from the fibre direction (0°/90°) in CFRP composite panel. The sensors mounted along the fibre direction (0°/90°) and on either sides of the stiffeners (R2 and R3) show reduction in the Lamb wave response compared to the response of R1 and R4 which lie within the stiffeners. The sensors R5-R8, which are bonded away from the fibre direction and after the stiffener show higher reduction in the Lamb wave response compare to response of R1 and R4.

CONCLUSION:

Structural health monitoring (SHM) is a key component of damage prognosis and detection systems. An SHM subsystem typically consists of an onboard network of sensors for data acquisition and some central processor to evaluate the structural health. It may utilize stored knowledge of structural materials, operational parameters, and health criteria. Peak response of the sensors in the Maximum Amplitude Spectra are used as parameters to assess the wave propagation in a stiffened aluminum and CFRP plate.

From the numerical and experimental studies carried out, we can observe that the experimental model shows more reflections from the stiffener than the numerical model, for the aluminum panel. The reason for this is that, in numerical model no contact exists between the stiffener and the panel. Contact condition may have to be adopted for numerical simulation. The sensors which are away from the stiffeners shows more reduction in the response compare to those closer to the stiffener. In case of CFRP panels, a reduction in response amplitude can be seen when the Lamb wave travels at an angle away from the fiber direction (0°/90°) and this reduction is more prominent in sensors located away from the stiffeners.

ACKNOWLEDGEMENTS

The authors are grateful to Structural Technologies department, NAL, Bangalore, India for providing necessary facilities required for the present study. Their appreciations extend to The Ministry of Science & Technology (DST), Government of India for their support to carry out the research (S-1-282).

REFERENCES

1) B. Masserey, Christian Raemy, Paul Fromme (2014); High-frequency guided ultrasonic waves for hidden defect detection in multi-layered aircraft structures, Ultrasonics 54(2014) Pg.1720-1728, Elsevier.
2) I.A. Viktorov (1967), Rayleigh and Lamb Waves, Plenum Press, New York.
3) Jeong-Beom Ihn and Fu-Kuo Chang (2008); Pitch-catch Active Sensing Methods in Structural Health Monitoring for Aircraft Structures; Structural Health Monitoring, vol. 7 no. 1 5-19
4) K.F Graff (1975), Wave motion in elastic solids, Dover Publications, INC New York.
5) Liang Chen, Yanlei Dong, Qingyuan Meng, Wei Liang (2012); FEM Simulation for Lamb Wave evaluate the defects of plates; Pg 1-4, IEEE 978-1-4673-1893-8.
6) Maciej Radzien, Lukasz Dolin, Marek Krawczuk, Magdalena Palacz (2013); Damage localization in a stiffened plate structure using a propagating wave; Mechanical Systems and Signal Processing vol. 39, 388–395, Elsevier.
7) Rathod V.T and D. Roy Mahapatra (2010); Lamb wave based monitoring of plate stiffener debonding using a circular array of piezoelectric sensors; International Journal on Smart Sensing and Intelligent Systems; Vol. 3, No. 1, 2;
8) W. Greve , J. J. Neumann , J. H. Nieuwenhuis, I. J. Oppenheim, N. L. Tyson (2008); Use of Lamb Waves to Monitor Plates: Experiments and

Simulations; Structural Health Monitoring, 2009-vol. 8 no. 1 5-15.
9) Yingtao Liu etal., (2011) - Structural Health Monitoring and Damage Detection in Composite Panels with Multiple Stiffeners.
10) Z. Q. Zhou, W. K. Chiu, M. K. Bannister (2006)-Health monitoring of aircraft fuselage structures using ultrasonic waves; 25th international congress of the aeronautical sciences; ICAS 2006
11) Zhongqing Su, Ling Ye, Ye Lu (2006), Guided Lamb waves for identification of damage in composite structures: A review, Journal of Sound and Vibration, 295:753-780.
12) Zhongqing Su and Lin Ye (2009); Identification of damage using Lamb waves, Vol 48, Springer.

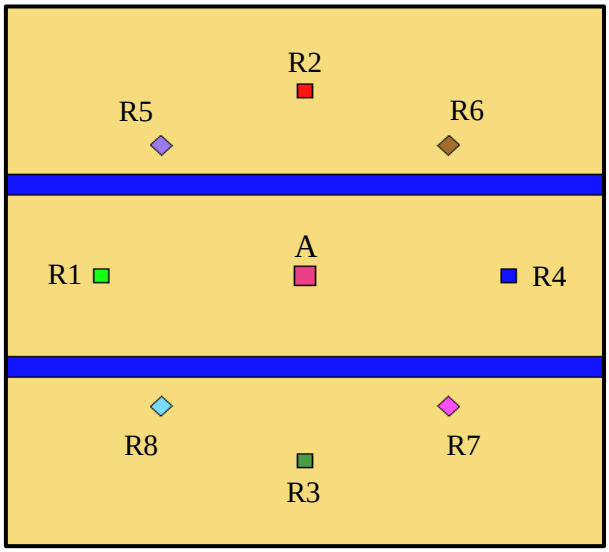

Fig 1. Stiffened plate with actuator 'A' and sensors 'R1-R8'

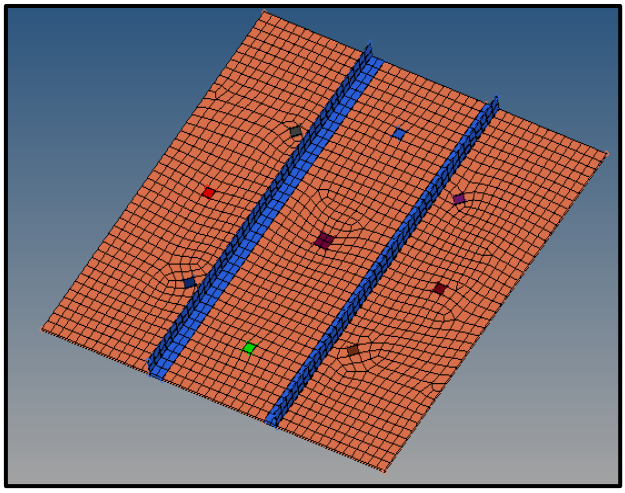

Fig 2. FE model of the stiffened plate

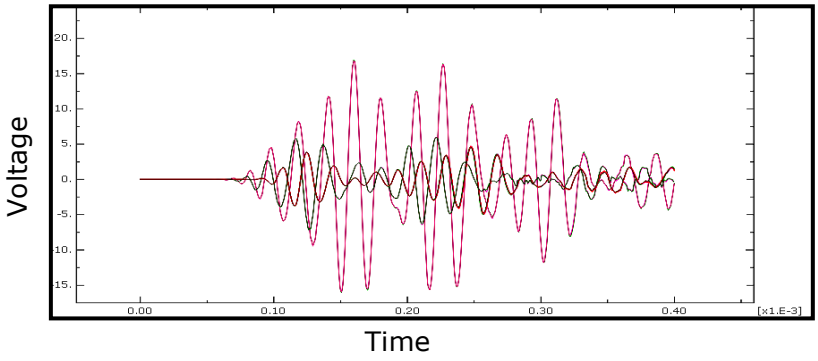

Fig 3. Voltage v/s time plot

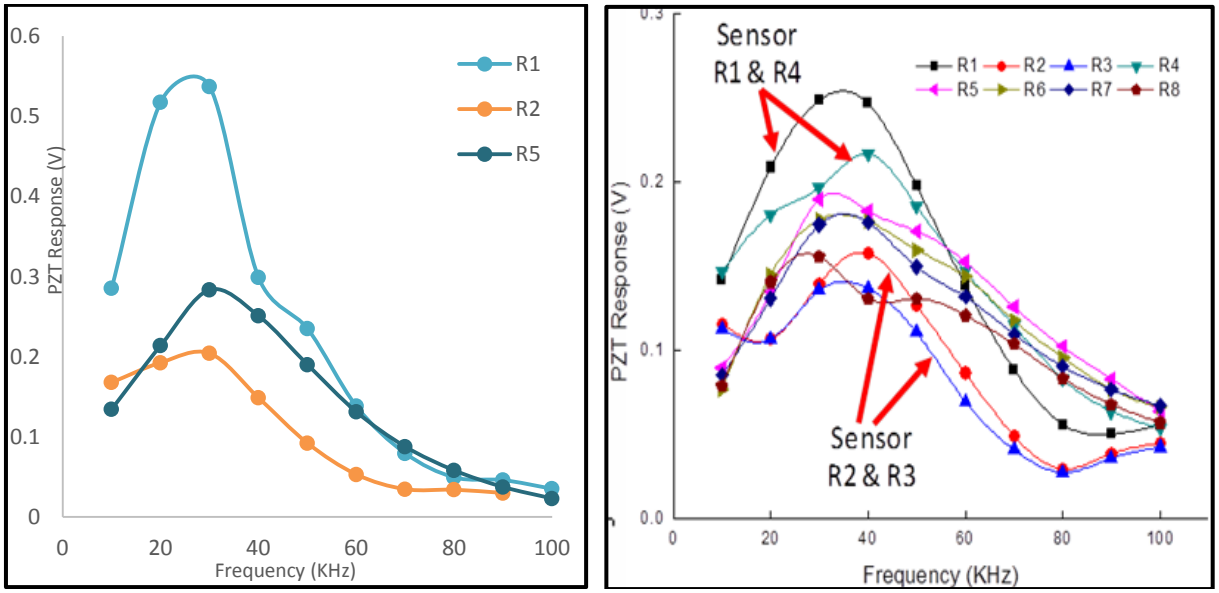

(a) by FEM **(b) by experimental**

Fig 4. MAS of riveted aluminum stiffened panel by FEM

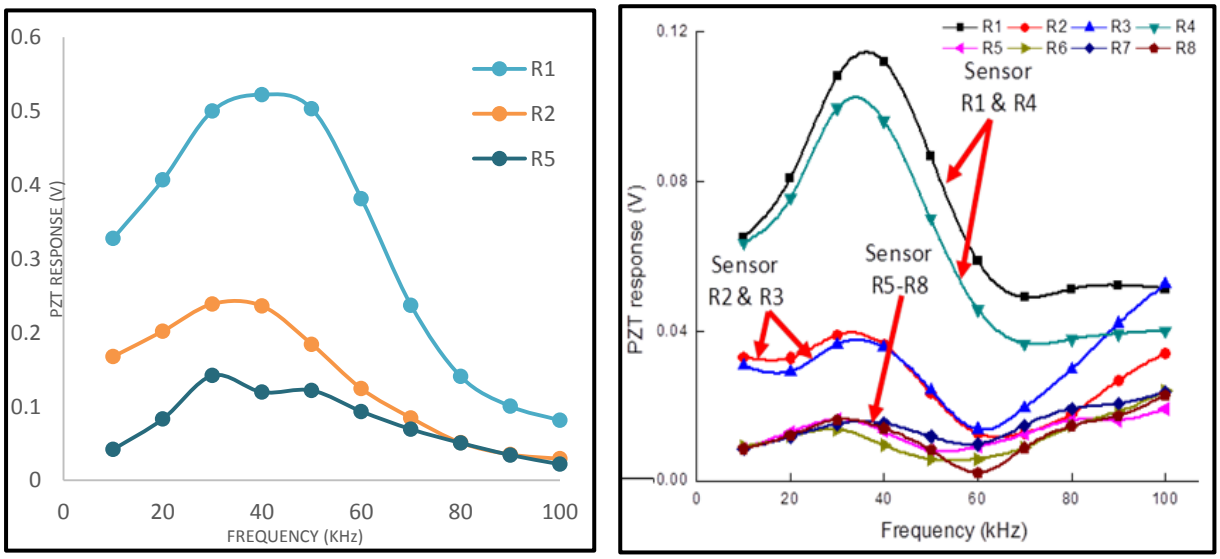

(a) by FEM **(b) by experimental**

Fig 5. MAS for stiffened CFRP panel

5thInternational Engineering Symposium - IES 2016
March 2-4, 2016, Kumamoto University, Japan

CLASSIFICATION OF CRACKS IN REINFORCED CONCRETE STRUCTURES USING ACOUSTIC EMISSION MONITORING TECHNIQUE

C Geetha[1] and R Vidya Sagar[2]

1 *Department of Civil Engineering, National Institute of Technology Karnataka, Surathkal, Mangalore, 575025, India.e-mail:12cv20.geetha@nitk.edu.in*
2 *Department of Civil Engineering, Indian Institute of Science, Bangalore 560012, India.email:rvsagar70@gmail.com*

ABSTRACT: In India, during the last 60-70 years several reinforced concrete (RC) structures were constructed. It is essential to maintain these RC structures and keep in useful condition. Because deterioration is a natural phenomenon and deterioration of these RC structures has started in these structures, a systematic approach is needed to assess the present damage condition. Non-destructive testing (NDT) such as acoustic emission (AE) technique is useful to monitor the ongoing fracture process of in-service RC structures. This article reports on classification of cracking in RC structures using AE monitoring technique. AE frequency parameters such as average frequency (AF), rise angle (RA) are used for characterizing the tensile cracking and shear cracking. It was observed that during tensile cracking there was an increase in the average frequency and during shear cracking average frequency decreases. A Gaussian mixture modelling (GMM) technique was used for classification of cracks in RC structures and the results are useful to distinguish between dominance of tensile cracks, shear cracks and the transition stage between tensile and shear cracking during the fracture process.

Keywords*: Acoustic emission, Concrete, Gaussian mixture modelling, cracking, Structural health monitoring.*

INTRODUCTION

It is known that AE monitoring technique is one of the non-destructive technique (NDT) method which is useful to test the structure without impairing its functionality or serviceability [4]. The main advantages of AE monitoring techniques are determination of event source location, characterizing and classification of types of cracks and health monitoring of safety operation of the structure. AE parameters such as frequency, rise angle, rise time, amplitude, and duration are crucial in classification of cracks in reinforced concrete structure [3]. RC structures could deteriorate due to heavy traffic loads and fatigue. The damages of such RC structures such as bridges, docks and buildings in service are qualified by applying cyclic load test (CLT) and monitoring AE activity. The released AE can be useful to locate the crack, the density of cracks, as well as the status of the damage condition.

Another aspect is the correlation of AE indices to the cracking mode. For most cases of materials and loadings until failure, tensile cracks are developed at the initial stage of loading, while shear cracks dominate later. This is typical for RC members that undergo bending. The initial cracking comes from the tensile load on the surface of concrete, while the member ultimately fails with diagonal shear cracks. Therefore, it is beneficial to characterize the mode of the cracks as it can lead to early assessment of the damage condition.

LITERATURE REVIEW

Classification method developed by the Japan Construction and material standard (JCMS-III B5706, 2003) of which results

were confirmed under the four-point bending tests and the direct shear tests of concrete specimens [5]. However, a defined criterion has not been confirmed. RA (Rise angle) and AF (Average Frequency) are parameters that can be used to readily classify the cracks into tensile and shear (Ohno and Ohtsu, 2010).

Initially when there is a micro cracking tensile cracks dominates and results in AE waveforms with shorter rise time and high frequency which includes opposing movement of the crack side's perpendicular to the crack plane. As the fracture progresses later shear cracks dominates with longer waveforms with high rise time and low frequency which includes opposite movement of cracks sides parallel to the crack plane. Thus, Crack propagation incidence has different AE signatures depending on the mode of the crack. This is mainly due to the larger part of energy transmitted in the form of shear waves, which are slower (Aggelis et al., 2010b). Therefore, the maximum peak of the waveform delays considerably compared to the onset of the initial longitudinal arrivals. This has been demonstrated in different kinds of materials, like concrete, fibre composites and rock [1].

A new approach based on Gaussian mixture modelling was presented to perform crack mode classification in RC structures in an experimental study carried out on a full scale RC shear wall subjected to reverse cyclic loading [2]. In Gaussian mixture models, clusters (i.e. tensile and shear respectively) are modelled with Gaussian distributions and maximize the likelihood of the GMM by expectation maximization (EM) algorithm [2].

AE PARAMETRE ANALYSIS

Extracting features from the AE signal is usually referred to as parameter based technique. Fig 1. Shows a typical AE signal with its main features. One of the crucial parameters which are influenced by the mode of crack is the average frequency (AF) and rise angle (RA) and AE energy.

RA (μs/dB) and AF (kHz) are defined as

RA = Rise time/Peak amplitude(1)

AF = Counts/Duration (2)

Thus the classification of cracking as shear and tensile was done by analysing the parameters AF and RA. The behaviour of some typical AE parameters with time for the same experiment is depicted in Fig. 2. The symbols stand for the value of the parameters, while the line is the moving average of 500 AE hits. Moving average of AF and RA value were plotted against time and were seen that, when there was sudden release of large number of AE hits (i.e. Fig.2), decrease in the AF and increase in the RA value can be seen.

AIM OF THE PRESENT STUDY

In this report, we would mainly focus on classification of cracking in reinforced concrete using Acoustic emission (AE) monitoring technique. Frequency parameters such as average Frequency (AF), Rise angle (RA) are used for characterizing the tensile cracks and shear cracks. The aim is to test the validity of a simple cracking mode characterization scheme based on Gaussian mixture modelling (GMM) and specific AE parameters in laboratory.

GAUSSIAN MIXTURE MODELLING

Tensile and shear clustering was obtained based on probability density estimation using Gaussian mixture models (GMM) and expectation maximization (EM) algorithm. A GMM is parametric probability density function represented as a weighted sum of M component Gaussian densities. For a *D*-dimensional measurement, feature vector $\vec{x}$, the mixture density defined as

$$p(\vec{x}|\lambda)=\sum_{i=1}^{m} p_i N(\vec{x}|\vec{\mu}_i),\sum_i) \quad (3)$$

i=1, 2, 3 … m

Where p_i are the mixture weights and $N(\vec{x}|\vec{\mu}_i), \sum_i)$ are unimodal component Gaussian (normal densities).
Each component density is *D*-variate Gaussian function of the form

$$N(\vec{x}|\vec{\mu}_c, \sum_c) = \frac{1}{(2\pi)^{D/2}|\sum|^{1/2}} \exp\{-\frac{1}{2}(\vec{x}-\vec{\mu})^T(\sum)^{-1}(\vec{x}-\vec{\mu})\} \quad (4)$$

With *D* X 1 mean vector $\vec{\mu}$, and DXD covariance matrix $\sum_c$. The complete Guassian mixture model is parameterized by the mean vectors and covariance matrices.

The EM algorithm is an efficient iterative procedure to compute the Maximum Likelihood (ML) estimate in the presence of missing or hidden data. In ML estimation, model parameter(s) are estimated for which the observed data are the most likely. In the expectation, the missing data are estimated given the observed data and current estimate of the model parameters. This is achieved using the conditional expectation, explaining the choice of terminology. In the Maximisation, the likelihood function is maximized under the assumption that the missing data are known. Convergence is assured since the algorithm is guaranteed to increase the likelihood at each iteration. Given a Gaussian mixture model the goal is to maximise the likelihood function with respect to the parameters comprising mean and covariance of the components and mixing coefficients.

Initialize the means $\vec{\mu}_c$, covariances $\sum_c$, and mixing coefficients π_i and evaluate the initial value of the log likelihood. In E-step, for each data point i and each cluster c, r_{ic} measures the relative probability that data point x_i belongs to the cluster c

$$\vec{r}_{ic} = \frac{\pi_c N(\vec{x}|\vec{\mu}_c,\sum_c)}{\sum_{c=1}^{K} \pi_c N(\vec{x}|\vec{\mu}_c\sum_c)} \quad (5)$$

If x_i is very likely under the c^{th} Gaussian, it gets high weight. In M-step, r_{ic} probabilities are assigned and parameters mean $\vec{\mu}_c$, covariances $\sum_c$, and mixing coefficients π_i are re-estimated using the current responsibilities. Total responsibility allocated to cluster c is given by

$$\vec{r}_c = \sum_i \vec{r}_{ic} \quad (6)$$

and fraction of total assigned to cluster c is given by

$$\vec{\pi}_c = \frac{\vec{r}_c}{N} \quad (7)$$

and the weighted average of the data is given by

$$\vec{\mu}_c = \frac{1}{\vec{r}_c}\sum_i \vec{r}_{ic}\vec{x}_i \quad (8)$$

Using this new weighted average of the data, weighted covariance of the assigned data is determined

$$\sum_c = \frac{1}{\vec{r}_c}\sum_i \vec{r}_{ic}\vec{x}_i\vec{x}_i^T - \vec{\mu}_c\vec{\mu}_c^T - \vec{\mu}_c\vec{\mu}_c^T \quad (9)$$

Thus log-likelihood of the model is evaluated, then iterated till convergence.

$$\vec{l}(\vec{\mu}|\vec{x}, \sum, \vec{\pi}) = \sum_i \ln \vec{\pi}_c N(\vec{x}_i; \vec{\mu}_c, \sum_c) \quad (10)$$

Iterations strictly increase the log-likelihood of the model, increasing of which fits the data.

EXPERIMENTAL SETUP

The experimental setup consisted of a servo hydraulic loading frame (1200 kN) with a data acquisition system and the AE monitoring system. A steel I-beam was placed beneath the actuator to transfer the load as two point loads. The load was applied (in four point bending) till failure of the specimen. The specimen was simply supported and the released AE signals were recorded using an 8 channel AE monitoring system. Resonant type AE differential sensors, pre-amplifiers, data acquisition system and processing instrumentation were used. The AE signals were amplified with a gain of 40 dB in preamplifier. The threshold value of 40 dB was selected to ensure a high signal to noise ratio.

ACI 437-12 proposed the cyclic load test (CLT) as a usual procedure for assessment of structural behaviour of RC members. By following ACI 437-12 guidelines the loading pattern was applied on the RC flanged beam specimen (assumed as a RC girder in a bridge) is shown in Fig. 3.In this article, specimen LC1M37 is used for AE parametric analysis and cracking mode characterization based on GMM technique.

RESULTS AND DISCUSSION

It is reasonable that the AE activity recorded at the different stages exhibits distinct characteristics. Before the main crack, any hit originates from small events of matrix cracking [1]. This cracking

occurs due to the tensile load at the bottom of the specimen. At the stage of the main crack formation, which is shortest in duration, a quite high rate of incoming AE signals are recorded. At that time the cracking events are more frequent and much stronger rupturing of the brittle matrix with a visible crack, accompanied by several side cracks takes place.

The variation of average AF against average RA for each cycle is plotted, a trend is observed along the depicted curve (i.e. Fig.4 (a) and Fig.4 (b)).Thus, the negative slope of the trend line is decreasing as the damage progresses and eventually comes to zero. The clustering of the data points towards the top left (i.e. Fig.4(a)) shows that during early stage emissions exhibit higher AF and lower RA and as the as fracture progresses, AF decreases and RA increases(i.e. Fig.4(b)) gradually.

From the GMM technique, we can cluster the tensile and shear region. AF versus RA graph(i.e. Fig.5) clearly defines two regionsthat is tensile and shear regions. A contour plot of Gaussian misture density function (i.e. Fig.6) implies two mutually exclusive categories of shear and tensile, where these regions are intersected and have a mixed Gaussian density function with a larger weight for tensile class in the load cycle 10. Cluster boundaries are defined by keeping the data points with higher likelihood into tensile or shear cluster and associate the rest of the data into other cluster named 'mixed' that is the transition stage(i.e. Fig.7) between tensile region and shear region . The mixed cluster is the one which includes the data with less probabilty of being associated to specific clusters.

CONCLUSION

Based on the above experimental results the given below conclusions can be drawn.

.

- AE parameters like the AF and RA exhibit strong sensitivity to the fracture mode (tensile micro-cracking, macro-cracking), showing that they can be included in a simple but reliable characterization scheme concerning the mode of damage in concrete.

- Tensile cracks are developed at the initial stage of loading, while shear cracks dominate later.

- GMM was able to identify three stages during the test: (a) dominance of tensile or flexural cracks during initial loading cycles, (b) transition stage during intermediate loading cycles, and (c) dominance of shear cracks during the final loading cycles.

REFERENCES

1Aggelis DG (2011) Classification of cracking mode in concrete by acoustic emission parameters. Mech Res Commun 38(3):153–157.

2) Alireza Farhidzadeh, et al, "A Probabilistic approach for damage identification and crack mode classification in Reinforced concrete structures", Journal of Intelligent Material Systems and Structures 0(0) 1-14. (DOI 10.1177/1045389X13484101).

3)Behnia,et al(2014) Advanced structural health monitoring of concrete structures with the aid of acoustic emission., Const and Buil Mat, 65, 282-302.

4) Grosse.C.U., Ohtsu.M,(2008) "Acoustic emission testing". Springer-Verlag. Berlin Heidelberg.

5) JCMS-IIIB5706 (2003) Monitoring method for active cracks in concrete by acoustic emission, construction materials standard, Federation of Construction Materials Industries, Tokyo.

6) Ohno K, Ohtsu M (2010), Crack classification in concrete based on acoustic emission. Const Build Mat 24(12):2339–2346.

7)R. Vidya Sagar • B. K. Raghu Prasad (2013) "Laboratory investigations on cracking in reinforced concrete beams using on-line acoustic emission monitoring technique", J Civil Struct Health Monit 3:169–186.DOI 10.1007/s13349-013-0036-5

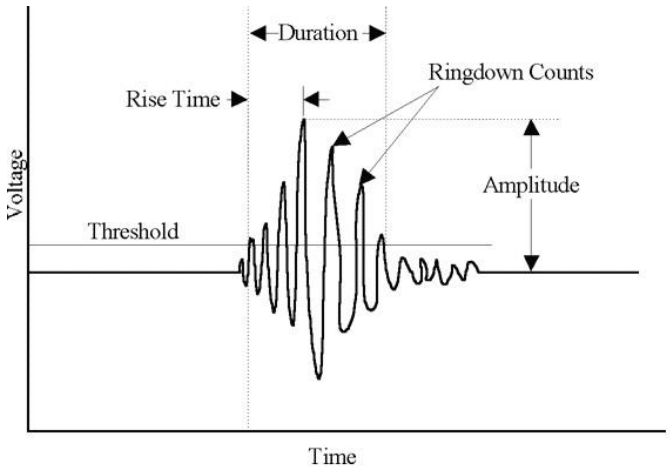

Fig.1. Schematic representation of a typical acoustic emission signal

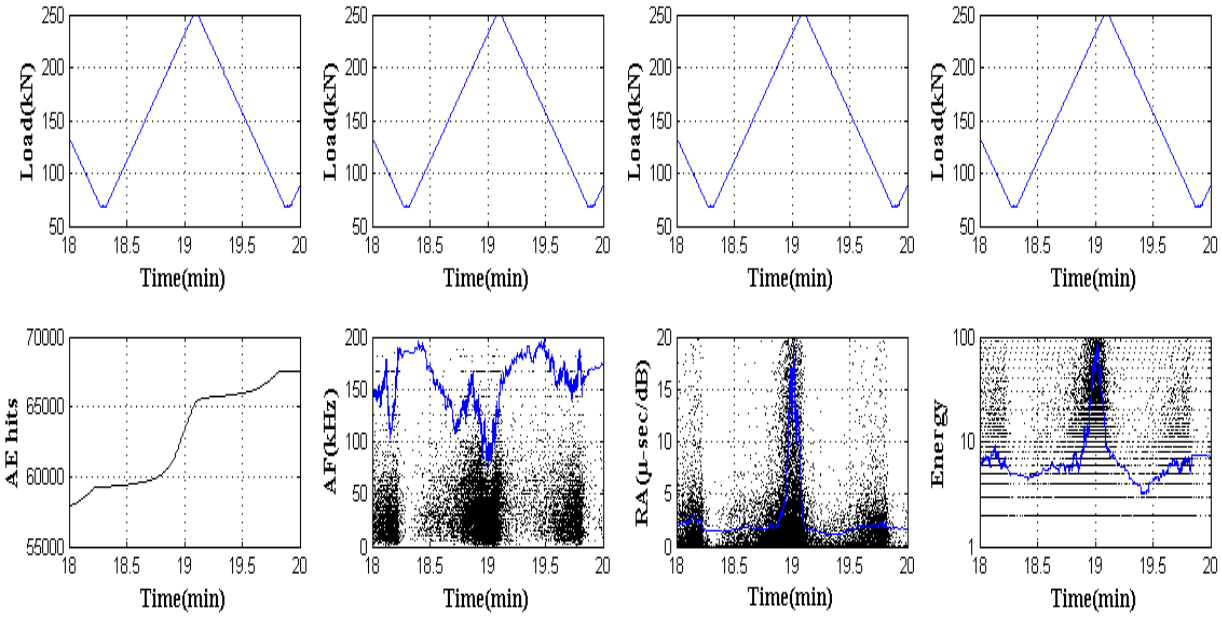

Fig.2. Time history of AE hits, Average Frequency, Rise Angle, and Energy for RCC concrete beam

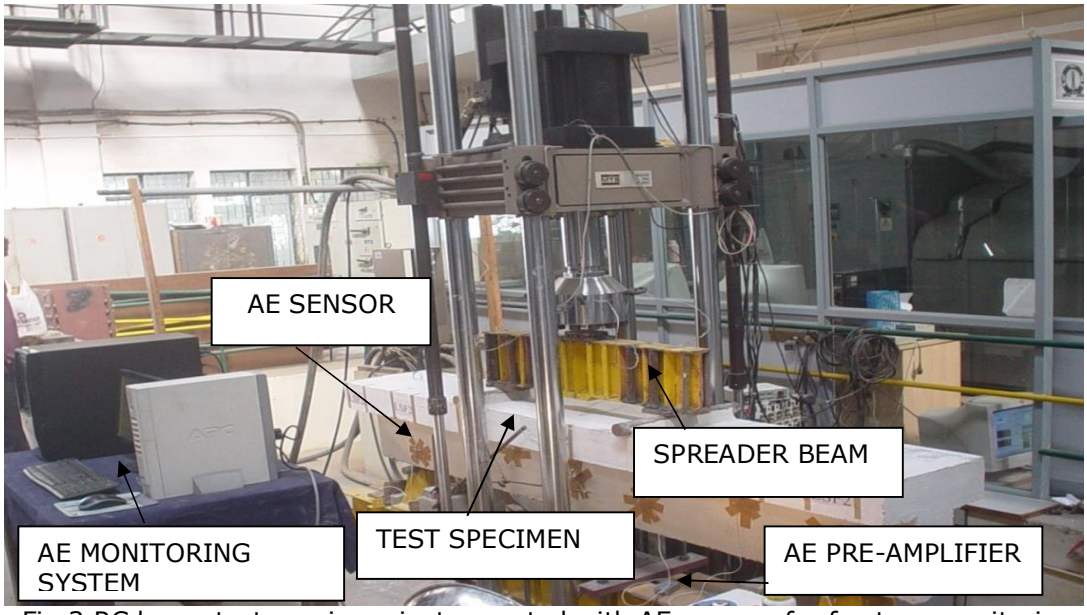

Fig.3.RC beam test specimen instrumented with AE sensors for fracture monitoring

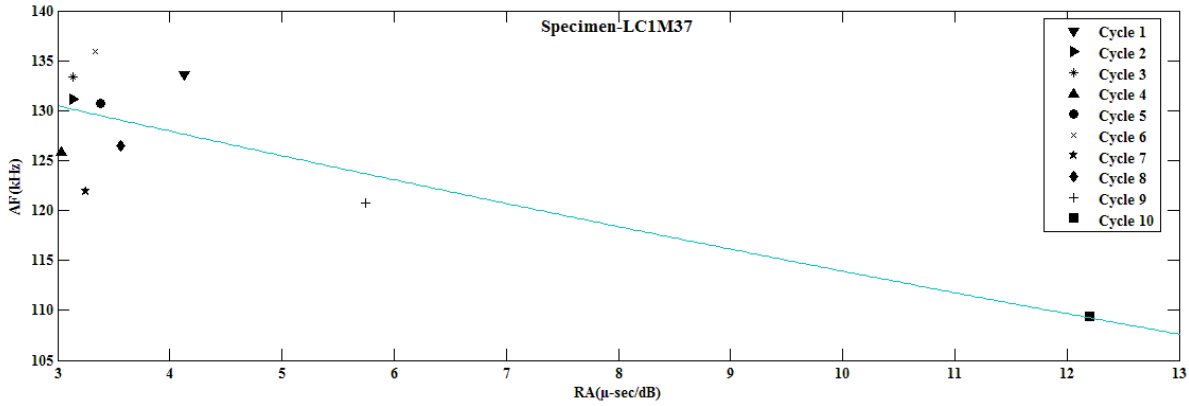

(a)

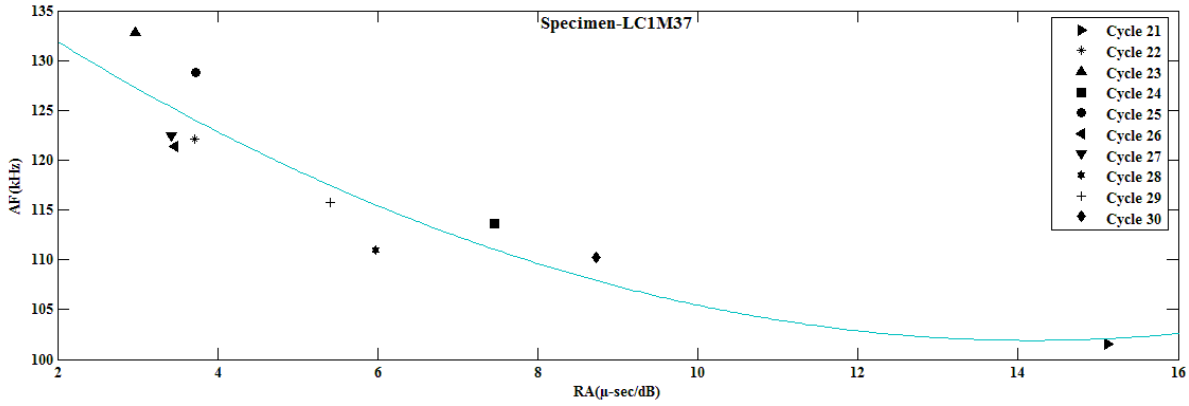

(b)

Fig.4. Graph of average AF(Average Frequency) v/s average RA(Rise angle) for each cycles (a) first ten cycles, (b) last ten cycles

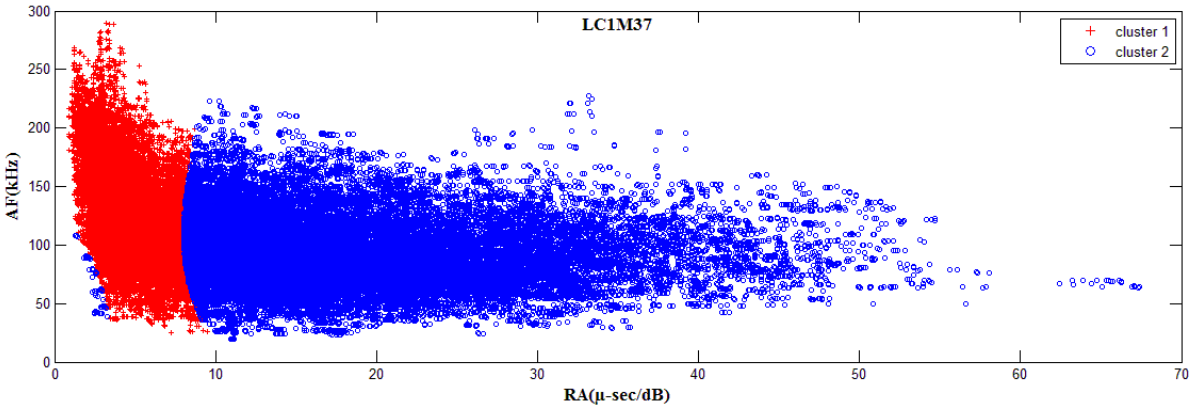

Fig.5.Average Frequency v/s Rise Angle showing tensile and shear region

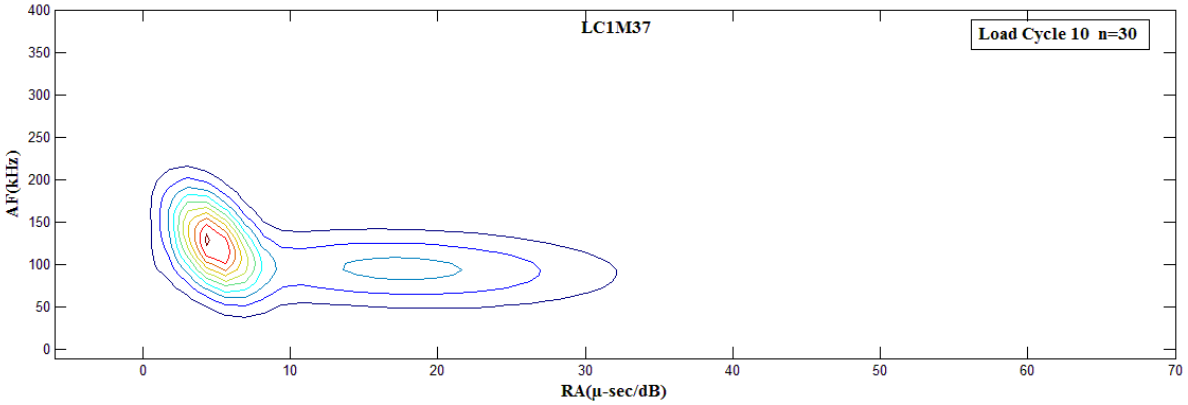

Fig.6. Contour plot of Gaussian mixture density function

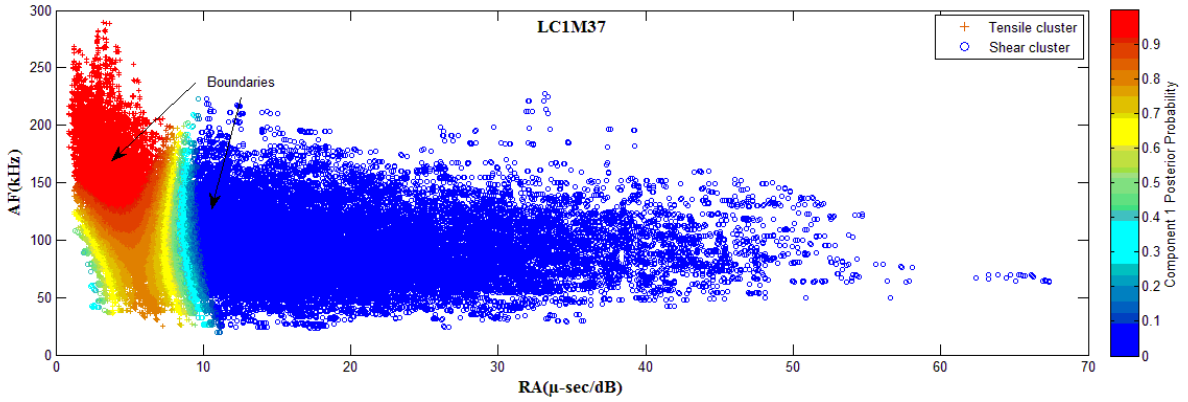

Fig.7.Average Frequency v/s Rise Angle showing the tensile, transition and shear region

5th International Engineering Symposium - IES 2016
March 2-4, 2016, Kumamoto University, Japan

Effect of Width of Gallery and Depth of Working on Stability of Coal Pillar

Shailaja M.[1], K. Ram Chandar[2] and Yamini Saraswathi[3]

1 UG Student, Department of Mining Engineering, National Institute of Technology Karnataka, Surathkal, Mangalore 575025, India email: shailaja.mallikarjun06@gmail.com
2 Assistant Professor, Department of Mining Engineering, National Institute of Technology Karnataka, Surathkal, Mangalore 575025, India. email: krc_karra@yahoo.com
3 Former UG Student, Department of Mining Engineering, National Institute of Technology Karnataka, Surathkal, Mangalore 575025, India. email: yamuub64@gmail.com

Abstract: Bord-and-Pillar is the most widely used method of underground coal mining in India. Stability of pillars is the major concern in underground mining as many fatal accidents in mines occur due to pillar failure. Factor of Safety is the measure of stability of coal pillars. The main objective of this study is to determine the stability of coal pillar for wide range of depth of working and width of galleries. Stress acting on the pillar is determined using Tributary area approach. The strength is obtained using empirical formulas like Salamon-Munro formula, Bieniawski and CMRI formula. Ratio of stress acting on the pillar to strength of the pillar gives Factor of Safety. Numerical analysis of the pillars is carried out in 2D using Comsol software to estimate stress acting on coal pillar.

Keywords: *Bord-and-Pillar, Stability, Factor of Safety, Tributary area approach, Numerical modelling.*

INTRODUCTION

Bord-and-pillar method of mining accounts has been the most widely used to extract coal from underground earlier. The governing factors of Bord and Pillar mining is the design of pillars. The design of pillars not only affects the support of the roof but also determines the percentage of extraction and design of the ventilation network (Zipf, 1997). If the stress of a pillar in a room-and-pillar mine exceeds its strength, it will fail, and the load that it carried will be transferred to the neighboring pillars. The additional load on these pillars may lead to their failure. This mechanism of pillar failure, load transfer and continuing pillar failure can lead to the rapid collapse of very large area of a mine.

Pillar failure occurs when the load on the pillar is more than the strength of the pillar. Crushing of pillar occurs due to increase in existing loads, chemical oxidation of coal, mine fires, and due to flooding of mines. In addition to pillar strength, the pillar width to height ratio (w/h) is also important (Mark, 2006).

For slender pillars, failure often results in nearly complete loss of load-bearing capacity, sometimes with sudden and total collapse. Pillars with w/h between about 4 and 10 are largely elastic and failures tend to occur gradually with post failure residual strength essentially constant. The pillars deform until they have shed enough load to stop the process. Pillars with w/h greater than 10 have a plastic core and may strain harden once the loss of initial strength due to crushing or yielding of the outer elastic portion of the pillar occurs (Zipf, 1997).

Various geotechnical factors like depth of mining, inclination of seam, in situ properties of coal, height of working and gallery width are taken into

consideration while designing of a pillar. The load on the pillar is generally calculated based on the tributary area approach and pillar strength is determined through various empirical equations given by different researchers. The ratio of strength of pillar to the stress on the pillar gives the safety factor. An optimum correlation between safety factor and extraction percentage determines the feasibility of working.

INVESTIGATIONS

Investigations are carried out in two phases, namely analytical modelling and numerical modelling taking the field conditions of a coal mine in south India.

EMPIRICAL ANALYSIS

Empirical analysis of the factor of safety of a coal pillar is done in the study to find the factor of safety of the coal pillar for different range of width and depth of working. Tributary approach is used to find out the load acting on the pillar and the strength of the coal pillar is found by using Salmon-Munro formula, CMRI and Bieniawski equations which are described below.

Tributary area approach is used to find out the load acting on the coal pillar and it is calculated using the following formula (Pati, 2011).

$$S_p = 1.1\mathrm{H}\left(\frac{(\mathrm{W+B})(\mathrm{L+B})}{\mathrm{W\times L}}\right) \quad (1)$$

Where, S_p is stress on the pillar psi, H is depth below surface in ft, w is pillar width in ft, L is pillar length in ft, and B width of gallery in ft.

Salmon-Munro conducted a survey of failed and standing coal pillars in South Africa and based on the study he proposed the following formula (Salamon.M.D.G., 1967) to determine the strength of the coal pillar.

$$\mathrm{S} = 7.2\left(\frac{\mathrm{w}^{0.46}}{\mathrm{h}^{0.66}}\right) \quad (2)$$

Where,
S = Shear strength (psi)
w = Width of pillar (feet)
h = Height of pillar (feet)

Central Mining Research Institute (CMRI-presently known as Central Institute of Mining & Fuel Research) developed the following formula for pillar strength taking into account the pillar w/h ratio, uniaxial compressive strength of coal, height of the seam and depth of cover (Peng.S.S., 1984).

$$\mathrm{S} = (0.27 \times \sigma_c \times \mathrm{h}^{-0.36}) + \left(\frac{\mathrm{H}}{160}\left(\frac{\mathrm{w}}{\mathrm{h}} - 1\right)\right) \quad (3)$$

Where,
S = Pillar strength (MPa)
σ_c = Uniaxial compressive strength of coal (UCS) (MPa)
h = Working height or seam height (m)
H = Depth of cover (m)
w = Width of pillar (m)

Bieniawski formula is based on large-scale in situ tests on coal pillars. Such tests were first undertaken in the United States by (Greenwald.H.P., 1939) during the period 1933–1941 (Bieniawski.Z.T., 1984).
The general normalized form of the Bieniawski equation is

$$S = \sigma_1\left(0.64 + 0.36\left(\frac{w}{h}\right)\right) \quad (4)$$

Where,
S = Pillar strength (Psi)
σ_1 = Strength of a cubical specimen of critical size or greater (e.g., about 3 ft or 1 m for coal).
w = Width of pillar (feet)
h = Height of pillar (feet)

Factor of safety is the ratio of Stress to the strength of the pillar.

NUMERICAL MODELING:

Numerical modeling of the Bord-and-Pillar method of working is done for wide range of depths of working and width of pillar is using COMSOL software and the results are mentioned below.

The properties of materials used for building the Comsol model are given in Table 1.

RESULTS AND DISCUSSION:

Factor of safety (FOS) of coal pillar at different depths of working with different width of openings and different size of pillars is found out using the equations

1, 2, 3 and 4. The calculated FOS are given in Table 2. FOS 1, FOS 2, FOS 3 are the factor of safety values obtained using Bieniawski formula, Salamon-Munro formula and CMRI formula respectively. FOS 4 is the factor of safety obtained using numerical modelling.

Twenty numerical models are developed, typical out is given in Fig. 1, which shows the stress distribution from the coal seam to the surface before the excavation is being done where the coal seam is present a depth of 80m from the surface. The stress that is acting on the coal seam is 1.3×10^6 N/m^2.

Fig.2 shows stress distribution from the excavation to the surface where depth of working is at 80m from surface, width of pillar is 13.5m, width of gallery is 2.8m and height of gallery is 2.7m. Figure 2 also shows enlarged view of stress distribution around the pillars and opening of gallery for clear understanding of stress distribution. Maximum stress acts at the edges of the pillar along the walls of the pillar which is 3×10^6N/m^2.

Fig.3 shows the comparison of FOS values obtained using different methods at different width of gallery at depth of working 80m. Among all, the numerical modeling resulted higher factor of safety and CMRI equation gave a lower factor of safety. But under all the conditions, the pillars are found to be stable.

CONCLUSIONS

Based on the above studies to assess the stability of pillars, the following conclusions are drawn.

1. It was found that as width of galley increases FOS of the pillar decreases.
2. As the width of pillar increased FOS of pillar increases.
3. Numerical modeling found to give higher FOC compared to analytical models.

REFERENCES

[1]. Bieniawski.Z.T. (1984). Rock Mechanics Design in Mining and Tunneling. A.A.Balkema.
[2]. Greenwald.H.P., H. H. (1939). Experiments on strength of small pillars of coal in the Pittisburgh bed. Washington, U.S. Bureau of Mines, 605.
[3]. Mark, C. (2006). The Evolutio of Intelligent Coal Pillar Design. Pittsburgh: Rock Mechanics Section NIOSH-Pittsburgh Research Laboratory.
[4]. Pati, N. K. (2011). Evaluation of Underground Coal Pillar Design. Rourkela: National Institute of Technology Rourkela.
[5]. Peng.S.S., C. (1984). Longwall Mining Wiley. New York.
[6]. Salamon.M.D.G., M. (1967). A study of the strength of coal pillars. J Sth Afr Inst Min Metal, 56-67.
[7]. Zipf, R. K. (1997). TOWARD PILLAR DESIGN TO PREVENT COLLAPSE OF ROOM-AND-PILLAR MINES. Spokane: Spokane Research Laboratory.

Table 1 Material properties used in numerical model in this study

Material Property	Lime stone	Sand Stone	Shale	Coal
Young'S Modulus (GPa)	8.45	5.12	3.5	21.9032
Poisson Ratio	0.24	0.22	0.23	0.26
Cohesion (MPa)	3.21	1.23	0.98	2.11
Internal angle of Friction (°)	34	30	30	48.6
Unit Weight (KN/m^3)	25.947	22.131	23.211	14.03
Density (Kg/m^3)	2645	2256	2356	1430

Table 2 Factor of safety values from empirical approach and numerical modelling

Width of pillar(m)	Depth of working(m)	Width of gallery(m)	FOS 1	FOS 2	FOS 3	FOS 4
13.5	80	2.8	5.5	5.1	3.7	13.8
16.5	80	3.4	6.3	5.6	4.4	16.8
19.5	80	4.0	7.2	6.1	4.9	14.7
21.0	80	4.4	7.4	6.3	5.3	15.2
16.5	120	2.8	4.5	4.0	3.3	14.5
19.5	120	3.4	5.0	4.3	3.7	14.6
22.5	120	4.0	5.7	4.5	4.2	11.6
25.5	120	4.4	6.3	4.9	4.7	10.3
22.5	220	2.8	3.4	2.7	3.0	9.5
25.5	220	3.4	3.7	2.8	3.3	11.2
30.5	220	4.0	4.3	3.1	3.9	10.0
34.5	220	4.4	4.8	3.3	4.4	9.8
28.5	350	2.8	2.7	2.0	3.0	7.3
34.5	350	3.4	3.2	2.2	3.6	7.8
39.5	350	4.0	3.6	2.3	4.1	9.0
45.0	350	4.4	4.0	2.5	4.7	9.4
39	480	2.8	2.7	2.8	3.7	8.3
42	480	3.4	2.8	2.9	3.9	7.8
45	480	4.0	3.0	3.2	4.1	7.3
48	480	4.4	3.2	3.5	4.4	7.5

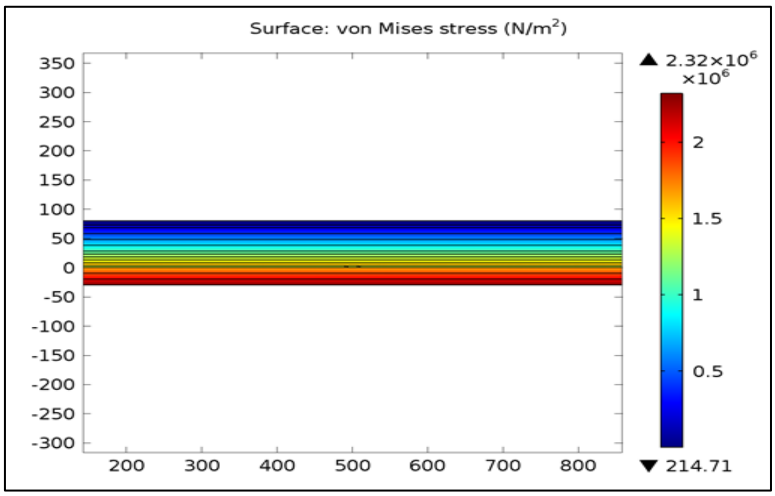

Fig.1 Stress distribution before the excavation is being done

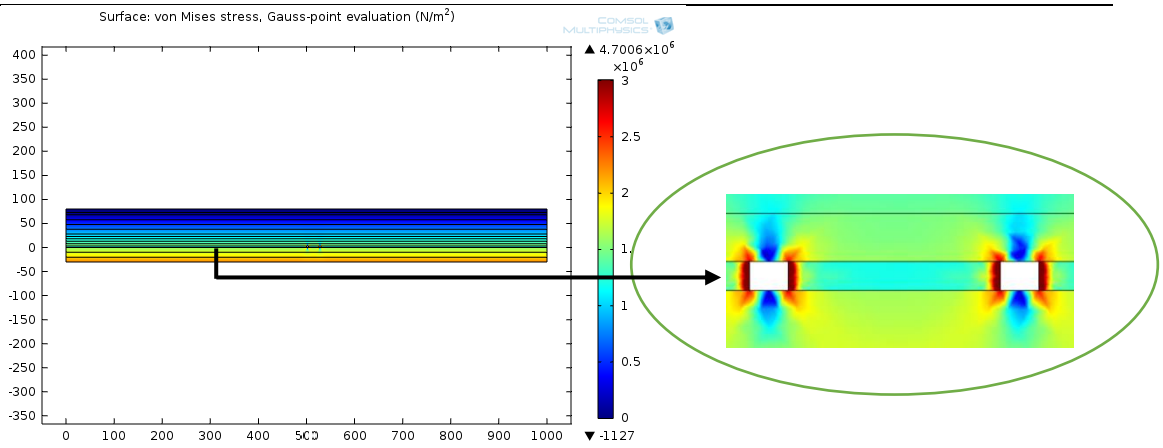

Fig.2 Stress distribution where depth of excavation is 30m, width of pillar is 13.5m and width of gallery is 2.8m

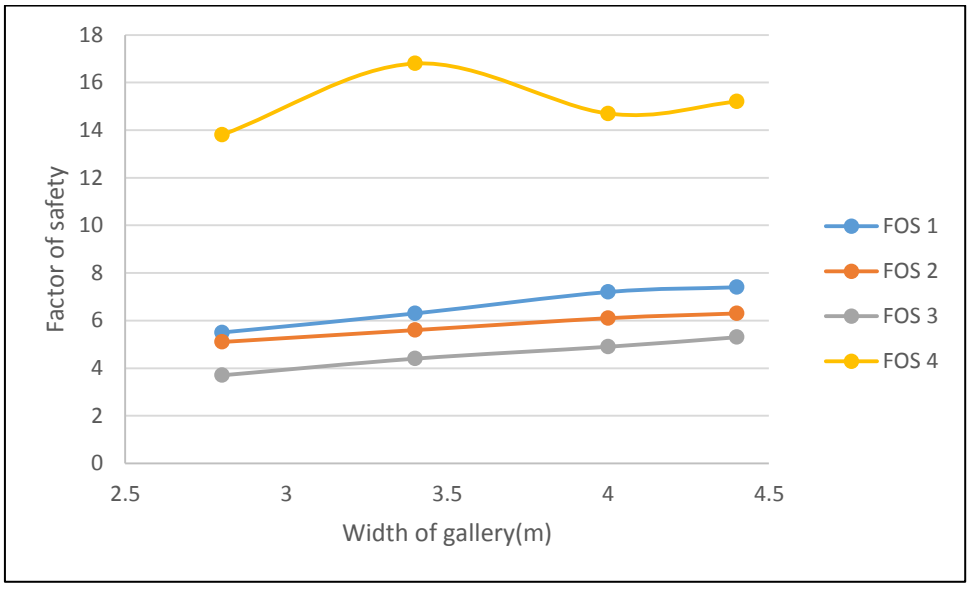

Fig.3 Comparison of variation of factor of safety with width of gallery of different empirical equations and numerical model

5th International Engineering Symposium - IES 2016
March 2-4, 2016, Kumamoto University, Japan

Modeling service life of reinforced concrete structures by simulating corrosion induced cover cracking

Resmy, V R[1] and **Rajasekaran, C**[2]

1 *MTech Student, Department of Civil Engineering, National Institute of Technology Karnataka, Surathkal, Mangalore 575025, India. Email: resmy.raveendra@gmail.com*
2 *Assistant Professor, Department of Civil Engineering, National Institute of Technology Karnataka, Surathkal, Mangalore 575025, India. Email: bcrajasekaran@gmail.com*

ABSTRACT: Corrosion of concrete structures is a problem which is common and it should be addressed for the long term life of structures. The time of repair or replacement of concrete structure due to corrosion is controlled by cracking on the concrete cover. Thus it is very important to predict cracking time due to corrosion with suitable accuracy which will help the timely maintenance of structure without affecting structural integrity. Rebar corrosion is one of the major causes of deterioration of concrete structures which seriously affects the durability of structures. Corrosion causes reduction in steel cross section, decrease in bond strength between steel and concrete and cover cracking. Once the maximum tensile strain of the concrete due to its hoop and radial strain exceeds its deformation capacity cracking, spalling and even de-lamination of concrete cover can occur. This study investigates the amount of corrosion products for crack initiation in terms of expansive pressure by modeling reinforcement corrosion using a 2-D plane strain formulation. In the proposed model, the penetration of corrosion produced, into concrete pores and micro cracks do not taken into account. The results of precise modeling of corrosion cracking can be exploited to simulate real life structures.

Keywords*: Corrosion, Service life, Crack initiation, Concrete deterioration.*

INTRODUCTION

Concrete is the powerful construction material available and Concrete structures are designed to satisfy requirements of safety, serviceability and durability during their design service life. Concrete is produced with considerable expense of energy thus it will undergo chemical changes under aggressive exposure conditions. The durability of a structure is its resistance against the actions from the environment surrounding the structure. Durability problems reduce the merits of concrete as a construction material. Concrete degradation occurs as a result of sulphate attack, frost action, action of acids, alkali aggregate reaction and in case of reinforced concrete chloride diffusion and carbonation causes corrosion of rebar which eventually leads to deterioration.

Rebar corrosion is one of the major causes of deterioration of concrete structures which seriously affected the durability of structures. Corrosion causes reduction in steel cross section, decrease in bond strength between steel and concrete and cover cracking. Concrete protects the embedded steel from corrosion by providing a highly alkaline environment (pH >13.5) which keep the steel in passive state. High alkalinity results in the transformation of a surface layer of steel into tightly adhering film. Deterioration process in concrete commonly occurs in the presence of moisture and due to the ingress of aggressive agents. Porous nature of concrete facilitates the ingress of aggressive agent which may cause the chemical changes in alkaline environment. In coastal zone, deterioration occurs as a result of corrosion mainly due to chloride attack. Carbonation and chloride attack may reduce the alkalinity in the vicinity of reinforcement leads to the disruption of

passive protective film around rebar. The entire reinforcement corrosion process can be divided into three stages. First phase is characterized by depassivation of protective film around rebar and corrosion initiation. Propagation, which is the second phase is characterized by rust expansion and rust accumulation around the porous zone of steel concrete interface. Rust which has relatively lower density occupies two to four times the volume of original steel. After filling porous zone any further accumulation of corrosion products will lead to development of internal pressure. During the third phase, internal pressure is strong enough to cause concrete cover cracking and eventually leads to spalling. Total service life is the sum of time for corrosion initiation, time for propagation and time required for cover cracking. Among all the phases first one is the longest one and third phase is the shortest phase. This study is focused on the variation of crack initiation pressure with geometrical parameters.

BACKGROUND OF STUDY

There are lots of studies with reasonable results regarding corrosion induced cover cracking of concrete structures. A large number of models have been proposed to predict the time to crack initiation which can be broadly divided into three main groups, Empirical models, Analytical models and Numerical models.

Empirical models are based on the results of experimental data, which includes determination of major parameters controlling corrosion induced cracking and then derivation by a regression analysis of a formula relating these parameters. Andrade and Alonso(Part-1,1993) conducted some preliminary experiments in which small reinforcement are artificially corroded by impressed current and the amount of current needed to induce crack at the surface are monitored. Andrade and Alonso (Part-2, 1993) used smeared crack approach to model the concrete finite elements, while the corrosion which is understood as the applied load on the structure. Corrosion is modelled by a combination of initial strains and change of elastic properties which is equivalent to the expansion and the softening of the steel elements at the rebar surface when they rust. Williomson and Clark(2000) measured cracking resistance of cover concrete experimentally by pressurizing the holes. Failure pressures were influenced by cover/diameter ratio, aggregate size, bar diameter and bar location.

There are lot of analytical models to predict the time to cracking of cover concrete and weight loss of reinforcing bar in the corroded reinforced concrete structures. Two famous analytical models are thick walled double cylinder (TWDC) model and thick walled uniform cylinder (TWUC) model. Development of analytic models enabling to account for formation of partial cracks in the concrete cover was based on the partition of the cylinder into two parts: a cracked inner cylinder and an un-cracked outer one. Most of numerical studies of corrosion-induced cracking of concrete have been either on finite element or boundary element analysis. Usually two-dimensional (2-D) constitutive models with plane strain formulation have been used to describe nonlinear behavior and cracking of concrete. The expansive nature of corrosion products was modeled by applying uniform or non-uniform internal pressure, or uniform or non-uniform radial expansive displacements, or using thermal analogy (Chernin and Val, 2011).They used the FE model to estimate the amount of corrosion products penetrating into concrete pores and microcracks. Dong Chen and Mahadevan (2006) developed a finite element based methodology to simulate entire degradation process from chloride penetration to reinforcement rust expansion to concrete cracking. A reinforcement corrosion and rust expansion model based on Faraday's law is developed, and the rust expansion is characterized by an equivalent time-varying radial displacement boundary condition. Xiao Pengwei et al. (2011) analysed the expansive behaviour of the concrete cover subjected to reinforcement corrosion using finite element. Four material parameters such as cover depth, rebar radius, elastic modulus and tensile strength of concrete are recognized as significant parameters in determining the

cracking behavior. Mirzaee et al. (2015) investigated the effects of various parameters on corrosion cover cracking via extended Finite Element Method in ABAQUS software.

EXTENDED FINITE ELEMENT METHOD

The extended finite element method (XFEM), is a numerical technique based on the generalized finite element method (GFEM) and the partition of unity method (PUM). It extends the classical finite element method (FEM) approach by enriching the solution space for solutions to differential equations with discontinuous functions. The extended finite element method was developed to ease difficulties in solving problems with localized features that are not efficiently resolved by mesh refinement. One of the initial applications was the modeling of fractures in a material. A key advantage of XFEM is that in such problems the finite element mesh does not need to be updated to track the crack path. XFEM can be utilized in conjunction with two approaches-the cohesive zone model and the virtual crack closure technique (VCCT). As XFEM based LEFM approach (VCCT) is appropriate for modeling failure of brittle materials, concrete fracture can be modeled using this method.

FINITE ELEMENT MODELING

In this model crack initiation and propagation are idealized as a 2D plain strain problem with uniform corrosion around the reinforcement. Crack initiation occurs in the direction of maximum tensile stress. The concrete beams have been modeled and analyzed using ABAQUS Finite element software. The dimensions are 150 mm width and 225 mm depth with three different covers adopted in mild, moderate and severe exposure condition in beams. Four node bilinear plain strain elements with reduced integration and hourglass control are used to model concrete. Concrete directly along the sea-coast shall be at least M30 in case of reinforced concrete which is more prone to reinforcement corrosion. The modulus of elasticity of concrete (E_c) and tensile strength(f_t) properties of concrete can be calculated using the following equations in accordance with IS 456:2000.

$$E_C = 5000\sqrt{f_{ck}} \quad (MPa) \qquad (1)$$

$$f_t = 0.7\sqrt{f_{ck}} \quad (MPa) \qquad (2)$$

Fracture energy 0f 80 N/m is adopted in this model and XFEM with LEFM is used to model concrete fracture behavior. The Finite element model in ABAQUS is shown in Fig.1. Faraday's law can be utilized to formulate corrosion process. The mass of iron consumed is related to the amount of current that flows through the electro chemical corrosion cell. At a certain stage corrosion products exert certain pressure which is large enough to initiate cracking in reinforcement concrete interface. This crack initiation pressure is strongly dependent on the concrete cover, rebar diameter and tensile strength of concrete.

RESULTS

1. Effect of concrete cover on crack initiation: The influence of cover thickness on crack initiation is examined by adopting 20mm, 30mm and 45mm cover. The crack initiation pressure is increasing with increase in cover. More pressure is needed to crack concrete with thicker concrete cover.

2. Effect of rebar diameter on crack initiation: The expansive pressure required for crack initiation is reducing with increase in rebar diameter. The variation of expansive pressure with different covers is represented in Fig.2.

CONCLUSIONS

The following conclusions are deduced from this study:

- The material parameters concrete cover and rebar diameter are identified as the important parameters controlling cracking due to corrosion.
- Expansive pressure increases with increase in concrete cover and decrease with increase in rebar diameter. This result qualitatively matches with the results of other researcher's.

REFERENCES

[1Andrade, C et al (1993), Cover cracking as a function of bar corrosion: Part I-Experimental test. Materials and structures, Vol. 26, No.8,pp. 453-464.
[2] Chen, D and Mahadevan, S (2008), Chloride-induced reinforcement corrosion and concrete cracking simulation, Cement and Concrete Composites, Vol. 30, No.3,pp. 227-238.
[3] Chernin, L and Val, D V (2011), Prediction of corrosion-induced cover cracking in reinforced concrete structures. Construction and Building Materials,Vol. 25, No. 4,pp. 1854-1869.
[4] Mirzaee M J et al (2015), Numerical Simulation of through-thickness cracking of concrete cover due to steel reinforcing bars corrosion. Sustainable Buildings and Structures, pp. 37-43.
[5] Molina, F.J. et al (1993). Cover cracking as a function of rebar corrosion: part 2—numerical model. Materials and structures,Vol. 26, No.9,pp. 532-548.
[6] Pengwei, X et al (2011), Finite element analysis of expansive behaviour due to reinforcement corrosion in RC structure, Procedia Engineering, Vol. 12, pp. 117-126.
[7] Williamson, S J and Clark, L A (2000), Pressure required to cause cover cracking of concrete due to reinforcement corrosion. Magazine of Concrete research, Vol. 52, No.6,pp. 455-467.

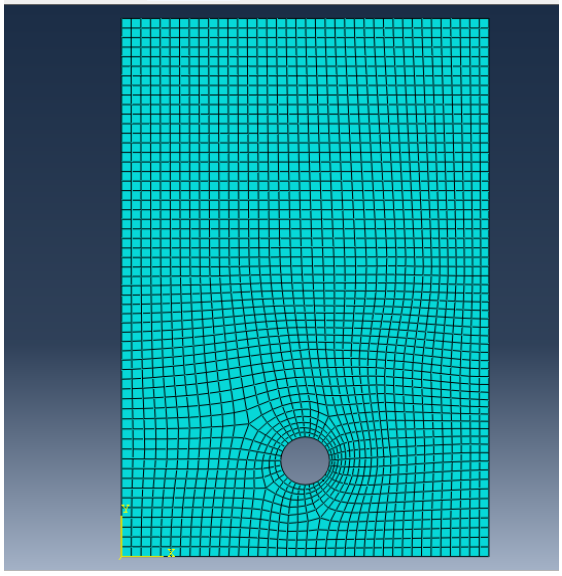

Fig.1 Finite Element model in ABAQUS

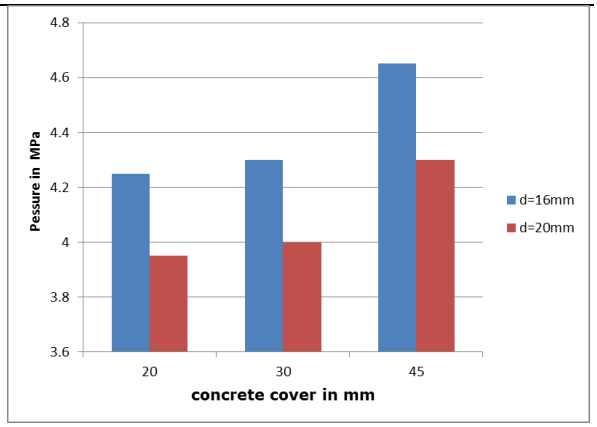

Fig.2 Effects of cover and diameter on expansive pressure

5th International Engineering Symposium - IES 2016
March 2-4, 2016, Kumamoto University, Japan

FUZZY STRUCTURAL ANALYSIS USING HDMR

A. S. Balu

Assistant Professor, Department of Civil Engineering, National Institute of Technology Karnataka, Surathkal, Mangalore 575025, India. email: asbalu@nitk.ac.in

ABSTRACT: Uncertainties are unavoidable in dealing with real world problems. In order to model engineering systems, it is important that we recognize the presence of all major sources of uncertainty. The knowledge-based uncertainty associated with imperfect knowledge of the real world may be reduced through application of better prediction models and/or improved experiments. The fuzzy finite element method consists of the application of the fuzzy arithmetic procedure through the sublevel strategy on the numerical procedure. This paper presents a practical approach based on High Dimensional Model Representation for analyzing the response of structures with fuzzy parameters. The merit of the proposed methodology is computational efficiency without compromise on accuracy in addition to fixing the dependency problem associated with the nonlinearity of the function.

***Keywords**: Fuzzy variables, HDMR, Surrogate model, Possibility theory*

INTRODUCTION

The exponential growth of computational power during the last few decades has enabled the finite element analysis of many real-life engineering systems which are too complex to be analytically solved in a closed form. In the traditional deterministic finite element analysis, system parameters such as mass, geometry and material properties are assumed to be known precisely and defined exactly. However, in practice most of the data used in the solution process of many practical engineering systems are either collected from experiments or acquired as empirical data from the past, which are usually ill defined, imprecise and uncertain in nature. The uncertainty present in the problem can be categorized into randomness and fuzziness.

Probabilistic methods are especially suitable in case of uncertainty due to randomness for which the information on both the range and the probability density function are available. The probabilistic concept is already well established for the extension of the deterministic FEM.

Fuzzy set theory [1] provides a concept for the description of linguistic or subjective knowledge and incomplete data in a non-probabilistic manner. The use of fuzzy set theory concept in the finite element context has led to the development of the fuzzy finite element method for the solution of engineering problems [2-4]. Its aim is to obtain the membership function of an output quantity, based on the fuzzy description of the uncertain input parameters. Over the last decade, several techniques have been reported, such as the vertex method [5−7], the global optimization approaches [8, 9] and the interval arithmetic approaches [10, 11]. However, each of these techniques has its specific limitations when applied to realistic engineering problems, and none of them has been established as standard interval procedure, and the choice of technique depends on the type of the conducted FE analysis.

This paper presents a practical approach based on High Dimensional Model Representation (HDMR) [12, 13] for analyzing the response of structures with fuzzy parameters. The proposed methodology involves integrated finite

element modelling, HDMR based response surface generation, and both, implicit and explicit fuzzy analysis procedures. The uncertainties in the material, geometric, loading and structural parameters are represented using fuzzy sets. To facilitate efficient computation, a HDMR based response surface generation is employed for the approximation of the fuzzy finite element response quantity.

In the proposed implicit formulation, the fuzzy response is expressed as a closed form expression using HDMR. The binary combinations of the fuzzy variables that result in the extreme responses at an α-level are obtained by applying combinatorial optimization to the approximated response function using HDMR. The membership function of the fuzzy response is then obtained by carrying out the full finite element analysis for the binary combinations that resulted in the extreme responses. In the proposed explicit formulation, using HDMR the response is expressed in a separable closed-form expression as a linear combination of the fuzzy variables through the definition of intervening variables, then using the transformation technique [14] the bounds on the response at each α-level are obtained.

APPLICATION OF HDMR IN FUZZY STRUCTURAL ANALYSIS

Let the *N*–dimensional vector $\mathbf{x} = \{x_1, x_2, \cdots, x_N\}$, represent the input variables of the model under consideration, and the response function as $g(\mathbf{x})$. Since the influence of the input variables on the response function can be independent and/or cooperative, HDMR [12, 13] expresses the response $g(\mathbf{x})$ as a hierarchical correlated function expansion in terms of the input variables as

$$g(\mathbf{x}) = g_0 + \sum_{i=1}^{N} g_i(x_i) + \sum_{1 \le i_1 < i_2 \le N} g_{i_1 i_2}(x_{i_1}, x_{i_2}) + \ldots + \sum_{1 \le i_1 < \ldots < i_l \le N} g_{i_1 i_2 \ldots i_l}(x_{i_1}, x_{i_2}, \ldots, x_{i_l}) + \ldots + g_{12\ldots N}(x_1, x_2, \ldots, x_N) \quad (1)$$

where g_0 is a constant term representing the zeroth-order component function or the mean response of $g(\mathbf{x})$. The function $g_i(x_i)$ is a first-order term expressing the effect of variable xi acting alone, although generally nonlinearly, upon the output $g(\mathbf{x})$. The function $g_{i_1 i_2}(x_{i_1}, x_{i_2})$ is a second-order term which describes the cooperative effects of the variables x_{i_1} and x_{i_2} upon the output $g(\mathbf{x})$. The higher order terms give the cooperative effects of increasing numbers of input variables acting together to influence the output $g(\mathbf{x})$. The last term $g_{12,\cdots,N}(x_1, x_2, \cdots, x_N)$ contains any residual dependence of all the input variables locked together in a cooperative way to influence the output $g(\mathbf{x})$. Once all the relevant component functions in Equation 2 are determined and suitably represented, then the component functions constitute HDMR, thereby replacing the original computationally expensive method of calculating $g(\mathbf{x})$ by the computationally efficient model. Usually the higher order terms in Equation 1 are negligible such that HDMR with only few low order correlations, amongst the input variables are typically adequate in describing the output behavior resulting in rapid convergence of HDMR expansion.

In this work, cut-HDMR procedure is used to approximate the original response function with an explicit performance function to estimate the response of structural/mechanical systems subjected to fuzzy variables after defining a reference point $\mathbf{c} = \{c_1, c_2, \cdots, c_N\}$ in the variable space. The first order approximation of the function,

$$\tilde{g}(\mathbf{x}) = \sum_{i=1}^{N} \sum_{j=1}^{n} \phi_j(x_i)\, g(c_1, \ldots, c_{i-1}, x_i^j, c_{i+1}, \ldots, c_N) - (N-1) g_0 \quad (2)$$

Along each of the fuzzy variable x_i having triangular membership function with the triplet number $[x_{iL},\ x_{iM},\ x_{iU}]$, $n\ (=3, 5, 7 \text{ or } 9)$ sample points x_{iL}, $x_{iM} - (n-3)(x_{iM} - x_{iL})/(n-1)$, $x_{iM} - (n-5)(x_{iM} - x_{iL})/(n-1)$, …, x_{iM}, …, $x_{iM} + (n-5)(x_{iU} - x_{iM})/(n-1)$,

$x_{iM} + (n-3)(x_{iU} - x_{iM})/(n-1)$, x_{iU} are deployed to obtain the first-order component functions.

If *n* is the number of sample points taken along each of the variable axis and *s* is the order of the component function considered, starting from zeroth-order to *l*-th order, then total number of function evaluation for interpolation purpose is given by, $\sum_{s=0}^{l}\left(N!(n-1)^s\right)/\left((N-s)!s!\right)$ which grows polynomially with *n* and *s*. As a few low order component functions of HDMR are used, the sample savings due to HDMR are significant compared to traditional sampling. Hence uncertainty analysis using HDMR relies on an accurate reduced model being generated with a small number of full model simulations. The tremendous computational savings result from just having to perform interpolation instead of full model simulations for output determination.

NUMERICAL EXAMPLES

Two numerical examples are presented to demonstrate the accuracy and efficiency of the proposed methodology. If *N*, *n*, and *m* respectively denote the number of fuzzy variables, the number of sample points taken along each of the variable axis, and the number of α -cuts, then using first-order HDMR approximation the total cost of original function evaluation entails a maximum of $N \times (n-1) + 2 \times (m+1)$ and $N \times (n-1) + 1$ by the proposed implicit and explicit formulations, respectively. It can be easily verified that the total computational cost of the proposed formulations is far less than $2^N m + 1$ number of function evaluations required for the crude vertex method fuzzy analysis in conjunction with combinatorial optimization, especially for large number of fuzzy input parameters and large finite element models. This clearly demonstrates the computational efficiency of the proposed formulations. The efficiency and robustness of the proposed formulations is expected to increase with increase in the complexity of the structure, number of fuzzy variables and number of alpha-cuts. If first-order HDMR approximation is not sufficient second-order HDMR approximation may be adopted at the expense of additional computational cost.

Closed-form Example

To illustrate the accuracy and the applicability of the transformation technique in the proposed explicit formulation to obtain the bounds on the response, the following nonlinear response function is considered.

$$\begin{aligned} f(\mathbf{x}) = {} & 16x_1^4 - 96x_1^3 + 216x_1^2 - 216x_1 \\ & -64x_2^3 + 240x_2^2 - 300x_2 \\ & +36x_3^2 - 84x_3 - 8x_4 + 264 \end{aligned} \qquad (3)$$

where $x_1 = [1,\ 2,\ 3]$, $x_2 = [-1,\ 0,\ 1]$, $x_3 = [-5,\ 0,\ 5]$, and $x_4 = [10,\ 15,\ 20]$ are assumed to have triangular membership functions and the triplet number for each fuzzy variable $[x_L,\ x_M,\ x_U]$ defines a triangular membership function. As Equation 3 represents closed form nonlinear function, in the proposed implicit and explicit formulations, the HDMR approximation of the original response function is skipped. In the proposed implicit formulation combinatorial optimization is carried out at each alpha-level. Ten alpha-levels ranging from 0 to 1 are chosen. Figure 1 shows the membership function of $f(\mathbf{x})$ obtained by the crude vertex method fuzzy analysis in conjunction with combinatorial optimization. Figure 1 also presents the membership function of $f(\mathbf{x})$ obtained by adopting interval arithmetic techniques [15] directly on Equation 3. As Equation 3 represents closed form nonlinear function, in the proposed explicit formulation, skipping the HDMR approximation of the original response function, the membership function of $f(\mathbf{x})$ is obtained by suitable transformation of the variables $x_1 - x_4$ into a linear combination of intervening variables, as follows

$$f(\mathbf{z}) = z_1 + z_2 + z_3 + z_4 \qquad (4)$$

where $z_1 = (2x_1 - 3)^4$, $z_2 = -(4x_2 - 5)^3$, $z_3 = (6x_3 - 7)^2$ and $z_4 = -8x_4 + 9$.

Figure 1 includes the membership function of $f(\mathbf{x})$ obtained by the proposed explicit formulation. As expected due to the problem of dependency, the membership function of $f(\mathbf{x})$ obtained by adopting interval arithmetic techniques resulted in wider bounds. The differences in the membership function of $f(\mathbf{x})$ obtained by the crude vertex method fuzzy analysis in conjunction with combinatorial optimization and the proposed explicit formulation is mainly due to the reason that the membership function obtained by using the vertex method fails to capture the minimum value of the response because it calculates the minimum and maximum values of the response only at the lower and upper limits of the variables at each alpha-level. Therefore, it does not identify the minimum of the response, which is located inside the design space.

Edge-cracked Plate

This example involves the edge-cracked plate shown in Figure 2, which is fixed at the bottom and subjected to far-field shear stress of τ^{∞} unit applied on top. The plate has length $L = 16$ units, width $W = 7$ units and crack length a. The elastic modulus is assumed to follow a hyperbolic-tangent gradation function which can be expressed with respect to the local (x_1, x_2) Cartesian coordinates

$$E(x_1) = \frac{E_1 + E_2}{2} + \frac{E_1 - E_2}{2}\tanh(\eta x_1) \quad (5)$$

where $E_1 = E(x_1 = -0.5W)$, $E_2 = E(x_1 = 0.5W)$, η is gradation parameter. E_1 =[0.5, 1.0, 1.5], E_2 =[2.5, 3.0, 3.5], η =[2.5, 3.0, 3.5], τ^{∞} =[0.5, 1.0, 1.5], and a=[2.5, 3.0, 3.5] are assumed to be fuzzy variables having triangular membership functions. A plane strain condition was assumed. A domain size $2b \times 2b$ ($b = 3.0$ units) is used to calculate the mixed-mode SIFs. FEM discretization involved 2711 nodes, 832 8-noded quadrilateral elements, and 48 focused quarter-point 6-noded triangular elements, as shown in Figure 2.

The possibility distributions of the mixed-mode SIFs K_I and K_{II} are shown in Figure 3. Again, (i) for all cases the proposed first-order HDMR based implicit and the combinatorial approach yield exactly the same results for all the possibility distributions of the responses; (ii) however explicit formulation estimates a narrow bound for the response and with increase in the order of approximation κ the bounds for the response are observed to become still narrower.

CONCLUSIONS

In this paper a practical approach based on HDMR for analyzing the response of structures with fuzzy parameters is presented. The proposed methodology involves integrated finite element modelling, HDMR based response surface generation, and both, implicit and explicit fuzzy analysis procedures. To facilitate efficient computation, a HDMR based response surface generation is employed for the approximation of the fuzzy finite element response quantity. In the proposed implicit formulation, the binary combinations of the fuzzy variables that result in extreme responses at an alpha-level are obtained by applying combinatorial optimization to the approximated response obtained using HDMR. Once the combinations are obtained, full finite element analyses are then carried out to determine the extreme values of the responses. In the proposed explicit formulation, using HDMR the response is expressed in a separable closed-form expression as a linear combination of the fuzzy variables through the definition of intervening variables, then using the transformation technique the bounds on the response at each alpha-level are obtained. The proposed explicit formulation is free from the problem associated with dependency of the fuzzy variables.

REFERENCES

[1] L. Zadeh, "Fuzzy sets," Inf. Contr., 1965; vol.8, no. 3, pp. 338–353.

[2] S. Valliappan, and T. D. Pham, "Fuzzy logic applied to numerical modeling of engineering problems," Comp. Mech. Adv., 1995, vol. 2, pp. 213–281.

[3] L. Chen, and S. S. Rao, "Fuzzy finite element approach for the vibration analysis of imprecisely defined systems," Finite Elem. Anal. Design, 1997, vol. 27, pp. 69–83.

[4] U. O. Akpan, T. S. Koko, T. R. Orisamolu, and B. K. Gallant, "Practical fuzzy finite element analysis of structures," Finite Elem. Anal. Design, 2001, vol. 38, pp. 93–111.

[5] W. M. Dong, and H. C. Shah, "Vertex method for computing function of fuzzy variables," Fuzzy Sets Sys., 1987, vol. 2, pp. 201–208.

[6] M. Hanss, "The transformation method for the simulation and analysis of systems with uncertain parameters," Fuzzy Sets Sys., 2002, vol. 130, no. 3, pp. 277–289.

[7] S. Donders, D. Vandepitte, V. Peer, and W. Desmet, "Assessment of uncertainty on structural dynamic responses with the short transformation method," J. Sound Vibr., 2005, vol. 288, no.3, pp. 523–549.

[8] B. Möller, W. Graf, and M. Beer, "Fuzzy structural analysis using α-level optimization," Comp. Mech., 2000, vol. 26, no.6, pp. 547–565.

[9] L. Farkas, D. Moens, D. Vandepitte, and W. Desmet, "Application of fuzzy numerical techniques for product performance analysis in the conceptual and preliminary design stage," Comp. Struc., 2008, vol. 86, no.10, pp. 1061–1079.

[10] S. S. Rao, and L. Berke, "Analysis of uncertain structural systems using interval analysis," AIAA J., 1997, vol. 34, no. 4, pp. 727–735.

[11] R. L. Muhanna, R. L. Mullen, "Uncertainty in mechanics problems interval based approach," J. Engg. Mech., ASCE, 2001, vol. 127, no. 6, pp. 557–566.

[12] H. Rabitz, and O. F. Alis, "General foundations of high dimensional model representations," J. Math. Chem., 1999, vol. 25, no. 2–3, pp. 197–233.

[13] R. Chowdhury, B. N. Rao, and A. M. Prasad, "High dimensional model representation for piece wise continuous function approximation," Commun. Num. Meth. Engg., 2008, vol. 24, no. 12, pp. 1587–1609.

[14] P. R. Adduri, and R. C. Penmetsa, "Confidence bounds on component reliability in the presence of mixed uncertain variables," Int. J. Mech. Sci., 2008, vol. 50, no. 3, pp. 481–489.

[15] R. E. Moore, "Methods and applications of interval analysis," SAIM Publication, Philadelphia 1979.

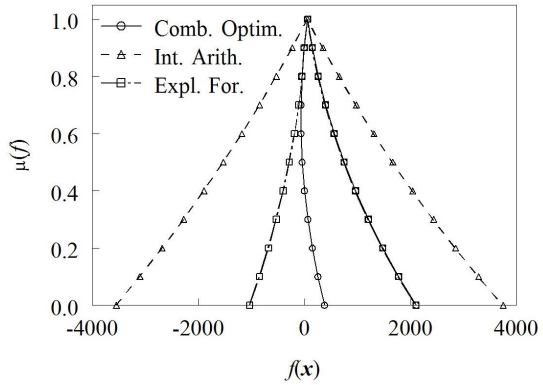

Figure 1. Comparison of membership function of response

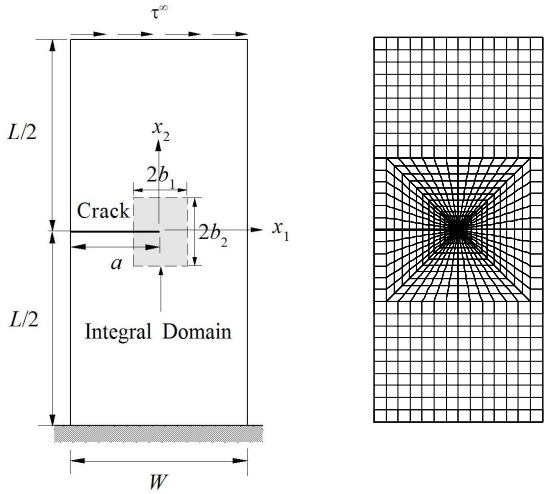

Figure 2. Edge-cracked plate with FEM discretization

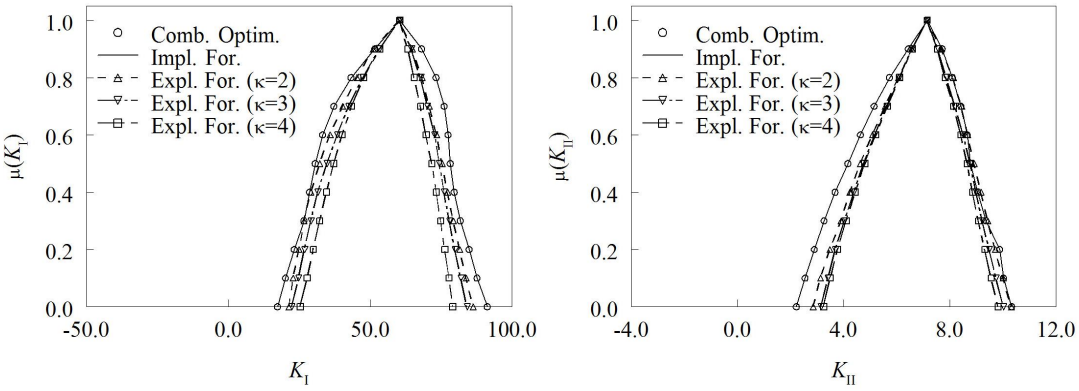

Figure 3. Possibility distributions of K_I and K_{II}

5th International Engineering Symposium - IES 2016
March 2-4, 2016, Kumamoto University, Japan

A CASE STUDY ON DELAY ANALYSIS OF STADIUM CONSTRUCTION PROJECT USING IMPACTED AS-PLANNED METHOD

Deepak Koshy Mathew[1], Rajasekaran, C[2] and **Shree Vidhya, R[3]**

1 *Former Post Graduate Student, Department of Civil Engineering, National Institute of Technology Karnataka, Surathkal, India. Email: deepakkoshymathew@gmail.com*
2 *Assistant Professor, Department of Civil Engineering, National Institute of Technology Karnataka, Surathkal, Mangalore 575025, India. email:bcrajasekaran@gmail.com*
3 *Assistant Lecturer, Department of Civil Engineering, National Institute of Technology Karnataka, Surathkal, Mangalore 575025, India. email: shreevidhyaramamoorthy@gmail.com*

ABSTRACT: Construction projects are subjected to various uncertainties and frequently cause delays, resulting in unanticipated extra costs being incurred by both contractors and clients. The main purpose of this study is to investigate the causes of construction schedule delays and the methods of schedule delay analyses. In this context, construction works of an international stadium project in Kerala, India was chosen and Impacted as-planned method was applied to the case study project in order to determine the construction schedule delays; to measure the impacts of these delays on the project completion duration; and to allocate responsibility amongst the project participants for preventing delay claims. After the application of the Impacted as-planned method it was observed that the delays in the critical activities extended the project duration by 101 days in total i.e. by 11.8% of the estimated construction period.

***Keywords**: Construction management, Project management, Time Impact Analysis, Schedule Delays.*

INTRODUCTION

Construction delays are widespread and are the biggest problems construction firms face. To recover the damage caused by delays, both the delays and the parties responsible for them should be identified. The analysis of these delays involves not only the calculation of the delay time but also the identification of the root causes and the responsibility for delays. Schedule delay analysis is used in order to identify delays and to measure the net impacts of delays on a project. Developments in computer technology along with the availability of more advanced and user-friendly project planning software have enhanced the capabilities of these techniques over the past decade (Pickavance, 2005). The aim of this paper is to use the most appropriate schedule delay analysis technique to the case study project in order to analyze the net impacts of construction delays on project completion duration and to assign responsibility amongst the project stakeholders for such delays.

SIGNIFICANCE

In the study of Ndekugri and Braimah (2008), delay analysis is defined as "the task of investigating the events that led to project delay for the purpose of determining the financial responsibilities of the contracting parties arising from the delay". According to Trauner et al. (2009), there are four main groups of construction delays: Critical or noncritical, excusable or non-excusable, compensable or non-compensable and concurrent or non-concurrent delays. The analysis of delays in construction projects is difficult and complicated because of the large number of

individual activities that have to be dealt with.(Menesi, 2007).

The Society of Construction Law (SCL) Protocol refers to this technique as the 'impacted as-planned. The SCL Protocol states that impacted as-planned is based on the effect of employer risk events on the planned programme of work. This is thought to be a simple form of delay analysis since it involves the least number of variables. This approach uses only the as-planned schedule based on the theory that the earliest date that a project could have been completed can be determined by adding the delays into the as-planned schedule. The time extension sought by the claimant is the duration between the planned completion and the new impacted completion.

MATERIALS AND METHODOLOGY

This study was conducted for analyzing construction schedule delays in order to recommend steps to eliminate or minimize their negative effects on construction completion duration and to apportion responsibility of delays amongst all project participants. A delay analysis was carried out on an under-construction project of a stadium in Trivandrum, India which had suffered delays during its construction. Details on the project participants and the project are not given in this paper for ethical reasons.

In the context of this project, a FIDIC based contract was signed between the contractor and the owner. The owner had assigned a consulting company to oversee the project and deal with the contractor. The scope of work consisted of the completion of the construction works of a stadium as per the activities determined in the as-planned schedule, in compliance with the technical specifications of the contract. This as-planned schedule was attached to the FIDIC based contract.

According to the original as-planned method schedule, the construction works were to be carried out in 851 days from 4 April 2012 to 2 August 2014. However, some disputes, delays and failures occurred which prevented adherence to the as-planned schedule.

For the successful application of this method, the daily records and diaries had been noted meticulously during the construction process. This study was conducted in three stages; which are explained in detail in the following sections. Collection of Information and Data; Determination of Causes, Types and Liability of Delays; and Conducting the Schedule Delay Analysis with Impacted as planned method. The construction site and the related companies were visited. and the information on the specific problems and the delayed events of the stadium project were gathered through informal interviews.

DELAY ANALYSIS

The causes of delays were determined by analyzing the official correspondence between consultant and contractor, time extension requests of the contractor, payment bills and project change orders by the owner during the construction period. These causes were studied to understand which party was responsible for their occurrences. Finally, the delay types according to their compensability were determined and presented alongside.

The as-planned schedule, which had been added to the contract documents, was obtained in order to start the delay analysis. After identification of construction delays and allocation of liabilities to parties, the delay analysis method was applied. Microsoft Project (MSP) software was used. and only durations were analyzed in the context of this research; costs and other resources were excluded. The impacts of the delays on the critical activities were seen in terms of project completion duration. Accordingly, the delayed events were entered into the as-planned schedule chronologically to ascertain the changes and delays in the progress of the construction. The delayed events in the critical activities were selected to be analyzed in Impacted As-planned method since these delays extended the project duration.

RESULTS AND DISCUSSION

Determination of Delays

In application of the Impacted As-planned method, the accuracy of records which were used in the delay analysis was very important to provide reliability. Project changes, changing site conditions, official correspondences between project participants, time extension requests of the contractor were approved under the control of parties. Therefore, these records did not require any reliability control. In this study, only approved records were collected and analyzed, as well interviews with the project parties were conducted at the construction site. The total float of the schedule was zero.

Handing over of construction site

In this project, signing of lease agreement for the project land was a critical activity as it affected the handing over of construction site which affected subsequent activities in the schedule because of its total float being zero. There occurred 25-days delay in the as-planned schedule caused by the owner. It is found that this delay event is beyond the reasonable control of the contractor and hence it is fair and reasonable that the contractor is compensated for the same.

Unanticipated Rain

The foundation works of the north pavilion building was a critical activity. The ground was wet due to heavy rains, and the excavators and dumpers could not operate in those conditions. Collapse of loose soil also occurred along the area excavated for the footing. This delayed event was a result of external factors. The rain during this period was unanticipated and this adverse weather condition is found to be a delay event. In accordance with the conditions of contract, reasonable extension of time may be granted by the client for such delays

Temporary suspension of works due to contractor's financial difficulties

The contractor was facing financial difficulties which led to a temporary suspension of activities at the site. The slab shuttering at 37.5m level was delayed by 45 days. The owner overcame this issue by off-loading some works from the main contractor.

Labour unavailability

The employees has left for holidays and the restarting of activities was also delayed as the labourers returned in batches. A delay of 12 days was caused to the slab shuttering works at 37.5m level of the north pavilion because of this contractor delayed activity. Since this activity was critical, the project completion duration extended.

Shortage of sand

The slab concreting works at 46.5m level was delayed by 15 days due to shortage of sand. This contractor delay event is due to the reduction in sand supply followed by a lorry owners' strike in Tamil Nadu, protesting against an increase in taxes.

Soil Improvement Works

The contractor has excluded soil improvement from his scope of work but as per the recommendations of the geotechnical consultant some of the plot land required soil stabilization. The work was subsequently executed by the contractor. It is found that a delay event which is beyond the reasonable control of the contractor has occurred. Soil stabilization was done for the club house and convention center. Activities in the critical path were not delayed and the project duration remained unchanged as a result of this delay.

Stoppages caused by road closures and obstructions

The road works were done by a different contractor. This resulted in the access road work and the stadium works progressing parallel to each other. The main contractor claimed that the closure of access roads disrupted the progress of his work. Access was denied due to the deep excavation of roads. Conditions of contract state that reasonable extension of time may be granted to contractor for such delays that are caused by other contractors employed by the client. However only activities on the non-critical path were affected, which did not extend the total project duration.

Revision in floor plan
The client revised the plan of west stand at +41m level. Spaces for retail were changed to corporate boxes. The contractor claimed that he is eligible for a time extension for the preparation and approval of the new drawings. However after analysis it is found that there was no extension to the project duration.

Shortage of cement and sand
There was a shortage of cement and sand towards the end of financial year. However none of the activities in the critical path were affected. Hence this delay did not cause any overall delay to the project.

Concrete plant breakdown
Concreting of raker beams in upper tier were delayed due to breakdown of concrete batching plant. Problems in organizing concrete subcontractors and delays in material procurement were main causes of these delays. This activity was not on the critical path or the near critical path. Hence total project duration remained unaffected. Consequently, the delays were researched from related records and causes of delays were identified.

Allocation of Liability to Parties and Determining Types of Delays
From related records, the causes of delays were researched and determined in the first step and listed in the second column of Table 1. Then, types of delay factors were determined and given in the fourth column of the below table 1. After allocation of liabilities to parties, types of delays according to their compensability were determined**.**

Schedule Delay Analysis with Impacted as-planned
it was seen that the project duration was changed when the activities on the critical path were delayed. While the project duration was extended because of construction schedule delays in the critical activities, inevitably cost and resources of the project were impacted from these delayed events. However, these impacted issues were not evaluated in this delay analysis.

SUMMARY
Results of allocation of project delays among the parties are presented in Table 2. As it can be seen from this table, the owner caused delays extended the project by 25 day; while contractor caused delays were 72 days in total. Also, there had been 4 day delays caused by external factors such as unforeseeable weather conditions. Consequently, the project finish date was postponed from 2 August 2014 to 11 November 2014; i.e. the project was delayed by 101 days due to these five construction delays. This means that the project duration was extended by 11.8 % or in other words more than 1/10 of the estimated construction period.

These delays can further be categorized as 25-days excusable compensable delays, 72-days non-excusable delays and 4-days excusable non-compensable delays. Consequently, liquidated damages should have been paid by the contractor according to the related clauses of the contract because of 72-days non-excusable delays. On the other hand, the contractor should have been given a time extension of 29 days due to 25-days excusable compensable delays and 4-days excusable non-compensable delays which were beyond the control of the contractor.

The delayed events of this case study which extended the project duration were caused due to lack of consensus within governmental organisations, owner caused delays, contractor's financial difficulties, problems in material procurement, shortages of labour and. unforeseeable weather conditions. It was observed that most of these delay causes correspond to the important causes of delays as reported in the relevant literature.

Table 1: Causes, Types , Liability of Delays

Causes of Delay	Type of Delay Factors	Liable Party	Type of Delay
Late start of handing over of construction site	Delay (Access to site)	Owner Related	Excusable compensable
Unforeseeable weather conditions	Unanticipated Events	External Factor	Excusable Non-compensable
Contractor's financial difficulties	Cash flow	Contractor Related	Non-excusable
Unavailabilty of labour	Procurement Delay	Contractor Related	Non-excusable
Sand shortage	Procurement Delay	Contractor Related	Non-excusable

Table 2: Allocation of Project Delays to Parties

No	Causes of delay	Compl-etion Durati-on	Project Delay
As planned		851	
1	Late start of handing over of construction site	876	25
2	Unforeseeable weather conditions	880	4
3	Contractor's financial difficulties	925	45
4	Unavailability of labour	937	12
5	Sand shortage	952	15

CONCLUSION

Construction schedule delays in a project can cause major problems for contractors and owners, resulting in costly disputes, controversial issues and adverse relationships between all the project participants.

There were 10 delays caused due to both critical and non-critical activities. Most of these correspond to the causes of delays mentioned in the literature in the previous sections. In the case of the project analyzed in this study, the causes of the delayed events can be listed as follows:

1. Late start of handing over of construction site
2. Unforeseeable weather conditions during foundation activities
3. Contractor’s financial difficulties
4. Labour shortage
5. Shortage of sand due to strike by lorry owners
6. Soil Improvement Works
7. Stoppage of work due to road closure and obstruction
8. Revised plan of West stand at 41.0m level
9. Lack of availability of cement, sand towards the end of the financial year,
10. Concrete plant breakdown at the site

According to the IAP schedule delay analysis, the delays due to the critical activities extended the project duration by 101 days in total i.e. by 11.8 % of the estimated construction period. On the other hand, the delays due to the noncritical activities did not impact the total duration. The delayed events are entered into the as-planned schedule respectively to see the changes on the project. Therefore, this analysis method is very realistic. On the other hand, the most important constraint of Impacted as planned method is that the available records, related data and as-planned schedule should be accurate in order to obtain accurate and clear results; otherwise, the analysis will be incorrect. Another drawback of the method is that the analysis of concurrent delays is difficult in terms of understanding the net portion of the liability. Despite these drawbacks, this selected method is reliable as recommended by many researchers and the technique for determining amount of time extension caused by construction schedule delays.

For a more detailed analysis, Time Impact Analysis needs to be done. TIA is more accurate compared to IAP method and requires regularly updated schedules which was not available at this case study project. Based on this case study, the following can be inferred for a more reliable analysis: finalization of the project design, allocation of sufficient time and adequate finance, qualified contractor and efficient labourers. These are some of the general suggestions for minimizing or avoiding the construction delays.

REFERENCES

[1] Arditi, D and Pattanakitchamroon T (2008), Analysis Methods in time-based Claims, Journal of Construction Engineering and Management, Vol. 134, pp. 242-252.
[2] Braimah, N et al (2008), Delay Analysis within construction contracting organizations, Journal of Construction engineering and management, Vol. 134, pp. 692-700.
[3] Braimah, N and Ndekugri I (2009), Consultants' Perceptions on Construction, Journal of Construction engineering and management, Volume 135, 1279-1288.
[4] Callahan, M D et al. (1992), Construction Project Scheduling, McGraw-Hill, USA.
[5] Caletka, A F and Keane, P J (2008), Delay Analysis in construction contracts, Wiley Blackwell Publications.
[6] Cooke, B and Williams, P (2009), Construction Planning, Programming and Control, Wiley Blackwell Publications.
[7] Dayi S (2010), Schedule Delay Analysis In Construction Projects - A Case Study Using Time Impact Analysis Method, Middle East Technical University, Ankara, Turkey.
[8] Kartam S (1999), Generic Methodology For Analyzing Delay Claims, Journal of Construction engineering and management, Vol. 125, pp. 409-419.
[9] Menesi W (2007), Construction Delay Analysis under Multiple Baseline Updates, University of Waterloo, Ontario, Canada.
[10] Pickavance K (2005). Delay and disruption in Construction Contracts, LLP Reference Publishing, London.
[11] The Society of Construction Law (SCL) (2002), Delay and Disruption Protocol.
[12] Trauner et al. (2009), Construction Delays: understanding them clearly and Delay Analysis in Construction Analyzing them correctly, London: Elsevier Inc.

5th International Engineering Symposium - IES 2016
March 2-4, 2016, Kumamoto University, Japan

EXPERIMENTAL STUDY ON FEASIBILITY OF RICE HUSK ASH IN PRODUCTION OF ECOFRIENDLY CONCRETE

Puttaraju K O[1], Shree Vidhya R[2] and **Rajasekaran C[3]**

1 *Former Post Graduate Student, Department of Civil Engineering, National Institute of Technology Karnataka, Surathkal, India. Email: puttu1112@gmail.com*
2 *Lecturer, Department of Civil Engineering, National Institute of Technology Karnataka, Surathkal, India. Email: shreevidhyaramamoorthy@gmail.com*
3 *Assistant Professor, Department of Civil Engineering, National Institute of Technology Karnataka, Surathkal, India. Email: bcrajasekaran@gmail.com*

ABSTRACT: The utilization of any discarded by-products as supplementary cementing materials in construction industry, without affecting the strength and performance of concrete will lead to low cost, eco-friendly and sustainable design of structures. Rice Hush Ash (RHA) is a-product obtained from combustion of rice husk. RHA contains non-crystalline silicon dioxide with high specific surface area and high pozzolonic reactivity, which makes it appropriate to be used as supplementary cementing material in concrete. The research is an investigation of the performance of concrete by partially replacing cement with RHA at 10%, 20% and 30% by weight of cement to make concrete. Comparison of strength was made with Ordinary Portland Cement (OPC) and Pozzolonic Portland Cement (PPC) with and without replacement of RHA at different proportions using M20 grade concrete for 7 and 28 days respectively. Incorporation of RHA in concrete provides better compressive, flexural and tensile strength for 10% and 20% replacement. The strength for 30% replacement was less when compared to the strength of normal concrete. From the experimental study, it is found that PPC mixes are more consistent, hence the 20% replacement of rice husk can be used for PPC than OPC to achieve high strength concrete.

***Keywords**: Rice Husk Ash, OPC, PPC, Compressive Strength.*

INTRODUCTION

The need to reduce the use of Ordinary Portland Cement (OPC) has intensified the research into the use of some locally available materials that could be used as partial replacement for OPC in construction works. Supplementary cementitious materials have been proven to be effective in meeting most of the requirements of durable concrete and blended cements are now used in many parts of the world. Various research works have been carried out on the binary blends of OPC with different pozzolans in making cement composites (Saraswathy and Song, 2007).

Rice husk ash is the byproduct of burned rice husk at higher temperature are commonly used as a raw material in concrete nowadays in order to improve the mechanical properties of concrete. Rice husk ash is a highly reactive pozzolanic material produced by controlled burning of rice husk. India is the second largest rice paddy cultivating country in the world. Rice husk is increasingly used as biomass to fuel and co-fuel the power plants. Both the technical advantages offered by structural concrete containing rice husk ash and the social benefits related to the decrease in number of problems of ash disposal in the environment have simulated the development of research into the potentialities of this material.

RHA is a promising pozzolanic material that can be blended with portland cement for the production of durable concrete, and

is also a value added technology (Mehta 1977). Approximately 1,000 kg of rice can produce 200 kg of husk, which on combustion produces approximately 40 kg of ash (Mehta 1986). Rice husk has high ash content, varying from 18–20% (Mehta 1992). Higher temperatures and longer durations of controlled burning produce RHA with higher pozzolanic properties (Boateng and Skeete ,1990). RHA is reported to have a pozzolanic index of 108%, which is higher than that of flyash (Class F).

SIGNIFICANCE

Al Khalaf and A.Yousif (1984) have investigated the effect of rice husk on pozzolanic behavior of rice husk ash. They investigated that up to 40% replacement of cement with RHA can be made with no significant change in the compressive strength as compared to the controlled mix, if the rice husk is burnt under optimum temperature condition.

Ismail and Waliuddin (1996) had worked on effect of rise husk ash on high strength concrete. They observed that optimum replacement of cement by RHA was 10–20%. It was also observed that when cement was replaced in different proportions of RHA, the workability decreased with increasing quantity of RHA.

Ramezanianpour et al. (2010) concluded that burning rice husks at temperature below 700°C produces rice husk ash with high pozzolanic activity.Mehta et al. (1977) observed that when the burning temperature, to get RHA, is high, the RHA goes into the crystalline stage while low burning yields RHA in amorphous form which is highly pozzolanic in character as compared to the crystalline form of RHA.

Zhang et al. (1996) noted that the incorporation of the RHA in cement paste did not increase its compressive strength compared with that of the control. The higher compressive strength of the RHA concrete compared with that of the control is due to probably to the reduced porosity, reduced $Ca(OH)_2$, and reduced width of the interfacial zone between the paste and the aggregate. However, with increase in the percentage of RHA replacement the flexural strength also decreased.

Gemma (2006) used cylinders for testing compressive strength with different w/c ratios (0.32,0.4 and 0.5) and observed that the RHA concrete had higher compressive strength at 91 days in comparison with that of the concrete without RHA, although at 7 and 28days a different behavior was observed between the concretes with the two RHA proportions considered. The increase in compressive strength of concrete with residual RHA is better justified by the filler effect (physical) than by the pozzolanic effect (chemical/physical). The increase in compressive strength of concrete with RHA produced by controlled incineration is mainly due to the pozzolanic effect.

Hendriks et al (2003) provided an estimation of 0.93 kg CO_2 emissions/kg of cement produced in India with a world average of 0.81 kg CO2/kg cement. if the amount of cement required per kg of concrete is reduced using supplementary material, it would reduce the quantity of CO_2 emissions into the atmosphere.

The aim of this present study is to reduce the environmental problems due to depletion of the natural resources. This aim can be achieved by using the Rice Husk Ash to produce concrete mixes for structural elements with required performance as conventional cement concrete. The objectives of the present study are

- To find the optimum mix design with regards to the amount of water, RHA and cement ratio.
- To investigate the physical properties of the RHA
- To study the relative strength development of RHA concrete with conventional concrete mix.
- To study the mechanical properties of RHA concrete

EXPERIMENTAL INVESTIGATIONS

The following materials are used in the production of eco-friendly concrete. A brief description of the materials used in the investigation are given below

Cement

The most common cementitious material used is Ordinary Portland Cement (OPC) and Portland Pozzolona Cement (PPC). OPC of grade 43 conforming to IS: 8112-1989 and PPC conforming to IS: 1489 - 1991 (Part1).Many tests were performed on OPC and PPC in order to find out the properties of the materials.

Table 1 Properties of OPC

Sl. No	Property	Results	Standard Values
1	Consistency	29%	-
2	Initial Setting Time	90 min	30 min minimum
3	Final Setting	225 min	Maximum 600 min
4	Specific Gravity	3.15	-

Table 2 Properties of PPC

Sl. No	Property	Results	Standard Values
1	Consistency	31%	-
2	Initial Setting Time	55 min	30 mins minimum
3	Final Setting	170 min	Maximum 600 min
4	Specific Gravity	2.83	-

AGGREGATES

Locally available river sand conforming to zone II as per IS: 383:1970 was used as fine aggregate in this investigation. The properties of fine aggregates are given in the table 3. Crushed granite type aggregates, having 20mm and down size were used as coarse aggregates in the experimental work. The properties of coarse aggregates are as given in table 4.

Table 3 Properties of Fine aggregates

Sl. No	Property	Results
1	Fineness modulus	2.78
2	Specific gravity	2.60
3	Grading Zone	II
4	Water absorption	1.30 %

Table 4 Properties of Coarse aggregates

Sl. No	Property	Results
1	Fineness modulus	6.70
2	Specific gravity	2.75
3	Water absorption	0.8 %

Rice Husk Ash (RHA)

Rice husk ash used in the present study was obtained from the Pranamya Biofuel plant near **Udupi, Karnataka state, India**. The specific gravity of rice husk ash is 2.11 and bulk density is 0.781 g/cc RHA, produced after burning of Rice husk (RH) has high reactivity and pozzolanic property. IS 456-2000 recommends use of RHA in concrete but does not specify quantities. The percentage of Silicon dioxide and Calcium oxide are 87-97% and 0.-2.2% respectively. Average specific gravity of rice husk ash is calculated as 2.11.

Water

Water is an important ingredient of concrete as it actively participates in chemical reaction with cement. The water used for mixing and curing should be clean and free from injurious quantities of alkalis, acid, oils, salt, sugar, organic materials, vegetable growth and other substances that may be deleterious to concrete or steel. The pH value of water should be not less than 6.

MIX PROPORTIONS

M20 grade mix was suggested in this study and a reference mix was prepared using OPC, PPC and conventional ingredients in accordance with IS 10262:1982 to achieve the target strength of 20MPa. The final mix proportion for the present study for M20 mix is 1:1.82:3.16 with a water-cement ratio of 0.50. Using the same mix proportion, concrete cubes for aggressive environment were casted as partial replacement of cement by RHA in terms of 10%, 20%, 30% on volume basis. The concrete cube of sizes (150 x 150 x 150) is casted in the laboratory.

RESULTS AND DISCUSSIONS

In the present investigation, an attempt has been made to study in detail, the behaviour of concrete mixed with different percentages (10%, 20% and 30%) of rice husk ash. The results of tests performed on rice husk concrete are discussed. The variations in compressive strength, split tensile strength and flexural strength are discussed in detail and presented in the figures 1a - 1c.

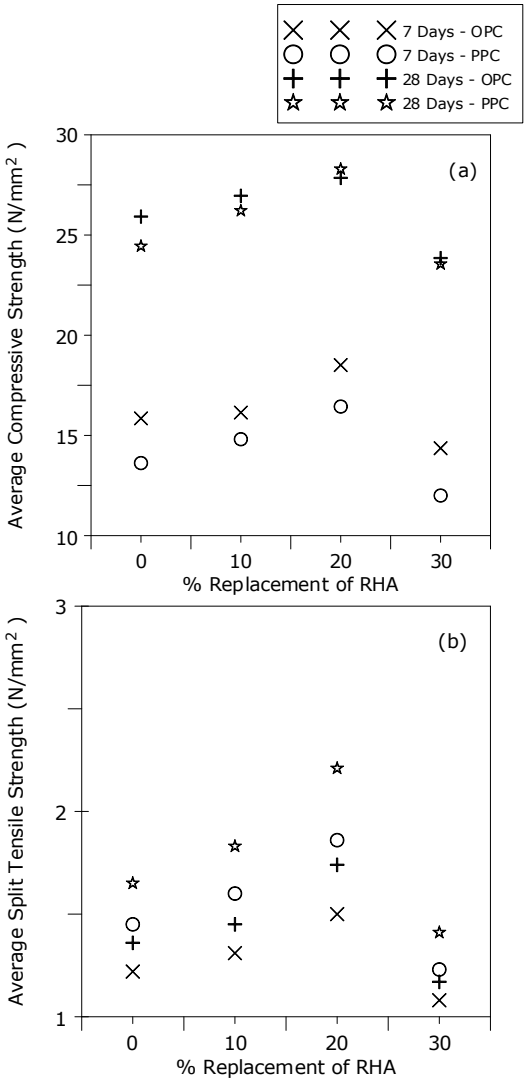

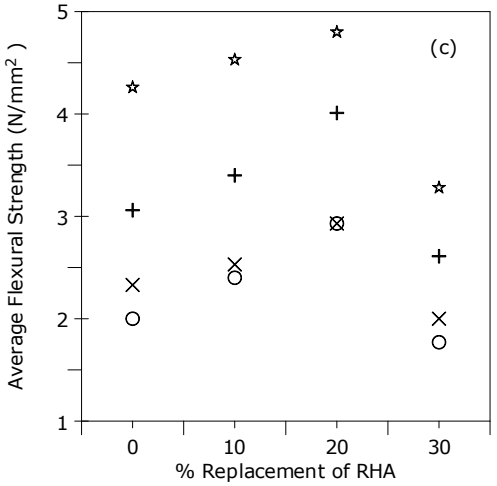

Fig.1 Properties of concrete with various proportions of RHA

Average Compressive Strength

It is seen that from figure 1(a), the 7 days compressive strength of concrete made with replacement of RHA with cement shows the increase in strength upto 20% replacement, beyond 20% replacement, the strength of concrete reduced than the original normal (conventional) concrete. Also it can be seen that as percentage of RHA replacement with cement increases, the strength of concrete decreases. Percentage increase in the strength at 20% replacement is nearly 20% for PPC mixes and 17% for the OPC mixes. 30% replacement mixes shows decrease in the strength by 10% to 15% for the both mixes. The results of 28 days compressive strength of mixes with 10% and 20% replacement of RHA with cement gives the better results than normal mix. But the mix of 30% replacement shows lesser strength. Percentage increase in the strength in OPC mixes at 10 % & 20% replacement is nearly 3 to 5%. Also for the PPC mixes the strength increased percentage at 10% and 20 % replacement is nearly 8 to 10%.

Average Split Tensile Strength

From the figure 1(b), it can be seen that the tensile strength of the concrete made with the RHA shows same variation as that of compressive strength. The tensile strength obtained at 10% and 20% replacement shows more strength than the normal mix strength. Percentage increase

in the strength in OPC mixes at 10 % and 20% replacement is to be 7.3% and 23%. Also for the PPC mixes the strength increased percentage at 10% and 20 % replacement is 10% and 28%. The 28 days tensile strength, as percentage of RHA in concrete increases the tensile strength increases upto 20% replacement and then beyond 20% replacement it shows the decrease in the tensile strength. Percentage increase in the strength in OPC mixes at 10 % & 20% replacement is 7% and 28%. Also for the PPC mixes the strength increased percentage at 10% and 20 % replacement is 11% and 30%.

Average Flexural Strength

From the figure 1(c), It was observed from the 7 days flexural strength comparison graphs that at 10% and 20% replacement, it shows more value than the normal mix but beyond 20% replacement it shows lower flexural strength than the normal mix. At 10% and 20 % replacement the increase in the flexural strength in OPC is 8.5% and 25% respectively and in PPC is 20%and 32% have been seen respectively. After 20% replacement the concrete strength decreased for OPC and PPC. Considering the 28 days flexural strength, as RHA replacement increases beyond 20%, the flexural strength decreases. Maximum increase in the flexural strength is observed at 20% replacement which is nearly 30% in OPC and 17% in PPC.

CONCLUSIONS

An experimental investigation on the effects of RHA in concrete regarding the compressive, split tensile, and flexural strength has been studied. Based upon the detailed analysis, the following important conclusions are summarized.

- It can be observed that, for 28 days compressive strength graphs, mixes of 10 % and 20% replacement of RHA with cement give better results than normal mix. But the mix of 30% replacement shows lesser strength than the normal mix.
- At 20 % replacement there is no significant change in the concrete strength. So maximum replacement upto 20% can be done without compromising with the strength.
- Percentage increase in the split tensile strength in OPC mixes at 10 % & 20% replacement is 7% and 28%. Also for the PPC mixes the strength increased percentage at 10% and 20 % replacement is 11% and 30%.
- At 10% and 20 % replacement the increase in the flexural strength in OPC is 8.5% and 25% respectively and in PPC is 20% and 32% have been observed.
- After 20% replacement the concrete strength decreased for both.
- From the overall results and comparison, 20% replacement of rice husk ash in the concrete gives the optimum results. It is well suitable to use the PPC instead of OPC as PPC mixes' results are more consistent and concrete obtained in PPC mix is more homogenous than OPC.
- By using one of the waste materials like RHA as partial replacement to cement, a better solution to produce eco-friendly concrete is provided and this approach also reduces the waste disposal problems of rice husk ash.

REFERENCES

[1] Al-Khalaf, M N and Yousif, H A (1984), Use of Rice husk ash in Concrete, Int. Journal of Cement Composites and Lightweight Concrete, Vol. 6, pp.123-126.

[2] Basha, E A et al (2005), Stabilization of residual soil with RHA and cement, Construction Building Materials, Vol. 5, No. 12, pp. 448–453.

[3] Bhanumathidas, N and Kalidas, N (2000), CO_2 abatement and conservation of natural resources through industrial byproduct utilization for cement and building materials, Workshop on Climate Change Mitigation Projects in the De-Centralized Energy Section and Building Material Sector: Developments, Alternatives and USAID, Pune, India.

[4] Boateng, A A and Skeete, D A (1990), Incineration of rice hull for use as a cementitious material: The Guyana experience, Cement Concrete Research, Vol. 20,pp. 795–802.

[5] Ephraim et al (2012), Compressive Strength of Concrete with RHA as partial replacement of ordinary Portland Cement, Scholarly Journal of Engineering Research, Vol. 1, No. 2, pp. 32-36.

[6] Gemma, R S (2006), Strength development of concrete with Rice-husk ash, Cement & Concrete Composite, Vol. 28,pp. 158-160.

[7] Hendriks et al (1998), Emission reduction of greenhouse gases from the cement industry, Proceedings of the 4th International Conference on Greenhouse Gas Control Technologies, Interlaken, Austria.
[8] IS 10262:1982, Recommended Guidelines for Concrete Mix Design, Bureau of Indian Standards, New Delhi, India.
[9] IS 383:1970, Specification for coarse and fine aggregates from natural sources for concrete (2nd rev), Bureau of Indian standards, New Delhi, India.
[10] IS 456:2000, Code of Practice for Plain and Reinforced Concrete, Bureau of Indian Standards, New Delhi, India
[11] IS 516:1959, Methods of Tests for strength of concrete, Bureau of Indian Standards, New Delhi, India.
[12] IS 8112:1989. Specification for OPC-43 grade cement. Bureau of Indian Standard, New Delhi, India.
[13] Ismail, M S and Waliuddin, A M (1996), Effect of rice husk ash on high strength concrete, Construction and Building Material, Vol. 10. No. 7, pp. 521-526.
[14] Shetty, M.S. (1997), Concrete Technology., S. Chand & Co. Ltd, pp. 50-70.
[15] Maeda, N et al (2001), Development of a new furnace for the production of rice husk ash, Proc. of 7th CANMET/ACI International Conference on Fly Ash, Silica Fume, Slag and Natural Pozzolans in Concrete, Chennai. Madras, pp.835–852.
[16] Malhotra, V M and Mehta, P K (1996), Pozzolanic and cementitious materials, Advanced Concrete Technology, Vol. 1. Canada: Gordon and Breach Publ., pp. 223-230.
[17] Mehta, P K (1977), Properties of blended cements made from rice husk ash, J. Am. Concr. Inst, Vol. 74, No. 9,pp. 440-442.
[18] Mehta, P K (1986), Structure, properties, and materials, Prentice-Hall, Englewood Cliffs, NJ, 382.
[19] Mehta, P K and Pirtz, D (2000), Use of rice husk ash to reduce temperature in high strength mass concrete, ACI Journal Proceedings, Vol. 75, pp. 60-63.
[20] Mehta, P K (1994), Rice-husk Ash – A Unique Supplementary Cementing Material, CANMET, Ottawa, Canada, MSL report 94-1 (R), pp. 419–444.
[21] Ogunbode et al, (2012), An evaluation of compressive Strength of Concrete made with RHA obtained by open air burning, www.academia.edu.
[22] Ramezanianpour, A A et al (2010), Mechanical properties and durability of concrete containing rice husk ash as supplementary cementing material, International Journal of Civil Engineering, Vol. 7, No. 2, pp. 180-186
[23] Salas, J (1988), Crucial curing of rice husk concrete.″ Building research and practices, Vol. 21, No. 6, pp. 367–376.
[24] Saraswathy, V and Ha-Won, S (2007), Corrosion Performance of Rice Husk Ash Blended Concrete, Construction and Building Materials, Gale Group, Farmington Hills, Michigan. www.encyclopedia.com/doc/1G1163421748.html.
[25] Zhang, M H and Mohan, M V (1996), High-Performance Concrete Incorporating Rice Husk Ash as a Supplementary Cementing Material, ACI Materials Journal, Vol. 93, No. 6, pp. 629-636.

5th International Engineering Symposium - IES 2016
March 2-4, 2016, Kumamoto University, Japan

AN EXPERIMENTAL STUDY ON OPTIMAL MIX DESIGN FOR PERVIOUS CONCRETE

Archana Harikrishnan [1], Rajasekaran, C [2] and Jeenu, G[3]

[1] Post Graduate Student, Department of Civil Engineering, National Institute of Technology Karnataka, Surathkal, India. Email: archanahari1992@gmail.com
[2] Assistant Professor, Department of Civil Engineering, National Institute of Technology Karnataka, Surathkal, India. Email: bcrajasekaran@gmail.com
[3] Assistant Professor, Department of Civil Engineering, College of Engineering Trivandrum, Kerala, India. Email: jeenu_shaj@yahoo.com

ABSTRACT: In this paper, the effect of size of coarse aggregates and the presence of fine aggregates on the properties of pervious concrete is investigated. The properties of sample blocks having different proportions of cement, coarse aggregate, fine aggregate and water were reviewed. The compressive strength, flexural strength, split tensile strength and permeability of the different trial mixes were determined. Results of the experimental study indicated that with a decrease in the size of coarse aggregates, the compressive strength increases in the absence of fine aggregates. The addition of calculated proportions of fine aggregates resulted in significant increase in the strength properties and a decrease in the permeability.

***Keywords**: Pervious concrete, Mix design, Pavement, Permeability*

INTRODUCTION

Pervious concrete is a special type of concrete having high porosity. It consists of Portland cement, coarse aggregate, little or no fine aggregate, admixtures, and water. Combination of these ingredients when mixed, placed, compacted and cured properly, produce a hardened material that not only has sufficient strength and durability to bear the specified load and to resist environmental conditions, but also have interconnected pores that provide adequate permeability to the material. Pervious concrete pavement is expected to reduce the impact of development on environment by allowing rain water to percolate to the soil below, recharging the ground water aquifers, reducing the volume of direct water runoff from the pavement and enhancing the quality of storm water. It reduces or eliminates the need for additional control structures, such as retention ponds for storing the runoff water.

Various studies have been conducted investigating the properties and possible applications of pervious concrete. The addition of fine aggregate results in better strength properties than the mix without fine aggregate (Lian et al, 2010). Pervious concrete can be successfully used in the construction of low volume pavements, parking lots, sidewalks, sub-base for conventional concrete pavements etc (Tennis et al, 2004).

OBJECTIVES

The main objective of this study is to prepare an optimal mix design for pervious concrete having a minimum compressive strength of 10-15 N/mm^2 and a permeability of 0.2-0.5 cm/s. The influence of size of coarse aggregates and presence of fine aggregates is also investigated.

RESEARCH SIGNIFICANCE

Large urban areas are covered by impervious concrete pavements resulting in increased runoff which has long term effects such as depletion of ground water, increased pollution in water bodies, lack of clean drinking water etc. The use of pervious concrete will reduce these issues as the pores in them will help in the

percolation of rain water thus replenishing ground water and reducing runoff. Though pervious concrete has got these advantages, the use of this material is not prevalent in Indian construction industry due to many reasons such as requirement of high maintenance and the possibility that the pores might get clogged due to the Indian road conditions.However as it is an eco friendly technique it is worth studying so that the advantages of pervious concrete can be exploited.

EXPERIMENTAL PROGRAM

The focus of the experimental research reported in this study is the investigation of the influence of aggregates on the properties of pervious concrete. Totally seven different concrete compositions were tested in this study.20mm,12mm and 6mm aggregates were used as single sized aggregates with 0%,2% and 4% fine aggregate content. Details of the mixture proportions used in this study are provided in the next section.

MIXTURE PROPORTIONS

From previous studies, the mix design approach based on determination of paste volume was adopted.

Required paste volume(%)=aggregate void content (%) + compaction index (%) – design void content (%) (Obla, 2010)

Aggregate void content was determined by doing laboratory experiments as shown in Table 1. Compaction index depends on the anticipated consolidation in the field. For greater consolidation effort, a compaction index value of 1 to 2 % may be adopted. For lighter level of compaction, a value of 7 to 8 % can be used. A compaction index of 5% was chosen for design purpose. A design void content of 30 % was adopted.
Table 2 gives the mix proportion adopted for this study.

MIXTURE CONSTITUENTS

The materials used in the test program are as follows:
Cement - Commercially available 53 grade Ordinary Portland cement conforming to IS 12269-1987 is used throughout the experimental program.
Coarse aggregate – Crushed rock of sizes 20mm, 12mm and 6mm is used as coarse aggregate. The different tests to determine the properties of the aggregate are conducted as per IS 2386: 1963 (Reaffirmed 1990) and the results are tabulated in Table 1.
Fine aggregate: River sand passing through IS 4.75 mm sieve conforming to IS 2386: 1963(Part III) is used as fine aggregate.

MIXING AND CASTING

Machine mixing was done to prepare the trial mixes. Dry mixing was done at first and the water was poured into the mixture gradually.The specimens used for the study included nine standard cubes, cylinders, three discs and a slab from each mix. The specimens were demoulded after 24 hours and were subjected to water curing.

EXPERIMENTAL TEST PLAN

The properties of the pervious concrete prepared in the designed mix proportions were determined by conducting tests on hardened concrete.
Compressive strength
The compressive strength test was performed on standard cubes at the age of 7, 14 and 28 days. The testing was done in accordance with IS 516-1959. The specimens were tested for compressive strength using 1000KN capacity compression testing machine.
Split tensile strength
Direct tensile strength tests were carried out on cylinders of diameter 150mm and height 300mm conforming to IS 5816: 1999.
Flexural strength
Flexural strength test was carried out on 250mm*250mm*50mm slabs in accordance with IS 516:1959.
Permeability
Permeability test was done on disc specimens of 100mm diameter and 50mm height using a variable head permeameter setup.

RESULTS AND DISCUSSION

Compressive strength
For all the concrete mixes prepared, the 28 day strength was found to be in the required range of 10-25 N/mm^2. Figure 1

shows the variation of compressive strength of mixes without fines with respect to the aggregate size. As the aggregate size decreases from 20mm to 6mm, about 130% increase in the 28 day strength is observed. This can be attributed to the better packing effect of the smaller sized aggregates. Figure 2 illustrates the variation of strength of specimen with fines. For 20mm aggregate mixes, no appreciable increase in the compressive strength was observed due to the addition of fines. For 12mm aggregate mixes, there is considerable increase in the 7, 14 and 28 day compressive strengths as compared to the mix without fines.

Split tensile strength

Table 4 shows the split tensile strength obtained for the different mixes. 20 mm aggregate with 4% fines gave the maximum split tensile strength followed by 12mm mix with 2% fines.

Flexural strength

The flexural strength obtained for the different mixes is given in Table 3. The required flexural strength for pervious concrete to be used in pavement construction is 1-3.6 MPa. From the results obtained it can be seen that the flexural strength of all the mixes were in this range. Maximum flexural strength was exhibited by 20mm with 4% fines mix.

Permeability

Table 4 gives the permeability obtained for the different mixes. The permeability required for pervious concrete to be used in pavement construction is 0.2-0.5cm/s. Except for the 6 mm mix, all other mixes exhibited permeability in this range. Maximum permeability was observed for 20mm aggregates without fines. This can be attributed to the larger sized pores present in it due to the uniform grading and the absence of fine aggregates. The mix with 6 mm exhibited the least permeability. This is due to the dense packing effect of the small sized aggregates.

CONCLUSIONS

Based on the work presented in this paper, the following conclusions can be drawn:

- As the size of the uniformly graded aggregate decreases, the strength properties improve while the permeability decreases.
- The addition of small percentages of fine aggregates resulted in better strength properties.
- The mix with 12 mm uniformly graded aggregates and containing 2% fines was found to be optimum mix with the required strength and permeability.

REFERENCES

[1] Beecham, S et al (2011), The relationship between porosity and strength for porous concrete, Construction and Building materials, Vol. 25, pp. 4294-4298.

[2] Lian, C and Zhuge, Y (2010), Optimum mix design of enhanced permeable concrete – An experimental investigation, Construction and Building materials , Vol. 24, pp. 2664-2671.

[3] Neithalath, N and Deo, M (2011), Compressive response of pervious concrete proportioned for desired porosities, Construction and Building materials, Vol.25, pp. 4181-4189.

[4] Obla, K H (2010), Pervious concrete – An Overview, The Indian Concrete Journal, August edition, pp. 9-18.

[5] Tennis, P D et al (2004), Pervious Concrete Pavements, First edition, Portland Cement Association, USA.

[6] Yang, J and Jiang, G (2003), Experimental study on properties of pervious concrete pavement materials, Cement and Concrete research, Vol. 33, pp. 381-386.

Table 1 Properties of coarse aggregates

Property	20 mm	12 mm	6 mm
Bulk density (gm/cc)	1.56	1.494	1.506
Void ratio (%)	53.06	64.15	87.5
Porosity (%)	34.67	39.08	46.67
Specific Gravity	2.387	2.453	2.825

Table 2 Mix proportions used in this study

Size of aggregate	Mix	Coarse aggregate(kg/m^3)	% fines	Fine aggregate(kg/m^3)	Cement (kg/m^3)	Water (kg/m^3)
20 mm	1	1001.13	0	-	454.42	136.34
	2	981.1	2	21.81	454.42	136.34
	3	961	4	43.62	454.42	136.34
12 mm	4	755.36	0	-	633.79	190.2
	5	721.66	2	16.04	633.79	190.2
	6	706.93	4	32.08	633.79	190.2
6 mm	7	318.20	0	-	464.49	139.32

Table 3 Split tensile and flexural strength test results

Mix	Split tensile strength (N/mm$^{2)}$	Flexural strength (N/mm$^{2)}$
1	1.17	1.76
2	1.41	2.11
3	1.85	2.77
4	1.36	2.05
5	1.58	2.37
6	2.11	3.16
7	1.14	2.88

Table 4 Permeability test results

Mix	Permeability(cm/s)
1	1.1457
2	0.7274
3	0.0375
4	0.6365
5	0.5241
6	0.5310
7	0.2023

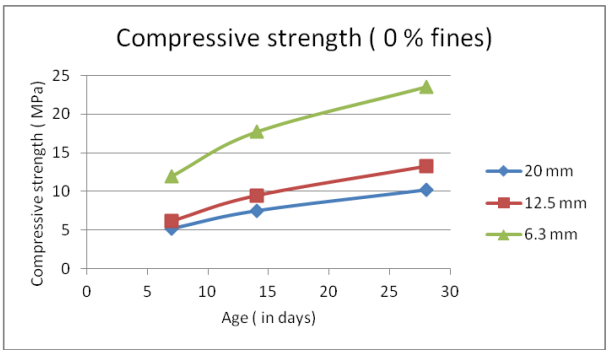

Figure 1 Variation of compressive strength of mixes without fines

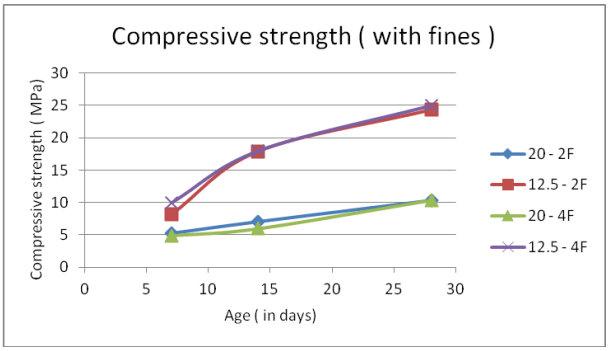

Figure 2 Variation of compressive strength of mixes with fines

5th International Engineering Symposium - IES 2016
March 2-4, 2016, Kumamoto University, Japan

PERFORMANCE OF FLYASH BASED CONCRETE WITH SPECIAL REFERENCE TO MARINE ENVIRONMENT

Sarfaraz Ahmed K [1] and Rajasekaran, C. [2]

1 *Mtech Student, Department of Civil Engineering, National Institute of Technology Karnataka, Surathkal, India. Email: ksarfaraz7@gmail.*
2 *Assistant Professor, Department of Civil Engineering, National Institute of Technology Karnataka, Surathkal, India. Email: bcrajasekaran@gmail.com*

ABSTRACT: The severity of marine environments varies depending on the locations and has a major bearing on the durability performance of marine structures. In this paper, an attempt has been made to assess the performance of concrete in severe marine environmental condition. The concrete specimens have been exposed to the marine water for curing and comparing with the normal curing conditions for different proportions of fly-ash based cement concrete. Fly ash is used to partially replace OPC at 0%, 15%, 30%, 50% and 60% by weight of cementitious material. Concrete specimens are casted and removed from the mould after one day of casting and exposed to two curing conditions: 1) specimens are cured for 28 days in normal water 2) specimens are directly exposed to marine water after demoulding. The mechanical and durability properties of concrete exposed to marine environment has been investigated and compared to normal curing conditions.

***Keywords**: Marine concrete, Durability, Concrete deterioration.*

INTRODUCTION

Concrete is the most widely used man-made material in the world, owing to its versatility and relative low cost. For a long time, concrete was considered to be very durable material requiring a little or no maintenance. The assumption is largely true, except when it is subjected to highly aggressive environments. We build concrete structures in highly polluted urban and industrial areas, aggressive marine environments, harmful sub-soil water in coastal area and many other hostile conditions where other materials of construction are found to be non-durable. Since the use of concrete in recent years, have spread to highly harsh and hostile conditions, the earlier impression that concrete is a very durable material is being threatened, particularly on account of premature failures of number of structures in the recent past.

One of the main reasons for deterioration of concrete in the past is that too much emphasis is placed on concrete compressive strength. As a matter of fact, advancement in concrete technology has been generally on the strength of concrete. It is now recognized that strength of concrete alone is not sufficient, the degree of harshness of the environmental condition to which concrete is exposed over its entire life is equally important. Therefore, both strength and durability have to be considered explicitly at the design stage. It is interesting to consider yet another view point regarding strength and durability relationship.

Generally, construction industry needs faster development of strength in concrete so that the projects can be completed in time or before time. This demand is catered by high early strength cement, use of very low W/C ratio through the use of increased cement content and reduced water content. The above steps result in

higher thermal shrinkage, drying shrinkage, modulus of elasticity and lower creep coefficients. With higher quantity of cement content, the concrete exhibits greater cracking tendencies because of increased thermal and drying shrinkage. As the creep coefficient is low in such concrete, there will not be much scope for relaxation of stresses. Therefore, high early strength concretes are more prone to cracking than moderate or low strength concrete. Of course, the structural cracks in high strength concrete can be controlled by use of sufficient steel reinforcements. But this practice does not help the concrete durability, as provision of more steel reinforcement, will only results in conversion of the bigger cracks into smaller cracks. All the same even these smaller cracks are sufficient to allow oxygen, carbon dioxide, and moisture get into the concrete to affect the long term durability of concrete.

1. Field experience have also corroborated that high early strength concrete are more cracks-prone. A point for consideration is that, the high early strength concrete made with modern Portland cement which are finer in nature, containing higher sulphates and alkalis, when used 400 kg/m^3 or more, are prone to cracking. Therefore if long-term service life is the goal, a proper balance between a too high and a too low cement content must be considered. This is where the use of mineral admixtures comes in handy. The objective of the present study is To determine the durability and strength of concrete for different fly-ash proportion replacements in concrete exposed to normal curing and marine environment. To minimize the use of cement in concrete and hence reducing carbon footprints in atmosphere. To determine the permeability of concrete for different proportion of flyash.

Materials Used

Cementitious materials – Cement, Alccoffine and Flyash are used as cementitious materials in different proportion.

Cement: In the present study, Ordinary Portland Cement (OPC) 43 grade is used and its properties are tabulated in table 1.

Alccoffine: Alccoffine 1203 is a supplementary cementitious material suitably replaces silicafume used in high performance concrete and its properties are tabulated in table 2.

Flyash: Flyash is collected from Udupi Power Corporation limited and its properties are tabulated in table 3.

Aggregates: The details of Fine Aggregate and Coarse Aggregate used are tabulated in table 4.

Water: Potable water available in the laboratory satisfying the codal requirements(IS 456-2000) is used.

METHODOLOGY

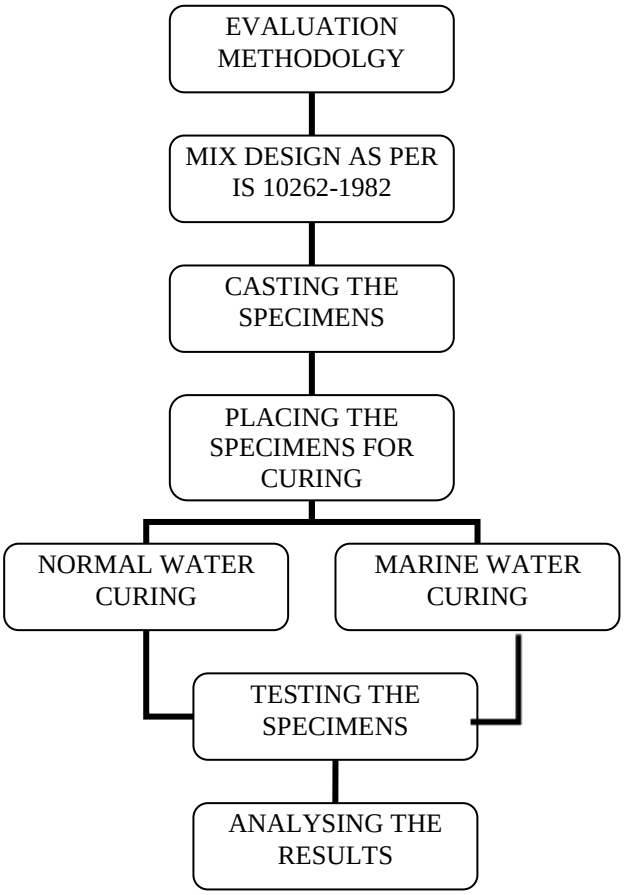

MIX PROPORTIONS

In order to study the behaviour of concrete in marine environment, concrete samples with varied percentage of flyash is used by adapting suitable mix design.

For the present study, OPC concrete with flyash proportions of 0%, 15%, 30%, 50% and 60% is used. The cement is replaced with 5% Alccoffine in all the mixes.

Concrete specimens are casted and removed from the mould after one day of casting and exposed to two curing conditions: 1) specimens are cured for 28 days in normal water 2) specimens are directly exposed to marine water after demoulding.

Cubes, cylinders and slabs were casted and subjected to two curing conditions. Then the samples are periodically collected and tested for mechanical and durability properties such as compressive strength and weight loss. The cylinders were tested for split tensile strength at 28 days. The slabs were tested for knowing the permeability of concrete using Permit Ion-Permeability apparatus.

EXPERIMENTAL PROCEDURE

The concrete cubes are tested in compressive testing machine. The permeability of the concrete is determined by Permit Ion-Permeability apparatus. The Permit Ion-Permeability test unlike other test is a Non Destructive Test. It measures the rate at which the ions are passing through the specimen and thereby providing diffusion ion migration coefficient, permeability coefficient, which is indirectly indicative of durability of concrete. The working principle behind this test is that the ions in the inner catholyte chamber are forced to migrate to outer anolyte chamber due to potential gradient acting as driving force.

The amount of ions reaching the outer cell is monitored indirectly by change in conductivity of the anolyte using conductivity probes. When the conductivity readings indicate the establishment of flow of ions into a anolyte chamber the slope of a steady state conductivity is determined. Using the slope of the steady state conductivity curve in the Nernst-plank equation we obtain the diffusion migration coefficient. The diffusion migration coefficient is given by the equation below

$$D_{mig-in-situ} = -\left(\frac{dc}{dt}\frac{T}{E}\right)\left(\frac{R}{zCF}\right)\left(\frac{L}{A}V\right) \quad (1)$$

$D_{mig\text{-}in\text{-}situ}$ = diffusion migration coefficient, m^2/s

$\frac{dc}{dt}$ = rate of change in concentration of anolyte, mol/m^3s^1

T = absolute temperature(average during steady state) K

R = universal gas constant (8.31 J/k-mol)

z = valency of the ions (chloride ion-1)

C = concentration of ion source solution ($0.55*10^3 mol/m^3$)

F = Faradays constant ($9.65*10^4$ C/mol)

E= Electrical potential apllied between cathode and anode(60V)

V = volume of the anolyte ($6.5*10^{-4}$ m^3)

$\frac{L}{A}$ = ratio of the flow length to exposed area(3.74 m^{-1})

RESULTS

1. Effect of compressive strength for different proportion of flyash : The influence of compressive strength for different proportion of flyash i.e. 0%,15%, 30%, 50% and 60% is determined. In all these, 5% Alccoffine is used as cement replacement in all the mixes. Fig 1 and Fig 2 represents the compressive strength for 7 days and 28 days respectively.

2. Effect of permeability of concrete for different flyash proportions : The permeability of concrete reduces with increase in flyash proportions. Higher the flyash proportions lesser will be the permeability and hence more durability is achieved.

TABLE 1 : Properties of cement

PROPERTY	RESULT OBTAINED	REQUIREMENT AS PER IS CODE
Specific gravity	3.1	In the range of 3.00- 3.15
Fineness cm^3/g	3713	not lessthan 2250
Setting times min	Initial 90 Final 210	not less than 30 not more than 600

TABLE 2 : Properties of alccoffine

PROPERTY	RESULT OBTAINED
Specific gravity	2.9
Fineness cm^2/g	12000
Bulk density kg/m^3	800

TABLE 3 : Properties of flyash

PROPERTY	RESULT OBTAINED
Specific gravity	2.16
Fineness cm^2/g	4260

TABLE 4 : Properties of fine aggregates and coarse aggregates

PROPERTY	FA	CA
Specific gravity	2.6	2.65
Loose bulk density g/cc	1.45	1.46
Compact bulk density g/cc	1.65	1.64

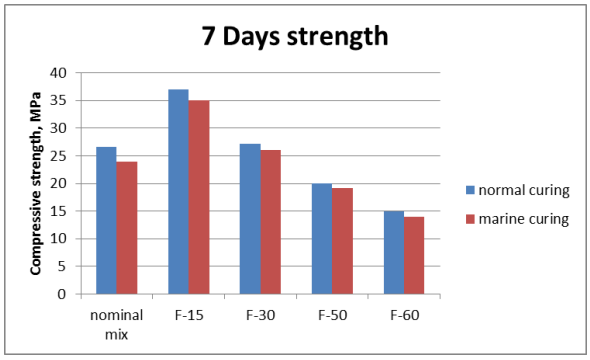

FIG 1: 7 Days Compressive Strength

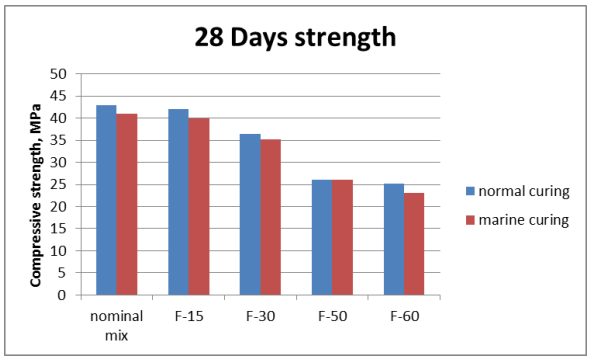

FIG 2: 28 Days Compressive Strength

CONCLUSIONS:

The following conclusions are drawn from this study

- Durability is not directly related to the strength of concrete. It depends on the microstructure of the concrete.
- The material properties, flyash proportions are identified as important parameters controlling the strength of concrete.
- On the basis of experimental results, flyash based concrete subjected to aggressive environment are more durable.

Admixtures may lead to substantial savings in the consumption of cement and also reduce the carbon footprint in atmosphere.

REFERENCES

[1] Bader, M. A. (2003). Performance of concrete in a coastal environment. *Cement and Concrete Composites*, *25*(4), 539-548.

[2] Chalee, W et al (2010). Utilization of fly ash concrete in marine environment for long term design life analysis. *Materials & Design*, *31*(3), 1242-1249.

[3] Dhir, R. K. et al (1997). Developing chloride resisting concrete using PFA. *Cement and Concrete Research*, *27*(11), 1633-1639.

[4] Hassan, K. E. et al (2000). The effect of mineral admixtures on the properties of high-performance concrete. *Cement and Concrete Composites*, *22*(4), 267-271.

[5] Leng, F et al (2000). An experimental study on the properties of resistance to diffusion of chloride ions of fly ash and blast furnace slag concrete. *Cement and Concrete Research*, *30*(6), 989-992.

[6] Lopez-Calvo, H. Z. et al (2012). Compressive strength of HPC containing CNI and fly ash after long-term exposure to a marine environment. *Cement and Concrete Composites*, *34*(1), 110-118.

[7] Mackechnie, J. R., & Alexander, M. G. (1997). Exposure of concrete in different marine environments. *Journal of materials in civil engineering*, *9*(1), 41-44.

[8] Shashiprakash, S. G., & Thomas, M. D. A. (2001). Sulfate resistance of mortars containing high-calcium fly ashes and combinations of highly reactive Pozzolans and fly ash. *ACI Special Publication*, *199*.

[9] Safehian, M., & Ramezanianpour, A. A. (2013). Assessment of service life models for determination of chloride penetration into silica fume concrete in the severe marine environmental condition. *Construction and Building Materials*, *48*, 287-294.

5th International Engineering Symposium - IES 2016
March 2-4, 2016, Kumamoto University, Japan

Experimental Study on Water Absorption and Accelerated Curing Properties of Recylced Aggregates in Concrete

Seeram Apoorva[1], Suman Saha[2] and **Rajasekaran C[3]**

1 *Under Graduate Student, Department of Civil Engineering, Easwari Engineering College, Chennai, India. Email: seeram94@gmail.com*
2 *Research Scholar, Department of Civil Engineering, National Institute of Technology Karnataka, Surathkal, India. Email: sumansaha.civil@gmail.com*
3 *Assistant Professor, Department of Civil Engineering, National Institute of Technology Karnataka, Surathkal, India. Email: bcrajasekaran@gmail.com*

Abstract: Demolition of concrete structures produces significant amount of solid waste. There has been an overwhelming promotion for need of environmental management and sustainable development in the recent years as a result of various environmental issues caused by the deterioration of the environment. The usage of Recycled Coarse Aggregate cannot be implemented as such in concrete. It is mandatory to study the water absorption characteristics since the water absorption of RCA will directly affect the water- binder ratio of the mix and which in turn affects the workability of concrete. The utility of ascertaining strength after 28 days is often questioned since by this time considerable concrete would have been placed and work may have progressed. It is then rather too late for remedial measures. It is therefore of tremendous advantage to predict 28 days strength within a few hours of casting the concrete so that, we have a good idea about the strength of the concrete. An attempt has been made to study the water absorption property and the compressive strength of the accelerated curing of concrete made with recycled coarse aggregates.

Keywords **-** *Accelerated curing, curing temperature, Recycled aggregates, water absorption, compressive strength.*

INTRODUCTION

Construction waste is a large percentage of solid waste. There has been an overwhelming promotion of environmental management and sustainable development in recent years. As a result, there is a growing awareness of environmental issues and the likely problems from deterioration of the environment. Construction by nature is not an environmentally friendly activity. These effects include - Land use and Land deterioration, Depletion of natural resources, Waste generation, and High consumption of Portland cement and high emission of carbon-di-oxide.

Owing to the depletion of solid waste disposal areas, it has been necessary to reduce waste generation in recent years. Construction, one of the most resource-consuming has to actively participate in waste reduction. The use of recycled aggregate for the production of concrete is one such way.

Recycled aggregates are composed of original aggregates and adhered mortar. The adhered mortar is a porous material; its porosity depends upon the w/c ratio of the recycled concrete employed. Unlike ordinary aggregate, recycled aggregate is coated with patches of cement mortar remains that increase water absorption, prolong the mixing time and affect the strength of the *RAC*.

Aggregates are the important constituents in concrete. They give body to the concrete, reduce shrinkage and effect economy. Aggregates occupy 70-

80 percent of the volume of concrete their impact on various characteristics and properties of concrete is considerable. As a result, the properties and behaviours of recycled aggregate need to be explored and fully understood. The absorption capacity is one of the most significant properties which distinguish recycled aggregate from raw aggregates, and it can have an influence both on fresh and hardened concrete properties. Thus absorption capacity of recycled aggregates must be known prior to the utilization of recycled aggregates in concrete production in order to control properties of fresh and hardened concrete.

Accelerated curing is useful in the prefabrication industry wherein high early age strength enables the removal of the formwork within 24 hours thereby reducing the cycle time resulting in cost saving benefits. The most commonly adopted curing techniques are **steam curing at atmospheric pressure, warm water curing, boiling water curing and autoclaving.** The Hot Water accelerated curing method is a modification of the Boiling Water Method, involving temperatures of 70°C for approximately 20 hours. Accelerated curing is the process by which the temperature of the concrete is raised artificially by applying external heat to speed up the rate of gain in strength.

CONSTRUCTION AND DEMOLITION WASTE

Construction and demolition (C & D) waste is defined as the solid waste generated by the construction, remodeling, renovation, repair, alteration or demolition of residential, commercial, government or institutional buildings etc. There is a high potential for recycling and re-use of C & D, since some of its components have a high resource value. In particular, there is a re-use market for aggregates derived from C & D waste in roads, drainage and other construction projects. The quantity of C & D wastes is increasing day by day due to the rapid growth in the construction industry. The main reasons for the increase of the volume of demolition concrete waste are Building waste created from the natural calamities, Demolition and Renovation of the buildings for the introduction of new facilities, Old buildings and structures have to be demolished as they overcome their usage limit, Building waste resulting from manmade disaster/war. The types of C & D wastes are shown in Fig 1.

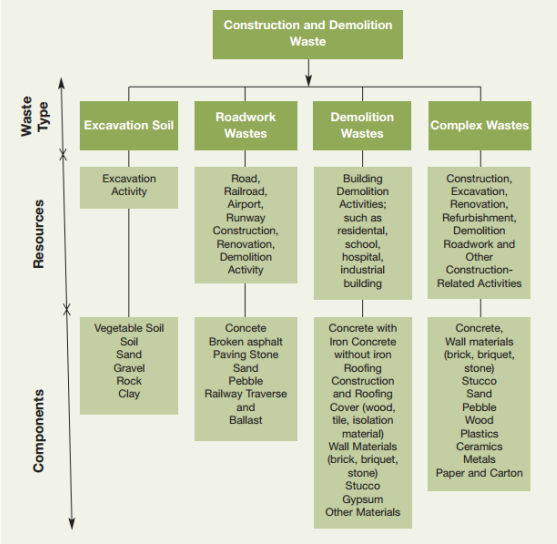

Fig.1 Types of C & D Waste

METHODOLOGY

The following activities were carried out:

- The tested cubes, cylinders which are available in the laboratory were crushed.
- Sieve analysis of the recycled aggregates was done and coarse (retained on 4.75mm sieve) and fine aggregates (passing through 4.75 mm sieve) were separated.
- Water absorption test was carried out for the following time periods for both Natural Aggregates and Recycled Aggregates for 1 Hour, 3 Hour, 6 Hour, 24 Hour, 48 Hour, 72 Hour and 7 Days.
- Concrete mixes with 30 percent replacement of the natural aggregates with recycled aggregates were prepared.
- Accelerated Curing was done for the prepared concrete mixes and

the Compressive Strength was conducted.

- Conclusions of the test result are given below.

Fig 2 Recycled Fine Aggregate

Fig 3 Recycled Coarse Aggregate

EXPERIMENTAL MATERIAL CEMENT

The most common cement used is Ordinary Portland Cement and Portland Pozzolona Cement. OPC of grade 43 conforming to IS: 8112-1989 and PPC conforming to IS: 1489 - 1991 (Part1). Many tests were performed on cement.

Natural Coarse Aggregates
Coarse Aggregates are particles than 4.75mm but generally between 9.5mm to 37.5mm in diameter. Locally available aggregate of maximum 20mm has been used.

Recycled coarse Aggregates
Large amounts of tested specimens such as cubes; cylinders etc. available in the concrete laboratory have been used. The specimens without reinforcement have been crushed by machine and then broken down by hammer manually into small pieces. The broken pieces are separated into two fractions. The pieces retained on 20mm sieve are used. The

Table 1 Properties of Ordinary Portland cement

sl. No.	Property	Results	Standard Values
1	Consistency	30%	-
2	Initial Setting Time	2 hours 5 min	30 mins minimum
3	Final Setting Time	5 hours	Maximum 10 hours
4	Specific Gravity	2.9	-

Table 2 Properties of Portland Pozzolona Cement

sl. No.	Property	Results	Standard Values
1	Consistency	31%	-
2	Initial Setting Time	55 min	30 mins minimum
3	Final Setting Time	2 hours 50 mins	Maximum 10 hours
4	Specific Gravity	2.828	-

Natural Fine Aggregates
The aggregate material which passes through 4.75 mm IS sieve and retained on 75 micron IS sieve is termed as fine aggregate. Table 3 gives the properties of Natural aggregates.

Table 3 Properties of Aggregates

sl. No	Property	Values	
		Fine Aggregate	Coarse Aggregate
	Specific Gravity	2.61	2.68
	Grading Zone	II	IV
	Water Absorption	1.0%	0.5%

pieces passing through 4.75mm have been left out (Recycled Fine Aggregate). The properties of recycled coarse aggregate are presented in table 4.

Table 4 Properties of Recycled Coarse Aggregates

sl. No.	Property	Value
1	Specific Gravity	2.55
2	Water Absorption	3.31 %

Water

Water is an important ingredient of concrete as it actually participates in the chemical reaction with cement. Since it helps to from the strength giving cement gel, the quantity and quality of water is required to be looked into very carefully. Casting and Curing of specimens were done with the potable water that is available in the university premises.

EXPERIMENTAL DETAILS

Water Absorption

Water absorption test was done using pycnometer method. The empty weight (w_1) of the pycnometer, along with the brass cap and washer was noted. Samples were filled up to one third of the pycnometer and the weight (w_2) was noted. Weight of the pycnometer (w_3) brim along with sample with water up to the brim is noted. Samples were prepared for the various time periods (1h, 3h, 6h, 24h, 48h, 72h and 7days) and are kept in observation. The samples are then taken are surface dried and oven dried at 100°C for 24 hours. The weight of the oven dried sample is noted (w_6). The specific gravity and water absorption is found by the equations

$$G = \frac{w_2 - w_1}{[(w_2 - w_1) - (w_3 - w_4)]} \quad \text{(Eq 1)}$$

$$\text{Water absorbed} = \frac{w_5 - w_6 \times 100}{w_5} \quad \text{(Eq 2)}$$

Design Mix

A mix of M25 and M30 grade with OPC and PPC was designed as per IS 10262:2009 and the same was used to prepare the test samples. The design mix proportion is shown in Table 5.

Accelerated Curing Method

The specimens were casted with the calculated proportions. They are stored in a place free from vibration, in moist air of at least 90 percent humidity and at temperature of 27±2°C for 23 hours ±15 minutes from the time of addition of water to the ingredients. The specimens are then gently lowered into the curing tank and shall remain totally immersed for a period of 3 ½hour ± 5 minutes. The temperature of the water in the curing tank shall be boiling (100°C) at sea level. The temperature shall not drop more than 3°C after the specimen are placed and shall return to boiling within 15 minutes. After curing for 3½ hours ± 5 minutes in the curing tank, the specimen are removed from the boiling water, removed from the moulds and cooled by immersing in cooling tank at 27 ±2°C for 2 hours. The cubes were tested immediately at the end of curing period. The compressive strength obtained is referred to henceforth as the "early compressive strength". The 28th day compressive strength is calculated by the equation

$$R_{28} = 8.09 + 1.64\ R_a \quad \text{(Eq 3)}$$

EXPERIMENTAL RESULTS

Table 6 and 7 gives the water absorption test results of the natural and recycled aggregates. Table 8 and 9 gives the compressive strength of OPC Mixes and PPC Mixes respectively.

Table 5 Quantity of materials required for 1 m^3 Concrete

Mix Name	Grade	W/C Ratio	Cement (kg)	FA (kg)	NCA (kg)	RCA (kg)	Water (kg)
OPC	M25	0.50	372	8.74	10.03	3.97	2.28
	M30	0.45	413.33	8.14	9.81	3.90	2.28
PPC	M25	0.50	372	8.32	10.01	3.99	2.29
	M30	0.45	413.33	8.12	9.79	3.91	2.28

Table 6 Specific Gravity and Water Absorption of Natural and Recycled Coarse Aggregates

Time period	Specific Gravity		Water Absorption (%)	
	Natural Coarse Aggregates	Recycled Coarse Aggregates	Natural Coarse Aggregates	Recycled Coarse Aggregates
1 h	2.76	2.62	0.28	3.59
3 h	2.67	2.73	0.56	3.31
6 h	2.68	2.71	0.28	2.38
24 h	2.75	2.55	0.28	3.31
48 h	2.05	2.57	0.57	3.64
72 h	2.78	2.68	0.01	3.72
7 days	2.81	2.65	0.28	2.38

Table 7 Specific Gravity and Water Absorption of Natural and Recycled Fine Aggregates

Time period	Specific Gravity		Water Absorption (%)	
	Natural Fine Aggregates	Recycled Fine Aggregates	Natural Fine Aggregates	Recycled Fine Aggregates
1 h	2.02	2.36	9.56	12.34
3 h	2.68	2.36	9.78	14.24
6 h	2.12	2.36	9.77	21.46
24 h	2.68	2.33	8.78	14.98
48 h	2.35	2.34	8.76	13.89
72 h	2.68	2.35	8.47	23.63
7 days	2.58	2.36	8.02	12.34

Table 8 Compressive Strength of OPC Mixes

Mix Name	Sample No	Weight (Kg)	Failure Load (KN)	Early Compressive Strength, R_a (N/mm^2)	28th day strength, R_{28} (N/mm^2)	Average 28th day strength (N/mm^2)
MOPC25	I	8.460	290	12.88	29.21	28.49
	II	8.622	280	12.44	28.49	
	III	8.470	270	12.00	27.77	
MOPC30	I	8.344	150	6.67	19.03	18.78
	II	8.306	150	6.67	19.03	
	III	8.482	140	6.22	18.29	

Table 9 Compressive Strength of PPC Mixes

Mix Name	Sample No	Weight (Kg)	Failure Load (KN)	Early Compressive Strength, R_a (N/mm^2)	28th day strength, R_{28} (N/mm^2)	Average 28th day strength (N/mm^2)
MPPC25	I	8.5	130	5.78	17.57	16.59
	II	8.36	100	4.44	15.37	
	III	8.49	120	5.33	16.83	
MPPC30	I	8.548	150	6.67	19.03	19.03
	II	8.466	150	6.67	19.03	
	III	8.428	150	6.67	19.03	

CONCLUSIONS

Based on limited experimental investigation concerning the water absorption and accelerated curing, the following observations are made regarding the compressive strength of 30% replacement of Recycled Coarse Aggregates of both OPC and PPC mixes:

- Quality of recycled coarse aggregate plays an important role to gain proper strength of concrete.
- Water Absorption capacity of recycled coarse aggregate is more than that of natural aggregates. It ranges from 2 to 4 percent whereas for natural coarse aggregates it's almost zero.
- Water Absorption capacity of recycled fine aggregate is in the range of 12 to 24 % whereas for natural fine aggregates its only 9%.
- The higher water absorption of the coarse aggregate resulted from the higher absorption rate of cement mortar attached to the aggregate particles. This high absorption of the water may affect the strength and durability of the concrete.
- Physical differences between Recycled Aggregate and natural aggregate results from higher water absorption rate.
- It was found that accelerated curing for recycled coarse aggregates is good method for OPC mix. Also extended studies have to done with various mixes and with various proportions to find out better results.

ACKNOWLEDGEMENT

The authors thankfully acknowledge to **Dr. KATTA VENKATARAMANA,** Dean (Academics) & Professor, **Dr. K N LOKESH**, Professor and Head, Department of Civil Engineering, National Institute of Technology Karnataka, Surathkal for their motivational and infrastructural support to carry out this study.

REFERENCES

1. IS: 383 (1987) "*Specification for Coarse and Fine aggregates from natural sources for concrete*", Bureau Indian Standards, New Delhi.
2. IS: 9013 (1978) "*Methods of making, curing and determining compressive strength of accelerated cured concrete test specimens*", Bureau Indian Standards, New Delhi.
3. Krishna Raju, "*Design of Concrete Mixes*", CBS Publishers.
4. M. Etxeberria, E. Vázquez, A. Marí, M. Barra (2007) "Influence of amount of recycled coarse aggregates and production process on properties of recycled aggregate concrete".
5. Shetty.M.S. (2003), "*Concrete technology - Theory and Practice*." S. Chand & Company Ltd., Ram Nagar, New Delhi.
6. Suman Saha, Rajasekaran, C. and Vinayak Pai, T (2015). Use Of Recycled Coarse Aggregates As An Alternative In Construction Industry – A Review. Proc. 4th International Engineering Symposium (IES 2015), Kumamoto University, Japan. March 4-6. C6-2-1 to C6-2-6.

5th International Engineering Symposium - IES 2016
March 2-4, 2016, Kumamoto University, Japan

Upgradation of Rural Township in India to a Smart City

Syra Habeeb [1] and S. Shrihari [2]

1 *Department of Civil Engineering, National Institute of Technology Karnataka, Surathkal, Mangalore 575025, India. email:syrahabeeb@gmail.com*
2 *Department of Civil Engineering, National Institute of Technology Karnataka, Surathkal, Mangalore 575025, India.*

ABSTRACT: Ordinary cities are dealing with difficulty in waste management, scarcity of resources, air pollution, human health concerns, traffic congestions and many more problems. Solution to most of these problems can be brought out by upgrading normal city in to a smart city. Smart city will give us live status updates on traffic patterns, pollution, waste management, water, power etc. The main application domains in this paper are water supply, housing and solid waste management. Data required for formulating these components of a smart city are jurisdiction map, master plan, GIS data, ward maps, slum locations, JNNURM implementations, STP locations, landfill sites and capacity. With the help of above mentioned datas a smart city model can be developed for these 3 components. Hence this work focus on developing a model incorporating these aspects which will help upgradation of a rural township (Mangalore) in India to a smart city.

Keywords*: Waste Management, Sensors, Water Supply , Mass Housing*

INTRODUCTION

The conceptualisation of Smart City, varies from city to city and country to country, depending on the level of development, willingness to change, resources and aspirations of the city residents. A smart city would have a different connotation in India than, say, Europe. The focus is on sustainable and inclusive development and the idea is to look at compact areas, create a replicable model which will act like a light house to other aspiring cities. A smart city celebrates and promotes its unique identity and culture. It has a robust and resilient economic base and growth strategy that creates large scale employment and increases opportunities for the majority of its citizens.

The core infrastructure elements in a smart city would include:

(i) Adequate water supply
(ii) Assured electricity supply
(iii)Sanitation, including solid waste management
(iv)Efficient urban mobility and public transport
(v)Affordable housing, especially for the poor
(vi)Robust IT connectivity and digitalization in the city.
(vii)Good governance, especially e-governance and citizen participation
(viii)sustainable environment
(ix)Safety and security of citizens, particularly women, children and the elderly, and
(x) Health and education.

In this paper we are discussing about elements like housing, water supply and solid waste management of Mangalore City. Housing is available at most income levels but is highly segregated across income levels. The poor live in informal settlements with limited to no access to basic services. A Smart City has sufficient housing for all income groups and promotes integration among social groups. The city has intermittent water supply and

availability. Water wastage is very high. A smart city has a reliable, 24/7 supply of water that meets national and global health standards. It has advanced water management programs, including smart meters, rain water harvesting, and green infrastructure to manage storm water runoff. Waste collection systems do not pick up waste on a frequent basis and waste often enters in to water bodies. A smart city has a waste management system that removes household and commercial garbage, and disposes of it in an environmentally and economically sound manner.

Accordingly, the purpose of the Smart Cities is to drive economic growth and improve the quality of life of people by enabling local area development and harnessing technology that leads to Smart outcomes. Application of Smart Solutions will enable cities to use technology, information and data to improve infrastructure and services. Comprehensive development in this way will improve quality of life, create employment and enhance incomes for all, especially the poor and the disadvantaged, leading to inclusive Cities.

WATER SUPPLY

Water Supply Status

There are two existing water supply schemes in Mangalore City , one was commissioned in 1956 (11.35MLD) and other was commissioned in 1971 (81.7MLD). Water connections is taken from existing water supply distribution network. The new water supply distribution system will be interlinked with the existing distribution system at various locations to improve water supply in the underserved and un-served areas. The domestic connections amount to 86.26% of total connections and 62.9% of total households. There are around 5000 free public stand posts. Out of total water connection 5.5% is un-metered.

Population covered under piped water supply is 80%. Presesnt water production is 91 MLD, corresponding to which available storage capacity 0f 50.73 is sufficient. Current per capita water consumption is 129 LPCD which is less than the prescribed Norm. As the new water production gets commissioned new service reservoirs are required.

Ongoing projects and service levels

It has been proposed to consider the water demand of Ullal, Mulki and six enroute villages. These towns/villages could buy water from Mangalore City Corporation (MCC) on prorate basis. Total Water Demand is 160MLD. Water available from 1971 scheme is 80MLD. So Balance required for ongoing project is 80MLD. Presently the frequency of water supply varies from ward to ward.

Key Issues

- In the old system, nearly 40% of water loss is due to leakages and unauthorized connections (illegal house connection and unauthorised connection through political pressure), breakage of pipes because of poor road maintenance. The distribution losses are accounting more than designed losses.
- At the consumer end there is no water quality monitoring system. Because of that water quality in many places are very low.
- No initiative for reuse of wastewater.
- Frequent contamination of water affected the public health especially urban poor and overall unsatisfied citizen services.
- Non-availability of spare parts at the time of breakdown of the pumping.
- Disparity in water supply rates and pressure is observed in certain areas due to lack of proper distribution of storage tanks, leakages in pipelines, contour, etc.
- High consumption of power for water supply bears a huge burden on the income and expenditure pattern of MCC.
- Only 63% of the households are connected to the water supply system indicating a sizeable gap between the total number of properties and the number of house service connections.
- Wastage of treated water due to lack of awareness and more number of public stand posts.
- Lack of technical and managerial skills of the ULB.

Strategies

- Improving the per capita supply through sustainable augmentation & management of water supply system.
- Whole water supply system should be brought in to a network where it can be connected and accounted for. Increase the coverage of individual house service connections to 100% and discourage public stand posts.
- 100% metering should be provided. Use smart metering. Devices can be calibrated to monitor water quality parameters.
- Reduction in losses at every level and reducing unaccounted for water, controlling unauthorized connections, losses and thefts by carrying out regular water audit and leak detection studies.
- Proper assessment of requirement and taking timely action to procure the spare parts or other materials solve problems at the time of breakdown of pumping.
- Sustain 24x7 supply with pressure higher than 2m with the help of pressure sensor.
- Water quality with residual chlorine greater than 0.2ppm.
- Better way to reduce leakage is to lay a new distribution network rather than interlinking new water supply distribution system with the existing distribution system.
- Capacity building of the water supply personnel in GIS, MIS, creating and updating utility maps, efficient preventive maintenance, etc.
- Improving the collection efficiency of the ULB and undertaking regular revisions of tariffs and connection charges.
- Adopting energy efficient measures to reduce the power consumption.
- Initiating water shed planning at regional level to protect the catchment areas, replenishing ground water and water conservation.
- Improve ground water table through aquifer recharge and rain water harvesting measures.
- Adopting recycling and reuse of wastewater.

HOUSING

Present housing scenario

Current population in mangalore city is about 575000. The total area of the town is 132.45km², with a gross density of 2843 persons per km². Males constitute 50.2% of the total population and females constitute 49.8%. The sex ratio is 991. Projected population of Mangalore city is shown in Fig.2. In Mangalore city urban agglomeration, which includes the city corporation area, there are 82925 households .As per Census of India, 2001, the share of permanent, semi-permanent and temporary houses in Mangalore city accounts to 75.17%, 24.04% and .75% respectively. Housing shortage is estimated as 33257.

The residential use encompasses an area of 5833.19 hectares (accounts for 19.06% of total LPA) which includes all types of dwelling units, detached units, apartments and residential plots. Majority of the concentration of residential development can be found in the ward nos. 16 & 17, 25 to 34, 38 to 48, 54 to 60 and are located between the Gurupur and Netravati River. Nearly 60% of the houses are in the form of scattered houses and are connected by narrow paths & streets.

Strategies

- Give more focus on green and energy efficient buildings.
- All new buildings should have rainwater harvesting. Green roofing or solar roof panels in each new houses should be made compulsory.
- Use temperature sensor and air quality sensor in buildings. Implement smart lighting system in common areas.
- Use concrete vibration sensors .
- Piezoelectric energy harvesting can be done by employing PZT patch as generator and converting mechanical strains in to electrical energy. Building construction utilizing recycled materials wherever possible
- Waste water is recycled and utilized in toilets, cooling towers and for irrigating the landscape
- Water-efficient fixtures and toilets help in conserving water

•Use of energy saving methods helped in reducing the energy demand by 35 %.

•Storm water management with the help of water retention layer at site, collection of storm water runoff in basement storage tanks.

• Employ mass housing by factory production to meet the demand of 33257 houses. Various ways of mass housing are modular homes, panelised homes, log homes and concrewall.

• Modular homes system comprises of various housing components manufactured in a controlled factory environment and simply assembled at site. Almost 90% of the housing are made in the factory . Besides savings in cost and time excellent quality and finish can be obtained.

• Panelised homes system involve advanced Construction Techniques to develop energy efficient durable houses built in a factory environment. It is recognised in several green building certifications.

• Log home construction earns points as a green building material and are also energy efficient and thermally comfortable.

• Concrewall Construction system is based on modular elements made of shaped polystyrene panels that are contained between two sheets of galvanized welded meshes.

SOLID WASTE MANAGEMENT

Solid Waste Generation, collection and disposal

The three major solid waste streams generated in Mangalore are (a) municipal solid waste, (b) biomedical waste and (c) hazardous industrial waste. The latest entrant is the e-waste in the city. Composition of solid waste is shown in Fig.1. MCC currently produces an average of 220TPD, with a daily collection of 200TPD. The Bio-medical Waste Rules make mandatory for all healthcare facilities, to treat bio-medical waste generated by them. Mangalore is a major industrial centre of Karnataka. It is estimated by KSPCB that around 4058MT of hazardous waste is generated in the Mangalore District. At present, there exists no information regarding the generation of electronic waste in MCC.

In Primary Waste Collection, Door-to-Door collection is practiced in about 30 areas, each of them collect the waste from 150 to 300 houses. In Secondary Collection, the waste from primary collection is transferred to 58 metal containers (with a capacity of 4.5m³ each). Manual handling of waste is avoided. Every day the waste is collected and disposed to processing site which is 9 km from the city. The waste is transported using twin container dumper placers, Compactors (Back Loaders) and Side Loaders.

MCC disposal site spread over an extent of 15.1Ha is located on top of a hill. Presently MCC is handling the operation and maintenance of aerobic compost plant which is generating 4 to 5 tons of compost through windrow method of aerobic composting. Areal view of processing and disposal site is shown in fig.3. In Mangalore, one SWM worker is available for a population of 383 persons. This is above the prescribed norms.

Key Issues

•Lack of awareness among the community.

•Waste is disposed in an unscientific manner, with crude open dumping being the prevalent in many areas.

•Foul smell, breeding of flies & other pests and generation of liquid runoffs (Leachate), which pose a serious threat to the underground water reserves.

• Sometimes due to conflict between government and agency, agency refuse to collect waste. Because of this garbage keeps lying in cities for extended periods.

• Staff lacks proper training on solid waste handling to advocate and collect the solid waste.

• Lack of resident's interest and support especially in the segregation of waste.

• Only 40 per cent of MSW is collected though door-to-door solid waste collection system in the city.

• The waste collection facilities, waste cleaning equipments, waste storage bins and waste transportation vehicles are not adequate. Such inadequacy is further accentuated by poor primary collection and waste disposal practices by citizens.

•Leachate generated from the dumping site contaminates the ground water in the area. There is no control over

encroachment and entry of rag pickers at the disposal site.

- Bio-medical waste from smaller hospitals find their way into MSW.
- There is no industrial/ hazardous waste management facility in the region.
- The waste collection, loading and unloading operations have been done manually. The sanitary workers are not provided with any protective equipment posing health hazards.
- There is indiscriminate burning of waste, illegal disposal of waste and solid waste dumping into the sea; which will cause serious public health and environment issues.

Strategies

- It is proposed to recycle waste up to maximum extent.
- The system of segregation at source and storage be encouraged through public participation, community education and awareness campaigns.
- It is always advised to have completely automated solid waste management system so that we can completely reduce the chances of govt. being blackmailed by waste collection agency and can see that proper waste management is done.
- Install tracking devices on each vehicle
- Geo-fencing of area and marking of important points and routes.
- Bin monitoring with RFID tags.
- CCTV cameras at dumping sites.
- It is recommended to introduce Auto tippers and reduce number of secondary collection points and multiple handling.
- It is also recommended to maintain information on vehicle movement, through a vehicle register at the dump site.
- Non-recyclable waste can be collected via a Pneumatic Waste Collection System and can be incinerated to generate electricity.
- Biodegradables can be composted and the by-product i.e biogas shall be utilized for lighting of common areas and manure for community parks.
- Remains and by–products of green organic waste could be fed to cheap, unproductive cattle. Cow-dung thus obtained serves as a fertilizer equivalent to 'black gold' when stored under perfect bacterial growth enhancing conditions.
- Fish remains are a feed for ducks and are said to increase their fertility by a factor of 1.5. This prevents fish waste from getting dumped in to landfills.
- Replace plastic for coal and pitch for road making purposes. Roads thus made are durable and inexpensive.
- Frequent levelling of garbage mountain , plantation and beautification can transform landfill sites into recreational parks , as has already been done in Israel.
- Combustible fraction can be taken to waste to energy facility.
- Authorized vendors shall be responsible for handling, collection and treatment of Bio- medical wastes at an appropriate site using modern technology.
- Set up a centralized hazardous waste processing plant.
- Construction Waste for Embankment and filling-up of Low lying areas.
- E-waste mostly consisting of computers, monitors, scanners, other electronic equipment, gadgets need to have a centralized processing plant.
- Industries that look into reprocessing of lead acid batteries and reprocessing discarded containers should be used effectively.
- Communities should be metering their trash just like they meter their other utilities.

DISCUSSION

Fully automated smart city in a developed country is different from still developing country like India. In India where we have so much operations available and people can do the job of automated machine, people will be satisfied by providing them jobs rather than employing a machine. But then full objective can fail because of this. So these things are taken in to consideration when we think of smart city solutions. In our country we used to have conflicts between agency and government. Because of that waste collection didn't happen for extended periods. In smart city human resources will be less and functions should be automated where there should not be any possibility for any such things to happen. We would like to present the problem with mass construction through siting an example. In Bombay they implemented mass construction while

replacing slum dwellers. They occupied it for few days , then later when they found that it fetches very good rent , they rented that houses and went back to slums. So slums where not cleared and apartments did not serve its purpose. For housings we can always insist that solar roof panels, smart lighting system, installation of sensors etc should be done. If we want to implement these in our houses cost of electricity is much cheaper than sensors and panels. Only when all these becomes cost even we can implement it compulsorily. Then everything will become smart enough. So smartness of our city should be of slighter smaller level when compared to that of fully developed countries.

CONCLUSIONS

Following conclusions are deduced from the study:

- Mangalore will have a systematically planned housing system which is safe, efficient and sustainable with improved liveability.
- Sufficient housing for all income groups can be obtained by mass housing.
- By following suggested strategies we will be able to build up green housings.
- 24/7 supply of water that meets national and global health standards can be obtained .
- A smart waste management is proposed.
- Due to the practical difficulties of completely automated system , the smartness of our smart cities will be slightly less than that of smart cities in developed countries.

REFERENCES

[1] ASCI, Hyderabad (2012), "Use of effective Urban Governance and service delivery in India: A selection of cases".
[2] Begg (1999), "Cities and Competitiveness" in Urban Studies, Vol. 36, Nos 5-6, S. 795-810.
[3] Chong, Chee-Yee. "Sensor Networks: Evolution, Opportunities, and Challenges." Proceedings of the EEE, 91.8. August 2003.
[4] CPHEEO-1999,Manual on water supply and treatment, published by ministry of urban development.
[5] CPHEEO-2005,Manual on operation and maintenance of water supply systems, published by ministry of urban development.
[6] Goldstein (1974), Basic data needed for the study of urbanization, IUSSP Committee on Urbanization and Population Redistribution.
[7] Kirby, Terry (2013). "City design: Transforming tomorrow." The Guardian. N.d. Web.
[8] Larson, Kent (2012). "Brilliant designs to fit more people every city." TEDxBoston, Boston, MA.
[9] Lombardi, P., Giordano, S., Farouh, H., Yousef, W. (2012) "Modelling the smart city performance", nnovation – The European Journal of Social Science Research, vol. 25, no. 2, June 2012, pp. 137-149.
[10] MCC(2015) , CDP for Mangalore draft final report, published by Mangalore City Corporation.
[11] MoEF (2006), manual on building construction, published by government of India.
[12] OECD (1997), "Better Understanding our Cities", The Role of Urban Indicators.
[13] Szczech-Pietkiewicz (2013), "Poland's urban competitiveness in the European context", The Polish Review, University of Illinois Press, vol. 58 no. 2, pp. 15-36.
[14] Taylor (1999), 'So-called 'world cities'; the evidential structure within a literature', Environment and Planning, Vol. 31, pp. 1901 – 1904.
[15] Taylor, P.J., Ni, P., Deruder, B., Hoyer, M., Huang, J., Witlox, F(2011) Global Urban Analysis. A Survey of Cities in Globalization, London, Washington D.C.: Earthscan.
[16] Thornley A(2000), Strategic Planning in the Face of Urban Competition, The Revival of Strategic Spatial Planning. Proceedings of colloquim. Royal Netherlands Academy of Arts and Sciences, Amsterdam.

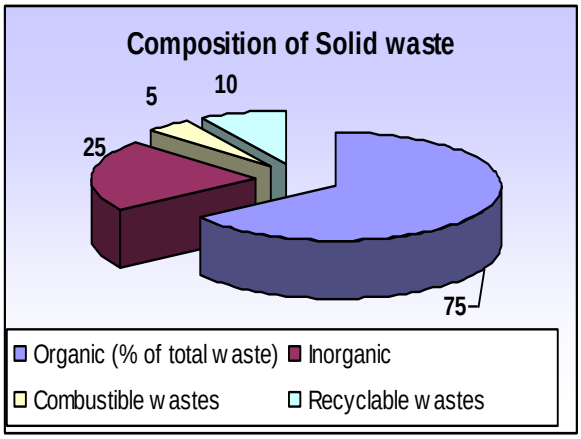

Fig.1. Composition of Solid Waste

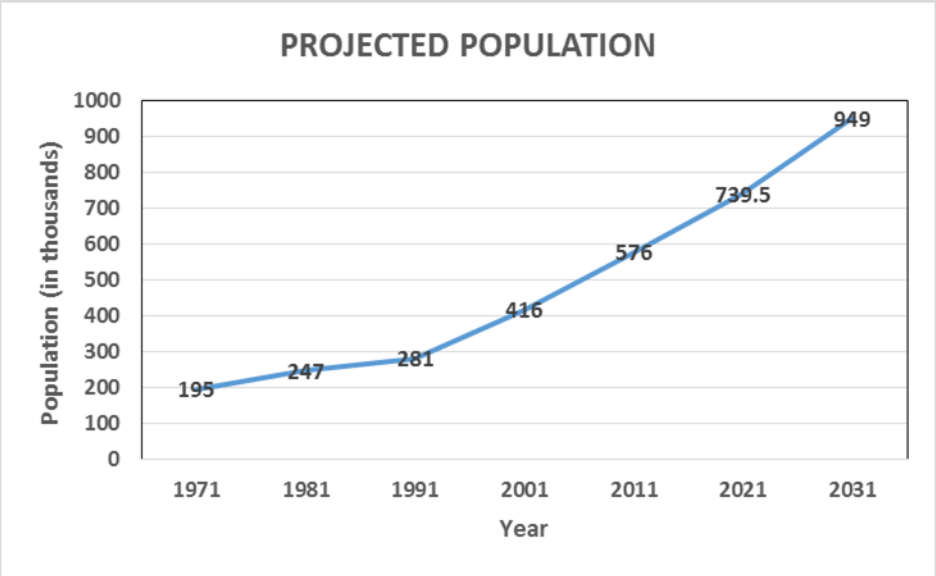

Fig.2. projected Population

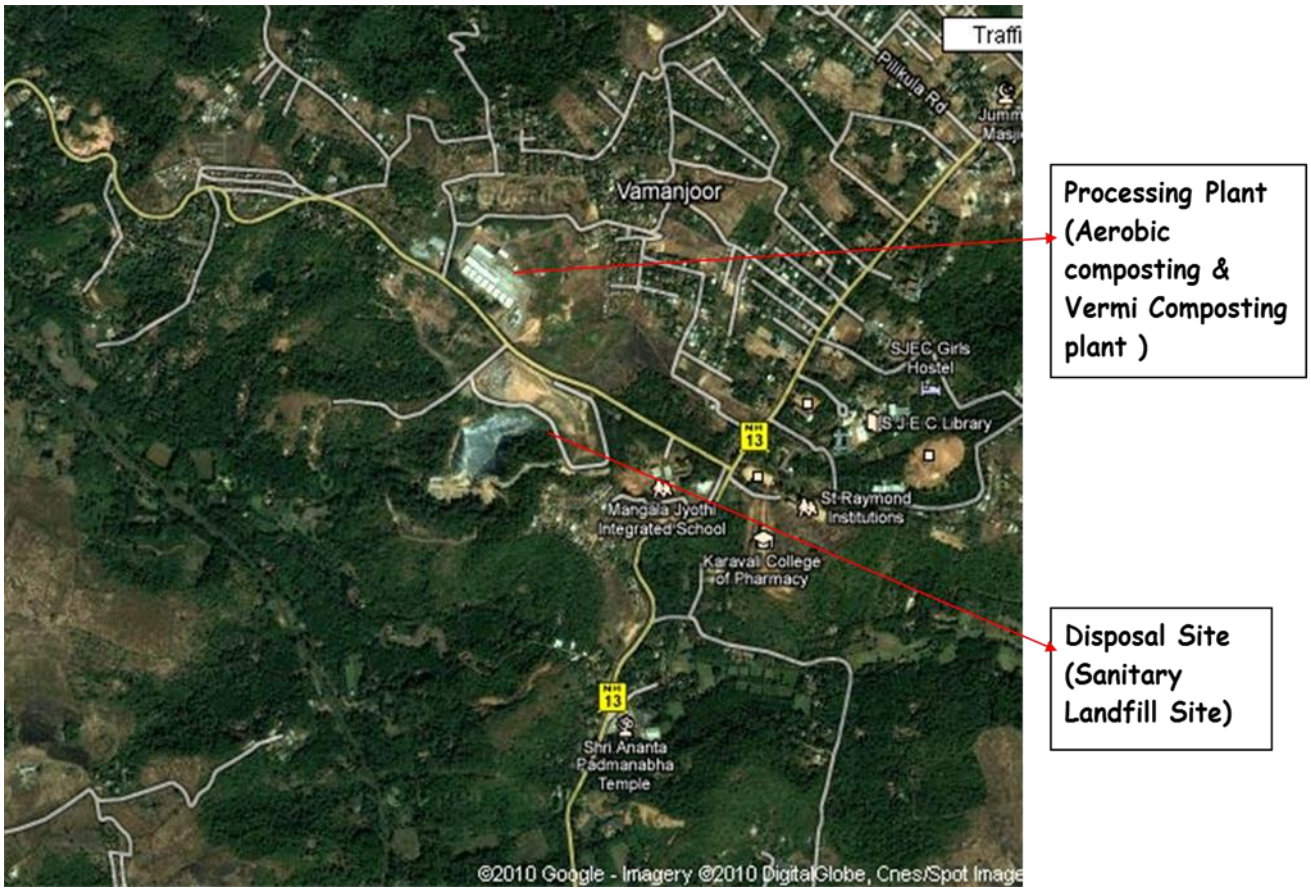

Fig.3.Areal view of processing and disposal site

5th International Engineering Symposium - IES 2016
March 2-4, 2016, Kumamoto University, Japan

LATERAL DISTRIBUTION OF VEHICLES ON URBAN UNDIVIDED ROADS IN NON-LANE BASED MIXED TRAFFIC CONDITIONS

Pooja Raj [1], Punith B. Kotagi [2] and **Gowri Asaithambi [3]**

1 *Post Graduate Student, Department of Civil Engineering, National Institute of Technology Karnataka, Surathkal, Mangalore, India. Email:poojarajhere@gmail.com*
2 *Research Scholar, Department of Civil Engineering, National Institute of Technology Karnataka, Surathkal, Mangalore, India. Email: punithk@nitk.edu.in*
3 *Assistant Professor, Department of Civil Engineering, National Institute of Technology Karnataka, Surathkal, Mangalore, India. Email: gowri_iitm@yahoo.co.in*

ABSTRACT: Vehicle placement being an important logic in simulation, it is required to assign the position of vehicle within a lane. In this study, an attempt is made to analyze the lateral distribution of vehicles on urban undivided roads in non-lane based mixed traffic conditions. For this purpose, traffic data collected on an urban undivided mid-block section using video-graphic technique was analyzed to investigate the lateral position of vehicles based on their types. Also, a relationship between lateral positions and speeds for different types of vehicles were studied. The analysis shows that majority of the cars and heavy vehicles (HV) are distributed near the middle of the road whereas two-wheelers and auto-rickshaws (three-wheelers) occupy almost the entire width of the road. Graphs plotted between speeds and lateral positions show that all vehicle types followed a second degree polynomial relation.

***Keywords**: Lateral Distribution, Undivided Roads, Non-lane Discipline, Mixed Traffic*

INTRODUCTION

Simulation models play a significant role to evaluate complex traffic situations that cannot be assessed with the help of analytical methods. In this model, it is required to assign the position of vehicles within a lane. To study the distribution of vehicles across the pavement width, it is necessary to analyze the characteristics of lateral placement of vehicles. Lateral placement of a vehicle is defined as the closest lateral position of the vehicle from the edge of the pavement when the vehicle is in motion. In India, traffic is highly mixed in nature with widely varying static and dynamic characteristics of vehicles. Also, due to weak lane discipline, vehicles occupy the entire road space without any confinements for manoeuvring. Moreover, majority of urban roads in India are undivided where the traffic flow in a particular direction is influenced by the prevailing traffic on the opposing lane. This often leads to complex vehicular interactions with road users, which makes it difficult to model traffic flow under mixed traffic conditions. Hence, this work mainly focuses on the study of lateral distribution of vehicles on urban undivided roads under mixed traffic conditions. This study investigates whether there is any significant difference in the lateral position of vehicles based on vehicle types and also examines the relationship between the lateral position and speed of different types of vehicles.

LITERATURE REVIEW

(a)Homogeneous Traffic Conditions:

Woods (1972) determined the effect on lateral placement of vehicles due to restrictions imposed by bridge abutments on rural two-way, two-lane highways. The results showed that by increasing the

amount of offset between the traffic lane edge and the bridge abutment and by reflectorizing the bridge abutments, drivers positioned their vehicle more correctly within their lane. Summala and Merisalo (1978) reported that with the decrease in speed there is a greater shift towards the right (left in Indian traffic conditions), particularly during night driving. Armour (1985) studied the effect of road cross section on vehicle lateral placement. He identified that the main factors influencing lateral placement are shoulder type and lane width. Lennie and Bunker (2005) compared the behavioural characteristics of passenger car drivers surrounding multi-combination vehicles using lateral position characteristics. It showed that passenger car behaviour changes around heavy vehicles when compared to passenger cars. Bunker and Parajuli (2006) investigated the influence of heavy vehicles on lateral movement characteristics due to oncoming vehicles. It was shown that the lateral positions of cars, utility vehicles and semi-trailers are statistically different when opposed than when unopposed, while the lateral positions of B-doubles were not.

(b)Mixed Traffic Conditions:

Dey et al. (2006) studied the lateral position of vehicles under mixed traffic conditions. They found that the placement of vehicles may follow a unimodal or a bimodal curve depending upon the percentage of slow and fast moving vehicles. They introduced two parameters such as Placement Factor (PF) and Skewness Range (SR) to describe the placement of vehicles and they concluded that the placement data follow a unimodal curve if PF and SR are less than 1.30 and 0.54 respectively**.** Balaji et al. (2013) studied the relation of placement and speed of different vehicles on two lane state highways. The analysis showed that three-wheelers, heavy vehicles and slow moving vehicles follow a linear relation, while two-wheelers and cars follow a second degree polynomial relation. The vehicles as a whole followed a second degree polynomial relation. Mahapatra and Maurya (2015) analysed the impact of different lane positions on average travel speed, time headway and lateral clearances for 4 lane, 6 lane and 8 lane divided highways. They concluded that there exists a wide variation in the lane specific vehicular speed, traffic composition, time headway and lateral gap in mixed traffic condition of Indian highways.

Based on the review, it was found that there were only limited studies on lateral placement of vehicles on urban undivided roads in mixed traffic and hence, this study aims to analyse the lateral distribution of vehicles in non-lane based mixed traffic conditions.

DATA COLLECTION AND EXTRACTION

The data for this study was collected using video-graphic technique during morning peak hours on a midblock section of a 12m wide two-way urban undivided road located in Bangalore city, India. A road section of 30 m length which is free from the effect of intersection, bus-stops, parked vehicles and pedestrians was chosen for this study. The carriageway width was divided into segments of 50 cm each for determining lateral position of vehicles. The on-going traffic (left-hand drive rule in India) at the section comprises about 3541 motorized vehicles, where two-wheelers accounted for the largest share of 63.7% and heavy vehicles with the least share of 1.9%. The traffic composition of the study section is shown in Fig.1. The videos recorded were then processed in image processing software, Irfanview to extract the required data. This software helps to obtain the (x, y) coordinates of all the points in terms of pixels on the image. Gridlines were drawn in AUTOCAD with obtained (x, y) image coordinates and was overlaid on video by using Ulead Video Studio 10.0 editor. Fig.2 shows the snapshot of the video image with overlaid gridlines showing the study stretch. Correction factors (screen to ground) were worked out by knowing distances on the ground and corresponding coordinates on the screen. These correction factors reduce the parallax effect due to camera height and angle change. When the vehicle touches the reference line on the middle of the road section, the closest lateral position of the vehicle from the edge of the pavement

was noted down and also, the time taken to travel the trap length was recorded.

ANALYSIS AND RESULTS

Speeds of different types of vehicles were calculated from the time taken for the vehicle to cross the known section of the road. Lateral positions of the vehicles were also calculated from the image coordinates using correction factors. Frequency distribution for lateral position of vehicles is shown in Fig.3. It was found that majority of the vehicles (62.9%) are preferred to travel in the middle of the road (4-7 m). Two-wheelers and auto-rickshaws occupy almost the entire width of the road as they have a tendency to occupy every lateral gap available on the road due to their smaller sizes and higher manoeuverability. Most of the cars (70.9%) prefer to travel near the middle of the road compared to two-wheelers (56.3%) and auto-rickshaws (66.9%) so as to maintain higher speeds. All the heavy vehicles (HV) are concentrated near the middle of the road (4-8 m) so as to avoid side interferences from other vehicles.

Descriptive statistics of lateral position and speed of each type of vehicles were shown in Table 1. The mean speed of two-wheelers is higher (13.1 m/s) because of their smaller sizes and higher manoeuverability whereas heavy vehicles (HV) travel at a lower mean speed (9.0 m/s) due to their larger size and lower manoeuverability. It was also found that the mean lateral position of all types of vehicles is in the range of 5-6 m from the edge of the pavement which indicates that most of the vehicles prefer to travel in the middle of the road. The one way ANOVA test indicates that the lateral positions of vehicle types are significantly different ($F_{observed}$= 8.35, $F_{critical}$=2.61) from each other at 5% level of significance.

Graphs were plotted between the lateral position (m) and speed (m/s) of different types of vehicles (Fig.4). Regression analysis was done and its goodness was checked by the value of coefficient of correlation. For the development of model, 75% of the total data was considered and the remaining 25% was used for validation. The graphs show that all the four types of vehicles followed a second degree polynomial relation. Most of the two-wheelers have higher speeds near the middle of the road because of their tendency for overtaking and also, they are not much influenced by the opposing vehicles, due to their higher manoeuverability. The speeds of auto-rickshaws and cars are not varying much up to the middle of the road and then start decreasing when they move in the opposing lane due to the influence of opposite vehicles. As the motion of heavy vehicles is not disturbed by the presence of other vehicles and also due to their lower manoeuverability, they travel at lower speeds. The predicted speed values from the model were compared with the speed values observed from the field for different lateral positions. Mean Absolute Percentage Error (MAPE) was calculated for each lateral position and they were found to be less than 15% for all the vehicle types, which conform the limits (15%) as proposed by Mathew and Radhakrishnan (2010) and Gowri and Sivanandan(2015). This indicates that the model replicates the field conditions reasonably.

CONCLUSIONS

The following conclusions were obtained from this study:

- It was observed that lateral positions of vehicles are different for different types of vehicles.
- Since lane discipline is not strictly enforced, it is found that two-wheelers and auto-rickshaws are distributed almost over the entire width of the road because of their smaller sizes and higher manoeuverability.
- Cars are mostly distributed near the middle of the road so as to maintain higher speeds. Heavy vehicles are also concentrated near the middle of the road so as to avoid side interferences and also due to their larger sizes and lower manoeuverability.
- The variations in speeds of auto-rickshaws and cars are relatively less up to the middle of the road but it is significant when they move

further towards the opposing lane due to the presence of opposing vehicles.

- Speeds of two-wheelers increases when they travel towards the middle of the road for the purpose of overtaking whereas heavy vehicles travel at relatively lower speeds as their motion is not disturbed by the presence of other vehicles and due to lower manoeuverability.

REFERENCES

[1] Armour, M (1985), Effect of Road Cross-Section on Vehicle Lateral Placement, Australian Road Research Board, Vol.15, No.1, pp. 30-40.
[2] Balaji, K et al. (2013), A Study on Lateral Placement and Speed of Vehicles on Two-Lane Roads, Indian Highways, Indian Roads Congress, Vol.41, No.9, pp. 49-53.
[3] Bunker, J M and Parajuli, A (2006), Examining Lateral Positions of Cars and Heavy Vehicles on a Two Lane Two Way Motorway, Transport Engineering in Australia, Vol.10, No.2, pp. 129-139.
[4] Dey, P P et al. (2006), Lateral Distribution of Mixed Traffic on Two-Lane Roads, Journal of Transportation Engineering, ASCE, Vol.132, No.7, pp.597-600.
[5] Gowri, A and Sivanandan, R (2015), Evaluation of Right-Turn Lanes at Signalized Intersection in Non-Lane-Based Heterogeneous Traffic using Microscopic Simulation Model, Transportation Letters: the International Journal of Transportation Research, Vol.7, No.2, pp. 61-72.
[6] Lennie, S C and Bunker, J M (2005), Using Lateral Position Information as a Measure of Driver Behaviour around MCVs, Road & Transport Research, Vol.14, No.3, pp. 62-77.
[7] Mahapatra, G and Maurya, A K (2015), Study on Lateral Placement and Speed of Vehicles under Mixed Traffic Condition, Proceedings of the Eastern Asia Society for Transportation Studies, Vol.10.
[8] Mathew, T V and Radhakrishnan, P (2010), Calibration of Microsimulation Models for Non-Lane Based Heterogeneous Traffic at Signalized Intersections, Journal of Urban Planning and Development, ASCE, Vol.136, No. 1, pp. 59–66.
[9] Summala, H and Merisalo, A (1978), Measuring the Lateral Position of Vehicles on the Road-System and Preliminary Results, Traffic Engineering and Control, Vol.19, No.7, pp. 328-330.
[10] Woods, W C (1972), A Study on the Lateral Placement of Automobiles due to Restrictions on Two-Lane Rural Highways, Masters Thesis, Paper 5060.

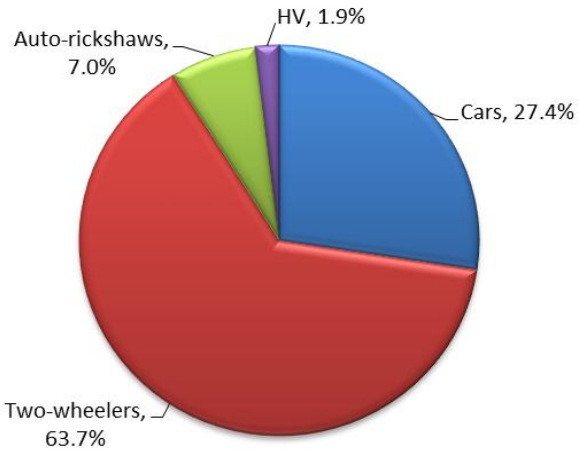

Fig.1 Traffic composition at the study section

Fig.2 Gridlines overlaid on the video image

Table 1 Descriptive statistics of lateral position and speed of vehicles

Vehicle Type	Lateral Position (m)				Speed (m/s)				Sample size
	Mean	SD	Min	Max	Mean	SD	Min	Max	
Two-wheelers	5.4	1.9	1.3	11.5	13.1	1.2	9.8	16.0	486
Auto-rickshaws	5.3	1.5	1.3	9.6	10.7	0.6	8.5	11.7	106
Cars	5.9	1.7	1.3	11.8	12.9	1.1	9.0	15.3	275
Heavy vehicles	5.8	0.9	4.2	7.1	9.0	0.7	8.1	10.4	19

*SD = Standard Deviation

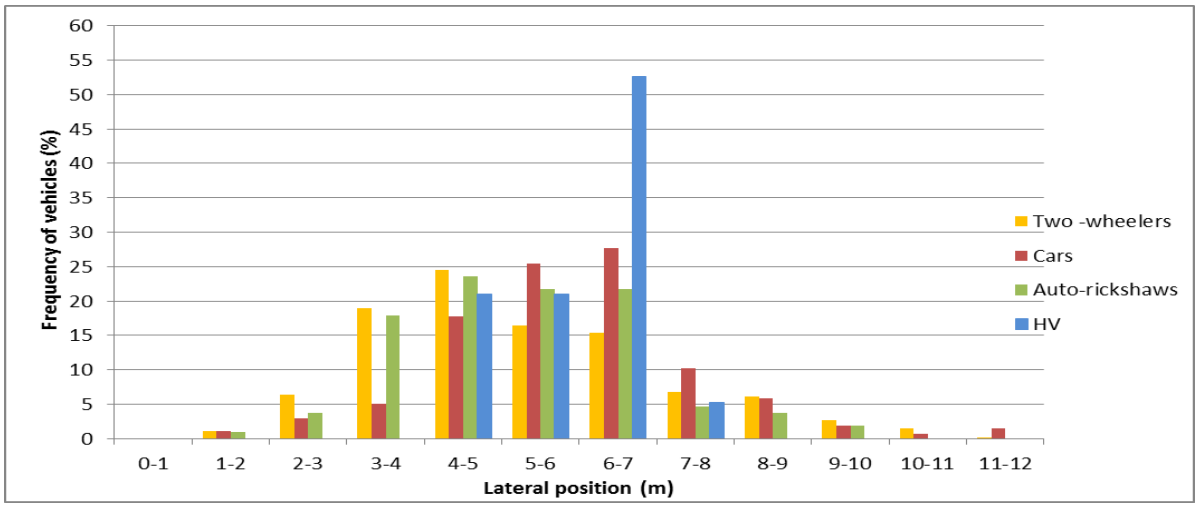

Fig.3 Frequency distribution for lateral position of different types of vehicles

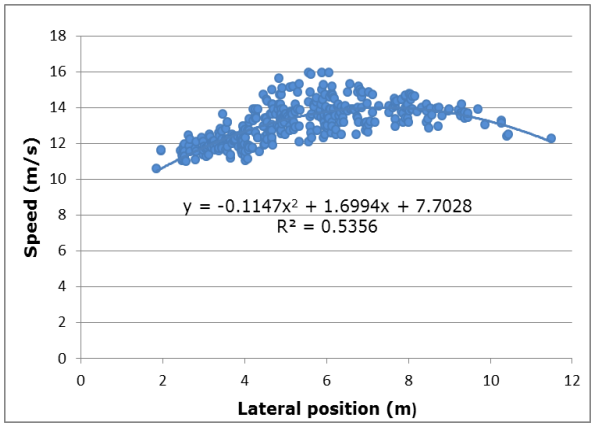

(a) Two-wheelers

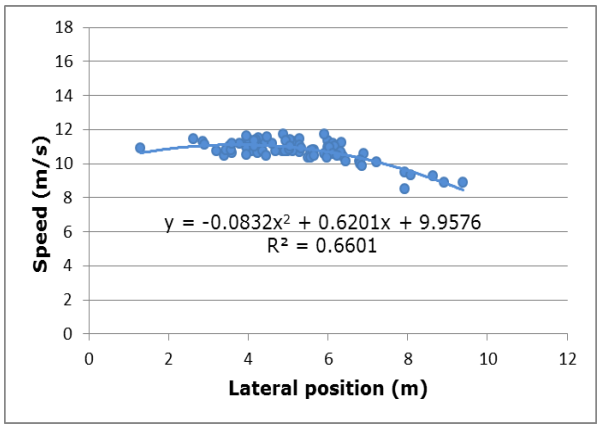

(b) Auto-rickshaws

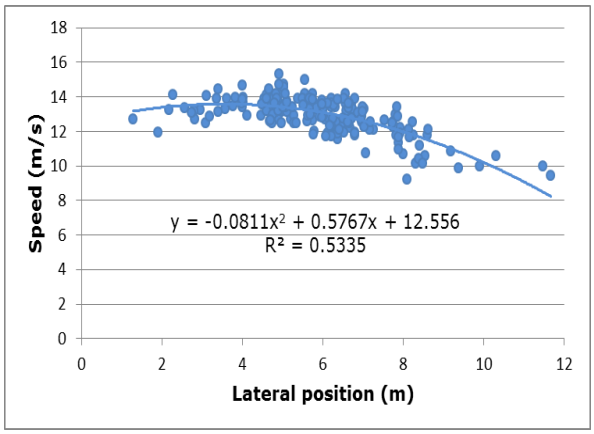

(c) Cars

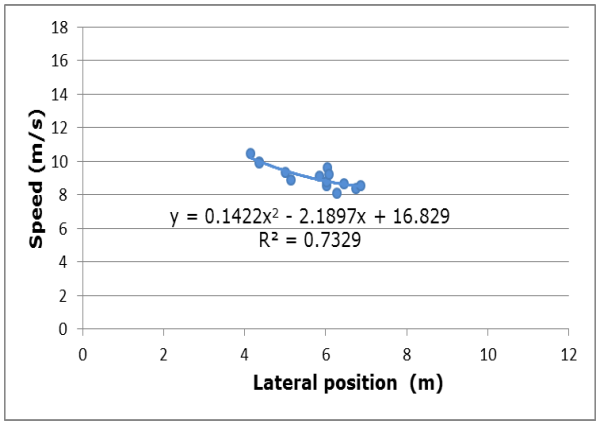

(d) Heavy vehicles

Fig.4 Relationship between speed and lateral position of vehicles

5th International Engineering Symposium - IES 2016
March 2-4, 2016, Kumamoto University, Japan

Emergency Vehicle Allocation- 108 Ambulances

Kunal Pathak

Department of Civil Engineering, National Institute of Technology, Tiruchirappalli-620015, India.email:kunalpathak125@gmail.com

ABSTRACT: The importance of emergency vehicles is widely known and also the fact that their role in the modern society is undoubted. Fire trucks or police vehicles, these are easily spotted and very efficient machines in situations demanding quick response. This paper will focus on the 108 Ambulance that works in Tamil Nadu and their performance over a period of one year. Their positional data, times were studied and maps were plotted. The need for their static positioning is an area of concern for the authorities as they really want to assess their performance and improve. The main objective of Emergency Medical Services (EMS) is to save lives but the potential of such systems to reduce mortality is related to paramedics training and to the time needed by a paramedic team to arrive on scene. In a real-time context, EMS managers are faced with two main problems: allocation problem and redeployment problem.
***Keywords**: Static Positioning, allocation, redeployment*

1. INTRODUCTION

The broad objective of the project was to analyse the number and location of the ambulances. The ambulances of three districts Chennai, Kancheepuram and Thiruvallur were studied forthe same. We were looking at the best way to place the ambulances to serve the calls better(static positioning). However, the call records vary according to the location and position and a dynamic re-allocation policy is needed to reach out to more callers.

Static positioning refers to deciding on home bases for ambulances where the number and location of bases are given and response times to calls are kept as small as possible.

Dynamic redeployment concerns the real-time relocation of idle ambulances so as to ensure better preparedness. The demand for ambulances fluctuate throughout the week, depending on the day of the week, and even the time of day, therefore EMS operators can improves system performance by dynamic relocation/redeployment of ambulances in response to fluctuating demand patterns. The objective of the model is to determine the minimum number of ambulances and their locations.

2. LITERATURE REVIEW

The topic of Emergency Vehicle Allocation has captured the imagination of traffic engineers, computer engineers and Operations Research experts. Their collaboration has led to several publications in this field to develop the best possible algorithm. Over the years many models have been developed. The earliest approach to this was in 1981, developed by Daskin and Stern (1981), who used a hierarchical model and assigned weights to certain zones. Another approach developed was by Bianchi and Church (1988), who developed Facility Location and Equipment Emplacement Technique (FLEET) model for determining the coverage area. They drew trade-off curves and used linear and integer programming to solve the problem of Maximal Expected Coverage Location Problem (MEXCLP). Over the 1990s Leclerc et al (1997)developed a genetic algorithm to the vehicle dispatching problem using a weighting scheme for the attributes that best reproduce the expert's decision process. Geographic Information System (GIS) was used by Peters and Hall

(1999)to assess the response of the ambulance and their performance.

However, the dynamic re-positioning problem was effectively tackled with the advent of heuristic techniques. Heuristic is any approach to problem-solving, learning, discovery using practical methods not guaranteed to be optimal but sufficient for practical purposes. Bianchi and Church (1990) used heuristic approach to their previously developed FLEET model. Restrepo (2008)used the Erlang Loss Formula and queueing theory for the static allocation of the ambulances. He resorted to Dynamic Programming technique for the dynamic allocation of ambulances.

Another recent approach is the "tabu search heuristic" method. In this technique, the programme is run even if the solution becomes non-optimal in the intermediate stages. It has been developed along the lines of Hill Climbing method and Traveling Salesman Concept. Gendreau et al (2001)have worked on this line to develop the best algorithm for dynamic allocation of the ambulances. Simulations confirm to the real-time data. The algorithm consists of a sequence of adjacent solution obtained by repeated removal and insertion of routes. Rajagopalana and others (2008)have used a Jarvis hypercube algorithm along with Tabu Search heuristic model for easing the computational burden.

This paper will keep the approach used by Marla (2012) as the background. She has proposed a Greedy algorithm which uses the maximum possible value as the basis for computation. The paper describes methods for both static and dynamic allocation of the ambulances. The simulation is data driven, input is taken from the data coming in and a count loop is channelized. This count manages the number of free ambulances and the request log which in turn enables the dispatch policy to function. The Greedy algorithm is used for the dynamic redeployment of a penalty function. The penalty function is nothing but a subset of the request function. The maximal optimal gain relative to the current solution is the working principle behind the Greedy algorithm.

3. OBJECTIVES

- Generate visualizations of GPS traces from ambulances.
- Check the extent of the data that is available (consistency).
- Explore the call records data (CRD).
- Develop distribution model for call origination.

4. METHODOLOGY

4.1.SIMULATOR

The simulator developed by Marla(2012) takes the following inputs

1. A request log A= $\{r_1+r_2+..r_N\}$.
2. An allocation W of ambulances to bases.
3. A redeployment policy$\mathrm{P}$ (W,Â) that takes as input the current allocation of free ambulances W and currently active requests Â.

Four major things happen in the processing of request arrival data:-

- Request r_n is processed and added to the active requests (y_r).
- Assigned ambulance is removed from the set of free ambulances (W).
- A job is added to event queue.
- Redeployment policy π is considered.

Input=(R,W,π,t_d) //For taking in input

Â←Â + y_r //Addition of requests

W ← W- y_r //Free Ambulance counter

The reverse happens in case of job completion

Â ← Â– y_r //Removal of requests

W ← W+ y_r //Free Ambulance counter

4.2.DATA-SETS

There were two major data-sets available: Ambulance GPS Data and the Call Records Data (CRD) courtesy: the Tamil Nadu Health Systems Projects (TNHSP).

The ambulance data consisted of the GPS locations of the ambulances in three districts: Chennai, Kancheepuram and Thiruvallurfor 27, 36 and 30 ambulances respectively for a yearlong period from April 2014 to March 2015. The GPS data had the latitudes, longitudes along with a date and time stamp. The aim was to check for the consistency of the data. This was done by subtracting the hour readings of the consecutive data points and plotting them. The values closer to zero show that the data received was continuous and consistent as shown in Plot 1. The data

was then sorted using the RStudio Software according to the registration number of the vehicles. The work on the visualization part of the project was done by plotting and tracing the path of an ambulance for a particular day. For developing an algorithm a certain number of ambulances were picked at random and their behavior, pattern and movement were studied. Plot 2 which was made using RStudio shows us the trace of an ambulance on a particular day. 'H' represents the hospitals and we notice that the concentration of points near the hospitals is high suggesting that the data is accurate. Similar plots were made by using GoogleMaps package in RStudio as shown in Plot 3. Different color coding for different hours was used to trace the path of the ambulance.The consistency of the data was checked by relating the two data-sets. The concentration of the points and the time of arrival at the spot from CRD was used to locate the victim as shown in Plot 4.

The CRD provided parameters like availed cases, un-availed cases, odometer readings, call type, emergency type etc. This was used in Plot 6 to show the number of cases where the ambulance was availed, un-availed, busy and En-route Service Not Required (SNR). Apart from this, using the odometer readings a plot between the number of incidents and the distance to reach the victim and distance to reach the hospital was made. A lower value of peak suggests that the ambulances are sufficient as they had to travel lesser distance as shown in Plot 5. Qualitative analysis like these from CRD gave us the idea whether new ambulances are needed or not.

4.3.ALGORITHM

The major points considered in the algorithm are:

1. Count the number of GPS points.
2. Start a loop for checking each time stamp.
3. Start an interior loop to set the time difference.
4. Store the values of time and GPS.

The GPS value of a particular ambulance was exported from RStudio Software in the form of .txt or .csv file. The subset is found for a particular working day of the ambulance. From this the number of GPS values available for the particular day was counted and saved in N.

4.4. SAMPLE PROGRAM

```
int i,j,k=0;
for(i=0;i<N;i++)
{
for(j=0;j<N;j++)
{
If(Tj-Ti<5 minutes && Ti=Spot Arrival Time)
{
Tk=Ti;
Latk=Latitudei;
Longk=Longitudek;
k++;}}}
```

This program provides a cluster of points for call origin. We can obtain the various clusters for hospitals, base stations and even signal stops by suitably changing the "if" condition. By studying 11 ambulances picked at random from the data-set it was seen that on an average each ambulance took 5 minutes to accurately locate the victim. The "and" criteria in the "if" condition eliminates the case when the ambulance was stuck up in a congestion or stationary. A more vigorous search of the data might lead to a finer value and better results, but for initial purposes, the accuracy level was considered as acceptable.

5. CONCLUSIONS

The major objective of the paper was to analyze the number and location of ambulances and the best way of positioning them to serve calls better. The need for new ambulances, their positioning and base stations was studied.

Preliminary plots of the data gave us a trace of the ambulance path which was used to pin-point the location of the victim. Manual plots were used to develop the algorithm and sample program.

A few points gave us erroneous values because of typing error in the entry of the data.

With an algorithm in place the simulation can now be suitably applied to our data-set and both dynamic and static allocation of the ambulances can be done.

5.1.FUTURE SCOPE

A lot of opportunity is available to increase the scope of this project. For example, the

distance between two points can be studied from the GPS data using the Haversine formula

$$hav\left(\frac{d}{R}\right) = hav(\phi 2 - \phi 1) + \cos(\phi 1)\cos(\phi 2)hav(\lambda 2 - \lambda 1)$$

where,
d is the distance between two points(along the greater circle);
R is the radius of the sphere;
$\phi 1,2$ is latitude of point 1 and latitude of point 2respectively;
$\lambda 1,2$ is longitude of point 1 and longitude of point 2 respectively;
and $haversine(\theta) = \frac{1-\cos\theta}{2}$.
With the time stamp available for each point, speed variation of the ambulances can be studied. The Call Records Data offers us a lot of parameters to study and choose from. The cases are divided as Emergency Type, Social Status, Economic Status, Gender, Age, and Region which can be studied to give us an idea of the ambulance response.

6. ACKNOWLEDGEMENTS

I am deeply indebted to Dr. Gitakrishnan Ramadurai of IIT Madras for guiding and mentoring me throughout this project. The author would like to thank Tamil Nadu Health Systems Project (TNHSP) for involving IIT Madras with this project along with Dr. Lavanya Marla from UIUC, IL for sharing her valuable experience in the field. Finally the author thanks Dr.Shuichi Torii and Dr. Katta Venkataramana for providing us with the unique opportunity to be a part of this symposium.

7. REFERENCES

[1] F. Leclerc, J.-Y. Potvin, and J.-Y. Potvin, "Genetic algorithms for vehicle dispatching," International Transactions in Operational Research, vol. 4, no. 5-6, pp. 391-400, 1997
[2] G. Bianchi and R. L. Church, "A heuristic for a hybrid fleet model," Computers & operations research, vol. 17, no. 5, pp. 481-494, 1990
[3] G. Bianchi and R. L. Church, "A hybrid fleet model for emergency medical service system design," Social Science & Medicine, vol. 26, no. 1, pp. 163-171, 1988
[4] H. K. Rajagopalan, C. Saydam, and J. Xiao, "A multiperiod set covering location model for dynamic redeployment of ambulances," Computers & Operations Research, vol. 35, no. 3, pp. 814-826, 2008
[5] J.-F. Cordeau, G. Laporte, A. Mercier, et al., "A unified tabu search heuristic for vehicle routing problems with time windows," Journal of the Operational research society, vol. 52, no. 8, pp. 928-936, 2001
[6] J. Peters, "An evaluation of ambulance service performance using a geographic information system," 1998
[7] J. Peters and G. B. Hall, "Assessment of ambulance response performance using a geographic information system," Social Science & Medicine, vol. 49, no. 11, pp. 1551-1566, 1999
[8] M. Gendreau, A. Hertz, and G. Laporte, "A tabu search heuristic for the vehicle routing problem," Management science, vol. 40, no. 10, pp. 1276-1290, 1994
[9] M. Gendreau, G. Laporte, and F. Semet, "A dynamic model and parallel tabu search heuristic for real-time ambulance relocation," Parallel computing, vol. 27, no. 12,pp. 1641-1653, 2001
[10] M. Restrepo, "Computational methods for static allocation and real-time redeployment of ambulances". PhD thesis, Cornell University, 2008
[11] M. S. Daskin and E. H. Stern, "A hierarchical objective set covering model for emergency medical service vehicle deployment," Transportation Science, vol. 15, no. 2, pp. 137-152,1981.
[12] Y. Yue, L. Marla, and R. Krishnan, "An Efficient simulation-based approach to ambulance fleet allocation and dynamic redeployment"in AAAI, 2012

8. TABLES AND FIGURES

Table 1: Operational details in days

AMBULANCE NO.	REGION	1ST HALF	2ND HALF
TN04XXX98	CHENNAI	137	170
TN04XXX00	CHENNAI	170	154
TN04XXX13	CHENNAI	162	137
TN04XXX16	CHENNAI	183	163
TN04XXX97	KANCHEEPURAM	61	83
TN04XXX03	KANCHEEPURAM	0	85
TN04XXX19	KANCHEEPURAM	76	60
TN04XXX25	KANCHEEPURAM	15	102
TN04XXX01	THIRUVALLUR	74	87
TN04XXX04	THIRUVALLUR	76	36
TN04XXX10	THIRUVALLUR	54	99

Table 2:Cases Handled By the Ambulances

AMBULANCE NO.	REGION	DATE	CASES
TN04XXX98	CHENNAI	04-11-2014	6
TN04XXX00	CHENNAI	11-07-2014	6
TN04XXX13	CHENNAI	16-03-2015	2
TN04XXX16	CHENNAI	03-12-2014	3
TN04XXX97	KANCHEEPURAM	15-01-2015	4
TN04XXX03	KANCHEEPURAM	19-03-2015	2
TN04XXX19	KANCHEEPURAM	04-06-2014	4
TN04XXX25	KANCHEEPURAM	16-08-2014	1
TN04XXX01	THIRUVALLUR	05-09-2014	5
TN04XXX04	THIRUVALLUR	04-05-2014	3
TN04XXX10	THIRUVALLUR	25-02-2015	2

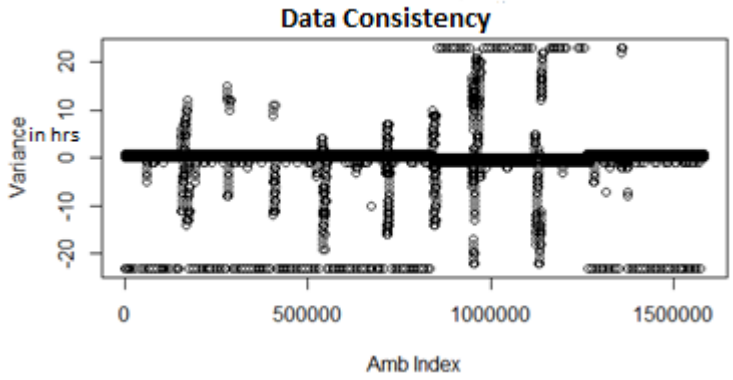

Fig.1: A plot to show the inconsistency in GPS values

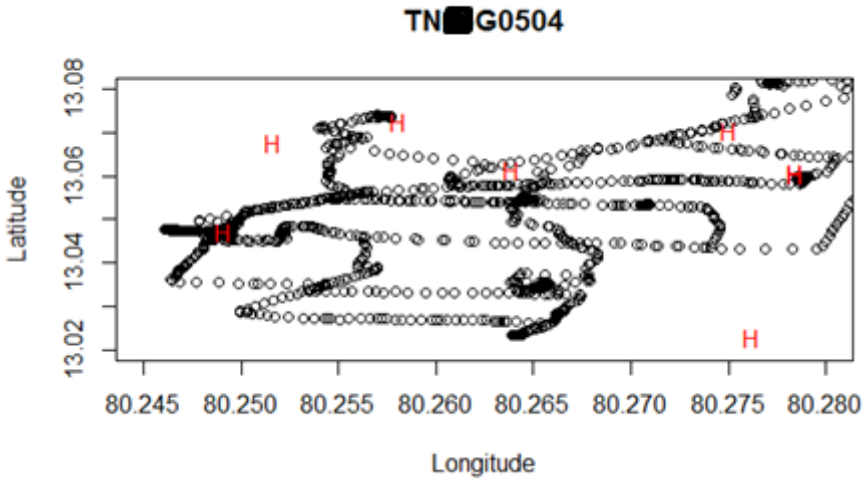

Fig.2: Ambulance GPS points plotted using RStudio

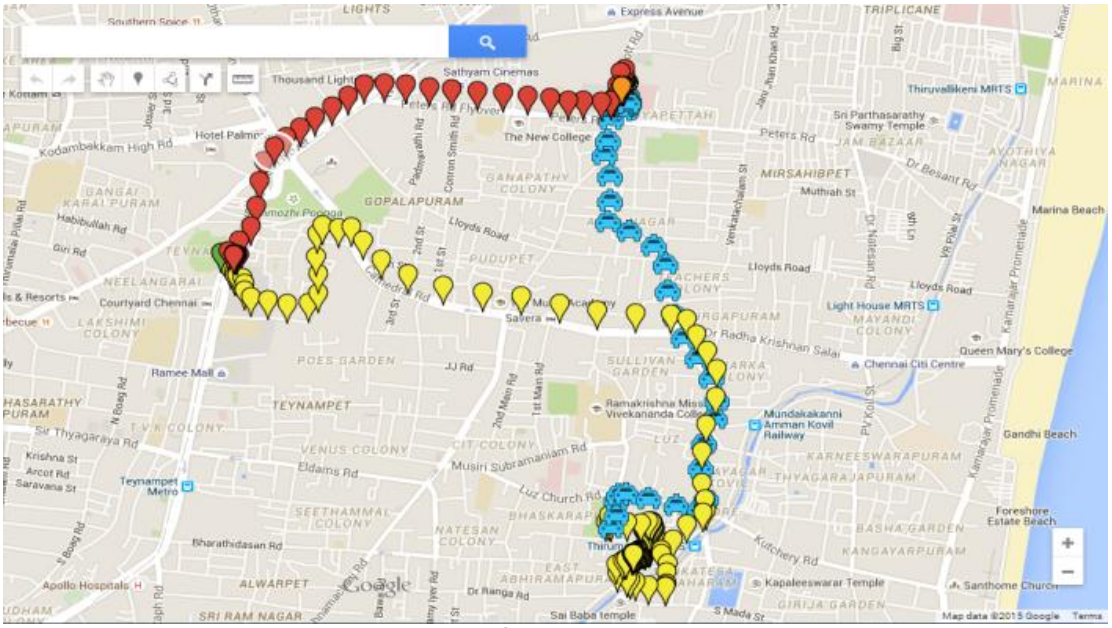

Fig.3: Ambulance TN04XXX13 on 1st March 2015 using GOOGLEMaps package.

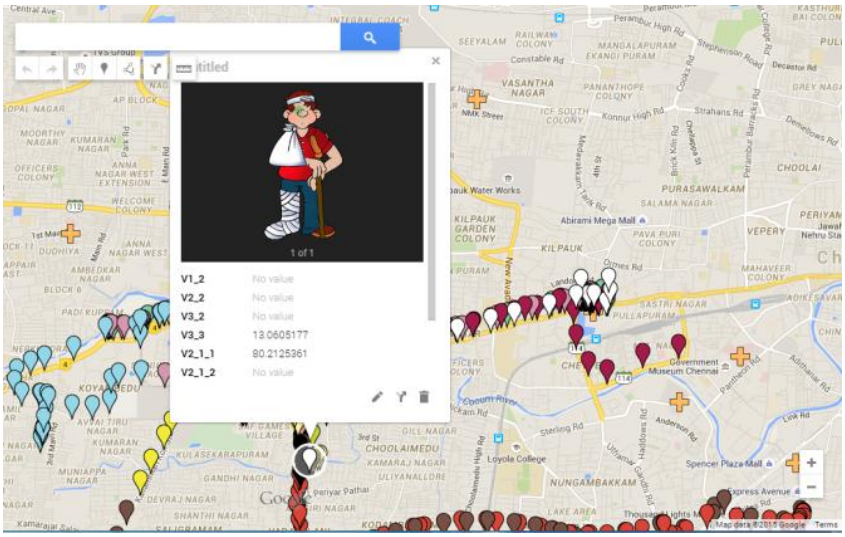

Fig.4: Locating the victim using both the data-sets

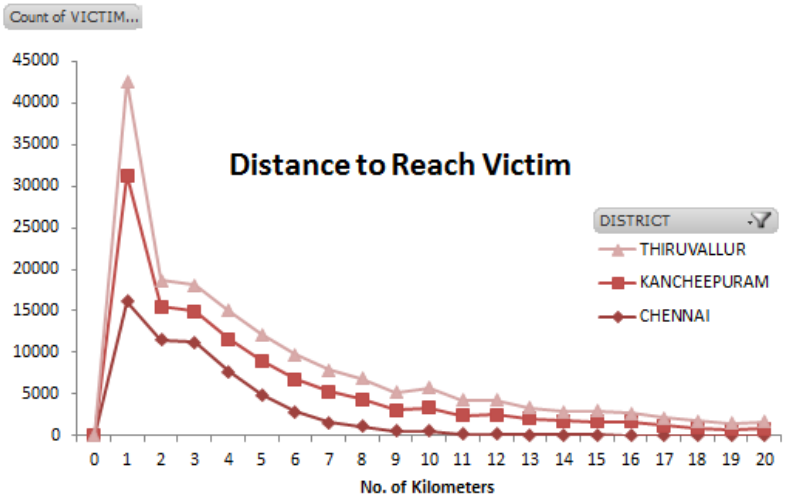

Fig.5: Sufficiency of ambulances

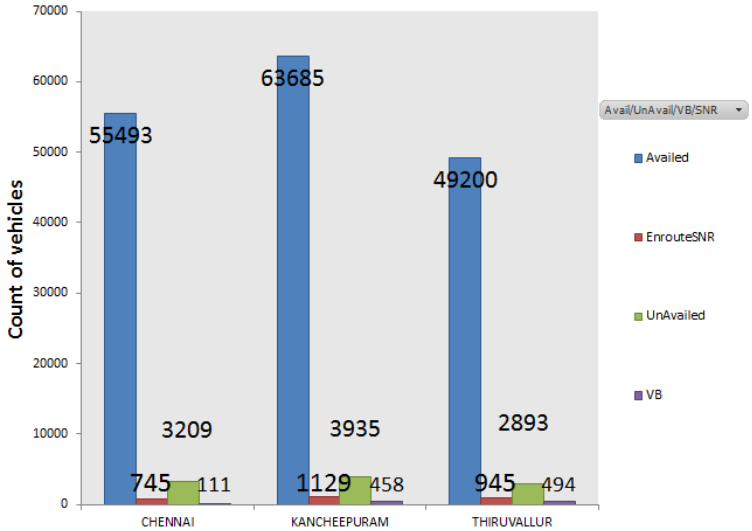

Fig.6: Cases of vehicles engaged during new request using CR

FLOODS AND RISK ASSESSMENT TOOL OF RAJAHMUNDRY

[1]D.Pranaya,[2] D V.Reddy[3] and D.NeelimaSatyam[1]
UG Student, Department of Civil Engineering,NITK. doddapanenipranaya@gmail.com
[2]Professsor, NITK Surathkal. 1952dvr@gmail.com
[3]Associate professor, IIIT Hyderabad. neelima.satyam@*iiit ac.in*

ABSTRACT: Flood has always been a recurrent phenomenon in India with more than 12% of the total land area in India prone to flood it is necessary to understand the concept of flood. This section on floods will help us understand the term better. The terms associated with floods are the types of floods, the causes of floods, the impact of floods, floods and development process, the mitigation measures, flood shelters, flood prone areas in India. Risk analysis has become a top priority for authorities and the population concerned" presents the basis to estimate current risk from a social perspective and identify tendencies in the way floods are understood by citizens. In this context, flood risk data and map of Rajahmundry is provided.

***KEYWORDS*:** Channel capacity, Floodplain, Flash floods, Coastal floods, Slope of water, Hydraulic efficiency

INTRODUCTION

India's first Prime Minister Jawaharlal Nehru believed that dams to produce power, irrigation and control flooding would be temples of a modern secular state. Since his day 400 large dams have been built in India, along with thousands of smaller levees as well as 16000 km of river embankments, but the area affected by floods has expanded from 2- 9 million hectares due to deforestation, poor urban drainage and other factors.Floods can arise from abnormally heavy precipitation, dam failures, rapid snow melts, river blockages. Floods become a disaster when areas are exposed to hazard without adequate warning and the community suffers loss of life, livelihood, assets and environmental security. Flash floods happen very quickly when lots of heavy rain falls over a short period of time and cause a biggest loss to human life than any other type of flooding. The worst cases of flooding may occur if there is a combination of storms, spring tides and low atmospheric pressures.

THE TYPES OF FLOODS:

Floods are prevalent throughout Asia presenting great challenges for disaster risk managers. The following are the three types of flood hazards confront the physical planners.

1. RIVER FLOODS: are also referred to in Asia as monsoon floods. These floods normally build up slowly and are often seasonal and may continue for days and weeks. These floods are associated with long rivers such as Indus. Natural action by the Riverine floods provides livelihood security for farmers and food security for people.

2. FLASH FLOODS: As the name suggests, flash floods are events with little time occurring between the start of the flood and the peak discharge. These floods normally occur within six hours of the beginning of heavy rainfall and are usually associated with intensive localized shower and severe thunderstorms. These. Flash floods occur in dry torrents of arid regions.

3. COASTAL FLOODS/STORM SURGES: Coastal floods occur in coastal regions. These floods are associated with cyclones and high tides. As in the river floods, intense rainfall over a large geographic area also produce flooding in coastal river basins.

THE CAUSES OF FLOODS:

Meteorological Causes such as prolongedrainfall, Cyclones, Typhoons, storms and tidal surges are the most flood damages. Ice and snowmelt, Impermeablesurfaces, saturatedland, Poor infiltration rates, Land erosion are the hydrological causes. Finally Anthropogenic Causes are the human activities in water catchments, which drastically intensify floods such as Population growth, deforestation and Global warming.

THE IMPACT OF FLOODS:

Buildings, Sewer systems, Roads, Railway lines, Canals are the primary effects, physical damage of property. Soil erosion and land degradation, Sedimentation, Traffic, Water pollution, Water logging, Land values, Trees, Landslides are Secondary effects. Decline in tourism, Rebuilding costs, Food shortage leading to price increase etc., Loss of production and provision of services, Impact on country's debt position, Loss of economic growth, Delay in development programs are tertiary effects

MITIGATION MEASURES:

REDUCING FLOODING:

Dams and reservoirs: Dams are the Classic engineering solution to flooding problem. It impedes its flow across the river. This helps keep discharge downstream of dam low even during prolonged heavy rainfall.

Construction of levees: Unlike natural levees, artificial levees are significantly larger and are generally constructed out of a material that is resistant to erosion. The main advantage of an artificial levee is that it allows the floodplain to be built on.

Wing dykes: Behind dykes, sediment builds up and the channel is narrowed, forcing water to flow faster. This helps reduce the risk of flooding by getting water away from an area at risk of flooding as quickly as possible, preventing a build-up of water.

Channel straightening: Like with wing dykes, this moves water through the river faster preventing it from pooling and so reducing the risk of a flood. A straightened channel is faster to navigate too, a nice benefit of channel straightening. In addition; erosion is stronger downstream because the river has a lot more kinetic energy.

Diversionspillways:When the river discharge rises, these channels move water around an area at risk of flooding and send it either back into the river or into another river. In addition, spillway pathcan take water around areas not usually used to flooding.

Floodplain Zoning: If no one is allowed to build on a floodplain then the damage caused by the river flooding will be greatly reduced because there isn't much to damage. In addition, floodplain zoning ensures that land on the floodplain isn't urbanized so infiltration can occur and surface run off is reduced. This reduces the likelihood of a river flooding.

Afforestation: This reduces a river's discharge and so makes it less likely to flood. When combined with floodplain zoning, afforestation can be very effective at reducing the risk of flooding. Afforestation has the benefit of creating new habitats for animals and improving water quality by filtering pollutants out of rainwater.

Wetland restoration: Wetlands are able to store large volumes of water which helps to reduce the discharge in a river. Wetlands don't reduce flooding where they are located but rather downstream of the river.

DETERMINING FLOOD RISK INDEX:

All data was integrated in a GIS environment using the Analytical Hierarchical Process (AHP) method which is a multi-criteria decision making technique based on a 9-point scale (Saaty, 1980; Siddique et al., 1996). This method involved a pair-wise comparison of the relative preferences of a small number of 'decision factors' for flood risk assessment after constructing a 'decision hierarchy'(table.1) Finally, a flood risk index (FRI) was computed using overlay analysis in Model Builder of Arc View 3.2 software as follows:

$$\mathrm{FRI} = \sum_{I=1}^{N}[(RIWi)^2 * (RIWij^3)] \qquad (1)$$

Where, RIW=relative importance weight of level2 decision factor, N=number of level2 decision factor, FRI=flood risk index

Flood prone areas in India: India is a peninsular country quite prone to flood. As per geological survey of India, flood prone areas cover about 12.5% area of our country. Intense monsoon rains from southwest causes rivers like Brahmaputra, Ganga, Yamuna etc. to swell their banks, which in turn floods the adjacent area. Past few decades, central India has become familiar with torrential rains and flash floods. The major flood prone areas in India are the river banks and deltas of Ravi, Yamuna-sahib, Gandak, Sutlej, Ganga, Gagger, Kosi, Brahmaputra, Mahanadhi, Mahananda, Damodhar, Godavari, Sabarmati, Mayurakshi and their tributaries. An overview about state wise flood prone areas can be gained by the following (table.2)

CONCLUSIONS

Flood is the overflow of water through any water body like ponds, rivers, lakes, streams etc. It has harmful as well as beneficial effects. Harmful effects such as loss of property, deaths of animals, humans whereas beneficial effects are groundwater recharge,fertilelandetc.Rajahmundry areas surrounding Godavari river basin with high flood risk are Katheru,Dhawaleswaram, Rajavolu,Bommuru,Chakradwarabandam,etc .inconsideration of decision factors like Population density (49%), Elevation (15%), Distance from active channels (23%), and Landcover (7%), Agriculture (4%), Geomorphic features(2%).

References

1.https://www.floodsmart.gov/floodsmart/pages/flooding_flood_risks/ffr_overview.jsp

2. https://en.wikipedia.org/wiki/Floods_in_India

3.http://www.nrsc.gov.in/Earth_Observation_Applications_Disaster_Management_Floods.html

4. http://timesofindia.indiatimes.com/topic/floods

5. https://www.savethechildren.in/85-latest-news/390-floods-in-india-top-10-risks-children-are-exposed-to.html

6. http://topyaps.com/5-worst-floods-india-seen-since-independence

7. http://www.oneindia.com/feature/have-a-look-at-9-deadliest-floods-in-indian-history-1517017.html

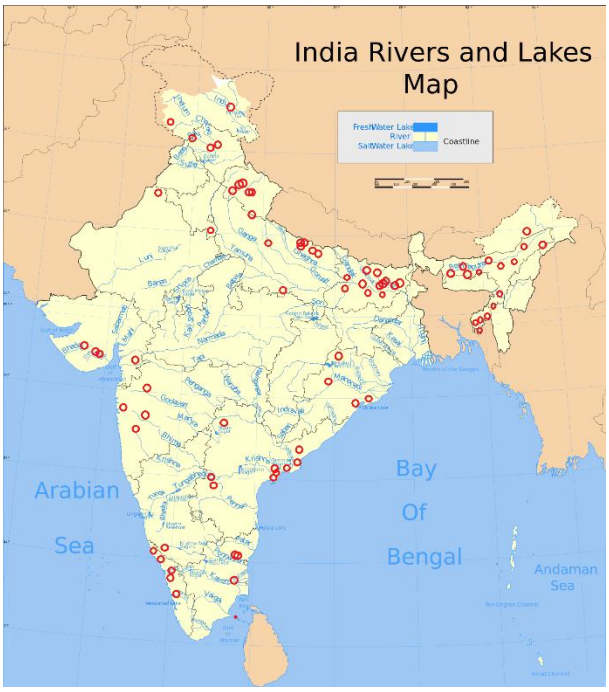

Fig.1: flood risk map of India

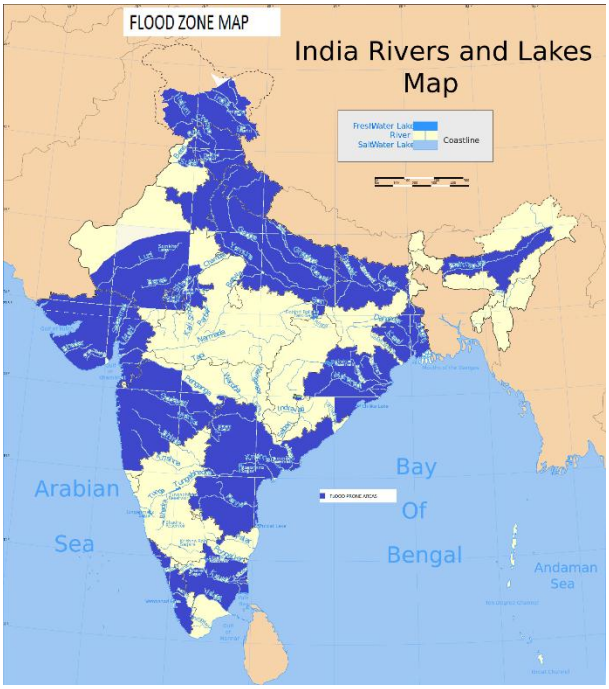

Fig.2: Indian flood map

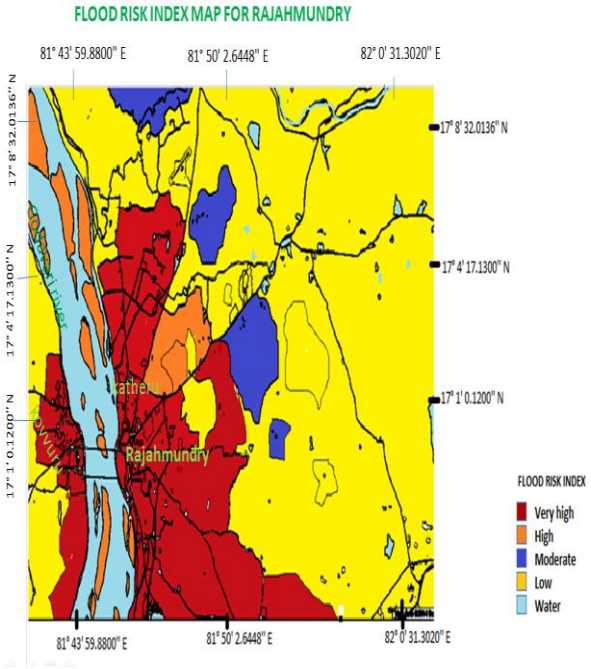

Fig.4: Flood risk map of Rajahmundry

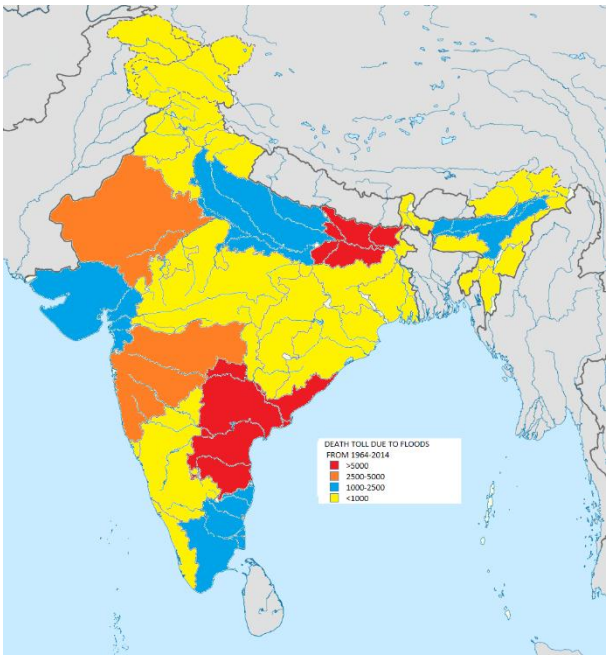

Fig.3:Death toll map of india

Table.1: Decision hierarchy and Relative Importance Weightage (RIW) for level 2 and 3 factor

Flood Risk Index (Level 1)						
Decision factors (Level 2)						
Decision factors	Population density	Distance to active channels	Elevation	Land cover	Agriculture	Geomorphic features
RIW²	0.49	0.23	0.15	0.07	0.04	0.02
Sub- factors (Level 3)						
Classes	**Cell attribute**	**RIW³**	**Classes**	**Cell attribute**	**RIW₃**	
Population density (no.)			**Distance to active channels (m)**			
A	> 1001	0.77	A	0 – 6.5	0.51	
B	701 - 1000	0.17	B	6.5 – 13	0.26	
C	401 - 700	0.05	C	13 – 20	0.13	
			D	20 – 27	0.06	
			E	27 – 34	0.03	
Geomorphic features			**Elevation (m)**			
A	Active Channels	0.34	A	33 – 35	0.35	
B	Channel Bars	0.26	B	35 – 37	0.23	
C	Inactive Channels	0.15	C	37 – 39	0.15	
D	Crevasse Deposits	0.11	D	39 – 41	0.10	
E	Water-logged areas	0.06	E	41 – 43	0.07	
F	Oxbow-lakes	0.05	F	43 – 45	0.05	
G	Sand Patches	0.02	G	45 – 47	0.03	
H	Flood Plain	0.01	H	47 – 49	0.02	
Land Cover			**Agriculture**			
A	Running Water	0.52	A	Dense	0.62	
B	Fresh Sand	0.27	B	Moderate	0.24	
C	Moist Sand	0.13	C	Less	0.08	
D	Water-logged areas	0.05	D	Barren	0.05	
E	Agriculture	0.02				

Table.2: State wise Flood prone Areas

STATE	AREA (MILLION ha)	STATE	AREA (MILLION ha)
UTTARPRADESH	7.336	TRIPURA	0.33
BIHAR	4.26	MADYAPRADESH	0.26
PUNJAB	3.7	HIMACHAL PRADESH	0.23
RAJASTHAN	3.26	MAHARASTRA	0.23
ASSAM	3.15	JAMMU AND KASHMIR	0.08
WEST BENGAL	2.65	MANIPUR	0.08
HARYANA	2.35	DELHI	0.05
ORISSA	1.4	KARNATAKA	0.02
ANDHRA PRADESH	1.39	MEGHALAYA	0.02
GUJARAT	1.39	PONDICHERRY	0.01
KERALA	0.87		
TAMILNADU	0.45		

5th International Engineering Symposium - IES 2016
March 2-4, 2016, Kumamoto University, Japan

PAN-sharpening the spatial resolution of Resourcesat-1 LISS-IV image

Jagalingam P[1] and Arkal Vittal Hegde[2]

1 Department of Applied Mechanics and Hydraulics, NITK, Surathkal, Mangalore 575025, India. email:lingam.jai10@gmail.com; arkalvittal@gmail.com

ABSTRACT: Image fusion combines the high spatial resolution panchromatic (PAN) image with low spatial resolution and high spectral resolution multispectral (MS) image to obtain both high spatial resolution and rich spectral resolution in a single image. In the present study, panchromatic image acquired from Cartosat-1 of high spatial resolution 2.5m and Resourcesat-1 LISS-IV MS image of high spectral resolution and low spatial resolution 5.8m are fused using various image fusion techniques such as Principal Component analysis (PCA), Modified Intensity Hue and Saturation (M-IHS), Brovey Transform (BT), Gram-Schmidt (GS) and High pass filter (HPF) to obtain the fused image which will have both high spatial resolution 2.5m and rich spectral resolution in a single image. The fused images are evaluated by using both Qualitative (Visual) and Quantitative analysis methods such as Root mean square (RMSE), Correlation coefficient (CC), Structural Similarity index method (SSIM), Peak signal noise ratio (PSNR), and Signal to noise ratio (SNR). The evaluation of results obtained from the analysis of fused image revealed that GS technique ranked first, followed by HPF method.

***Keywords**: Image fusion, Qualitative analysis and Quantitative analysis, Fusion techniques*

INTRODUCTION

Image fusion is the method of merging appropriate information from both PAN and MS images to develop a single picture with more information than any of the two images. All the earth observing satellites such as Landsat series, IRS series, Quickbird, Ikonos, Spot series etc., provides two images 1) PAN image with high spatial resolution, 2) MS image with high spectral and low spatial resolution Yun Zhang (2004). PAN image with high spatial resolution has the advantage of identifying and differentiating the small features, but the image appears in black and white, whereas the MS image is spectrally rich and has the advantage of differentiating and identifying the features based on colour Ranchin and Wald (2000). Many remote sensing applications such as wetland mapping, Land use Land cover (LULC), Change detection analysis require both high spatial and spectral rich resolution in a single image. Due do the two technical limitations of satellites 1) Resolution trade-offs, 2) System trade-offs all the earth observing satellites launched till date cannot afford single image with both high spatial and high spectral resolution Nikolakopoulos (2008). In-order to overcome the limitation of satellites, various image fusion (or) PAN-sharpening techniques are developed such as Principal Component analysis (PCA) Chavez and Kwarteng (1989), Modified Intensity Hue and Saturation(M-IHS) Siddiqui (2003), Brovey Transform(BT) Hallada and Cox(1983), Gram-Schmidt(GS) Zhang (2004) and High pass filter(HPF) Gangkofner et.al (2008) to achieve the single image with both high spatial and high spectral resolution.

In the present study image fusion techniques such as PCA, M-IHS, GS, HPF, BT are used to fuse the multisensor imagery, Cartosat-1 PAN image of high spatial resolution 2.5m and Resourcesat-1 LISS-IV MS image with high spectral resolution and low spatial resolution 5.8 m. The results of all the fused images are evaluated using both quantitative analysis and qualitative analysis.

FUSION METHODS

Principal Component analysis (PCA)

In this method, PCA transformation is performed on the MS image and produce images as PC1, PC2 and PC3.Generally PCA method assumes that the PC1 is a good estimate of PAN image, where PC2 and PC3 collect the spectral information of MS image. The first PC1 image is replaced with the high spatial resolution of PAN image and resampling the PAN image to match spatial resolution of PC1 image. And, inverse transformation is applied on Resampled PAN, PC2, PC3 to obtain image in the RGB color mode. Later, RGB image is resampled to high spatial resolution of the PAN image to obtain a fused image with both high spatial and high spectral image.

Modified Intensity Hue Saturation (M-IHS)

The M-IHS method is developed to overcome the limitation of IHS method is that it can only process three bands at a time. The M-IHS method works by estimating the spectral overlap between each low resolution multispectral band and high resolution panchromatic band and weighting the merge based on these relative wavelengths. Thus, this technique performs better when merging images cover significant overlap of the wavelengths.

Brovey Transform (BT)

The BT method first multiplies each low resolution multispectral band by the high resolution panchromatic band and then divides each product by the sum of the MS bands. It is a mere method to fuse images acquired from different sensors. This method well preserves the spectral information of MS image and also improves overall brightness of the MS image with the high spatial resolution image. Nevertheless, this method is good for creating visually appealing pictures.

Gram-Schmidt (GS)

In this method, spatial resolution of PAN image is simulated to lower spatial resolution PAN image by forming a linear combination of the lower spatial resolution of MS image. GS transformation is done along the simulated lower spatial resolution PAN image and MS image. The simulated lower spatial resolution PAN image is employed as the first band in the GS transformation. The statistics of the higher spatial resolution of PAN image are adjusted to match the statistics of the first transform band, resulting from GS transformation and higher spatial resolution PAN image (with adjusted statistics) is substituted for the first transform band to produce a new set of transforming bands. Lastly, the inverse GS transformation is done on the new set of transformed bands to create the enhanced spatial resolution of MS image.

High pass filter (HPF)

The HPF method initially sets the Ratio (R) between the cell sizes of MS image and PAN image. The process involves a convolution using an HPF on the PAN image to reduce the low-frequency spectral information. Resample the original MS image to pixel size of PAN image. Add filtered PAN image to each resemble the MS band, to enhance the pixel size of the MS image to a pixel size of PAN image.

QUALITY ASSESSMENT

The primary aim of the PAN - sharpening technique is to transmit the high spatial resolution from the PAN image into high spectral resolution MS image, to get a single picture with both high spatial and high spectral resolution. During the transformation of information from PAN image of MS image, the image fusion techniques may generate spatial distortion and spectral distortion in the combined image. In order to appraise the character of the fused image two different approaches are taken such as qualitative and quantitative analysis.

QUALITATIVE ANALYSIS

The best and most uncomplicated path to evaluate the fused image is the quantitative analysis or Visual analysis. In this analysis, a group of people will compare the fused image with original PAN and MS image to measure the character of the fused image by taking the various optical parameters such as spatial details,

geometric design, size of objects, colour information etc. Fonseca et al (2011).

QUANTITATIVE ANALYSIS

The analysis is grounded on mathematical modelling and it is also recognized as objective analysis. In this analysis, the fused images are evaluated by adopting the quality metrics such as RMSE, CC, SSIM, PSNR, and SNR. This metric assesses the character of the fused image by taking a set of pre-defined quality indicators for evaluating the spectral and spatial similarities between the merged image and reference image. The reference image is the MS image at the spatial resolution of PAN image. The availability of ultimate reference image is challenging; Duplicate reference image is obtained by resampling the original MS image spatial resolution to PAN image spatial resolution (Fig.3)

RMSE

Zoran (2009) states that Root Mean Square Error (RMSE) is a good indicator of the spectral quality of fused image. The combined image is close to the reference image when RMSE value is null. The following equation is adopted for determining the RMSE value of fused image.

$$\text{RMSE}=\sqrt{\frac{1}{MN}\sum_{i=1}^{M}\sum_{j=1}^{N}\left(I_r\ (i,j)-I_f\ (i,j)\right)^2} \qquad (1)$$

Where, $I_r(i,j)$= the pixel value of reference image, $I_f(i,j)$ = the pixel value of fused image and M, N are the image size.

Correlation Coefficient (CC)

According to Zhu and Bamler (2013) CC is applied to calculate the similarity of spectral characteristics between the reference and fused images. The value of CC should be close to +1, which indicates the reference and fused images are similar.

$$CC=\frac{2\ c_{rf}}{c_r\ +c_f} \qquad (2)$$

Where $c_r\ =\sum_{i=1}^{M}\sum_{j=1}^{N}I_r\ (i,j)^2$, $c_f\ =\sum_{i=1}^{M}\sum_{j=1}^{N}I_f\ (i,j)^2$

$$c_{rf}\ =\sum_{i=1}^{M}\sum_{j=1}^{N}I_r\ (i,j)I_f\ (i,j)$$

Structural Similarity Index measure (SSIM)

Wang Z et al. (2004) It is employed to compare the local forms of pixel intensities between the reference and fused images. The value 1 indicates the reference and fused images are similar.

SSIM

$$=\frac{(2\ \mu_{I_r}\ \mu_{I_f}\ +c_1\ )\left(2\ \sigma_{I_r\ I_f}\ +c_2\ \right)}{\left(\mu^2\ I_r\ +\mu^2\ I_f\ +c_1\ \right)\left(\sigma^2\ I_r\ +\sigma^2\ I_f\ +c_2\ \right)} \qquad (3)$$

Where μ_{I_r} ,μ_{I_f} are the mean value of reference and fused images and σ_r ,σ_f are standard deviation of reference and fused images. c_1 & c_2 is a constant added to the value of $\mu^2_{I_r}\ +\mu^2_{I_f}$, $\sigma^2_{I_r}\ +\sigma^2_{I_f}$ when their value is close to 0. It is added to avoid the instability.

Peak Signal to Noise Ratio (PSNR)

Naidu (2010) states that PSNR is calculated by the number of gray levels in the image divided by the corresponding pixels in the character and the fused images. When the value is high, the fused and reference images are alike.

PSNR=

$$20\log_{10}\left(\frac{L^2}{\frac{1}{MN}\sum_{i=1}^{M}\sum_{j=1}^{N}\left(I_r\ (i,j)-I_f\ (i,j)\right)^2}\right) \qquad (4)$$

Where L=number of gray levels in the image, $I_r(i, j)$=the pixel value of reference image, $I_f(i, j)$=the pixel value of fused image and M, N is the image size.

Signal to Noise Ratio (SNR)

Alimuddin (2012) SNR is used to measure the ratio between information and noise of the fused image. Higher value indicates that both the reference and fused images are similar.

$$SNR = 10\log_{10}\left(\frac{\sum_{i=1}^{M}\sum_{j=1}^{N}\left(I_r\ (i,j)\right)^2}{\sum_{i=1}^{M}\sum_{j=1}^{N}\left(I_r\ (i,j)-I_f\ (i,j)\right)^2}\right) \quad (5)$$

I_r (i,j)=The pixel value of reference image, I_f (i,j)=The pixel value of fused image and M, N is the image size.

RESULTS AND DISCUSSION

The fused image obtained from image fusion techniques such as PCA, M-IHS, BT, GS and HPF method are shown in the (Figures 4 to 9). The original PAN, MS and resampled MS image are shown in the (Figures 1 to 3). The problem of image fusion techniques produces spectral and spatial distortions in the combined image. In order to analysis the performance of fused image, both quantitative and qualitative analyses are employed.

Qualitative analysis

In this analysis, all the fused images and original MS and PAN images were exposed in the same zoom level. A group of people with both remote sensing specialization and non-remote sensing specialization was adopted to visually compare the fused images with MS and PAN images and evaluated the performance of different fused images. The PCA and M-IHS images looked similar by preserving spatial information and spectral information. However, the fused images of PCA and M-IHS was not very close to the original images. BT fused image showed less spatial detail, but preserved maximum colour information. HPF image preserved high spatial information compare to PCA and BT image, but slight colour variation occurred. GS image can preserve both spatial and colour information and was slightly better than PCA, BT, HPF and W-HIS images. The result of quantitative analysis reveals that GS image looked similar to the original image by preserving both spatial details and colour information.

Quantitative analysis

The quality metric indices such as RMSE, CC, SSIM, PSNR and SNR were used to assess the performance of the fused image. This metric evaluates the fused image by comparison with the reference image (Fig.3). The results of the metrics are shown in the (Figure 9 to 13). In each quality metrics certain attribute to be satisfied for selecting the best fused image which preserves the maximum colour information of MS image and pixel size of PAN image: a) RMSE value close to zero, b) CC value close to 1, c) SSIM value close to 1, d) Higher value of PSNR, e) Higher value of SNR. In the (Fig.9) RMSE metric value indicates that the GS method outperforms the other methods. The value of CC (Fig.10) indicates that the GS method best preserves the colour information original MS image followed by HPF method. The SSIM (Fig.11) metric indicates that the GS method performed well. The results of PSNR (Fig.12) revealed that the GS method performs best. The result of SNR (Fig.13) metric showed that HPF method performs better followed by GS method. The result of four, out of five quality metrics indicates that GS method can preserve both colour information and spatial details in the fused image.

Fig.1 LISS IV original image

Fig.2 PAN original image

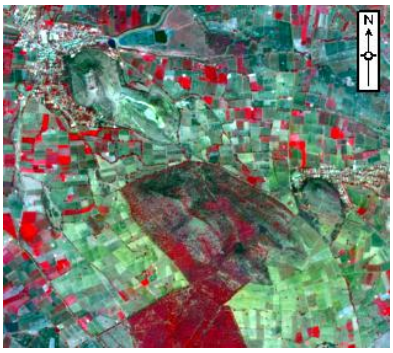

Fig.3 Resampled LISS IV Image

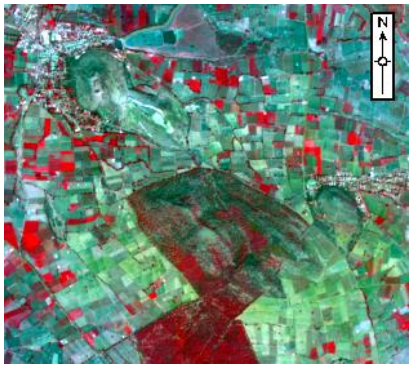

Fig.4 PCA fused image

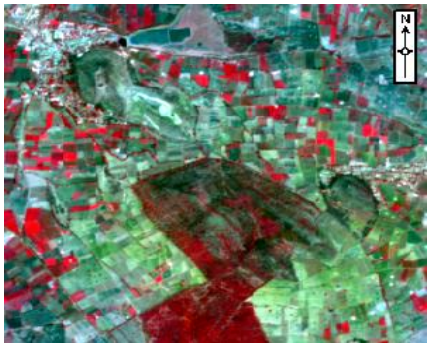

Fig.5 M-HIS fused image

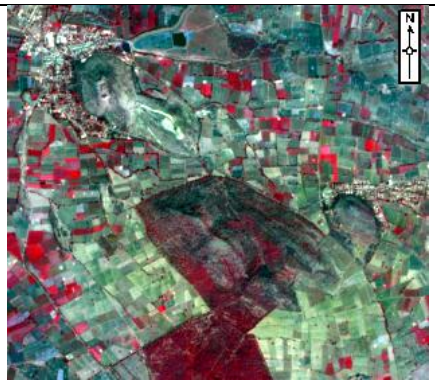

Fig.6 BT fused image

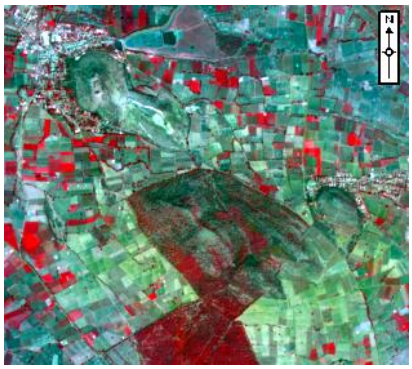

Fig.7 GS fused image

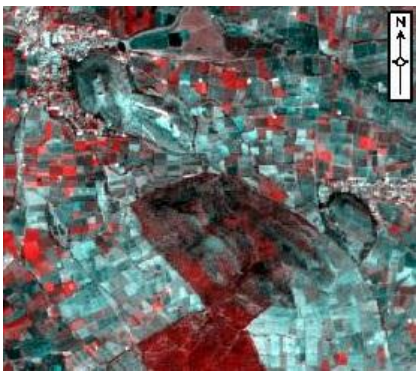

Fig.8 HPF fused image

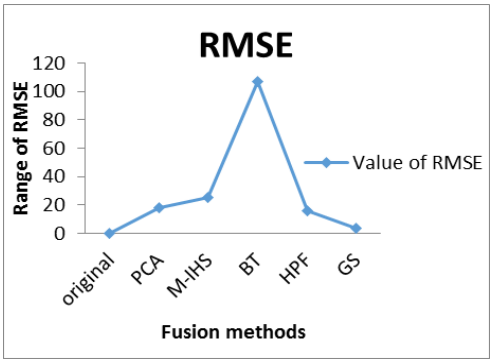

Fig.9 RMSE vs Fusion methods

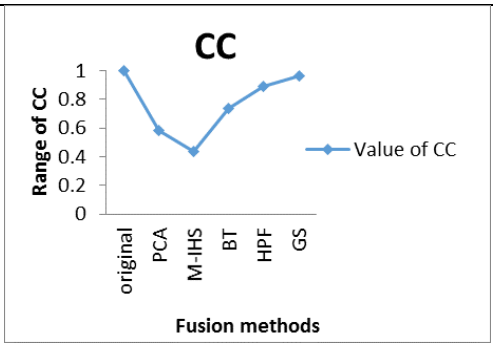

Fig.10 CC vs Fusion methods

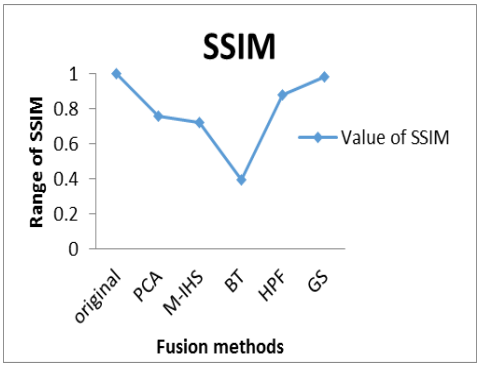

Fig.11 SSIM vs Fusion methods

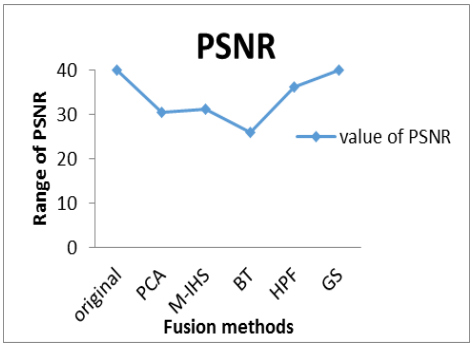

Fig.12 PSNR vs Fusion methods

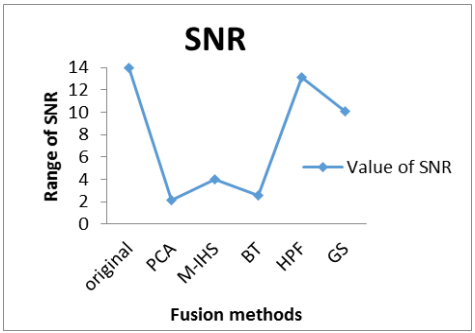

Fig.13 SNR vs Fusion methods

CONCLUSION

In the present study, MS image with high spectral resolution and PAN image of high spatial resolution is fused to enhance the pixel size of MS image and at the same time while preserving the colour information of MS image by using various image fusion or PAN-sharpening techniques such as PCA, M-IHS, BT, HPF and GS. All the fused images are evaluated and compared taking two quality metrics such as quantitative and qualitative analysis. The outcome of both metrics revealed that the GS method ranked first, followed by HPF methods for best enhancing the pixel size of the MS image while preserving the color information of multispectral image.

REFERENCE

[1] Alimuddin I, Sumantyo, J T S, Kuze H (2012), Assessment of pan-sharpening methods applied to image fusion of remotely sensed multi-band data. Int. J. Appl. Earth Obs. Geoinf, Vol.18, pp 165–175.

[2] Aniruddha, G and Joshi, P K (2013), Assessment of pan-sharpened very high-resolution WorldView-2 images, Int. Journal of remote sensing, Vol.34, No.23, pp 8336-8359.

[3] Chavez, P S and Kwarteng (1989), A Extracting spectral contrast in Landsat Thematic Mapper image data using selective principle component analysis, Photogramm.Eng. RemoteSens, Vol.55, No.3, pp 339-348.

[4] Fonseca, L et al, (2011) Image Fusion for Remote Sensing Applications. InTech, pp. 153–158.

[5] Gangkofner, U G et al (2008), optimizing the high-pass filter addition technique for image fusion. Photogrammetric Engineering and Remote Sensing, Vol.74, No.9, pp.1107-1118.

[6] Hallada, W A and Cox, S (1983) Image sharpening for mixed spatial and spectral resolution satellite system, 17th International symposium on remote sensing of the environment, May 9-13, Ann arbor, pp.1023-1032.

[7] Naidu V P S, (2010), Discrete Cosine Transform-based Image Fusion, Def. Sci. J, Vol.60, pp 48–54.

[8] Nikolakopoulos, K G (2008), Comparison of Nine Fusion Techniques for Very High Resolution Data," Photogramm. Eng. Remote Sens, Vol. 74, No. 5, pp. 647–659.

[9] Ranchin, T and Wald, L (2000), Fusion of High Spatial and Spectral Resolution Images: The Arsis Concept and Its Implementation, Photogramm. Eng. Remote sens, Vol. 66, No.2003, pp. 49–61.

[10] Siddiqui, Y (2003), The Modified IHS Method for Fusing Satellite Imagery, ASPRS 2003 Annual Conference Proceedings, May 5-9, 2003.

[11] Wang Z, Bovik A C, Sheikh H R, Simoncelli E P, (2004), Image Quality Assessment: From Error Visibility to Structural Similarity, IEEE Trans IMAGE Process, Vol.13, pp 1–14.

[12] Yun Zhang (2004), Understanding Image Fusion, Photogramm. Eng. Remote Sens, No. June, pp. 657–661.

[13] Zhang (2004), System and method for image fusion, Unite States Patent, 2008.

[14] Zoran L F (2009), Quality Evaluation of Multiresolution Remote Sensing Image Fusion, U.P.B. Sci. Bull., Ser. C 71, pp 38–52.

5thInternational Engineering Symposium - IES 2016
March 2-4, 2016, Kumamoto University, Japan

Limit state design of industrial chimneys – Comparison of international codal provisions

Muhammed Hassan Faisal K S[1] and **B R Jayalekshmi**[2]

1 *M.Tech Student, Department of Civil Engineering, NITK, Surathkal, Mangalore 575025, India. email:faisalkalathil@gmail.com*
2 *Associate Professor, Department of Civil Engineering, NITK, Surathkal, Mangalore 575025, India.email:br.jaya@gmail.com*

ABSTRACT: There is an impending demand for taller and structurally safe chimneys all around the world as the environment and pollution control boards enforce stringent regulations on air pollution nowadays. CICIND model code and IS 4998 (draft code 2013) recommends limit state method of design for chimneys. Comparisonof the design provisionsin these codes has been attempted in this study. Chimneys being tall and flexible structures, wind loads are more critical than earthquake loads. Limit state design of chimneys based on the response due to wind loads are also compared. It has been found that the design of chimney as per CICIND model code is economical while IS 4998 based design is conservative.

Keywords*: RCC Chimney, Limit State Method, IS 4998, CICIND, Wind analysis*

INTRODUCTION

Tall RC chimneys are commonly used to discharge pollutants at higher elevation. The enforcement of stricter air-pollution control standards has led to the construction of increasingly tall RC chimneys worldwide. Further, due to the availability of advanced construction materials chimney shell is being made with thinner wall. As a result, chimneys have become more slender and sensitive to wind-induced vibrations. The cross-section of the chimney is generally hollow circular, from aerodynamic considerations, and tapered, from considerations of structural economy and aesthetics. The chimney is subjected to gust buffeting in the along-wind direction due to drag forces, and also to possible vortex shedding in the across-wind direction. In the typical case of slender, tapered RC chimneys, it is the along-wind response which generally predominates and governs the design.

CICIND was founded in 1973 in Paris, under the Presidency of Marius Diver of France. The need for such a body had been demonstrated at the first International Chimney Symposium, held in Edinburgh earlier that year. This symposium highlighted the contradictory requirements of the various National Codes governing the design of industrial chimneys as well as a lack of knowledge about the processes leading to accelerated deterioration of chimneys at that time. CICIND Model Codes and Manuals represent the best available mix of international good practice in design provided by experts within the field. Unhampered by the constraints of national or regional practices, and with no particular political objective to achieve, the user can be assured of valuable, independent design advice. "Model Code for Concrete Chimneys - Part A; The Shell" - 2nd Edn., Rev. 1 - August 2001 is the latest version discussing limit state design of chimney shell. The Indian Standard was first published in 1968 as IS: 4998 and subsequently revised in 1975. The second revision was brought out in 1992 supposed to be in two parts, with the Part 1 (published in 1992) dealing with the assessment of loads and the Part 2 envisioned to deal with design criteria for reinforced concrete circular (RC) Chimneys. In the third revision (2013), both the above aspects of assessment of loads and design criteria are consolidated into a single standard. Only Chimneys of circular

cross section have been included. Attempt has been made to compare important codal provisions of CICIND model code and IS 4998(draft code, 2013). A RC circular chimney of height 275m has been analysed for wind loads as per IS 4998 and designed using both CICIND model code and IS 4998 for comparison of design results.

COMPARISON OF CODAL PROVISIONS

Material Law

Both IS 4998 and CICIND recommends parabolic stress block for concrete. IS 4998 enhanced the stress in concrete by introducing short term loading factorC_{sf}.

The stress-strain relationship for concrete in compression is taken as

$$f_c = \frac{0.67\, f_{ck} C_{sf}}{\gamma_c}\left\{2\left(\frac{\varepsilon}{\varepsilon_{cu}}\right) - \left(\frac{\varepsilon}{\varepsilon_{cu}}\right)^2\right\} \quad (1)$$

For $\varepsilon \le \varepsilon_{cu}$

Where

$\varepsilon_{cu} = 0.002$

f_{ck} =Characteristic cube strength of concrete

γ_c = 1.5

C_{sf} = short-term loading factor

$$= [0.95 - 0.1(P_u/P_{umax})]/0.85 \quad (2)$$

P_u = Factored axial load

$$\mathrm{P}_{umax} = 2\pi rt\left[\left(\frac{0.67 f_{ck}}{\gamma_c}\right)\left(1 - \frac{p}{100}\right) + f_s(\varepsilon_{cu})\left(\frac{p}{100}\right)\right] (3)$$

p = percentage reinforcement.

Here $f_s(\varepsilon_{cu})$is stress in steel corresponding to strain ofε_{cu}.

In CICIND, the ultimate strain for concrete ε_{cu} is limited to 0.003 at the centre of the wall for horizontal sections and 0.0035 at the edge for vertical sections. But in IS 4998, the maximum compressive strain in concrete in axial compression shall be limited to 0.002 under both axial and flexural compression.

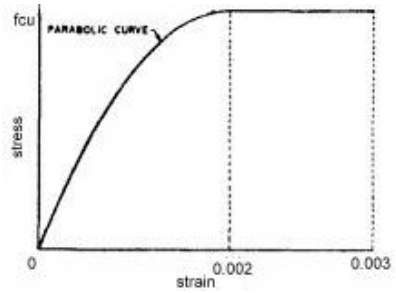

Fig.1 Design stress-strain curve of concrete (CICIND model code).

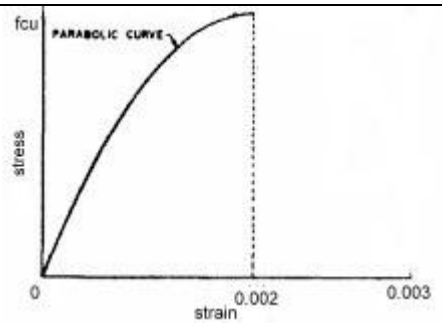

Fig.2 Design stress-strain curve of concrete (IS 4998).

Wind Load

Analysis procedure of along wind in both CICIND and IS 4998 is almost same, i.e. it consists of static part and a dynamic part.

The static part, the mean wind load per unit height is given by

$$W_m(z) = 0.5\, \rho_a v(z)^2 C_D d(z)$$

While IS 4998 explicitly giving the value of shape factor C_D to be taken as 0.8 for circular chimney, CICIND specifies C_D is a function of height and diameter of chimney given by

C_D = 0.6 if $^h/_d < 5$

$$C_D = 0.1\,\frac{\log_{10}\left(\frac{h}{d}\right)}{\log_{10}(5)} + 0.5 \quad if\ 5 < {}^h/_d < 25$$

C_D = 0.7 if $^h/_d \ge 25$

Where

h = height of top of shell above ground level

d = chimney diameter at 0.75h

Both the codes follows same formula for calculating the dynamic part.

In CICIND there is no entirely satisfactory way of calculating across wind. Instead the method of ACI 307-95 is recommended which is similar to the one followed in IS 4998.

Aseismic Design

Codes of practice around the world provide conservative guidelines for the aseismic design of tall reinforced concrete chimneys in the belief that such structures would behave in a brittle manner when subjected to severe earthquake excitation. This has resulted in reinforced concrete chimneys being prohibitively expensive in regions of high seismicity.

The CICIND model code makes a considerable deviation from the general seismic design philosophy. The seismic design approach recommended in CICIND is based on dual performance based design philosophy.

(a) Designing the chimney elastically to resist earthquake induced loads considered for a damageability limit state earthquake event, and
(b) Designing the chimney with sufficient ductility so that chimney will survive an extreme earthquake event without premature failure and collapse.

An importance factor of IF=1.4 is recommended for the ultimate limit state.
It is recommended that the seismic actions be calculated using the response spectrum method assuming uncracked properties with a structural response factor (R factor) dependent on the level of seismic detailing specified

R =1.0(no specified seismic detailing)
R =2.0 (capacity design & seismic detailing)

While, an importance factor of 1.5 and response reduction factor of 3 as per IS 1893 part IV (2005) have been recommended in IS 4998 for aseismic design.

Minimum requirements of design

Both CICIND and IS 4998 is almost identical regarding the minimum requirements of reinforcement. The minimum vertical reinforcement shall be 0.25 percent for deformed bars and 0.3 percent of concrete area under consideration for mild steel bars. Both codes specifythat the minimum diameter of bar shall not be less than 12mm and maximum centre to centre distance of reinforcement shall not exceed 300mm.
There is a slight difference in the provisions of horizontal reinforcement. As perIS 4998, the minimum reinforcement shall not be less than 0.2 percent for deformed bars and 0.25 percent for mild steel bars. But in CICIND, the minimum reinforcement should not be less than 0.1 percent. Also CICIND specifies that the bar diameter should not be less than 8mm.

As per CICIND, the maximum spacing of horizontal reinforcement should not exceed lesser of

(i) Wall thickness(ii) 10 times diameter of vertical reinforcement and (iii) 300mm.
Whereas in IS 4998, the spacing of bars shall not be more than 300 mm or shell thickness whichever is less.
Apart from this, CICIND also specifies that the minimum reinforcement should be distributed over a distance of 0.2 diameter or 2.5m whichever is greater, below the top of the shell if the shell top is not stiffened by concrete roof slab. IS 4998 specifies the minimum shell thickness to be 250mm while in CICIND the minimum thickness is 200mm.

DESIGN RESULTS FOR275m TALL CHIMNEY

Geometry of Wind Shield

The reinforced concrete Shell of wind shield starts from 1.5 m below finished ground level and extends for a height of 271.5 m. the outer diameter of the chimney tapers from 26 m at the base (-1.5 m) to 18.8 m at 150 m level. The outer diameter is maintained as 18.8 m from 150 m to 271.5 m level. The thickness of shell is 900 mm from base to 35 m level from where is reduces to 400 mm at150 m level. The thickness remains constant as 400 mm above this height.

Wind load

The intensity of wind at various heightsare calculated based on IS 875-3, 2003.Basic wind speed consideredis 39 m/s.The wind load calculation for chimney is done as per IS 4998 based on simplified method and tabulated in Table 1.

Design results

The design of reinforced concrete shell for the above chimney based on limit state method given in latest IS 4998 and CICIND are tabulated in Table 2. Factor of safety for wind load is 1.4 and for dead load is 0.9 (worst load case) for both cases as recommended.It has been found that minimum reinforcement (0.25%) is

adequate for the chimney height 200m and above.

Table 1. Design Loads at different elevations

Elevation (m)	Axial load (kN)	Bending moment (kNm)
0	237396.4	2902306.09
5	228628	2827747.57
10	221579.6	2753463.94
15	214602.1	2679388.88
25	204558.9	2531547.01
55	160613.2	2092366.17
105	102251.2	1396660.95
155	64998	787099.97
205	38998.8	304220.18
255	12999.6	30257.35

Table 2. Design Results at different elevations

Elevation (m)	thickness (m)	Reinforcement percentage (%)	
		IS 4998	CICIND
0	0.90	0.32	0.29
5	0.90	0.32	0.29
10	0.90	0.32	0.29
15	0.90	0.32	0.29
25	0.90	0.32	0.29
55	0.85	0.28	0.25
105	0.60	0.32	0.25
155	0.40	0.27	0.29
205	0.40	0.01*	0.01*

**provide minimum reinforcement (0.25%).*

CONCLUSIONS

The following conclusions are deduced from this study:

- CICIND utilizes the material strength of concrete a little higher than IS 4998 by extending the strain at failure by 0.003 instead of 0.002 as specified in IS 4998
- Analysis procedure of wind load in CICIND and IS 4998 is almost same. No explicit method for across wind analysis has been published in CICIND, instead they recommend the method by ACI 307-95 which is quite similar to that in IS 4998.
- For earthquake analysis, CICIND makes a critical deviation from all codes by incorporating ductility and performance based design which results in economic sections in the regions of high seismicity.
- The minimum requirements of reinforcements and sectional thickness are almost same in CICIND and IS 4998.
- For a chimney of height 275m considered, it has been found that the design results by CICIND are economical as compared to IS 4998 which is conservative.

REFERENCES

[1]Draft code, BIS, CED 38 (7892) WC April 2013, Draft Indian Standard Code ofPractice for Design of Reinforced Concrete Chimneys Revision of IS 4998(Part 1)

[2] IS: 1893-1984, Criteria for earth quake resistant design of structures, (FourthRevision), BIS, New Delhi.

[3] John L. Wilson(2003), Earthquake response of tall reinforced concrete chimneys, ENGINEERING STRUCTURES, Vol.25, pp. 11-24.

[4]CICIND, Model codefor concrete chimneys (2001), Part A: the shell, second edition, revision 1, International Committee on Industrial Chimneys, Switzerland.

[5]CICIND, Commentaries for the Model code for concrete chimneys (2001), Part A: the shell, second edition, revision 1, International Committee on Industrial Chimneys, Switzerland.

5th International Engineering Symposium - IES 2016
March 2-4, 2016, Kumamoto University, Japan

Dynamic Response of Masonry Infill Panels under Earthquake loading

Deepa Venugopalan [1] and **Katta Venkataramana** [2]

1 *M.Tech Student, Department of Civil Engineering, NITK, Surathkal, Mangalore, 575025, India. email:deepa.venugopalan1@gmail.com*
2 *Professor, Department of Civil Engineering, NITK, Surathkal, Mangalore, 575025, India. email:ven.nitk@gmail.com*

ABSTRACT: Very often the open space in the RC frame system is separated with masonry filler walls constructed between the columns and beams of the main structure. The masonry filler walls are considered to be non-structural elements. When the RC frame with masonry infill is subjected to seismic load, the connection between the frame and the masonry develop interaction forces in the contact zone between them influencing the behaviour of infilled frame. The masonry infill increases the stiffness of the structure.
Finite Element Analysis of RC frame models without and with masonry infill walls with different aspect ratio is carried out in this study using ANSYS software and is validated by comparing the results with the shake table test conducted in Central Power Research Institute, Bangalore. It was concluded that the masonry infill in the RC frame improves its seismic behaviour and that the aspect ratio plays a significant role in the behaviour of the RC frame without and with masonry infill.

Keywords*: Masonry infill, ANSYS, Aspect ratio*

INTRODUCTION

Reinforced concrete frame buildings are the most commonly used type of construction of multi-storeyed buildings throughout the world. Masonry panels are used to build partition and enclose the structure. Masonry is considered as one of the oldest construction materials, which provides excellent insulation, fire resistance and isolation from climatic forces such as heat, sun, wind, rains, extreme cold etc. Masonry is a composite material that consists of masonry units and mortar joints, hence studying its behavior is difficult. Masonry units can be bricks, blocks, ashlars, adobes, irregular stones and others. Mortar can be clay, bitumen, chalk, lime/cement based mortar, glue or others.

When vertical load carrying capacity is considered the presence of masonry in the RC frame has no role, infact it causes additional weight on the structure due to the self-weight and do not contribute to the load bearing capacity. The masonry walls are brittle and weak in tension and are considered to be non structural members. However in case of lateral loading, the masonry infill panels have some role in the load transfer. The connection between the infills and the surrounding frame develops interaction forces in the contact zone.

Due to the presence of masonry infill, the stiffness and the lateral strength of the RC frame increases. The natural frequency of vibration increases and the lateral deflection of building decreases due to the increased stiffness. However, if the placing of infills is not uniform in plan or in elevation of the building the masonry infill panels become a disadvantage. When a storey has relatively lesser infills than adjacent storeys, short column effect occurs, where due to the variation of stiffness in the storeys, the storey with lesser stiffness undergo more deflection

compared to other storeys. If the infills are raised only upto a partial height of the column, short column effect takes place. And when the infills are unsymmetrically located in plan, plan- torsion effect comes into picture.

Influence of Masonry Infills

Murty and Jain (2000) explained that the change of frame mechanism to truss mechanism Infills interfere with the lateral deformations of the RC frame. Separation of frame and infill takes place along one diagonal and a compression strut forms along the other. Thus, infills add lateral stiffness to the building. The structural load transfer mechanism is changed from frame action to predominant truss action. It is schematically shown in Fig.1; the frame columns now experience increased axial forces but with reduced bending moments and shear forces.

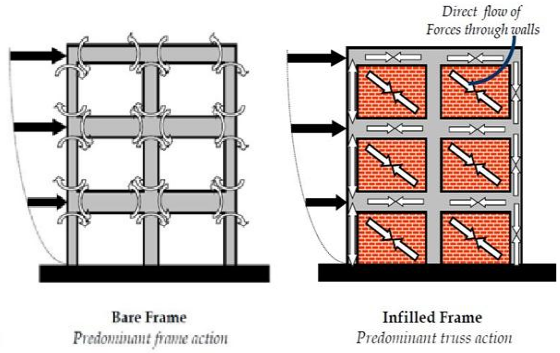

Fig.1 Predominant frame & truss action (Murty and Jain, 2000)

Even when the infills are structurally separated from the RC frame, the separation may not be adequate to prevent the frame from coming in contact with the infills after some lateral displacement; the compression struts may be formed and the stiffness of the building may increase. In a bare frame, inelastic effects in RC frame members and joints cause energy dissipation, while in an infilled frame inelastic effects in infills also contribute to it. Thus, energy dissipation in an infilled frame is higher than that in the bare frame. If both frame and infill are detailed to be ductile, then stiffness degradation and strength deterioration under cyclic loading are nominal. However, if inelastic effects are brittle in nature (*e.g.,* cracking of infill, bond slip failure in frame, or shear failure in frame members), the drop in strength and stiffness under repeated loading may be large. Masonry infill walls are normally subjected to two perpendicular forces i.e., in-plane forces and out-of-plane forces during an earthquake.

Equivalent Diagonal Strut Model

In the case of horizontal loading due to wind or seismic action, it is usual to assume that an equivalent compression strut can replace the action of the masonry panels. The consideration of stiffening effect of infill panel on the frame is often important as it can considerably alter the behavior of building in elastic range. The effect of infill from elastic to inelastic behavior of a building can be quite complex. Its effect can be represented by a diagonal strut having the same thickness as that of the infill panel. Many investigators have proposed various approximations for the width of the equivalent diagonal strut. The width of the strut depends on the length of contact between the wall and the columns, and between wall and the beam. Fig.2 shows the schematic representation of equivalent diagonal strut model.

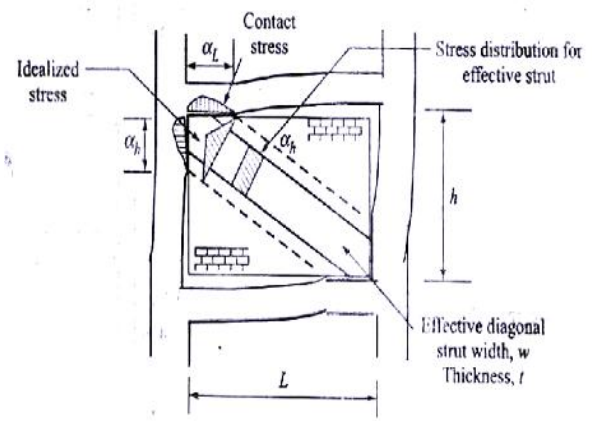

Fig.2 Equivalent Diagonal Strut (Pankaj Agarwal, 2007)

Stafford Smith (1966) developed the formulations for α_h and α_L on the basis of beam on an elastic foundation. The following equations are proposed to determine α_h and α_L, which depend on the

relative stiffness of the frame and infill, and on the geometry of the panel.

$$\alpha_h = \frac{\pi}{2}\sqrt[4]{\frac{4E_f I_c h}{E_m t \sin 2\theta}} \quad \text{..... (1)}$$

$$\alpha_L = \pi\sqrt[4]{\frac{4E_f I_b L}{E_m t \sin 2\theta}} \quad \text{..... (2)}$$

where,
E_m = Elastic modulus of the masonry wall,
E_f = Elastic modulus of the frame material,
t, h, L = Thickness, height, and length of the infill wall, respectively
I_c = Moment of inertia of the column of the frame,
I_b = Moment of inertia of the the beam of the frame,
$\theta = \tan^{-1}(h/L)$
Hendry (1998) has proposed the following equation to determine the equivalent or effective strut width w, where the strut is assumed to be subjected to uniform compressive stress

$$w = 1/2\sqrt{\alpha_h^2 + \alpha_L^2} \quad \text{..... (3)}$$

Modelling
The masonry infill panel can be modelled by any of the following modelling techniques depending on the level of accuracy, simplicity and its application:

a) Detailed micro-modelling
b) Simplified micro-modelling
c) Macro-modelling

In detailed micro-modelling the masonry units and mortar in the joints are represented by continuum elements whereas the unit-mortar interface is represented by discontinuous elements. Young's modulus, Poisson's ratio and other inelastic properties of both unit and mortar are taken into account.

In simplified micro-modelling the units are represented by continuum elements whereas the behaviour of the mortar joints and unit-mortar interface is lumped in discontinuous elements.

In macro-modelling, the units, mortar and unit-mortar interface are smeared out in the continuum.

The third approach does not make a distinction between individual units and joints but treats masonry as a homogeneous anisotropic continuum. This approach cannot be effective in case of masonry infilled panels with openings.

In the present work, detailed micro modelling approach is used and is modelled using ANSYS software.

STUDY DONE
In order to study the effectiveness of the masonry infill in the RC frame, the RC bare frame and the frame with masonry infill was modelled using ANSYS software by micro-modelling and also as equivalent diagonal strut model. For the equivalent diagonal strut model the width of the strut was computed using the formulae by Stafford Smith (1966). Modal analysis was carried out and the results were compared with the shake table test for the models, conducted in Central Power Research Institute, Bangalore to validate the models. The frequencies obtained from the analysis of the frame using ANSYS software were compared with the experimental results.

The models used for study are one bay one storey 2D frame structures with aspect ratio of 0.7, 1.0 and 1.3. The length of beam is 2.4m centre to centre between the columns, and length of the columns are 1.68m, 2.4m, and 3.12m for frames of aspect ratio 0.7, 1.0 and 1.3 respectively. The RC frame cross section is 230mm X 115mm. The brick dimension is 75mm x 115mm x 230mm.

The experimental set up of the shake table test conducted in Central Power Research Institute, Bangalore, on the bare and masonry infilled frame is shown in Fig.3. The ANSYS models of the bare and infilled frames are shown in Fig.4 and Fig.5 respectively.

Elements used in the model
For modelling concrete frame SOLID65 was used. SOLID65 is used for the 3-D modelling of solids with or without reinforcing bars (rebar). The solid is capable of cracking in tension and crushing in compression. The element is defined by

eight nodes having three degrees of freedom at each node: translations in the nodal x, y, and z directions. The most important aspect of this element is the treatment of nonlinear material properties. The concrete is capable of cracking (in three orthogonal directions), crushing, plastic deformation, and creep. The rebar are capable of tension and compression, but not shear. They are also capable of plastic deformation and creep.

The mortar and the brick units are meshed using SOLID 185 element. SOLID185 is used for 3-D modeling of solid structures. It is defined by eight nodes having three degrees of freedom at each node: translations in the nodal x, y, and z directions. The element has plasticity, hyperelasticity, stress stiffening, creep, large deflection, and large strain capabilities. It also has mixed formulation capability for simulating deformations of nearly incompressible elastoplastic materials, and fully incompressible hyperelastic materials.

Modal Analysis

Modal Analysis is the study of the dynamic characteristics of structures. This analysis characterizes the dynamic properties of elastic structures by identifying its modes of vibration. The response of the structure is different at each of the different natural frequencies. These deformation patterns are called mode shapes. Both the natural frequency (which depends on the mass and stiffness distributions in structure) and mode shape are used to design structural systems mainly for vibration applications.

After modelling, meshing and applying the boundary conditions the model is submitted to ANSYS solver. To perform modal analysis there are different mode of extraction methods available in ANSYS, among which Block Lanczos extraction method is used. Five modes were extracted and expanded. Table 1 shows the comparison of the natural frequencies of the RC frame without and with infill walls.

CONCLUSIONS

The following conclusions are deduced from this study:

- Out-of-plane vibration frequency of the RC frame decreases when masonry infill is present.
- As the aspect ratio increases, the frequency decreases for both bare frame and infill frame in out-of-plane and in-plane vibration.

ACKNOWLEDGEMENTS

The results of experiments carried out at CPRI Bangalore were used in this paper for validating the modelling.

REFERENCES

[1] Miha Tomazevic (1999), "*Earthquake Resistant Design of Masonry Buildings*", Imperial College press.

[2] Murthy C.V.R, Sudhir Jain (2000), "Beneficial Influence of Masonry infill walls on seismic performance of RC frame buildings", *12th World Conference on Earthquake Engineering.*

[3] Pankaj Agarwal (2007), "*Earthquake Resistant Design of Structures*", Prentice Hall of India Private Limited.

[4] Stafford- Smith (1966), "Behaviour of Square Infilled Frames", *Journal of the Structural Division*, Proceedings of ASCE, Vol. 91, No. ST1, pp. 381-403

Table 1 Comparison of fundamental frequencies of bare and masonry infill frames (Out- of- plane)

Aspect ratio	Bare frame		Frame with masonry infill		
	Experimental	FE Analysis	Experimental	FE Analysis- detailed micromodelling	FE Analysis- equivalent diagonal strut model
0.7	7.5	7.971	4.00	6.194	6.9537
1.0	4.00	4.9075	2.00	3.754	4.5114
1.3	2.00	3.2557	1.00	2.242	2.9505

Fig.3 Experimental setup of shake table test of bare frame and masonry infilled frame

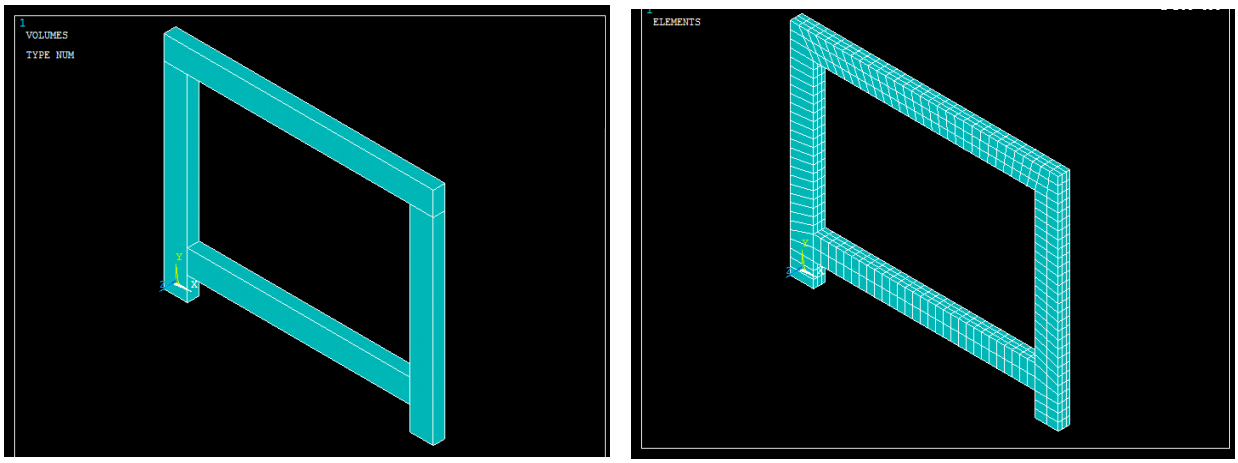

Fig.4 Bare frame modelled in ANSYS before and after meshing (Aspect ratio 0.7)

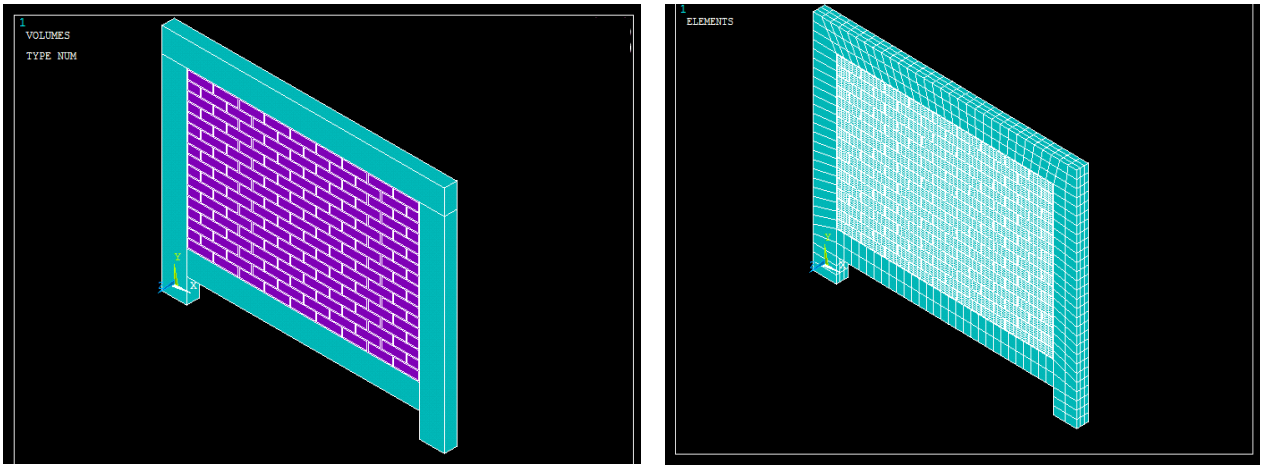

Fig.5 Frame with masonry infill modelled in ANSYS before and after meshing (Aspect ratio 0.7)

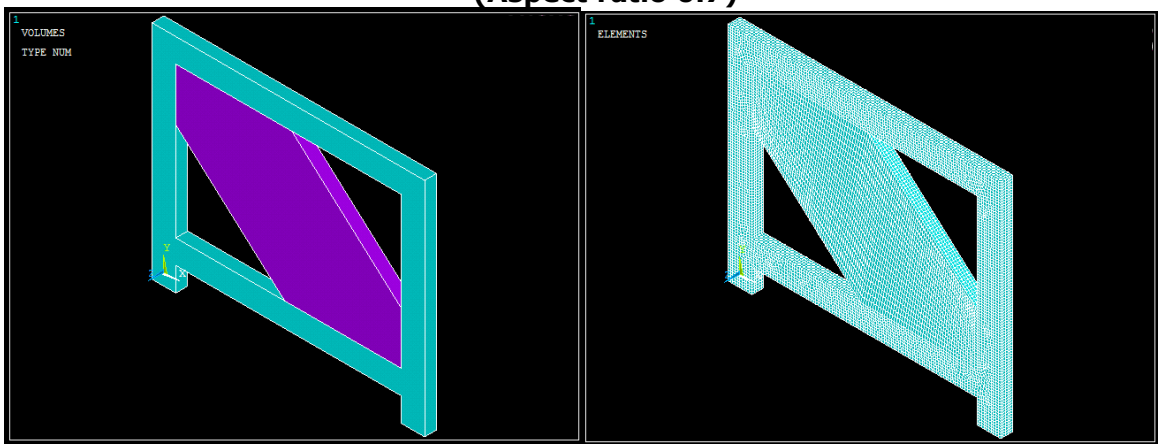

Fig.6 Frame with equivalent diagonal strut modelled in ANSYS before and after meshing (Aspect ratio 0.7)

5th International Engineering Symposium - IES 2016
March 2-4, 2016, Kumamoto University, Japan

Comparative study on the effects of earthquake loads on the structural dimensions of buildings with different heights and aspect ratios

P P Sivan [1], Mithila Bhagavathi M [2], Navas K[3], P V Gouri[3], Radeef K[3] and Sreelakshmi T M[3]

1 *Profesor, Department of Civil Engineering, Govt. Engineering College, Trichur 68009, Kerala, India. e-mail:ppsivan@yahoo.com*
2 *Master Course student, Department of Civil Engineering, National Institute of Technology Karnataka, Surathkal, Mangalore 575025, India. email:mithilabagavathi1993@gmail.com*
3 *Formerly under graduate student, Dept of of Civil Engineering, Govt. Engineering College, Trichur 68009, India*

ABSTRACT: This paper focuses on the effect of different aspect ratios i.e. A/B ratio, where A and B are the base width of the building frame in two directions, on the seismic performance of RC Framed structure. Aspect ratios ranging from 1 to 3 are considered for this study. The various heights chosen are 14.4m (4-storey), 18m (5-storey) and 25.2m (7-storey). Analysis and design are carried out according to Indian Standards in STAAD software. The effect of earthquake forces for different aspect ratios and heights are studied and compared. It is observed that as height of the building increases wind plays major role as compared to earthquake loads. However a similar trend is not seen in the case of beams.

***Keywords**: Aspect Ratio, Natural Frequency, Aisle Width, Storey drift*

INTRODUCTION

Vibration considerations are essential in engineering design and applications. In recent times, as earthquakes, and the destruction caused by them have become more common, it becomes critical for all the buildings to be built earthquake resistant. It is common practice to design buildings subjected to gravity loads and wind loads. The effects of these loads, in terms of bending moments and shear forces, on the members of a structure are well known. This is not the case when an earthquake acts on a building. Earthquake forces, being dynamic in nature, can strike the building from any direction, and hence make it difficult to generalise the effects caused on the structural members of the building. As a result, the sections designed for gravity and wind loads will not be sufficient to withstand an earthquake load.

A unique trait of earthquakes is that the ground motion moves in repeating frequencies. These frequencies are determined by the local geology of the area and can be determined from historical records. Therefore, engineers try to figure out what the frequencies for a particular fault and region are so they can make sure that buildings in those areas do not have natural frequencies that are the same as the earthquakes. If this can be avoided, buildings generally survive the earthquake better and will not have the extreme movement caused by resonance (Chopra A.K 2001).

The effects of an earthquake load on a building depend on the stiffness of the building in the direction of the load. The stiffness of a building defines the resistance to deformation in a particular direction, and it may be related to the building's aspect ratio and height (Xia Hongliu 2008, Kiran Kamath 2014).

Storey Drift is also an important phenomenon in the design of a building. Codes specify limiting values for storey drift. But when an earthquake strikes a building this may get exceeded. Plan dimension of a structure is the key factor for the overall structure lateral rigidity (Wei Lian 2006).

This is a research to find a correlation between the design sections required for an earthquake resistant building design and the aspect ratio or height of a building. Several typical examples are employed to analyze in this paper. The influence of earthquake forces on storey drift of a structure is also studied for all the examples.

The effect of earthquake forces on a building depends upon its natural frequency of vibration, which in turn depends on its dimensions. Thus, it may also be possible to relate the results of this research with the natural frequency of a building.

DESCIPTION OF THE STRUCTURE

In the present study regular Reinforced Concrete Framed structures of aspect ratios ranging from 1 to 3 (1, 1.25, 1.33, 1.5,1.67, 2, 2.33, 3), and heights ranging from 14.4 m to 25.2 m are considered. The storey height is taken as 3.6 m for typical floors and 4m for ground floor. Structural configuration of a four storey structure with aspect ratio 1.67 is shown in Fig 1.

Live load for all the floors are taken as 2.5kN/m^2 and that of roof is 0.75kN/m^2. Floor finish on the floor is 1kN/m^2 and weathering course on roof is 1.8kN/m2. The unit weights of concrete and masonry are taken as 25kN/m3 and 20kN/m^3 respectively. Wind load and seismic load calculations are done based on the respective Indian standard codes, i.e.IS875(Part3) and IS 1893:2002. In the seismic weight calculation only 25% of floor live load is considered. The building is ordinary moment resisting frame considered to be situated in seismic zone III. The medium type of soil is considered. Importance factor is taken as 1. Equivalent Static Method is used for the determination of storey shear. This shear is further distributed to different joints using Eq.1.

$$Qj = \frac{Qi \sum lj}{l} \quad (1)$$

Where Q_j is the design lateral force at joint j of floor i, Σl_j is the sum of aisle width on either side of joint j and *l* is the length of floor i considered in direction of the lateral force. The initial dimensions of the sections are taken arbitrarily for columns and based on deflection criteria for beams.

STUDY ON THE STRUCTURAL RESPONSES OF COLUMNS

Analysis is carried out for models with and without earthquake combination. The corresponding design sections are arrived at. The ratio of these sections is determined in order to compare and find a correlation between these ratios and aspect ratios. Results are tabulated and graphs are plotted between the section ratios and height of the building for constant aspect ratio and also between section ratios and aspect ratios with constant height (Fig 2, Fig 3).

It is observed that generally as the number of storey changes from 4 to 5, the aspect ratio decreases and then increases as the number of storeys becomes 7 for most of the aspect ratios. For a given height of the building, the section ratios do not show significant correlation with the aspect ratios. The section ratios for a 5 storey building are generally lesser, with values closer to 1. The ratios obtained for a 4 storey building are the largest compared to the other 2 storeys. From these observations, it can be inferred that for a 4 storey building, earthquake loads are more predominant than wind loads and as height increases the action of wind becomes significant.

STUDY ON THE STRUCTURAL RESPONSES OF BEAMS

Design of beams is done for combinations with and without seismic loads to arrive at the most economic depth. The corresponding section ratios were formulated. Comparisons are done for constant aspect ratio with different height and vice versa. Graphical representations

of the same are shown in Fig 4 and Fig 5 respectively.
It is seen that there is no significant relationship between the section ratios with respect to aspect ratio or height of the building. This may be because in general beam sections are dependent on the spans of the slabs on either side of the beam and are not affected by the aspect ratio or the number of storey in the building.

STUDY ON THE ASPECT RATIO AND HEIGHT BASED ON STOREY DRIFT

Storey drift is an important parameter in the design of multi-storeyed buildings. The largest story drift is commonly used as the main guidepost of high-rise buildings. A maximum value of H/500, where H is the total height of the building is recommended by the Indian Standard code, IS 456:2000. The storey drift is determined for all the models using STAAD. Comparison of the storey drift with respect to aspect ratio and height of the building are made. It is observed that maximum storey drift was caused due to earthquake loads than wind loads. The influence of wind load is found to increase with the height of the building. Graph showing the variation of storey drift with height and aspect ratio is shown in Fig 6.
It is seen that there is no much variation of storey drift with respect to aspect ratio. However significant variation is observed with respect to height of the building. The average values of storey drift of four storey, five storey and seven storey building are obtained as 4.968m, 5.859m and 7.653cm respectively. The story displacement values are obviously smaller than the limit value (1/500) defined by the code.

STUDY ON THE ASPECT RATIO AND HEIGHT BASED ON MODAL FREQUENCY

Engineers must design a structure such that resonance does not occur during regular operation. This is a major purpose of natural frequency (modal) analysis. Ideally, the first mode has a frequency higher than any potential driving frequency. The correlation of modal frequency with height of the building for various aspect ratios considered is studied. The results are presented in Fig 7.
It can be inferred that for a given height of the building the mode 1 frequency is nearly constant for all the aspect ratios. On an average the frequency is 2.08Hz Hz, 1.893 Hz and 1.4135 Hz for four storey, five storey and seven storey buildings respectively. This frequency can be related to stiffness of the structure. Lower the frequency, lesser is the stiffness value. Here it is seen that as height of the building increases from 14.4 to 25.2m the frequency decreases from 2.08 Hz to 1.4 Hz. This is why tall, slender structures having low stiffness have long return periods and low natural frequencies.

CONCLUSIONS

The following conclusions are deduced from this study:

- Aspect Ratio and height of the building play an important role in the performance of the structure during an earthquake.
- From the first study, it is observed that wind loads play important role in five storey building than other models, resulting in lower section ratios. This concludes that wind has influence in high rise buildings than low rise buildings. But earthquake has significant role even for low rise buildings. So it is important to consider earthquake resistant design even for low rise buildings.
- However in the second study, such a correlation is not established which concludes that beam sections do not depend on the aspect ratio or height of the building. They mainly depend on the span of beams and slabs.
- As the height increases the storey drift increases. But the drift values are constant for a given height of the building. Hence it is concluded that storey drift depends solely on the height of the building and not on the aspect ratios.
- Similarly modal frequency also remains constant with respect to aspect ratio. However it decreases with height of the building which

proves that taller buildings are less stiff than short structures.

- The stiffness the building, therefore, controls how the building will respond to an earthquake.

ACKNOWLEDGEMENTS

The authors are grateful to The Department of Civil Engineering, Government Engineering College, Trichur, Kerala, India for providing necessary facilities required for the present study. Their appreciations extend to The Ministry of Education, Government of India for their support to carry out the research.

REFERENCES

[1] Chopra A.K (2001), Dynamics of Structures: Theory and Applications to Earthquake Engineering. 2nd Edition, Prentice Hall, New Jersey.

[2] Kiran Kamath and Shruthi Grace (2014), Comparative Study on Effect of Aspect Ratio on Performance of Steel Frame Structure with and without infill using Pushover Analysis, *International Journal Of Innovative Research In Electrical, Electronics, Instrumentation And Control Engineering*, Vol. 3, Special Issue 1.

[3] Unikrishna Pillai S, Devdas Menon (2009), Reinforced Concrete Design, Third edition, ISBN 0-07-463331-7.

[4] Wei Lian, Wang Sen. (2006), High-rise Building Story Drift Control. Building Structure , 36, pp 49-55.

[5] Xia Hongliu, Gao Jie (2008), Study on Ihe Limit Value Of Plan Dimension For Frame-Corewall Structures, *The 14th World Conference on Earthquake Engineering*, Beijing, China.

[6] Yasser Alashker et al (2013), Effects of Building Configuration on Seismic Performance of RC Buildings by Pushover Analysis, *Open Journal of Civil Engineering*, 5, pp 203-213.

[7] The Indian Standard IS 456: 2000 "Plain and Reinforced Concrete – Code of Practice (Fourth Revision)", July 2000.

[8] The Indian Standard IS 1893 (PART 1): 2002 "Criteria for Earthquake Resistant Design of Structures, Part 1 General Provisions and Buildings (Fifth Revision)", June 2002.

[9] The Indian Standard IS 875 (PART 3): 1987 "Code of practice for design loads (other than earthquake) for buildings and structures, Part 3 Wind Loads (Second Revision)", November 1988.

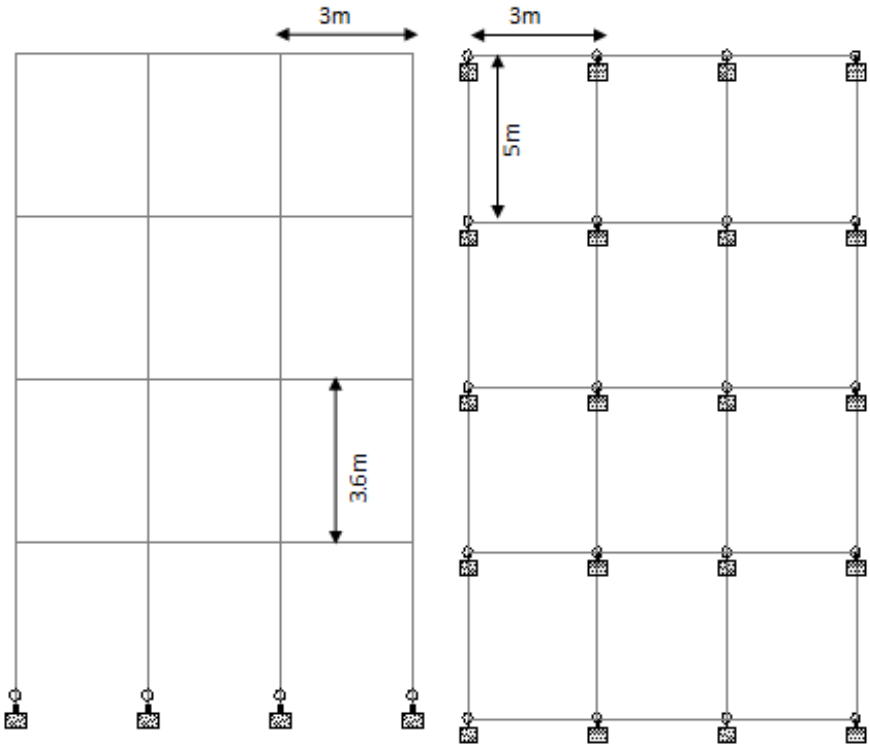

Fig.1 Elevation and plan (typical)

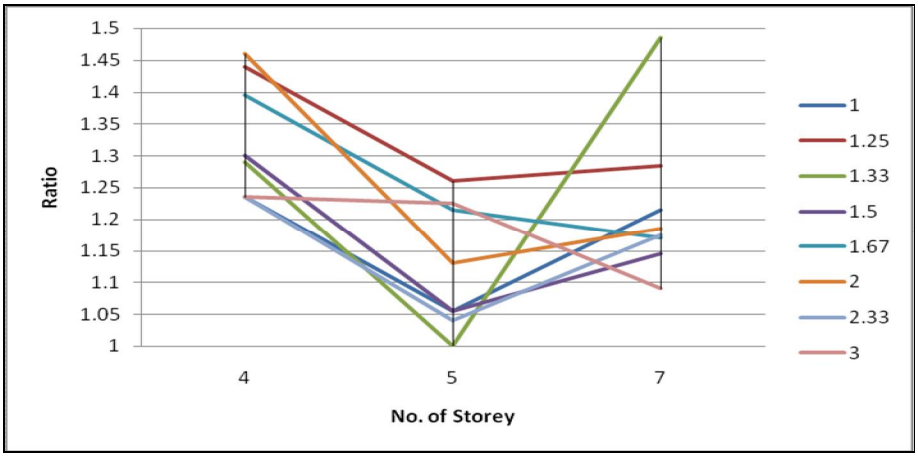

Fig 2 Variation of section ratios with height of the building (columns)

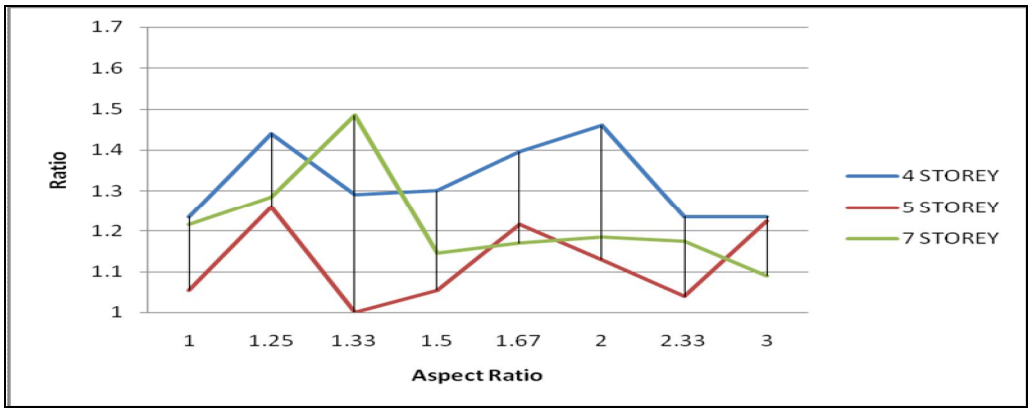

Fig 3 Variation of section ratios with Aspect Ratios (columns)

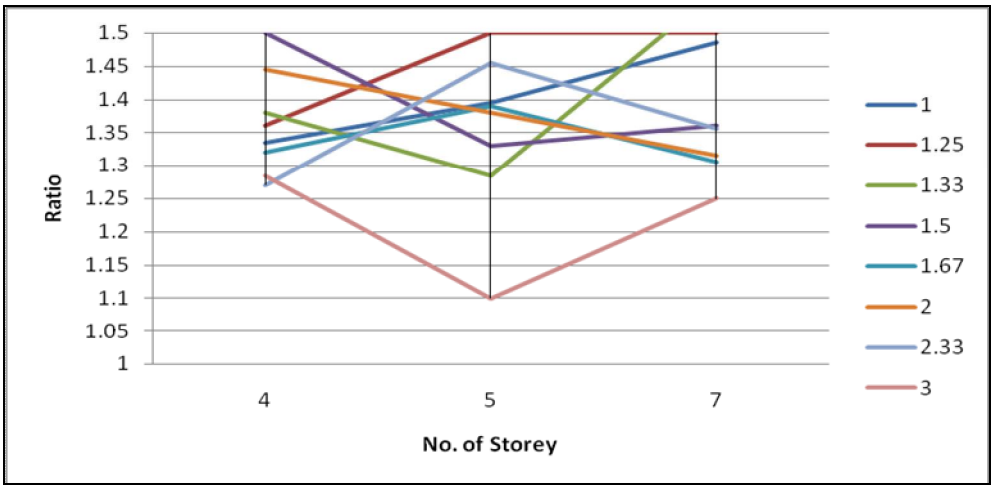

Fig 4 Variation of section ratios with height of the building (beams)

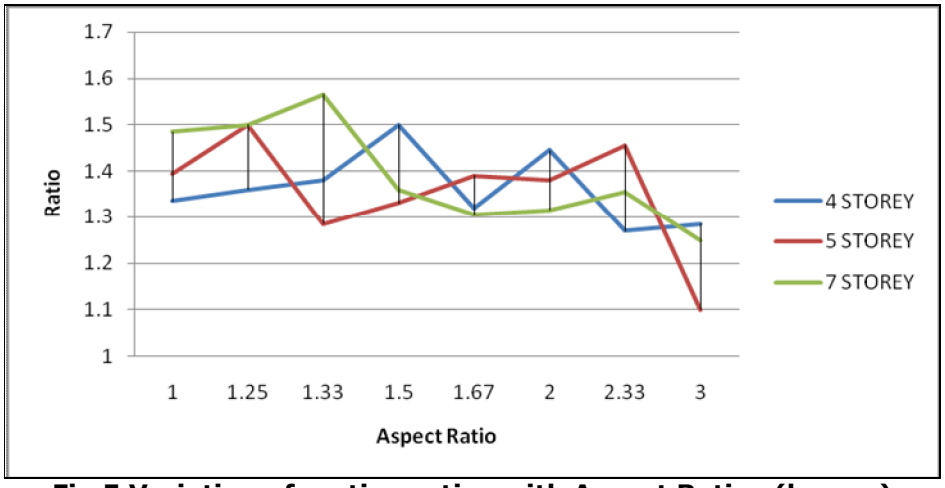

Fig 5 Variation of section ratios with Aspect Ratios (beams)

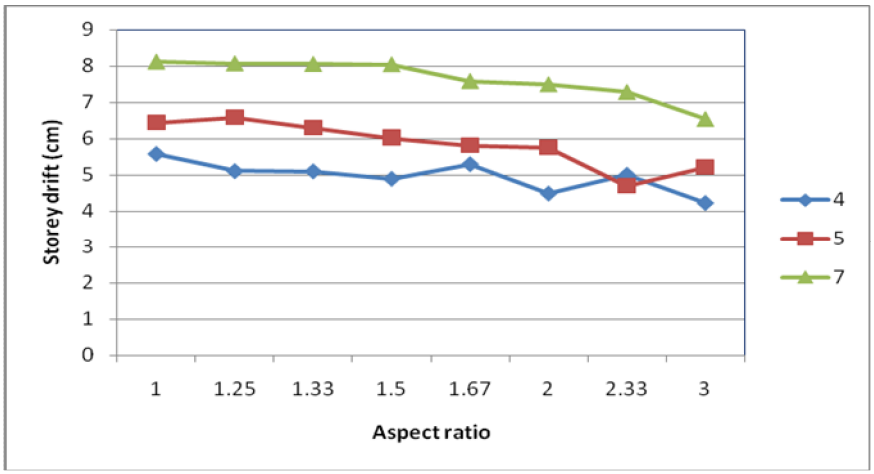

Fig 6 Variation of Storey drift with Aspect Ratios

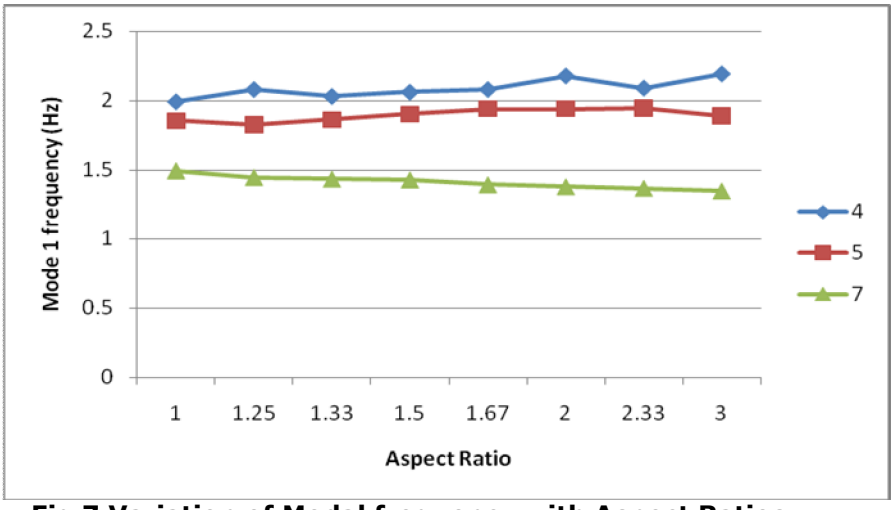

Fig 7 Variation of Modal frequency with Aspect Ratios

5th International Engineering Symposium - IES 2016
March 2-4, 2016, Kumamoto University, Japan

TORSIONAL RESISTANCE OF STRUCTURES WITH STIFFNESS ECCENTRICITY

Aravind R[1] and **B.R.Jayalekshmi[2]**

1 *M.Tech Student, Department of Civil Engineering, NITK, Surathkal, Mangalore 575025, India. email:arvr1991@gmail.com*

2 *Associate Professor, Department of Civil Engineering, NITK, Surathkal, Mangalore 575025, India.email:br.jaya@gmail.com*

ABSTRACT: A building is said to be symmetric if its centre of mass and centre ofrigidity coincides with each other at all floor levels in the same vertical axis. However, in real practice it is seldom the case. Most of the buildings that are constructed nowadays are asymmetric in some ways. This paper deals with the analysis of torsional resistance of structures with stiffness eccentricity when subjected to seismic forces. Non-linear static analysisof a set of RC building models having stiffness eccentricityis carried outto assess their seismic demands to a selected earthquake using SAP software. Torsional response variation based on stiffness eccentricity is evaluated.

Keywords*: Torsional resistance, stiffness eccentricity, seismic forces, pushover analysis, seismic demand.*

Earthquake is one of the most severe natural calamities that have affected the mankind. However, unlike other calamities earthquake doesn't result in the loss of life directly. It occurs through the destruction of natural and man-made structures. Numerous researches are going all over the world for several decades to find out the various types of failures in buildings due to seismic excitations.

Seismic surveys and studies conducted on the modes of failure of buildings during past earthquakes suggests that the most vulnerable buildings are those which are asymmetrical in nature. Studies have also been conducted on the study of both elastic and inelastic behavior of such buildings to find out the possible seismic vulnerabilities.The studies conducted by Chandler (1985), Chopra & Goel (1991), Goel (2001) illustratethat the asymmetry provides a serious threat. However most of these studies have used a simplified idealized model. These idealized models may not actually represent the real life buildings.

Asymmetrical buildings are most unavoidable in modern constructions due to various types of functional and architectural requirements. The lateral torsional coupling due to eccentricities between centre of mass (CM) and centre of rigidity (CR) in an asymmetrical building generates torsional vibrations in the structure even under purely translational ground shaking. During earthquake, inertia force acts through the centre of mass while resistive force acts through the centre of rigidity. Due to this non concurrency in the line of action of forces, a time varying twisting moment is generated which causes torsional vibrations in the structures along with lateral vibrations. Figure 1 shows the graphical representation of the torsional moment in asymmetric structures due to seismic excitations.

The design eccentricity given as per IS code is:

$$e_{di} = \begin{cases} 1.5\, e_{si} + 0.05 \\ b_i e_{si} - 0.05\, b_i \end{cases} \quad (1)$$

whichever of these gives the most severeeffect in the shear of any frame where

e_{di} = Static eccentricity at floor *i*, defined as the distance between centre of mass and centre of rigidity, and

Bi = Floor plan dimension of floor*i*, perpendicular to the direction of force.

From the equation (1) four possible Design Centre of Mass (DCM) locations are obtained in each floor of the building. To satisfy the provisions in the design code,the building has to be analysed multiple times considering all possible combinations of DCM locations. This is a time consuming and cumbersome exercise and not followed correctly in the design offices. To address this problem, behaviour of the structure based on the variation of eccentricity is to be known. This is the principal motivation of the present study.

The objective of this paper is to understand the torsional behavior of asymmetrical buildings having stiffness eccentricities when subjected to seismic forcesand its comparison to the symmetrical buildings. Through this comparison an overview on the torsional resistance of asymmetric structures is to be obtained.

Non-linear static analysisof RC building modelshaving stiffnesseccentricitysubjected to El Centro ground motion is carried out using SAP software.

MODELLING

7–storey and 15–storey RC frame buildings with and without stiffness eccentricity are designed as per IS 456:2000 and considered to study the torsional response variation. The buildings have a uniform storey height of 3m. The cross section of the beams and columns are equal in all frames in all floors (beams andcolumns 300mm x 600mm) for better comparison. The plan and frame dimensions are taken from literature (Kilar, 2001). Asymmetric buildings designed as per IS 456:2000 is used.Four asymmetric buildings with 7–storey and15–storey each are obtained by shifting the CR in the X direction by varying the span of the exterior bay (ASYM1, ASYM2, ASYM3, ASYM4).Figure 2 shows the plan dimensions of all the buildings (SYM, ASYM1, ASYM2, ASYM3, and ASYM4).

The columns are oriented considering the span, symmetry of the structure and major and minor axis of the structure as a whole. The beam–column joints are assumed to be rigid. The foundation is provided at a depth of 2m below the ground level and is considered as a fixed support. The structure is assigned with a constant live load of 5 kN/m^2 on all floors.The asymmetric buildings are obtained by varying the length of one bay in the direction of the earthquake. The stiffness eccentricity is the major parameter used here to compare the response. Load combinations are considered as per IS 456–2010. Torsional response of the corner most ground floor column are also studied.

M25 grade of concrete and Fe 415 grade of steel are used for all the frames. Modulus of elasticity values of all these materials are taken from IS 456:2000. The short term modulus of elasticity (Ec) of concrete is taken as

$$\mathrm{Ec} = 5000\sqrt{\mathrm{fck}}\mathrm{MPa} \qquad (2)$$

where f_{ck} is the characteristic compressive strength of concrete cube in MPa.For steel reinforcement modulus of elasticity (Es) and Yield strength (Fy) are taken as per IS 456:2000.

METHODOLOGY

Modal analysis of the structures gives the fundamental natural frequencies. The five buildings (7–storey and 15–storey) are analysed using modal analysis to find out the fundamental natural period, mass participation ratios and to know the variation in elastic modal properties due to the presence of asymmetry.

Response spectrum analysis is done on the buildings withthe design spectrum for a soft soil (Type III) and a peak ground acceleration of 0.36g (zone V). The

response reduction factor, R is equal to 5 (Special moment resisting frame). The importance factor, I is taken as 1.0. The SRSS method is adopted for the analysis. The acceleration is applied along the UYdirection to have the maximum effect on the structure.

In the implementation of pushover analysis, the buildings accounts for the non–linear behaviour of the structural elements. In the present study, the plastic hinges are assumed to be concentrated at specific points in the structure. Beam and column elements are modelled with flexure (M3 for beams and P-M2-M3 for columns) hinges at possible plastic regions under lateral load (*i.e.* both ends of the beams and columns). These flexural hinges are defined using FEMA 356 table 6–7 for concrete beams and table 6–8 for concrete columns. The properties of flexural hinges simulate the actual response of RC components under lateral loads. The dead load case is assigned as non–linear so that it can be used as the starting point for the pushover analysis. The pushover load is designed to continue from the dead load case. The load is applied as an acceleration in the UY direction. Here displacement control is used and a monitored displacement based on the permissible storey drift is considered. The analysis is done on multiple states to identify the propagation of hinges along the structure.

The Resultant base shear versus monitored displacement curve is plotted once the pushover analysis is done.

RESULTS AND DISCUSSIONS

This paper deals with the analysis of torsional resistance of structures having stiffness eccentricity when subjected to seismic forces.Response spectrum analysis andNon-linear static analysis are done using the software SAP on a set of RC building models having stiffness eccentricity, to find out their seismic demands to selected earthquake. Torsional response based on stiffness eccentricity is evaluated.

Table 1 shows the variation of roof deflection among the different buildings. The roof deflection is maximum for the ASYM4 in both 7 and 15 storey buildings. The roof deflection increases with increase in eccentricity.

Table 2 presents the fundamental natural period and the corresponding participating mass ratios of the buildings. Table 2 shows that the natural period of symmetrical buildings are lower than the asymmetrical buildings. ASYM4 shows the highest natural period making it the most flexible building configuration.

Table 3 shows variation in base shear for the buildings based on the eccentricity ratios (eccentricity/plan length). As the eccentricity ratio increases considerable variation of base shear occurs on the buildings. However as eccentricity ratio increases, percentage of base shearwith building weight decreases.

Figures 3(a) and 3(b) represent the base shear Vsroof displacement curves for the 15–storey and 7-storey buildings respectively. The asymmetrical buildings show higher base shear for the same monitored displacements.

CONCLUSIONS

The following conclusions are deduced from this study:

- The maximum roof displacement responses of the five buildings have considerable amount of variation subjected to the generated earthquake ground motion. The roof displacement responses for symmetric building is found to be lesser compared to the asymmetric buildings for all the cases studied here.
- There is considerable variation in the base shear for the buildings as the eccentricity ratio increases. However as eccentricity ratio increases, percentage of base shear with building weight decreases.
- The asymmetrical building ASYM4 shows the highest base shear for both 7-storey and 15-storey.

REFERENCES

[1] Chandler, A. M.,(1986). Building Damage in Mexico City Earthquake, *Nature*, 320(6062), 497-501

[2] Chopra, A. K. and Goel, R. K.,(1991). Evaluation of Torsional Provisions in Seismic Codes, Journal of Structural Engineering, ASCE, 117(12), 3762-3782.

[3] Goel, R. K.,(2001). Performance of building during the January 26, 2001 Bhuj earthquake. *EERI Special Earthquake Report in Earthquake in Gujarat*, India.

[4] Kilar, V.,(2001).Seismic response of asymmetric frame building designed accordingto euro codes. *Proceeding of the first international structural engineering and construction conference*, Honolulu, Hawaii, 681-686.

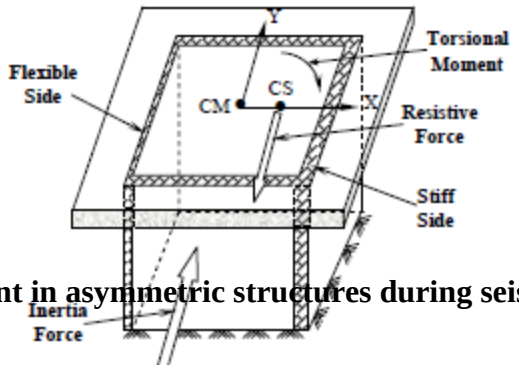

Figure 1 : Torsional moment in asymmetric structures during seismic excitations

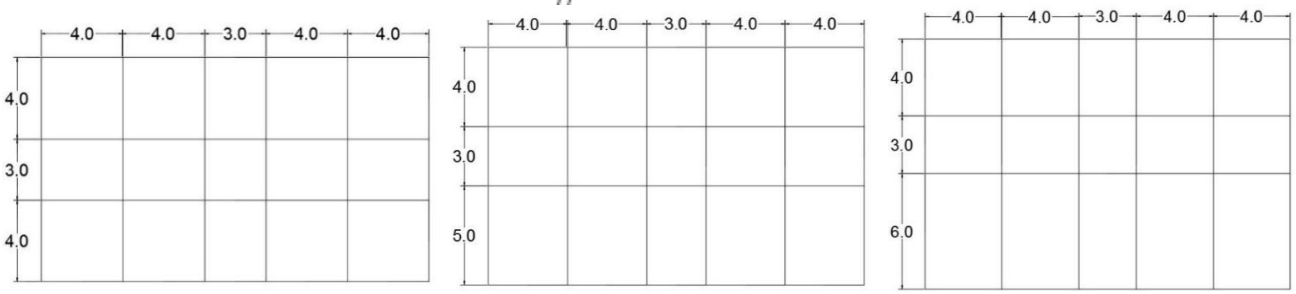

SYM ASYM1 ASYM2

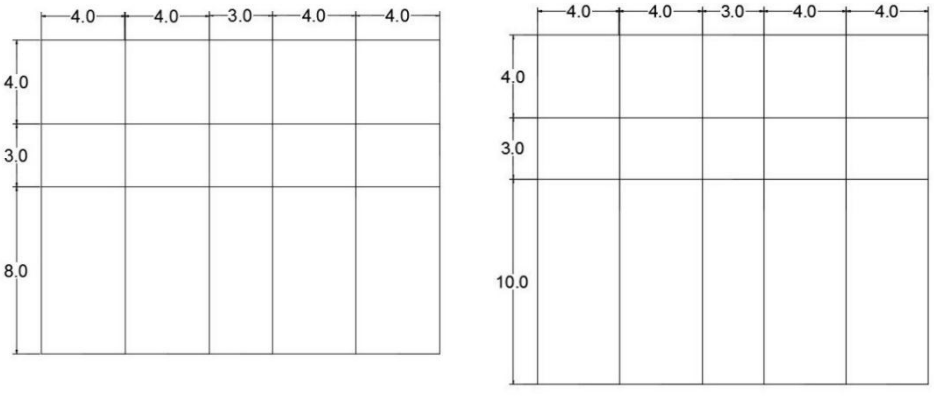

ASYM3 ASYM4

Figure 2: Plan Dimensions (in metres)

Table 1: Roof deflection

Model	Roof deflection (m)	
	7 Storey	15 Storey
SYM	0.0156	0.0435
ASYM1	0.0174	0.0478
ASYM2	0.0193	0.0527
ASYM3	0.0224	0.0628
ASYM4	0.0244	0.0731

Model	7 Storey		15 Storey	
	T(s)	UX (%)	T(s)	UX (%)
SYM	0.832	78.72	1.755	78.666
ASYM1	0.855	78.67	1.809	78.622
ASYM2	0.879	78.53	1.852	78.48
ASYM3	0.926	77.84	1.952	77.79
ASYM4	0.975	76.55	2.054	76.43

Table 2: Fundamental natural period

Table 3: Base shear

Model	Eccentricity Ratio (e/b)	7 Storey		15 Storey	
		Base shear (kN)	% of weight	Base Shear (kN)	% of weight
SYM	0	1228.19	7.22	1204.14	3.4
ASYM1	0.09	1270.44	7.03	1242.18	3.32
ASYM2	0.19	1308.99	6.84	1285.45	3.24
ASYM3	0.04	1381.59	6.49	1358.02	3.08
ASYM4	0.06	1444.21	6.16	1421.51	2.92

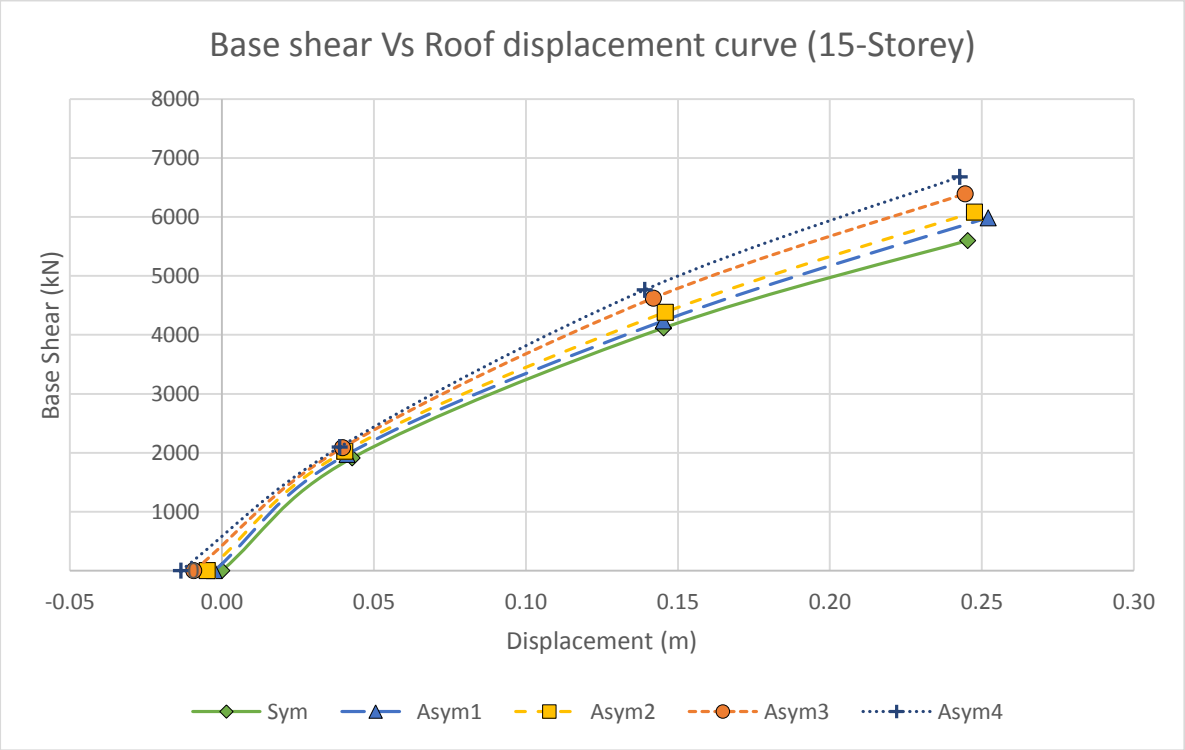

Figure 3(a): Baseshear Vs Roof displacement curvefor 15-storey

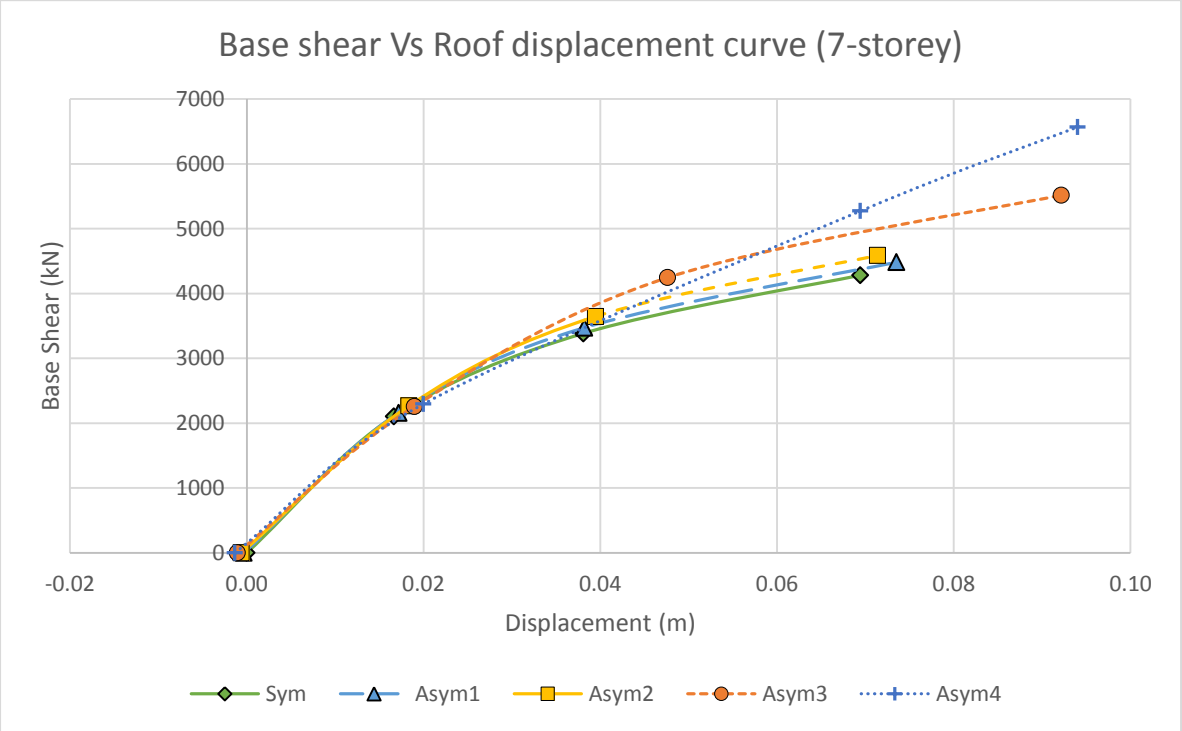

Figure 3(b): Base shear Vs Roof displacement curve for 7-storey

5th International Engineering Symposium - IES 2016
March 2-4, 2016, Kumamoto University, Japan

Seismic Response of Asymmetric Structures

R Eswar Reddy and **Katta Venkataramana**

Department of Civil Engineering, National Institute of Technology Karnataka, Surathkal, Mangalore 575025, India. email:reswar10@gmail.com

ABSTRACT: The seismic response of base-isolated structures, when eccentricities are set in the superstructure is presented. Linear dynamic analyses were used to study peak responses for different ratios of static eccentricities between the center of mass and the center of rigidity for the superstructure. The analysis of a typical 4 storeyed building is done using SAP2000. Unidirectional and bidirectional actions of selected ground were used in the study. The time history analysis has been carried out for the 1940 El Centro earthquake data. Peak dynamic response i.e., maximum isolator displacements were studied and compared to the ones obtained for symmetric systems of reference for the different ground motions under consideration, assessing the importance of the relative value of e_s on those response quantities.

***Keywords**: seismic response, asymmetry, stiffness, torsion, base isolation*

INTRODUCTION

Buildings with an asymmetric distribution of stiffness and strength in plan undergo coupled lateral and torsional motions during earthquakes. In many buildings the centre of resistance does not coincide with the centre of mass. The stiffness characteristics control the dynamic response of the building structure. The choice of the stiffness characteristics of structures is a crucial step in the theoretical design phase. The good behaviour of the structure can be provided with a well distributed lateral load resisting system.

Asymmetry in a structure produces torsional effects that are sometimes difficult to assess, and can be very dangerous. The preferred method of minimizing torsional effects is to select floor plans that are regular or symmetric and reasonably compact. The behaviour of buildings during earthquakes will be satisfactory only if all measures are taken to provide a favourable failure mechanism. A special account must be taken so that torsional effects do not endanger or preclude the global ductile behaviour of the structure. Buildings with an asymmetric distribution of stiffness and strength in plan undergo coupled lateral and torsional motions during earthquakes. Because of torsion, the seismic requirements of asymmetric buildings increase beyond those required by just translational or lateral deformation. An important aspect of the inelastic behaviour of asymmetric structures is the considerations of the degree of control over inelastic twist. One of the design aims should be to restrain the system against unrestricted inelastic twist. In the structures, which remain elastic during an earthquake, torsional vibrations may cause significant additional displacements and forces in the lateral load resisting elements. However, the design of the majority of buildings relies on inelastic response. In such situations, the torsional motion leads to additional displacement and ductility demands.

Torsion has been the cause of major damage to buildings subjected to strong earthquakes, ranging from visible distortion of the structure to structural collapse. In many past earthquakes this kind of collapse has occurred. Torsion occurs under the action of seismic forces

when the center of mass of a building does not coincide with its center of rigidity.

Some of the situations that can give rise to this situation in the building plan are positioning the stiff elements asymmetrically with respect to the center of gravity of the story i.e., the placement of large masses asymmetrically with respect to stiffness. A combination of mass as well as stiffness distribution results in the situations described above. It should be kept in mind that the infills attached to the panel are usually very stiff and, therefore, participate in the structural response to an earthquake and can cause torsion. The building rotates about its center of rigidity. This causes large increase in the lateral forces and displacement demands in lateral load resisting elements, in proportion to their distance from the center of rotation. The conventional analysis for torsion simply gives the force due to moment produced by an eccentric static force. It takes no account of the torsional vibrations and the associated accelerations. Under study, an eccentricity between the centers of mass and stiffness is considered significant when it exceeds 10% of the horizontal plan dimensions. In such cases, accurate measures should be taken in the structural design of the building.

Torsion may become even more complicated when there are vertical irregularities, such as setbacks. In effect, the upper part of the building transmits an eccentric shear to the lower part, which causes downward torsion of the transition level regardless of the structural symmetry or asymmetry of the upper and lower floors. Non symmetric or torsionally unbalanced buildings are prone to seismic damage due to coupled lateral and torsional movements producing non-uniform displacement demands in building elements and concentrations of stresses and forces on structural members. Current codes fall short of providing recommendations for irregular structures. Thus, there is an apparent need to develop a simple analysis procedure based on rigorous analytical and experimental information on the inelastic seismic response of irregular structures.

PROBLEMS WITH ASYMMETRY

i. Differential settlement
ii. Liquefaction
iii. Unexpected stresses due to torsion

Differential settlement is mainly caused to the structures which are asymmetric in nature because for their mass or stiffness distributions. Such structures are supposed to be settled differentially, which in turn lead to liquefaction of the soil in the sub-structure.

Due to torsional effect induced in the structure, some unexpected stresses get induced in the structural elements which lead to some dangerous consequences like stress reversals or magnifying the stresses beyond the allowable limits. This leads to the collapse of structure either partially or completely, depending on the load distribution path.

SOLUTION

i. Tie beams
ii. Raft foundation
iii. Base isolation

A typical muti-storeyed building is considered with details as mentioned in Table 1.

The number of modelled structures is three. Among which, one is symmetric in plan (i.e., model 1 with zero eccentricity (e1) as shown in Fig.1) and the other two are asymmetric in their plan (with eccentricities e1 and e2 for model 2 and model 3 respectively). These two asymmetric models are shown in Fig.2 and Fig.3. The eccentricities (e) of the models are increased by shifting their bays towards one side. Thus e1<e2<e3.

LOADS CONSIDERED

The primary loads which were considered for the analysis are:

a) Self-weight of the structure
b) A live load of 2 kN/m^2 as per IS 875-part II

1940 El Centro (Imperial Valley irrigation district) earthquake time history data with

peak acceleration is applied in both X-direction and Y-direction. The peak acceleration is 0.3186 m/sec2 at 2.0185 sec. The acceleration curve is shown in the Fig.4

To design the base isolator, the structure that gives the maximum support reaction must be considered. In this case, the third structure shown in Fig.3 would give the maximum vertical support reaction which is equivalent to 1542 kN. For that support reaction, a lead rubber bearing (LBR) isolator is designed using UBC (1997) provisions and that bearing is incorporated to all the supports of all the three structures considered.

DESIGN OF BASE ISOLATOR STIFFNESS

The design of the isolator is carried out to just obtain the effective stiffness of the bearing as below:

Load coming on each bearing from SAP2000, W_i = 1552 kN

Maximum admissible stress on LRBs = 15 MPa

To determine the diameter of the bearing:

Area required,

$$A = \frac{1542 \times 10^3}{15 \times 10^6} = 0.1028\ \text{m}^2$$

Therefore the minimum diameter,

$$D = \sqrt{\frac{0.1028 \times 4}{\pi}} = 0.362\ \text{m}$$

Say, D = 400 mm

Target Period, T_{eff} = 2 sec

Assuming Damping ratio, β = 0.15

Design Displacement,

$$d_{bd} = \frac{\left({}^{g}/_{(4 \times \pi^2)}\right) C_{VD} T_{eff}}{B_D} \quad (1)$$

Where,

C_{VD} = Seismic co-efficient (as per UBC Table 16-R)

Therefore, for assumed zone III and stiff soil type,

C_{VD} = 0.54

B_D = numerical co-efficient related to the effective damping of the isolation system at the design displacement (as per UBC Table A-16-C)

= 1.35

$$d_{bd} = \frac{\left({}^{9.81}/_{(4 \times \pi^2)}\right) 0.54 \times 2}{1.35} = 0.199\ \text{m}$$

Therefore, the effective stiffness

$$K_{eff} = \left(\frac{2 \times \pi}{T_{eff}}\right)^2 \frac{w_i}{g} \quad (2)$$

$$K_{eff} = \left(\frac{2 \times \pi}{2}\right)^2 \frac{1542}{9.81} = 1551.4\ \text{kN/m}$$

Thus, this effective stiffness is used for the base isolator while analysing the structures in SAP2000. After performing further design, the obtained thickness of the base isolator is

t_r = 300mm

So, in order to compare the results of all the three models, specific nodes were considered which are in common with all models. Those nodes are node number 324 and node number 353 as shown in the Fig.1, Fig.2 and Fig.3

CONCLUSIONS

The following conclusions are deduced from this study:

- The obtained peak absolute displacements after performing linear time history analysis were 207mm, 216mm and 220mm for model 1, model 2, model 3 respectively at node 324 after 2.6sec in Y direction.
- The peak relative displacements (i.e., the offset between the corresponding solid and dotted lines of the models) of node 324 with respect to node 353 are 42mm, 48mm, 49mm for model 1, model 2, model 3 respectively.
- It is observed that the nodal displacements (in both X and Y directions i.e., U1, U2 respectively) of the nodes, farther from the centre of rigidity are comparatively higher than those nearer to the centre of rigidity. Whereas, in this paper, the nodal displacements in only Y direction were compared.
- Because of providing the base isolators, the relative displacements are almost equal, as they reduce the seismic force transferred to the super structure.

REFERENCES

[1] Uniform Building Code (1997), Structural Design Requirements, Volume 2.
[2] IS 1893 (2002), Criteria for Earthquake Resistant Design of Structures, Part I
[3] IS 875 (1987), Code of Practice for Design Loads for Buildings and Structures, Part II

Table 1 Details of Structure

Element	Property	Value
Beams	Dimension	0.3mx0.6m
Columns	Dimension	0.5mx0.5m
Slab (floors)	Thickness	0.25m
Slab (roofs)	Thickness	0.15m
Shear walls	Thickness	0.25m
Bays	Width	6m
Storey	Height	3m

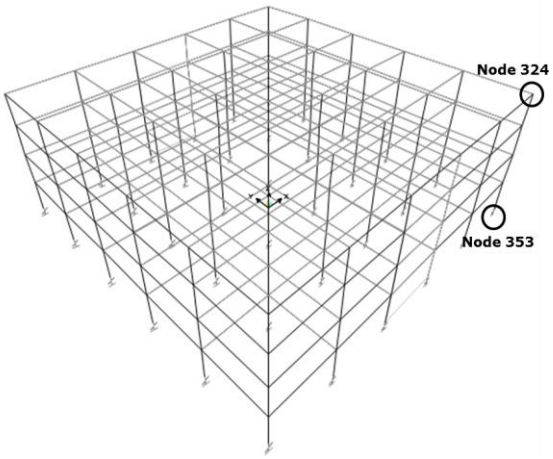

Fig.1 Model 1
(Symmetric structure with e1 = 0)

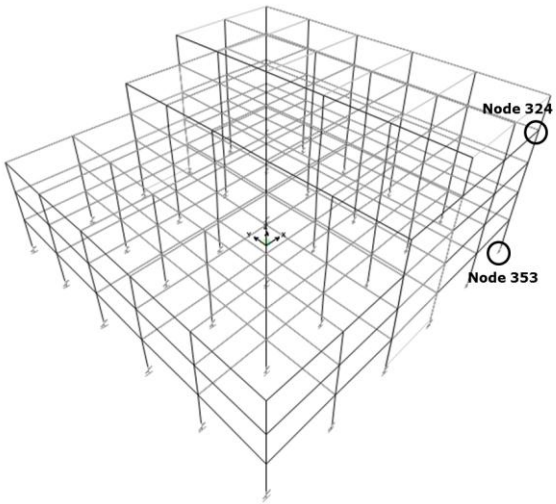

Fig.2 Model 2
(Asymmetric structure with e2 > e1)

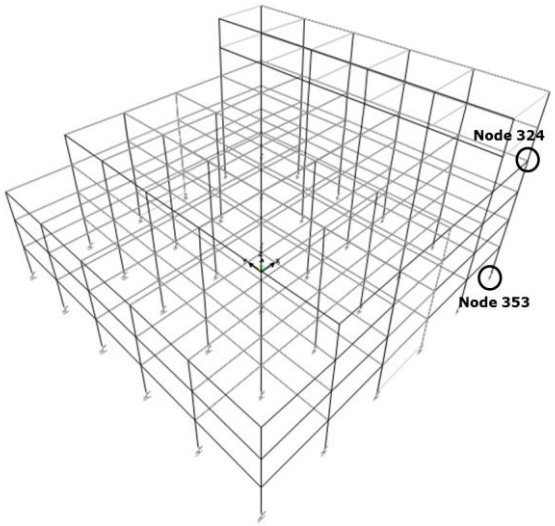

Fig.3 Model 3
(Asymmetric structure with e3 > e2)

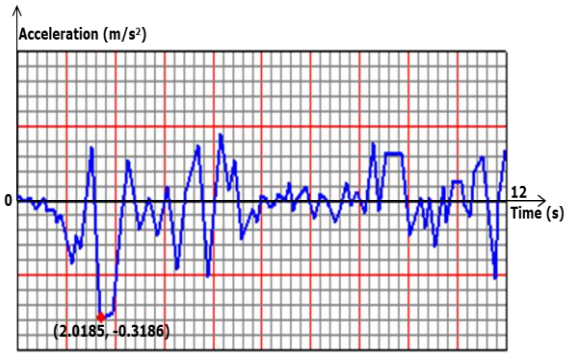

Fig.4 El Centro earthquake data

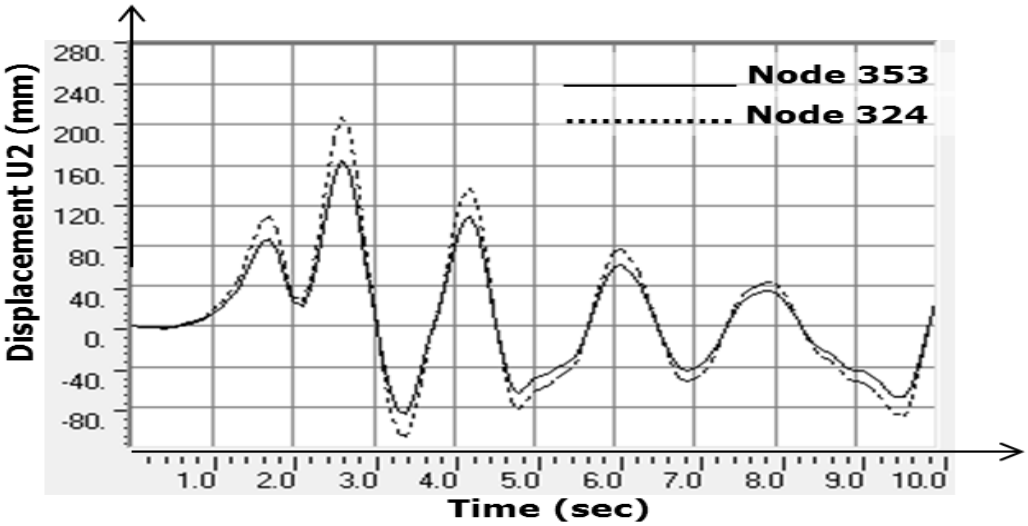

Fig.5 Displacement function for model 1

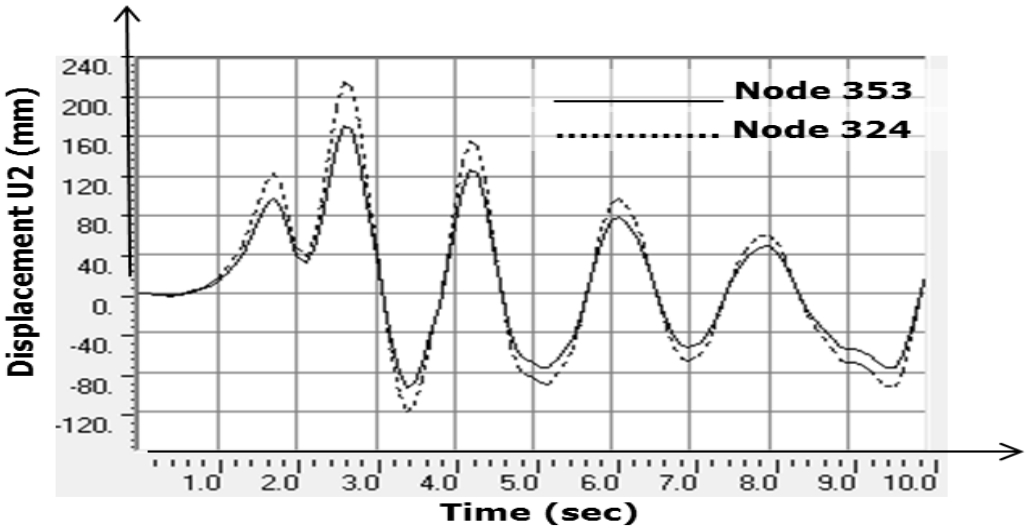

Fig.6 Displacement function for model 2

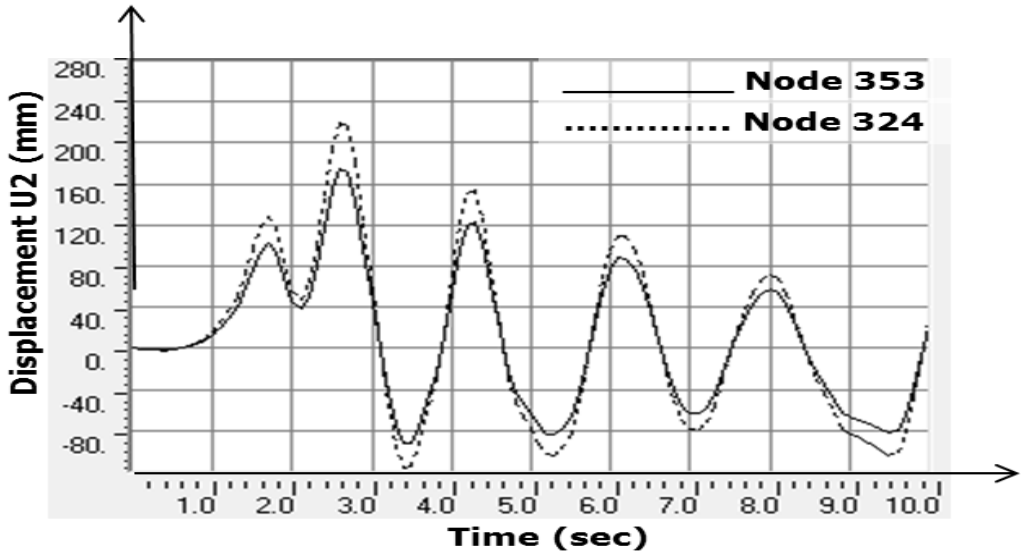

Fig.7 Displacement function for model 3

5th International Engineering Symposium - IES 2016
March 2-4, 2016, Kumamoto University, Japan

SOIL-STRUCTURE INTERACTION ANALYSIS OF CONICAL SHELL FOUNDATIONS

Vipin T K [1] and **B R Jayalekshmi** [2]

1 *M.Tech Student, Department of Civil Engineering, National Institute of Technology Karnataka, Surathkal, Mangalore 575025, India. email:vipintk13@gmail.com*
2 *Associate Professor, Department of Civil Engineering, National Institute of Technology Karnataka, Surathkal, Mangalore 575025, India. email:br.jaya@gmail.com*

ABSTRACT: Shell foundations are in general economic alternatives to plain shallow foundations in situations involving heavy super structural load transfer to weak soils. An upright cone in its larger form can serve as rafts for tower-shaped structures such as chimney shafts. This study focus on the comparison of finite element analysis of conical shells with available experimental results.
The two components of the interacting system; the soil and the shell foundation, are modelled using the finite element method. The soil-structure interaction between the foundation and the supporting soil medium are modelled using interface elements. Comparison between the results obtained is made with the results of tests done on the conical shell foundations. The investigation shows that the experiment results are mostly on the higher side when compared to the FEM analysis.

Keywords*: Shell foundations, conical shell, finite element, interface element.*

INTRODUCTION

Even though shells have wide and varied use as roof structures, they are newcomers to the family of structural foundations. The twin attributes of a shell which are recommended in roofs are economy and aesthetics. Since the latter aspect is of no concern in the case of a buried structure such as the foundation, it is the aspect of economy which holds the key to the acceptance and use of shells as economic alternatives to the conventional plain foundations. For foundations involving heavy column loads to be transmitted to weaker soils shells are economic alternatives to plain foundations. The economy with shells tends to increase with increasing column loads and decreasing bearing pressure of the soil.

Conical shell foundations are the simplest form in which a shell can be put to use in foundations. The provision of radial and circumferential reinforcement is as simple as for a circular flat footing, while the construction is probably only a little more difficult. Cones with larger dimensions can also serve as foundations for tall structures like chimney shafts, in place of the conventional circular or octagonal rafts.

An optimum design of a shell footing is one in which both the footing and the supporting soil fail simultaneously. However a better design would be one where the same fraction of the ultimate capacity of the optimum system is utilized in either component, at the working load [1]. Shell footing had a better load carrying capacity compared with the flat footing for a similar cross sectional area. Edge beams at the bottom of the shell footings increase the load carrying capacity [2].The load-settlement character of conical shell footing also improve with decrease in half–shell angle. The conical shell footing takes nearly 80% of the theoretical failure load obtained from membrane analysis [3].

An experimental investigation on conical shell foundation was conducted by Kurian

and Dierks [4]. The present study is an attempt to compare the response in shell foundation subjected to unit load obtained from available experimental results with those from finite element analysis.

METHODOLOGY

Experimental Setup

The experiment was conducted on elastic model of a conical shell footing in Berlin by Kurian and Dierks [4]. The dimensions of the model are given in Fig.1. The test was conducted on the model by loading it centrally with 1 kN load in the upright position. The material used for conical shell model had the following properties.

Young's modulus = 3000 N/mm^2
Poisson's ratio = 0.34

The tests were conducted on the conical shell foundation resting on a soil medium of moist sand compacted to a density of 19.11kN/m^3 in a cylindrical tank.

To conduct the present study, the conical shell footing used for the test conducted by Kurian and Dierks [4] was analysed using ANSYS software.

Finite Element Analysis

The conical shell foundation was modelled using ANSYS software and elastic continuum analysis was done. A vertical concentrated load 'P' of 1kN was applied at the top of the conical shell foundation model (Fig.1). FEM Analysis of the conical shell foundation considering fixed base and a compliant base of moist sand below the foundation was carried out. The results obtained were compared and plotted as graphs.

SHELL63 element was used for modelling the conical shell. SHELL63 element has both bending and membrane capabilities. Both in-plane and normal loads are permitted. The element has six degrees of freedom at each node: translations and rotations in the nodal x, y, and z directions. The soil was assumed to be elastic, homogeneous and isotropic. It was modelled using SOLID45 element. SOLID45 is used for the 3-D modeling of the soil. The element is defined by eight nodes having three degrees of freedom at each node: translations in the nodal x, y, and z directions. The soil was assigned with the following properties.

Young's modulus = 421.1 N/mm^2
Poisson's ratio = 0.35

The finite element models of conical shell foundation with fixed base and compliant soil base are shown in Fig.2

RESULTS AND DISCUSSION

The results obtained from the study are compared and plotted as shown in the Figs 3-6. The results obtained from the FEM analysis are similar to the available experimental result at the bottom half of the foundation. The resultant stresses Ns, N_θ obtained from FEM analysis vary 60-80% with the available experimental results at the top portion of the conical shell foundation. The moments Ms, M_θ obtained also differed by 50-60% at the top portion of the foundation. The soil-structure interaction caused variations of 20-30% from the response of fixed base model. Structural response in conical shell with fixed base is more than that with the compliant base except for the case of Ms.

CONCLUSIONS

The following are the conclusions of this study:

- The results of FEM analysis show close agreement with the available experiment results. But the FEM analysis results are conservative with higher values of resultant moments and stresses.
- Compared to fixed base model, the analysis considering the soil-structure interaction shows lower values of structural responses.

REFERENCES

[1] Nainan P.K, Varghese P.C. (1969), Discussion on Design & Testing of Cone and Hypar footings, Journal of Soil Mechanics & Foundation Div., Vol. 95, pp.415-416
[2] Al-Azzawi A.A (2013), A Study Behaviour of Shell Footings using FEM Analysis, IGCTE, Vol. 31, Part(A),No. 19.
[3] Ramesh M, Blessy Joy M (2015), Experimental Study on Conical Shell footing, IJERT, ISSN: 2278-0181, Vol. 4, Issue 06.
[4] Kurian N.P, Dierks k (1981), Behaviour of Conical Shell Foundation under Concentric and Eccentric Loads, Vol. 56, No. 2, pp61-65

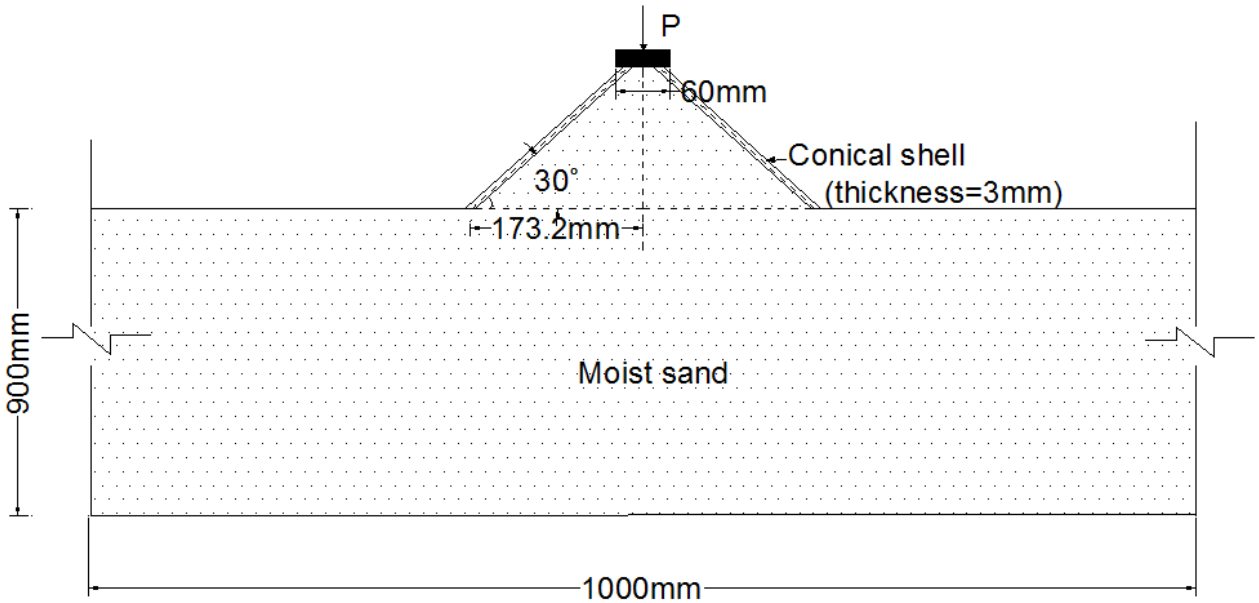

Fig.1 Sectional elevation of conical shell foundation model

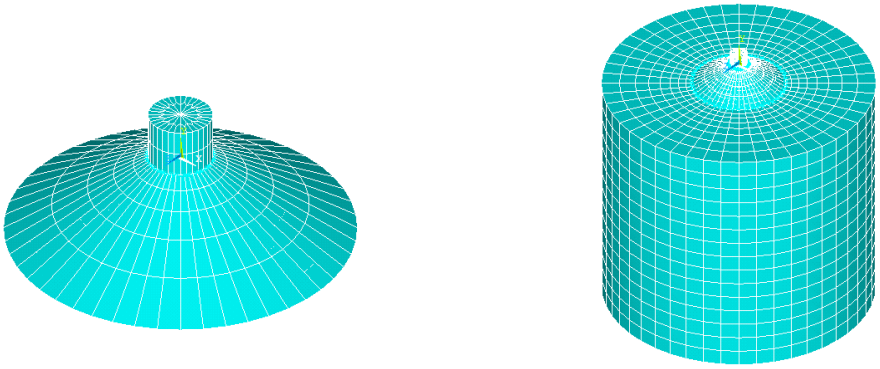

Fixed base ***Compliant base***

Fig.2 Finite element model of conical shell foundation

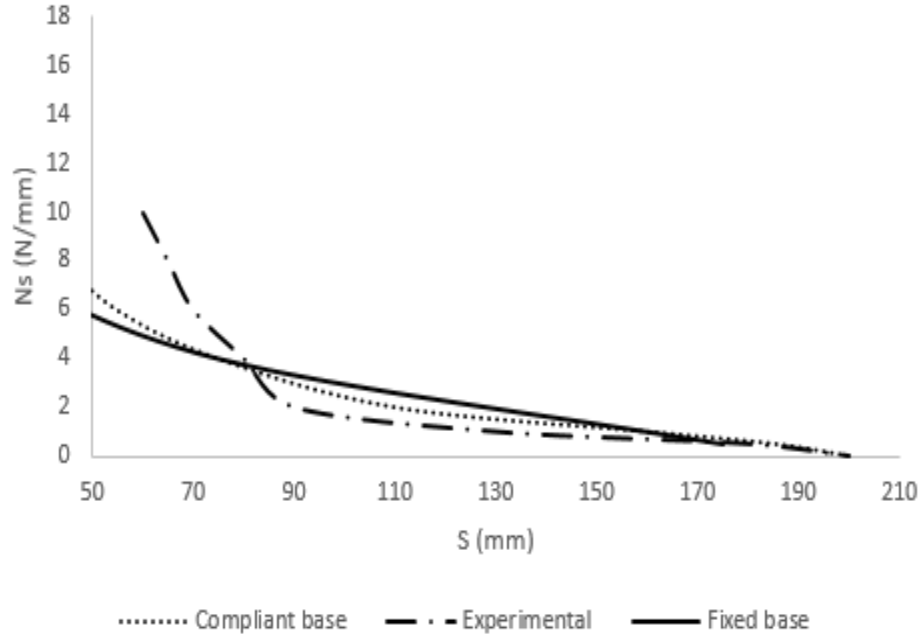

Fig.3 Variation of Ns along the shell surface

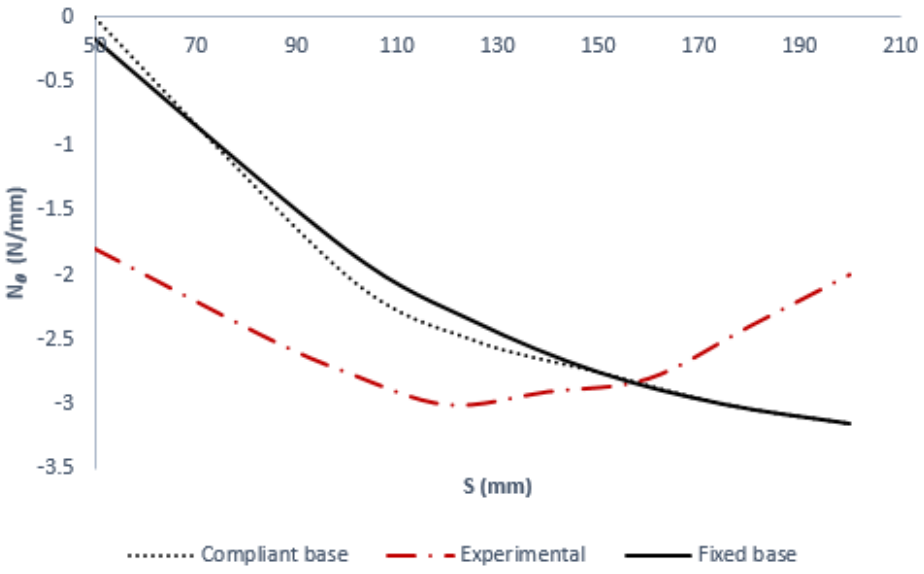

Fig.4 Variation of N_θ along the shell surface

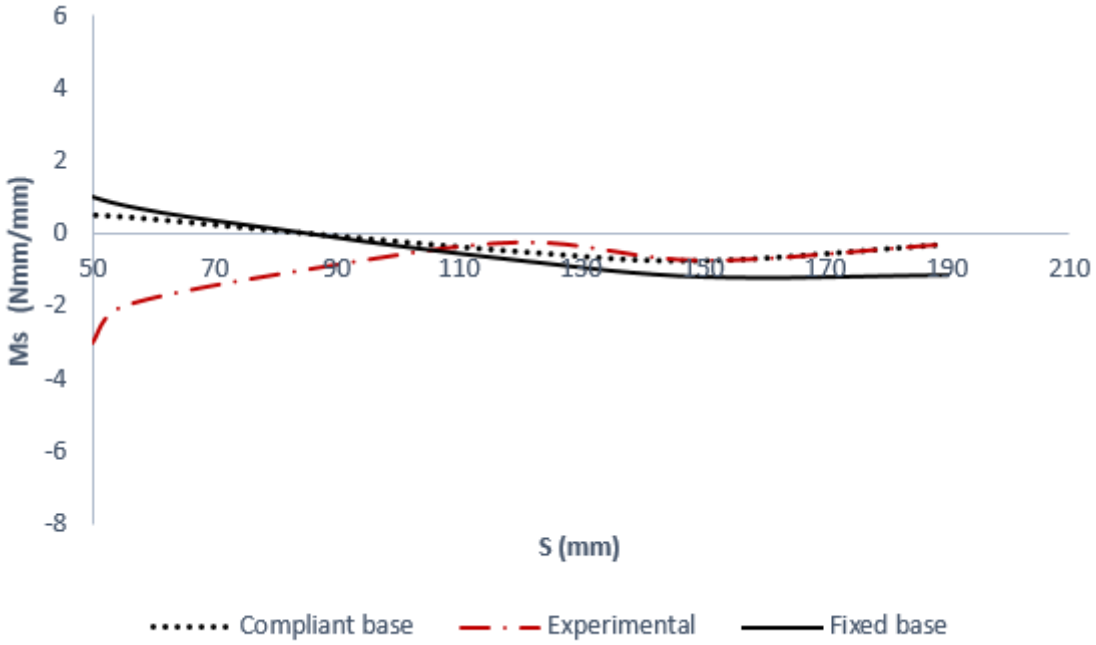

Fig.5 Variation of M_S along the shell surface

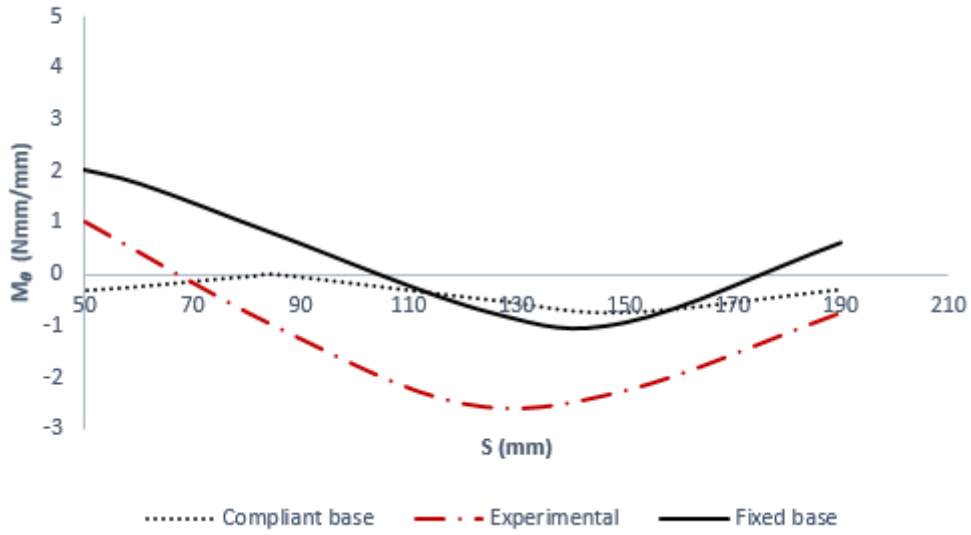

Fig.6 Variation of M_θ along the shell surface

5th International Engineering Symposium - IES 2016
March 2-4, 2016, Kumamoto University, Japan

UNDER-REAMED PILES FOR STABILISATION OF EXPANSIVE SOILS

Meera Susan Varghese [1] and Sitaram Nayak [2]

1 *M.Tech student, Department of Civil Engineering, National Institute of Technology Karnataka, Surathkal, Mangalore 575025, India. Email:meerasv.1993@gmail.com*
2 *Professor, Department of Civil Engineering, National Institute of Technology Karnataka, Surathkal, Mangalore 575025, India. email:snayak65@yahoo.co.in*

ABSTRACT: An under-reamed pile is a pile of shallow depth having one or more bulbs at its lower end. This when taken to a depth below the critical depth of expansive soils would anchor the foundation well and prevent the movement of the foundation along with the soil. Under-reamed piles provide an ideal solution for stabilising expansive soils like Black cotton soil. These piles are efficiently used in machine foundations, bridges, electrical transmission tower foundation, sand water tanks etc. Under-reamed piles are technically superior and also proves to be a more economical and better foundation scheme.

Keywords*: under-reamed pile, expansive soil, load carrying capacity, settlement*

INTRODUCTION

Under-reamed piles are concrete piles having one or more bulbs of diameter as much as 6m formed by enlarging the bore hole for the pile stem by an under reaming tool. These may be either (i) bored cast insitu concrete piles or (ii) bored compaction concrete piles. Under-reamed piles find application as foundations in different soil conditions to

(a) avoid undesirable effect of seasonal swelling and shrinkage in expansive soils.
(b) rest the foundation on a firm strata at a required depth with acceptable bearing capacity.
(c) obtain adequate resistance to upward, downward and lateral loads or moments.
(d) take foundations below scour depth.

PROBLEMS WIH EXPANSIVE SOILS

Expansive soils are usually inorganic clays of high compressibility composed mainly of minerals of smectite group like Montmorillonite, Saponite etc. which are characterized by excessive water absorption. Absorption of water causes an increase in volume as high as 10% or even more *[Gangadarapa et.al(1999)].* Similarly loss of water content during dry weather results in shrinkage. Alternate wetting and drying causes vertical movements in the soil mass. These movements lead to damages in the structure in the form of excessive settlements, cracks, structural distortions etc. Expansion of soil due to absorption of water leads to increased pressure on the vertical faces of foundations, basements retaining walls etc*. [Aleilahi et.al(2014*)]. An increase in the moisture content also leads to a decrease in the shear strength and leads to instability of the structure due to active foundation movements.

GENERAL DESIGN CONSIDERATIONS OF UNDER-REAMED PILES

Under-reamed pile foundations shall be designed in such a way as to transmit the load from the structure they support without causing any structural damage. The length of these piles may be 3.5m below the ground level if the expansive soil deposits are at greater depth and the length shall be smaller when the expansive soil deposits are of shallower depths and overlies strata of good bearing capacity. The diameter of stem varies from 20 to 50 cm. The diameter of bulbs can vary

between 2 to 3 times the pile stem diameter *[Punmia(2006)].* For piles of diameter less than 30cm the spacing of bulbs has to be greater than 1.5 times the diameter of the bulb. The top bulb is usually placed at a depth less than 1.75m and under-reamed piles having more than 2 bulbs are not generally advised. The center to center spacing should not be more than twice the bulb diameter.

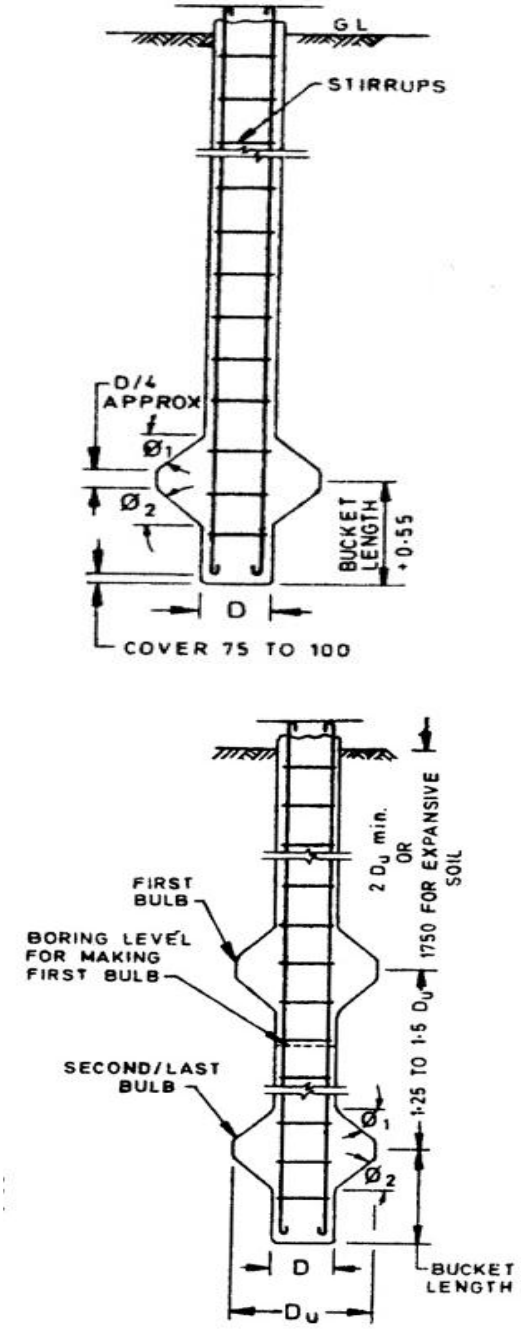

Fig.1 Typical details of bored cast insitu under-reamed pile

[www.engineerengineering.blogspot.in]

LOAD CARRYING CAPACITY

The properties of soil strata and the dimensions of pile determine the load carrying capacity of an under-reamed pile. Axial load component is transferred through bearing at the toe, projected area of the bulb and the skin friction developed along the pile. When the spacing between the piles is large the friction developed in the stem between successive bulbs may also contribute to load carrying capacity.
The load carrying capacity of an under-reamed pile is given by

$$Q_U = A_p N_c C_p + A_a N_c C'_s + C_{a'} A_{s'} + \alpha C_a A_s$$

Where,

Q_U = Ultimate bearing capacity of the pile
A_p = Cross sectional area of the pile stem at the toe level
N_c = Bearing capacity factor usually 9
C_p = Cohesion of soil around the toe
$A_a = \pi (D_u^2 - D^2)$
Where D_u and D are the under-reamed bulb and stem diameter respectively
$C_{a'}$ = Average cohesion of soil around and under bulbs
$A_{s'}$ = Surface area of cylinder circumscribing the under-reamed bulbs
α = Reduction factor (usually 0.5 for clays)
C_a = Average value of cohesion along the pile stem
A_s = Surface area of the stem

MERITS OF UNDER-REAMED PILES

(a)The length of the pile can be varied depending on the soil conditions.
(b) The soil bored out during the construction process may be used to determine the design parameters of the pile
(c) Penetration test can be carried out in the bore hole economically
(d)Bulbs of large diameters can be constructed in favourable soil conditions.
(e)The cost of construction of under-reamed piles are less since the diameter of the stem can be reduced considerably thus reducing the quantity of concrete required.

(f) The sound and vibration during the construction process is less.
(g) There is no ground heave.

DEMERITS OF UNDER-REAMED PILES

(a)In soft soils there are chances of squeezing and necking of the pile.
(b) In water bearing grounds the construction of under-reamed piles require special machinery and is not very economical.
(c) The concreting cannot be checked after the construction and hence poorly compacted spaces may adversely affect the performance of the piles.
(d)Enlarged bases cannot be formed if the soil is not self-supporting.
(e)The piles cannot be extended above the ground surface.
(f) Boring can lead to disturbances and settlements in the adjacent structures.

COMPARISON OF ORDINARY AND UNDER-REAMED PILES

The dimensions of ordinary piles and single bulb under-reamed piles of equal length and load carrying capacity were determined using Ansys *[Shetty et.al(2014)]* and Bentley geostructure foundation analysis softwares. The settlements of these piles under the loads were also determined. The properties of soil, pile dimensions and settlements are given in table 1, table 2 and table 3 respectively

Table 1 Soil properties

Depth(m)		c (kPa)	Ø (°)	ɣ (KN/m^3)
From	To			
0	10	55	18	18
10	20	50	20	18
20	-	45	22	19

Table 2 Dimensions of under-reamed and ordinary piles having equal load carrying capacity and lengths

load (KN)	Length of pile (m)	Diameter of pile(mm)		
		Under-reamed pile		ordinary Pile
		stem	bulb	
270	3.5	300	750	470
270	4	300	750	400
280	5	300	750	380
285	6	300	750	350

Table 3 Settlements of ordinary and under-reamed piles carrying equal loads

load (KN)	Length of pile(m)	Settlement(mm)	
		Under-reamed pile	Ordinary pile
270	3.5	15.744	25.23
270	4	14.351	35.3
280	5	15.948	28.7
285	6	15.325	19.1

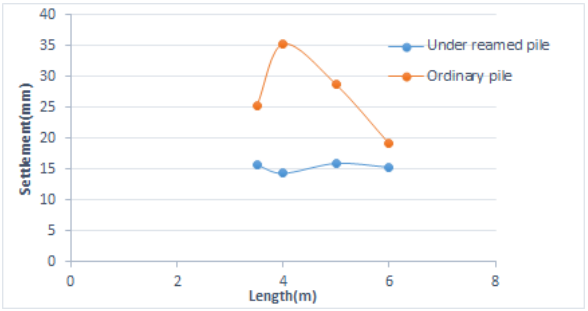

Fig.2 Settlements v/s length graph of ordinary and under-reamed piles under equal loads

COMPARISON OF SPREAD FOOTING AND UNDER-REAMED PILES

To make a comparison between spread footing and isolated footing a design was performed to determine the dimensions of a spread footing using Bentley geostructure foundation analysis software. For a load of 270KN the dimension of the footing was 4.1×4.1×.3 m. The volume of the footing is 5.043m^3 which is 15 times the volume of an equivalent under-reamed pile. Hence the use of spread footings in clays can be considered to be very uneconomical.

GEOMETRICAL PARAMETERS OF UNDER-REAMED PILES

To determine the optimum geometrical parameters of an under-reamed pile the load carrying capacity of piles were computed for different stem and bulb diameters. The results are shown in table 3.

Table 4 Load carrying capacity and settlement for varying geometric dimensions

Diameter (mm)		Length (m)	Load (KN)	Settlement (mm)
stem	bulb			
200	500	3.5	150	14.423
300	750	3.5	270	15.744
400	1000	3.5	420	14.678
500	1250	3.5	560	14.93

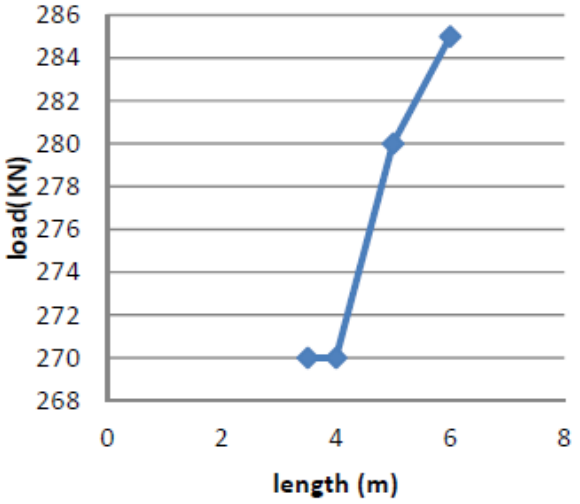

Figure.3 Variation of pile length Vs load

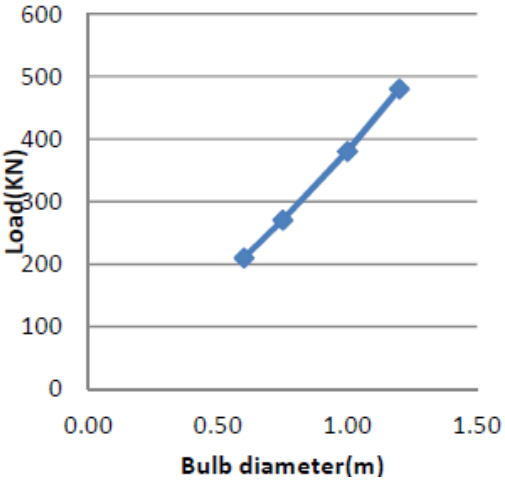

Figure.4 Variation of bulb diameter Vs load

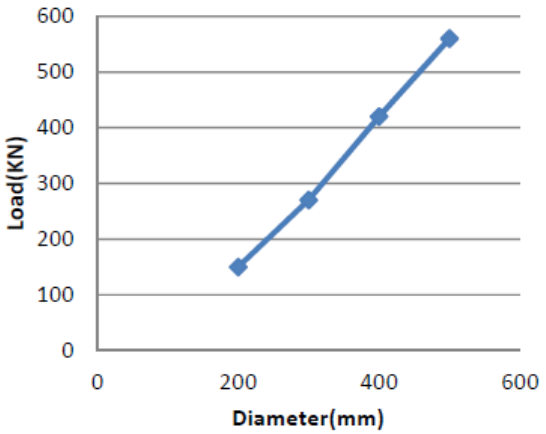

Figure.5 Variation of stem diameter Vs load

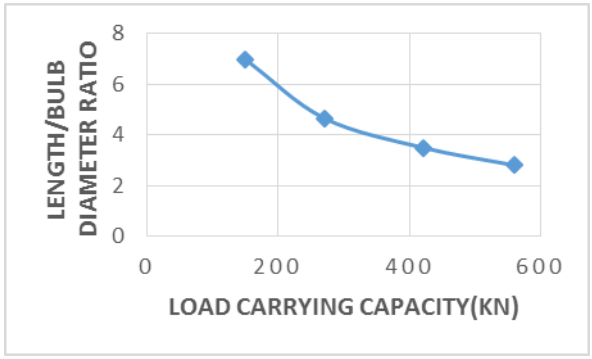

Figure.6 Variation of load carrying capacity Vs length/bulb diameter ratio

From the above graphs it can be seen that an increase in length does not produce a considerable increase in the load carrying capacity. However an increase in bulb and stem diameter causes a significant increase in load carrying capacity. Also increasing the bulb diameter increases the load carrying capacity at a higher rate when compared to increasing the stem diameter. Increasing the bulb diameter increases the total volume of the pile by a smaller amount and hence may be more economical. Also for a constant length a smaller length to bulb diameter ratio gives a higher load carrying capacity. Hence it may be concluded that in an under-reamed pile the load carrying capacity may be increased by increasing the bulb diameter . Increasing the length and stem diameter does not play a significant role in enhancing the performance.

COST COMPARISON OF ORDINARY AND UNDER-REAMED PILES

The volume of ordinary and under-reamed piles of equal load carrying capacity are tabulated below. The reduction in volume directly indicates savings in the material cost.

Table 3 cost comparison of ordinary piles and under-reamed pile

Length (m)	Volume of pile (m^3)		Savings in cost (%)
	Under-reamed pile	Ordinary pile	
3.5	0.29	0.61	52.3
4	0.32	0.51	35.4
5	0.40	0.57	30.2
6	0.47	0.58	19.2

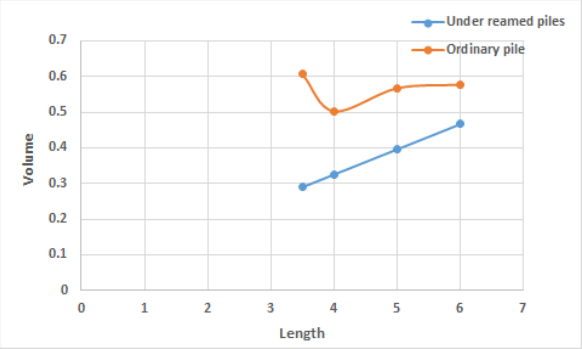

Fig.7 Volume v/s length of ordinary and under-reamed piles under equal loads

It can be seen that the reduction in cost is very high for short length of the pile. This is because as the length increases the frictional resistance offered by the stem becomes significantly large thereby reducing the contribution of the bulb. The above graph indicates the material costs and it can be seen that there is an average reduction in cost by 32%.

CONCLUSIONS

The following conclusions are deduced from this study:

- Under-reamed piles are an ideal and economical solution to stabilize expansive soils when compared to spread footing and ordinary piles.
- The cost of material can be reduced by an average of 32%
- The settlements of under-reamed piles are significantly low when compared to ordinary piles.

ACKNOWLEDGEMENTS

The authors are grateful to Prof, Katta Venkataramana, Dean and Professor, NITK Surathkal, Eldhose M Manjummekudiyil, and Anjana R Menon, M.Tech Students, NITK, Surathkal for the help and assistance provided throughout this work.

REFERENCES

[1] Alielahi, Hamid et al. (2014), Influence of under-reamed pile groups arrangement on tensile bearing capacity using FE method, EJGE, Vol 19 2014, pp.1398-1401

[2] Gangadharappa B.M. et al (1999), Study on under-reamed piles in cohesionless soil under tension, Journal of Geotechnical engineering, pp.235-243

[3]Punmia B.C., Soil mechanics and foundation, Laxmi Publications (P) Ltd. , 16th edition, pp.750-755

[4]Shetty Parikshith et al, (2015), Analytical study on geometrical features of under-reamed piles by Ansys, IJCAS, 2(3) pp.174-180

[5]Website:http://engineerengineering.blogspot.in/2013/02under-reamed-pile-foundation.html

5th International Engineering Symposium - IES 2016
March 2-4, 2016, Kumamoto University, Japan

A STUDY ON SOIL DYNAMICS AND SOIL-STRUCTURE INTERACTION

Priyanka Katta

Undergraduate Student, Department of Civil Engineering, PES Institute of Technology, 100 Feet Ring Road, Banashankari Stage III, Bengaluru, INDIA 560085.
e-mail:priyanka681702@gmail.com

ABSTRACT: The quakes have been taking place ever since the earth was formed 4.45 billion years ago. However, very little was known about the theory of earthquakes, their reasons and consequences. In the 19th century it was thought that the buildings collapsed into heaps of rubble because of the poor Structural engineering and intolerance of the building to withstand the frequency of the earthquakes. In the early 20th century it was found out that even if the building was structurally sound when the natural frequencies of the buildings were on par with those of the earthquakes the buildings undergoing lateral shear collapsed. This became the chief law of Earthquake Engineering. This answered many of the questions, vis-à-vis for the buildings to crumble during earthquakes. However, in late 20th century, the impact of earthquakes on the buildings was in an unusual manner and this changed the whole outlook towards earthquakes. It was found that even if the structures (super and sub) were structurally sound, if there is no adequate bond between the soil and the sub-structures, the damage would be fatal. This paper deals the phenomenal changes and activities that take place at the interface of the soil and the structures

INTRODUCTION

Soils and the sub-structures are subjected to many dynamic loads such as wheel loads, machines used in the construction activities, blasting, wave action, earthquakes etc. Of them, the earthquakes and their effects are the most critical threats to the foundations and the structures as it is difficult to predict its ground motion characteristics. This leads to many mishaps such as settlement of the foundations, liquefaction of the soil due to which the soil loses its ability to support the structures, the lighter structures, due to the effect of buoyancy, could float etc. The damage of the structures in many cases is not directly attributed to soil or structures purely, it's because of the interaction at the junction of soil and structure.

The soil–structure interaction does not become crucial when the loads are acting vertically. Not even the lateral loads such as wind loads which act always. This is prominent when an area is subjected to sudden vibrations namely quakes, bombings, blasting while quarrying etc. All these activities and their effects are time-dependent and that's why Soil-Structure interaction is a major concept in soil dynamics.

DYNAMIC BEHAVIOR OF SOILS

The behavior of soil varies from one kind of soil to another, under dynamic loading. Factors such as the strain magnitude, the strain rate and the number of cycles have great impact on the soil behavior. The strength of certain soils escalates when subjected to rapid cyclic loadings, or the saturated sand and clay which is highly dilative might lose strength with vibration.

SOIL- STRUCTURE INTERACTION

The buildings are constructed with an assumption that the soil is rigid and has the ability to take any kinds of loads. This assumption is mostly suitable for the hard soils like rocks where the soils are highly stiff and are rarely affected by the loads acting. However, the soils are not always completely rigid. There are soils which are soft too. These kinds of soils are less capable to take up heavy loads. They are susceptible to more lateral loads as the particle to particle interaction of the soil shall also be prominent.

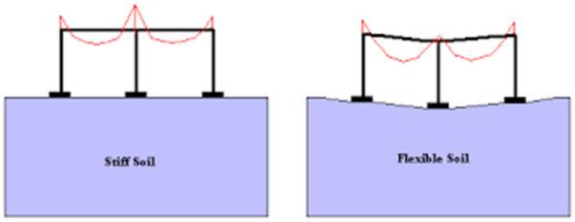

Figure 1. Behaviour of different kinds of soils when subjected to loads

This happens majorly due to two reasons. . This occurs firstly due to the inability of the foundation to conform to the deformations of free field motion that would deviate the response of structure from free field motion (Kinematic interaction). Secondly the dynamic response of the structure would induce deformation of the supporting soil (Inertial interaction). They will have low stiffness too. Hence, will undergo tremendous deformation. So, when the stiffness of the soil becomes lesser than the load magnitude, the soil fails.

While practicing, the structural part of the buildings are looked after by the Structural Engineers and the soil properties and their stiffness are dealt by the Geo-technical Engineers. They also generalize that loads act directly on the soil and the latter can take all kinds of loads. However, they do not consider the forces acting on the structural components which are in contact with the soil along the sides and at the base of the structures out of mere negligence unknowingly or economy point of view. This interface is one of the crucial points which will connote if the structure can fail or not when the soil is subjected to sudden dynamic loading conditions. If this interface is very weak then it can lead to damages especially during quakes costing many lives and properties.

Thus, *the process in which the response of the soil influences the motion of the structure and the motion of the soil influences the response of the soil is known as the SOIL-SRUCTURE INTERACTION*. (IS1893-1, 2002).

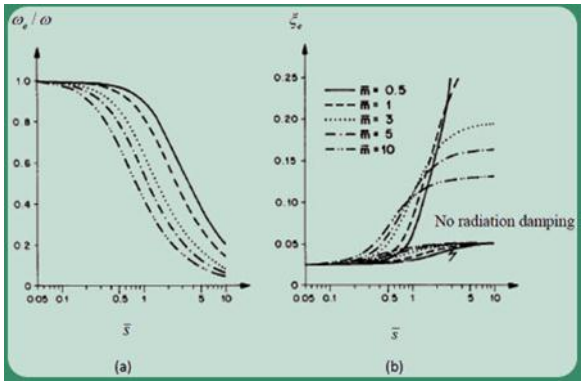

Figure 2. Effect of stiffness ratio and mass ratio on (a) natural frequency and (b) damping ratio of soil-structure system (Wolf, 1985).

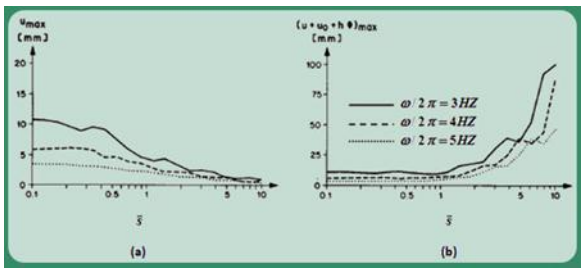

Figure 3. Response of equivalent SDOF system to artificial time history, considering SSI: (a) maximum structural displacement; (b) maximum displacement of mass relative to free field (Wolf 1985).

The above Figures illustrate the effect of SSI on natural frequency and damping ratio of equivalent SDOF system by comparing its response with fixed base system. Fig. 2(a) implies that when the stiffness ratio is high i.e. stiffness of foundation much greater than the stiffness

of the soil the natural frequency of equivalent SDOF system decreases, indicating the significance of SSI for stiff and massive structure supported on flexible soils. Fig. 2(b) shows that at high stiffness ratio the damping of equivalent SDOF system is high.

The effect of SSI on displacements is indicated in Fig.3(a) and reveals that as the stiffness ratio increases, the structural deformation decreases. It means that the considering effect of SSI results in reducing the distortion of the structure. On the other hand Fig. 3(b) shows that as the stiffness ratio increases, the overall displacement of the mass relative to the free field increases. It means that considering SSI effect results in increasing the overall displacement of the mass. Finally on one side the SSI tends to reduce the demand on the structure and on the other side as the foundation can rotate and translate, it increases the overall displacement.

CONSEQUENCES OF POOR SOIL-STRUCTURE INTERACTION

The major effects of the poor soil-structure interaction are:

- Settlement of dry sands.
- Liquefaction of saturated cohesionless soils.

Settlement of dry sands

Loose sands under vibration get compacted and partially consolidated. With seismic loads, such compaction causes settlement. It is indeed very important to evaluate and assess the vulnerability of the soil when subjected to such a condition. It is experimentally found that the sand with relative density lesser than 60% or standard penetration resistance lesser than 15, are likely to undergo settlement.

Figure 4. settlement during Niigata earthquake 1964, Japan

Liquefaction of saturated cohesionless soils

The major cause for the damages during earthquakes is the ground failure. The presence of the fissures, abnormal or unequal movements or the loss in the strength could be the reason for it. During earthquakes, when the soils are subjected to compaction and consolidation, there is inter-granular stress which get transferred from grains to pore water. This leads loss in soil shear strength and increase in pore water pressure. When the pore water pressure becomes equal to the total stress and effective stress of the soil goes zero, they tend to behave more like a liquid mud. This phenomenon is termed as LIQUEFACTION. As a result, the structures lighter than the soil, start floating.

Figure 5. Liquefied Ground in Bhuj, January2001 (Photo: Dr. T.G.Sitharam, IISc Bangalore)

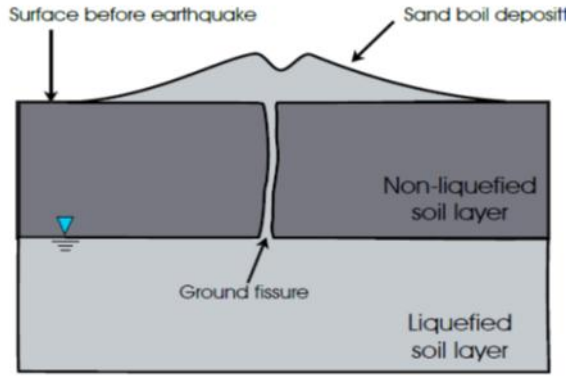

Figure 6. Schematic representation of liquefaction

Figure 7. Tohoku earthquake, Japan (2011)

CONCLUDING REMARKS

Soil-structure interaction is caused by mainly two phenomena- inability of the foundation to conform to the deformation of the soil and dynamic response of the superstructure that causes deformation in the supporting soft soil.

Soil-structure interaction analysis is important in case of structures built on soft soils and prone to seismic activities and vibrations like nuclear buildings, machine foundations, mining and tunnel boring sites.

The soil- structure interaction effect results in lowering the natural frequency of the soil-structure system as compared with natural frequency of structure alone. Also the total damping of soil-structure system is found to be greater than that of the structure alone resulting in conservative design. But, as the foundation can rotate and translate, the overall displacement is seen to increase.

REFERENCES

Kausel, E. (2010). "Early history of soil–structure interaction." Soil Dynamics and Earthquake Engineering, 30, 822–832.
Kramer, S., L. (1996). "Ground Response Analysis." Geotechnical Earthquake Engineering, 254-307.
Das, B., M., Ramana, G., V. (2011). "Fundamentals of vibrations." Principles of Soil Dynamics, 7-55.
Menglin,L.,Huaifeng,W., Xi, C.,Yongmei, Z. (2010). "Structure–soil–structure interaction: Literature review." Soil Dynamics and Earthquake Engineering, 31,1724–1731.
Boresi, A., P., Schmidt, R., J., Sidebottom, O., M., (1993). "Beams on Elastic Foundation." Advanced Mechanics of Materials, 404-439.

5th International Engineering Symposium - IES 2016
March 2-4, 2016, Kumamoto University, Japan

Purpose and Design of Retaining Walls

Nidhi Rao [1] and **Sitaram Nayak** [2]

1 *Student, Bachelor of Technology, Department of Civil Engineering, National Institute of Technology Karnataka, Surathkal, Mangalore 575025, India. email:nidhirao11@gmail.com*
2 *Professor, Department of Civil Engineering, National Institute of Technology Karnataka, Surathkal, Mangalore 575025, India. email:snayak65@yahoo.co.in*

ABSTRACT: Each type of retaining wall has its own characteristics and makes it suitable for a certain application. Gravity walls retain backfill soil using their own weight. They are huge structures and are usually used for small heights. RCC cantilever, RCC counter fort and RCC buttress walls are other types of conventional retaining walls. Soil nailing technique, involves reinforcing soil with elements such as reinforcing bars which are called as nails. These reinforcing bars are installed into pre-drilled holes and then grouted. Sometimes horizontal reinforcement in the soil in the form of geogrids is provided. Design of retaining wall involves finding the forces acting on the wall and applying stability checks on it. Along with these traditional methods, Erosion control blanket and Vetiver grass are also used as eco-friendly ways of controlling soil erosion.

***Keywords**: retaining wall, application, reinforcement, force, stability*

INTRODUCTION

Retaining walls are structures used to restrain movement of soil in slopes and gradients. It provides stability to soil and other materials and prevents them from assuming their natural slope. Usually, retaining walls are subjected to lateral earth pressure of soil that tries to move the walls from their position. While constructing a building on a hill, a retaining wall helps to prevent the soil from falling in on the structure ensuring safety. A retaining wall enables increase in the slope of the hill hence providing more usable land. Retaining walls built around the foundation helps to prevent rainwater or ground water from eroding the soil around the foundation. Based on the mechanism used by various kinds of retaining walls to stabilize the soil, they can be classified as

a) Externally Stabilized retaining walls
b) Internally Stabilized retaining walls

TYPES OF RETAINING WALLS

A) Externally Stabilized

Externally stabilized structures count on the strength and stability of wall elements to both resist lateral loads and also prevent erosion of the retained soil.

A few examples are:

i) Gravity walls

Gravity walls made of mass concrete or brick masonry or stone masonry to resist movement because of their heavy section.

ii) RCC Cantilever walls

Cantilever retaining walls are made of reinforced cement concrete conferring to IS 456-2000 and are thinner in section compared to gravity retaining walls.

iii) Counterfort Retaining walls

Counterfort walls are similar to Cantilever walls but the stem of the wall has vertical brackets called counterforts at regular intervals

throughout its span in the backfilled portion of the wall.

iv) Buttressed Retaining walls
Buttressed retaining walls have counterforts (buttress) on the opposite side of the backfill.

B) Internally stabilized Retaining walls
Internally stabilized structures depend on friction developed between closely-spaced reinforcing elements and the backfill to resist lateral soil pressure. A separate, non-structural element in the form of facing, erosion control mat and/or vegetation is attached to prevent erosion of the retained soil.

i) Soil Nailed Retaining wall
Involves reinforcing the soil with bars which essentially work in tension. These are usually parallel to one another and slightly inclined downward. The skin friction between the soil and the nails puts the nails in tension.

ii) Geogrid Reinforced retaining wall
Geogrid is a mat like element made of polymers like polypropylene. These are placed horizontally in the soil at specified intervals. Horizontal reinforcement of these geogrids provides enough tensile strength to hold the soil mass together.

DESIGN OF RETAINING WALL

I. CALCULATION OF LATERAL EARTH PRESSURE

There are a number of theories that help us to calculate the lateral pressure exerted by soil on the wall. Here two of the main theories are discussed.

A) Rankine's Earth pressure theory

Assumptions
1) The backfill should be dry, homogenous, and semi-infinite.
2) The ground surface is considered to be plane
3) The backfill of the wall is vertical and smooth(No wall friction)
4) The wall if yields, yields about the base

i) Case I- Active State

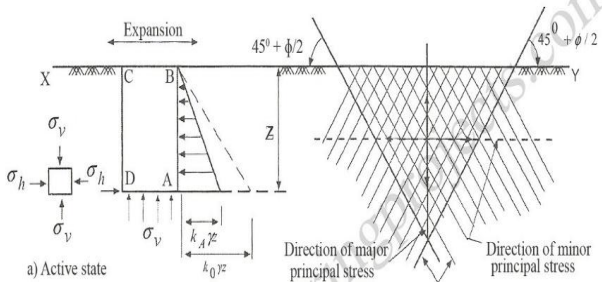

Fig 1. Development of active state

Major principal stress = $\sigma_1=\gamma z$
Minor principal stress = $\sigma_3=p_a$ (lateral earth pressure)
According to Mohr's principle,
$\gamma z = p_a \tan^2(45+\phi/2)+2c \tan(45+\phi/2)$

$p_a = k_a\gamma z - 2c\, k_a^{-1/2}$ (1)

where $k_a=\frac{1-\sin\phi}{1+\sin\phi}$

When c=0

$p_a = k_a\gamma z$, where $k_a=\frac{1-\sin\phi}{1+\sin\phi}$

P_a=Lateral Earth force

$=\frac{1}{2}\, p_a H$

$P_a=\frac{1}{2}\, k_a\gamma H^2$ (2)

ii) Case II- Passive State

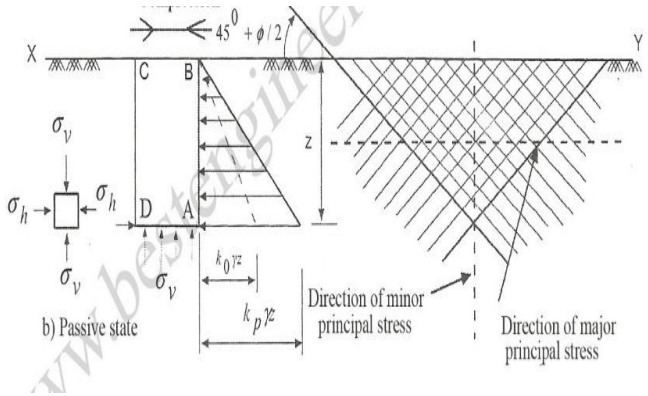

Fig 2. Development of passive state

Major principal stress = $\sigma_1 = p_p$ (lateral earth pressure)

Minor principal stress = $\sigma_3 = \gamma z$

According to Mohr's principle,

$p_p = \gamma z \tan^2(45+\phi/2) + 2c \tan(45+\phi/2)$

$p_p = k_p \gamma z + 2c\, k_p^{-1/2}$ (3)

where $k_p = \frac{1+\sin\phi}{1-\sin\phi}$

When c=0

$P_p = k_p \gamma z$, where $k_p = \frac{1+\sin\phi}{1-\sin\phi}$

P_p=Lateral Earth force

$= \frac{1}{2} p_p H$

$P_p = \frac{1}{2} k_p \gamma H^2$ (4)

B) Coulomb's Earth pressure Theory

Assumptions

1) The backfill should be dry, homogeneous, and semi-infinite.
2) There is wall friction between the wall and soil
3) The failure wedge is considered to be a rigid body
4) The equilibrium of the failure wedge by constructing a force polygon is used to find the lateral earth pressure.

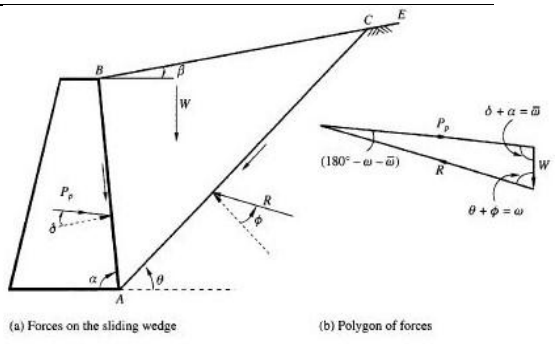

Fig 3. Coulumb's failure wedge

$P_p = \frac{1}{2} k_p \gamma H^2$ (5)

Where $k_p =$

$$\frac{\sin^2(\alpha-\phi)}{(\sin^2\alpha)(\sin(\alpha+\delta))\left(1-\sqrt{\frac{\sin(\phi+\delta)\sin(\phi-\beta)}{\sin(\alpha-\delta)\sin(\alpha+\beta)}}\right)^2}$$

II. STABILITY CALCULATIONS

A) Internal stability

In case of internally stabilized retaining walls, two stability criteria have to satified:

i) Check for Tension Failure

It depends on the spacing between the reinforced elements. A factor of safety of 1.5 is used to calculate the spacing.

ii) Check for Pullout Faulire

This depends on the lateral length of the reinforcement. Again a factor of safety of 1.5 is used here.

B) External stability

External stability needs to be checked for both internally and externally stabilized walls.

i) Check for Sliding

Factor of safety against sliding =Resisting force/Actuating force

$$= \frac{(cB+\sum V \tan\delta)}{Pa}$$

≥ 1.5

where c-Cohesion

B- Breadth of the wall

V- Downward forces on the

Wall
δ- Wall friction
P_a- Lateral earth pressure

ii) Check for Overturning
=Resisting moment/Actuating Moment
≥1.5

iii) Check for safety against bearing failure

$$\sigma_{max} = \frac{\Sigma V}{B}\left(1 + 6 * \frac{e}{B}\right)$$

≤SBC

where B- Breadth of the wall
V- Downward forces on the wall
e- Eccentricity of the resultant earth pressure
SBC- Safe Bearing capacity of soil

iv) Check for tension

$$\sigma_{min} = \frac{\Sigma V}{B}\left(1 - 6 * \frac{e}{B}\right)$$

≥0

where B- Breadth of the wall
V- Downward forces on the wall
e- Eccentricity of the resultant earth pressure

ADDITIONAL NOTES

a) For a RCC Cantilever Retaining wall, reinforcements (main steel and distribution steel) needs to be designed for the stem, heel and toe of the wall.

b) Weep holes of about 75mm diameter shall be provided at about 1m c/c both ways (staggered). At the mouth of the weep holes, filter material shall be provided.

c) Alternate Retaining structures like Gabion walls can also be used in places prone to differential settlement as the flexibility on the gabion walls allows settlement without damaging the wall.

CONCLUSIONS

Retaining walls are important structural elements in the civil engineering world. They are necessary as they permit greater usage of land. They also reduce the cost of filling or excavating to make a level surface for construction to carry on. It is important to choose the right kind of retaining wall based on its purpose and prevailing soil conditions in the area. There are a number of types of retaining walls to choose from. The design of any retaining wall mainly revolves around the amount of lateral earth pressure exerted by the soil on the wall. Hence determination of this pressure is vital in the design process. Stability of a structure is given highest priority in the construction process. Therefore it is essential to carry out various stability checks on to wall to rule out possibility of failure in any manner.

REFERENCES

References should be given in alphabetical order. (font to be used: Verdana 8)
[1] B C Punmia, Ashok Kumar Jain and Arun Kumar Jain (1970), Soil Mechanics and Foundations, 16th ed., Laxmi Publications Ltd, New Delhi,pp.500-540
[2] Su Yang et al Int. Journal of Engineering Research and Applications ISSN : 2248-9622, Vol. 3, Issue 6, Nov-Dec 2013, pp.1012-1021
[3]VNS Murthy (2002), Geotechnical Engineering-Principles and Practices of Soil Mechanics and Foundation Engineering, Marcel Dekker, New York,pp 420-475
[4] Terzaghi, K and Peck, R B, (1987), Soil Mechanics in Engineering Practice, 2nd ed., McGraw Hill, New York, pp.85-100.

5th International Engineering Symposium - IES 2016
March 2-4, 2016, Kumamoto University, Japan

COMPACTION AND STRENGTH BEHAVIOUR OF SOFT CLAY COIR PITH MIXES

Dr.Kodi Rangaswami[1], Siddarth Sasi N K[2], Nikhil K Baby[3], Nikhil VR[3], Nithin P S[3], Nithin Austin[3]

1 *Asst.Profesor, Department of Civil Engineering, NIT Calicut, Kozhikode 673601, Kerala, India. Email : ranga@nitc.ac.in*
2 *Master course student, Department of Civil Engineering, National Institute of Technology Karnataka, Surathkal, Mangalore 575025, India. Email:siddarth1605@gmail.com*
3 *Formerly undergraduate student, Department of Civil Engineering, NIT Calicut, Kozhikode 673601, Kerala, India.*

ABSTRACT: Nowadays coir pith utilization for different applications is to be investigated to prevent unwanted stagnation of coir pith deposits. How to utilize such natural waste by products is the challenging task to every engineering discipline. Therefore present study is to be focused on suitability of coir pith as a soil stabilizer in improving the geotechnical properties of clayey soil. It is proposed to conduct compaction and UCC test on un-stabilized and stabilized soil mixes. The optimum level of coir pith is to be evaluated based on maximum compaction density and UCC strength. The timing effect also should be tested on durability of coir pith mixed soils. The compaction strength of soil specimen is to be compared under both UCC and UTM testing conditions to develop the relations. Finally the improvement of soil strength is to be quantified.

Keywords: *Coir pith, Strength, Compaction*

INTRODUCTION

Structures are meant to stand firm for many years to come and more importantly, could provide great strength to support loads within the structure. The unstable properties of soft clay are believed to be the major circumstances for any structure to be built on it. The major challenge of problems with soft clay soil is the stability of the soil and settlement. All soils are compressible and could undergo volume changes when they are subjected to changes in the stress applied to them. Foundation settlements are the most emergence problems happened in building constructions. Many commercial and residential buildings have become distressed due to settlement.

The high compressibility properties of soft clay are one of the major factors that could lead to high settlement. This is happened from the fact that soft clay are finer in particles and being too cohesive with the presence of water. High settlement is as dangerous as it could affect the movement of whole structure and would end up with structure failures and cracks. Soft clay has the lowest value of permeability where water is hard to get through particles and this is the reason why soft clay has high moisture content. The presence of water could have made the soil become more unstable. Water could be the main agent that makes the soil become unstable especially with the high ability of the soft clay soil to trap huge amount of water within its particles. The soil particles have high tendency to bond closely with one another that make soft clay become easily compressed when undergoing compaction activity.

By the weak conditions of the soil, the stiffness of the soil could easily be affected and this has made the soil become weak in strength. Strength of soil is the most vital part of any soil properties. Soil with weak strength could not sustain massive and high load on it. It becomes more dangerous when structures are built on the soft clay soil without having made proper

design and analysis on the soil. The structures are more subjected to fail. Coir pith is a by-product of the coir industry (Fig 1). Coir pith is a biomass residue generated during the coir extraction of coir fibre from coconut husk.

PHASE 1: CHECKING THE SOIL PROPERTIES

Specific gravity was determined by using pycnometer. It is found using Eq.1. The specific gravity of soil was found to be 2.64 and that of the coir pith was 0.7.

$$G = \left(\frac{W2 - W1}{(W2 - W1) - (W3 - W4)} \right) \quad (1)$$

Where,
G = specific gravity
W1 = wt of jar
W2 = wt of jar+soil
W3 = wt of jar+soil+water
W4 = wt of jar+water

Dry density and water content were found out by compaction test. The apparatus had a volume of 1120.4cm^3.Five samples were taken. The results were found out and the graph of dry density versus water content was plotted.

PHASE 2: CHECKING THE COIR PITH PROPERTIES

Sieve analysis was carried out on the coir pith. 135g of coir pith was taken and grain size analysis distribution was found out. Water absorption of coir pith was found to be 280%.

PHASE 3: CHECKING THE PROPERTIES OF SOIL MIXES

Four mixes were taken. 0.1% coir by weight of clay, 0.2%, 0.5% and 1% (Fig 2, 3, 4, 5). The dry density and water content was obtained as shown in Fig 6. Graphs were plotted. Unconfined compression tests were performed on soft clay as well as soft clay mixed with coir pith (Fig 7, 8). The sample mixed with 0.2% coir pith was found to have obtained max UCC strength of 85%.

Tests on the specimen with change in time

The strength and volume change tests were conducted with reference to the time. The time period considered was 2,4,7 and 14 days. The variation in properties of the specimen were found at certain intervals (Fig 9, 10)

CONCLUSIONS

The following conclusions are deduced from this study:

- The 0.2% coir pith mix was found to be the most efficient mix with maximum dry density of 1.95gm/cc and UCC strength of 85KPa.
- The maximum dry density of clay was found to be 1.64 and the maximum dry density of the 0.2% coir pith mix was found to be 1.95. The large difference in the specific gravity was due to the filling up of voids by the coir pith.
- The water absorption of coir pith is found to be 280% and the specific gravity is 0.7.
- The volume change of the UCC test specimen was found to be very high initially and decreases gradually till the 7th day and then approaches a constant value.
- The UCC strength of the coir pith mix of 0.2% is less at initial day and then increases and reaches a value of 128KPa.
- The water content value at maximum dry density increases with increase in coir pith content.
- The specific gravity of soil is found to be 2.66 and the dry density is 1.64.
- There was an increase in UCC strength of 95% when the clay was reinforced with coir pith (0.2%-most efficient mix)
- The UCC strength of clay is 47KPa but the strength value decreases to a value lesser than 47KPa when the mix is 0.5%. This may be because of the high absorption value of coir pith.
- The strength of the specimen increased gradually with the ageing effect.

ACKNOWLEDGEMENTS

The authors thank the Ministry of Education, Government of India and TEQIP which provided financial support to carry out this research.

REFERENCES

1. Nadarajan G. 1995. Commercial exploitation of coconut pith problem and prospects. *Indian Coconut Journal* 9:11.
2. Namsivayam, Kadirvelu K (1994). Coir pith, an agricultural waste byproduct, for the treatment of dyeing waste water. *Bio-resource technology* 48(1):79-81.
3. Prasad S.V. et al., 1983. Alkali treatment of coir fibres for coir-polyester composites. *Journal of Material Science*18 :(1443-1484).
4. Thampan P.K, 1991. *Hand book on Coconut*. New delhi, India: Oxford and IBH publishing co., Pvt. Limited.

.

Figure 1: Typical coir pith

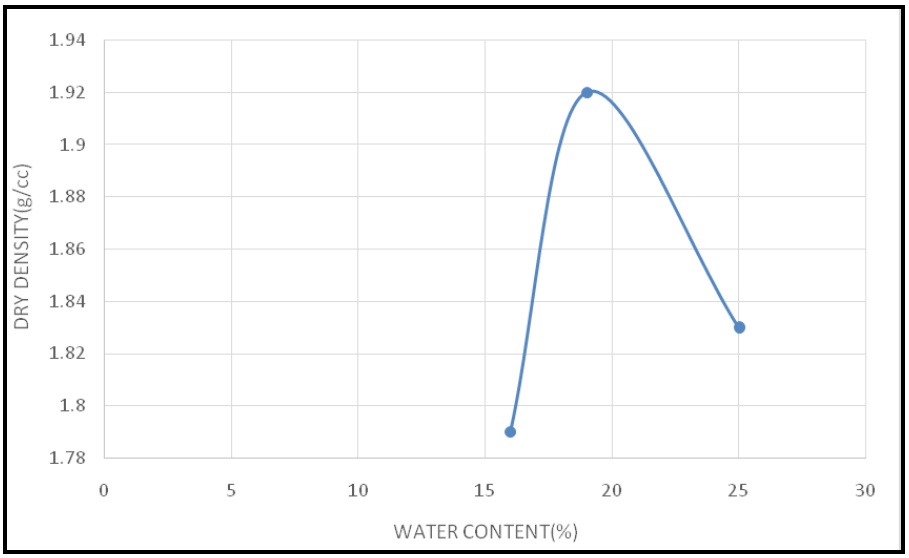

Figure 2: Compaction curve for 0.1 % coir pith content

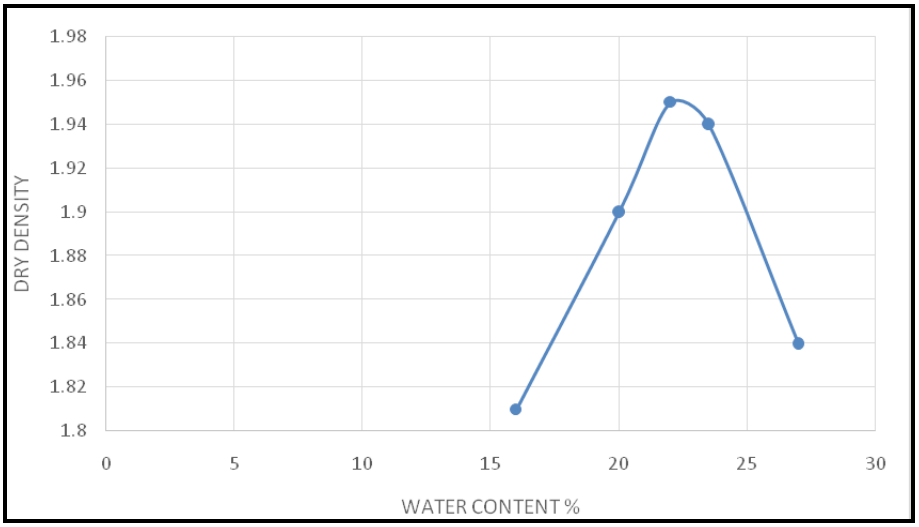

Figure 3: Compaction curve for 0.2 % coir pith content

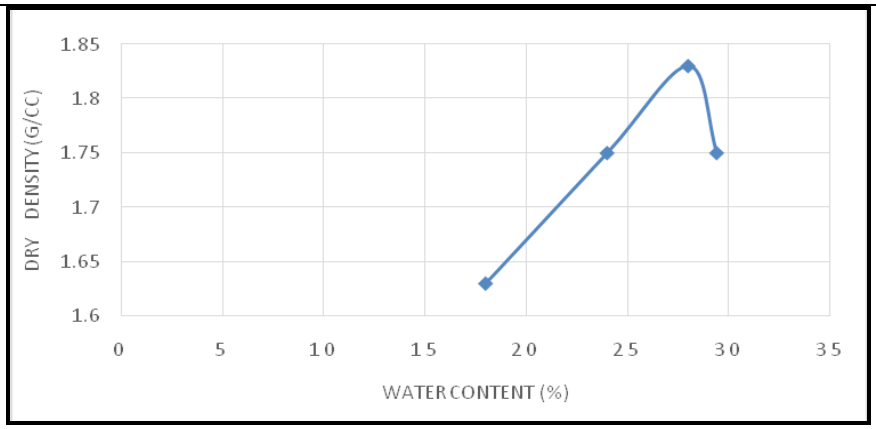

Figure 4: Compaction curve for 0.5 % coir pith content

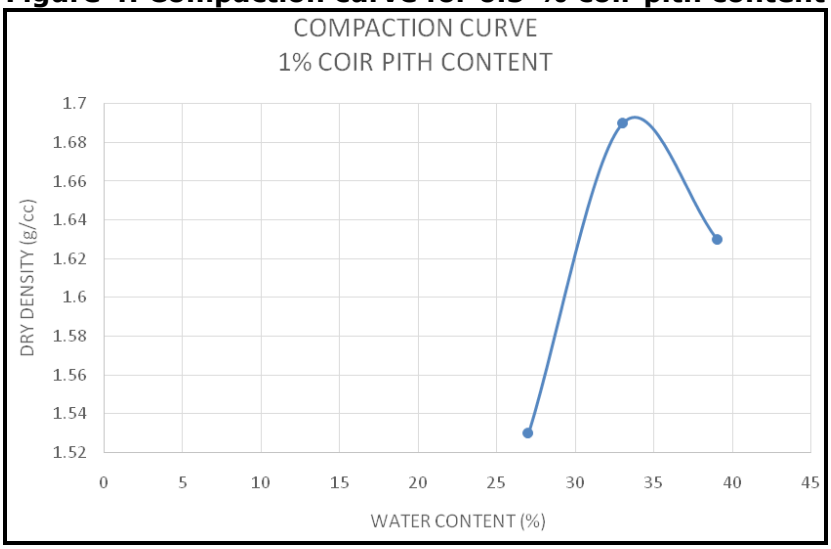

Figure 5: Compaction curve for 1 % coir pith content

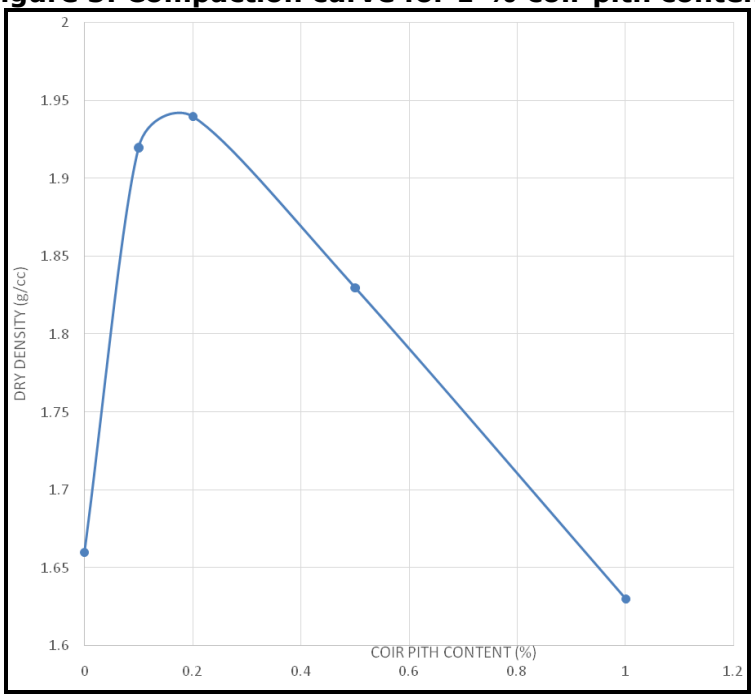

Figure 6: Coir pith content vs Maximum Dry Density

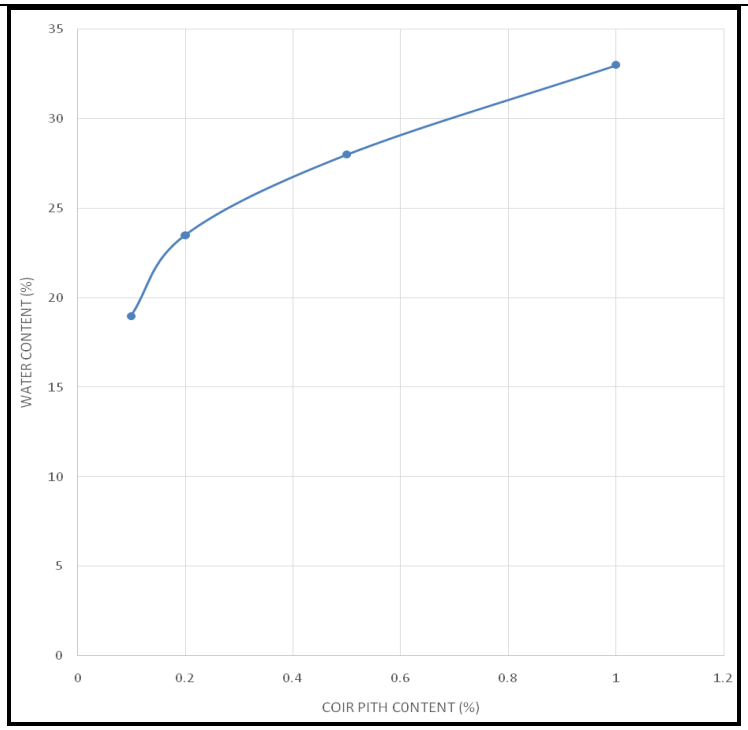

Figure 7: Coir pith content vs water content at maximum dry density

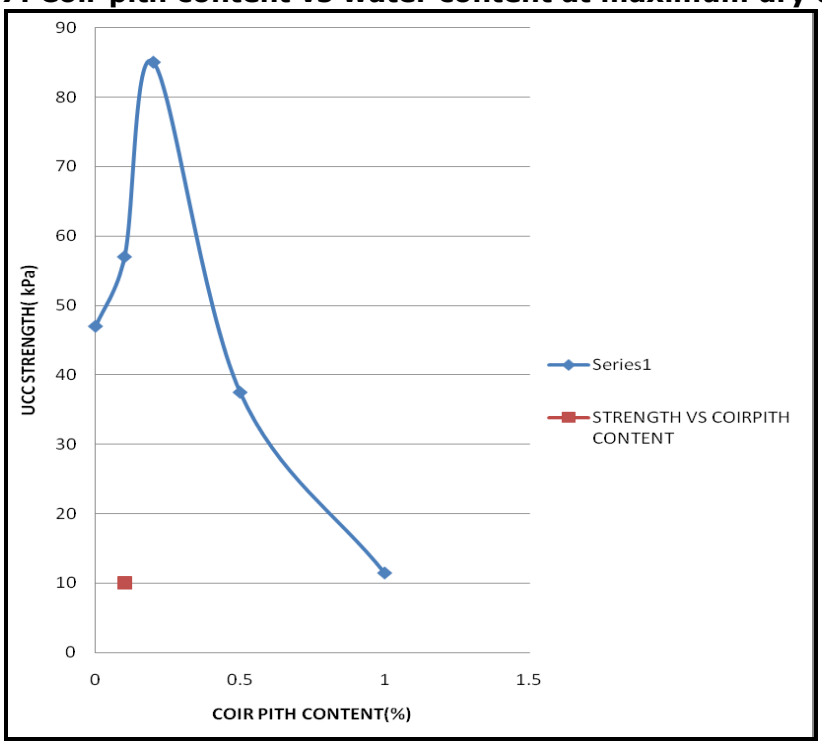

Figure 8: Strength vs coir pith content

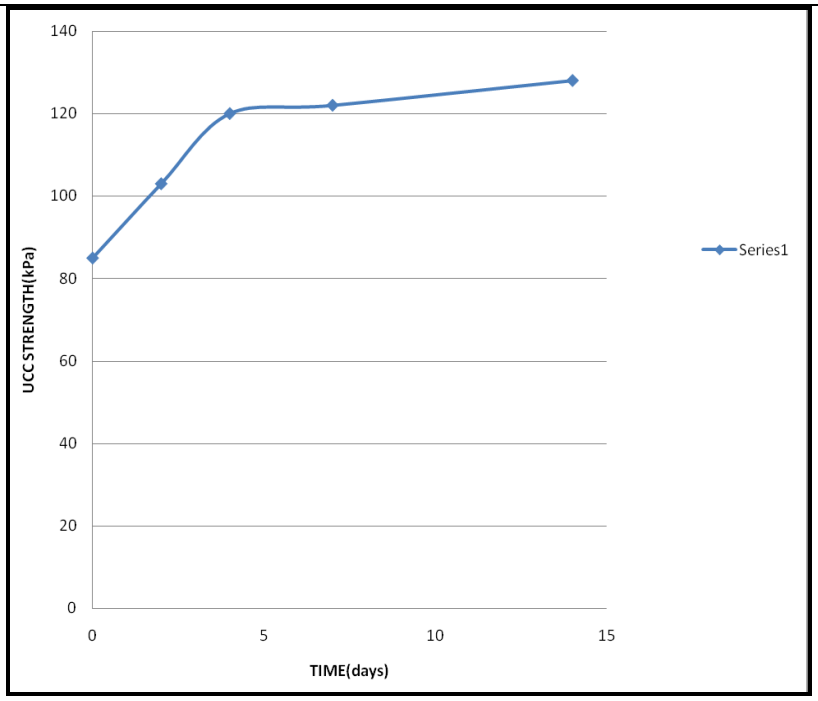

Figure 9: Strength vs Time (0.2 % mix)

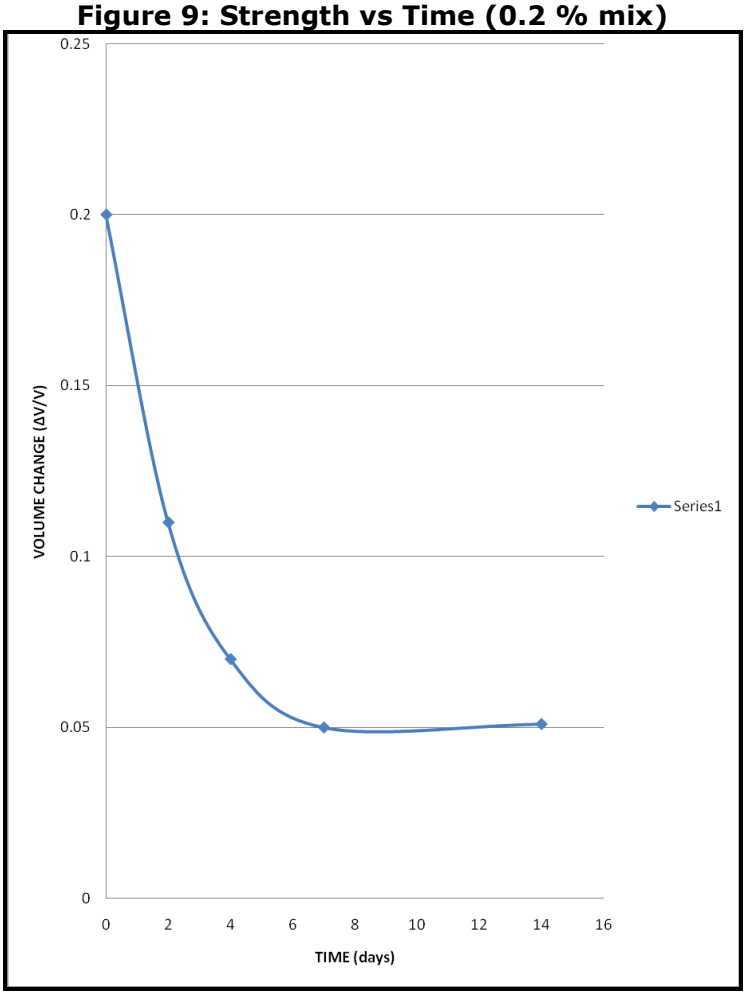

Figure 10: Volume change vs Time (0.2 % mix)

5th International Engineering Symposium - IES 2016
March 2-4, 2016, Kumamoto University, Japan

A STUDY ON SEISMIC ANALYSIS OF STRUCTURES

Shrish Gopal Upadhyay[1] and Katta Venkataramana[2]

1 *Department of Civil Engineering, PES Institute of Technology, 100 Feet Ring Road, Banashankari Stage III, Bengaluru 560085, INDIA*
e-mail:shrishupadhyay7747@gmail.com
2 *Department of Civil Engineering, National Institute of Technology Karnataka (NITK), Surathkal, Srinivasnagar 575 025, Mangalore, INDIA*
e-mail:ven.nitk@gmail.com

ABSTRACT: Modern construction involves analysis of structures subjected to dynamic loads such as wind load and seismic load which cause fatigue in structures, resulting in loss of strength and stiffness of the structure. The havoc due to earthquakes could be mitigated by following the standards in the code books and design aids meticulously. The present study is intended to understand seismology, the response of structures in seismic zones, and their design aspects as per the Indian code book IS-1893 (Part 1)-2002. The base shear in a given structure within a seismic zone and the storey shear at each floor level are obtained using equivalent lateral force procedure and dynamic analysis procedure. On the basis of the past investigations and reports, an attempt has been made to comment on the practical applicability of the various provisions given in the code book.

Keywords*: base shear, seismic load, seismology, stiffness.*

INTRODUCTION

Traditional building design involved static analysis of the structure, however modern construction practise mandates designing the building for even dynamic loads. Dynamic actions are caused on buildings by both wind and earthquakes. In wind design, the structure is subjected to a pressure on the exposed surface area; this is force-type loading. However, in earthquake design, the building is subjected to random ground motion at its base, inducing inertial forces in the structure; this is displacement-type loading (Fig.1). Seismic load causes severe vibratory motion in the structure. Also, being cyclic in nature, they induce fatigue and hence loss of strength of structure and stiffness deterioration. Hence, we must design the buildings efficiently to ensure safety of a structure as well as its occupants with minimum usage of resources. Bureau of Indian Standards (BIS) have made codes and provisions to ensure proper analysis and detailing of structures subjected to seismic loads. The Seismic behaviour of a structure depends upon various parameters like intensity, duration and frequency content of ground motion, geologic and soil condition, quality of construction, etc. Observation of structural performance of structures during an earthquake can clearly identify the design strengths and weaknesses, as well as, the desirable qualities of materials, techniques of construction, site selection etc.

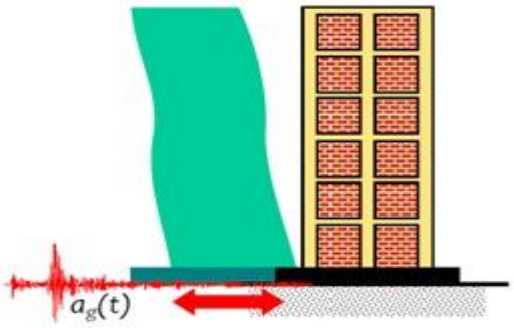

Fig.1 Earthquake Loading
(Source: Some Concepts in Earthquake Behaviour of Buildings, C V R Murty)

Several theories have evolved to explain the cause of earthquake. Two of most

widely used theories include those of Reid's Elastic Rebound Theory and Theory of Plate Tectonics. The former states that the earthquakes are the shock waves generated because of tremendous amount of energy released due to slip of rocks across the fracture. The later states that the earthquakes are result of relative movement between various tectonic plates along their boundaries.

The earthquakes are quantified by two terms namely, Intensity and Magnitude. The Intensity is the qualitative measure of its damage potential, represented by Modified Mercalli Intensity (MMI) Scale. The Magnitude is quantitative measure of amount of energy released at the source, expressed as Richter Magnitude (M).

BASIC ASPECTS OF SEISMIC DESIGN

The seismic design of a structure is basically governed by mass of the structure in addition its stiffness, because ground vibration induces inertial forces that are proportional to the mass of the structure. It is economically unviable to design structures to behave elastically during earthquakes without damage. Therefore, structures are designed only for a fraction of the force that they would experience, if they were designed to remain elastic during the expected strong ground shaking, and thereby permitting damage. But, sufficient stiffness must be ensured to avoid structural damage under minor shaking. As such, design against earthquake effects is called as earthquake-resistant design and not earthquake-proof design.

Thus, in seismic design, a careful balance between cost and acceptable damage is achieved through extensive research and detailed post-earthquake damage assessment studies. The results of this study are then incorporated into precise seismic design provisions.

The traditional earthquake-resistant design philosophy requires that normal structures should be able to resist:

a) Minor (and frequent) shaking with no damage to structural and non-structural elements;
b) Moderate shaking with minor damage to structural elements, and some damage to non-structural elements; and
c) Severe (and infrequent) shaking with damage to structural elements, but with NO collapse (to save life and property inside/adjoining the structure).

An earthquake resistant building has following four virtues in it:

a) Good Structural Configuration: The building's size, shape and structural system carrying loads are such that they ensure a direct and smooth flow of inertia forces to ground.
b) Lateral Strength: The maximum lateral force that it can resist is such that the damage induced in it does not result in collapse.
c) Adequate Stiffness: Its lateral load resisting system is such that the earthquake-induced deformations in it do not damage its contents under low-to-moderate shaking.
d) Good Ductility: Its capacity to undergo large deformations under severe earthquake shaking even after yielding is improved by favourable design and detailing strategies

The seismic design demands ductile behavior of structures wherein structure is stable enough to withstand large displacement demand through structural damage without collapse and undue loss of strength. It is relatively simple to design structures of given lateral strength and initial stiffness by appropriately proportioning the size and material of the members. But, achieving sufficient ductility requires extensive laboratory tests on full-scale specimen to identify preferable methods of detailing.

CHARACTERISATION OF GROUND MOTION

The ground motion is characterised in order to assess the seismic demand of the structure. The two important parameters used to characterise the ground motion are Response History and Response Spectrum.

The *Response History* is a plot of acceleration, velocity and displacement of

a point on the ground surface as a function of time for the entire duration of earthquake. It is also known as *Time History* (Fig. 2). However, the Response Spectrum is a plot of the peak value of a response quantity such as acceleration, velocity or displacement of an SDOF system as a function of natural vibration period T_n of the system with a particular ratio. It provides a convenient method of estimating the response of the structure with known natural period to specific ground motion. The individual plots represent Response spectrum in Fig. 3.

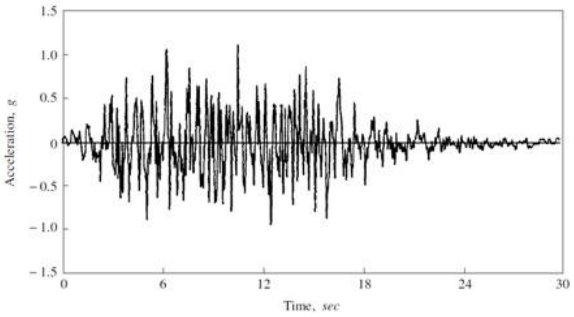

Fig.2 Response History
(Source: Clough and Penizen, Dynamics of Structures, 3rd Edition.)

The individual spectrum, used to assess response to a particular earthquake, is quite irregular and hence is not convenient to use for designing the structures. In order to design structures, we use Design Response Spectrum, which is rather smooth plot and represents the average of spectra of several ground motions. The envelope in Fig.3 represents the Design Response Spectrum.

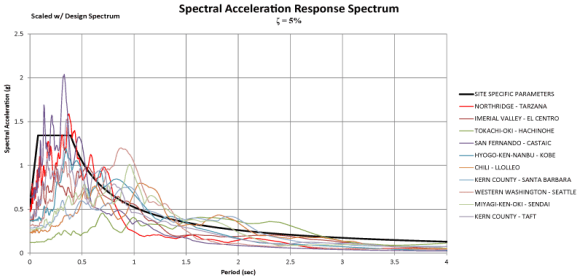

Fig.3 Response Spectrum
(Source: http://www.structuremag.org/wp-content/uploads/0313-ps-1.gif)

DYNAMICS OF STRUCTURES

The ground shaking due to earthquake induces oscillations and inertial forces in the structure, the duration and intensity of same is function of dynamic characteristics of the structure along with the characteristics of ground motion. The dynamic characteristics of a structure are governed by its modes of oscillation and damping. The mode of oscillation of a structure can be defined by associated Natural Period and Deformed Shape.

NATURAL PERIOD

Natural Period (T_n) of a structure is the time taken by it to undergo one complete cycle of oscillation. It is inherent property of a structure controlled by its mass m and stiffness k; mathematically,

$$T_n = \sqrt{\frac{k}{m}} \qquad (1)$$

The heavier and the flexible structures have larger natural time period as compared to those lighter and stiffer. The reciprocal of natural period of a structure ($1/T_n$) is called the Natural Frequency. The structure offers least resistance, and hence undergoes larger oscillation when shaken at its natural frequency. If the frequency of ground motion applied over a period of time is in close range of natural frequency of the structure, the structure undergoes resonance. However, earthquake ground motion departs from this condition and hence, generally even when ground motion frequencies are close to natural frequency of the structure, in spite of resonance, the structure undergoes increased response.

DEFORMED/MODE SHAPE

Mode shape of the oscillation associated with a natural period of the structure is the deformed shape of the structure when shaken at the natural period. There are three basic modes of oscillation, namely, pure translational along X-axis, pure translational along Y-axis and pure rotation about Z-axis (Fig.4). As a structure might have infinite numbers of natural period, it has infinite mode shapes. In order to analyze structure mathematically we assume a structure having N nodes, would have 6N modes of oscillation and 6N natural periods & mode shapes of oscillation. The deformed shape of the structure associated with oscillation

at fundamental natural period is termed its first mode shape. Similarly, the deformed shapes associated with oscillations at second, third, and other higher natural periods are called second mode shape, third mode shape, and so on, respectively (Fig.5).

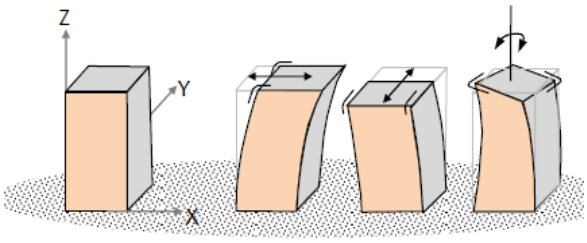

Fig.4 Basic Modes of Vibration
(Source: Some Concepts in Earthquake Behaviour of Buildings, C V R Murty)

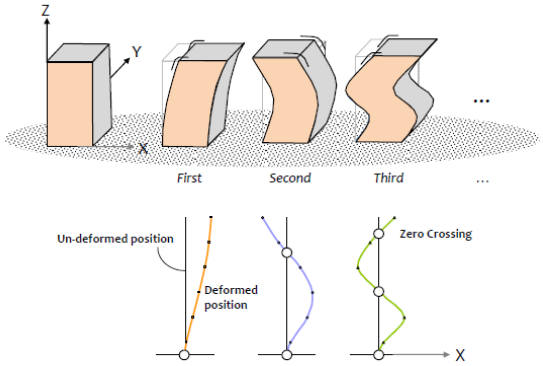

Fig.5 Fundamental and two higher translational modes of oscillation along X-direction of a building
(Source: Some Concepts in Earthquake Behaviour of Buildings, C V R Murty)

DAMPING

Damping is a phenomena in which the structures set to oscillation by earthquake shaking eventually come back to rest with time due to dissipation of the oscillatory energy through conversion to other forms of energy, like heat and sound. The damping in the structure due to structural elements is called structural damping. The damping that arises from these inelastic actions is called hysteretic damping. The damping that occurs in the structure due to soil characteristics is called as radiation damping.

Damping is expressed as a fraction of the critical damping (which is the minimum value of damping at which the structure gradually comes to rest from any one side of its neutral position without undergoing any oscillation). Damping is said to be different for different natural modes of oscillation of a structure. But, Indian seismic codes recommends the use of 5% damping for all natural modes of oscillation of reinforced concrete structures, and 2% for steel structures.

DESIGN CHARACTERISTICS

Earthquake ground motion is random and time variant. However, for design purpose, most of the design codes represent the earthquake-induced inertia forces as the net effect of the random shaking in the form of design equivalent static lateral force. This force is called as the Seismic Design Base Shear V_B and remains the primary quantity involved in force-based earthquake-resistant design of structures.

As per the Indian Seismic Code IS: 1893 (Part 1) - 2007, Design Base Shear VB is given by:

$$V_B = A_h W = \frac{ZI}{2R}\left(\frac{S_a}{g}\right)W \qquad (2)$$

where, Z is the Seismic Zone Factor , I the Importance Factor, R the Response Reduction Factor, and S_a/g the Design Acceleration Spectrum Value, W is the seismic weight of the structure calculated as per provisions in IS 1893-1 (2002).

While there is lesser control on design acceleration spectrum value A_h, seismic weight W could be reduced by choosing light and efficient materials. Also, the distribution of this mass in plan and elevation of the structure renders earthquake-induced inertia forces to be uniformly distributed throughout the structure, instead of being localized at a few parts of the structure.

RESPONSE OF BEAM COLUMN JOINT

Beam column joints significantly affect the response of the structure subjected to large forces during severe ground shaking. They are assumed to be rigid for designing and as such the shear forces developed in the joint remains unconsidered leading to brittle failure at the joints which is

undesirable. In Indian practice, the joints are not specifically designed and the attention is given to provide sufficient anchorage to beam longitudinal reinforcement. This may be acceptable only when the frame is not subjected to seismic loads. This poor design practice of joints is compounded by the high demand imposed by the adjoining flexural members (beams and columns). Unsafe design and detailing within the joint region jeopardize the entire structure, even if other structural members conform to the design requirements. Lu X. et al. (2012) showed that beam column joint is the weakest link in the structure and that most of the observed structural failure has been initiated by a damage or failure in the beam-column joint.

The main function of a joint is to enable the adjoining members to develop and sustain their ultimate capacity (Nelson et al. 2004). The response of beam-column joint is controlled by bond and shear failure mechanisms. In order to dissipate the seismic energy induced in the structure by the ground shaking, the structure must have sufficient ductility, which is in turn obtained by ensuring ductility of structural members in the form of inelastic rotations also known as plastic hinges. The basic seismic design requires the formation of plastic hinges in beams rather than in columns.

The shear force induced in the joint is resisted by truss and strut mechanism. The diagonal concrete strut action mechanism (MacGregor 1988) is formed by the major diagonal concrete compression force in the joint. This force is produced by the vertical and horizontal compression stresses as well as critical section of shear stresses on concrete of the beam and column. The truss mechanism (Park and Pauley 1975) is formed by a combination of the bond stress transfer along the beam and column longitudinal reinforcement, the tensile resistance of lateral reinforcement and compression resistance of uniform diagonal concrete struts in the joint panel. The strength of the strut mechanism depends on the comprehensive strength of concrete and that of the truss mechanism on the tensile yield strength of the lateral reinforcement crossing the failure plane. The design codes recommends adequate anchorage to longitudinal bars and confinement of core concrete (close ties both above and below the joint) for proper transfer of the shear forces induced in the joint.

Hooda N. et al. (2013) showed congestion of bars near the joint results in increase in deflection. The use of fibre reinforced concrete would resolve the problem of congestion and provide post-cracking ductility, thus improving the seismic response of structure.

Lu X. et al. (2012) proposed other non conventional methods of improving the response of the beam column joint, such as use of RC jackets and inclined bars. The shear resistance of beam column joint has increased with the provision of diagonal bars within the core and the plastic hinges were formed in beam far from the joint.

CONCLUSION

Earthquakes are one of nature's greatest hazards of life. The impact of this phenomenon is sudden with little or no warning to make preparations against damages and collapse of buildings/structures. The hazard to life in case of earthquake is almost entirely associated with man-made structures such as building, dams, bridges, etc. Prevention of disasters caused by earthquake has become increasingly important in recent years.

Bureau of Indian Standards (BIS) published various codes and guidelines in order to meet the seismic demands of not only the new structure but also to retrofit the old structures. The building planning and detailing must comply with the provisions given in the standards and codes to ensure safety of the structure and its occupants.

REFERRENCES

[1] Cheung, P.C., Paulay, T. and Park, R. (1993), "Behavior of beam column joints in seismically-loaded RC frames", Struct. Eng., 71(8), 129-138.

[2] Chopra, A. K. Dynamics of Structures. Theory and Applications to Earthquake Engineering. 3rd ed. New Jersy: Pearson.
[3] Hooda, N., Narwal, J., Singh, B., Verma, V. and Singh, P. (2013), An Experimental Investigation on Structural Behaviour of Beam Column Joint, IJITEE ISSN: 2278-3075, Volume-3, Issue-3.
[4] Hosur, V. (2013). Earthquake-Resistant Design of Building Structures, 1st ed. Delhi: Wiley.
[5] IS 1893 (Part 1):2002, "Criteria for Earthquake Resistant Design of Structures".
[6] Lu, X., Urukap, T. H., Li, S. and Lin, F. (2012), Seismic behavior of interior RC beam-column joints with additional bars under cyclic loading, Earthquakes and Structures, Vol. 3, No. 1, 37-57.
[7] MacGregor, J.G. (1988), Reinforced concrete mechanics and design, Prentice-Hall, Englewood Cliffs, NJ
[8] Nelson, A.H., Darwin, D. and Dolan, C.W. (2004), Design of concrete structure-thirteenth edition, McGraw-Hill, New York.
[9] Paz, M. Structural Dynamics. Theory and Computation .2nd ed. Delhi: CBS.

5th International Engineering Symposium - IES 2016
March 2-4, 2016, Kumamoto University, Japan

EFFECT OF RICE HUSK ASH ON SHEDI SOIL

Sharada K [1], Anjana Bhasi [2] and Katta Venkataramana[3]

1 *Undergraduate Student, Department of Civil Engineering, NMAMIT, Nitte 574110, India. Email: sharada.kakunje@gmail.com*
2 *Professor, Department of Civil Engineering, National Institute of Technology Karnataka, Surathkal, Mangalore 575025, India. email:anjanabhasi@yahoo.com*
3 *Professor and Dean(Acadamics), Department of Civil Engineering, National Institute of Technology Karnataka, Surathkal, Mangalore 575025, India. e-mail:ven.nitk@gmail.com*

ABSTRACT: The strength of weak soils can be improved by the addition of admixtures. Shedi soil is one of the locally available weak soils in the coastal region of Karnataka. Rice Husk Ash (RHA) is a waste from rice mills which causes dumping problem. In this paper, RHA is used as a stabilizer in different percentages to evaluate the properties of Shedi soil. The effect of Rice Husk Ash on index and engineering properties of Shedi soil was evaluated by liquid limit, plastic limit, standard proctor compaction test, unconfined compression test. Variation of optimum moisture content and dry density with different percentages of Rice Husk Ash was studied. The optimum amount of Rice Husk Ash was found to be 2%. Developed stabilized soil has shown satisfactory results.

***Keywords**: Rice Husk Ash, Shedi Soil, Soil Stabilization*

INTRODUCTION

Soft soils have problems like slope instability, large vertical settlement, differential vertical settlement and difficulty to move construction equipment. Shedi soil is considered to be soft soil. This soil can be improved by many methods such as replacing of soil, dynamic compaction, dynamic consolidation, vibration methods, soil reinforcement , grouting. Use of these ground improvement methods has kept the cost of construction financially high. A considerable amount of research concerning stabilisation of soil with additives such as cement, lime, lime – fly ash, bitumen and polymers is also available in the literature (Al-Amoudi, 2010; Muntohar, 2013). But recently, the use of agricultural waste such as Rice Husk Ash (RHA) which is produced in abundance and considered a worthless by–product of the rice mills, is found to considerably reduce the construction cost when used as a soil stabilizing material.

OBJECTIVES OF THE STUDY

- To characterize the soil by conducting routine laboratory tests like specific gravity, Atterberg Limits and grain size analysis. Also to determine engineering properties like Optimum Moisture Content (OMC), Maximum Dry Density (MDD) and Unconfined Compressive Strength (UCS).
- To determine the applicability, effectiveness and suitability of Rice Husk Ash (RHA) as soil stabilizing material.
- To find out the optimum content of RHA which gives maximum strength to stabilized soil compared to that of the original soil.

SHEDI SOIL

The coastal area of Karnataka has top hard layer of laterite. Below this, we can find the Shedi soil (Fig.1). During monsoon, when water gushes through this layer, Shedi soil dissolves and flows with water.

This creates cavities and heavy settlement and sliding of top layer after application of load.

Fig.1 Shedi Soil

Fig.2 Rice Husk Ash (RHA)

RICE HUSK ASH (RHA)

India is a major rice producing country. About 20 million tons of RHA (Fig.2) produced annually. This much of RHA is a great environmental in terms of dumping. Lots of ways are being thought of for disposing them by making commercial use of this RHA.

During milling of paddy, 78% by weight is rice and 22% is husk. Husk is used as fuel in mills. By burning Husk, 75% organic volatile matter and 25% is Rice Husk Ash. So for every 1000 kg of paddy grains, 220 kg of Husk will be generated and for this 220 kg of husk, 55 kg of Rice Husk Ash will be generated. The Rice Husk Ash is a silica rich material. The chemical composition of RHA (Table 1.1) as follows

Table.1 Chemical composition of RHA (Khandaker et al. 2011)

Oxide compounds	**%**
Calcium oxide (CaO)	2.4
Silica (SiO_2)	91.3
Alumina ($Al2O_3$)	1.4
Iron oxide (Fe_2O_3)	0.6
Magnesia (MgO)	2.1
Sodium oxide (Na_2O)	0.3
Potassium oxide (K_2O)	1.9

Based on the burning conditions, RHA is categorized as active ash (A-RHA), carbon ash (C-RHA) and crystallized ash (Cr-RHA) (Table 1.2).

Table 2 Classification of RHA (Vinh Pham 2012)

Ash	**Burning Condition**	**Color**	**Expectation**
A-RHA	500 'C in 2 hours, quick cooling	Grey	Highly active
C-RHA	Open- air and quick burning	Black	Averagely active due to high amount of carbon
Cr-RHA	Slowly burning and cooling in range of 600'C and 700'C	Pink	Averagely active due to crystallized silica

METHODOLOGY

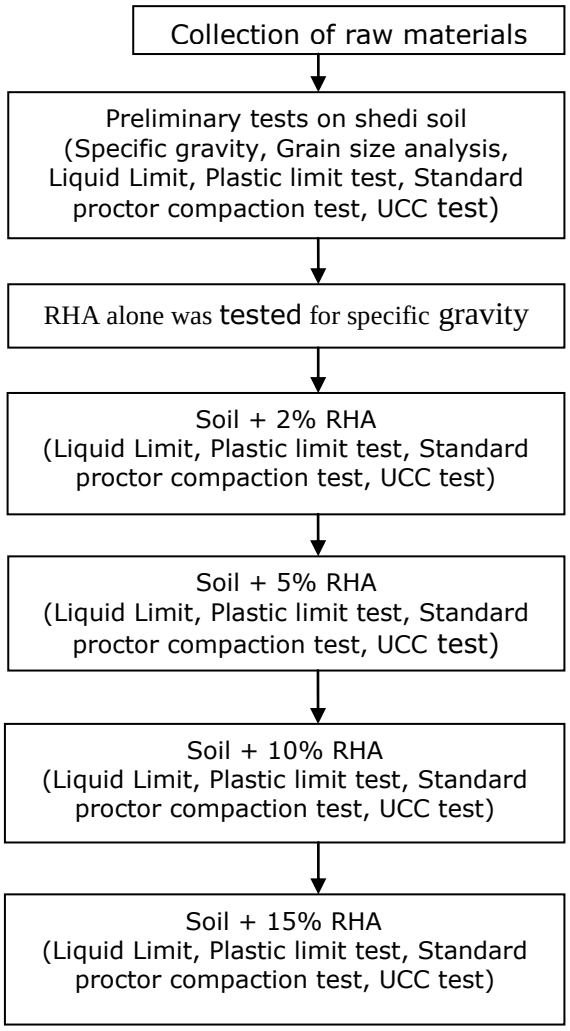

BASIC PROPERTIES OF SHEDI SOIL

Initially, basic properties of the Shedi soil (Table 3.1) were found out by conducting different tests.

Table 3 Basic property of shedi soil

Characteristics	**Description**
Specific Gravity	2.55
Particle Size Distribution	Fine grained
Liquid Limit (%)	46
Plastic Limit (%)	30.97
Plasticity Index (%)	15.42
Maximum Dry Density(g/cm^3)	1.41
Optimum Moisture Content (%)	29.2
Unconfined Compressive Strength (KN/m$^{2)}$	282

BASIC PROPERTY OF RHA

Specific Gravity of RHA was found out by density bottle method.

Table 4 Basic property of RHA

Characteristic	Description
Specific Gravity	2.3

TESTS ON DIFFERENT PROPORTIONS OF RHA

4.1. LIQUID LIMIT

Soil was mixed with different percentages of RHA (2%, 4%, 5%, 10%, and 15%). The effect of adding different proportions of RHA on the properties of Shedi soil was studied. The first property studied was Liquid Limit.

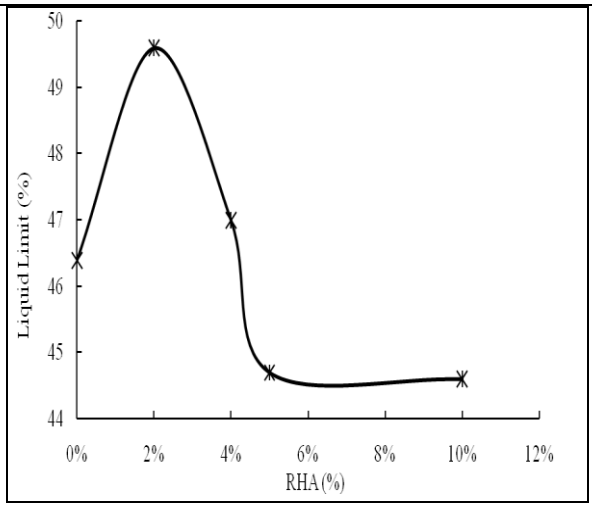

Fig 4.1 Influence of RHA on liquid limit parameter

According to the Fig 4.1, adding RHA to the soil caused an increase in the liquid limit parameter till 2% of RHA.The reason is the need for extra water for reactions to take place.

Above 2% of RHA, liq limit decreased. This maybe due to the reduction in pores due to the formation of cementatious material which formed closer bond between the soil particles.

4.2. PLASTIC LIMIT

The effect of RHA on plastic limit was studied.

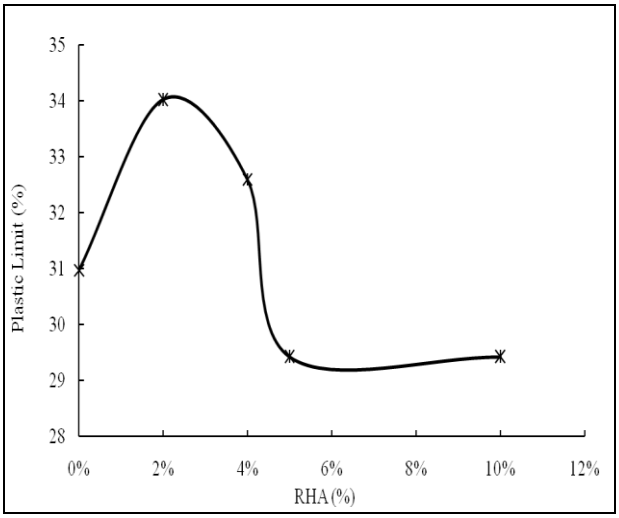

Fig 4.2 Influence of RHA on plastic limit parameter

According to Fig 4.2, adding RHA to the soil caused an increase in plastic limit up to 2%. Above 2%, with increase in RHA, plastic limit decreased. This is due to the same reason as given in the case of liquid limit.

4.3. STANDARD PROCTOR COMPACTION TEST

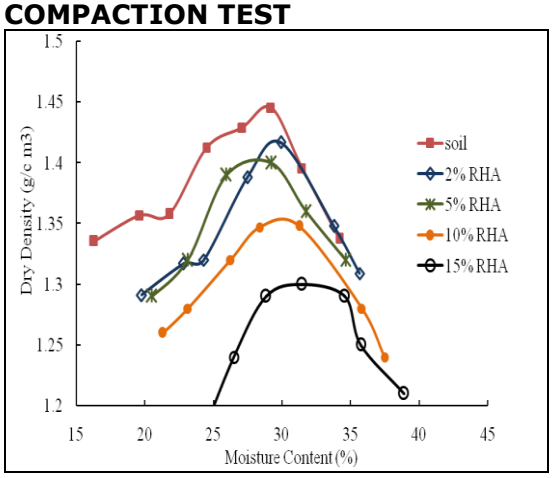

Fig. 4.3 Variation of dry density with moisture content

(a) Variation of OMC with RHA content

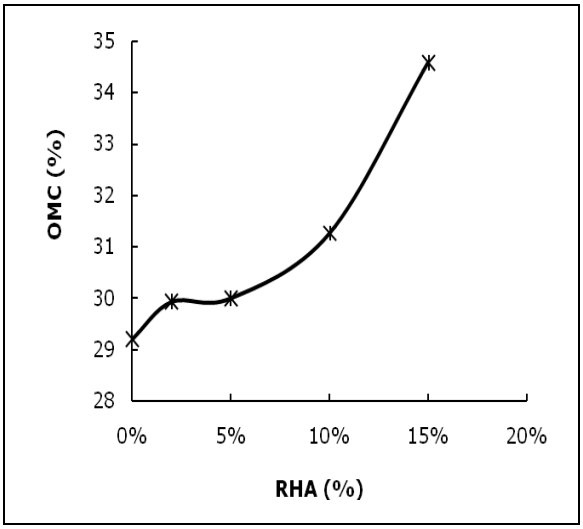

Fig 4.4 Variation of OMC with RHA

Increase in OMC is caused by the absorption of water by the additives to precede the chemical reaction.

(b) Variation of dry density with RHA content

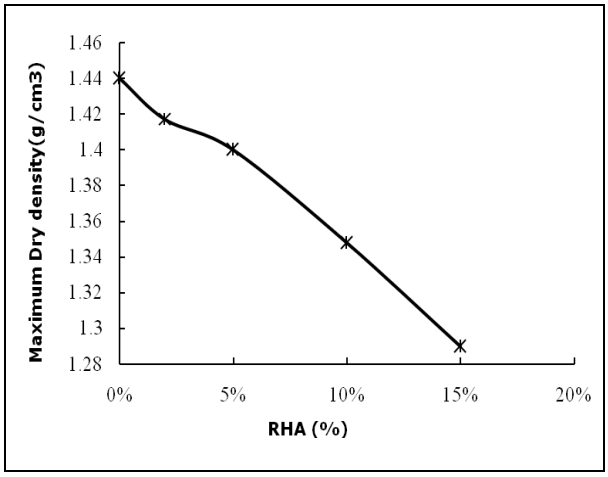

Fig. 4.5 Variation of MDD with RHA

Dry density is reduced by the presence of additives owing to its relatively low specific gravity (Table 3.2).

4.4. UNCONFINED COMPRESSION TEST (UCC TEST)

In general, compressive strength increases with the increase in the stabilizer content. Fig.4.6 shows the development of unconfined compressive strength of stabilized soil with varying percentages of RHA. RHA increases the silica content of the soil. This increases the pozzolanic reaction of the soil. Hence the strength is increased till 2% of RHA. Later as the percentage of RHA increases beyond 2%, RHA makes the soil brittle and hence the failure of the specimen happens.

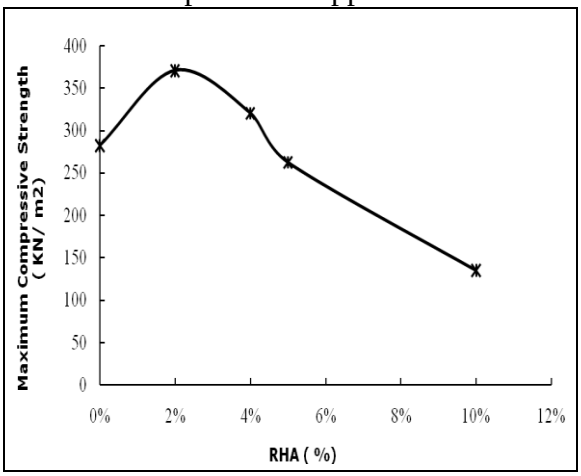

Fig. 4.6 Influence of RHA content on Unconfined Compressive strength

Fig. 3 UCC test apparatus

CONCLUSIONS

A series of tests have been performed to study the effects of RHA on the strength of shedi soil. The following results were obtained from the tests conducted on soil mixtures with RHA content varying from 0% to maximum 15%.

1) Up to 2% of RHA, Liquid limit and plastic limit were found to increase. Above 2% of RHA, Liquid limit and plastic limit were found to decrease.

2) Increasing treatment with RHA showed a decrease in the dry density of the treated soil. The reason is that the specific gravity of RHA is less than soil.
3) An increase in the Optimum Moisture Content (OMC) was caused with increase in the RHA content. The reason is the activation of pozzolan reaction of soil and RHA, which needs more water.
4) The potential benefit of stabilization is found to depend on the amount of stabilizers. For the combination of soil and 2% RHA, the maximum strength was obtained. The increase in strength was found to be 31 % when compared to normal Shedi soil.
5) High percentage of siliceous materials in the RHA makes it a good material for stabilization and use of RHA with lime-Cement mixes for further improvement of strength can be thought of.

REFERENCES

[1] Al-Rawas, A. A., Hago, A., and Al-Sarmi, H. (2005) Effect of lime, cement and Sarooj (artificial pozzolan) on the swelling potential of an expansive soil from Oman. Building and Environment, 40(5), 681–687.
[2] Al-Amoudi, O. S. B., Khan, K., and Nasser Saban Al-Kahtani, N. S. (2010) Stabilization of a Saudi calcareous marl soil. Construction and Building Materials, 24(10), 1848–1854.
[3] Anwar Hossain, K. (2011) Stabilized Soils Incorporating Combinations of Rice Husk Ash and Cement Kiln Dust. Journal of Materials in Civil Engineering, 23(9), 1320–1327.
[4] Choobbasti, A. J., Ghodrat,H., Vahdatirad, M. J., Firouzian,S., Barari,A., Torabi,M., and Bagherian,A. (2010) Influence of using rice husk ash in soil stabilization method with lime. Frontiers of Earth Science in China, 4(4), 471–480.
[5] IS 2720 (1964). Methods of test for soils, Bureau of Indian Standards, New Delhi.
[6] Muntohar, A. S., Widianti,A., Hartono,E., and Diana,W.(2013) Engineering Properties of Silty Soil Stabilized with Lime and Rice Husk Ash and Reinforced with Waste Plastic Fiber . Journal of Materials in Civil Engineering, 25(9), 1260-1270.
[7] Singhai,A.K., and Singh,S.S. (2014) Laboratory Study On Soil Stabilization Using Fly Ash And Rice Husk Ash. International Journal of Research in Engineering and Technology, 3(11), 348-351.
[8] Vinh Pham (2012) Utilization of Rice husk ash in GeoTechnology. *A MSc thesis submitted to the* Delft University of Technology, Netherlands.

5th International Engineering Symposium - IES 2016
March 2-4, 2016, Kumamoto University, Japan

Statistical Downscaling of Precipitation from GCM output using SVM in Nethravathi River Basin

Syed Ameena[1] , Dr.Paresh Chandra Deka[2]

1 *M.Tech Student, Department of Applied Mechanics& Hydraulics, National Institute of Technology, Surathkal-575025, India. e-mail: ameenarahman1991@gmail.com*
2 *Associate Professor, Department of Applied Mechanics& Hydraulics, National Institute of Technology, Surathkal-575025, India. e-mail: pareshdeka@yahoo.com*

ABSTRACT: Global climate models (GCMs) are considered to be the ultimate contrivance to simulate the doom of anthropogenic de-gradation of climate. However the GCMs cannot be directly applied to hydrological models because of the mismatch in the data resolution. Thus downscaling is considered to be a solution to present the coarse GCM data to finer resolution. This research concentrates on two statistical downscaling techniques namely LS-SVM (Least square support vector machine) and ANN (artificial neural network) to downscale CMIP5 GCM output to obtain daily simulations of precipitation for monsoon period in future. This study also undertakes rigorous evaluation and comparison of the two downscaling techniques.

Keywords*: Climate change, Statistical downscaling, Support Vector Machine(SVM) , Artificial Neural Network(ANN).*

INTRODUCTION

GCMs are gaining popularity and reliability to replace the method of hydrological modelling to study climate change impacts (Tofiq and Guven, 2014)**.** Impact of climate change on hydrologic variables can be studied by downscaled data from the atmospheric circulation patterns induced with specific external forcing like sea level rise, land use changes and changes in green house gases, developed at global scale of the order of 10^6 km^2.

Downscaling is the process of interpolating regional-scale atmospheric processes occurring at incongruent spatial and/or temporal scales (predictor variables) to station-scale meteorological series (predictand variables).High resolution rain fall data could be projected by integrating spatio-temporal downscaling (Lu and Qin, 2014). The most recent developed model is the Coupled Model Intercomparison Project Phase5 (CMIP5). Representative Concentration Pathway (RCP) with irradiative forcing levels of 8.5, 6, 4.5 and 2.6 W/m^2 (Vuuren et al., 2011) are considered as the external driving force.

Climate modeling is just a mere Baedeker and not an exact itinerary. It is heuristic in projecting precipitation taking into account the effects of global warming and subtropical drying robustly, but failing in simulating the effects of El-Nino and the inter tropical convergence zone relocation (Anon,2012).

The use of data mining (DM) techniques in downscaling generally classified under the Statistical downscaling technique, is found beneficial in many ways (USAID, 2014). Some of the important data mining techniques are artificial neural networks and support vector machines.

Artificial neural network (ANN) is based on the functioning of brain theory. (Behzad et al., 2009) employed multi-layer feed forward and back-propagation algorithm. (Snell et al., 2000) used ANN to interpolate surface air temperature. ANN model is superior both in terms of predictive precision and encompass model.

Support vectors act as informative variables (Chen, 2015). Support Vector

Machines is used for studying linear and nonlinear cluster data (Suykens, 2001). Different kernels of Support Vector Machine like Least Square Radial Basis Function (Tripathi et al., 2006) and Polynomial (Aksornsingchai and Srinilta, 2011). Several regression techniques in SVM has also been studied like Least Square Regression (Sachindra et al., 2013) , Smooth Support Vector Machine (Chen et al., 2012) and Relevance Vector Machine(RVM) (Ghosh and Mujumdar, 2008). (Chen et al., 2010) used support vector classification (SVC) to determine whether the day is dry or wet and support vector regression (SVR) to estimate the amount of precipitation conditional on the occurrence of a wet day.

STUDY AREA

Nethravathi River is one among the perennial west flowing rivers of Karnataka with many hydroelectric projects and diversion schemes. Hence, climate change impact study may also give the insight to future availability of water coupled with GCM Scenario outputs. The average annual rainfall of the basin is found to be 4113.1mm with a range of 2970.1mm to 5585.1 mm. The maximum temperature ranges from 26.4 °C to 36.5 °C and minimum temperature ranges from 15.8°C to 27.2 °C , on an average of 27.4 °C . The humidity of the basin is more than 85% with Tropical Moist Climate.

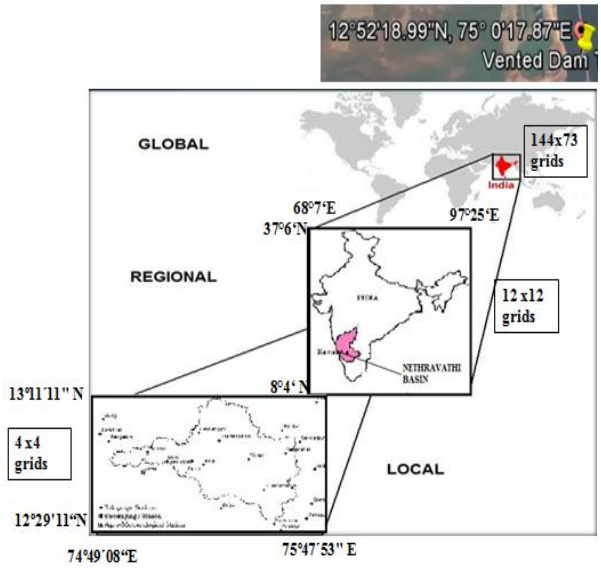

Fig.1 Study area showing grid points

The extent of scaling down of GCM grid data to national and basin data grids is shown in the Figure 1. Fig. 2 depicts box-plot of daily precipitation for Bantwal station at basin outlet. The monsoon arrives in June first week and rains heavily till September. Other months receive less than 100 mm. About 90% of annual rainfall occurs in June to October due to the southwest monsoons.

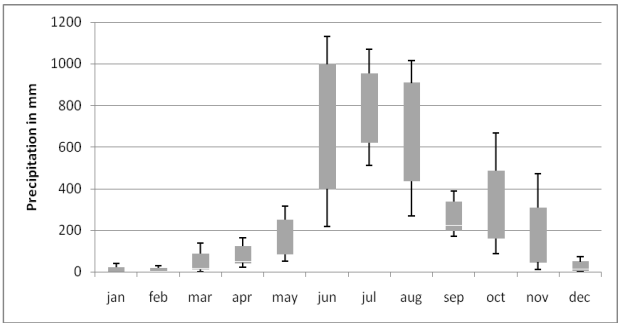

Fig.2 Mean daily precipitation at Bantwal.

DATA PROCUREMENT

The following listed datasets have been used for downscaling precipitation on a daily basis at a site resolution.

Table 2 Data set and Source

DATA TYPE	BASE PERIOD	RESOLUTION	SOURCE
Rainfall	1981-2013	0.25°X 0.25°	IMD
Predictor	2006-2050	2.81°X 2.81 °	CCCM3
Predictor	1981-2010	2.5 °X 2.5 °	NCEP/ NCAR Re-analysis

The National Center for Environmental Prediction (NCEP) and National Center for Atmospheric Research (NCAR) have created a 50year historical database in terms of atmospheric fields for climate studies at global scale. The NCEP & NCAR Reanalysis is considered as a proxy to observed data. Station data was used for the calibration (1981-2006) and validation (2007-2010) of the downscaling model with the NCEP-NCAR data and the Canadian Coupled Climate Model (CCCM3) from CMIP5 project for the RCP4.5 scenario respectively.

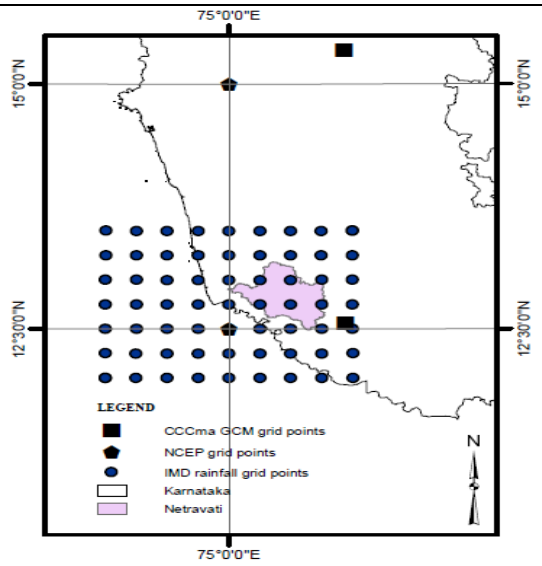

Fig.2 Study area

METHODOLOGY

The methodology adopted for downscaling precipitation from Global climate models using data mining techniques is as explained in the following sections:

1. Selection of predictors
2. Data processing
3. Seasonal stratification
4. Training and validation

From Table 1, the most common grid size is 4x4 and similarly about 5 predictor variables namely Hgt, shum, uwnd, vwnd, Tair and mslp are considered.

Table 1 Selection of Predictors

Author	Predictor
Tripathi et.al (2006). 6x6 grid	Air, hgt, shum, uwnd. (5 variables)
Raje& Mujumdar (2011) 6x6 grid	mslp, shum, ,Ts, uwnd, vwnd. (6 variables)
Chen et.al (2010). 4x4 grid	Mslp, geotropic air velocity, uwnd, vwnd, vorticity, divergence, rhum, shum, Tmean (26 variables)
Manjula et.al (2015) 3x3 grid	Ta, hgt, shum, uwnd, vwnd,sp,Ts (15 variables)

Air-air temperature (°K), hgt – geopotential height (m), shum- specific humidity, uwnd- meridional wind speed (m/s),Ts – surface temperature ,vwnd – zonal windspeed (m/s) , mslp –mean sea level pressure, sp – surface pressure ,rhum – relative humidity.

Data processing includes interpolation, Standardization, Bias removal and Principal component analysis. Daily large scale atmospheric data of GCM are interpolated to NCEP grid points using 3rd order (4-point) Bessel interpolation to overcome the resolution mismatch (Srinivas et al., 2014). Each variable is then normalized by subtracting the mean from it and then dividing the result by the standard deviation of the original variable.

Training large data sets hinders the performance of the data modelling techniques and hence the a data reduction technique called principal component analysis is followed as explained by Mujumdar and Nagesh Kumar (2012).

Chen et al.(2010) stratified the seasons into dry and wet days in order to select the predictors for regression. If the statistical property of predictor from the Two-sample Kolmogorov Smirnov test for the zero precipitation is different from that of non zero precipitation, then that predictor was chosen for the regression model developed to quantify the amount of precipitation.

ANN is a cognitive machine learning techniques consisting of three basic layers –input, hidden and output with interconnected neurons in each layer. The present study adopts as single hidden layer feed forward neural network. The training is done using back propagation algorithm is used to train the network. Sigmoid and purline activation functions are used in the hidden and output layers, respectively, Noori et al (2014).

Support Vector Machine (SVM) works on statistical learning theory and structural risk minimization.In the SVM technique, least square LS-SVM regression model has two tuning parameters -regularization parameter which determines the magnitude for penalty of the soft margin and the kernel parameter for the RBF kernel selected. Tuning of these parameters has been done by the cross validation technique using LIB-SVM.

RESULTS AND DISCUSSIONS

From the PCA in figure 3, it is found that the first 3 variables contributed to more than 90% of the variability. Therefore the first three variables are retained for model development.

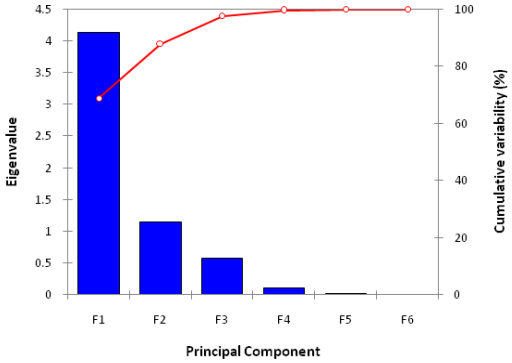

Fig.3 Variance explained by the PCs

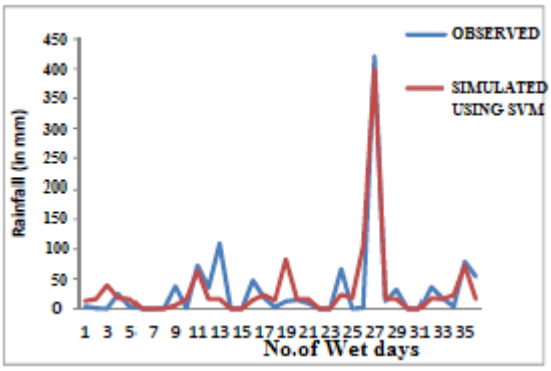

Fig.4 Validation of the model

Table 2 Model Performance

γ,σ^2	100,0.5
Nash –Sutcliffe coefficient	0.81
Daily extreme rainfall observed	446.7mm
Daily extreme rainfall simulated	442.86mm

CONCLUSIONS

The following conclusions are deduced from this study:

- LS-SVM performs better than ANN due to its ability to capture peaks and extreme rainfall events.
- Nash-Sutcliffe coefficient and the total sum of the rainfall proved as the best measures performance evaluation of the downscaling model.
- The daily precipitation was generated and it was determined to be on the rise

REFERENCES

[1] Aksornsingchai.P and Srinilta. C (2011), Statistical Downscaling for Rainfall and Temperature Prediction in Thailand In.
[2]Bader et.al (2008), Climate Models: An Assessment of Strengths and Limitations. A Rep. by U.S. Clim. Chang. Sci. Progr. Subcomm. Glob. Chang. Res. 124 pp.
[3] Behzad et al (2009), Generalization performance of support vector machines and neural networks in runoff modeling. Expert Syst. Appl. 36,pp 7624–7629.
[4]Chen et al (2012), Comparison and evaluation of multiple GCMs, statistical downscaling and hydrological models in the study of climate change impacts on runoff. J. Hydrol. 434-435, 36–45. doi:10.1016/j.jhydrol.2012.02.040
[5]Chen et al (2015), Mining Informative Hydrologic Data by Using Support Vector Machines and Elucidating Mined Data according to Information Entropy. Entropy 17, pp 1023–1041.
[6]Chen et al (2010), Statistical downscaling of daily precipitation using support vector machines and multivariate analysis. J. Hydrol. 385, pp 13–22.
[7]Devak et al (2015), Dynamic coupling of support vector machine and K-nearest neighbour for downscaling daily rainfall, J. Hydrol. 525, pp 286–301.
[8]Ghosh and Mujumdar (2008), Statistical downscaling of GCM simulations to streamflow using relevance vector machine. Adv. Water Resour. 31, pp 132–146.
[9]Lu, Y., Qin, X.S.(2014), Multisite rainfall downscaling and disaggregation in a tropical urban area. J. Hydrol. 509, pp 55–65.
[10]Mujumdar, P.P., Nagesh Kumar, D (2012), Floods in a changing climate, 1 ed. international hydrology series, United Kingdom.
[11] Noori, (2014), Assessment of input variables determination on the SVM model performance using PCA, Gamma test, and forward selection techniques for monthly stream flow prediction. J. Hydrol. 401, pp 177-189.
[10]Sachindra et al (2013), LS support vector and multi-linear regression for statistically downscaling general circulation model outputs to catchment streamflows. Int. J. Climatol. 33, 1087–1106.
[11]Snell et.al (2000). Spatial interpolation of surface air temperatures using artificial neural networks: Evaluating their use for downscaling GCMs. J. Clim. 13, 886–895.
[12]Srinivas et al (2014), Multi-site downscaling of maximum and minimum daily temperature using support vector machine. Int. J. Climatol. 34, 1538–1560.
[13]Suykens (2001), Nonlinear modelling and support vector machines. IMTC 2001 Proc. 18th IEEE Instrum. Meas. Technol. Conf. Rediscovering Meas. Age Informatics Cat No01CH 37188 1, 287–294.
[14]Tofiq and Guven(2014), Prediction of design flood discharge by statistical downscaling and General Circulation Models. J. Hydrol. 517, 1145–1153.
[15]Tripathi et al (2006), Downscaling of precipitation for climate change scenarios: A support vector machine approach. J. Hydrol. 330, 621–640.
[16]Vuuren et al (2011) The representative concentration pathways : an overview 5–31.

5th International Engineering Symposium - IES 2016
March 2-4, 2016, Kumamoto University, Japan

Groundwater Modeling Using GMS-10 For Gurupura Sub-Basin Comprising of Wetlands

Reenu Siby Aricatt [1], Chingka Kalai [2] and Subrahmanya K.[3]

1 *M.Tech Student, Department of Applied Mechanics, NITK, Surathkal, 2-39-1, Mangalore 575025, e-mail:reenusiby18@gmail.com*
2 *Master course student, Department Applied Mechanics, National Institute of Technology Karnataka, Surathkal, Mangalore 575025, India. Email:chingkalai@gmail.com*
3 *Asst.Profesor, Department of Applied Mechanics, NIT Karnataka, Mangalore 575025, India. Email : subrahmanyakundapura@gmail.com*

ABSTRACT: The sustainable use and management of groundwater resources is now a great challenge for many countries. Recently groundwater modelling has been an effective way to address this challenge. There are a number of modelling softwares that exist to simulate groundwater flow. Among them modelling software MODFLOW is used to determine the interactions between the surface water and groundwater and to develop a model for the study area. To combat the threats,like the excess groundwater extraction,reclamation activities and protection of the wetlands in the coastal regions of Dakshin Kannada district,it is necessary to develop a groundwater management model.In the present study a numerical groundwater model using GMS MODFLOW for a wetland present in Gurupura sub-Basin is developed which can help in predicting the future groundwater levels.The boundary of the study area was determined from Bhuvan 2D and ArcGIS was also used for data preparation to feed the model input.The transient models which are data intensive but more reliable in exploring the groundwater flow regimes due to spatial-temporal nature of flux input was chosen. The study focused on development of transient Groundwater model of the study area,comparing the model results with the field data collected and analyze the water quality of the study area.
Keywords*:MODFLOW,Transient model,Bhuvan 2D, Conceptualization*

INTRODUCTION

Groundwater is considered to be one of the major drinking water resources many countries. Therefore, it requires best possible management and protection measures to preserve to its utmost quality and put it to its beneficial use. With growing development of the resource and with growing human impact on the aquifers, the management of this essential source is important. Problems like over-pumping and groundwater pollution result in the drastic depletion of the resource. To mitigate conflicts of interests and avoid severe environmental damage, we must be able to predict the reactions of aquifers to human impact with respect to both groundwater quality and quantity. Groundwater models are computer models of groundwater flow systems, are used by hydro-geologist. Aquifer conditions can be predicted using groundwater models. They can also be defined as a powerful management and prediction tool which combines the appropriate physical laws in a self-consistent mathematical model with the available hydro-geological data, to understand the response to externally applied stress and its behavior and properties of the system. Numerical groundwater model are computer based representation of the characteristics of a real hydro-geological system that uses the laws of science and mathematics. Groundwater modeling in recent years has become one of major part of many projects dealing with groundwater

exploitation, remediation and protection. The role of numerical models in groundwater investigation will increase accordingly, as computer hardware and software continue to be upgraded and become more affordable. It is essential, to interpret groundwater model, understand its limitations and use properly.

Groundwater Modelling

Groundwater modeling has been proved to be an economical and important tool that conceptualize the groundwater strategies. Studies conducted in various regions using Groundwater Modelling Systems have been discussed here**.**

A recent study conducted using MODFLOW includes Lakshmi Priya et al(2015) uses Visual MODFLOW to study and simulate the behavior of complex aquifers including the effects of irregular boundaries, heterogeneity and different processes such as groundwater flow, and solute transport. Mathematical models are tools, which are frequently used in studying groundwater systems. In general, mathematical models are used to simulate (or to predict) the groundwater flow and in some cases the solute and/or heat transport.(C.P.Kumar)

STUDY AREA

GENERAL

Gurupura river is one of the major west flowing river of Dakshin Kannada district. The present study area is a sub-basin of Gurupura River and is heavily urbanized and industrialized, for this reason fresh water is more acute. The groundwater quality and quantity in this study area is highly affected due to excessive groundwater extraction for industrial, agriculture and domestic purpose.

LOCATION

The present study area is a sub-basin of Gurupura river around 17-23 km from Surathkal. The areal extent of the study area is approximately 57.73 km^2. It lies between longitude of 74°48'24.16"E to 74°56'23.08"E and latitude of 12°56'0.18"N to 12°59'31.97"N. The study area is combination of 2 small watersheds. The first watershed is covering areal extent of 36.8 km^2, lies between longitude of 74°48'24.16"E to 74°53'28.42"E and latitude of 12°56'0.18"N to 2°59'31.97"N. The second watershed is covering area of 21km^2, lying between longitude of 74°51'39.64"E to 74°56'23.08"E and latitude of 12°56'16.59"N to 12°58'50.85"N.

METHODOLOGY

1. Delineate the study area **.**
2. Create a groundwater model of the study area using GMS
3. Field visit to the site and check if the delineation is correct
4. Note the study area, the location of wells using GPS & collect water.
5. Run the model a get the groundwater contours of the study areas also the head at each observation wells
6. Verify the model results with the field values
7. Model values almost similar to field values
   - If the model values are similar to field values,the model developed is correct.
   - If the model values are not similar to the field values,model needs to be checked .

Groundwater flow modeling using MODFLOW

Groundwater model using MODFLOW with comprehensive graphical interface is included in GMS. MODFLOW is a 3-D, cell-centered, finite difference, saturated flow model developed by the United States Geological Survey (McDonald & Harbaugh, 1988). Both steady state and transient analyses can be performed in MODFLOW and has a wide variety of boundary conditions and input options.

Data Used

Boundary of the study area ,Data of source and sink ,Layer Elevation,Aquifer parameters, Recharge rates

Equations

The governing equation for groundwater flow is the theoretical basis of the model. The three-dimensional, non-equilibrium movement of groundwater of constant density through anisotropic, porous and

heterogonous medium can be described by the following partial differential equation:

$$S_s \frac{\partial h}{\partial t} + W(x,y,z,t) = \frac{\partial}{\partial x}\left(K_{xx}\frac{\partial h}{\partial x}\right) + \frac{\partial}{\partial y}\left(K_{yy}\frac{\partial h}{\partial y}\right) + \frac{\partial}{\partial z}\left(K_{zz}\frac{\partial h}{\partial z}\right) \quad (1)$$

CONCLUSIONS

The study carried out was an attempt towards development of ground water flow model, using software called Groundwater Modelling Systems (GMS) 10. In the above study a transient model was developed for Gurupura Sub-Basin, considering constant pumping all through the year. The recharge rate was fed to the model considering the rainfall during each month.

- The model developed would give the change in ground water contour for each day, within the stress period. The field data collected for a particular day in a month could be compared with the simulated value for that same day.
- The model results were compared with actual water level for the months of January, February, March and April (Year 2015).
- The correlation coefficient (R^2) of simulated vs observed water levels for the month of January, February, March and April for the year 2015 are 0.9573, 0.9547, 0.9527 and 0.9359 respectively.
- The Root Mean Square of Errors (RMSE) value of simulated vs observed water levels for the month of January, February, March and April are 8.15, 23.45, 7.97 and 8.59 respectively.
- The overall R^2 and RMSE values of simulated vs observed water levels for the four months are 0.95 and 8.17 respectively.
- The Ground water model developed for the study area can be used for predicting future water table depending on the rainfall pattern.
- From the field observation it can be concluded that the water table remains very close to the ground surface
- The difference between the water table level and the ground surface increases from January to April in the year 2015.

ACKNOWLEDGEMENTS

The authors thank the Ministry of Education, Government of India and TEQIP which provided financial support to carry out this research.

REFERENCES

References should be given in alphabetical order. (font to be used: Verdana 8)

[1]C.P.Kumar.Concepts and Modeling of Groundwater System, IJISET - International Journal of Innovative Science, Engineering & Technology, Vol. 2 Issue 2, February 2015

[2]Lakshmi Priya,Narayanan RM, Study on Groundwater Modelling of Aquifers using Visual Modflow. International Research Journal of Engineering and Technology, Vol 2,Issue 2,May 2015

[3] Chinga Kalai, 2014. Groundwater Modelling using GMS 10 ,M.Tech Thesis,Department of Applied Mechanics and Hydraulics,National Institute Of Technology,Surathkal

[4] Magnus. U. Igboekwe, N. J. Achi, Finite Difference Method ofModelling groundwater Flow, Journal of Water Resource and Protection, 3, 192-198

[5]SG.Sindhu,2012.Groundwater Management of coastal aquifers in Trivandrum, International Conference on Modelling Optimization and Computing, Volume 38, 2012, Pages 3434–3448

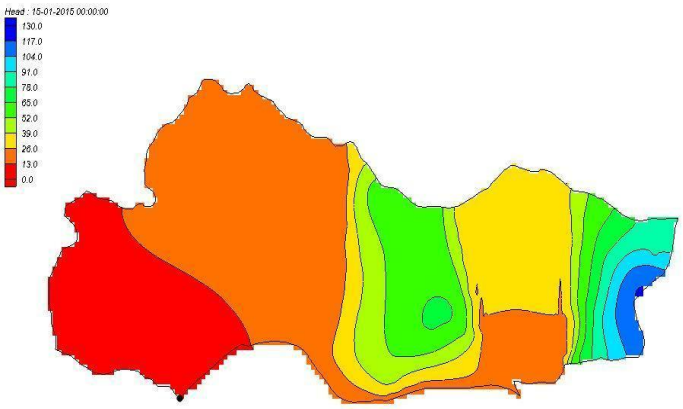

Figure1.Simulated Groundwater Contour(m) of January

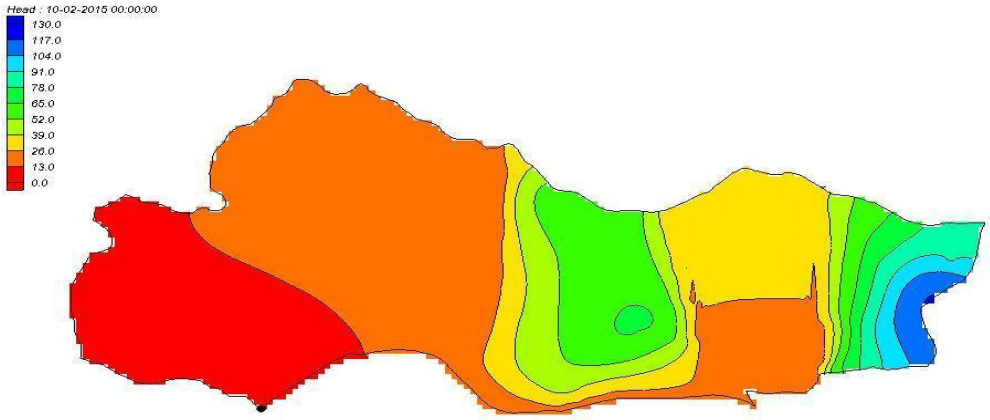

Figure2.Simulated Groundwater Contour(m) of February

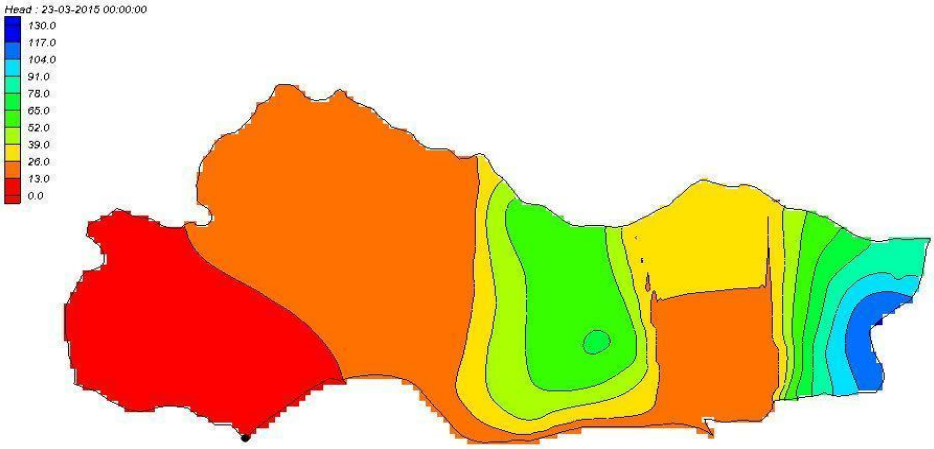

Figure3.Simulated Groundwater Contour(m) of March

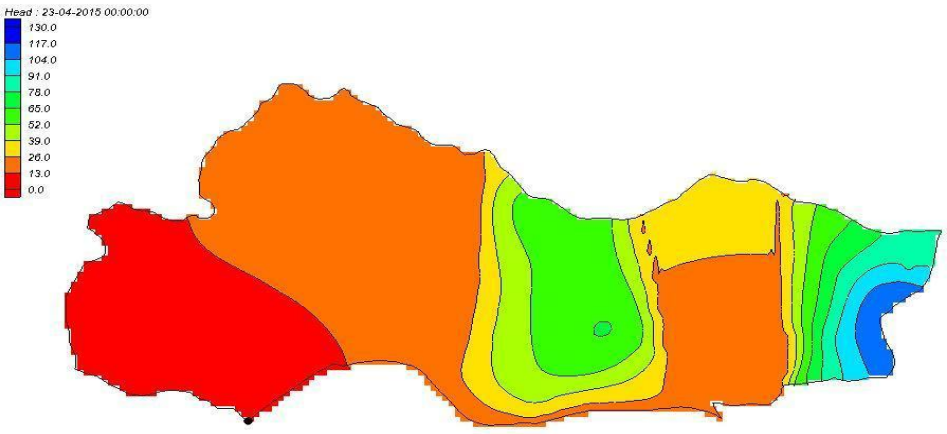

Figure4.Simulated Groundwater Contour(m) of April

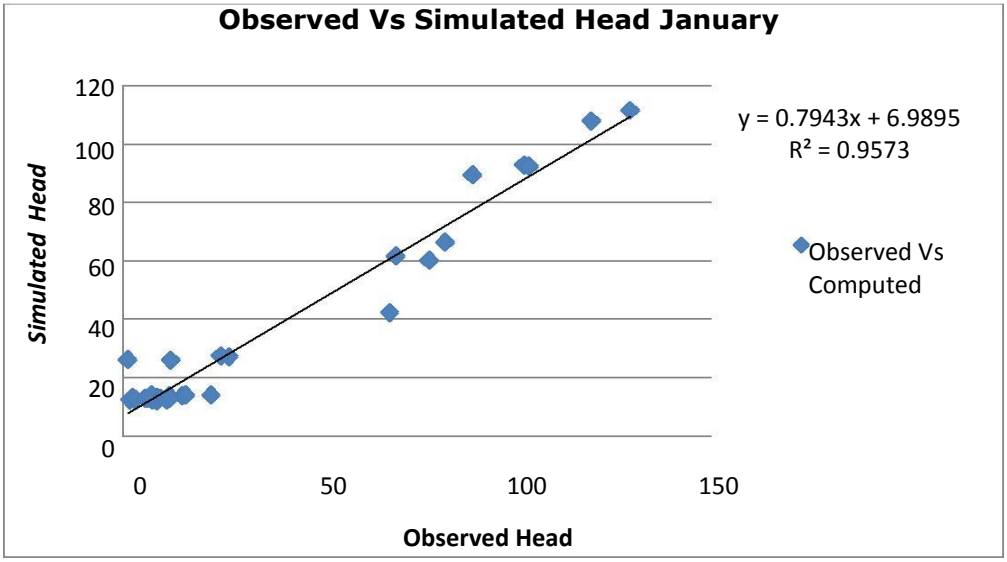

Figure5.Observed Vs Simulated Head Values at 31 Wells for the month of January

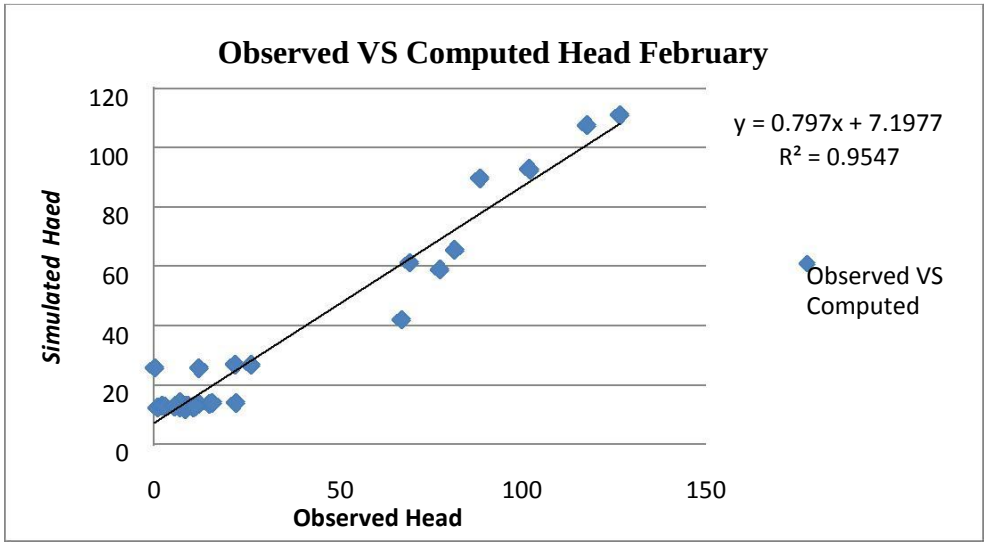

Figure6.Observed Vs Simulated Head Values at 31 Wells for the month of February

Figure6.Observed Vs Simulated Head Values at 31 Wells for the month of March

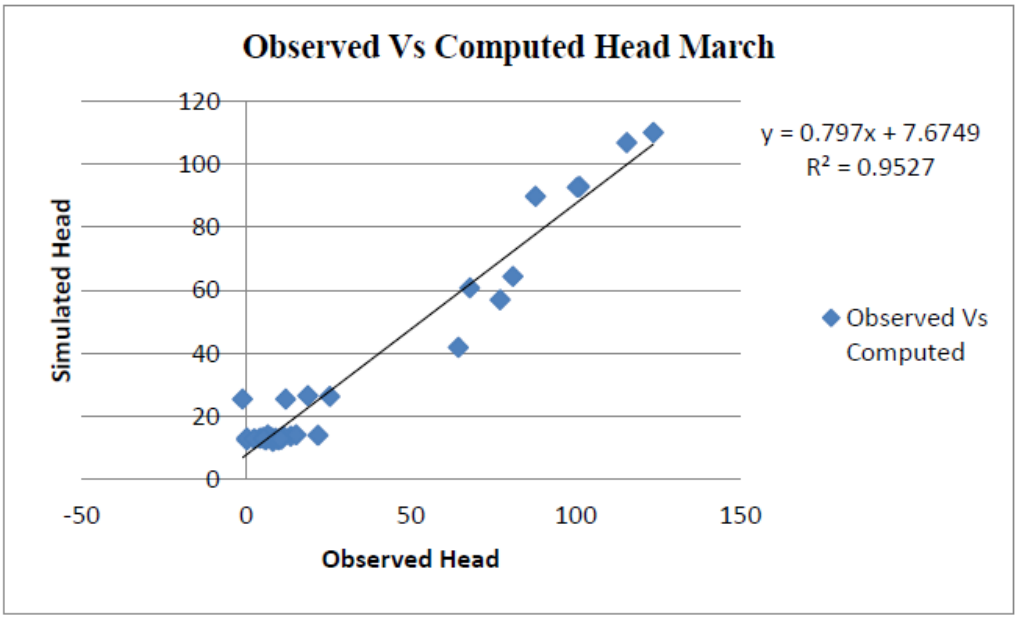

Figure7.Observed Vs Simulated Head Values at 31 Wells for the month of March

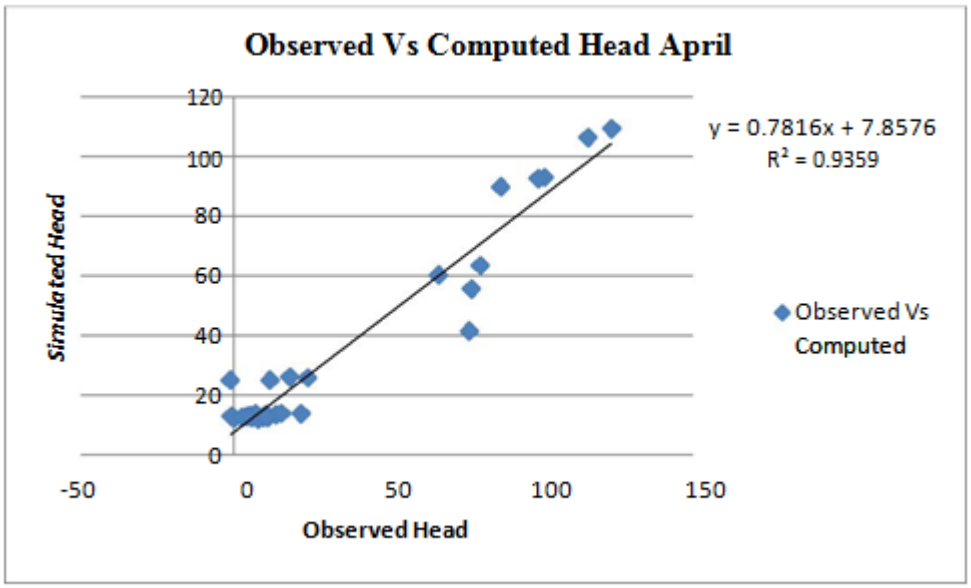

Figure8.Observed Vs Simulated Head Values at 31 Wells for the month of April

5th International Engineering Symposium - IES 2016
March 2-4, 2016, Kumamoto University, Japan

REUSE TECHNIQUE FOR DOMESTIC WASTE WATER IN MULTI-STORIED BUILDINGS

Mohammed Mohiuddin Asad[1], Rajasekaran, C[2] and Shree Vidhya, R[3]

1 *Post Graduate Student, Department of Civil Engineering, NITK, Surathkal, India. Email:* mohdasad36@gmail.com
2 *Assistant Professor, Department of Civil Engineering, NITK, Surathkal, India. Email:* bcrajasekaran@gmail.com
3 *Lecturer, Department of Civil Engineering, NITK, Surathkal, India. Email:* shreevidhyaramamoorthy@gmail.com

ABSTRACT: Increasing water demand has become a significant issue of concern due to population explosion and water scarcity. To avoid water crisis, there is a need for reducing the generation of wastewater and reusing the water. This paper deals with one such technique. Two pipe system is used to collect night soil and sullage separately and the sullage is made to pass through a gully trap. A collecting pond collects the wastewater from the top floor and is used for flushing toilets in lower floors. The flushing cistern is modified and has two inlets with individual floats, one for drawing the water from the collection pond and the other from the normal water system. The reason for providing two inlets is that in case the upper floor is vacant for reasons, the residents can use the water from normal supply system for flushing. The inlets can be controlled by control values.

Keywords*: Flushing cistern, Sullage, Domestic Waste water, Reuse.*

INTRODUCTION

Rainwater harvesting (RWH) for urban sustainability gives benefits and it is emerging as a key concern in order to clip with water scarcity in cities. Due to lack of knowledge regarding the most adequate scale in financial terms for RWH infrastructures particularly in dense areas. Water is a vital element for human life and for the development of communities, without which economical and social development are not possible. To assure its sustainability, the actual tendency of increase the extraction to supply the rising demand for potable water has to be reverted. The overexploitation of water resources has been leading to water stress and restrictions on water supply in many countries (EEA Signals, 2009). The importance of securing water supply necessitates that all options be explored. Research has indicated that demand on water catchments can be substantially decreased when a large proportion of households reuse grey water and/or install rainwater tanks (Anthony M R et al, 2009).

Water scarcity (Blue crisis) is not new problem in under developed or developing countries. It may be either due over exploitation of ground water due to lack of awareness, contamination of available water, poor planning and allocation of funds by local authorities, environmental effects etc. As sources of water are limited every attempt should be made to supply potable water to the farthest consumer and that to free from pathogens, because 780 million people lack access to an improved water source; approximately one in nine people and every 21 seconds, a child dies from a water related illness. Rainwater utilization may be one of the best available methods for recovering natural hydrological cycles and aiding in sustainable urban development (Kim, R H et al., 2005). Thus is appropriate to say

"No clean water, No life" than "No water, No life". Hence people should use water in effective way i.e., by proper use of available water and using waste water for less important industrial and domestic purposes.

The main purpose of providing a flushing cistern (tank) to a water closet is to push the soil waste (night soil) from one side of the trap to the other (as shown in Fig. 1 & 2), "to prevent the entry of foul sewer and drain gases into the houses". The single model flushing cistern requires 10 – 15 litres of water per flushing (Arora and Bindra, 2010) while latest Dual model cistern may need 3 - 9 litres. But we can also do this using sullage. Sullage is used water resulting from washing clothes and kitchen utensils, shower or bath and other domestic water not containing excreta (Fact Sheet 3.10).

MATERIALS AND METHODS

The waste water collecting tank, flushing cistern (tank) with extra float, brackets, and control valves are required. In this method the two pipe system is used where one pipe collects soil waste from water closet (soil pipe) and other collects sullage (waste pipe).The soil pipes are connected directly to the drain whereas waste pipes are connected through a trapped Gully (Arora and Bindra, 2010). These connections are shown in fig.3. In this method waste water from top floor is collected in a collecting tank provided in the bathroom of lower floor as shown in Fig.4. The collecting tank is basically a grease trap (in this type of trap lighter matter like oil, soap latter, detergents etc., which floats on the surface are allowed to escape through the outlet) where excess waste water flows out through the outlet and joins the waste pipe. The tank is provided at a suitable height (as shown in Fig.5) and dimensions are decided based on the quantity of waste water to be stored. The water stored in the collecting tank is to be used for flushing. Unlike a conventional flushing cistern which has one inlet and one outlet, in this method flushing cistern is to be provided with two inlets, one outlet, an extra float for extra inlet (as shown in Fig.6) and larger plan width to accommodate extra float. As shown in Fig.7 one inlet draws water from the waste water collecting tank and other draws water from the normal water supply system. The reason for providing two inlets is that in case the upper floor is vacant for any reason, the residents can use water from normal supply system for flushing. The inlet supply from each inlet can be controlled by control valves provided.

CHEMICAL TREATMENT

Disinfection of sullage prior to reuse is important to prevent the transmission of pathogens. Chlorine is a widely utilized disinfectant and as such is a leading contender for disinfection of sullage. Regrowth of pathogenic bacteria after chlorination of sullage with a long retention time could threaten people health security during reuse but this threat may not be serious as water is not retained for long time. The load on this treatment can be reduced by decreasing the organic matter in the sullage especially from kitchens by using floor traps of smaller opening to arrest the entry of food particles.

CONCLUSIONS

By using this technique a family of five can save about 70-100 liters of water every day and if a community or society is adopting this method, the total water saved can be supplied to localities where quantity of water is less and quality is inferior. It's high time that people understand the value of water and do their bit to humanity by saving water. This is a simple cost effective technique, which is easy to adopt and has no secondary problems thus giving us a "Green solution to blue crisis".

REFERENCES

[1] Anthony, M R et al (2009), Socio-economic and psychological predictors of domestic greywater and rainwater collection: Evidence from Australia. Journal of Hydrology, Vol. 379, pp.164–171.
[2] Arora, S P and Bindra, S P (2010),The text book of Building Construction, ISBN: 8189928805, Dhanpat Rai Publications, New Delhi. India.
[3] EEA Signals (2009): Key Environmental Issues Facing Europe. European Environment Agency. Copenhagen. ISBN 978-92-9167-391-9.pp. 38.

[4] Fact Sheet 3.10, Water Sanitation Health, World Health Organization.
[5] Kim R H et al (2010), Developing technologies for rainwater utilization in urbanized areas, Environmental Technology, Vol. 26, pp. 401–410.
[6] www.water.org/water-crisis/water-sanitation-facts/

Fig.1 Western Style Water Closet

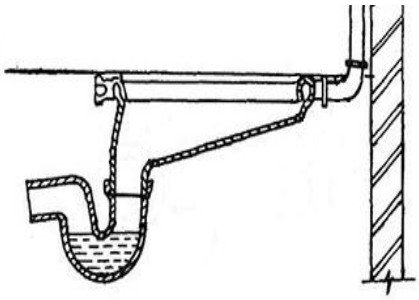

Fig.2 Indian Style Water Closet

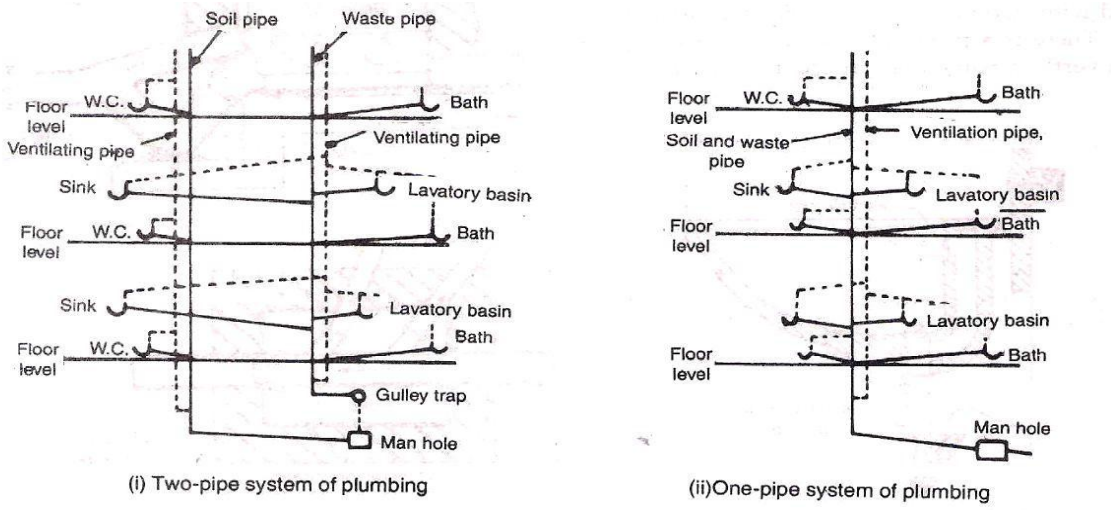

Fig.3 Plumbing Pipe Systems

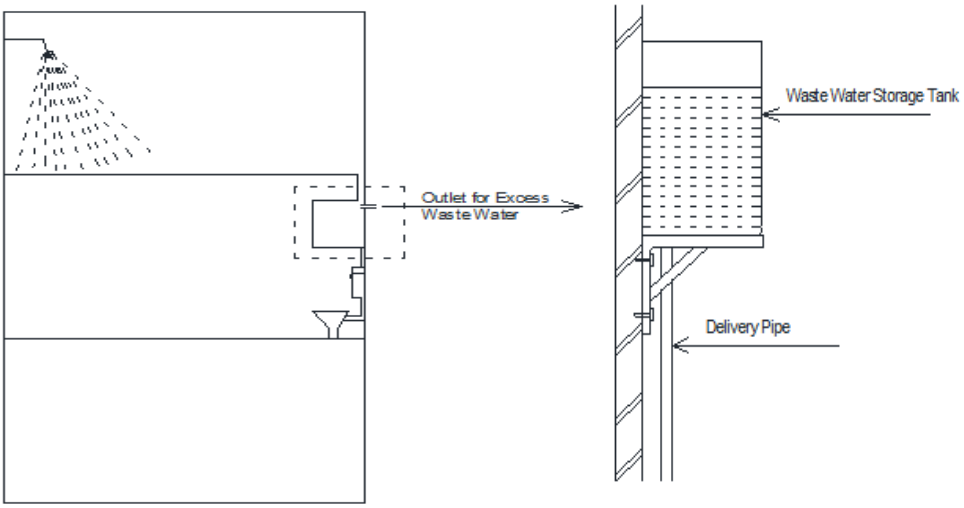

Fig.4 Waste Water Collecting System **Fig.5 Setting up of Storage Tank**

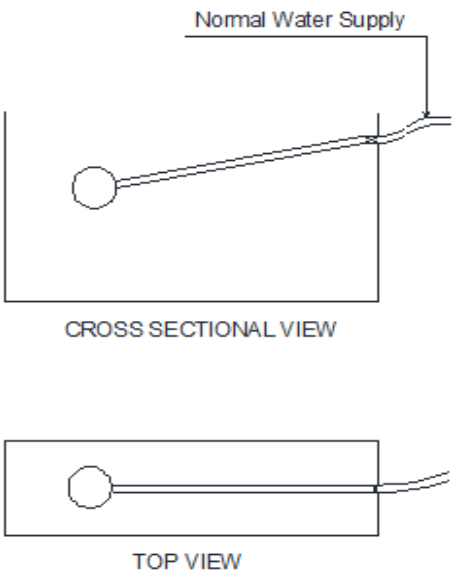

Fig.6 Views of Normal Flushing Cistern

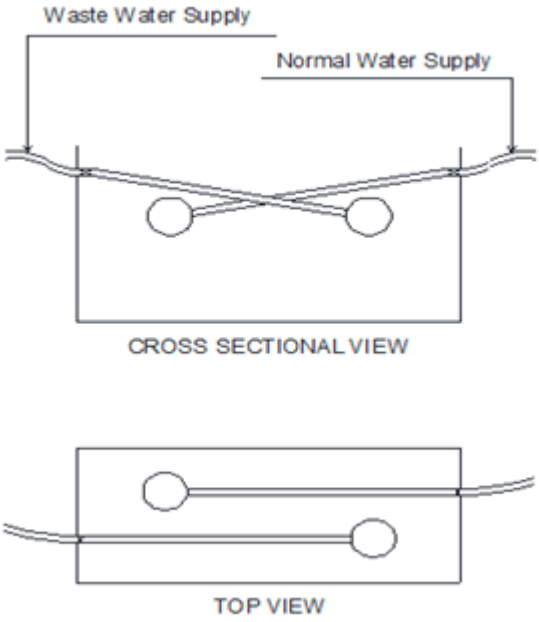

Fig.7 Views of Flushing Cistern to be used in this Technique

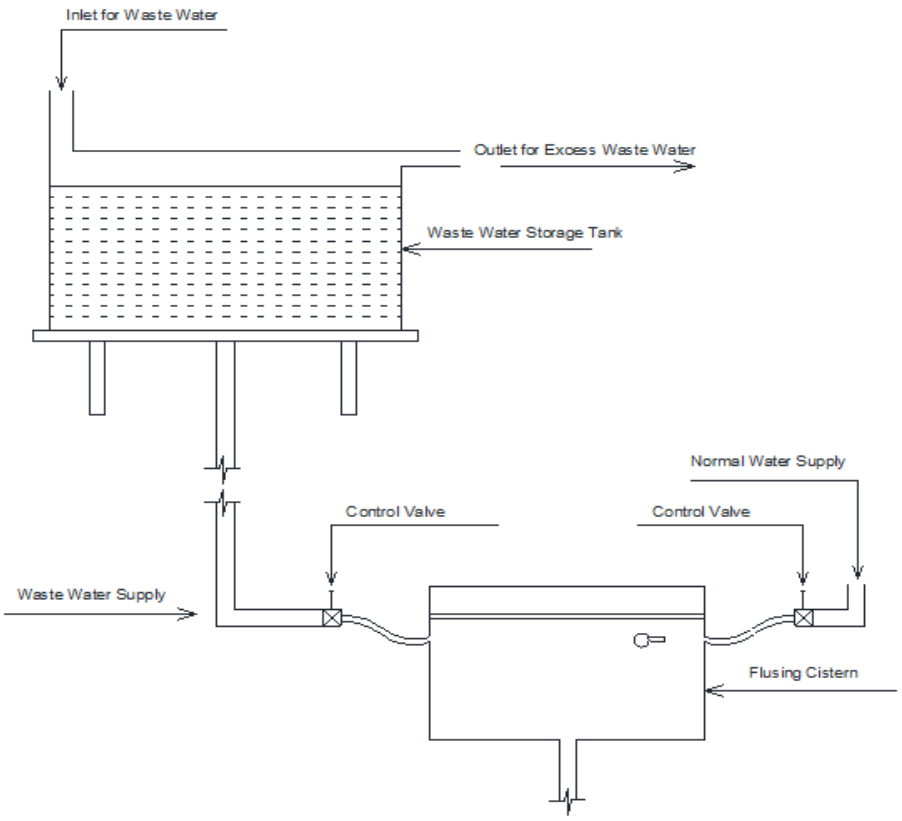

Fig.8 Pictorial representation of Domestic Waste Water Reuse Technique

5th International Engineering Symposium - IES 2016
March 2-4, 2016, Kumamoto University, Japan

Utilization of Iron Ore Mine Waste for Vegetation by Adding Different Natural Additives

S. Sirisha [1] and **K. Ram Chander** [2]

1 *UG Student, Department of Mining Engineering, National Institute of Technology Karnataka, Surathkal, Mangalore 575025, India. e-mail:sirisha.ssr@gmail.com*
2 *Assistant Professor, Department of Mining Engineering, National Institute of Technology Karnataka, Surathkal, Mangalore 575025, India. Email: krc_karra@yahoo.com*

ABSTRACT: Mining activities disrupt the natural ecosystem and lead to nutritionally deprived habitats. It often leads to contamination of natural soils with metals and toxic substances. The prominent nutrition determining characteristics of soil such as: Nitrogen, Phosphorus, Potassium and Organic Carbon were found through experimentation to be much lesser in iron ore overburden as compared to natural soil. Naturally, it takes several years for the over burden to convert back to the quality of natural soil. Hence, mine spoil genesis during early stages of restoration is essential. In an attempt to increase the fertility of the mine overburden soil, Lignin, sandstone waste and rice husk were added in 25% V/V, 50%V/V and 75%V/V proportions. After laboratory study of the altered samples, it was found that these additives adjust the pH and reduce the salinity and density along with showing a significant increase in phosphorus, organic carbon and potassium content. The additives, especially lignin, also contributed in release of nitrogen which is immensely beneficial for improving soil fertile quality permanently.

Keywords*: Soil nutrition, iron ore overburden, lignin, sandstone waste, mine spoil geneis, rice husk*

INTRODUCTION

Mining industry provides raw materials to many other industries and is bigger than all the other industries. Despite of its importance, mining activities are often frowned upon by the society due to the damage it causes to the natural ecosystem producing large amounts of inevitable wastage. Soil degradation is one of the most prominent environmental damages caused by mining. Degradation of soil refers to a significant loss of the soil quality that requires specific and vital remedial measures to restore soil functions (Bouma, 1997).

A variety of solid wastes are produced during mining such as: Overburden rock, mill tailings and processing wastes. These solid wastes cannot just be dumped on the surface as they form a barren land not supporting vegetation due to its low nutritional value. Land degradation of terrestrial habitats due to extensive iron mining activities often results in loss of natural ecosystem and associated bio-diversity (Ezeaku and Davidson, 2008), which even lead to geo-environmental disasters such as soil erosion, landslides due to slope failures and many more. The best way to recover these wastelands harboring overburden dumps is to scientifically grow a cover of thick vegetation thus restoring the natural ecosystem of the region. This also prevents the occurrence of the disasters mentioned above.

Overburden soil is generally the material that needs to be extracted in order to reach the economically exploitable ore.

The ratio of overburden excavated to the amount of mineral extracted is known as the stripping ratio.

For example, a stripping ratio of 6:1 means 6cu.m of overburden needs to be excavated to uncover 1tonne of mineral. Lower this ratio, the more productive the

mine. The overburden ratio for surface mining of metal ores generally ranges from 2:1 to 8:1 depending on local conditions. The ratio for solid wastes from underground mining is typically around 0.2:1.13 According to the data generated by the Indian Bureau of Mines (IBM), average stripping ratio for limestone mines in India is found to be 1:1.05. For iron ore mines, the stripping ratio ranges around 5.15:2.5 (World Bank, 1996). This implies that for every tonne of iron ore produced, double the quantity of waste is generated.

PROPERTIES OF THE MINE OVERBURDEN

The quantity and composition of overburden rock changes greatly with site, but it essentially mimics a few properties associated with both the ore and host rock. The parameters that determine the soil quality suitable for vegetation are broadly classified into:

i. Physical Properties
ii. Chemical Properties
iii. Biological Properties

Physical Properties

Physical properties of soil, in this case mine spoil, such as its texture, bulk density, compaction, particle size, moisture content, water holding capacity, pH and electrical conductivity have a significant role to play in the soil quality and its ability to support vegetation. The soil needs to have the capacity to hold water in the root zone and the particle size and texture should not be harsh and unsupportive for the growth of plants. Maintaining appropriate pH and salinity of the soil is also significant. Very low soil pH indicates presence of toxic environment for the plants to survive and this is known as acidic soils. Higher values of pH are harmless for many types of vegetation. Large amount of soluble salts indicating electrical conductivity imply that these salts will disrupt the natural flow of water into the plants' xylem due to common osmosis phenomenon. Thereby defying support for growth of plants in this soil.

Chemical Properties

Chemical properties are the most vital indicators of soil quality. These properties of mine waste are majorly to evaluate the values (in percentages) of nitrogen, potassium and phosphorus, metal levels, and deficiency of macronutrients. Tailings and other wastes from metalliferous ores contain some metals (i.e. Al, Mn, Fe, Cr, Cu, Ni, Pb, Cd, Zn) and lack in N-P-K values. These metal concentrations are much greater than those normally found in soils (Baker 1991, McGrath, 1998).

Biological Properties

Biological properties are also important for proper and natural vegetation on any soil. This generally indicates presence of certain plant supporting soil enzymes and various microbes that either help the vegetation or destroy it. Their presence must be checked and enhanced or reduced whichever seems appropriate. The basic indicator for biological properties is the presence of organic matter in the soil.

Limiting Factors of Mine Spoil for Re-vegetation

Soil quality is the ability of the soil to support plant growth. It is not possible to express the quality of soil in terms of a single parameter. There are a set of physical, chemical and biological parameters or factors that decide the soil quality and its ability to support vegetation. These soil parameters are listed below:

a. Soil grain size and texture
b. Bulk Density
c. Moisture content
d. Soil pH
e. Electrical conductivity
f. Soil Organic Carbon (SOC)
g. Nutrient content (N, P, K)

Some researchers have tried to use the mine waste for various purposes. Ram Chander et. Al., 2015, studied various properties of coal mine waste to assess the suitability for vegetation.

INVESTIGATIONS

Samples of iron ore overburden were collected from three areas in a magnetite ore mine in Karnataka State, India. The samples collected were brought to the laboratory and limiting properties were determined. Moisture content and density were determined as per the suggested methods in Indian Standard codes (IS:

2720(Part II)-197, 1975, IS: 2720, Part XXIV, 1973). The pH and electrical conductivity were determined according to BIS: 2720 part XIXX (1973) and 2720 part XIX (1977). The total Nitrogen was determined by the Kejhdhal Method and Potassium and Phosphorus were determined through K_2O and P_2O_5 which were estimated using a flame photometer as shown in **Fig 1**. Finally, the soil organic carbon was determined by Walkley-Black Method. The results of all the experiments to determine the properties of overburden are tabulated in **Table 1**.

Hence, the iron ore overburden was found to be majorly lacking organic carbon content, moisture and nutrients (N, P and K). In an attempt to improve the nutrient content and other properties of soil enabling it to support plant growth, different additives were added and tested. Lignin, a waste product from the Kraft process of paper pulping industry, rice husk, a waste product from the rice mills and sandstone, overburden waste from a coal mine, were found to be the most suitable and have increased the soil quality to the levels that can support vegetation.

PROPERTIES OF OVERBURDEN WASTE WITH ADDITIVES

Lignin

Lignin is an organic substance binding the cells, fibers and vessels which constitute wood and the lignified elements of plants (Ex: Straw). It is the most significantly available source of renewable carbon after cellulose on earth. It is estimated that around 40 to 50 million tons per annum of lignin is produced as a non commercialized waste product around the world. It is generally defined as a dendritic network polymer of phenyl propene basic units. Lignins differ in chemical composition depending on their source. Kraft lignins are sulphur bearing and over 100,000 tons of this type of lignins are produced every year from the kraft pulping process in the paper mills. (El-Mansouri, N.-E., and Salvado J., 2007)

As a natural and renewable raw material obtained at low costs, it has an application potential in various areas including agriculture. Lignin and lignin derived products play a vital role in formation of soils and in plant and animal nutrition.

Once added to the iron ore overburden, it helped to increase the soil quality tremendously. It was also observed that lignin helps slow release of nitrogen into the soil. This helps preserve the soil fertility for a longer duration of time.

Rice husk

Rice husk (replaceable by wheat husk, waste pulp from an oil mill, etc) plays the role of improving the organic carbon content and phosphorus content of soil simultaneously decreasing the density of the soil (which is very high in case of iron ore overburden).

Sandstone

Sandstone is the major component of infertile coal mines overburden. It is a waste material by itself but was found to stabilize the pH and EC of iron ore overburden also helping the fertility of the soil by increasing phosphorus content and lowering the density.

The properties of all the additives are compiled in **Table 2**.

Sample of overburden was taken with each of these additives, added 25%v/v, 50%v/v and 75%v/v. The changes in the limiting parameters of soil quality were observed.

The samples mixed with different volumes of additives are shown in **Fig 2**. The experimental procedures are same as performed on the overburden sample. The results are compiled in histograms. **Fig 3** shows the variation of properties of limiting properties by adding different percentages of lignin to the overburden. **Fig 4** shows the variation of properties of limiting properties by adding different percentages of rice husk to the overburden. **Fig 5** shows the variation of properties of limiting properties by adding different percentages of sandstone to the overburden.

Significant variation of pH and EC were not observed in any case whereas all the additives helped lower the density of the highly dense iron ore overburden. Lignin shows increase in organic carbon content and nitrogen whereas rice husk reduces density and sandstone increases

potassium and phosphorus content majorly. Hence, the additives have practically shown increase in limiting factors to a level close to normal vegetation supporting soil. Rice husk shows a vital increase in SOC, P, K and even N. It lowers the density to a great extent. Hence, it is vitally contributing to soil fertility when added 25% or above to the overburden.

CONCLUSIONS

- The overburden dumped during mining causes various problems including scarring of landscape, slope stability problems, degradation of land and many more.
- Sample iron ore overburden soil, when studied, was found to be lacking in many required properties for vegetation.
- Lignin, rice husk and sandstone are waste products from different industries. These were found to improve the soil quality effectively and efficiently.
- From these limited studies, it was found that the additives: rice husk, lignin and sandstone show a significant difference in the fertile characteristics of overburden. Lignin contributes to release of nitrogen and increased organic content along with P and K is achieved through rice husk and sandstone when added above 25% by volume.

ACKNOWLEDGEMENTS

Authors are thankful to the managements of the mine, paper mill, rice mill for providing us with required samples, various laboratories for providing facilities for conducting all the experiments.

REFERENCES

[1] Baker, A.J.M.; Reeves R.D. and Mcgrath S.P.(1991), In Situ Decontamination of Heavy Metal Polluted Soils using Crops of Metal-Accumulating Plants: A Feasibility Study, R.L. Hinchee and R.F. Olfenbuttel eds. In situ bioreclamation. Boston, Butterworth - Heinemann, pp. 600-605.

[2] Bouma, J. (1997), Soil environmental quality: A European perspective, J. Environ. Qual., Vol. 26, pp. 26-31.

[3] DeMartini, N., Forssen, M., Hupa, M., Niiemela, K.,(2004), Release of Nitrogen Species from the Recovery Process of Three Kraft Pulp Mills, Tappi Journal, Vol. 3(10), pp. 3-8.

[4] Ezeaku, P.I., and Davidson, A. (2008), Analytical Situations of Land Degradation and Sustainable Management Strategies in Africa, Journal of Agricultural Society of Science, Vol. 4, pp. 42-52.

[5] El- Mansouri, N.E., and Salvado J. (2007), Analytical Methods of Determining Functional Groups in Various Technical Lignins, Industrial Crops and Products vol 26(2), pp 116-124.

[6] ISRM 1979, Suggested Methods for Determining Water Content, Density, International Journal of Rock Mechanics and Mining Sciences & Geomechanics Abstracts, Vol. 16, pp141-150.

[7] Mcgrath, S.P. Phytoextraction for Soil Remediation (1998), Brooks, R.R., ed. Plants that Hyperaccumulate Heavy Metals: their Role in Phytoremediation, Microbiology, Archaeology, Mineral Exploration and Phytomining. New York, CAB International, pp. 261-288.

[8] Ram Chandar, K., and Chaitanya, V., and Raghunandan, ME., (2015), Experimental Study for the Assessment of Suitability for Vegetation Growth on Coal Overburden. Int. Jl. Mining and Mineral Engineering, Vol-6, No. 3, pp 218-233.

[9] World Bank (1996), Pollution Prevention and Abatement: Base Metal and Iron Ore Mining., Draft Technical Background Document. Environment Department, Washington, D.C.

Table 1 Various Properties of iron ore overburden

Property		Sample 1	Sample 2	Sample 3
Soil texture (%)	Sand	86.02	85	85.8
	Silt	6.6	10.2	7.5
	Clay	5.81	4.8	5.31
Specific Gravity		2.62	2.43	2.49
Moisture Content (%)		22	24	28
Soil pH		8	7.5	7.3
Electrical Conductivity		0.2	0.2	0.3
Soil Organic Carbon(SOC)%		0.44	0.32	0.44
Nitrogen (N)%		0.41	0.38	0.34
Phosphorus (P)%		2.25	1.97	2.21
Potassium (K) (meq/100g)		13.5	13.6	12.1

Table 2 Properties of various additives

Properties	Lignin	Rice Husk	Sandstone
Specific Gravity	0.52	1.27	2.2
pH	7.7	6.7	8.2
Electrical Conductivity	0.5	1.7	0.1
Nitrogen	12.38	0.71	0.83
Phosphorus	2.1	7.12	7.12
Potassium	0.56	0.56	0.56
SOC	0.98	2.8	0.3

Fig. 1: Flame photometer used during the estimation of K_2O and P_2O_5.

Fig. 2: Samples of overburden mixed with various additives in different proportions

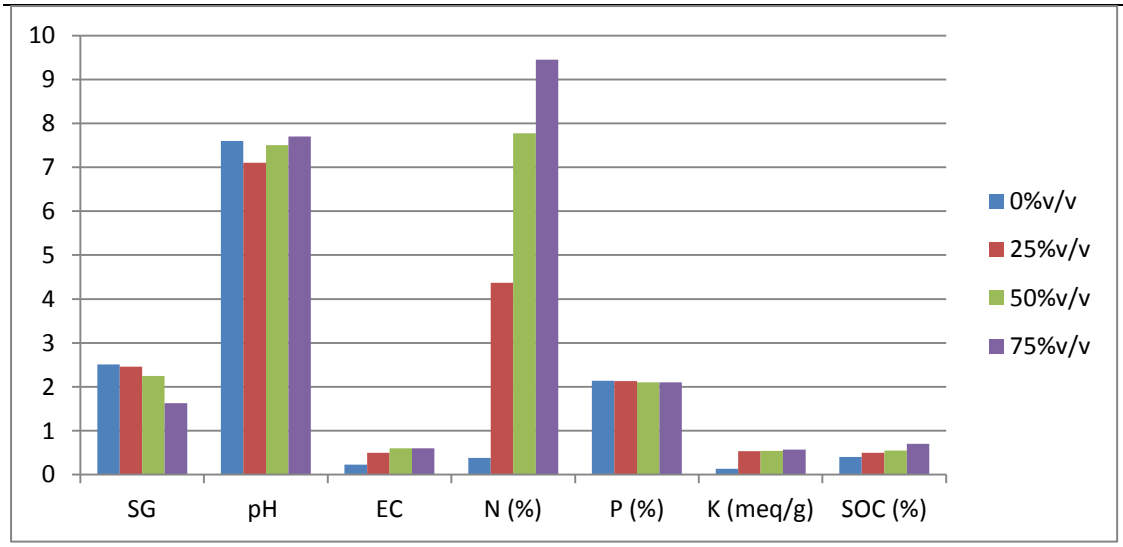

Fig. 3: Changes in limiting factors with addition of different volumes of lignin

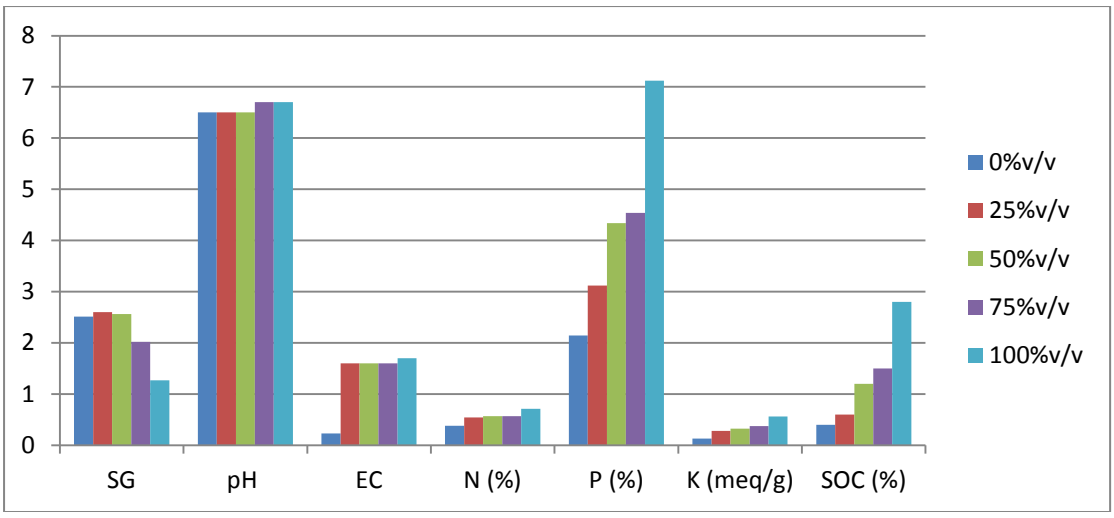

Fig. 4: Changes in limiting factors with addition of different volumes of rice husk

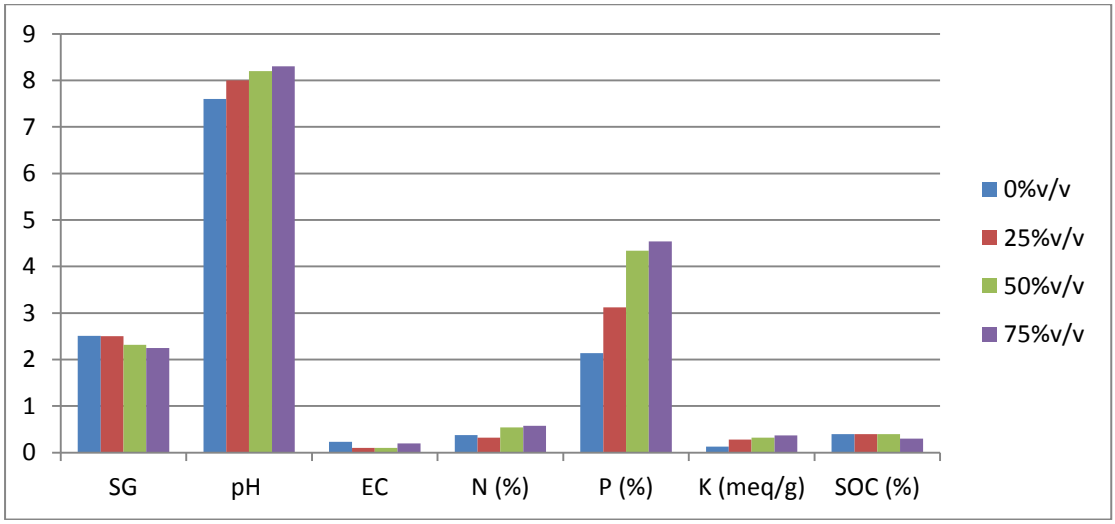

Fig. 5: Changes in limiting factors with addition of different volumes of sandstone.

5th International Engineering Symposium - IES 2016
March 2-4, 2016, Kumamoto University, Japan

ANAEROBIC TREATABILITY OF SWITCH GRASS FOR BIOGAS PRODUCTION

Arun Kumar Thalla [1], Uma S[2] and **Devatha C P[3]**

1 *Assistant Professor, Department of Civil Engineering, NITK Surathkal, Mangalore 575025, INDIA. e-mail:thallpce@gmail.com*
2 *Research Scholar, Department of Civil Engineering, NITK Surathkal Mangalore 575025, INDIA. email:uma.nitk@gmail.com*
3 *Assistant Professor, Department of Civil Engineering, NITK Surathkal, Mangalore 575025, INDIA. e-mail:revacp@gmail.com*

ABSTRACT: The present study deals with the study of anaerobic digestibility of switch grass for producing biogas. Switch grass is a type of lignocellulosic biomass rich in cellulose and hemicellulose (sugars) and is abundantly available in the Western Ghats of south Karnataka District, INDIA. Switch grass for the present study is collected from NITK Surathkal campus, Mangalore India and it is cut into pieces of about 5-10 cm size, dried at a temperature of 110°C for 24 hour in a hot air oven. Dried biomass/grass is shredded to a size of 3-5 mm and stored in a plastic air tight container and kept in the refrigerator for further study. Anaerobic sludge (Inoculum) collected from Kavoor treatment plant was mixed in four different proportions viz. 3:1, 1:1, 1:3 and 0:1 ratio on a mass basis (Sludge : Switch grass). The series of experiments were conducted in 1-litre air tight glass bottles under mesophilic conditions. The pH, temperature, moisture content, volatile solids, nitrogen, COD/N ratio were monitored at the start and end of the digestion test, where as volume of biogas produced every day was measured by volume-displacement method. From the results obtained, it is observed that 1:3 proportion yielded a maximum gas production i.e. 350 L/kg of VS from which it can be concluded that anaerobic digestion of switch grass could be a technically viable alternative for producing bio-energy (biogas).

***Keywords**: Biogas, Lignocellulosic biomass, switch grass, Mesophilic, volatile solids*

INTRODUCTION

The demand for energy is continuously increasing because of over growth of population and industrialisation. Eventhough fossil fuel are important source of energy are diminishing as well as expensive. The anaerobic digestion is considered as key technology for sustainable use of biomass as a renewable source (Fig. 1). Biogas composed of methane and carbon dioxide produced from different solid waste (Kalamaras et al. 2014)

Anaerobic digestion of treating solid waste/biomass producing methane can be an important energy source for the generation of heat and power. The various biomasses have been considered to generate renewable methane gas, particularly municipal solid wastes, agricultural and animal wastes. Several perennial grasses have been identified as hopefully as energy crops, such as miscanthus, reed canarygrass and switchgrass (Panicum virgatum L.). These grasses require less nutrient and pesticide inputs than annual crops. The grasses have been predictable as more promising energy crops because of a more efficient photosynthetic pathway. Switchgrass has supplementary advantages such as superior biomass yield across worldwide geographical range, flexibility to borderline quality land, low water and nutrient requirements (Masse et al 2010). Furthermore, switchgrass roots enhance soil structural stability and require relatively low inputs of energy, water and agrochemicals per unit of energy produced

based on methane yield of crops i.e. in litres of gas per unit of biomass per day. The aim of this present study is to assess the treatability/potentiality of switch grass for efficient production of biogas in terms of methane and carbon dioxide.

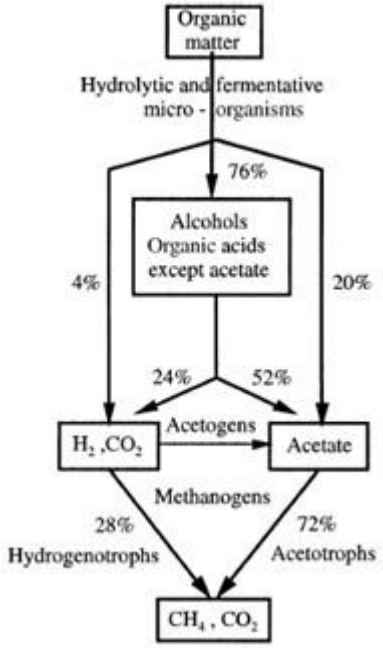

Fig.1 Stages of Anaerobic Digestion

MATERIALS AND METHODS

The method of collecting switch grass biomass, analysing the characteristics of feedstock for easy biodegradable as well as parameter utilised for the biogas production were discussed in this section.

Characterisation of Inoculum and feedstock

The initial seeding of the reactors were done using anaerobic sludge collected from UASB reactor functioning at Kavoor treatment plant, located in Kavoor, Mangalore. This sludge was selected considering the fact that the reactor is used to treat municipal solid waste which has very high COD and lignocellulose biomass, the initial total solid content of the sludge was moderate so it was allowed to settle and the supernatant was removed to obtain a total solid content level of around 12.95% (13%) to be used as inoculum in AD.

Switch grass, type of herbaceous substrate utilized for the biogas production. The switch grass used for the present study is collected from NITK campus. The biomass composed of cellulose, hemicellulose and lignin which cannot be exploited as the palatable crops, so it can used for the conversion of energy that is in the form of biogas. The collected raw substrate is chopped to reduce its sizes upto the length of 10 cm and it for drying in hot air oven at 45°C for 8-16 hours. After drying, it is further chopped/ blended so as to reduce its size passes through 425 µm sieve using hand blender/home mixer for the effective utilization. It is stored in the plastic containers maintaining moderate temperature for the further use. The inoculum, feedstock used in the experiment and the characteristics are presented in table-1

Experimental Setup and Operation

Experiments performed at batch anaerobic co-digestion with mesophilic temperature were carried out in 1L glass bottles with working volume of 60%. Anaerobic sludge and switch grass mixed in terms of volatile solids with the ratios of 3:1, 1:1, 1:3 and 0:1 respectively. The reactors filled with inoculum and switch grass expressed in terms of VS and tap water to fill liquor volume of 600 ml. The reactors were mixed vigorously by hand. Each experiment performed in duplicate. All the treatment performed at hydraulic retention time of 25-30 days least upto less than 5% respectively.

Analytical Methods

Dry matter content, volatile solids, Nitrogen were analysed according to standard methods (APHA, 1999). The pH of the each proportions measured by potentiometrically pH meter. Biogas production was monitored by volumetric displacement method connected to anaerobic reactor. The composition of biogas determined using gas chromatography with model TRACE1110. The biogas and methane are produced from inoculum was measured and subtracted from the total production of samples. Chemical oxygen demand determined based on APHA method.

RESULT AND DISCUSSION

Characteristics of feedstock and inoculum

The characteristics of UASB inoculum obtained from kavoor treatment plant and switch grass analysed respectively (Table 1)

Table 1 Characteristics of Inoculum and feedstock

Characteristics	Inoculum	SG	Digestate
	Initial	Initial	Final
pH	6.92	7.01	7.54
Temperature (*°C)	30-33	30-33	30
Moisture Content (%)	87.05	4.51	ND
TS (%)	12.95	95.49 (DW)	3.16 (WW)
VS (%)	3.689	83.02 (DW)	12.03 (WW)
COD/N ratio	20.15	25.1	25.2

Anaerobic Digestion Experiments

Batch co-digestion experiments of inoculum with switch grass were performed to investigate biogas and methane production. To examine the treatability of these wastes can be potential substitute for methane production. Biogas varies from 0-1.1 L/d. The average methane content in the biogas production produced in all reactors was around 57.95% (Fig 3). Switch grass was used as substrate in co-digestion with inoculum is a eco-friendly, effective technology for crop conservation. The cumulative biogas productions are 4.11, 3.63, 4.22, 2.4 L respectively (Fig. 4). In first 15 days of anaerobic digestion more than 60% of the total biogas produced in 0:1 &1:1 and more than 65% observed in 3:1 and 1:3. Highest methane yield observed from switch grass as well as inoculum at 3 times more at co-digestate. Biogas production of inoculum and switch grass was 341.56, 301.48, 350, 200 L/kg VS substrate added respectively (Fig.2). Methane production is significantly higher at 1:3 ratio with switch grass than other ratio. Among various ratios, switch grass as promising feedstock for biogas production.

A comparison between all co-digestion treatments shows methane yield of all substrates shows their potentiality. It is noticed that comparative advantage instead of single substrate used as digesting substrate. Inoculum is used a substrate bedding material to initiate the digestion activity. The advantage in combinations with higher methane yield observed for switch grass.

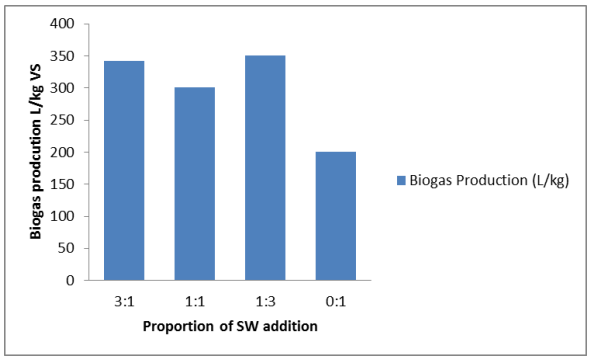

Fig. 2 Biogas production

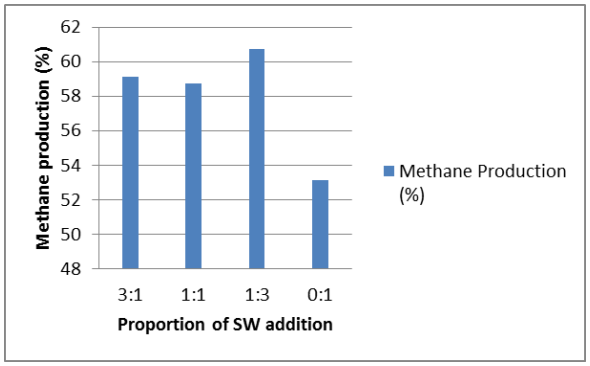

Fig. 3 Methane production

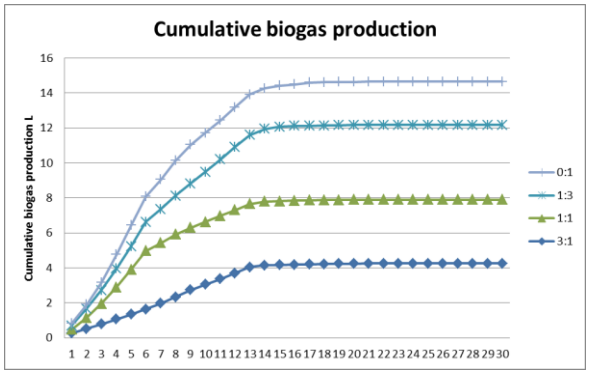

Fig. 4 Cumulative Biogas production

Solids and pH variation

It can be assumed that variation in biogas production between different mixes caused by differences in pH (Fig. 7). Among the different mixes, pH maintained around seven. In this study after digestion, slight increase in pH from the initial pH. The decrease in pH is absorbed at the ratio 3:1 results in slightly less biogas production compared with 1:3 respectively.

All the proportion shows similar trend of decrease in total and volatile solids which indicates the effective hydrolysis of substrate (Fig 5&6). Less methane yield observed at 0:1 compared with all other mix ratios due to presence of only substrates without inoculum also one portion of waste considered. This supports the earlier literature by Rao et al. (2011) stating crop used as anaerobic co-digestion at different mix ratio for bioenergy production

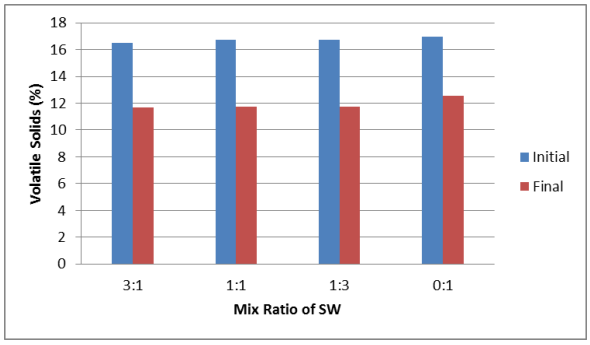

Fig. 5 Variation in Volatile solids in (%)

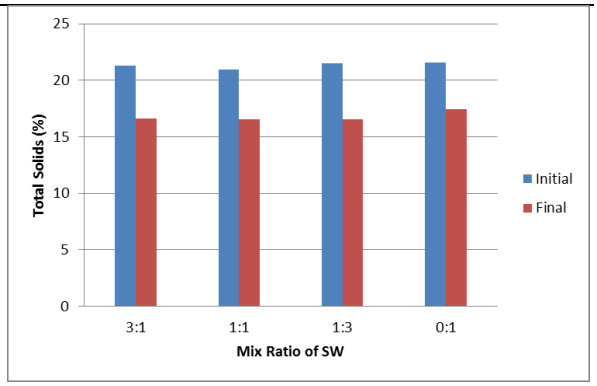

Fig. 6 Variation in Total solids in (%)

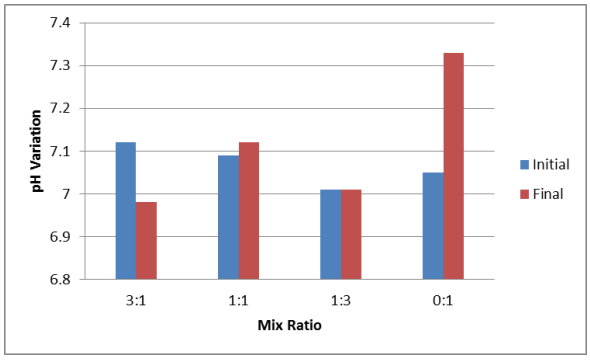

Fig. 7 Variation in pH

Table 2 Initial and final solids and pH of anaerobic digestion

Parameter		**3:1**	**1:1**	**1:3**	**0:1**
VS (%)	Initial	16.49	16.74	16.75	16.98
	Final	11.707	11.75	11.73	12.56
Total Reduction (%)		29.01	29.82	30.11	26.12
TS (%)	Initial	21.32	20.95	21.48	21.57
	Final	16.63	16.55	16.53	17.47
Total Reduction (%)		22.01	21.04	23.04	19.06
pH	Initial	7.12	7.09	7.01	7.05
	Final	6.98	7.12	7.01	7.33

CONCLUSION

The experimental study was carried out for the treatability nature of switch grass for its biogas production.

The volatile solids conversion to methane and carbon dioxide was found to be 60.75% which is higher compared with other proportion.

Based on the results obtained, it is observed that 1:3 proportion yields biogas of 350 L/kg of VS_{added}/d concluded that technically feasible for biogas production with 25-30 days HRT of digestion process.

REFERENCES

[1] APHA (1999), Standard methods for the examination of water and wastewater," American Public Health Association Washington, DC., 1999.
[2] Chandra et al. (2012), Improving biodegradability and biogas production of wheat straw substrates using sodium hydroxide and hydrothermal pretreatments, Energy.
[3] Masse et al. (2010,) Methane yield from switchgrass harvested at different stages of development in Eastern Canada, Bioresource Technology, vol.101, pages 9536-9541.
[4] Kalamaras et al. (2014) Anaerobic Co-digestion of cattle manure and alternative crops for the substitution of maize in south Europe vol.172, pages 68-75.
[5] Rao et al. (2011), Experimental design of mixture for anaerobic co-digestion of sewage sludge, Chemical Engineering Journal, Vol. 172, pages-977-986.

5th International Engineering Symposium - IES 2016
March 2-4, 2016, Kumamoto University, Japan

LIVING WITH THE RISK NEPAL EARTHQUAKE- 2015

Binita Thapa[1] and Katta Venkataramana[2]

1 *Undergraduate Student, Department of Civil Engineering, National Institute, of Technology Karnataka ,Surathkal ,Mangalore 57025, India. Email:binita2012.bt@gmail.com*
2 *Professor, Department of Civil Engineering, National Institute of Technology Karnataka, Surathkal, Mangalore 575025, India. email: ven.nitk @gmail.com*

ABSTRACT: A major earthquake of magnitude 7.8 and Mercalli scale IX hit Nepal recently on 25 April 2015, killing 9000 people and injuring thousands. Its epicentre was east of the district of Lamjung, and its hypocenter was at a depth of approximately 8.2km. According to the USGS, the temblor was caused by a sudden thrust, or release of built-up stress, along the major fault line where the Indian Plate carrying India, is slowly diving underneath the Eurasian Plate, carrying parts of Europe and Asia. The earthquake triggered avalanches on Mount Everest and many devastating landslides. A series of aftershocks began immediately after the main shock. Aftershock as high as magnitude of 7.3 was also recorded. Hundreds of thousands of people were made homeless, historical temples were brought down into rubbles and many villages were flattened down. Nepal has been struggling with its economy since the past few decades. It is indeed a big challenge for Nepal to overcome this traumatic event.

Keywords*: Nepal Earthquake, Indian Plate, Eurasian Plate, aftershocks, landslides*

1. INTRODUCTION

25th April, 2015- Children were flickering around, vehicles were bustling around the cities and mountaineers were on their way to conquer the top of the world. The day could have been a normal weekend but unfortunately tragedy struck when a major earthquake of magnitude 7.8 and Mercalli scale IX hit Nepal with its epicentre 80km northwest of the capital Kathmandu with the hypocenter at a depth of approximately 8.2km.

Nepal is a landlocked sovereign country located in South Asia. It has an area of 147,181sq.km and the population is approximately around 27million. It is bordered to the north by China and to the south, east and west by India and is located in the south of Himalayas. The Himalaya itself is the result of the collision of Indian plate and Eurasian plate. The geodynamics of the northward convergence of India beneath Eurasia generates high rates of seismicity that threaten millions of people in the mountainous regions of Nepal and within the Indian Gangetic plain. At present, the 40-50 mm/year of northward convergence of Indian plate relative to stable Eurasia (Patriat and Achache, 1984) is believed to be absorbed by a combination of horizontal shearing and crustal shortening. Crustal thickening, primarily under the Tibetan Plateau, has also been debated as a structural model for convergence. Across the Central Himalaya of Nepal nearly half of this convergence (estimated at about 20mm/year) is absorbed by convergence across the plate boundary decollement (Avouac, 2003). Convergence is also manifested by recurring small to moderate, large, and great earthquakes such as the large Kangra earthquake of 1905 (M7.8) (Hough and Billam, 2008), the great Bihar–Nepal earthquake of 1934 (M8.2) and now the Gorkha earthquake

(M7.8) which are associated with large reverse faults. Nepal has always been earthquake vulnerable zone. It had had a long history of destructive earthquakes. Earthquakes may be inevitable but the catastrophic losses in lives and properties can be avoided to the certain extent if we help communities to prepare. The unpredictability nature of earthquake is beyond our control. The only solution as of now is to be prepared and reduce the risk.

2. METHODOLOGY

This paper is based on the field visits of severely damaged area, different literature review, reports and books published on the related topic and data collected from the internet and newspapers.

2.1 Geology

Nepal lies towards the southern limit of the diffuse collisional boundary where the Indian plate under thrust the Eurasian plate central sector of the Himalayan arc of Nepal.
It is nearly one-third of the 2,400km long Himalayas. Based on the morphological, geological, and tectonic features, the Nepal Himalayas are sub-divided into five tectonic zones from south to north. These are extending east to west and almost parallel to sub-parallel.1)Terai Plain(Indo-gangetic-plain).2)Sub Himalaya(Sivalik-Range).3)Lesser Himalaya (Mahabharat-Range and mid valleys).4)Higher Himalaya and 5)Inner Himalaya.

2.2 Historical Earthquakes in Nepal

Nepal has a long history of destructive earthquakes. At least ten major earthquakes (Chitrakar and Pandey, 1986) were recorded in the historical archives.
1255 AD (June, 7): Oldest earthquake recorded. The magnitude of the earthquake is approximated to be around M7.8 in Richter scale. One-third of the populations were swiped.
1408 AD: Another major earthquake that hit the Kathmandu Valley which completely destroyed the buildings and temples.
1505 AD: Lo Mustang earthquake occurred on 6 June and had an estimated magnitude between 8.2 and 8.8 making it one of the largest earthquakes in Nepalese history. The earthquake resulted in damage from Tibet to India and killed an approximate 30 percent of the Nepalese population at the time
1833 AD: Its magnitude is reported to be of M7.8 with possible rupture length of more than 70km and the event is located at 50km North East of Kathmandu. Valley was hit by two main shocks in the late summer, one in the afternoon, 6pm, and the other in the night, 11pm. Most of the buildings, houses, public shelters, and temples had collapsed. The Tower of *Dharahara* was severely damaged. Records indicate 18,000 houses collapsed around the country
1934 AD (January, 15): Known as Great Nepal-Bihar-Earthquake, is the strongest earthquake of the 20th century which caused the highest number of casualties ever recorded in Nepal. The epicenter of this moment magnitude 8.1 earthquake was located in eastern region, 9.5km south of Mount Everest. The earthquake caused major damages at a widespread area, where the intensity of the earthquake varied from VII to X in Modified Mercalli scale, Mercalli Intensity X extended in to Kathmandu Valley, Kathmandu Valley experienced an extreme damage, and most of the buildings were destroyed. Due to the 1934 Earthquake 8,519 people lost their lives, 126355 houses were severely damaged, and more than 80,000 buildings were completely collapsed. Damage distribution reported during the 1934 event suggests that site effects must have played a major role in modifying the ground motion, particularly on the southern part of the Kathmandu basin (Dixit et al., 1998). One noteworthy phenomenon of this earthquake was that sand and water vents appeared throughout the central vents of the earthquake area. The ground around these sand fissures subsided, causing more damage. Extensive liquefaction of the ground took place over a length of

300km (called the slump belt), in which many structures went afloat.
1988 AD (August, 21) was M 6.9. Affected mostly the eastern region of the country. Earthquake resulted in 721 deaths, 6553 serious injuries, and damages in more than 65000 buildings,

2.3 Nepal earthquake-2015

The earthquake occurred on 25 April 2015 at 06:11:26 UTC with focus at a depth of 8.2km which is considered shallow, lasting about fifty seconds. The India Meteorological Department said two powerful quakes were registered in Nepal at 06:11 UTC and 06:45 UTC. The first quake measured M7.8 and its epicentre was at a distance of 80km to the northwest of Kathmandu. The second earthquake was M6.6. It occurred 65km east of Kathmandu and with focus at a depth of 10km. Over thirty-eight aftershocks of magnitude M4.5 or greater occurred in the day following the initial earthquake, including the one of magnitude M6.8. According to the USGS, the temblor was caused by a sudden thrust, or release of built-up stress, along the major fault line where the Indian Plate, is slowly diving underneath the Eurasian Plate. Kathmandu, situated on a block of crust approximately 120km wide and 60km long, reportedly shifted 3m to the south in 30 seconds.

2.4 Lessons Learned

- Government and communities should built their capacity to cope up with the consequence of the disasters.
- For disaster management process skilled human resources should be kept alert.
- Haphazard urbanization should be controlled.
- Earthquake resilient building codes must be implemented and the historical buildings must be renovated regularly.
- Rural areas should be provided with access, awareness and basic facilities of health and reliable communication.
- All the structures like dams, bridges, towers, roads should be earthquake resilient.

3. OBSERVATIONS

- The devastating earthquake resulted in the death of 8,857 people and injuring 22,309 people.
- Many properties including both government houses (Fully damaged - 2687, partially damaged - 3776) and private houses (Fully damaged - 602567, partially damaged - 284479) were affected.
- 32,000 classrooms were destroyed and 15,352 classrooms were damaged after the two major earthquakes in Nepal.
- The total amount of 1600million USD is required to rebuild the private damaged buildings and 600million USD is required to rebuild the damaged public infrastructures. Hence totalling the amount to 2.2billion USD.
- Right now there are 2million unsafe private buildings which will be completely damaged if similar type of earthquake strikes again. To renovate these buildings 2thousand USD per house is estimated. Hence the total amount required for the renovation is 4billion USD which is more than the total development budget of a year.

The earthquake has left millions still in need of food, clean water and shelter. Nepal is still reeling from the disasters.

4. CONCLUSIONS

Few days after the Nepal earthquake Japan was hit by the earthquake of same magnitude on 30th May 2015 but no damages or injuries were reported. The extensive damage and the high rate of death toll in Nepal were due to its poor infrastructure and lack of disaster management.
The overall distribution of seismically triggered damage resulting from this earthquake is asymmetrical, with pronounced damage to the east and little damage to the west. The major earthquake effects include infrastructure damages, landslides, and ground failures including liquefaction. Nearly all buildings constructed of stone rubble suffered complete collapse. However, modern reinforced concrete structures and wood-frame structures having thin sheet metal

siding typically survived the earthquake shaking with minimal damage. It is important that these behavioral tendencies be understood and incorporated into the overall rebuilding strategy of remote villages

The lack of sufficient data has severely limited the ability to understand how strong motions were distributed and how they correlate to distributions of landslides, ground failure and infrastructure damage. It is imperative that the engineering and scientific community continues to install strong motion stations so that such data is available for future earthquake events to gain insight to damage thresholds and expected future ground motions. Such information will benefit the people of Nepal through improved approaches to earthquake resilient design.

ACKNOWLEDGEMENTS

The authors are very much thankful to Er. Lok Bahadur Thapa, member of District Disaster Relief Committee (DDRC), Gorkha for the guidance to prepare the paper.

REFERENCES

- *Avouac, J. P. (2003) Mountain building, erosion, and the seismic cycle in the Nepal Himalaya, Adv. Geophys. 46, pp. 1–80.*
- *Bilham, R. (1995) Location and magnitude of the 1833 Nepal earthquake and its relation to the rupture zones of contiguous great Himalayan earthquakes. Curr. Sci. 69, 101–128.*
- *Central Disaster Relief Committee, Ministry of Home Affairs (MoHA),Nepal.*
- *Hough, S.E., and Bilham, R. (2008) Site response of the Ganges basin inferred from re-evaluated macroseismic observations from the 1897 Shillong, 1905 Kangra, and 1934 Nepal earthquakes, J. Earth Syst. Sci. 117, S2, pp. 773–782*
- *Patriat, P., and J. Achache(1984), India-Eurasia collision chronology has implications for crustal shortening and driving mechanisms of plates, Nature, 311, 615–621.*

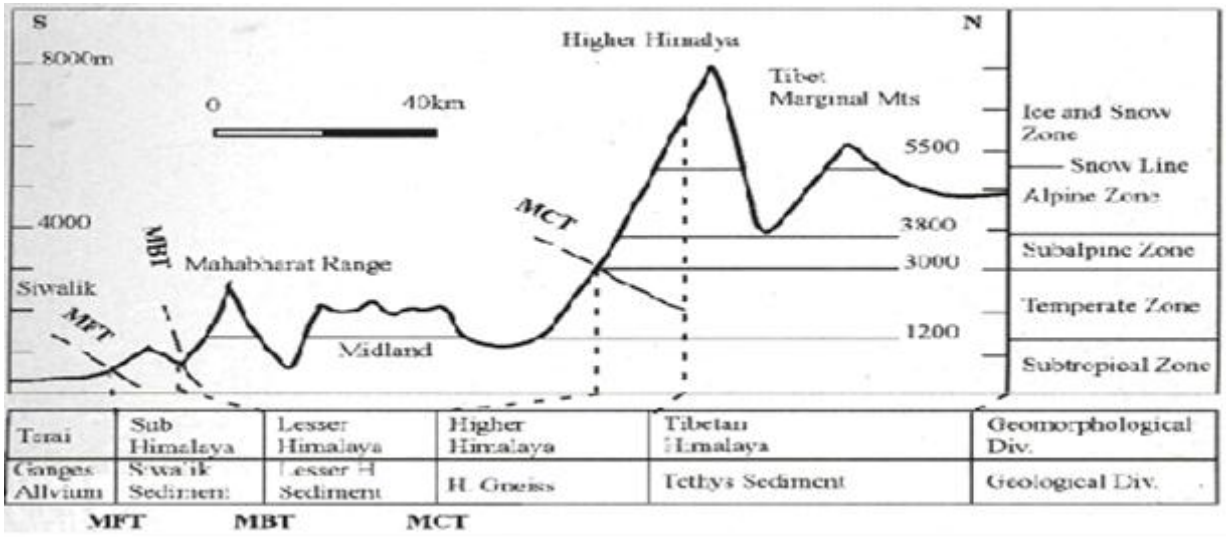

Fig 1- Simplified Physiographic and Geologic Cross-section of the Himalaya along with corresponding Climatic Zones.

(Source: https://www.google.co.in/imgres?imgurl=http://www.sabo-int.org/projects/images/pic_nepal01.gif&imgrefurl=http://www.sabo-int.org/projects/nepal.html&h=308&w=500&tbnid=LAQ69zUKxirk0M:&docid=MeYwgX6mvDjC-M&ei=7zKdVvnpMZeOuASGl72wDA&tbm=isch&ved=0ahUKEwi5ne_TgrTKAhUXB44KHYZLD8YQMwgcKAAwAA)

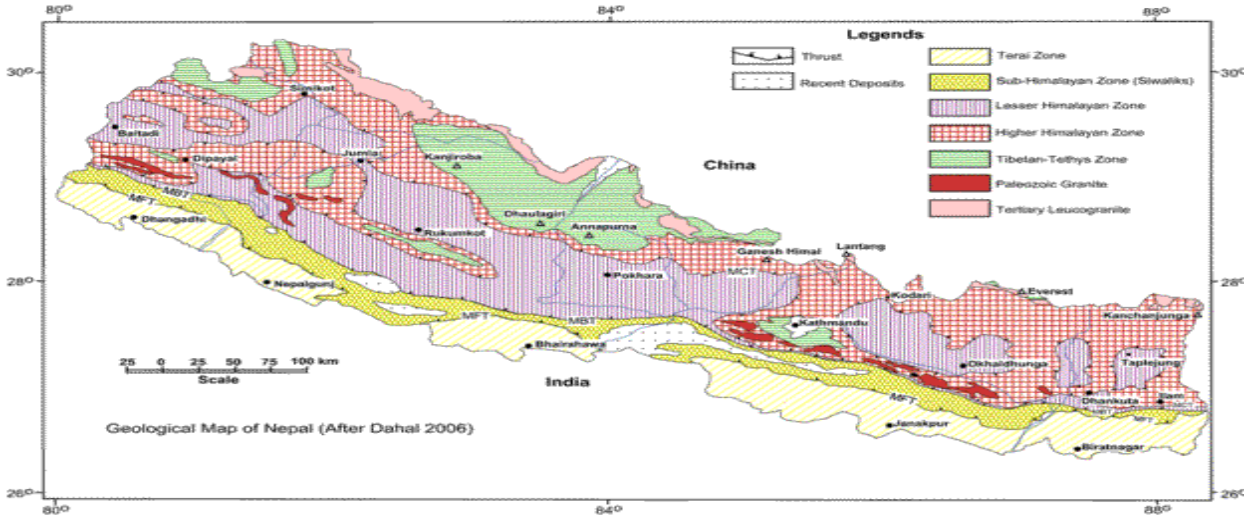

Fig 2- Geological Map of Nepal.

(Source: https://www.google.co.in/search?q=geology+of+nepal&espv=2&biw=1366&bih=667&tbm=isch&imgil=ixEYvczZKUB3NM%253A%253BH8r_rHaSr_A4BM%253Bhttp%25253A%25252F%25252Fwww.ranjan.net.np%25252Franjan%25252Findex.php%25252Fresources%25252Fgeology-of-nepal&source=iu&pf=m&fir=ixEYvczZKUB3NM%253A%252CH8r_rHaSr_A4BM%252C_&usg=__MXlo5D3mISkEMdeLFOiSNIMKvU%3D#imgrc=ixEYvczZKUB3NM%3A&usg=__MXlo5D3mISkEMdeLFOiSNIM-KvU%3D)

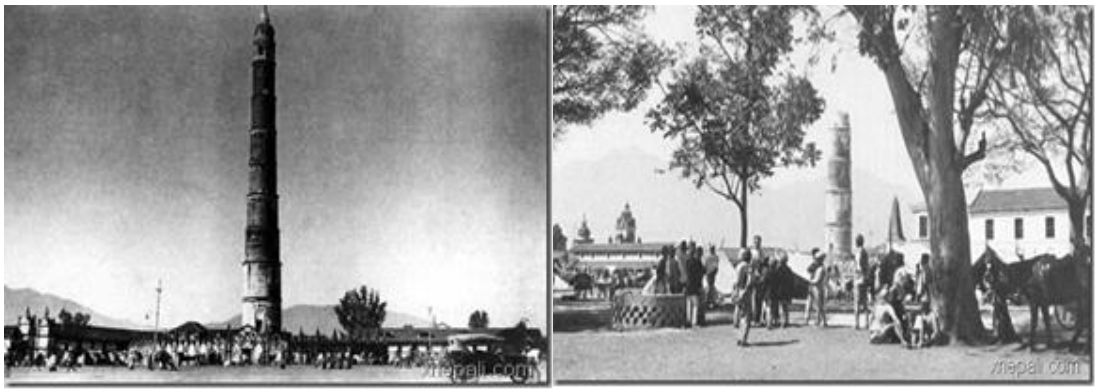

Fig 3-Pre and Post-Earthquake: Dharahara (Tallest tower of Kathmandu at that time) being destructed by the 1934 AD earthquake

(Source: 1st picture)
https://www.google.co.in/search?q=dharahara+before+1934+earthquake&tbm=isch&imgil=EpGgkgv8LXCVjM%253A%253B69LwLwVicWVu-M%253Bhttp%25253A%25252F%25252Fxnepali.net%25252Fmovies%25252Fearthquake-history-of-nepal%25252F&source=iu&pf=m&fir=EpGgkgv8LXCVjM%253A%252C69LwLwVicWVu-M%252C_&usg=__Wu-9tJ5idmKpNMM7X7UgW_H55gY%3D#imgrc=EpGgkgv8LXCVjM%3A&usg=__Wu-9tJ5idmKpNMM7X7UgW_H55gY%3D
(Source: 2nd picture)
https://www.google.co.in/search?q=dharahara+before+1934+earthquake&tbm=isch&imgil=EpGgkgv8LXCVjM%253A%253B69LwLwVicWVu-M%253Bhttp%25253A%25252F%25252Fxnepali.net%25252Fmovies%25252Fearthquake-history-of-nepal%25252F&source=iu&pf=m&fir=EpGgkgv8LXCVjM%253A%252C69LwLwVicWVu-M%252C_&usg=__Wu-9tJ5idmKpNMM7X7UgW_H55gY%3D#imgdii=lMARyuZvbUcPIM%3A%3BlMARyuZvbUcPIM%3A%3BPMC-zdTAIMV3CM%3A&imgrc=lMARyuZvbUcPIM%3A&usg=__Wu-9tJ5idmKpNMM7X7UgW_H55gY%3D)

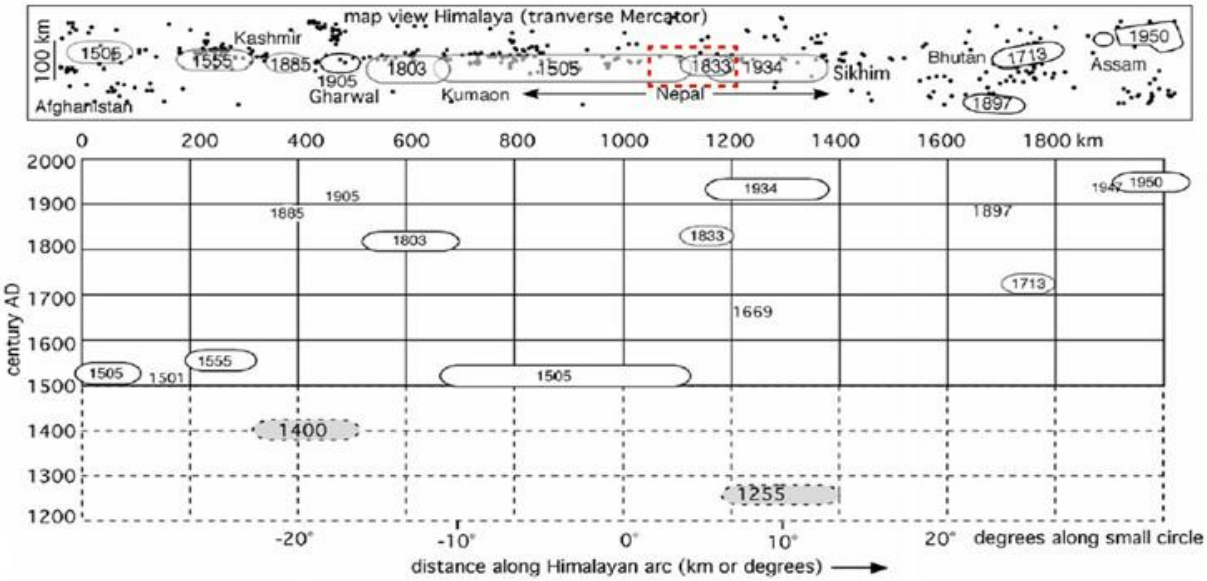

Fig-4 Time-position plot of earthquakes along the Himalayan frontal thrust. The distances are along the small circle of the arc of the Himalayan frontal thrust. (Bilham,1995).

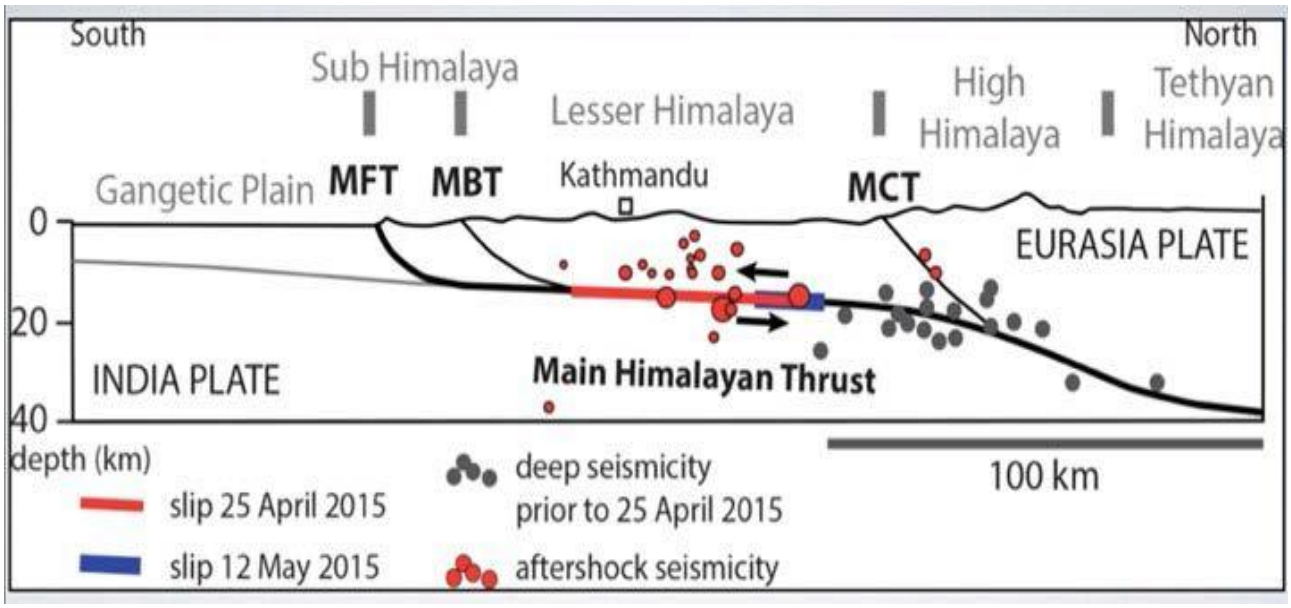

Fig-5 Generalized Cross section through the Central Himalayan showing the MHT and the modelled slip of Nepal Earthquake-2015 and the aftershock of 12th May 2015(USGS,2015)

5th International Engineering Symposium - IES 2016
March 2-4, 2016, Kumamoto University, Japan

THE NEPAL EARTHQUAKE 2015: A CASE STUDY

Swathi S [1], Katta Venkataramana[2]

1 *Post Graduate Student, Department of Civil Engineering, National Institute of Technology Karnataka, Surathkal, India. Email: swathisraju94@gmail.com*
2 *Professor of Civil Engineering, National Institute of Technology Karnataka, Surathkal, India. Email: ven.nitk@gmail.com*

ABSTRACT: The Gorkha (Nepal) earthquake of magnitude 7.8, occurred at 11:56 NST on 25 April 2015 with an epicenter 77 km northwest of Kathmandu, the capital city of Nepal, that is home to nearly 1.5 million inhabitants, and at a focal depth of approximately 10-15km. The mainshock destroyed a large number of buildings and infrastructure in urban and rural areas, and triggered numerous landslides in the mountain areas, blocking roads, and hampering rescue and recovery activities. Buildings in Nepal are vulnerable to seismic actions. Due to poor seismic performance, many buildings were damaged or collapsed and these structural failures caused many fatalities. Historical monuments as well as religious structures suffered tremendous damage induced by this earthquake. The earthquake damage observations indicate that the majority of the damaged buildings were stone or brick masonry structures with no seismic detailing underwent serious damages, whereas the most of RC buildings were undamaged. Although the majority of the existing buildings in Kathmandu were not directly affected by the long-period ground motions, such seismic waves can pose serious risks to high-rise buildings. Adequate earthquake engineering design considerations are essential for reducing potential seismic risk to these structures.

Keywords*: Aftershocks, subduction zone*

INTRODUCTION

The Nepal earthquake of magnitude 7.8, with an epicenter 77 km northwest of Kathmandu, occurring at an approximate depth of 15km, claimed the lives of 9000 people and injured more than 23,000. It occurred at 11:56 Nepal Standard Time on 25 April, with a maximum Mercalli Intensity of IX (*Violent*) (Fig. 1). The Gorkha earthquake appears to have been stronger than the 1934 earthquake, possibly making it the largest earthquake recorded in Nepal in almost a century. The earthquake occurred at the subduction interface between the Indian plate and the Eurasian plate along the Himalayan arc. The earthquake rupture propagated from west to east and a strong shaking was experienced in Kathmandu and the surrounding areas. The capital was not completely taken by surprise as the country sits astride a massive continental subduction zone. The occurrence of Gorkha earthquake, less than 200 years after the 1934 event, provides further evidence that large intra-plates underlie the country. Kathmandu, which is situated on a block of crust approximately 120 km wide and 60 km long, reportedly shifted 3 m to the south in a matter of just 30 seconds.

The destruction due to the mainshock included damage to number of buildings and infrastructure in urban and rural areas. The observations of the damage pattern indicate that the majority of the damaged buildings were stone or brick masonry structures with no seismic detailing. On the other hand, most of the RC buildings were undamaged. This was a clear indication that adequate structural design is the key to reduce the earthquake risk in Nepal.

AFTERSHOCKS

A series of aftershocks began immediately after the mainshock, at intervals of 15–30 minutes. A major aftershock of magnitude 6.9 M_w occurred on 26 April 2015 in the same region at 12:54 NST , with an epicenter located about 17 km south of Kodari, Nepal. Over thirty-eight aftershocks of magnitude 4.5 M_w or greater occurred in the day following the initial earthquake, including the one of magnitude 6.8 M_w. The major aftershocks include that of 7.3 M_w on 12 May and 6.7 M_w on 26 April. A total of 417 aftershocks of 4M_w and above have been recorded as of 25 Nov 2015. The aftershocks triggered numerous landslides and rock or boulder falls in the mountain areas, blocking roads, and hampering rescue and recovery activities leading to further loss of life and property.

A major aftershock occurred in Nepal on 12 May 2015 with a moment magnitude of 7.3, 18 km southeast of Kodari. The epicenter was on the border of the two districts of nepal, dolakha and Sindhupalchowk. This occurred on the same fault as the larger magnitude 7.8 earthquake of 25 April, due east to the original quake. It struck at a depth of 18.5 kilometres and the tremors were felt as far as about 2400 kilometers away from the epicenter, in Chennai.

This earthquake induced many mass movements in mountainous areas and resulted in landslide lakes, which could be another cause of secondary disasters. In addition, the earthquake also triggered a major avalanche on the south slopes of Mt. Everest, located approximately 160 km east-northeast of the epicentre.

BUILDING TYPOLOGY OF NEPAL

In Nepal, most of the masonry buildings are constructed with walls made of sun-dried or fired bricks or stone with mud mortar, and the building frame is made of wood. These types of buildings generally have flexible floors and roof, and are prevalent in rural areas. The masonry materials are of low strength and thus are seismically vulnerable. With the advancement of the cement in Nepal, brick or stone buildings are constructed with cement mortar. Wooden buildings are popular near the forest areas in Nepal. In these buildings, wooden pillars are made out of tree trunks and walls are constructed with wooden planks or mud mortar plaster.

According to the data obtained from the census, mud-bonded brick or stone masonry buildings account for a major portion of about 44.2%, followed by wooden buildings accounting for 24.9%. In urban areas for example, in Kathmandu valley, buildings with cement-bounded brick or stone account for 17.6%, followed by cement concrete at 9.9%. The reinforced concrete (RC) building concept being a modern form of construction in Nepal, began in late 1970s. Most of the conventional RC constructions are non-engineered that is, not structurally designed, and thus lack sufficient seismic resistance. The engineered RC buildings, which are relatively new, often adopt the Indian standard code with seismic provisions.

EFFECT OF EARTHQUAKE

INFRASTRUCTURAL DAMAGES

The earthquakes caused widespread damages to transportation infrastructures (Fig. 2), primarily to that of roads. According to the Nepal Department of Roads the country has 15,000 kilometers of strategic roads, which includes 21 highways and 208 feeder roads. The road and highway network across Nepal was heavily affected, with more than 2,000 kilometers, either damaged or destroyed. Sindhupal chowk, Dolakha and Nuwakot were the worst affected districts. The severe cracking and debris-covered roadways made it very challenging for relief and rescue teams to initially reach some of the hardest-hit remote areas.

Tribhuvan International Airport, which is Nepal's only international airport, near Kathmandu, closed briefly following both earthquakes and some of the larger aftershocks. The damage in the airport worsened immediately after the first earthquake due to the increased number

of planes bringing aid and relief workers into the country. The runway sustained cracks, but was able to be almost fully utilized.

National Society for Earthquake Technology (NSET) reported that out of 35,000 public and private schools, only 350 to 400 have been retrofitted. 160 public school buildings survived the earthquake in Kathmandu valley because they were part of a school safety program, which includes retrofitting. It has also been reported that 400 health posts, or community health centers were destroyed in the 2015 Gorkha earthquake, with an additional 300 damaged and three district hospitals which collapsed. However, the World Health Organization reported that the 2015 Gorkha earthquake and its aftershocks failed to disrupt the services at Kathmandu's largest public hospitals, as these hospitals had been retrofitted for safety, which involves everything from repairing cracks in walls to installing seismic belts and roof bracing, and has been an important part of preparedness plans.

STRUCTURAL DAMAGES

(a) Damages to Buildings

Most of the damaged buildings were stone or brick masonry structures with wooden frames. The RC frame buildings performed well in this earthquake. This indicates that ground motion intensity experienced in Kathmandu was not so intense, in comparison with those predicted from probabilistic seismic hazard studies for Nepal. Majority of the existing buildings in Kathmandu were not directly affected by the long-period ground motions, but such seismic waves can pose serious risks to high-rise buildings (Fig. 3).

Some buildings that were severely damaged by the mainshock collapsed during major aftershocks. In the mountain areas, numerous villages were devastated by the sequence of aftershocks and major landslides were triggered. These landslides blocked roads, disconnecting remote villages.

The shallow depth of the earthquake and the nature of Kathmandu valley have contributed to the high losses in the capital of Nepal. It is noticeable that the quality of construction and materials of buildings is very poor. Many recently built reinforced concrete structures failed in a pan-cake mode due to improper column-beam connections. Furthermore, many brick structures collapsed or heavily damaged due to the use of poor mortar material and tie-beams and slabs within the walls.

(b) Damage to Monuments and Cultural Heritage

In Kathmandu, earthquake damage to old historical buildings was severe, whereas damage to the surrounding buildings was limited. Historic buildings and temples were destroyed, leaving massive piles of debris in streets (Fig. 4). In the Durbar Square of Kathmandu, a large number of heritage sites and structures were destroyed, except a few survived, such as the Kumari House, and the Pashupatinath Temple which survived.

Studies showed that many temples and monuments that were restored in the recent past performed much better in this earthquake. There were also many historic structures that were resilient because of their design, the type materials of used and the engineering of their construction. The impacts provide an insight to some improvisations in reducing risks to infrastructures such as retrofitting, good design and engineering, and use of good building materials.

Also destroyed in Kathmandu was the nine-story Dharahara (Bhimsen) Tower that once stood more than 60 meters (200 feet) tall. The tower which was originally built in 1832 and had a viewing deck on the eighth floor. It was reconstructed following the earthquake that struck Kathmandu in 1934.

Historical monuments as well as religious structures associated with Buddhism suffered tremendous damage induced by the 2015 Gorkha earthquake (Fig. 5). Most of these structures were of masonry type using bricks and earth-mortar as a

bonding agent. However, three of the monument zones - the Durbar Squares at Kathmandu, Patan, and Bhaktapur - were almost fully destroyed as they suffered extensive and irreversible damage. Inspite the tremendous losses, a surprising number of the ancient monuments withstood the tremors and are still standing today.

REFERENCES

[1] Ömer Aydan and Resat Ulusay (2015), "A Quick Report On The 2015 Gorkha(Nepal) Eartquake And Its Geo-engineering Aspects"
[2] "25 April 2015 Gorkha Earthquake Disaster Risk Reduction Situation Report", *DRR sitrep 2015-002 – June 2, 2015, UNISDR The United Nations Office for Disaster Risk Reduction.*
[3] B. Gutenberg and C. F. Richter (1942), "Earthquake Magnitude, Intensity, Energy, and Acceleration (Second Paper)"
[4] T.G. Sitharam, J.S. Vinod (2015), "Nepal Earthquake of April 25, 2015", *International Journal of Geotechnical Earthquake Engineering, 6(1),81-90, January-June 2015*
[5] Ben Ramalingam and David Sanderson (2015), "Nepal Eartquake Response: Lessons for operational agencies"
[6] R. C. Kandeli, B. H. Pandey and A. M. Dixit, "Investing in future generation: The School earthquake safety program of Nepal", 13th World Conference on Earthquake Engineering Vancouver, B.C., Canada August 1-6, 2004, Paper No. 1730
[7] Bandita Sijapati, et. al. "Migration and Resilience : Experiences from Nepal's 2015 Earthquake", Center for the study of labour and mobility.
[8] "Humanitarian crisis after Nepal earthquakes 2015", World Health Organization (2015).
[9] Katsuichiro Goda, Takashi Kiyota, Rama Mohan Pokhrel, Gabriele Chiaro, Toshihiko Katagiri, Keshab Sharma and Sean Wilkinson, "The 2015 Gorkha Nepal earthquake: insights from earthquake damage survey", *Front. Built Environ., 22 June 2015*
[10] F. Jouanne, J. L. Mugnier, J. F. Gamond, P. Le Fort, M. R. Pandey, L. Bollinger, M. Flouzat and J. P. Avouac (2003), "Current shortening across the Himalayas of Nepal"
[11] H. Chaulagain, H. Rodrigues, J. Jara, E. Spacone, H. Varum (2012), "Seismic response of current RC buildings in Nepal: A comparative analysis of different design/construction"
[12] Revathy M. Parameswaran, Thulasiraman Natarajan, Kusala Rajendran, C.P. Rajendran, Rishav Mallick, Matthew Wood, Harish C. Lekhak (2015), "Seismotectonics of the April–May 2015 Nepal earthquakes: An assessment based on the aftershock patterns, surface effects and deformational characteristics"
[13] Hemchandra Chaulagain Hugo Rodrigues Enrico Spacone H. Varum(2015), "Seismic response of current RC buildings in Kathmandu Valley"

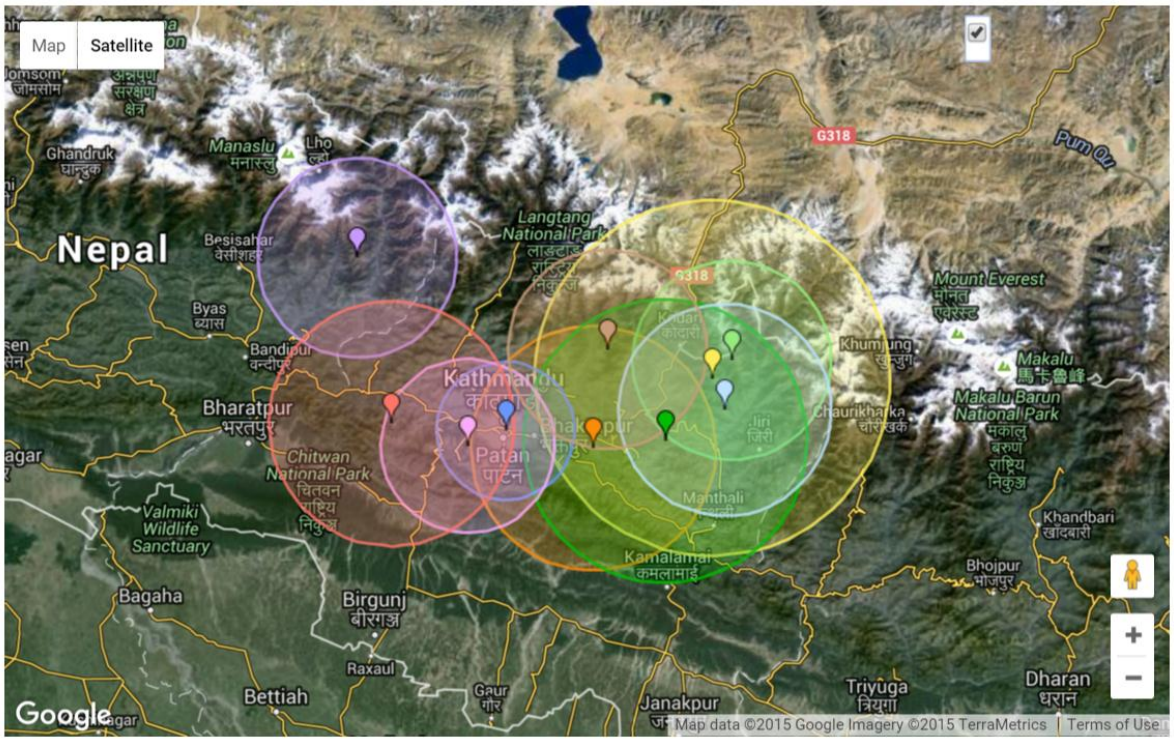

Fig.1 Satellite imagery of the earthquake affected areas

Fig.2 Bridge failure (Infrastructural Damage)

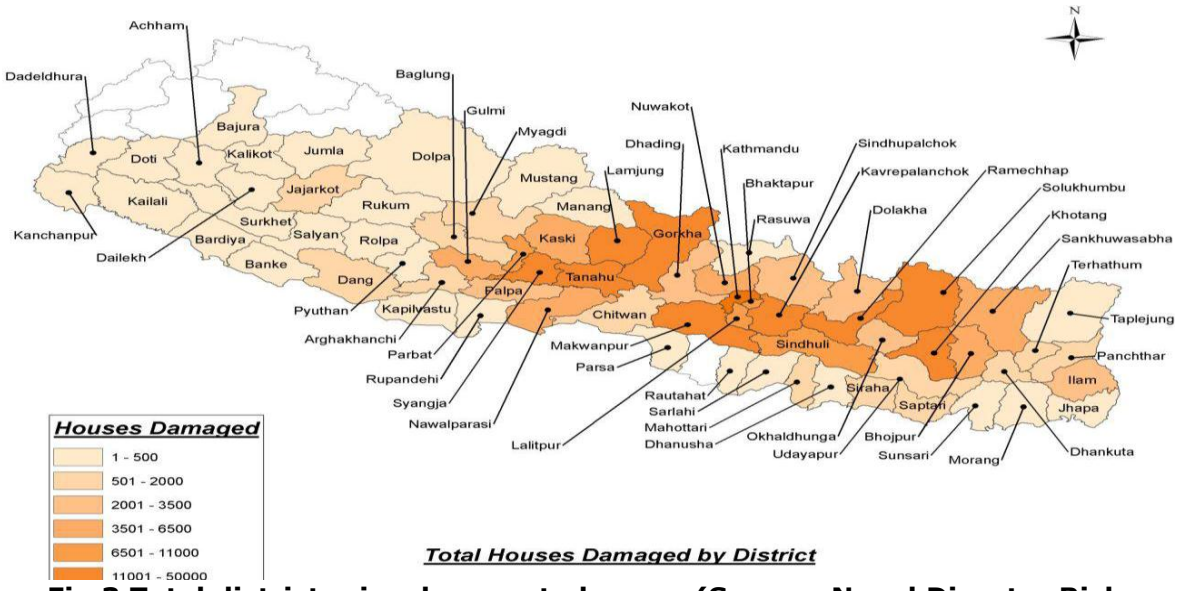

Fig.3 Total district-wise damage to houses (Source: Nepal Disaster Risk Reduction Portal & Impact Forecasting)

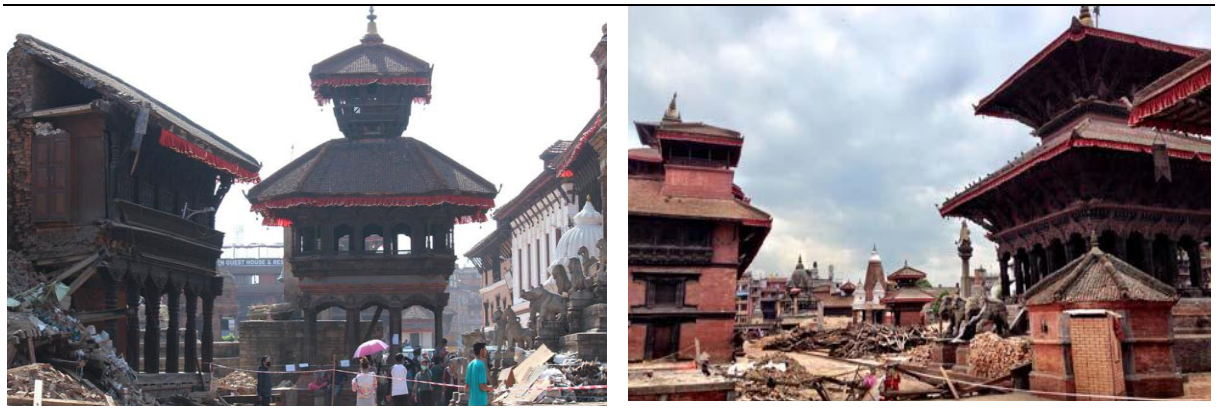

Fig.4 Damaged heritage site at Bhaktapur Darbar square.

Fig.5 Kal Mochan Ghat: before and after (ICIMOD)

5th International Engineering Symposium - IES 2016
March 2-4, 2016, Kumamoto University, Japan

PAPERCRETE- "AN ALTERNATIVE BUILDING MATERIAL"

Seethu K*, BELL V S, DILSHA A D, LAYANA K V and Arun Das P H
Department Civil Engineering, College of Engineering Trikaripur, Cheemeni, Kerala, 671313, India.

** Corresponding author. Presently Master course student, Dept of Civil Engg, NITK, Surathkal, Mangalore 575025, India. email: seethuk01@gmail.com*

ABSTRACT: This project is mainly concerned with the efficient usage of waste paper in construction material. For this purpose brick made of papercrete is considered. Papercrete includes paper pulp, cement and sand. In this project, four proportions of papercrete were made and tested for its weight,compressive strength and water absorption etc. The weight and compressive strength were found to be low and decreased with increasing waste paper content while water absorption was high.The developed bricks can be used as partition walls in high-rise buildings.This project will definitely give solutions for the solid waste management.

***Keywords**: Papercrete, Waste paper, Compressive strength, Water absorption*

I.INTRODUCTION

Our planet is priceless and we, as her caretakers need to be aware of ecological ramification our action have .Now searching for an eco-friendly way to complete building projects."Papercrete "offers a versatile alternative to commercial building materials. Papercrete is a material originally developed 85 years ago but it is only recently rediscovered. It consists of re-pulped paper fiber with Portland cement and sand . Papercrete was independently invented by Eric Patterson and Mike McCain. First patented in 1928, it was revived during the 1980s .Paper mainly consists of cellulose fiber and inorganic materials .So it was expected that fiber combine well with cement paste. Actually what papercrete offers is, freedom and personal empowerment. Because of cheapness and ease of testing,the average person is able to attempt very low cost design .There is also the freedom to create economic as alternative ,acceptable housing. From the last decade large demand has been placed on building material industry because of the increasing population which has caused shortage of building materials. Because of this crisis the need for converting the industrial wastes to useful building and construction material has increased. By doing so not only the industrial waste will be recycled and used as building materials but there will be economic design of buildings.One of the most advantageous properties of papercrete is it can be produced using solar energy. The only power needed is for pulp generation.

II. MATERIALS AND METHODS

Papercrete is a new material,there are no written mixing and sampling standards"-Centre of Alternate Building Studies in Engineering Research Report, 2005. So the procedure that is given below was followed by our own. The equipments which were used in this project is for our convenience only.

A)MATERIALS

1. Paper

Paper is the main ingredient for the manufacturing of papercrete.Paper is a natural polymer which consists of wood cellulose.Cellulose is made of units of monomer glucose.The hydrogen bonding is the basis of papercrete's strength. In each sector amount of waste paper is increasing day by day. The waste paper was collected from our college including news paper,answer sheets,etc.By using paper as a main ingradient we can reduce the amount of waste and providing a new economically feasible building blocks.

2.Cement

Cement is one of the binding materials in the papercrete. Cement is the important building material in today's construction world. In this project Portland pozzolana cement was used.

3.Water

Water is an important ingredient of papercrete as it actively participates in the chemical reaction with cement. It should be free from organic matter.

4.Sand

Sand ,which is passed through 4.75mm sieve is used.It is free from dirt and organic matters.

B)MOULD

Fig.1 Mould

This mould was made with a non water absorbing plywood material having size of 195 mm length, 95mm wide and 95mm deep. The bricks shrink during drying; hence the mould was prepared larger than the standard size of the brick.

C)MIX PROPORTION

Table 1 Mix proportion

Sl no	Mix	Proportion (Cement:sand:Paper pulps)
1	M_1	1:4:8
2	M_2	1:3:6
3	M_3	1:2:4
4	M_4	1:1.5:3

D)PULP GENERATION

The paper pulp generation is the main step in the manufacturing process of papercrete. Forgeneration of pulp followings steps are followed.

- First collected papers were teared into small pieces of papers. And it is stored in buckets .
- Water was added to buckets. The paper pieces were immersed individually not in a bulky manner in order to make the pieces completely wet. Before immersing it into the water, the papers were weighed.
- The papers were kept in the tank for 6 to 7 days otherwise until the paper degrades in to a paste like form.
- After the particular period, the papers were taken out and hammered.
- The hammered papers were scratched manually on the ground.
- Then the papers were mixed with required water and then, papers were grinded using mixer grinder.
- Now the paper pulp was ready and it was stored in suitable container.
- Then excess water was removed by squeezing
- Finally dried paper pulp stored in a container.

Fig.2 Paper pulp

The above pulp generating process was tedious and uneconomical. For the lab purpose only these procedures were followed. While going for mass production, the Tow mixers were recommended to reduce the cost. The tow mixers have sharp blades and it can operate mechanically or electrically.

E)MIXING

After all the ingredients were collected, the mixing was done. In this mixing was done manually. The mixing process of papercrete brick is different, and the processes are given below. The exact mix proportion was not known. So, trial proportions were used in this project.

The following steps explain how the mixing process was done:

- Volume batching was carried out in this project. According to the particular proportion the materials were measured & kept separately. This was done just before the mixing starts. The Glows, shoes, masks were weared before the mixing.

- Then, the non-water absorbing and smooth surface was made for mixing.
- Water was sprinkled over that surface. And this mixing place was selected nearer to the casting place.
- First the ingredients like sand, cement &paper pulp were taken.
- Cement and sand were dry mixed with trowel thoroughly still uniform colour was formed.
- The dried paper pulp was placed over dry mixed cement and sand,mixed thoroughly to get the uniform mix.
- Then water was poured into the dry mix for obtaining sufficient workability.
- After the mix, the required amount of papercrete was taken to the site and the remaining amount was kept free from evaporation.

F)MOULDING

After mixing, it should be placed in the mould before 30 minutes. So, two moulds were used at a time to make the process very fast. In this project, the bricks were moulded manually by hand.

The following are the steps involved in moulding:

- A ground was selected, which was nearer to the mixing place and having smooth surface.
- Then, the ground was made in to uniform level and plastic sheet was placed over it.
- After that, the oil was applied in the inside surface of mould for papercrete bricks.
- Now the mould was placed over the plastic sheet on ground.
- The mix was taken and it was placed in the mould.
- Then the mix was pressed or forced in such a way that it fills all the corners of the mould.
- The extra or surplus mix was removed either by wooden strike or the metal strike or frame with wire.
- The mould was lifted and the raw brick was left on the ground.
- The mix number of the brick was marked on the top.
- Then the next brick was prepared nearer to the previous brick continuously.

G)SOLAR DRYING

For solar drying, the brick kept in direct sunshine until the brick face turned white. Then, the brick should be turned on a different face.

Fig.3 Solar drying

III.RESULTS AND DISCUSSIONS

After casting the bricks, they were analysed for using as a building material. The following tests were carried out to check the brick.

A)Compressive strength

It is the main and important test. This test only decides the strength of the brick. This test was carried out by Universal Testing Machine. This test was carried out on the 28th days from the date of casting of papercrete brick.While testing the papercrete brick great care must be taken, because papercrete bricks never failed catastrophically, it just compressed like squeezing rubber. So the load was applied up to full compression. When the papercrete brick failed at higher load at the structure was not fully collapsed. Only the outer faces cracked and peeled out. So the papercrete bricks are having elastic behavior and little brittleness.

Fig.4Compressive strength test

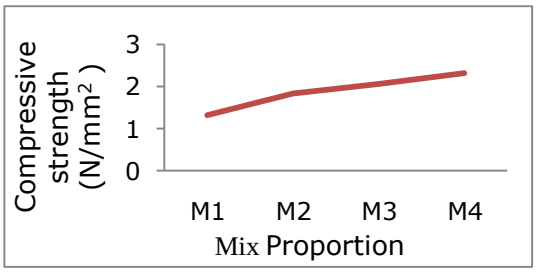

Fig.5 Compressive strength v/s Mix proportion

Experiment results shows as paper content increases compressive strength decreases and ductile behavior of papercrete increases.

C)WATER ABSORPTION TEST

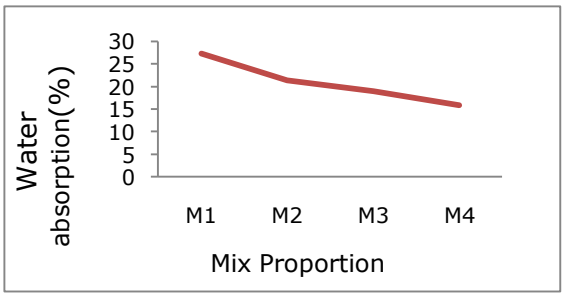

Fig.6 Water absorption v/s mix proportion

The results shows that water absorption is greater than 20%.it is because paper pulp absorb water and water occupies in the pores .but it can be made waterproof by using concrete sealer.

D)Weight

Light weight bricks are also the important objective of this project.All the bricks were weighed in a well conditioned electronic weighing machine. The following are the weight of papercrete bricks.

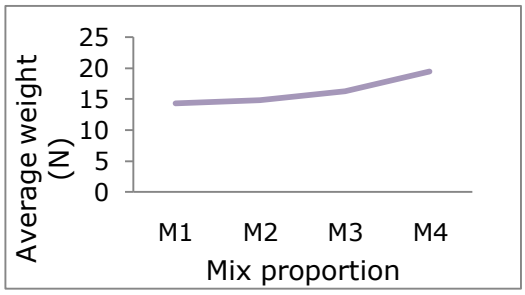

Fig.7 Average weight v/s mix proportion

The ordinary conventional bricks weight various from 30N to 35N. but the papercrete brick weight various from 14N to 20N. The maximum weight is less than 20N only. So this bricks are light weight.

D)Fire test

In this test, a sample of papercrete block must perform successfully during exposure to a controlled fire for the specified period of time, followed by the impact of a stream of water from a hose. By perfoming fire test on papercrete it is found that fire resistance rating of papercrete is about 1hr.

Fig.8 Papercrete brick after fire test

Other tests such as nailing,cutting,drilling and soundness test were also carried out and results proves that papercrete bricks can be used as building material.

II.CONCLUSIONS

- Papercrete brick is an alternative to building material. It is suitable for non-load bearing walls only.
- Due to less weight, the total dead load of the building will be reduced.
- It reduces the amount of waste paper and helps in solid waste management.
- From the results M3 is the favourable mix. Because as the paper content is increases compressive strength and weight decreases but along water absorption increases .M3 has a compressive strength 2.05MPa.
- Papercrete is more flexible ,used in earthquake prone areas.

IV.FUTURE SCOPE

Properties can be modified by the following

1. Code suggest that papercrete has no proper mix proportion ,it is based on commensence only .So you can go for other convenient proportion .
2. By adding waste material such as fly ash ,rice husk ash, glass fibre etc you can improve the properties of papercrete.
3. Papercrete can be made fireproof by coating boric acid and borax
4. In papercrete ,quarry dust can replace sand and become economical

ACKNOWLEDGEMENTS

Authors gratefully acknowledge the encouragement and guidance by Prof. Katta Venkataramana, NITK, while preparing this research paper.

REFERENCES

1. B J Fuller, A Fafitis and J L Santamaria. (May 2006) "The Paper Alternative", ASCE Civil Engineering Vol. 75 No.5 pp. 72-77.
2. M O'Farrell and S Wild. (2006) "A New Concrete incorporating Watepaper Sludge Ash (WSA)" Cement &Concrete Composites Vol.17, No.3 pp 149-158.
3. Chandana Sukesh, Katakam Bala Krishna, P.Sri Lakshmi Sai Teja, S.Kanakambara Rao(2013)-" Partial Replacement of Sand with Quarry Dust in Concrete", ISSN: 2278-3075, Volume-2, Issue-6, May
4 Isaac I. Akinwumi, Olasunkanmi M. Olatunbosun, Oluwarotimi M. Olofinnade, Paul O. Awoyera(2014)-'' Structural Evaluation of Lightweight Concrete Produced Using Waste Newspaper and Office Paper'', Vol.6, No.7
5 J. S. Manuel., 2002. "How Do Paper Houses Stack Up", Journal of environmental health perspective, Vol. 110, No. 3, A 126.

5th International Engineering Symposium - IES 2016
March 2-4, 2016, Kumamoto University, Japan

EFFECT OF DYNAMIC RESPONSE ON SOFT STOREY OF MULTI STORIED BUILDINGS

Ashwitha Gopi [1,2], R.Sajeeb[1], Domin T K[1] ,Karthika MG[1] ,Lekshmi S[1] , Praseetha P [1] ,Swathy S[1] ,Salman ul Faris [1]

1 *Department of Civil Engineering, TKM College of Engineering,Kollam,Kerala-691005*
2 *Master course student, Department of Civil Engineering, National Institute of Technology Karnataka, Surathkal, Mangalore 575025, India. email:ashwithagopi1992@yahoo.co.in.*

ABSTRACT: The increasing unbalance of required space to availability has led to a situation where in providing open ground storey(OGS) in commercial and residential buildings has become a need of time. These provisions reduce the stiffness of the lateral load resisting system and a progressive collapse becomes unavoidable in a severe earthquake for such buildings due to the presence of soft storey. Soft storey behaviour exhibits higher stresses at the columns and the columns fail as the plastic hinges are not formed on predetermined positions. The objective of this work is to study the effect of soft story on structural behaviour of high rise buildings and seismic response of soft story structures. A multi storied (G+9) building, located in the seismic zone III is considered for the study.

***Keywords**: Open ground storey, Soft Storey, seismic response*

1.INTRODUCTION: Due to increasing population, since the past few years, car parking space for residential apartments in populated cities, is a matter of major concern. Hence, the trend has been to utilize the ground storey of the building itself for parking. These types of buildings (Fig.1) having no infill masonry walls in ground storey, but infilled in all upper storeys, are called Open Ground Storey (OGS) buildings.

Fig. 1 Typical Example of OGS Building

There is significant advantage of these category of buildings functionally, but from a seismic performance point of view, such buildings are considered to have increased vulnerability. From the past earthquakes, it is evident that the major type of failure that occurred in OGS buildings included snapping of lateral ties, crushing of core concrete, buckling of longitudinal reinforcement bars etc. Due to the presence of infill walls in the entire upper storeys except for the ground storey, the upper storeys are much stiffer than the open ground storey. Thus, the upper storeys move almost together as a single block, and most of the horizontal displacement of the building occurs in the soft ground storey itself. In other words, this type of buildings sways back and forth like an inverted pendulum (Fig.2) during earthquake shaking, and hence, the ground storey columns and beams are heavily stressed. Therefore, it is required that the ground storey columns must have sufficient strength and adequate ductility(Setia and Sharma,2012). The vulnerability of this type of building is attributed to the sudden lowering of lateral stiffness and strength in ground storey,

compared to upper storeys with infill walls.

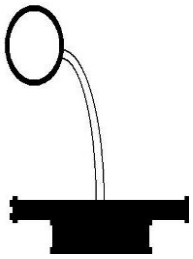

Fig. 2 Behaviour of OGS Buildings like an Inverted pendulum

2. OBJECTIVE OF THE STUDY

The objective of this project work is to study the effect of soft story on the structural behaviour of high rise buildings. The present study focuses on the seismic vulnerability of the large number of the special class of reinforced concrete multi-storey buildings being constructed in the urban areas of the country having open ground storey to accommodate parking. The study investigates the effect of soft storey on the structural response such as displacement, velocity, acceleration and base shear of a multi-storeyed building. The numerical investigation is planned using a dedicated computer program developed using inbuilt routines available in the software MATLAB (ver. R2007b). Parametric studies will be carried out on the equivalent dynamic model of a multi storeyed (G + 9) building, located in seismic zone III. The effect of the stiffness of first storey on the dynamic response of the structure also needs to be investigated.

3. METHODOLOGY

- Modeling of a 10 storey high rise building for dynamic analysis. Here modeling is done using spring-mass damper system.
- Parametric studies to investigate the effect of first storey stiffness on displacement, velocity, acceleration and base shear of the developed model, using time history analysis.
- The dynamic analysis is carried out using the computer program developed in MATLAB and the response of the building due to an earthquake ground motion as well as a harmonic base motion is obtained for different values of first storey stiffness.
- An OGS type multi storeyed building, located in the Zone III is considered for case study.
- Important results and conclusions, on the response of high rise buildings to varied stiffness values, are arrived at.

4.MODELLING OF THE BUILDING FOR ANALYSIS

For the purpose of performing the dynamic analysis**,** the continuous degree of freedom is discretized by assuming that the mass of each storey is concentrated at the respective floor levels. The discretization yields a finite multi degree of freedom system (here the ten storeyed building gives a ten degree of freedom system). Then, the ten storeyed building model chosen for the study, is transformed into its equivalent shear model, using the assumptions. Finally, the building is analysed as a mass spring damper system, thereby using the equations of motion in structural dynamics and the respective solutions are obtained as follows.

5. EFFECT OF SOFT STOREY - ANALYTICAL STUDY

Various models of the buildings have been modelled and the dynamic analysis has been done by varying the value of ' stiffness ratio'. The value of 'stiffness ratio' is defined as the ratio of the stiffness of the first floor to the floor immediately above it. The ratio was varied from 0.5 to 1.1, thus making a total of twelve models. Each of the models was analyzed for its behaviour under the action of an earth quake data: El Centro.dat and a harmonic loading. The dynamic analysis of each model also gives the values of the top floor maximum displacement ($X_{10,\ Max}$), top floor maximum velocity ($V_{10,\ Max}$), top floor maximum acceleration ($X_{dd\_10,\ Max}$), maximum base shear ($V_{b,\ Max}$) and the natural frequency (ω_1). Using the values, variations showing the maximum dynamic response with stiffness ratio are obtained.

Plots

Variation of maximum displacement, velocity and acceleration of Top floor, maximum base shear and natural

frequency with the stiffness ratio are shown in Fig. 3 to7.

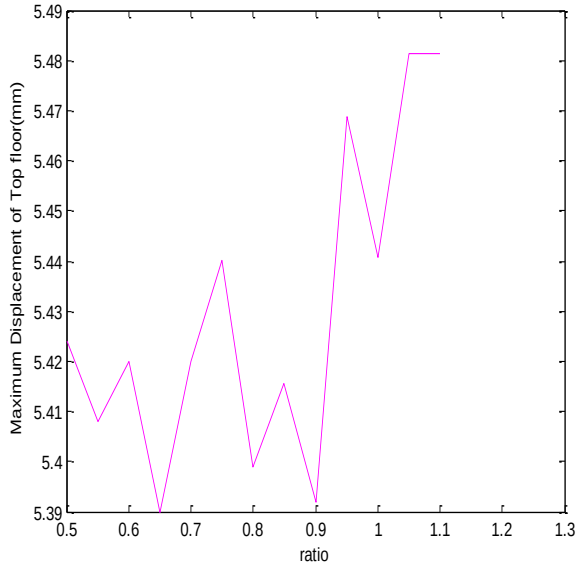

Fig. 3 Variation of Maximum Displacement of Top Floor with Stiffness Ratio

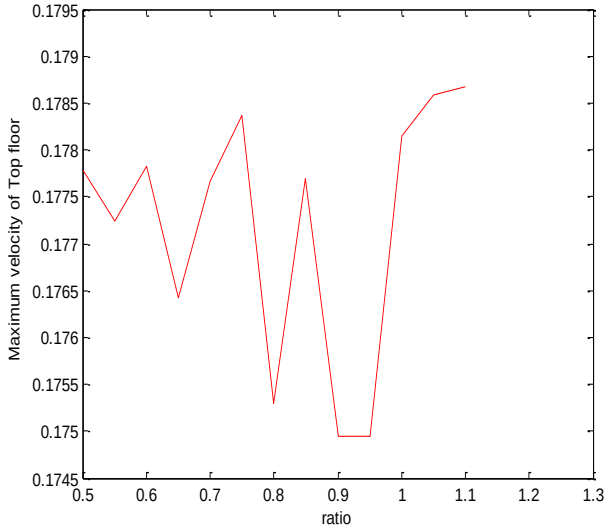

Fig.4 Variation of Maximum Velocity of Top Floor and Stiffness Ratio

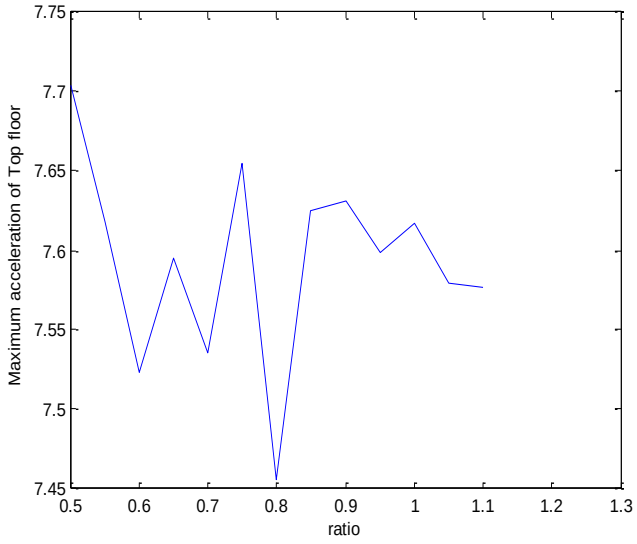

Fig.5 Variation of Maximum Acceleration of Top Floor with Stiffness Ratio

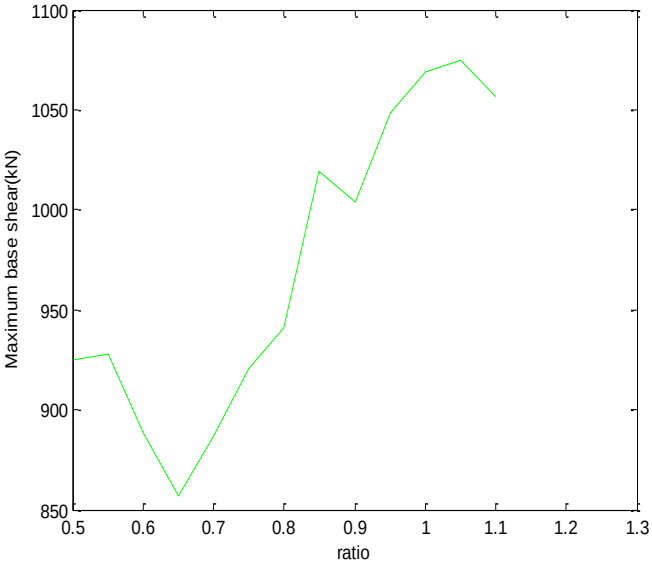

Fig.6 Variation of Maximum Base Shear and Stiffness Ratio

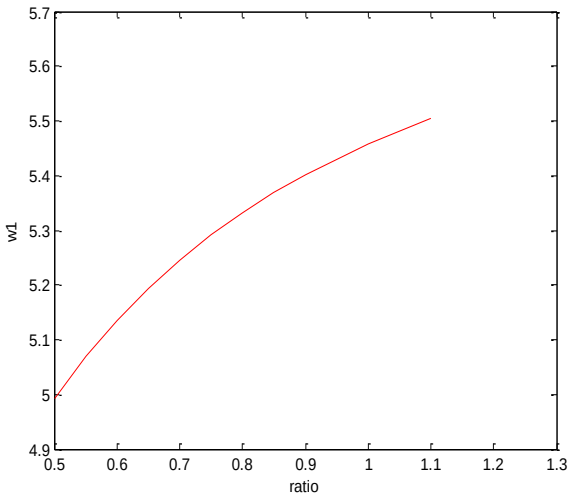

Fig.7 Variation of Natural Frequency with Stiffness Ratio

5.1 DYNAMIC ANALYSIS DUE TO HARMONIC BASE MOTION

Maximum Response Obtained under Harmonic Base Acceleration for Different Stiffness Ratios were obtained. Using the values response plots were obtained.

Plots : Variation of maximum displacement, velocity and acceleration of Top floor, maximum base shear and natural frequency with the stiffness ratio.

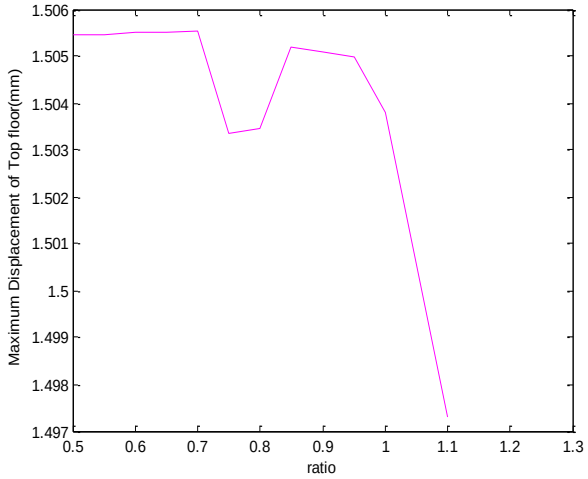

Fig. 8 Variation of Max Displacement of Top Floor and Stiffness Ratio

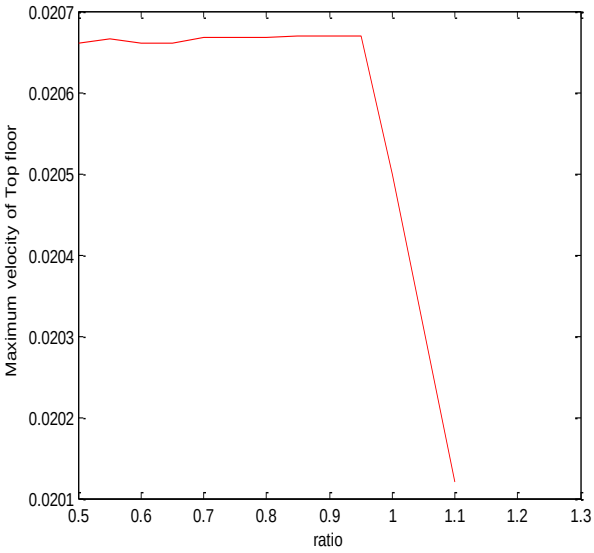

Fig. 9 Variation of Max Velocity of Top Floor with Stiffness Ratio

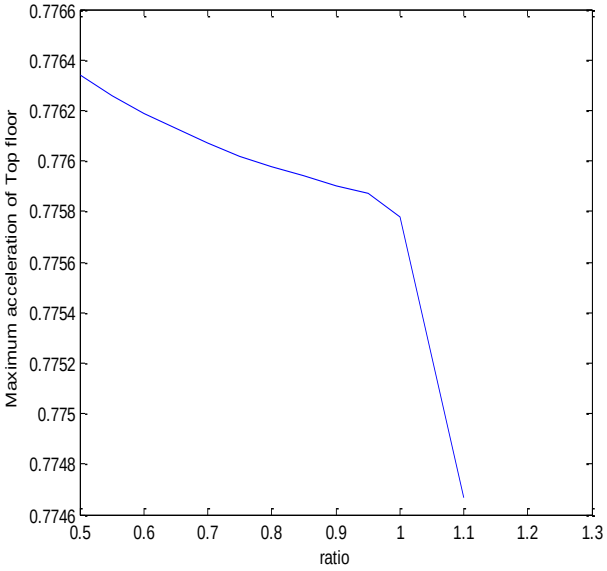

Fig. 10.Variation of Max Acceleration of Top Floor with Stiffness Ratio

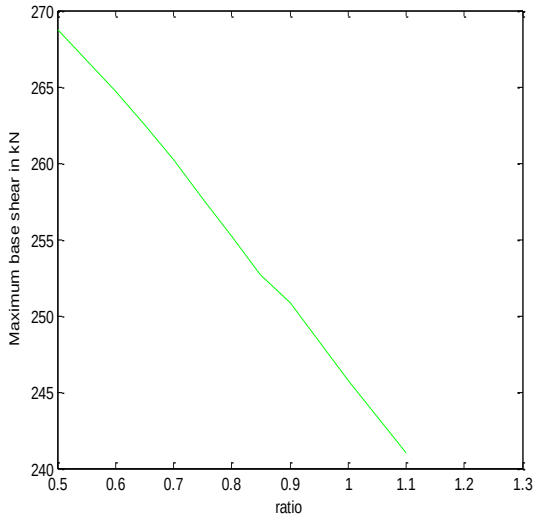

Fig.11 Variation of Maximum Base Shear with Stiffness Ratio

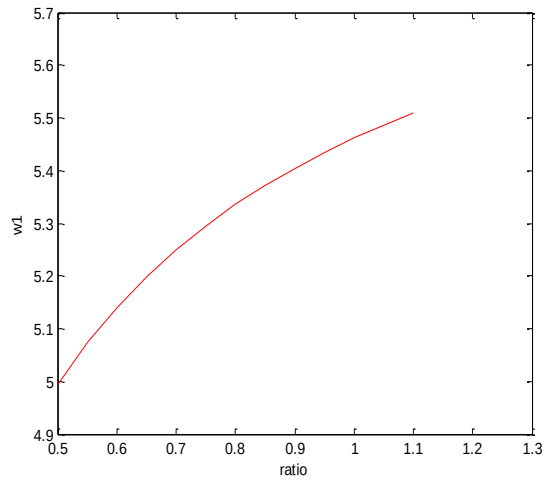

Fig.12 Variation of Natural Frequency with Stiffness Ratio

From the results obtained under ElCentro earthquake, one may observe that the maximum response is not increasing with reduction in the stiffness ratio except for floor acceleration. However, the increase in maximum response with reduction in stiffness ratio is observable for the case of system subjected to harmonic base motion.

6. CASE STUDY :

The building which is used for analysis is a G+9 storied official cum commercial building located near Manjeri town at Malappuram district which comes under seismic zone III. The ground floor has an area of 442.127m^2, the storey above has an area of 393.09 m^2 up to the level of 7th storey and 8th and 9th floors have an area of 442.127 m^2. The basement floor is used as the Parking Area. So the no. of columns is less compared to the other floors. Thus the building acts as an Open Ground Storey building(OGS). The head room of each storey is 3.60 m .and each floor has 2 stair cases and one lift well.

Table 1 Properties for Example Building

Properties	Dimensions
Plan dimensions	26.2m x 17.5m
Total height of building	36m
Height of each storey	3.6m
Size of transverse beams	0.23m x 0.4m
Size of longitudinal beams	0.23m x 0.6m
Size of columns	0.23m x 0.4m
Size of external column	0.3m x 0.6m
Thickness of slab	0.12m
Live load at roof levels	3.5kN/m^2
Grade of Concrete	M20
Density of Concrete	25kN/m^2

6. 1 PLOTS: ElCentro loading

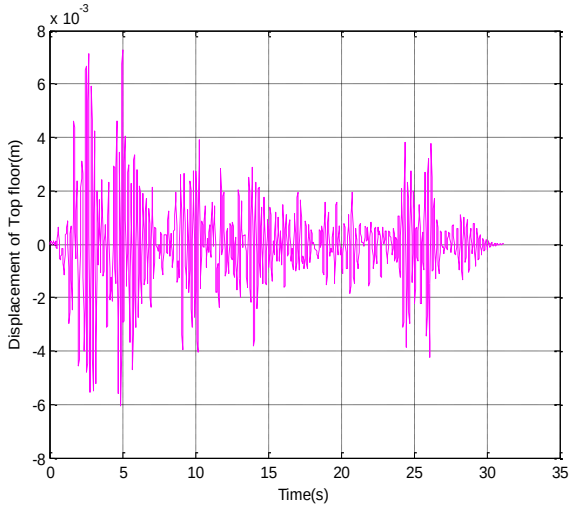

Fig.18 Variation of Displacement of Top Floor with Time

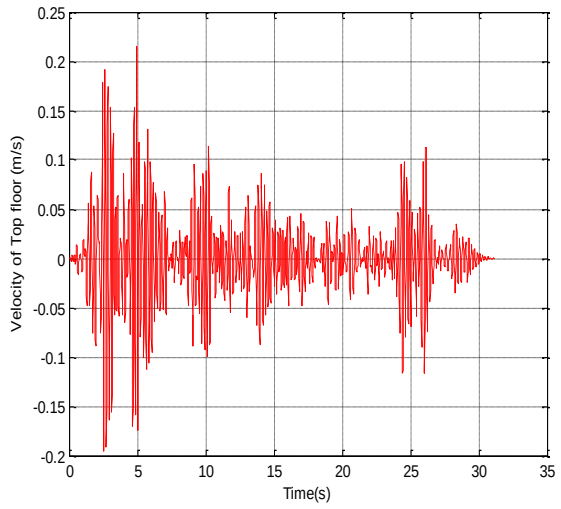

Fig.19 Variation of Velocity of Top Floor with Time history

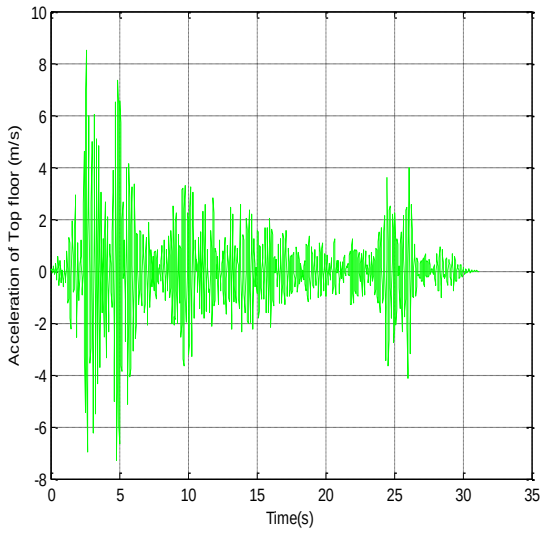

Fig.20 Variation of Acceleration of Top Floor with Time history

These figures show the time history of responses. The maximum values of the responses can be easily picked from these time histories.

CONCLUSION

The effect of soft storey on the dynamic response of a multi storied RC building modelled as a 10 degrees of freedom system is studied. From the parametric study it is observed that reduction in the stiffness of first storey adversely affects the performance of the system. Responses such as floor acceleration and base shear are found to be increasing with a reduction in the stiffness of the first storey. However, this aspect could not be observed for system subjected to an earthquake ground motion. If the dominant frequency of the earthquake motion is away from the frequencies of the system under consideration the earthquake effects may not be prominent.

REFERENCES

1. IS 1893 (Part 1): 2002, *Indian Standard Code of Practice for Criteria for Design of Earthquake Resistant Structures*, Bureau of Indian Standards, New Delhi, 2002.

2. Setia S. and V Sharma, (2012) Seismic Response of R.C.C. Building with Soft Storey, *International Journal of Applied Engineering Research*, 7 (11), Research India Publications. ISSN 0973-4562.

STUDY ON EARTHQUAKES AND DIFFERENT HOUSING TYPES IN NORTH EAST INDIA

[1]L.Sri Vaishnavi, [2] D.V. Reddy, [3] D.Neelima Satyam

[1] Undergraduate Student, Dept of Civil Engineering, NITK, India. vaishu.2895@gmail.com
[2] Professor ,NITK Surathkal, India. dvr1952@gmail.com
[3]Assistant Professor , IIIT Hyderabad, India.neelima.satyam@iiit.ac.in

ABSTRACT: The Indian Sub-Continent has a history of devasting earthquakes .The major reason for the high frequency and intensity of the earthquake is that the Indian plate is driving into Asia .The latest version of seismic zoning map for India given in the earthquake resistant design code of India assigns four levels of seismicity for India .In other words, the earthquake zoning map of India divides India into four zones(2,3,4,5) and zone 5 expects the highest level of seismicity. The regions of Kashmir, the central Himalayas and North East Indian regions fall in this region. This report consists of a study on frequency of occurrence of earthquakes in the North East India in the past 80 years and it describes the housing types in the North Eastern part of India namely traditional housing , concrete structures and their foundation types . The comparison between these two structures based on the extent of magnitude they can resist during earthquakes , repairs and the effect of slopes on these structures . The report also discusses on the reliability of structure with respect to surrounding structures.

KEY WORDS: *Devasting ,Seismicity ,Zoning*

INTRODUCTION

Arunachal Pradesh, Assam, Manipur, Mizoram, Nagaland, Tripura, Meghalaya, and Sikkim comes under the North eastern part of our country. North East India has micro climatic conditions and natural calamities including Earthquakes. Seismicity of this region is very high in our country. Most of the North East states have a humid sub-tropical climate with hot, humid summers, severe monsoons and mild winters. By observing past 80 years Earthquake data and plotting these points on a map (figure 1) we can conclude that the North east India experiences the major devasting Eathquakes. Also, Earthquake motion excitation can induce pounding in adjacent buildings with inadequate separation distance. Pounding between closely spaced building structures can be a serious hazard in seismically active areas. Therefore, seismic pounding between adjacent buildings may induce unwanted damage even though each individual structure might have been designed properly to withstand the strike of credible earthquake events.

DESCRIPTION

Different type of construction in these areas are 1. Traditional type, 2. Concrete type.

1.TRADITIONAL HOUSES

1. Kutccha house
2. Semi pucca house

KUTCCHA HOUSE

Houses are constructed with organic renewable resources like bamboo, mud, grass, cane leaves, cane etc. Plinth and

foundation are made of consolidated earth with timber or bamboo posts. Walls are made of bamboo mats, grass, earth, cane leaves etc. Roof is thatched, made of wheat or maize straws, with split bamboo framing.

Types of Kutccha houses are

1. Bamboo and wooden Kutccha house
2. Silted Kutccha house and
3. High pitched roof Kutccha house

BAMBOO AND WOODEN KUTCCHA HOUSE

They are present in all states with small changes as per local climate. Materials used are bamboo posts driven into ground, bamboo trusses for sloped roof. Some times mud plaster is used for walls and mixed with cow dung. In cloudy and cold climatic areas walls are constructed with wood or stone masonry to retain heat. Houses are rectangular in shape with 3 to 4 rooms (figure 2). Plans and sizes vary as per requirements. Typical layout of the house consists of

1. Sora Ghar (Drawing Room)
2. Huwa Ghar (Bed Room)
3. Randhoni Ghar (Kitchen Space)

Construction materials used are bamboo posts and horizontal members, with wall infills with bamboo splits of sizes between 15 to 40 mm called as "KARNI". Frequent maintenance is required for mud plaster due to shrinkage and cracking in summer and washout in rainy season.

STILTED KUTCCHA HOUSES

These houses are also known as CHANG. Mostly constructed in areas of high precipitation and moisture content both in air and soil. Construction is mostly with bamboo or wood and thatch for roofs seen in mostly Assam and Arunachal Pradesh. Houses are rectangular in shape and similar to bamboo Kutccha houses, they are constructed over bamboo posts and bamboo diagonal bracings are tied to form the stilt areas. The structure above is formed by horizontal members tied across the bamboo posts with jute ropes and using dowel and tenon joints. Height is 1.5 to 2m from the ground. Stilted houses are typically designed to keep out the effects of heavy monsoon. The floor and wall inlays are mostly bamboo weaves, which allows the water of floods and heavy rains to pass rather than storing (figure 3). Roof height from floor is 3.5m.

HIGH PITCHED ROOF KUTCCHA HOUSE

These type of houses are characterised with a double pitched roof with high fronts and low backs. Materials used in construction are mostly timber or bamboo for structural elements, weaved bamboo sheets for walling, infill and thatch for roofing. Most of these houses are rectangular form with length 10 to 15m and breadth 5 to 6m with one or two entrances. To keep out the effects of cold and cloudy climates very less openings are left in the walls to retain heat inside the houses. Interior have five spaces mostly.

AKISHEKHOK or front room to store the rice pounding tables, public spaces.

ABIDELABO is a narrow room between AKISHEKHOH and AMIPHOKIBOH where the unmarried girls of the household sleep i.e; semi-private place.

The AKUZU-ABO is a private space where the head of the family and his wife sleeps.

The AZHI-BO or the liquor room forms the last room where rice beer is stored in bamboo jugs. The roofs are double pitched with a high front of about 4.6m and low back of about 3.6m. The front apex of the roof is mostly adorned with a horn, or a cross as per tribal customs and social statuses of the inhabitants (figure 4).

SEMI PUCCA HOUSES

These houses are made with mixture of organic and inorganic materials such Wood, bamboo, corrugated GI sheets etc. They have found place as an advancement of traditional kutccha houses. According to materials used they are classified as

MODIFIED KUTCCHA HOUSES

These type of houses bear close resemblance with the traditional kutccha houses and mostly being built in rural areas those days. They are modified for usage of modern materials in construction. The traditional thatch roof is replaced by corrugated GI sheets thereby reducing the maintenance of the roof during rainy days. The mud plaster is stabilised with added cement that adds onto the durability of the plaster.

ASSAM TYPE HOUSES

These type of houses are extremely good in several past earthquakes in the region, owing to the usage of light weight construction materials, flexible connections and good framing. Due to untreated wood based materials, these houses are vulnerable to fire and are used for both residential and commercial buildings. Mostly these houses are one storeyed with elevated plinths to keep off flood water and stray animals. Two storeyed versions are also found in some areas. For residencies, these type of houses having rectangular plan for single family units and typical 'L' or 'C' plan form for multi family units(figure 5). A continues verandah generally runs along the full length of front facade. If constructed in hills, the verandah is placed to face the slope. The materials used for this type of construction are sal woods for posts, wooden trusses for sloped roof and lakes and is plastered over with a mix of mud and cow dung. The wooden trusses are mounted with Ikra trees or corrugated GI sheets to form the roof.

2.CONCRETE STRUCTURES

Modern construction practices are Reinforced brick masonry system, Confined brick masonry system.

REINFORCED BRICK MASONRY SYSTEM

In this system, the construction is similar to the bamboo(IKra) housing. For modelling of reinforced masonry sap is used. In sap the wall is created by layered shell element. In shell element there are three different layers considered, first and third layer are made of bricks and second middle layer is made of rebars. The spacing of rebar is taken as 300mm.

CONFINED BRICK MASONRY SYSTEM

For confined masonry system, the dimensions of the model is taken same as above two systems. For this system wall is taken as brick wall, and for tie beam and column reinforced concrete is used. The dimensions of tie beam and column is as per EERI(Earthquake engineering research Institute).

COMPARING TRADITIONAL AND CONCRETE STRUCTURES

The structural elements that mainly fail during earthquake are walls, beams and columns. The structural elements bearing only vertical loads before earthquake, have now to carry horizontal bending and shearing effects as well (figure 6). When the bending tension due to earthquake exceeds the vertical compression, net tensile stress will occur. If the building material is weak in tension such as brick or stone masonry cracking occurs which reduces the effective area for resisting bending moment, thus causing failure. In case of wooden structures, wood frames without walls have almost no resistance against horizontal forces. Resistances are highest for diagonal braced wall. Buildings with diagonal bracing in both vertical and horizontal frame performs much better(figure 7). The traditional wood frame IKra construction of Assam wooden

piles separated from ground performed very well during Earthquakes. Hence wooden structures resist well when compared to concrete structures.

MAGNITUDE

From the model of different structural systems, the seismic force on different houses is determined. Hence from the seismic force data and from stresses experienced we conclude that bamboo type housing system is advantageous (table1 & table 2).

REPAIRS

During earthquake connections between the joints are effected and foundations are taken off in wooden structures. Therefore, bracings are placed diagonally to support the structure. In concrete structures cracks develop during earthquake and these cracks are firstly cleaned and then filled by cement-sand or lime-sand mortar. Water is sprinkled on the cement mortar, the wall will then become strong again and this repaired area will not act as a weak point in the wall for future earthquakes. In case of severe damage both type of structures are reconstructed, but the reconstruction of concrete structures is complex and expensive when compared to wooden structures.

North eastern parts of India have large scale of hilly region. During past earthquakes, Reinforced concrete frame buildings that have columns of different height within one storey, suffered more damage in shorter columns as compared to taller columns in same storey. Due to this irregular deformation of columns failure of buildings on slopes occur. Vernacular practices are developed with locally available, easily workable, natural building materials and have less impact on failure. Hence concrete structures are more effected than wooden structures in hilly terrain.

Regarding the reliability of structures and seismic pounding, there are many buildings worldwide which already built in contact or extremely close to another that could suffer pounding damage in future earthquakes. The simplest and the effective way for reducing damage due to pounding is to provide enough separation but it is sometimes difficult due to high cost of land. An alternative to minimise the effect of pounding is through decreasing the lateral motion, which can be achieved by joining adjacent structures at critical locations so that their motion could be in phase with one another or by increasing the pounding buildings damping capacity by means of passive structural control of energy dissipation system.

According to IS 1893-1(2002): criteria for earthquake resistant design of structures of two adjacent buildings, or two adjacent units of the same building with separation joint in between should be separated by a distance equal to the amount R times the sum of the calculated storey displacements of each of them, to avoid damage in contact when the two units deflect towards each other. When floor levels of two similar adjacent units or buildings are at the same elevation levels, factor R on this requirement may be replaced by R/2. Here, R is response reduction factor.

CONCLUSION

The traditional houses in North Eastern part of India has several advantages compared to concrete structures which include temperature control, enhancing natural ventilation, protection from natural calamities such as floods, earthquakes etc. But it has several disadvantages like fire proneness, termite infestation due to usage of non-treated bamboo and wood lack of damp proofing and washouts during rainfall. Regarding pounding we conclude that, by constructing structures specified by IS codes, the damaging effects due to seismic pounding can be reduced. As the magnitude of seismic forces and stresses experienced by wooden houses is much less and the repairing cost is too low when compared

to concrete structures we conclude that wooden houses perform well in regions of high seismicity when compared to concrete structures.

REFERENCES

[1] Hemant kaushik K.R. (2009). Housing report: Assam type House. World Housing Encyclopedia.

[2] Khan A.A. (2009). Housing report: Traditional Naga type House. World Housing encyclopedia.

[3] Manoj kumar singh, S.M. (2011). Bioclimatism and vernacular Architecture of North East India.

[4] Nath R, Dr.J.Pathak, Dr.B.Sharma, "Assam type House – Traditional Earthquake resistant construction practice in Assam. (2010).

[5] Padhi B.K. (2009). Religious art and Architecture in North east India : Agam kala prakashan.

[6] Steele, J. (1988). Hassan Fathy by James Steele. St. Martin's Press.

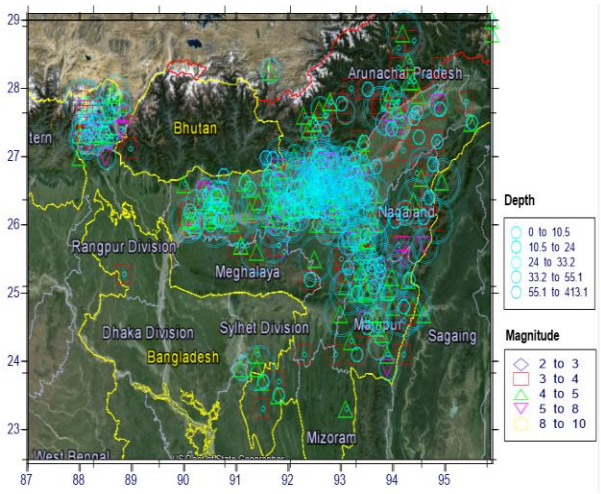

Fig 1. MAP SHOWING THE DEPTH AND MAGNITUDE OF PAST 80 YEARS EARTHQUAKES IN NORTHEAST INDIA

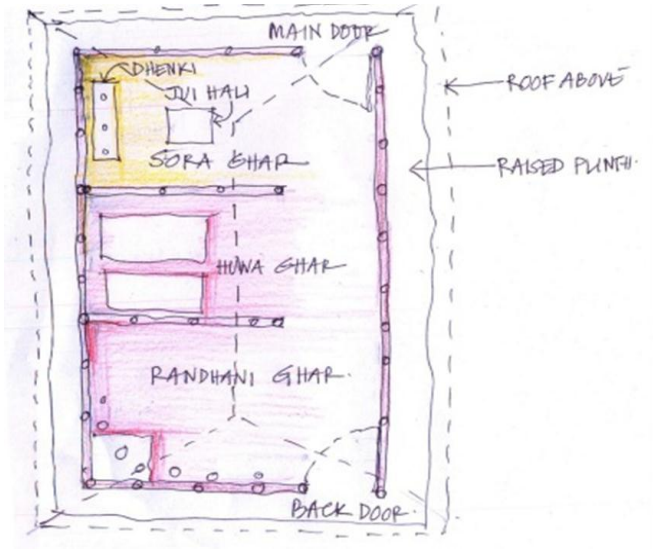

Fig 2. PLAN OF TYPICAL KUTCCHA HOUSE FOR ASSAM

Fig 3. TYPICAL STILTED HOUSE

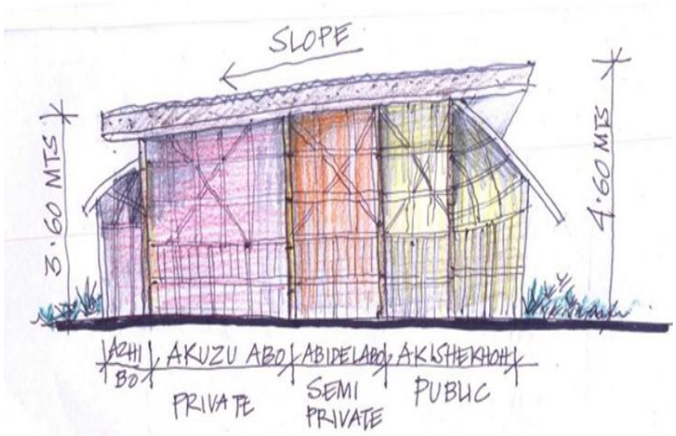

Fig 4(a).TYPICAL NAGA HOUSE SECTION

Fig 4(b).NAGA HOUSE WITH DOUBLE PITCHED ROOF

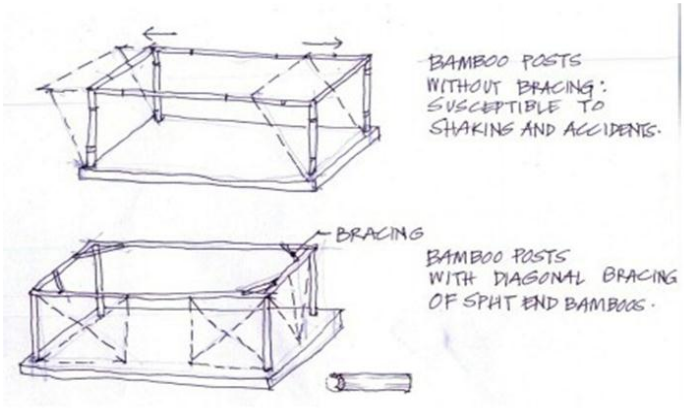

Fig 7.BAMBOO POSTS WITH AND WITHOUT BRACINGS

Fig 5. ASSAM TYPE HOUSE

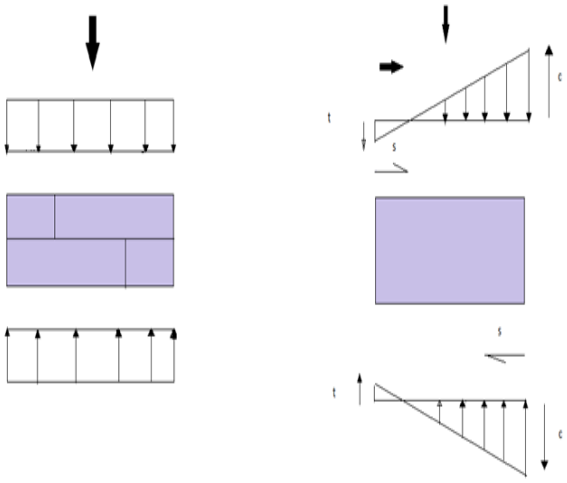

Fig 6. FORCES ACTING ON THE WALL BEFORE AND AFTER EARTHQUAKE

Table 1. COMPARISON OF SEISMIC FORCES

HOUSING TYPE	**SEISMIC FORCE (KN)**
BAMBOO	*14.55*
REINFORCED BRICK	*112.00*
CONFINED BRICK	*124.13*

Table 2. COMPARISON OF STRESSES

HOUSING TYPE	*PRINCIPAL MAJOR STRESS (MPa)*	*PRINCIPAL MINOR STRESS (MPa)*	*SHEAR STRESS (MPa)*
BAMBOO	*3.82*	*0.464*	*1.37*
REINFORCED BRICK	*1.28*	*0.29*	*0.24*
CONFINED BRICK	*1.18*	*0.188*	*0.54*

MECHANICAL ENGINEERING
&
RELATED FIELDS

5thInternational Engineering Symposium - IES 2016
March 2-4, 2016, Kumamoto University, Japan

Some Studies on the Performance and Emission Characteristics of a Diesel Engine Fuelled with Bio-fuel Blends

Mohanan P.[#], Dinesha P.[*]

Department of Mechanical Engineering, National Institute of Technology Karnataka, Surathkal, India
[#]Email: profmohanan@gmail.com
[*]Email: dinesh123mech@gmail.com

ABSTRACT: The present investigation deals with the performance and emission characteristics of cardanol based B10M10 (10% cardanol + 80% diesel+10% Methanol), B20M10 (20% cardanol + 70% diesel+10% Methanol) and B30M10 (30% cardanol + 60% diesel+10% Methanol) bio-fuel blends. The experiments are conducted on a four-stroke single cylinder diesel engine with 29.5 deg. bTDC injection timing (IT) and 220 bar injection pressure (IP) at 25%, 50%, 75%, and 100% full load conditions. The experiments have been carried out with B10M10, B20M10 and B30M10 bio-fuel blends and the results are compared with baseline diesel fuel. Results have shown that the blend of B20M10 gives lower BSEC and higher BTE at all loads compared to B30M10 biofuel blend. Lower NOx, CO, HC and Smoke emissions are observed for B20M10 over B30M10. When compared to diesel, B20M10 results slightly lower performance and higher emissions. The results reveal that blend of 20% cardanol - in diesel with 10% volume methanol provide acceptable engine performance and improved emission characteristics compared to higher cardanol biofuel blends.

***Keywords**: Biofuel, cardanol, diesel, methanol, performance, emission*

INTRODUCTION

The modern world is enhancing the demand for petroleum products with increased industrialization and use of vehicles. There are few options available from which to obtain petroleum- based fuels, and these options are concerted to some areas in the world. Hence, countries which lack these resources have to import crude oil leading to foreign exchange crisis. Therefore, it is imperative to produce alternative fuels from materials indigenous to the country, leading to the emergence of bio-fuel. It was in this context that vegetable oil and animal fats, which are renewable biological sources, helped in the production of bio-fuel as an option for diesel fuel (Ramadhas A.S. et al. 2004). This fuel is not only biodegradable, harmless, and has low emission profiles, but it is also environment friendly. Rudolf Diesel tested vegetable oil as fuel for his engine more than a century ago. With the availability of cheap petroleum, suitable crude oil fractions were refined to serve as fuel, and thus, diesel fuels and diesel engines started to develop together. In the 1940s, to tide over certain difficult situations, vegetable oils were used as fuel during World war-II. Vegetable oils and animal fats are regaining the attention of the world in their capacity to produce bio-diesel fuel because of increased worry over the environment, rising fuel prices, and minimal availability of fossil fuel. Bio-diesel fuels will help in lowering the levels of contamination and greenhouse gas effects(Narayan C.M. 2002, Dinesha and Mohanan 2015).

Many investigations have been carried out all over the world, which shows that biodiesel will minimize environmental

pollution. Das and Ganesh (2003) studied the methods of extraction of CNSL from cashew nut shell. The authors studied the yield of CNSL at low temperature pyrolysis (CNSL-1) and high temperature pyrolysis (CNSL-2). They did not report much difference in properties like ash content, moisture, and density. Also, it was observed that the viscosity changed drastically as the temperature rose from room temperature to higher temperature (at 60 °and 80 °C). They noticed a slightly higher calorific value and lower flash point in the case of CNSL-2 compared to CNSL-1 and the100% miscibility with methanol and diesel showed good indication for blending with these fuels. da Silva and de Matos (2009) conducted an experimental study on physical, viscous, and thermal properties of CNSL at different percentage compositions of gasoline-CNSL, diesel-CNSL, and Ethanol + CNSL blends. These blends were characterized and reported on their physical properties (density, viscosity, and calorific value).

Pushparaj and Ramabalan (2013) conducted experiments a single cylinder, four-stroke direct injection diesel engine with B20 CNSL blend and ethanol percentages of 5%, 10%, and 15%. The results showed lower exhaust emissions for 10% ethanol with B20 CNSL blend. The NO emission was reduced by 57% compared to B20. Kasiraman G. et al. (2011) studied the effect of blending 30% by volume of alcohol with cashew nut shell oil. The blends were prepared by mixing 30% volume of methanol and 30% volume of ethanol separately with CNSO (or CNSL).

The present study cardanol is selected as a biofuel for the fuelling of diesel engine after blending with diesel and 10% methanol as an additive. Cardanol is a naturally occurring phenol manufactured from CNSL. It is a mono hydroxyl phenol having a long hydrocarbon chain in the meta position. The experiments have been conducted to investigate the effect of cardanol-methanol-diesel blends on the performance and emission characteristics of the single cylinder diesel engine at different loading conditions.

EXPERIMENTAL SETUP

The engine tests are conducted on a computerized single cylinder four-stroke, naturally aspirated, open chamber (Direct Injection) and water-cooled diesel engine test rig as shown in Fig. 1. The specification of diesel engine used for experiments is given in Table 1. It is directly coupled to an eddy current dynamometer. The engine and the dynamometer are interfaced to a control panel, which is connected to a computer. Test rig is provided with necessary equipment and instruments for combustion pressure and crank angle measurements with accuracy. These signals are interfaced to computer through an analog to digital converter (ADC) card PCI-1050 which is mounted on the motherboard of the computer.

RESULTS AND DISCUSSION

A wide range of experiments were carried out at different load conditions to examine the effect of cardanol diesel blends on the performance and emission characteristics of the test engine. The tests have been carried out for various blends of B10M10, B20M10, and B30M10 at 25%, 50%, 75%, and full load. The performance and emission characteristics are investigated at injection timing of 29.5 deg. bTDC and the fuel injection pressure is kept at 220 bar. The results are compared with baseline diesel operations.

BRAKE SPECIFIC ENERGY CONSUMPTION (BSEC)

Figure 2 shows the variation of brake specific energy consumption (BSEC) for the various fuel blends at different load conditions. For all the blends, specific energy consumption decreases up to part load and increases thereon. The BSEC at full load for diesel is 11.53 MJ/kW-hr, whereas it is 12.41 MJ/kW-hr, 12.5 MJ/kW-hr, and 13.09 MJ/kW-hr, respectively, for B10M10, B20M10, and B30M10 fuel blends. The BSEC increases by 7.6%, 8.3%, and 13.5%, respectively, for B10M10, B20M10, and B30M10 blends when compared to diesel as the biofuel

percentage is increased in the fuel blend. The test results show that diesel has lower BSEC compared to other fuel blends. A marginal increment in BSEC is observed for B10M10 blend and B20M10 has 3% higher BSEC compared to B10M10 blend. This may be due to the lower calorific value of the bio-fuel blends compared to diesel. Another reason for higher BSEC is the increased fuel consumption of higher bio-fuel blends.

BRAKE THERMAL EFFICIENCY (BTE)

Figure 3 shows the variation of brake thermal efficiency (BTE) at varying engine loads. The BTE generally increases with increasing engine load for all fuels, and is maximum for 75% load. It is observed from the figure that the BTE of the bio-fuel blend decreases as the percentage of cardanol is increased. The BTE of diesel is 32% at 75% load, whereas it is 30.3%, 30%, and 28.6% for B10M10, B20M10, and B30M10 blends, respectively, at the same load. At part load conditions, the BTE is lower than of diesel be due to the higher fuel viscosity, density, and higher latent heat of vaporization required to get combustion. The higher viscosity and lower evaporation of biodiesel results in the formation of large size fuel droplets during atomization, which leads to inadequate mixing of air and fuel. At higher load condition, the high temperature of the air helps the bio-fuel blend to evaporate and mix properly, resulting in improved BTE of the engine.

NOX EMISSION

Figure 4 shows the variation of NOx emission for various fuel blends at different load conditions. The NOx emission increases as the load is increased, and maximum NOx is obtained at full load condition. The NOx of diesel is 643 ppm at 100% load, whereas it is 684 ppm, 693 ppm, and 727 ppm for B10M10, B20M10, and B30M10 blends, respectively, at the same load. The NOx level increases as the cardanol bio-fuel percentage is increased from B10M10 to B30M10. It is observed that 6.4%, 7.8%, and 13% higher NOx is obtained respectively for B10M10, B20M10, and B30M10 blends compared to diesel. NOx is formed through high temperature oxidation of nitrogen (N_2) in the combustion chamber. The formation of NOx depends on in-cylinder temperatures, oxygen concentration, and residence time for the reaction to take place. In addition, at high combustion (flame) temperatures, N_2 and O_2 in the combustion chamber disassociate into their atomic states and participate in a series of reactions. When compared to diesel, the cardanol blends have higher NOx emission. At 29.5 deg. bTDC advanced injection timing, the NOx level increases as the cardanol composition is increased from 10% to 30%. The higher NOx emission at higher temperature can be attributed to various reasons, such as fuel spray characteristics, combustion of biodiesel due to its oxygen content, and higher temperature in the cylinder.

CO EMISSION

It is observed from Fig. 5 that CO emission increases as the engine load is increased due to rich mixture requirement during higher load conditions. The CO of diesel is 0.35% at full load, whereas it is 0.45%, 0.47%, and 0.7% for B10M10, B20M10, and B30M10 blends, respectively, at the same load.When compared to diesel, all the cardanol blends tested have higher CO emission, and B30M10 has maximum CO emission. It is observed from the figure that 28.5%, 34%, and 100% more CO emission is obtained for B0M10, B20M10, and B30M10 fuels, respectively, compared to diesel. Diesel operation gives lower CO emissions as it undergoes complete combustion compared to bio-fuel blends. The CO emissions increase as the fuel-air ratio becomes greater than the stoichiometric value. With increasing cardanol percentage, CO emission level increases, and the higher emissions observed at full load condition is due to the higher biofuel concentration.

HC EMISSION

The variation of HC emission at different loads for different blends is shown in Fig. 6. Hydrocarbon emission increases as the

engine load is increased and maximum HC emission is obtained for 100% load condition. Moreover, the HC emission increases as the cardanol composition is increased in the fuel blend. It is observed from the figure that 15%, 40%, and 80% more HC emission is obtained for B0M10, B20M10, and B30M10 fuels, respectively, compared to diesel at full load condition. At 29.5 deg. advanced injection timing, diesel has lower HC emission, since more time is available for the combustion. A marginal variation in HC emission is observed for B10M10 and B20M10 at all load conditions. In addition, the higher cetane number of biodiesel reduces the combustion delay period, which helps to decrease the HC emissions. Alcohol blended fuels show slightly higher HC emissions in some cases because alcohols have lower cetane numbers, which result in longer ignition delay and decomposition of the blended fuels.

SMOKE EMISSION

The variation in smoke opacity of the engine is depicted in Fig. 7. It is observed from the figure, that smoke opacity values tend to increase for biofuel blends compared to diesel for all loading conditions. It is also observed from the figure, that 21%, 28.5%, and 46% more smoke is obtained for B0M10, B20M10, and B30M10 fuels, respectively, compared to diesel at full load condition. The smoke emission is mainly due to the poor combustion of the biofuel blend. Higher viscosity and poor atomization of the fuel may cause incomplete combustion causing the formation of smoke.

CONCLUSIONS

From the above findings it can be concluded that B20M10 blend gives improved performance and emission characteristics over B30M10 fuel blend and it is recommended that B20M10 is the best fuel blend for the CI engine when operated with 29.5 deg. bTDC fuel injection timing and 220 bar fuel injection pressure. B20M10 blend results 4.5% lower BSEC at full load compared to B30M10 fuel blend. B20M10 gives higher BTE with an increase of 4.6% at 75% load compared to B30M10. Biofuel blend with 20% cardanol results lower UBHC emission over other fuel blends. 4.7% lower NOx emission obtained for over B30M10 at full load operation. B20M10 gives 32.8% lower CO, 22% less HC and marginal reduction in smoke opacity is observed for over B30M10 full load conditions.

REFERENCES

[1] da Silva F.J.A. and de Matos J.E.X. (2009), A note on the potential of CNSL in fuel blends for engines in Brazil, Rev. Tecnol., Vol 30, No.1, pp.89-96.
[2] Das P. and Ganesh A. (2003), Bio-oil from pyrolysis of cashew nut shell—a near fuel, Biomass and Bioenergy, Vol. 25, No.1, pp.113-117.
[3] Dinesha P. and Mohanan P. (2015), A Study of the Effect of Injection Pressure on the Combustion, Performance, and Emission Characteristics of Cardanol Biofuel blend fuelled CI Engine, Asia Pacific Journal of Chemical Engineering, Vol. 10, No. 1, pp. 56-64.
[4] Kasiraman G. et al. (2011), Effect of alcohol blending with cashew nut shell oil (CNSO) on the performance, emission and combustion characteristics of a direct injection diesel engine, Proc. 22nd National conference on IC Engines and Combustion, pp. 84-90.
[5] Narayan C.M. (2002), Vegetable oil as engine fuels-prospect and retrospect, Proceedings on Recent Trends in Automotive Fuels, Nagpur, India
[6] Pushparaj T.and Ramabalan S. (2013), Green Fuel Design for Diesel Engine, Combustion, Performance and Emission Analysis, Procedia Engineering, Vol.64, pp.701-709.
[7] Ramadhas A.S. et al. (2004), Use of vegetable oils as I.C. engine Fuels - A review, Renewable Energy, Vol. 29, pp. 727–742.

Table 1Specifications of the experimental setup

Engine	Four-stroke, single cylinder, constant speed, water cooled CI engine
Make	Kirloskar
Model & BHP	TV1 5.2kW@ 1,500 RPM
Compression Ratio	17.5:1
Dynamometer Type	Eddy Current
Load Measurement	Strain Gauge Load cell
Interfacing	ADC card- PCI 1050

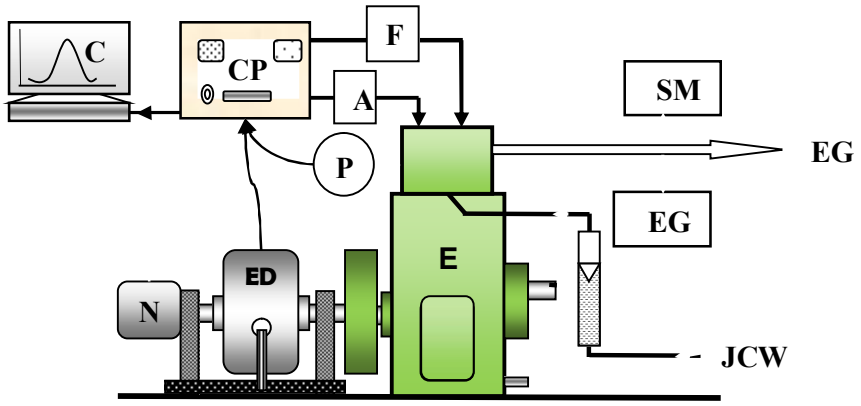

Fig. 1. Experimental engine setup
A-Air flow sensor; C-Computer; CP- Control panel; E-Engine; ED-Eddy current dynamometer; EG- Exhaust gas; EGA- Exhaust gas analyzer; F-Fuel flow sensor; JCW- Engine jacket cooling water; N-rpm sensor; P-Pressure transducer; SM- smoke meter

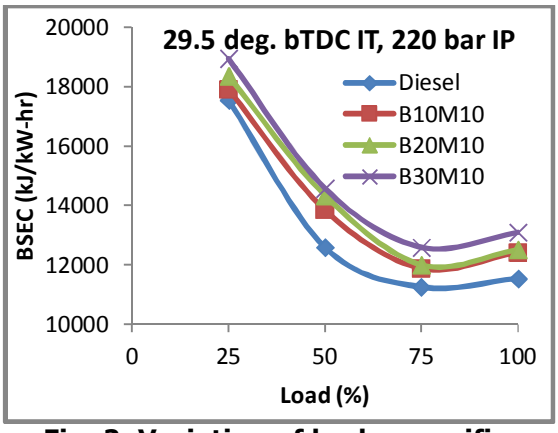

Fig. 2. Variation of brake specific energy consumption for the fuel blends

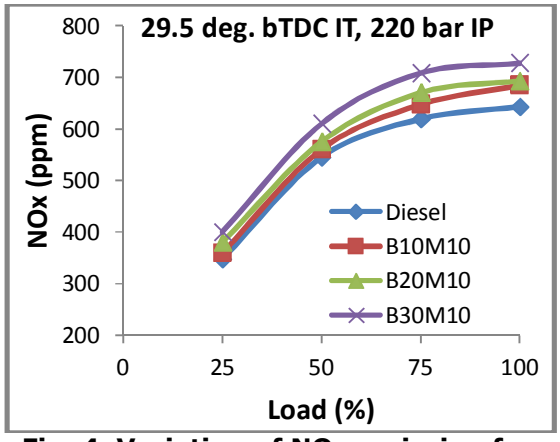

Fig. 4. Variation of NOx emission for the fuel blends

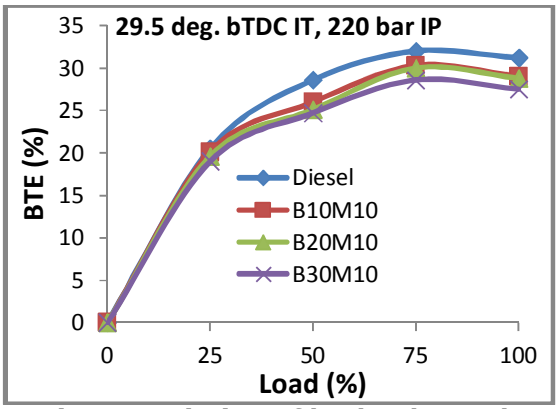

Fig. 3. Variation of brake thermal efficiency for the fuel blends

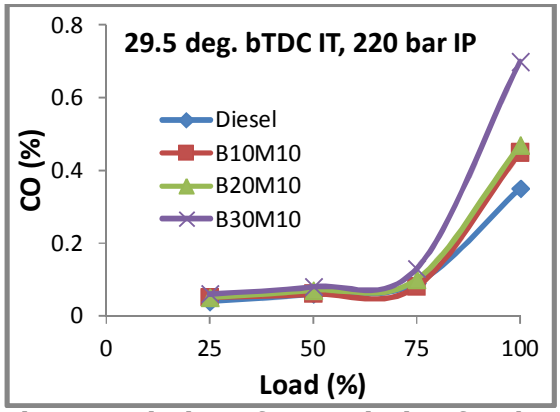

Fig. 5. Variation of CO emission for the fuel blends

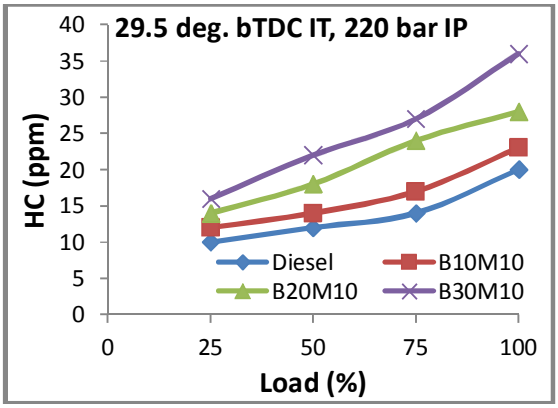

Fig. 6. Variation of HC emission for the fuel blends

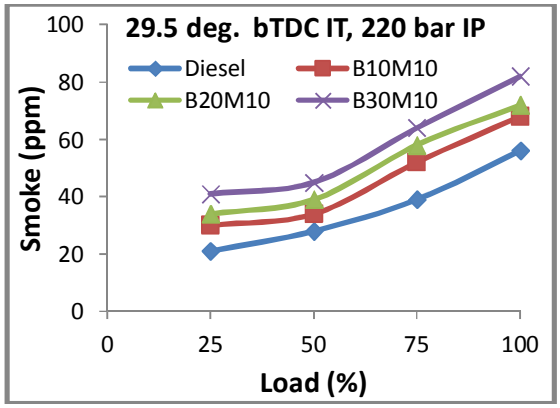

Fig. 7. Variation of smoke emission for the fuel blends

5th International Engineering Symposium - IES 2016
March 2-4, 2016, Kumamoto University, Japan

Effect of Melt Pool Behaviour on Solidification Microstructure in Laser Additive Manufacturing of Ti-6Al-4V Thin-Wall Structures

Srikanth Bontha[1] and Nathan W. Klingbeil[2]

1 *Department of Mechanical Engineering, National Institute of Technology Karnataka, Surathkal, Mangalore, Karnataka 575025, India.*
e-mail:srikanth.bontha@nitk.edu.in; srikanth.bontha@gmail.com
2 *College of Engineering and Computer Science, Wright State University, Dayton, Ohio, USA 45435.*

ABSTRACT: Laser Additive Manufacturing (LAM) processes have found many applications in the aerospace industry. Some of these applications include: low volume production, adding features to components, component repair and fabrication of functionally graded structures. Generally, components used in aerospace applications have very strict guidelines for consistency in geometry, dimensions and microstructure. Therefore, the primary obstacles to the widespread commercialization of these LAM processes include the control of melt pool size, residual stress and microstructure. While the control of melt pool size and solidification microstructure have been addressed individually in the literature, their interconnection is yet to be thoroughly investigated. This work aims to understand the effect of melt pool behavior (primarily in the vicinity of a free edge) on solidification microstructure in laser additive manufacturing of Ti-6Al-4V thin-wall structures using transient thermal finite element analysis. Numerical results are also interpreted in the context of a solidification map for predicting trends in solidification microstructure in laser-deposited Ti-6Al-4V.

Keywords*: Laser Additive Manufacturing, Melt pool, Microstructure, Transient thermal finite analysis, Thin-wall structures, Ti-6Al-4V*

INTRODUCTION

In Laser Additive Manufacturing (LAM), a solid metallic object can be fabricated directly from a three-dimensional Computer-Aided Design (CAD) representation of the object. Right from the time of their initial development, LAM processes have proved beyond doubt that they can be useful manufacturing techniques. However, the primary obstacles to the widespread commercialization of these processes as viable manufacturing alternatives for metallic components include the control of melt pool size, residual stress and microstructure (Beuth and Klingbeil (2001)).

The control of melt pool size and residual stress in these processes have been addressed by Vasinonta et al. (2001, 2002). The control of solidification microstructure in LAM processes was addressed by Bontha et al. (2006, 2009).

Of the three process characteristics listed above, the control of melt pool size assumes the highest priority (Bontha (2006)). This is because a consistent melt pool size is needed to allow a specific feature to be built using these laser-based material deposition processes. Therefore, transient response of the melt pool must be understood to build an effective system for feedback control of melt pool size in LAM processes. This work focuses on understanding the effect of melt pool behavior near a free edge on solidification

cooling rates and thermal gradients (and thereby on the resulting microstructure).

Rangaswamy et al. (2003) observed via direct thermal imaging of the melt pool that an increase in melt pool size occurs upon approaching a free edge, without any changes in the process variables (laser power or velocity). Aggarangsi et al. (2003) developed thermo-mechanical finite element models to both understand and control the increase in melt pool size in the vicinity of a free edge. Further, they concluded that in order to control the melt pool size effectively when approaching a free edge, a power reduction needs to be initiated before the melt pool size begins to increase.

In a recent study Aggarangsi et al. (2004) have extended the steady-state process map approach developed by Vasinonta et al. (2001, 2002) to investigate the transient changes in melt-pool size due to step changes in laser power and velocity. Further, progress has been made in developing real time feedback control for the LENS™ process using thermal imaging techniques for a better understanding and control of the thermal behavior during fabrication (Griffith et al. (1999), Hofmeister et al. (2002)).

Despite all this progress, the effect of transient changes in melt pool size on solidification cooling rates and thermal gradients (and thereby on the resulting microstructure) have not yet been addressed. The current work addresses this problem through thermal finite element analysis of 2-D thin-wall geometry. The research on transient effects presented in this work, only addresses the effect of transient melt pool response in the vicinity of the free edge.

MODELING APPROACH

In this section, the thin-wall geometry of Fig. 1 is considered. The chosen geometry is representative of thin-wall structures commonly built using the LENS™ and other small-scale laser deposition processes.

The thermal Finite Element (FE) models used in this study consider only the problem of heat conduction within the melt pool and the surrounding thin-wall geometry, with all free surfaces assumed to be insulated. Thus the FE models used here, do not include the effects of: Radiation from the surface of the melt pool, Convective heat transfer between the free surfaces of the wall and the surrounding air, Convective flows within the melt pool and Evaporation of the molten metal. Dobranich and Dykhuizen (1998) suggested in their work that these other modes of heat transfer (convection, radiation and evaporation) are generally small compared to conduction in laser deposition processes and hence their effects can be neglected. Finally, the thermal finite element models do not explicitly include material addition (i.e., the powder feed rate) during the laser pass. While the effect of material addition can be grossly approximated through the fraction of the absorbed laser power Ŭ, the current modeling approach is most strictly applicable for a single laser pass across an existing thin-wall.

In the thermal finite element models presented here, the laser is modeled as moving point heat source, so that the actual distribution of power is neglected. Such an assumption is most appropriate for cases in which the melt pool is sufficiently large relative to the laser beam width, and has been previously found to provide reasonable predictions of melt pool size in thin-wall LENS™ deposits (Vasinonta (2002)).

The finite element modeling was carried out using the commercial software package ABAQUS. A representative 2-D thermal finite element mesh and boundary conditions for the thin-wall geometry of Fig. 1 is illustrated in Fig. 2. The model uses 4-noded bi-linear thermal elements as part of the ABAQUS software package. The finite element model approximates the laser deposition process as a moving point heat source Ŭ*Q*, which is successively applied to adjacent nodes (beginning at the left end) at time intervals corresponding to the laser velocity *V*. The

parameter Ŭ represents the fraction of the laser power absorbed by the deposit, and based on previous results in the literature has been estimated as 35 % (Kummailil et al. (2005)). This value gives reasonable agreement with melt pool sizes observed for the LENS™ process (Brown, 2003). The remaining boundary conditions are approximated as insulated (q = 0) on the top and both vertical edges, with a fixed temperature condition on the bottom (T = 25◦C). The fixed room temperature condition on the bottom neglects any inherent preheating of the base during material deposition. Finally, the finite element model uses temperature-dependent specific heat, density and thermal conductivity, and also includes latent heat effects for Ti-6Al-4V.

The finite element models presented here have a higher mesh density near the right free edge (Fig. 2). This is done to facilitate the investigation of the effect of melt pool behavior in the vicinity of the free edge on solidification cooling rates and thermal gradients. The finite element models used have three different mesh densities going from left to right (in the x-direction). A coarser mesh is used for the first sixth of the model, while the element size in the next sixth of the model is one half of the coarser region element size. Finally, the remaining portion of the model has a finer mesh where the element size is one fourth of the coarser region element size.

In this work, thermal finite element analysis is carried out to model, the movement of the laser beginning at the left free edge of the wall, traveling left to right across the wall and reaching the right free edge. Once the laser reaches the right free edge it is turned off. Here, the effects of steady-state, transient and stationary melt pool (when the laser is turned off) behavior on solidification cooling rates and thermal gradients is investigated. The results from simulations with temperature-dependent properties for Ti-6Al-4V material are plotted on the solidification map of Ti-6Al-4V to provide predictions of grain morphology.

PROCEDURE FOR EXTRACTION OF COOLING RATES AND THERMAL GRADIENTS

The solidification cooling rate and thermal gradient at the onset of solidification have been extracted from the 2-D nonlinear finite element results at various nodal locations through the depth of the melt pool (Bontha, 2006). At each nodal location the solidification cooling rate is determined as

$$\frac{\partial T}{\partial t} = \left| \frac{T_s - T_L}{t_s - t_L} \right| \qquad (1)$$

In equation (1), T_L = 1654°C and T_S = 1620°C are the liquidus and solidus temperatures reached at times t_L and t_S respectively. The thermal gradient evaluated at t = t_L is determined directly from the nodal heat flux output and is obtained from Fourier's law as

$$G = \left| \vec{\nabla} T \right| = \frac{\left| \vec{q} \right|}{k} \qquad (2)$$

In equation (2), $\left| \vec{q} \right|$ is the magnitude of the heat flux vector and k is the thermal conductivity at the liquidus temperature. Now solidification velocity R is determined from solidification cooling rate and thermal gradient as

$$R = \frac{1}{G} \frac{\partial T}{\partial t} \qquad (3)$$

Following the calculation of G and R, the expected grain morphology can be calculated as either equiaxed, columnar or mixed by plotting points in G vs. R space (i.e., on the solidification map) (Kobryn, 2003).

RESULTS AND DISCUSSION

This section presents the results for the case when the laser is turned off upon reaching the free edge. Here the effects of steady-state, transient and stationary melt pool behavior on solidification cooling rates and thermal gradients are presented. Figure 3 illustrates the increase in melt

pool size as the laser approaches the free edge. An important point to note here is that the melt pool region is zoomed in Fig. 3 for a better view. Further, in Fig. 3, the location of the laser is evident from the intensity of the temperature distribution.

As the laser moving with a constant power and velocity reaches the center of the wall (Fig. 3 (a)), the melt pool size reaches a steady-state configuration. Throughout this paper, this melt pool is referred to as steady-state melt pool. As the laser begins to approach the free edge, there is a slight increase in temperatures at all depths within the melt pool, without any noticeable change in melt pool size. Throughout this paper, this melt pool is referred to as a transient melt pool. The size of the transient melt pool is the same as the steady-state melt pool, however the temperatures at all depths in the transient melt pool are slightly higher than the corresponding steady-state melt pool temperatures. Upon approaching the free edge, there is a considerable increase in melt pool size (Figs. 3 (b), (c) and (d)). This increase in melt pool size upon approaching the free edge is due to the decreased ability of the thin-wall to conduct the heat away from the melt pool.

As discussed earlier, this paper also considers the situation where the laser is turned off upon reaching the free edge. Throughout this paper this melt pool is referred to as a stationary melt pool.

Values of cooling rates and thermal gradients are extracted through the depth of the melt pool using equations (1) and (2) at four different x-locations in the model represented by $\frac{\bar{a}}{\bar{l}}$. Here $\bar{a}$, is the normalized distance from the right free edge and $\bar{l}$, is the steady-state melt pool length determined using the Rosenthal solution (Bontha, 2006). The spacial normalization is analogous to the ones used in Bontha et al. (2006, 2009). The value of $\frac{\bar{a}}{\bar{l}}$ = 17.22 corresponds to a location at the center of the wall where the melt pool behavior has reached a steady-state configuration (Fig. 3 (a)). Whereas, the value of $\frac{\bar{a}}{\bar{l}}$ = 1.03 corresponds to a location near the right free edge, where the temperatures at all depths within the melt pool increase slightly without any noticeable change in the melt pool size as the laser begins to approach the right free edge. This value of $\frac{\bar{a}}{\bar{l}}$ = 1.03 represents the last x-location where the nodes through the depth of the melt pool solidify before the laser is turned off. The melt pool at this location is therefore referred to as a transient melt pool. Finally, the values of $\frac{\bar{a}}{\bar{l}}$ = 0.34 and $\frac{\bar{a}}{\bar{l}}$ = 0 correspond to locations near and at the free edge of the wall which solidify as part of the stationary melt pool after the laser is turned off. The melt pool at these locations is referred to as a stationary melt pool.

The effect of melt pool behavior (steady-state vs. transient vs. stationary) on grain morphology in the Ti-6Al-4V material system is presented next. As discussed earlier, results for solidification thermal gradient and cooling rate can be interpreted in the context of a solidification map to provide predictions of grain morphology in laser-deposited Ti-6Al-4V. Upon extracting the solidification cooling rate $\frac{\partial T}{\partial t}$ and thermal gradient | ∇T | from the finite element simulations the solidification velocity R is determined using equation 3. Next, by plotting the points on the G vs. R space, the expected grain morphology can be predicted as either equiaxed, columnar or mixed (Kobryn, 2003).

Solidification map showing the effect of melt pool behavior on grain morphology is shown in Fig. 4. From Fig. 4, it is clear that the data points from the steady-state melt pool behavior fall in the fully columnar region. This result is in agreement with that presented in Bontha et al. (2006). Next, the data points from the transient melt pool behavior also fall in the fully columnar region. This can be reasoned as

follows: for the transient melt pool behavior there is a decrease in cooling rates without any noticeable change in thermal gradients (when compared to the steady-state melt pool). This results in a very small leftward movement in *G* vs. *R* space, and therefore all the data points from the transient melt pool also fall in the fully columnar region.

However, for the case of a stationary melt pool, there is a clear movement of the data points into the fully equiaxed region. This trend can be reasoned as follows: the significant increase in melt pool size upon reaching the free edge is analogous to increasing laser power under steady-state conditions. An increase in laser power acts to reduce the thermal gradients at all depths within the melt pool, which for a fixed cooling rate would move the data down and to the right in the *G* vs *R* space. At the same time, the solidification rate *R* decreases with an increase in laser power, which is a competing effect. However, the decrease in thermal gradients is more pronounced (by an order of magnitude) and dominates the effect.

CONCLUSIONS

The focus of this work has been to investigate the effect of melt pool behavior in the vicinity of a free edge. Cooling rates and thermal gradients extracted from 2D thermal finite element models have been interpreted in the context of a solidification map for the Ti-6Al-4V material system. Results suggest a transition from columnar to mixed or fully equiaxed microstructure at the free edge.

ACKNOWLEDGEMENTS

This work has been supported by the National Science Foundation, grant number DMI-0224517, by the Joint AFRL/DAGSI Research Program, project number ML-WSU-01-11, and by Wright State University and the Ohio Board of Regents.

REFERENCES

[1] Aggarangsi, P. Beuth, J. and Griffith, M., "Melt Pool Size and Stress Control for Laser- Based Deposition Near a Free Edge," in Solid Freeform Fabrication Proceedings, pp. 196–207, Solid Freeform Fabrication Symposium, August 2003.

[2] Aggarangsi, P. Beuth, J. and Gill, D., "Transient Changes in Melt Pool Size in Laser Additive Manufacturing Processes," in Solid Freeform Fabrication Proceedings, pp. 163-174, Solid Freeform Fabrication Symposium, August 2004.

[3] Beuth, J.L. and Klingbeil, N.W., "The Role of Process Variables in Laser-Based Direct Metal Solid Freeform Fabrication," JOM, Vol. 53, No. 9, pp. 36-39, 2001.

[4] Bontha, S., "The Effect of Process Variables on Microstructure in Laser Deposited Materials," PhD Thesis, Wright State University, 2006.

[5] Bontha, S. Klingbeil, N.W. Kobryn, P. and Fraser, H.L., "Thermal Process Maps for Predicting Solidification Microstructure in Laser Fabrication of Thin-Wall Structures," Journal of Materials Processing Technology, vol. 178, no. 1-3, pp. 135–142, 2006.

[6] Bontha, S. Klingbeil, N.W. Kobryn, P. and Fraser, H.L., "Effects of Process Variables and Size-Scale on Solidification Microstructure in Beam-Based Fabrication of Bulky 3D Structures," Materials Science and Engineering A, vol. 513-514, pp. 311–318, 2009.

[7] Brown, C.J., "Modeling of Solidification Microstructure in Laser-Deposited Ti-6Al-4V," Master's thesis, Wright State University, June 2003.

[8] Dobranich, D. and Dykhuizen, R., "Scoping Thermal Calculations of the LENS Process," Sandia National Laboratories Internal Report, 1998.

[9] Griffith, M. Schlienger, M. Harwell, L. Oliver, M. Baldwin, M. Ensz, M. Essien, M. Brooks, J. Robino, C. Smugeresky, J. Hofmeister, W. Wert, M. and Nelson, D., "Understanding the Thermal Behavior in the LENS Process," Materials and Design, vol. 20, no. 2, pp. 107–113, 1999.

[10] Hofmeister, W. Griffith, M. Ensz, M. and Smugeresky, J., "Solidification in Direct Metal Deposition by LENS Processing," JOM, vol. 53, pp. 30–34, September 2001.

[11] Kobryn P. and Semiatin, S., "Microstructure and Texture Evolution during Solidification Processing of Ti-6Al-4V," Journal of Materials Processing Technology, vol. 135, pp. 330–339, 2003.

[12] Kummailil, J. Sammarco, C. Skinner, D. Brown, C. and Rong, K., "Effect of Select LENS™ Processing Parameters on the Deposition of Ti-6Al-4V," Journal of Manufacturing Processes, vol. 7, pp. 42–50, January 2005.

[13] Rangaswamy, P. Holden, T. Rogge, R. and Griffith, M., "Residual Stresses in Components Formed by the Laser Engineered Net Shaping Process," Journal of Strain Analysis for Engineering Design., vol. 38, pp. 519–527, November 2003.

[14] Vasinonta, A. Beuth, J. and Griffith, M. "A Process Map for Consistent Build Conditions in the Solid Freefrom fabrication of Thin-Walled Structures," ASME Journal of Manufacturing Science and Engineering, vol. 123, pp. 615–622, 2001.

[15] Vasinonta, A., "Process Maps for Melt Pool Size and Residual Stress in Laser-based Solid Freeform Fabrication". Ph.D. Thesis, Carnegie Mellon University, 2002.

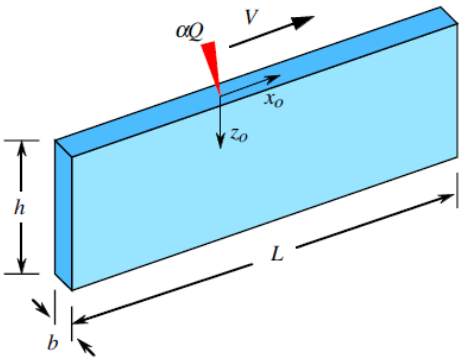

Fig.1 Thin-Wall Geometry

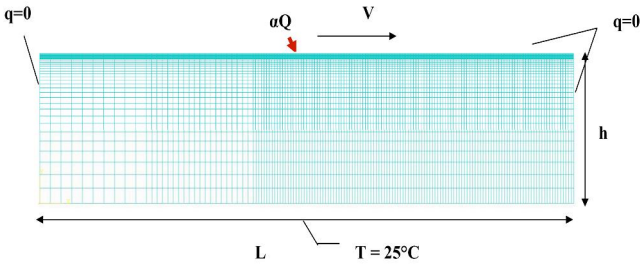

Fig.2 Representative 2-D Thermal Finite Element Mesh for Transient Analysis

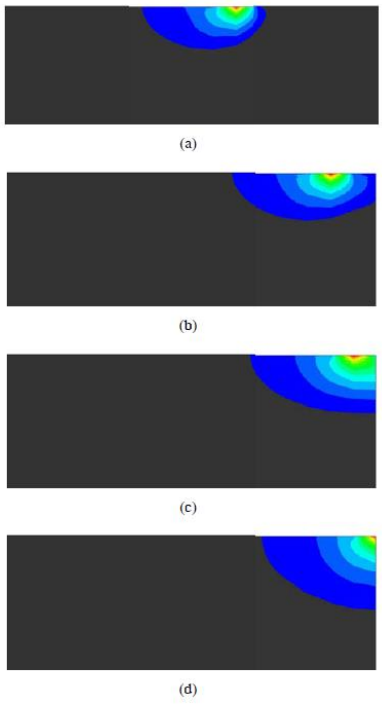

Fig.3 Illustration of the Increase in Melt Pool Size as the Laser Approaches the Free Edge of the Wall

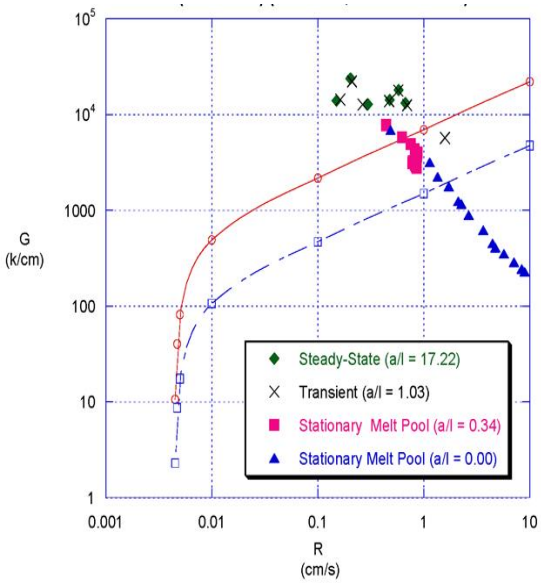

Fig.4 Effect of Melt Pool Behavior on Grain Morphology in Ti-6Al-4V (Q = 350 W, V = 8.47 mm/s)

5th International Engineering Symposium - IES 2016
March 2-4, 2016, Kumamoto University, Japan

Steady State modelling of Cryogenic Loop Heat Pipes

Arun Ashok Rao [1], Prashanth Ramesh [2], *Somesh Bhatia*[3] and Ajay Kumar Yadav [4]

1. *Undergraduate Student, Department of Mechanical Engineering, National Institute of Technology Karnataka, Surathkal, Mangalore -575025, India email:aunashok_rao@yahoo.co.in*
2. *Undergraduate Student, Department of Mechanical Engineering, National Institute of Technology Karnataka, Surathkal, Mangalore -575025, India email:prashanthramesh06@gmail.com*
3. *Undergraduate Student, Department of Mechanical Engineering, National Institute of Technology Karnataka, Surathkal, Mangalore -575025, India email:someshbhatia@ymail.com*
4. *Assistant Professor, Department of Mechanical Engineering, National Institute of Technology Karnataka, Surathkal, Mangalore -575025, India email:ajaykyadav@nitk.edu.in*

ABSTRACT: Loop heat pipes are efficient and reliable heat transfer system whose operation is based on the liquid-vapour phase change phenomenon. They use the capillary pressure generated in a porous structure to passively circulate the fluid from a heat source to a heat sink. Cryogenic loop heat pipes (CLHP) operate at ranges which are much below that of conventional loop heat pipes. CLHPs possess high pumping capability and good heat transfer performance that are important for effective and efficient cryogenic heat transport with considerable applications in space and terrestrial surroundings. The present work aims at numerically modelling a CLHP to obtain its operating characteristics which in turn can aid in the optimization of the CLHP.

Keywords: Cryogenic loop heat pipe, heat transfer, parametric study, Numerical modelling

INTRODUCTION

According to J Ku (1999), Loop Heat Pipes (LHPs) are two phase heat transfer devices that transfer heat by the evaporation and condensation of a working fluid which is transported in the system by means of capillary forces generated by fine porous wicks. LHPs can be categorized based on the operating temperature as Ambient Loop Heat Pipe (ALHP) and Cryogenic Loop Heat Pipe (CLHP). A CLHP typically operates at a temperatures of less than 200 K whereas ALHPs operate at temperatures of 0-60 °C. LHPs have the capability to transport large quantities of heat over large distances. Moreover, due to the capillary action, it has strong antigravity properties, Bai et al (2015). CLHPs which have little to no vibrations due to lack of moving parts, inherit the properties of ALHPs. As a result, CLHPs are capable of transferring heat at cryogenic temperatures without producing the vibrations that are traditionally associated with cryocoolers. Moreover, due to the compact size and the lack of a pump, they have a lot of potential for applications in space. A CLHP consists of the following components – Evaporator, Compensation Chamber (CC), Condenser, wick, liquid line and vapour line. The operating fluid used in a CLHP depends upon the operating range of the CLHP. Table 1 lists the operating range and the corresponding working fluid.

A lot of research has been carried out in the field of ALHPs resulting in various numerical modelling techniques. However, limited work has been carried out in the

modelling of CLHPs. The present work utilizes a model developed for ALHPs by L. Bai et al (2009) for type-A CLHP. Type-A, shown in figure 1, was selected due to its simplicity and ease of modelling. The model developed by Bai et al is capable of accurately predicting two phase flows and the heat transfer associated with it. Moreover, it provides a robust method of modelling the thermal conductivity and pressure loss associated with a porous wick. Knowledge of the operating characteristics of a CLHP aids in system optimization and experimental evaluation. The present work extends the model developed by Bai et al for a nitrogen charged CLHP. The model uses the laws of mass, momentum and energy conservation, to carry out a steady state analysis of the CLHP. Here, the variation of temperature and pressure drop of characteristic points of a CLHP with increase in heat load is studied in detail.

MATHEMATICAL MODEL

The working of a CLHP is similar to that of an ALHP, wherein, the heat is transferred due to evaporation and condensation of the working fluid. The working fluid is circulated due to capillary forces. The loop operating temperature is calculated as a function of the input heat load. In this CLHP model, the following assumptions are made

1. Heat transfer in the wick is only along the radial direction
2. The CLHP is under steady condition for a given load
3. The heat transfer between the CLHP parts and the ambient occurs via natural convection alone

For a given input condition, the loop operating temperature (saturation temperature) is calculated by solving the energy balance equation for each component of the LHP, T Kaya et al (1999). To solve these equations, thermophysical properties of the working fluid (nitrogen) are needed. These properties are functions of the loop operating temperature. Hence an iterative solution method is employed to obtain the loop operating temperature.

The liquid and vapour lines (transport lines) are modelled as small bored smooth pipes. Here, axial conduction of heat is neglected. Hence, the energy conservation equation for the transport lines can be written as a function of the temperature (T) in standard notations as,

$$-\dot{m}C_p\frac{dT}{dL} = (UA/L)_{p-a}(T - T_{amb}) \qquad (1)$$

Where,

$$\frac{1}{(UA/L)_{p-a}} = \frac{1}{h_i\pi d_i} + \frac{\ln\left({}^{d_o}/_{d_i}\right)}{2\pi k_w} + \frac{1}{h_o\pi d_o} \qquad (2)$$

And the subscripts *i, o, p-a, w* indicate inner, outer, pipe to ambient and wall respectively. The heat transfer coefficient at the inner wall (h_i) can be calculated based on the Nusselt number (*Nu*) as follows,*Nu* can be considered as 4.36 for a fully developed laminar flow. However, if the flow is turbulent, it can be determined by the Dittus-Boelter as follows,

$$Nu = .023Re^{.8}Pr^{n} \qquad (3)$$

As natural convection is assumed at the outer boundary of the vapour and liquid lines, h_o is calculated as follows

$$h_0 = 1.32\left(\frac{T - T_{amb}}{d_0}\right)^{0.25} \qquad (4)$$

The pressure drop that occurs across the transport lines is calculated using the Darcy-Weisbach equation as shown below.

$$-\frac{dP}{dL} = f \times \frac{1}{2}\rho u^2 \times \frac{4}{d_i} \qquad (5)$$

Where the friction factor *f*, is calculated as function of the Reynold's number (*Re*) as follows,

$$f = \begin{cases} 16/Re & Re < 2200 \\ .0791Re^{-0.25} & 2200 < Re < 10^5 \end{cases} \qquad (6)$$

Figure 2 shows the schematic of an evaporator and figure 3 shows the network diagram of a typical evaporator used in LHPs. Nodal temperatures are obtained by solving Fourier's Law of heat conduction.

Heat is initially transferred from the source to the evaporator wall via the saddle and is expressed as

$$Q = G_s\left(T_q - T_{w,e}\right) \quad (7)$$

Heat is then transferred along two paths. Part of the heat leaks into the compensation chamber (CC) (Eq.8) and the rest is transferred to the liquid vapour interface (Eq.9) as shown below,

$$Q_{e-cc} = G_{w,e-cc}\left(T_{w,e} - T_{w,cc}\right) \quad (8)$$

$$Q_{w,e-lv} = G_{w,e-lv}\left(T_{w,e} - T_{lv,e}\right) \quad (9)$$

The heat transferred to wick is primarily used for evaporating the liquid present in the liquid vapour interface and is given by equation 10. The rest of the heat is assumed to be transported along the wick in the radial direction.

$$Q_{evap} = \dot{h}_{fg}\dot{m}_v \quad (10)$$

Here, part of the heat is used for heating the fluid flowing through the wick, thereby, heating it from the CC saturation temperature to the evaporator temperature (Eq.11).

$$Q_{wick} = \dot{m}_l C_p\left(T_{lv,e} - T_{lv,cc}\right) \quad (11)$$

The remaining heat is radially leaked to the CC and is given as follows,

$$Q_{leak} = G_{lv,lv}\left(T_{lv,e} - T_{lv,cc}\right) \quad (12)$$

Most of the conductance values can be easily determined as they are mere functions of temperature. However, conductance terms involving interfaces have to be experimentally determined due to the complex nature of the heat transfer involved.

The condenser model was based on the work of Bai et al, 2009. Energy balance of the compensation chamber is used to obtain the loop operating temperature which is a characteristic parameter of a CLHP.

Properties of the working fluid are strong functions of temperature and in the present work all relevant fluid properties such as density, specific heat, latent heat, conductivity were modelled as polynomials (P(T)) in the form given below. The coefficients a_i were derived based on data available in literature, Marquardt et al (2002), J. E. Jensen et al (1980)

$$P(\mathrm{T}) = \sum_{\mathrm{i}} \mathrm{a_i T^i} \qquad \mathrm{i} = 0,1,2,\ldots \quad (13)$$

Solution algorithm of Bai et al, 2009 was adopted for the present work. By splitting the CLHP into control volumes corresponding to each part of the CLHP, energy balance for each of these control volumes is solved to obtain the relevant temperatures as well as the pressure drop. It is important to note that LHPs are driven by capillary forces and they operate only when the rise in capillary pressure is greater than the total pressure drop, J Ku (1999). The maximum rise in capillary pressure is given by

$$\Delta p_c = \frac{2\sigma\cos\theta}{R_p} \quad (14)$$

Where R_p refers to the maximum capillary radius and σ refers to the surface tension and θ refers to the contact angle. For the CLHP to work, this value must be greater than the total pressure drop, which is the sum of pressure drop across the grooves of the wick, the vapour line, liquid line, the condenser and the evaporator and is given by,

$$\Delta p_{tot} = \Delta p_g + \Delta p_v + \Delta p_l + \Delta p_c + \Delta p_e \quad (15)$$

RESULTS AND DISCUSSION

Table 2 shows the dimensional details of the CLHP model. The nitrogen charged CLHP was analysed at a sink temperature of 85 K and an ambient temperature of 300K. Figure 4 shows the variation of temperature of certain characteristic points with heat load. Here, it is very evident from the monotonic decrease of the evaporator temperature with increase in

heat load that the CLHP is operating in the Variable conductance regime. This is not the case with LHPs as there is a transition from constant conductance mode to variable conductance mode. This can be attributed to the large difference in the temperature of the cryogen and the ambient. The temperature of the working fluid gradually rises along the transport line due to ambient heating. Moreover, as the heat load increases, mass flow rate increases and this results in a reduction of temperature rise of the working fluid in the liquid line with increase in load. Figure 5 clearly shows the operating limit of the CLHP, where the rise in capillary pressure equals the total pressure drop. At a heat load of 14 W, the capillary limit is reached as a result, the CLHP cannot transport more heat. At very low heat loads, mass flow rates are too small. Moreover, figure 5 shows that the maximum drop in pressure occurs at the vapour line and the condenser suggesting the need for further design improvements.

From the analysis, it is very easy to note that the overall heat transfer capability of CLHP is lesser than that of an ALHP. This can be attributed to the fact that CLHPS reach the capillary limit very quickly when compared to ALHPs. This occurs as a result of small diameter pipes which cause large flow resistance, thereby, large pressure drops. Moreover, the maximum capillary pressure of a CLHP itself is less than ALHP due to the low values of surface tension of Cryogens.

CONCLUSIONS

The following conclusions are deduced from this study:

- Heat transport capacity of a CLHP is low when compared with that of a ALHP
- CLHP predominantly operates in the variable conductance mode
- Modelling of the system to study the variations in temperature and pressure drop of some of the characteristic points

REFERENCES

[1] Bai, Lizhan, et al. "Mathematical modeling of steady-state operation of a loop heat pipe." *Applied Thermal Engineering* 29.13 (2009): 2643-2654.

[2] Bai, Lizhan, et al. "Development of cryogenic loop heat pipes: A review and comparative analysis." Applied Thermal Engineering 89 (2015): 180-191.

[3] Bolz, Ray E. *CRC handbook of tables for applied engineering science*. CRC press, 1973.

[4] Jensen, J. E., et al. *Brookhaven National Laboratory Selected Cryogenic Data Notebook: Sections X-XVIII*. Vol. 2. Brookhaven National Laboratory, 1980.

[5] Kaya, Tarik, and Triem T. Hoang. "Mathematical modeling of loop heat pipes and experimental validation." *Journal of Thermophysics and Heat Transfer*13.3 (1999): 314-320.

[6] Ku, Jentung. *Operating characteristics of loop heat pipes*. No. 1999-01-2007. SAE Technical Paper, 1999.

[7] Marquardt, E. D., J. P. Le, and Ray Radebaugh. "Cryogenic material properties database." *Cryocoolers 11*. Springer US, 2002. 681-687.

Table 1 Typical CLHP working fluids and their temperature range

Cryogen	Temperature Range
Oxygen	90-140 K
Nitrogen	80-110 K
Neon	30-40 K
Hydrogen	20-30 K
Helium	2-4K

Table 2 Dimensions of the CLHP model

Part	Component	Dimension
Evaporator	Casing OD/ID X Length	φ 14/12 x 40 mm
	Wick OD/ID X Length	φ 12/5 x 25 mm
Main Loop	Liquid Line OD/ID X Length	φ 2/1 x 1000 mm
	Vapour OD/ID X Length	φ 2/1 x 1000 mm
	Condenser Line OD/ID X Length	φ 2/1 x 600 mm
Wick	Maximum Capillary Radius (Rp)	1.0μm
	Porosity	55%
	Permeability	>5x10-14
Volume of CC		2 ml
Volume of Gas Reservoir		500 ml

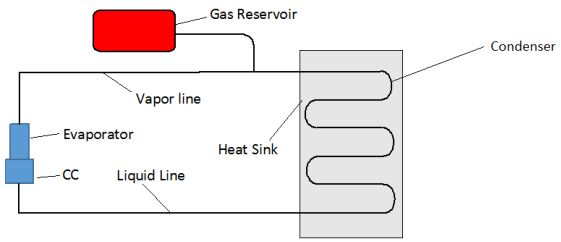

Fig.1 Schematic of Type A CLHP

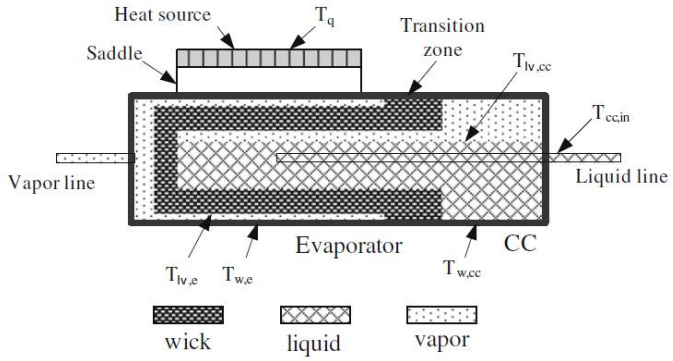

Fig.2 Schematic of an evaporator in a LHP, L. Bai et al (2009)

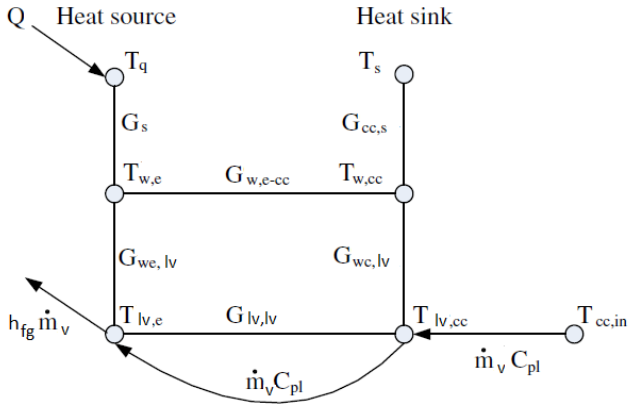

Fig.3 Network diagram of the evaporator shown in figure 2

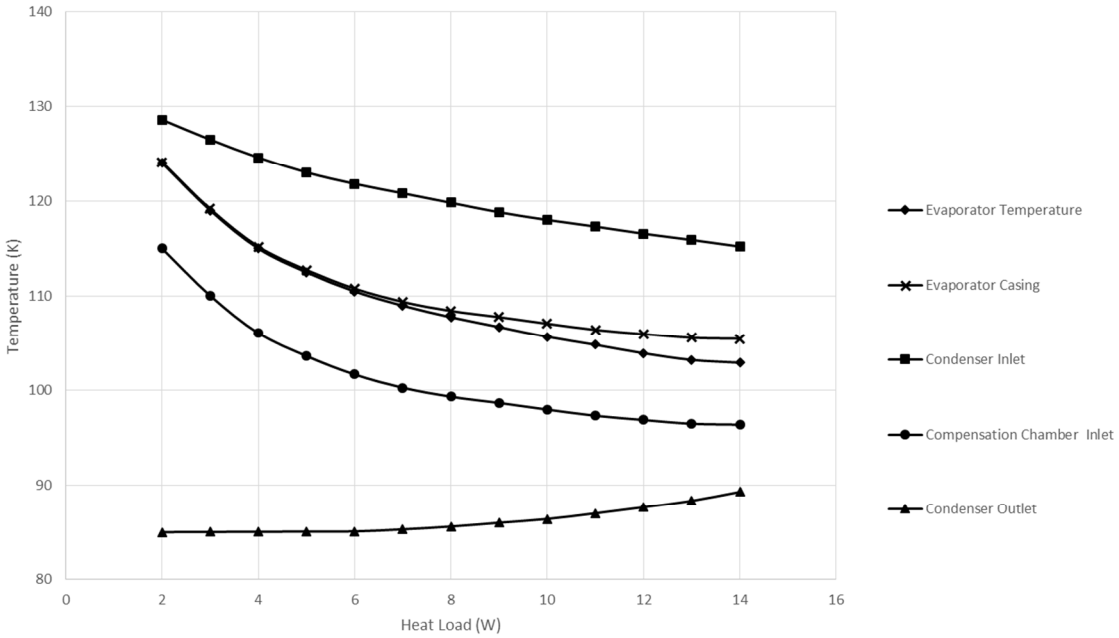

Fig.4Temperature of components of the LHP versus heat load

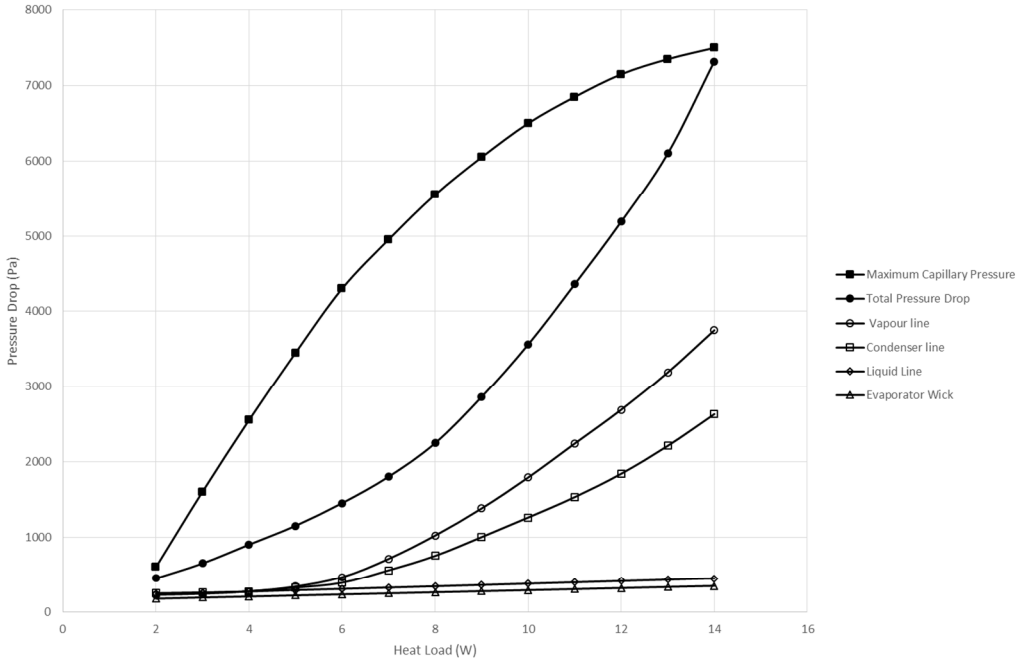

Fig.5 Pressure drop of each component versus heat load

5th International Engineering Symposium - IES 2016
March 2-4, 2016, Kumamoto University, Japan

An Innovative Renewable Energy Application for Algae and Fecal Sludge in the Combusted Boiler System

An-Peng Chen [1], Ouda Yusuke[2], Matsumoto Shota[2] and **Torii Shuichi[2]**

1 *Graduated School of Science and Technology, Kumamoto University, Kurokami, 2-39-1, Kumamoto 860-8555, Japan. e-mail:abc_10@kumamoto-u.ac.jp*
2 *Department of Mechanical System Engineering, Kumamoto University, Kurokami, 2-39-1, Kumamoto 860-8555, Japan. e-mail:abc_10@kumamoto-u.ac.jp*

Abstract: Biomass is a composition of various types of waste materials that can be utilized as useful form of energy. However this new kind of energy hasn't met its full potential in production of energy especially electricity generation due to its lower performance in terms of thermal efficiency. Algae and microalgae has been treated as the source of bio-fuel and some algae also used in fermentation for bio-gas and other phase of energy. In this paper we selected the freshwater microalgae "*Chlorella Vulgaris*" as the main material and mixture with fecal sludge. We used the mixture as biomass fuel and combusted in the boiler system to analysis its heating performance.
We found out the mixture material combusted in the boiler system, the outlet gas temperature is up to 700 ℃ and the emission gas components are in a trend with time serious. The results in this paper will be used as a reference material for microalgae multi-oriental energy application and biomass composition proximate and ultimate research development in the future.

***Keywords**: Biomass Energy, Microlgae, Fecal Sludge, Renewable Energy,*

Introduction

Since industrial revolution in 19th century, the artificial activities and modern industry with a huge quant usage of fossil fuel and emission of carbon dioxide into atmosphere had increased rapidly in 20th century, which it also related within the phenomena such as global warming and climate change. After the oil crisis in 1970s, scientists search for an alternative energy source and developing innovated technology to reduce the usage of fossil fuel and carbon dioxide emission [1]. Renewable energy seems to become the solution for the situation, and it includes hydropower, wind, solar, ocean (OTECs, wave, current, tide, etc.) and biomass energy. Biomass had been used since the mankind discovered fire and biomass energy has the mature technology and mostly using in the developing countries, such as in Africa and Asia using it for cooking and heating in daily life and the ratio might up to one-third in total energy supply [2]. Furthermore, biomass energy has the advantages with the flexibility and convinces, it also contributes 10% energy supply till today. Biomass includes a board range of biomaterials, such as wood, agricultural waste, energy grease, food industry waste, and algae (microalgae/ macro algae). Biomass energy could be used directly or converted into different phase for advanced energy device, engine or combustion boiler system, that as known as biofuel [3]. The 1st generation of biofuel extracts the oil crop or animal grease as the main material, which it has fully commercialized and developed by using convectional technology [4]. The debate of "food versus fuel" had been raised after food crisis in 2008, the concept for producing biofuel starting to investigate the material without competing

feedstock, the 2nd generation biofuel is fermented plant lignin, hemicellulose and cellulose and transforms into bioethanol [5]. However, the scientists search for an alternative material and with great potential and promising application. Algae have been considered as the 3rd generation biofuel, with lipid, protein and cellulose as the components, and no competition with food crop feedstock and land usage.

Microalgae and its Application

The concept using algae as biomass energy material researches started in 1978 till 1996, U.S. Department of Energy's Office of Fuels Development funded a project that is called ASP, Aquatic Species Project. The ASP aimed to develop the microalgae technology by using the waste carbon dioxide from power plant, to produce transportation fuel, select the potential microalgae strains and design the portal type of photo-bioreactor. Japan government (NEDO) also funded the project for carbon dioxide fixation and photo-bioreactor design, which used the *Chlorella*. sp as the main material. The programs established the fundamental principles such as, the basic design for photo-bioreactor, promising strain for lipid production (Table 1.) and open pond aquaculture system [6].

Table 1. Lipid content dry biomass of various species of microalgae

Microalgae Species	Lipid(%dry weight)
Monallanthus salina	*>20*
Nannochloropsis sp.(fresh water)	*20-35*
Nannochloropsis sp.(sea water)	*31-68*
Neochloris oleoabundans	*35-54*
Botryococcus braunii	*25-75*
Chlorella sp.	*28-32*
Crypthecodinium cohnii	*20*
Cylindrotheca sp.	*16-37*
Dunaliella primolecta	*23*
Isochrysis sp.	*25-33*
Nitzschia sp.	*45-47*
Phaeodactylum tricornutum	*20-30*

[7~13]

In recent studies, the using microalgae as other main purpose to biomass energy overcomes the low performance and increases the efficiency with certain transformation. In purpose of improving the efficiency effectively and cost down properly, those algae needed to be treated or pretreated before used in energy system or transform into other energy phase, such as syn-gas or liquidized. However, the algal biodiesel production has shown that lipid extraction and that might over use chemicals could jeopardize the environment and cause the energy waste during harvesting procedures. Some studies use the fermentation as the main approach, which is anaerobic reaction with a biological process in which sugars such as glucose, fructose, and sucrose are converted into cellular energy and thereby produce ethanol and carbon dioxide as metabolic waste products. Anaerobic digestion is a spontaneous process mediated by micro-organisms converting biomass into biogas, but it still needs more developed [14].

Biomass utilization is the trend for biomass energy related applications, thermochemical conversion is considered one of the promising routes, and these processes include gasification, pyrolysis, liquefaction and combustion. Combustion is high temperature chemical reaction between fuel and oxidant, and converted fuel to energy in the form of heat in the gas phase. Recently the microalgae energy-related researches focus on pyrolysis, such as bio-diesel. However, only a few studies about the microalgae in combustion behaviors, and mostly studied the *Chlorella* species. These studies analyzed the microalgae in different oxygen concentrations and N2/O2 ratio in thermogravimtric analysis (TGA) [15] [16]. In 2014, the Lopez-Gonzalez reported [17] that microalgae (*Chlorella. vulgaris*, *Nannochloropsis gaditana* and *Scenedesmus almeriensis* kinetic and analyzed in TGA-MS-DSC) is potential biomass for combustion application. In previous study, we analyze the two different microalgae in TGA and calorific meter, the calorie values from *Chlorella V.* and *Spirulina* are over 5000 Kcal/Kg, which is higher than most of the biomass materials, such as wood waste or crop

stein and the TGA result shows that decreased rapidly after the temperature reached 300 °C and 80% of the sample had been burned out after 900 °C [18]. In this study, we used the *Chlorella V.* mixed with fecal sludge to combust in the boiler system to analysis the heating value to be generated and the its heating behavior in the boiler system with time serious.

Material and Method

Microalgae have been studied for decades, and used in energy application depends on its property and composition. The chemical composition will be important for using in energy related researches. However, we also have to consider the quantity and potential in biomass energy. Therefore, in this study we selected *Chlorella V,*, that has been used in multi-applications and well known by the general consumers. Recently, *Chlorella V.* also is chosen as the raw material for produce bio-diesel or carbon fixation with its high growth rate, rich in lipid cell and the ability to synthesis long chain fatty acid. In this study, we mixed the *Chlorella V.* powder with fecal sludge (sample size under 2.5mm), also as known as night soil sludge that contain feces and urine, which is collected from Kyushu local area.

Fig 1. Microalgae (*Chlorella V.*) Powder Samples from Taiwan Chlorella Manufacturing Company

Fig 2. Fecal Sludge

The calorific value analysis method covers the determination of the gross calorific value of a prepared analysis sample of solid forms of biomass by the bomb calorimeter method. The calorific value, or heat of combustion, is a measure of the energy available from the microalgae. Calorific value is determined in this method by burning a weighed analysis sample in an oxygen bomb calorimeter under controlled conditions.

Fig 3. Calorific Meter, SHIMADZU Corp., model: CA-4J.

The structure of the combustion system as shown in Fig 4, the furnace has an inner cylinder and outer casing, which is called bi-cylindrical structure. The procedures as fellow:

1. Preheating the burner until the temperature reached 500℃.
2. Supplying the fuel and air into the combustor.
3. Burner stopped after temperature reached 800℃.
4. After the heating temperature is stable (over 800℃), which start to analyze gas components.

Temperature is measured in 4 places, ch1, ch2, ch3, ch4, and also sampling the gas components.

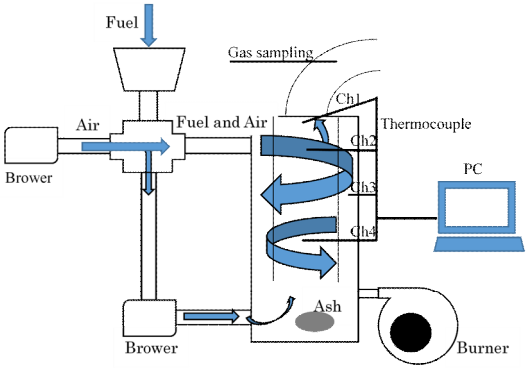

Fig 4. Combustion System Illustration Diagram

Results and Discussions

The atmosphere and sample condition as shown in Table 2., the water content and Calorific Value are the test from the mixed sample. The *Chlorella V.* calorific value is over 5000 Kcal/KG [18], and the water content is near 0%. The mixed sample due to fecal sludge lower the heating value and raised the water content.

Table 2. The atmosphere and sample condition during the combustion experiment

Atmospheric Temp(℃)	Atmospheric Pressure(Pa)	Water Supply Temp(℃)	Humidity(%)
7.8	102.3	8.5	72.4
Fuel Type		Water Content(%)	Calorific Value (Kcal/KG)
Microalgae (*Chlorella. V*) + Fecal Sludge		10.30%	4435.2

The combustion system is stable after temperature reached 800℃; we analyzed the gas emission in 5 times in different timing as shown in Fig 5., to construct a time serious.

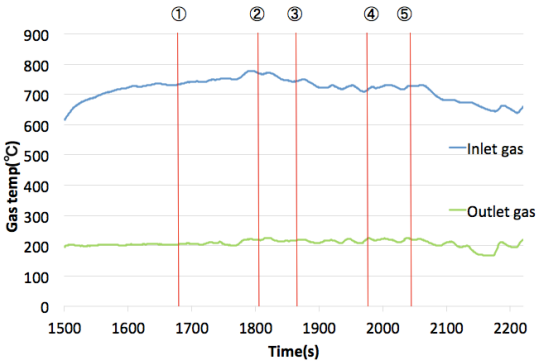

Fig 5. Gas sampling time serious

The concentration changes of gas emission have shown in Table 3. The concentration changes in O_2 and CO have the same trend increasing with time, but in NO, NOx shows in the other way, that decreasing with time. The microalgae is composed with cellulose, protein, and fatty acid. Also carbon plays an important role in the photosynthesis effect, the carbon is the main component in *Chlorella V.*. CO and CO_2 increase more and cause NO and NOx reducing. (Fig.6)

Table 3. List of gas emission concentration in combustion system time serious

	O_2 (%)	CO_2 (%)	CO (ppm)	NO (ppm)	NO_x (ppm)	SO_2 (ppm)
1	8.9	9.4	1.0	36.0	91.0	0.5
2	7.6	11.8	37.0	40.0	96.3	1.5
3	8.7	10.6	39.0	36.5	93.5	1.5
4	9.1	10.2	50.0	31.0	85.9	2.5
5	12.1	7.4	72.0	25.0	76.4	3.5

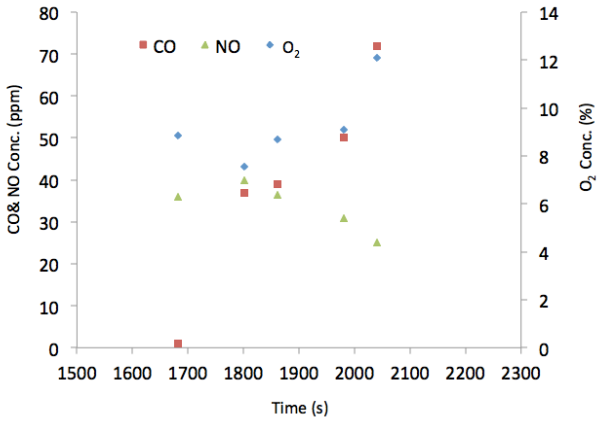

Fig 6. Time serious of CO vs. NO vs. O_2 in the combustion system

Conclusions

We analyzed *Chlorella V.* mixed with fecal sludge sample for its calorific value and heat performance in the combustion system:

- *Chlorella V.* obtains higher calorific value than fecal sludge.
- CO and CO_2 concentration increase with time.

- However NO and NOx decrease with time, perhaps the amount of carbon atom, competing for oxygen.

In Taiwan, and some other Southern Asian countries have the euphotic effects in the lakes, ponds or dams. Algae not only damage the ecosystem in the aquatic area and also become a waste treatment issue. In this study, we analyzed calorific value mixed microalgae and fecal sludge. Algae can provide higher energy than fecal sludge, and with NOx and COx emission concentration have totally different trends with time. Its behavior could use to simulate to combine microalgae with sludge for further studies. Algae and biomass energy related technologies still have a huge space for improvement and microalgae related researches would be even better optimized in the near future.
"

References

[1] L.C. Lau, K.T. Lee, and A. R. Mohamed. "Global warming mitigation and renewable energy policy development from the Kyoto Protocol to the Copenhagen Accord—A comment" Renewable and Sustainable Energy Reviews. Volume16., PP 5280–5284., 2012

[2] I. Dincer. "Renewable energy and sustainable development: a crucial review" Renewable and Sustainable Energy Reviews. Volume 4., PP 157-175., 2000

[3] S. Heidenreich, P. U. Foscolo "New concepts in biomass gasification" Progress in Energy and Combustion Science Volume 46 ., PP 72-95., 2015

[4] R. Saidura, E.A. Abdelaziz, A. Demirbas, M.S. Hossain, S. Mekhilef "A review on biomass as a fuel for boilers" Renewable and Sustainable Energy Reviews. Volume 15., PP 2262–2289., 2011

[5] R. Sims, M. Taylor, j. Saddler, and W. Mabee "From 1st to 2nd generation biofuel technologies, an overview of current industry and R&D activities". IEA Report

[6] R.H. Wijffels and M.J. Barbosa., "An outlook on microalgal biofuels." Science. Volume 379, Issue 5993. PP 796-799., 2010.

[7] Y. Chisti, "Biodiesel from microalgae. ", Biotechnology Advances, Volume 25, PP 294-306., 2007

[8] A.M. Illman, A.H. Scragg, and S.W. Shales, "Increase in Chlorella strains calorific values when grown in low nitrogen medium. ", Enzyme Microbial Technology, Volume 27, Issue 8, PP 631-635., 2000.

[09] P.S. Nigam, and A. Singh, "Production of liquid biofuels from renewable resources. ", Progress Energ. Combust. Sci. Volume 37, Issue 1, PP 52–68, 2011

[10] O. Pulz, "Photobioreactors: production systems for phototrophic microorganisms. ", Appl. Microbiol. Biotechnol., Volume57, PP 287-293. 2001

[11] C. Ratledge, "Fatty acid biosynthesis in microorganisms being used for single cell oil production. ", Biochimie, Volume 86, Issue 11, PP 807-815., 2004

[12] J. M. S. Rocha, J. E. C. Garcia,, M. H. F.Henriques, "Growth aspects of the marine microalgae Nannochloropsis gaditana. " Biomol. Eng. Volume 20, 2PP 37-242., 2003

[13] A.h. Scragg, L. Spiller, and J. Morrison, J., "The effect of 2,4-dichlorophenol on the microalga Chlorella VT-1, " Enzyme Microbial Technology, Volume 32, Issue 5, PP 616-622., 2003

[14]M. Ras, L. Lardon, S. Bruno, N. Bernet, J. P. Steyer. , "Experimental study on a coupled process of production and anaerobic digestion of Chlorella vulgaris." Bioresource Technology, (2011). Volume 102., No.1., PP 200-206., 2011

[15] Y. Tang, X. Ma, Z. Lai. "Thermogravimetric analysis of the combustion of microalgae and microalgae blended with waste in N2/O2 and CO2/O2 atmospheres." Bioresource Technology. Volume 102., PP 1879–85. 2011

[16] L. Pane, E. Franceschi, L. De Nuccio, A. Carli. " Applications of thermal analysis onthe marine phytoplankton, Tetraselmis suecica." Journal of Thermal Analysis and Calorimetry. (2001), Volume 66., PP 145–154,. 2001

[17] D. López-González, M. Fernandez-Lopez, J.L. Valverde, L. Sanchez-Silva, " Kinetic analysis and thermal characterization of the microalgae combustion process by thermal analysis coupled to mass spectrometry," Applied Energy Volume 114, PP 227–237., 2014

[18] A.P. Chen., S. Torii " Characterized the Microalgae (Chlorella and Spirulina) and Macro Algae By Using TGA and Bomb Calorific Meter for the Biomass Energy Application" ICOPE-2016 conference, Yokohama, Japan.

5th International Engineering Symposium - IES 2016
March 2-4, 2016, Kumamoto University, Japan

Effect of Graphene Oxide Nanofluid on Thermal Performance of Multi-Heat Pipe

Mohamed Salem [1], Tarek A. Meachail[2], Magdy A. Bassily[3] and **Shuichi Torii [1]**

1 *Department of Mechanical System Engineering, Kumamoto University, Kurokami, 2-39-1, Kumamoto 860-8555, Japan. e-mail:Mohamed_salem@aswu.edu.eg*
2 *Department of Mechanical Power, Faculty of Energy Engineering, Aswan University, Aswan, Egypt.*
3 *Department of Mechanical Power, Faculty of Engineering, Minia University, Minia, Egypt.*

Abstract: A multi-heat pipe is a device for heat transmission. It is composed of a heating section, a cooling section and an adiabatic section. The heating and cooling sections are the same and both are connected by four circular parallel tubes. This experimental study is performed to investigate heat transfer performance of a multi-heat pipe using pure water and Graphene oxide (GO)/water nanofluid. GO/water nanofluids were synthesized by the modified Hummers method with 0.05%, 0.1%, 0.15%, and 0.2% volume concentrations. Five different heating power levels (10W, 15W, 20W, 25W and 30W) were used in the experiments. It is found that (i) the heating section wall temperature of the GO/water nanofluids were found to be lower than those of the pure water. (ii) heat transfer performance is enhanced by suspension of nanoparticles is a comparison with that of pure water.

***Keywords**: Nanofluid, Multi-heat pipe, Graphene Oxide, Heat transfer performance*

INTRODUCTION

With an ever-increasing thermal load due to smaller features of microelectronic devices and more power output, cooling for maintaining desirable performance and durability of such devices is one of the most important technical issues in many high-tech industries. Scientists have tried to find new techniques to solve the problems of increasing temperatures of electronic devices which limited their performances. Heat pipes are one of the most effective heat transfer devices that can transport thermal energy from one point (evaporator) to another (condenser) by utilizing the phase change of working fluid. A heat pipes are composed of three parts evaporator, adiabatic section, and condenser that are placed vertically one on top of the other. The evaporator section is filled with certain amount of working fluid which vaporizes, when the heat input is supplied and the vapour passes through the adiabatic section and gets condensed in the condenser section. The condensed liquid falls back to the evaporator through the walls of the heat pipe due the action of gravity.

Torri S. and Tung D. (2011) studied the effect of 0.1, 1.0, 5.0 vol% diamond/water nanofluids on a multi-heat pipe cooling device. They found that the heat pipes filled with diamond/water nanofluids show lower evaporator thermal resistances than a water-filled heat pipe, and the reduction of the thermal resistance was amplified as the concentration of nanofluid increased. Asirvatham L. et al. (2015) presented an enhancement in the heat transfer performance of a glass thermosyphon using graphene-acetone nanofluid with 0.05%, 0.07%, and 0.09% volume concentrations. Azizi M. et al. (2013) analyzed experimentally the thermal performance in a Two-Phase Closed Thermosiphon Using Graphene/Water Nanofluid. They found that the overall heat transfer coefficient and thermal efficiency

of the thermosyphone were enhanced with weight concentration.

Kim K. and Bang I. (2016) investigated the effects of 0.01 and 0.03 vol. % graphene oxide nanofluids on heat pipe performance and capillary limits. They found that the capillary limit of the heat pipes containing GO/water nanofluids was higher than for the water heat pipe. Also, the heat pipes charged with GO/water nanofluids showed lower evaporator thermal resistances by about 25% compared with the water-filled heat pipe. Noie S. et al. (2009) showed heat transfer enhancement by using Al2O3/water nanofluid in a two-phase closed thermosyphon. They showed that the efficiency of the two-phase closed thermosyphon increases up to 14.7% when Al2O3/water nanofluid was used instead of pure water. Guo W. and Nutter D. (2009) investigated experimentally the effect of the axial conduction through the pipe wall on the performance of a thermosyphone. They found that the axial conduction through the pipe wall caused an increase in the overall heat transfer coefficient, evaporation heat transfer coefficient and condensation heat transfer coefficient of the thermosyphone. Ghanbarpour M. et al. (2013) study experimentally effect of Al2O3/water nanofluid on the thermal performance of screen mesh heat pipe. The experimental results indicate that the thermal resistance of the heat pipe with nanofluid is lower than that of the base liquid and the temperature difference between evaporator and condenser decreases as well.

In this research, the heat transfer performance was investigated for various concentrations of Graphene oxide (GO)/water nanofluid with 100% fill charge ratio under different constant heat fluxes.

MATERIALS AND METHODS

Materials

Graphene oxide (GO) was synthesized from natural graphite powder by a modified Hummers method (1958). Graphite fine powders (45 μm) was purchased from Wako pure chemical industries (Japan), concentrated sulfuric acids (H_2SO_4), sodium nitrate ($NaNO_3$), potassium permanganate ($KMnO_4$), hydrogen peroxide (30% H_2O_2), hydrochloric acid (5% HCL) and deionized water were used throughout the experiment. H_2O_2), hydrochloric acid (5% HCL) and deionized water were used throughout the experiment. Four volume fractions was prepared for graphene oxide nanofluids 0.05%, 0.1%, 0.15% and 0.2% with different pH values 6.38, 4.95, 5.97 and 5.62 respectively (Fig.1) .

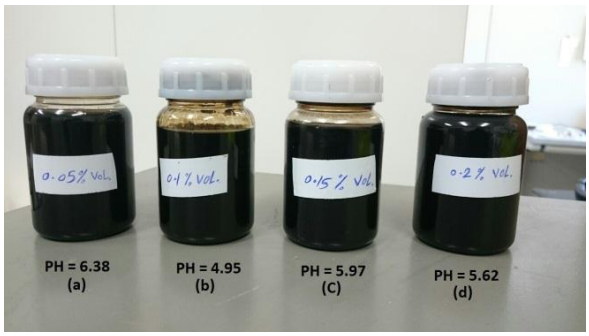

Fig.1 Graphene Oxide nanofluids. (a) 0.05 vol. %, (b) 0.1 vol. %, (c) 0.15 vol. % and (d) 0.2 vol. %

Experimental Method

A multi- heat pipe was made in laboratory of Kumamoto University-Japan (Fig. 2). It is composed of heating, cooling, and adiabatic section. The external dimensions for heating and cooling sections are 45 x 45 x 8mm, and the internal dimensions are 42 x 42 x 5mm. The adiabatic section is consisted of four parallel circular tubes whose dimension is ϕ6 (external diameter) x ϕ5 (inlet diameter) x 45 mm (length).

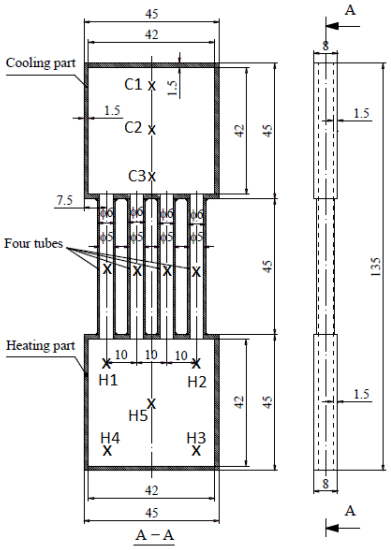

Fig. 2 Structure of the Multi-heat pipe

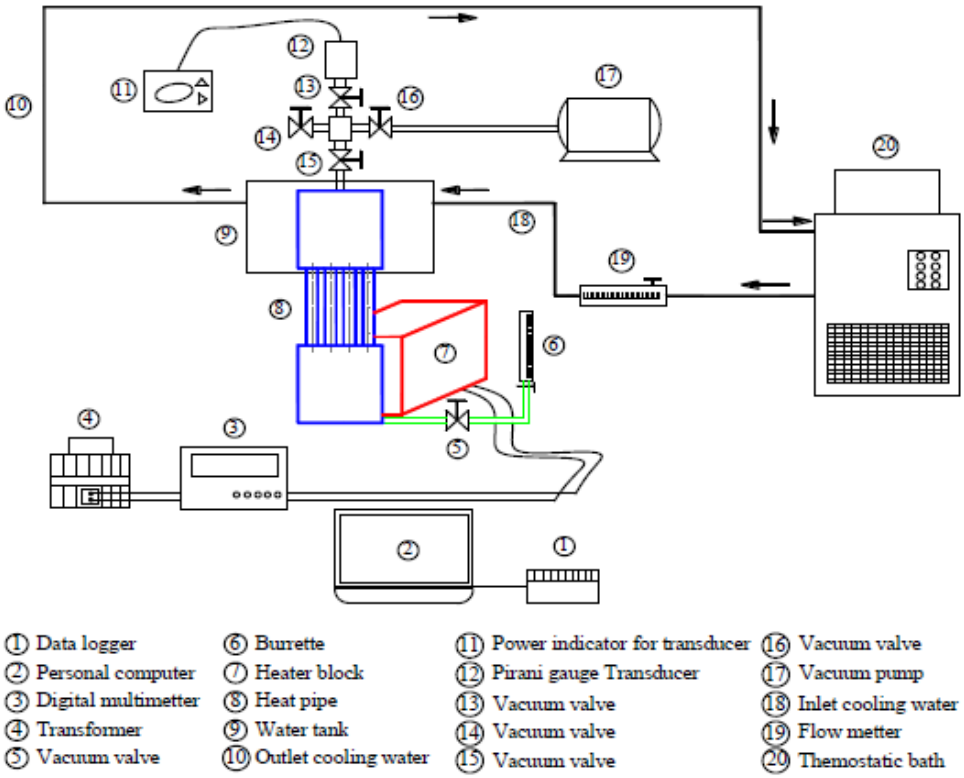

Fig. 3 Schematic diagram of experimental apparatus

A schematic diagram of experimental apparatus is described in Fig. 3. A multi-heat pipe is heated by heater block made from copper containing five heaters (HAKKO, Japan) which connected with transformer (YAMABISHI, Japan) and its voltage and power are measured by the digital multi-meter (HIOKI, Japan). An adequate amount of working fluid is filled inside of the heat pipe by burette (NALJENE, USA). Vacuum pressure inside the heat pipe is generated by the vacuum pump (ULVAC KIKO, Japan). The cooling section of the heat pipe is cooled by cooling water set at 15°C by thermostatic bath (NCC-1100, Japan) with the measurement of flow by flow meter (KOFLOC, Japan). The temperature of heat pipe is measured by twelve K-type thermocouples (Fig. 2), with five of them embedded in the heating section (H_1, H_2, H_3, H_4, and H_5), four in the adiabatic section (a_1, a_2, a_3, and a_4), and three in the condenser (C_1,C_2 , and C_3).

In this experiment, the working fluid was pure water and GO/water nanofluid with volume concentrations 0.05, 0.1, 0.15, and 0.2%. The test section was charged with the working fluid at 100% fill ratio (volume ratio of the working fluid to internal heating section volume). The pressure inside the test section was set to 9.5 kpa via vacuum pump for all cases. The test section is heated under constant heat fluxes (10, 15, 20, 25, 30 W) and the cooling water supplied to the water tank at a rate of 3.5 L/min. at 15 °C inlet temperature.

RESULTS AND DISCUSSION

The effect of employing GO/water nanofluids on the heat pipe thermal performance can be explained by measuring and calculating the variation of evaporator temperature, condenser temperature, and the thermal resistance of the heat pipe and comparing these parameters with those of the heat pipe with pure water. The mean temperature of evaporator section (T_H) and condenser section (T_C) were calculated as follow:

$$T_H = \frac{T_{H1} + T_{H2} + T_{H3} + T_{H4} + T_{H5}}{5} \qquad (1)$$

$$T_C = \frac{T_{C1} + T_{C2} + T_{C3}}{3} \quad (2)$$

Figure 4 shows the mean temperature of the evaporator section as a function of the input power (equation 3) and volume concentrations.

$$Q_{in} = V\,I \quad (3)$$

where V and I are the applied voltage and current, respectively.

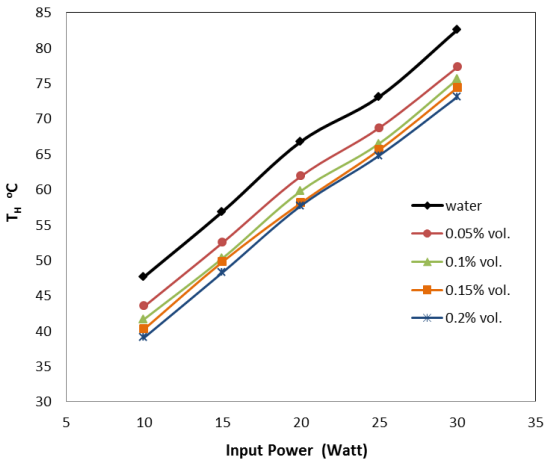

Fig.4 Evaporator temperature at different input power

As can be seen, the mean temperature of the evaporator increased with the input power increased for all concentrations. When the heat pipe charged with GO nanofluid, the wall temperature is less than pure water. It confirms that the thermal performance of multi-heat pipe is better when nanofluid is used instead of pure water. By increasing the concentration of GO/water nanofluids, the smaller rise in wall temperature of evaporator observed than pure water under various heat fluxes. It is also observed that the temperature reduces by 8.81%, 12.58%, 15.51%, and 18.03% for 0.05%, 0.1%, 0.15%, and 0.2 vol.%, respectively, at 10 W when compared with pure water.

Figure 5 presents mean wall temperature of condenser at different heat fluxes and volume fractions. From the figure, it is observed that the wall temperature increases when the concentration of GO particles increases. The percentage of increase in wall temperature of condenser at 10w was 7%, 12.52%, 14.38%, and 16.57%, respectively, for 0.05%, 0.1%, 0.15%, and 0.2% volume concentration.

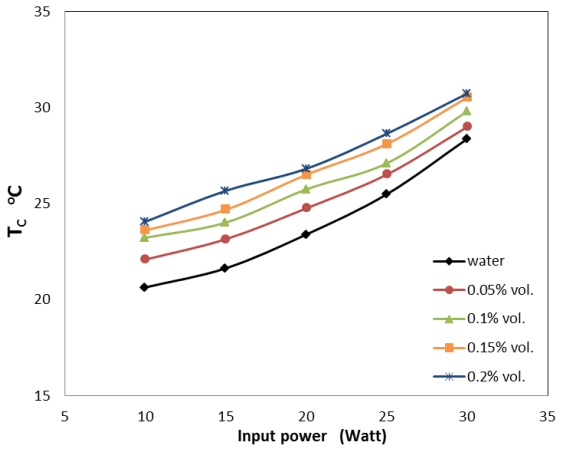

Fig.5 Condenser temperature at different input power

The overall thermal resistance of the heat pipe (R_{th}) is measured from the average temperature difference between the evaporator and the condenser sections and the input power (equation 4) [Azizi M. et al. (2013)].

$$R_{th} = \frac{T_H - T_C}{Q_{in}} \quad (4)$$

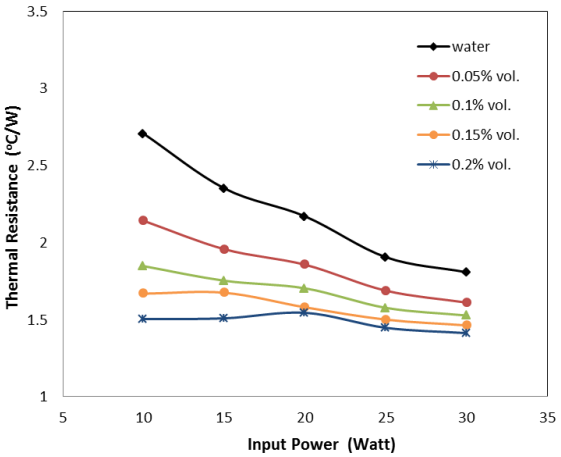

Fig.6 Thermal resistance as a function of input power

Figure 6 compares the measured overall thermal resistance (R_{th}) of nanofluid with various concentrations of GO particles for different heat fluxes with that of pure water. It is showed that the overall thermal resistance decreases with the

increase in heat flux. Also, Increase GO nanoparticles as the dispersed phase in water can significantly reduce the thermal resistance of the heat pipe. The overall thermal resistance reduces by 20.88%, 31.74%, 38.34%, and 44.45%, respectively, for 0.05, 0.1, 0.15, 0.2 % vol..

CONCLUSIONS

An experimental study was performed to investigate the thermal performance of multi-heat pipe using graphene oxide/water nanofluid. Graphene oxide was synthesized by modified Hummers method. The following conclusions are deduced from this study:

- The heat transfer performance of this multi-heat pipe is enhanced by suspension of nanoparticles in comparison with that of base fluid (pure water).
- The evaporator wall temperature of the heat pipe increases with an increase in concentration of nanoparticles and heat flux.
- The condenser wall temperature of the heat pipe increases with heat flux and reduces with increase the volume fraction of nanofluid.
- Thermal resistance values of the GO/water nanofluids-filled heat pipes were lower than those of the water heat pipe.

.

REFERENCES

[1] Shuichi Torii and Dao Danh Tung (2011), Effect of Diamond Nanofluid on Thermal Performance Of Multi-Heat-Pipe Cooling Device Heated Under Constant Heat Flux, International Journal of Earth Sciences and Engineering, vol. 4, pp. 757-761.

[2] Lazarus Godson Asirvatham, Somchai Wongwises, and Jithu Babu (2015), Heat Transfer Performance of a Glass Thermosyphon Using Graphene-Acetone Nanofluid, Journal of Heat Transfer, vol. 137, pp. 111502/1-111502/9.

[3] Mehdi Azizi, Maryam Hosseini, Samira Zafarnak, Mehdi Shanbedi, and Ahmad Amiri (2013), Experimental Analysis of Thermal Performance in a Two-Phase Closed Thermosiphon Using Graphene/Water Nanofluid, Industrial & Engineering Chemistry Research, vol. 52, pp. 10015-10021.

[4] Kyung Mo Kim, and In Cheol Bang (2016), Effects of Graphene Oxide Nanofluids on Heat Pipe Performance and Capillary Limits, International Journal of Thermal Sciences, vol. 100, pp. 346-356.

[5] S.H. Noie, S. Zeinali Heris, M. Kahani, and S.M. Nowee (2009), Heat Transfer Enhancement Using Al2O3/water Nanofluid in a Two-Phase Closed Thermosyphon, International Journal of Heat and Fluid Flow, vol. 30, pp. 700–705.

[6] Wei Guo and Darin W. Nutter (2009), An Experimental Study of Axial Conduction Through a Thermosyphone Pipe Wall, Applied Thermal Engineering, vol. 29, pp. 3536-3541.

[7] M. Ghanbarpour, N. Nikkam, R. Khodabanndeh, and M. Toprak (2013), Experimental Study of Nanofluid Effect on the Thermal Performance of Screen Mesh Heat Pipe, 13th UK Heat Transfer Conference, pp. 98/1-98/8.

[8] Hummers W., JR., and Offeman R., (1958), Preparation of Graphitic Oxide, J.Am.Chem.Soc., vol. 80, pp. 1339.

5th International Engineering Symposium - IES 2016
March 2-4, 2016, Kumamoto University, Japan

Rover with rocker-bogie linkage mounted with an ultrasonic sensor and Bluetooth module.

Meet Upadhyay [1], B. Suresh[2], Dr.Guruprasad K R[3], Asavari Limaye, Nischita Kaza, Prachi Shahi, Vedant Dhruv, Vignesh Radhakrishnan

Department of Mechanical Engineering, NITK, Surathkal, Mangalore 575025, India

1 email:meetupadhyay1@gmail.com
2 email:sureshbnarayan94@gmail.com
3 email:krgprao@gmail.com

ABSTRACT: An economical robot which utilises the Rocker-Bogie linkage, which is also used by NASA's Curiosity; to facilitate all terrain movement. The rover has 6 wheels with independent motors mounted to the linkage. The electronic components are mounted on a main chassis. The robot also consists of an ultrasonic sensor for obstacle detection and an android phone for live camera feed and accelerometer values transmitted via a Bluetooth module. While this is intended to model a space rover, it has terrestrial applications too. These include mapping and surveying unknown locations as well as locating survivors in wreckage and live feed.

***Keywords**: rover, rocker bogie, Arduino, path plotting*

INTRODUCTION

A planetary rover is a space exploration vehicle designed to move across the surface of a celestial body. The advantage of a rover over an orbiting spacecraft is its ability to make microscopic observations and conduct physical experimentation. A rover is required to be reliable, compact and autonomous as far as navigation and data acquisition are concerned.NASA's current design uses a two wheeled rocker arm on a passive pivot attached to a main bogie on the opposite side (Bickler, 2004). Miller et al (2002) discussed the need for rovers with higher traversal speeds for future planetary missions. They described a method of driving a rocker bogie linkage which can effectively step over most obstacles instead of impacting them, preventing high dynamic shocks. Barlas (2004) discussed the different types of suspension systems of wheeled locomotion which are required to be simple, lightweight, and have spring-less

connections to maintain equal traction and be able to distribute load equally to each wheel and prevent slipping. Tarokh et al. (1999) have described a rigorous method for the kinematic modelling of the Rocky 7 Mars Rover in terms of measured wheel velocities and certain rocker joint angles. Stone (1996)described the design of NASA's Mars Pathfinder and its various susbsystems.Patel et al. (2010) have provided the locomotion subsystem analysis of the ExoMars rover developed by ESA – a 3 bogie concept with flexible metallic wheels, body pose adjustment capability and 6 wheel steering. The paper focused on the suspension mechanism performance and wheel performance. Kim et al. (2011) presented an optimal design of a wheel type mobile robot with high stability and excellent adaptability while climbing stairs using the Taguchi model for optimization. Harrington et al. (2004) discussed the design of a lightweight, compact mechanism for the Mars Exploration Rover. It also highlighted the various latch and deployment mechanisms employed.

MOBILITY

Rocker Bogie Mechanism

The mechanism of the rover is based on a 6 wheeled rocker bogie suspension system. The mechanism allows the rover to traverse different kinds of terrains like rocks, sand and fine dust. The mechanism consists of a pair of rigid linkages on either side of the chassis attached to each other via a passive rotary joint. This joint is constructed by using two tubes, with internal and external threads respectively which allows the links to rotate about the tube's axis. Each linkage consists of two rigid links attached to each other by pivot joint. The front and middle wheels of are attached to the ends of the forward linkage known as the bogie. The rear wheel is attached to the rear end of the rear linkage known as the rocker. The forward end of the rocker is attached to the middle of the bogie and serves as a pivot point. The rocker is attached to the chassis ahead of the rear wheel by the tube arrangement. The advantage of the mechanism is the high degree of mobility. As the rover moves, the wheels are free to move up and down independently of the other wheels and hence can follow the contours of the terrain. It also maintains an almost equal weight distributionon each wheel (Stone, 1996). The bogie only passes a portion of its displacement to the rocker due to the pivot. When the rover encounters an obstacle, the front wheels are pushed against it by the rear wheels. The rotation of the front wheel lifts it up and over the obstacle. The other wheels move similarly. As a wheel encounters an obstacle, it comes to a dead stop. The rover must be operated at very low speeds, otherwise this shock would damage the vehicle frame and/or flip the vehicle (Miller et al., 2002). An important phenomenon observed while testing, was the lifting off of one of the wheels when it slipped and the other wheels maintained traction. This had to be checked otherwise it would flip over a bogie and disable the rover. Mechanical stops were added to limit the maximum rotation of the bogie. For the stability of the mechanism, the center of gravity must lie below the platform. Hence, majority of the components attached below the platform.

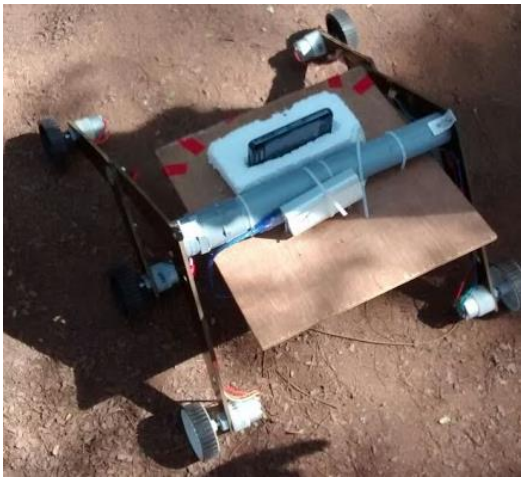

Fig 1: Completed rover.

Obstacle Capability

Obstacle capability is usually compared in terms of wheel diameter. The rover can climb obstacles up to 1.5 times its wheel diameter and climb slopes within 3 degrees of the angle of repose of the soil.

Material

Initially a flexible plastic was used to construct the links which did not perform well as it deformed excessively when the rover was in motion. It was replaced by a stiffer acrylic board. The tube joint was made of PVC. Wood was used for the platform because of its strength and light weight.

Table 1 Rover Specifications

Wheel base	475 mm
Wheel track	350 mm
Height of rover	300 mm
Platform dimensions	300mm x 300mm x 5mm
Rocker angle	90 deg
Bogie Angle	106deg
Wheel Diameter	70 mm
Motor speed	100 RPM
Battery	12 V, 1.5 A

NAVIGATION AND CONTROL

The rover's motors and ultrasonic sensors were controlled using an Arduino Uno. Arduino is an open source platform that

comes with its own IDE and is significantly simpler to code than many other microcontrollers, as it already has a vast set of libraries available. Hence an Arduino Uno board was preferred over an MSP 430 or other similar microcontrollers.

The motors were controlled using motor driver ICs. The motor driver works on the principle of a dual H-bridge. If the inputs to the motor driver are LOW and HIGH, the shaft rotates in a direction such that the rover moves forward, and vice versa. If both the inputs are LOW (or HIGH) the motor stops, since there is no current flowing through the motor. To turn the rover to the right, the wheels on the right side are made to rotate in the reverse direction and the ones on the left are moved forward. In the opposite manner, the rover is turned left. So the rover turns about its geometric centre.Due to limited availability of pins on an Arduino Uno board, the controls for the motors on each side were common. The motor controls were lumped so as to reduce the code size and adhere to the code limit of a Uno, which is 16KB.

Autonomous control was the default control state of the rover and can be manually controlled by an override via the app. An Ultrasonic sensor HC-SR04 was used to detect obstacles. The sensor has four pins – trig, echo, Vcc and GND. Trig emits ultrasonic pulses for 10 microseconds when the pin is set to HIGH. The echo pin is set to HIGH when it receives a pulse. The duration between two successive instances of echo becoming HIGH is measured; and the distance of the obstacle calculated. The rover moves forward by default. When it detects an obstacle in front, it again triggers the left and right sensors, measures the distances of the obstacles to its left and right, and finally moves in the direction in which it has more space.

An Android app was used to remotely control the rover via Bluetooth. The app was created using MIT App Inventor, an open source, web based platform. Communication between the rover and the app was established using the Bluetooth module, HC-05. Once the device's Bluetooth is turned on and the 'Connect to device' button is pressed, the app presents a list of visible devices. Upon successful connection, the buttons on screen can be used to control the rover's motion. The slider is used for speed control and is set to a default value, when the app is started up. When a button click is recognized, a string is sent to the serial buffer of the Uno, where it is received by the inbuilt function serialEvent().A set of characters is used to detect a button click as well as a termination character to indicate the end of the string. The character corresponding to the button click, say 'F' for front is extracted and the appropriate function is called in the Arduino code.

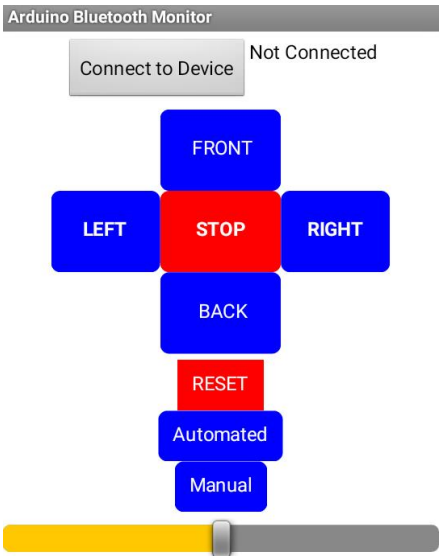

Fig 2: Bluetooth app GUI

PATH PLOTTING

The position of the rover (x and y coordinates) were plotted using the wireless Inertial Measurement Unit (IMU) of a mobile phone placed on the rover.
User Datagram Protocol (UDP) is an alternative communications protocol to Transmission Control Protocol (TCP) and was used to transmit data. It is primarily used for establishing low-latency and loss tolerating connections between applications on the Internet. It runs on top of the Internet Protocol (IP).

The following apps were used to obtain data and manipulate the path of the rover:

IMU+GPS Stream: A Stream containing the values of Accelerometer, Gyroscope, Magnetometer, GPS Position and other Sensor-Values in CSV- Format by WLAN to a Client and/or a Stream (using UDP interface) to a SD-Card can be started and stopped.

IP Webcam: The app turns the phone into a network camera with multiple viewing options. The camera feed can be viewed on any platform with a VLC media player or browser. This app was used to display the video feed from the rover.

The velocities in x, y and z directions are calculated by the product of the acceleration values obtained from the IMU and the difference in the time between two incoming data pulses.

$$v_x = v_x + a_x \cdot dt, \quad v_y = v_y + a_y \cdot dt, \quad v_z = v_z + a_z \cdot dt \quad (1)$$

The displacements are calculated as:

$$s_x = s_x + v_x \cdot dt, \quad s_y = s_y + v_y \cdot dt, \quad s_z = s_z + v_z \cdot dt \quad (2)$$

To account for sudden changes:

$$s_x = 0.1 s_x + 0.9 s_x^{prev} \quad s_x = 0.1 s_x + 0.9 s_x^{prev},$$

$$s_x = 0.1 s_x + 0.9 s_x^{prev} \quad (3)$$

s_x^{prev}, s_y^{prev} s_z^{prev} are the previous values of displacement along the fixed axis.
Rotation Vector Values x, y, z obtained from the IMU: x y z

$$\text{Rotation Vector} = x \sin\frac{\theta}{2} \quad \quad (4)$$

The angle of rotation of axis

$$\theta = 2\sin^{-1}\sqrt{x^2 + y^2 + z^2} \quad (5)$$

u, v, w are found using:

$$s_x = u \sin\frac{\theta}{2} \quad s_y = v \sin\frac{\theta}{2} \quad s_z = w \sin\frac{\theta}{2} \quad (6)$$

A rotation matrix was used to find the displacement along the fixed coordinate system (Ground) using the displacement in the phone's coordinate system, angle of rotation, and direction cosines of the line along which the system was rotated.
is the unit vector along axis of rotation and is the angle by which the axis is rotated. x, y, z are the displacements along the phone's axis in the time T_p *to* T_c. x, y, z are now updated to be the displacements along the fixed axis.The final displacements are obtained along the fixed coordinate axes which are used to plot the position of the rover.

CONCLUSIONS AND FUTURE WORK

Thus the various subsystems were integrated to construct a fully functional and robust rover.
Future plans for the rover include:

- A more robust design with double bogie arrangement
- Installation of temperature and pressure sensors
- Implementation of path planning algorithms
- Improve path plotting performance for quicker response

ACKNOWLEDGEMENTS

The members of the Amateur Astronomy Club, NITK and Astro Committee 2015 who contributed to the project and provided financial support.

REFERENCES

[1] Barlas, F (2004). Design of a Mars Rover suspension mechanism, Doctoral dissertation, Izmir Institute of Technology.
[2]Bickler, D (1993), The New Family of JPL Planetary Surface Vehicles, in Missions, Technologies and Design of Planetary Mobile Vehicles, pp. 301-306, D. Moura, Ed., Cepadues-Editions Publisher, Toulouse France.
[3] Harrington, BD and Voorhees, C (2004), The Challenges of Designing the Rocker-Bogie Suspension for the Mars Exploration Rover, 37th Aerospace Mechanisms Symposium, pp 185-195.
[4] Kim, D, Hong, H, Kim, HS, & Kim, J (2012). Optimal design and kinetic analysis of a stair-climbing mobile robot with rocker-bogie mechanism. Mechanism and machine theory, v. 50, pp. 90-108.
[5] Miller, D and Lee, T (2002) High-Speed Traversal of Rough Terrain Using a Rocker-Bogie Mobility System. Space 2002 and Robotics 2002: pp. 428-434.

[6] Patel, N, Slade, R, &Clemmet, J (2010). The ExoMars rover locomotion subsystem. Journal of Terramechanics, v. 47, n. 4, pp. 227-242.
[7] Stone, HW (1996). Mars pathfinder microrover-a small, low-cost, low-power spacecraft. Jet Propulsion Laboratory.
[8] Tarokh, M, McDermott, G, Hayati, S, & Hung, J (1999), Kinematic modeling of a high mobility Mars rover. In Robotics and Automation, 1999. Proceedings. 1999 IEEE International Conference on, v. 2, pp. 992-998.

5th International Engineering Symposium - IES 2016
March 2-4, 2016, Kumamoto University, Japan

Autonomous Wireless Vehicle for Object Avoidance and Target Tracking

Sandeep Kumar Nayak [1], Kiran A [2] and ***Gangadharan K V [3]***

Department of Mechanical Engineering, NITK Surathkal, Mangalore 575025, India

1. *e-mail: sandeepnayak1.618@gmail.com*
2. *e-mail: anginthayakiran@gmail.com*
3. *e-mail: kvganga@nitk.ac.in*

ABSTRACT: The paper elucidates a novel procedure to build an Autonomous wireless two wheel drive vehicle whose functionality, not limited to, would be detection of obstacles and avoiding it. The vehicle would indicate the presence of an obstacles by buzzing and is equipped with a solenoid to respond to traps and unmovable situation. Target identification and object tracking would be achieved subsequently through image processing.

Keywords*: Obstacle avoidance, Target Tracking, LabVIEW, Arduino, Image Processing*

INTRODUCTION

A wireless vehicle was to be made from scratch with capability to avoid obstacles, locate target and move towards the target.

The entire mission profile was systematically modularized beginning with the design of a sturdy mechanical chassis which would hold all the components, Table 1.

Then the choice of onboard sensors such as Ultrasonic sensor and IR sensor was being made.

Finally an overhead camera for the arena was chosen that, through image processing in LabVIEW, would help in tracking the vehicle and target identification and later simple procedure is developed to guide the vehicle to its target.

Mechanical Design

A square chassis was chosen with four 12V DC motors of 100 rpm. The dimension were so chosen to accommodate all components of table 1 and in such a way that the centre of gravity would be at the geometric centre of the chassis. The motors were then connected to the Arduino via H Bridge.

Obstacle Avoidance

An Ultrasonic sensor was chosen to be fixed at the front of the vehicle [4].The range of the sensor was approximately 3m.It was calibrated to detect obstacle within the range of 15cm from the vehicle. In order to detect obstacle near the corner of the vehicle, IR sensors were placed on either side of the vehicle.

Various scenarios were considered while making an algorithm for the vehicle response to one or more obstacles as shown in Fig. 1.

NI Wireless DAQ module (9191) was chosen for the Wi-Fi connectivity for communication between Arduino and LabVIEW.

Image Processing

For identifying the vehicle, a green coloured triangle shape was chosen to be stuck on the vehicle. Color detection,

Particle analysis and Pattern tracking is done in LabVIEW using the Vision assistant module [2].

Colour threshold properties were applied to the original image, to make the green colour more dominant and then

morphological features were applied to fill gaps and holes for better image.
The coordinate system were attached to the centre of mass of the triangular shape.
The final image is as shown in Fig. 2.
Using similar procedure, the target was also assigned specific colour and shape and CG calculated.
The pixels positions were mapped with the real world through image calibration feature of vision assistant to get the coordinate system of the vehicle and target.
The Distance and angle measurements between the vehicle and the target were calculated and monitored in real time, which are sent to LabVIEW for controlling the robot.
The entire algorithm is as shown in Fig. 3.

Path Planning

From Image processing, using the angle that is obtained from the target and the robot, the robot needs to be calibrated for the movement. The angle that is obtained is made as a function of time that a certain set of motor need to work in order to orient the robot at that angle.
To achieve this, the time taken by the vehicle to rotate 360 degree was noted and the experiment was repeated several times. The average of the time was then considered the time for the vehicle to rotate. It is denoted as T.
The calibration setup is as shown in Fig. 3.
The approximated time taken by the vehicle to move an angle θ is given by the equation:

$$t = \left(\frac{\theta}{360}\right) * T \qquad (1)$$

Assuming the vehicle rpm is constant.

The time t, would be fed to LabVIEW to control the amount of time, which either

Side of the motors would run, to orient itself to angle θ. The Path planning algorithm is shown in Fig. 5.

CONCLUSIONS

The vehicle could successfully detect obstacles and avoid it.
The image processing part was also successful in identifying the vehicle and target. The real time distance and angle were obtained. Therefore, the system could successfully track the position and orientation of the both the vehicle and the target.
However integrating the LabVIEW to signal Arduino was erroneous.
As a result, the vehicle movement towards the target were not agreeing with the algorithms.

FUTURE SCOPE

Improvising the path planning algorithm and implanting it into the vehicle.
Response to moving targets.
Designing and implementing a controller for better response from the vehicle.

ACKNOWLEDGEMENTS

Students Online Laboratory through Virtual Experimentation - SOLVE, NITK Surathkal, http://solve.nitk.ac.in/ for providing the facilities to work on the project.

REFERENCES

[1]Arduino Documentations and Examples: https://www.arduino.cc/
[2]LabVIEW Documentations and Examples: https://www.ni.com/manuals/
[3]Working Of Ultrasonic Sensor Principles:http://www.elprocus.com/obstacle-avoidance-robotic-vehicle/

Table 1 Hardware used

No	Item	Specification/use
1	NI Wireless CDAQ module (9191)	connectivity: Wi-Fi, 12V
2	NI DAQ card (NI 9375)	16 channel DI/DO Module Input:0-5V(Low);10-15V(high) Output: 12V
3	Arduino UNO	Power Supply – 9V Battery
4	Ultrasonic Sensor(HC-04)	Distance (0-3m)
5	DC – Motors	12V , 100RPM
6	Motor Drivers (H- Bridge)	LM293D
7	IR Sensor	Output (0-5V) - Analog
8	Rechargeable Battery	12V
9	Solenoid Plunger	12V
10	Buzzer	5V

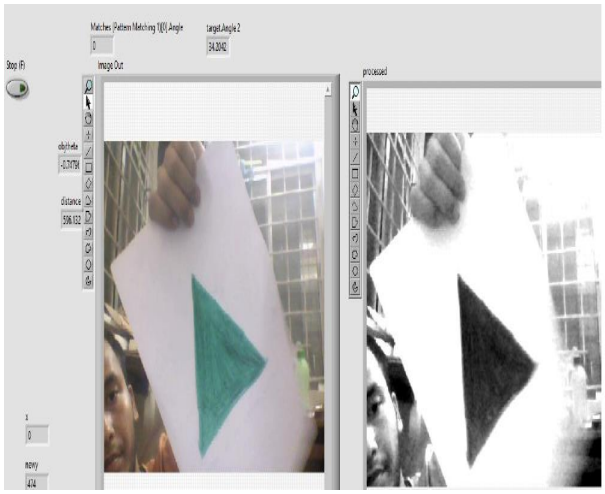

Fig. 2: Processed Image

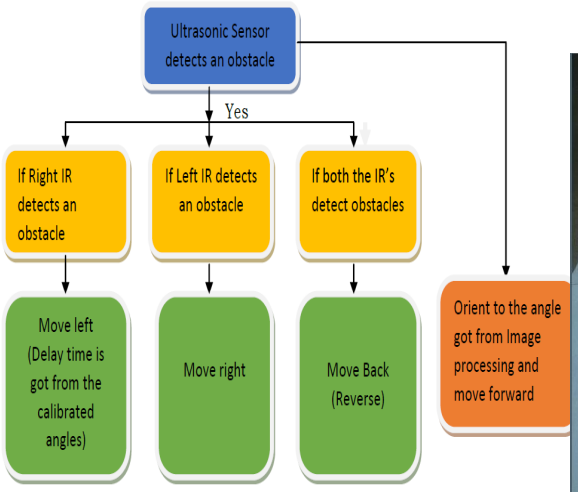

Fig. 1: Obstacle Avoidance

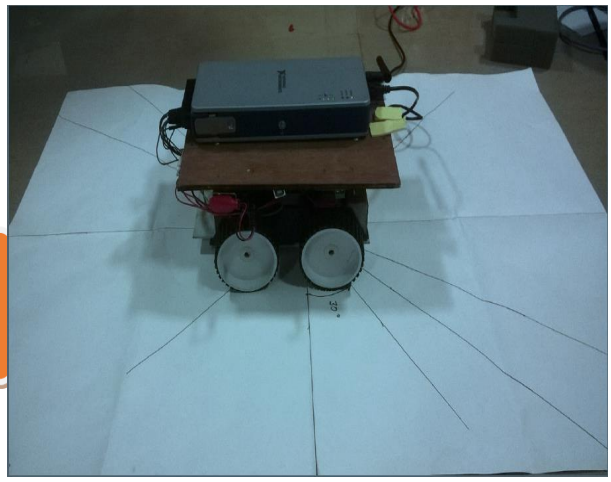

Fig. 3: Angle Calibration

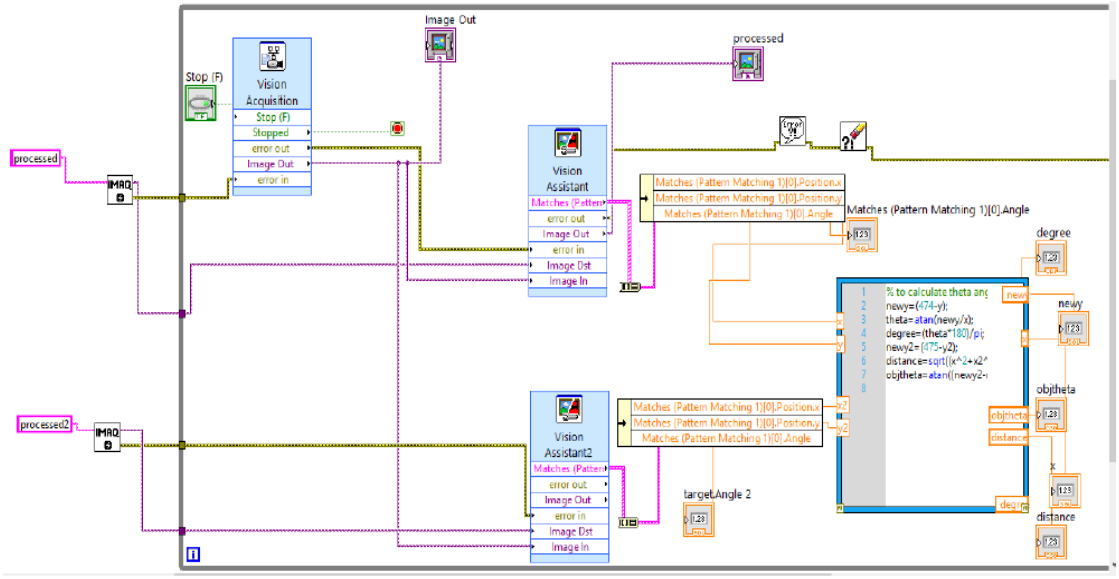

Fig. 4: LabVIEW code for Distance and Angle Measurement

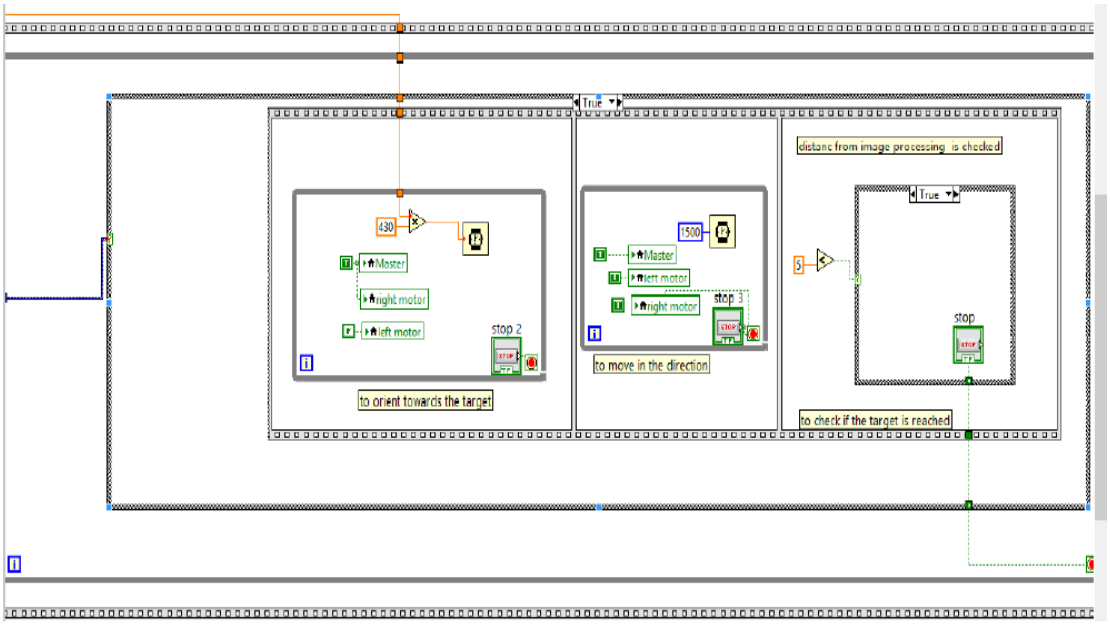

Fig. 5: Path Planning Algorithm

5th International Engineering Symposium - IES 2016
March 2-4, 2016, Kumamoto University, Japan

Multi-ferrocity of Bismuth-ferrite: A review of advances in analysis of properties and its application

Panigrahi Upasana [1], Shuichi Torii [2]

1 *Ph.d Student, Advanced Technology, Department of Mechanical System Engineering, Kumamoto University, Kurokami, 2-39-1, Kumamoto 860-8555, Japan. e-mail:154d9214@st.kumamoto-u.ac.jp*
2 *Profesor, Department of Mechanical System Engineering, Kumamoto University, Kurokami, 2-39-1, Kumamoto 860-8555, Japan. e-mail: thermal@mech.kumamoto-u.ac.jp*

ABSTRACT: Multi-Ferroics are imminent phenomenon having co-exist of unique and strong coupling of electric, magnetic and structure order parameter. This fascinating field has gained strong momentum over recent few years due to its significant influence in new strategy in science and technology. Yet much more insightful studies are required for full understanding of the physical mechanism of multi-ferroics. In this paper, a comprehensive review on Bismuth–Ferrite is presented. Summarizing the key observations and the trend of research, the literature has been meticulously surveyed, with occasional obligatory reference to a few pioneering studies on the multi-ferrocity. Detailed discussion on advancement in important application areas like solar applications and dielectric applications are presented. Identification of changes in properties with various doping method has gone through a series of modification, is analysed. A systematic analysis of future application is illustrated, considering the state-of-the-art knowledge base.

Keywords*: multi-ferroics, Bismuth-ferrite, pervoskite structure, BFO nano-powder, ferro-electricity, ferro-elasticity*

INTRODUCTION

Multiferroics is the phenomenon exhibited by certain materials in which atleast two ferroic order such as ferro-magnetism, anti-ferro magnetism, ferro-elasticity or ferro-electricity occur. This introduces a new fascinating field of science and research, with promising applications towards microwave devices, sensors, transducers, data storage, merimister, energy harvesting applications. The most important multiferroic is Bismuth-ferrite (BFO).The chemical formula is BiFeO3. BFO exhibits polymorphism with morphotropic phase boundary(MPB) phenomenon without insertion of misfit dislocation. The large displacement from rhombohedra like (R like) (4.05Å) to tetragonal like (T like) (4.64Å) with theoretical stain value of 15% approximately, has been observed.[1,2,3]. This accounts to wide application due to coupling of ferroelectric and magnetic order parameter with intrigue switchable polarization up too approximately 150μC/cm^2. This property is the function of temperature. BFO is eco-friendly with intrinsic polarization and high Curie temperature. It has been studied the pyroelectric behavior of BFO has coefficient of 90 μC/cm^2 at room temperature, which degraded abruptly with rise in temperature due to much higher ferroelectric polarization of T like BFO. This brings in the usage of BFO as thermal harvesting applications and pyroelectric sensor.

BiFeO3 is antiferromagnetic below the Neel Temperature T_N=643K and also ferroelectric below T_c=1143K.[4] It has long range 62nm cycloidal spin arrangement, that manifests net zero magnetization.

STRUCTURE INFORMATION OF BFO:

Large number of metastable structures of BFO with respective multiferroic property coupled with strong magneto-electricity is found at room temperature [5]. The α phase structure of BFO is distorted pervoskites with slight rhombohedral distortion having large octahedral tilt along [111] pseudo –cubic direction and strong ferroelectric polarization.

The phase transition from α to β and γ phases at 1098K and 1204K respectively, occurs before final decomposition which is after more 10K. The former phase change involves large volume contraction and latter phase change is iso-structural transition. Both β and γ are paraelectric orthorhombic phases incurring insulator to metal transition..

There have been 6 phase transition under application of high pressure only on BFO ranging from 1bar till 60GPa [6]. Orthorhombic structure is stable in range between 11 and 38 GPa. According to Glazer. et.al, the first four structural transition occurs at lower pressure itself i.e. at 4, 5, 7,11GPa. They are more complex like nanotwinned structures with very large unit cells. As the pressure is enhanced, BFO undergoes two more transition at 38 and 48 GPa. [7] The last one is insulator to metal transition but indifferent pattern as compared to rare earth orthoferrites transition. The total strain increases with pressure. The most remarkable note is that in both cases of high pressure and high temperature application on BFO, there is the absence of simple cubic phase transition. The table1 represents clarified structural parameters of BFO.

DOMAIN STRUCTURE OF BFO

the domain wall conductivity and magnetism has pulled in intensive research and studies recently. The ferroelectric domain structure of BiFeo3act as insulator but the domain walls involves in significant conduction [8]. Siedel.et.al observed that the conductivity is the consequence of structural induced charges in both electrostatic potential and local electronic structures attributing to decrease in band gap at domain walls and incurring carrier density at domain walls. As reported by Forikhipoor et.al [9], the thermal activation of electrons at trap states at lower voltage and Schottky emission at higher voltage lead to the conductivity. This can be enhanced by presence of strain driven migration of oxygen vacancies. Henceforth, both intrinsic and extrinsic method for conduction can be applied. The conductivity of ferroelectric vortices is appreciably higher than domain walls.[10]

The structure charges at domain wall leads to electrostatic potential and induces piezoresponse in mixed phase BiFeO3 films at phase domains and at domain walls in hexagonal magnetites [11]. The conduction due to charged walls can be easily controlled by external electric field. The domain walls act as dynamic tunable conductors. Being anti ferro magnetic domains are cross coupled with ferro electric domains, boh can be controlled by external electric field , where later is induced by electric field poling Figure-1 shows electrical control by poling of antiferromagnetic domain: (a) before and (b) after, (c) and(d) showing correlation of antiferromagnetic and ferromagnetic domain

MAGNETIC PROPERTIES

BFO is G type anti ferromagnet [12] fig 2 shows 3D reciprocal space mapping of crystal, with yellow peak representing nuclear origin and red peaks are magnetic. There is two rhombohedral twins with two ferroelectric domain in crystal with polarizing axes in [111] and [1$\bar{1}$1].Magnetism is due to partially filled d state. The properties is more infuelnced by the method of synthesis of BFO such as sol-gel method and hydrothermally growing method.

Even the doping of chemicals affects the saturation of magnetization. Mn doping in Bsite leads to interaction Fe ions with it, consequently refining the particle size, canting of antiferromagnetic ordered spins and enhancing ferromagnetic ordered spins.[13]

MAGNETO-ELECTRIC COUPLING

The strong direct magneto electric coupling phenomenon is exhibited by BFO. The slight changes in bond between

magnetic and oxygen ions cause the change in magnetic order and hence, induce an electric field. The indirect magnetic coupling can also be exhibited, if two different sub-lattices participate in magnetism and ferroelectricity. The interplay of electrostatic interaction with exponential spiral spin density at ferromagnetic surface, the s-d exchange interaction and spin diffusion leads to magneto-electric coupling. The dynamical coupling leads to magnetic damping.

FERROELECTRICITY

The $6s^2$ lone pair of electrons of Bi^{3+} has polar properties with high electronic polarizability. This leads to directional bonding. It is attributed by the O-2p-B-3d hybridisation having d^0 occupancy.[14] BFO shows magnetic property as magnetic cation sits on B site of the pervoskite. This leads to the phenomenon of multiferroics.
The chemical doping at A site(Bi^{3+}) results in better ferroelectric properties with lowering the noncollinearity of spin magnetic structure (example doping of La) or at B site (Fe^{3+}) aids in waning the leakage current by decreasing the formation tendency of oxygen vacancies.

BFO AS DIODE AND DIELECTRIC

The $6s^2$ lone pair of electrons of Bi^{3+} develops a symmetry-lowering structural distortion. The suitable chemical doping at A-sites improves the functional response of BFO as diode. With chemical doping of Mn, the diodic property improves. It shows an ohmic-current voltage
BFO film has p-type conduction, owing to Bi vacancies. It acts as capacitors with space charge limited current conduction. The shift critical voltage owing to ferroelectric polarization at asymmetric band modulation in depletion layer manifests diode property. The tunning of electro resistive effect, switchable diode effect leads in creating non-volatile memory. This property reflects BFO as promising candidate for resistive random access memory.
As studied by Graf.et.al [15], the intrinsic dielectric susceptibility of BFO along crystallographic direction is the function of temperature. At room temperature, the dielectric coefficient is small due to the saturated ferroelectric polarisation. Yet ε_{ij} coefficient rises with temperature. ε_{33} displays a sharp peak in temperature due to transition of phases from rhombohedra to orthorhombic.
The extrinsic method of La doping in A sites improves dielectric constant but not affect dielectric loss while Mn doping wanes the both.[16] Ti substitution enhance dc resistivity.[17] V improves the dielectric constant with temperature stability.[16]
Perhaps, the piezoelectric coefficients are found to be small at room temperature, though remain positive, increases with temperature.

PHOTOVOLTAIC EFFECT

This property has attracted extensive research to harvest energy via solar cells. It has been observed to have photovoltaic effect aligned at 71° and 109° domains. BiFeO3 is the efficient photocatalytic semiconductor with band gap energy of 2.0 eV. The chemical substitution of Ca, Sm, La, K and Ba [16,17,18],in BFO films enhanced the leakage current and consequently improve the photovoltaic effect. The report by Yang.et al, shows that the Nd and Co doping increase packing density by enhancing oprtical constants and band gap energy.[19]
BFO nanowire of 450nm with band gap 2.5eV is used as photoanode in dye synthesized solar cells as synthesized and analyzed by Lotey et.al. This has high energy conversion up about 3.02% [20]

CONCLUSIONS

The Bismuth-ferrite has garnered great attention due to its intriguing fundamental physics, chemical structures and future ventures. This intrigues development of new generation devices.

REFERENCES

[1] Chung-Hua Chiu, Wen-I Liang, Chun-Wei Huang , Atomic Visualization of the Phase Transition in Highly Strained BiFeO Thin Films with Excellent Pyroelectric Response, (2015) Nano Energy 17,pp.72–81
[2] R J Zeches, M.D Rossell, R ramesh, (2009)Science 326, pp 977-980
[3] A. R . Damodaran, CW. Liang, Q.He, C.Y Peng, (2011) Advanced Matter. 23 , 3170-3175
[4] Lebeugle D, Colson D, Forget A, Viret M. Appl Phys Lett 2007;91:022907.

[5] O. Diéguez, O.E. González-Vázquez, J.C. Wojdeł, J. Íñiguez, Phys. Rev. B 83 (2011) 094105.
[6] M. Guennou, P. Bouvier, G.S. Chen, B. Dkhil, R. Haumont, G. Garbarino, J. Kreisel, Phys. Rev. B 84 (2011) 174107.
[7] S. Prosandeev, D. Wang, W. Ren, J. Íñiguez, L. Bellaiche, Adv. Funct. Mater. 23 (2013) 234–240.
[8] A. L. Roitburd, Phys. Status Solidi A 37 (1976) 329.
[9] S. Farokhipoor, B. Noheda, J. Appl. Phys. 112 (2012) 052003.
[10] N. Balke, et al., Nat. Phys. 8 (2012) 81.
[11] E.B. Lochocki, et al., Appl. Phys. Lett. 99 (2011) 232901.
[12] G. Catalan, J.F. Scott, Adv. Mater. 21 (2009) 2463.
[13] Hiroki Matsuo, Yuuki Kitanaka, Yuji Noguchi, Masaru Miyayama, Electrical conduction mechanism in BiFeO -based ferroelectric thin-film capacitors: Impact of Mn doping, Journal of Asian Ceramic Societies 3 (2015) 426–431
[14] Julien Varignon, Nicholas C. Bristowe, Éric Bousquet, Philippe Ghosez, Novel magneto-electric multiferroics from first-principles calculations,
C. R. Physique 16 (2015) 153–167
[15] M. Graf, M. Sepliarsky , R. Machado, M.G. Stachiotti, Dielectric and piezoelectric properties of BiFeO from molecular dynamics simulations, Solid State Communications 218 (2015) 10–13
[16] Fuxue Yan , Gaoyang Zhao , Na Song, Nana Zhao, Yuanqing Chen, In situ synthesis and characterization of fine-patterned La and Mn co-doped BiFeO, Journal of Alloys and Compounds 570 (2013) 19–22
[17] Venkata Sreenivas Puli, Dhiren Kumar Pradhan, Sreenivasulu Gollapudi, Indrani Coondoo, Neeraj Panwar, Shiva Adireddy, Douglas B. Chrisey, Ram S. Katiyar, Magnetoelectric coupling effect in transition metal modified polycrystalline BiFeO, Journal of Magnetism and Magnetic Materials 369 (2014) 9–13
[18] Zhiwu Chen, JianqiangHu, ZhenyaLu, XinhuaHe, Low-temperature preparation of lanthanum-doped BiFeO3 crystallites by a sol–gel-hydrothermal method, Ceramics International 37 (2011) 2359–2364
[19] Shenghong Yang, Ning Yan, Sen Chen, Yueli Zhang, Structural and optical properties of the BiFeO3 system multiferroic films prepared by a sol–gel method, Ceramics International 41 (2015) S361–S364
[20] Gurmeet Singh Lotey , N.K. Verma, Synthesis and characterization of BiFeO nanowires and their applications in dye-sensitized solar cells, Materials Science in Semiconductor Processing 21 (2014) 206–211

Table 1: structural parameters of BFO

Formula	BFO
Cell type	R3c(161)
Initial cell (Å^3)	5.5810 x5.5810 x13.876
a	5.5790
b	
c	13.8705
Cell volume (Å3)	373.884
Average Bi-O band distance Å	2.41613
Average Fe-O bond distance Å	2.0235
Fe-O-Fe (deg)	156.854
Fract %	100.00
Bragg R-factor	1.19
Rf-factor	1.15

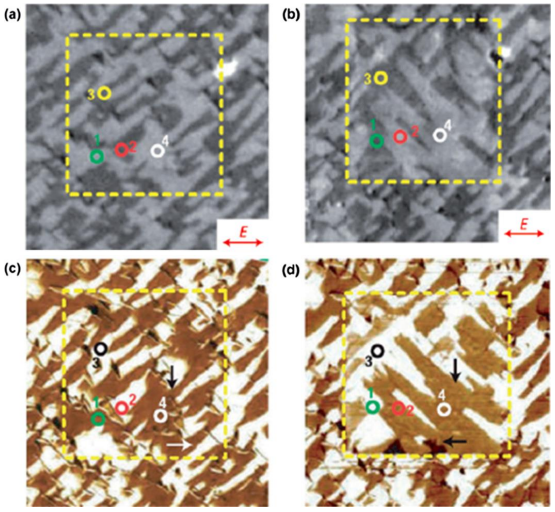

Fig1

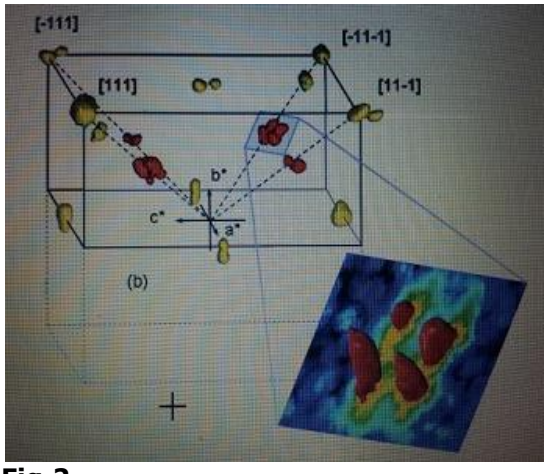

Fig.2

5th International Engineering Symposium - IES 2016
March 2-4, 2016, Kumamoto University, Japan

A State-of-the-Art to Identify Potential Sites for Biomass Resources Using Remote Sensing and Geographical Information System

Raju AEDLA[1], Ranipet Hafeez BASHA[2] and **Shuichi TORII[3]**

1 *Post-Doctoral Research Fellow, Kumamoto University, Kurokami, 2-39-1, Kumamoto 860-8555, Japan. e-mail:rajuaedla.nitk@gmail.com*
2 *Research Assistant, Graduate School of Science and Technology (GSST), Kumamoto University, Kurokami, 2-39-1, Kumamoto 860-8555, Japan. e-mail:hafeezbasha@gmailcom*
3 *Professor, Graduate School of Science and Technology (GSST), Kumamoto University, Kurokami, 2-39-1, Kumamoto 860-8555, Japan. e-mail: torii@mech.kumamoto-u.ac.jp*

ABSTRACT: The biomass is emphasized as an alternative to the conventional fossil fuels like coal and natural gas, even though the energy produced is considerably low. This is because of the easy availability of biomass from various natural sources, benefit of waste management and reduction of global warming. Biomass is any organic material which has stored sunlight in the form of chemical energy. As a fuel it may include wood, wood waste, energy crops, agricultural residues, forest residues, aquatic plants, human and animal wastes, municipal wastes. Biomass refers to recently living organisms, most often referring to plants or plant-derived materials. By conversion of biomass, biofuels are generated, which contains energy from geologically recent carbon fixation. Geospatial techniques such as Remote Sensing and Geographical Information System (GIS) can ensure optimum biomass resource potential sites for efficient renewable power generation. Biomass resources are identified using these geospatial techniques spatially as well as temporally. Geographic Information Systems (GIS) along with Remote Sensing (RS) advantages in mapping on spatial and temporal scales of the resources and are well appropriate for identifying of biomass resources potential zones. The present paper describes the importance and role of geospatial techniques in identification of biomass resources potential sites with existing studies. The study concludes that biomass resources can identify and assess by developing accurate geospatial model through database containing information about land cover, land use, regional cartography, administrative boundaries, populated areas, road network, a digital terrain model, lithological map, climatic data, industry, and a civil census.

***Keywords**: Biomass, Geospatial techniques, remote sensing, geographical information system*

INTRODUCTION

Biomass energy is most commonly used energy resource in developing countries and it is based on the biological materials derived from biological organisms. Biomass mostly referred as plants or plant-derived materials, waste from agriculture or animal husbandry, and other related materials. As an energy source, biomass can either be used directly, or converted into other energy products such as biofuel. The 1st generation of biofuel is fully developed and commercialized, because it is mainly extracted from food and oil crops (viz. rapeseed oil, palm oil, sugarcane, sugar beet, wheat, barley, maize, etc.) as well as animal fats using conventional technology [1]. 2nd

generation biofuel is fermented plant lignin, hemicellulose and cellulose and transforms into bioethanol.

Biomass material is used to generate power, heat, steam, and for producing transportation fuels and also used by the food processing industries, animal feed industry, and the wood products industry, which includes construction and fiber products (paper and derivatives). Along with chemical products made by these industries that have diverse applications including detergents, fertilizers, and erosion control products. Biomass providing approximately 14% of the world's energy needs and it ranks 4th in worldwide as an energy source. Especially in developed nations; biomass is the most important source of energy because it provides 35% of their energy [2][3]. Moreover it is estimated that by 2050 biomass can provide nearly 38% of the world's direct fuel use and 17% of the world's electricity [4]. The use of biomass fuels provides substantial benefits as far as the environment is concerned. Biomass absorbs carbon dioxide during growth, and emits it during combustion. Therefore, biomass helps the atmospheric carbon dioxide recycling and does not contribute to the greenhouse effect because biomass consumes the same amount of CO2 from the atmosphere during growth as is released during combustion [5].

According to IEA [6] statistical analysis of data, biomass energy is used in worldwide and also placed 4th quantity amount behind the gasoline, coal and gas. Biomass energy is not only a green technology, but also a renewable energy source that can replace coal quickly and cost-effectively, providing the same operational benefits while dramatically improving the environmental profile of energy generation. However this new kind of energy hasn't met its full potential in production of energy especially electricity generation due to its lower performance in terms of thermal efficiency. Based on the demand and importance of biomass resources, it is necessary to identify and assess the biomass resources to replace non-renewable resources. It is necessary to identify the potential sites of biomass resources, and then to assess the sites of resources spatially as well as temporally. Geographic Information Systems (GIS) along with Remote Sensing (RS) helps in mapping on spatial and temporal scales of the resources.

In view of this, the present study describes various studies for identification of biomass resources using remote sensing and geographical information system techniques.

Biomass resources generally assessed using direct and indirect relationship methods. In direct relationship methods, the relationship between spectral response and biomass using multiple regression analysis [7], k-nearest neighbor [8] and neural networks [9] were used for assessment of biomass. In indirect relationships, attributes data estimated from the remotely sensed data, such as Leaf Area Index (LAI), structure (crown closure and height) or shadow fraction were used in equations to estimate biomass.

REMOTE SENSING (RS)

Remote Sensing (RS) is the science and art of obtaining information about an object, area or phenomenon through the analysis of data acquired by a device that is not in contact with the object, area or phenomenon under investigation [10]. In Earth's perspective, remote sensing is the process of obtaining the information about the Earth's surface features using on-board sensors or camera systems from the satellite platform without being in direct contact with it. The data collected by these sensors are in the form of electromagnetic energy (EM) which are emitted or reflected by the object at different wavelengths depending on its physical properties.

A variety of remotely sensed data were used for biomass mapping including coarse spatial resolution data such as SPOT-VEGETATION and AVHRR [11] and MODIS [12]. To linkage of ground measurements to coarse spatial resolution remotely sensed data (e.g., MODIS, AVHRR, IRS-WiFS), studies have integrated multi-scale

imagery into biomass assessment methodology and also incorporated moderate spatial resolution imagery (e.g., Landsat, ASTER) as an intermediary data between the field data and coarser imagery [8]. Landsat TM and ETM+ data were the most widely used data of remotely sensed imagery for biomass estimation [13,14,15] and moderate spatial resolution imagery like ASTER and Hyperion data were also used for biomass estimation. Likewise, high spatial resolution data such as QuickBird and IKONOS have been used for biomass estimation. GIS-based modelling using ancillary data, such as climate normal, precipitation data, topography, and vegetation zones is another approach to biomass estimation and geostatistical approaches (i.e., kriging) are to generate spatially explicit maps for above-ground biomass (AGB) from field areas. More frequently, GIS is used as the mechanism for integrating multiple data sources for biomass estimation (e.g., forest inventory and remotely sensed data).

GEOGRAPHICAL INFORMATION SYSTEM (GIS)

The Geographical Information System (GIS) is "a powerful set of tools for collecting, storing, retrieving, transforming and displaying spatial data from the real world for a particular set of purposes" [16]. GIS is capable of handling both spatial data and attribute data of earth surface features. More significantly, a GIS also facilitates the query and analysis of the spatial data, effectively synthesizing multiple layers of information. The GIS can be used to distinguish relationships among the disparate data layers, and ultimately create new spatial data from the results of the queries and/or analyses. A Data Base Management System (DBMS) is built in GIS to store and manipulate attribute data of features and it is designed with user friendly commands in Structured Query Language (SQL). GIS has the ability to spatially interrelate multiple types of information stemming from a range of sources. GIS convert data from one coordinate system to another, to understand the characteristics of the various types of coordinate systems, either by using raster or vector data format. GIS also offers flexibility of adjusting parameters of customizing analyses to study possible changes associated with biomass resources [17].

In this view, geographical distribution of biomass potential has raised the interest of researchers in using GIS for the evaluation of the biomass supply and characteristics and estimation of the transportation cost to existing power plants as well as the site selection for energy production developments.

Biomass resource assessment using GIS-based approach provides a valuable methodology, which is very user friendly to adapt for various regions to estimate biomass resources. However, the importance is not on the specific results, but rather the significance of systematic biomass resource assessment is to better characterize the variation across the resource base [17]. With significant advantages of GIS, it is widely used in many bio-energy studies. One of the earliest applications was of the woody biomass production potential where a model of woody crop productivity was linked with county-level data on land availability and soil quality to produce county-level maps of potential biomass supplies [18]. At a finer spatial resolution, very sophisticated GIS-based studies of bio-energy have been done, where a GIS was developed to assess the potential of eucalyptus plantation grown on former sugarcane lands for supplying fuel to potential conversion facilities [19, 20]. In these analyses, roadmaps, soil maps, and land-use maps are linked with forest productivity and economic models to estimate the cost of delivering eucalyptus wood to specific locations. At a large scale, GIS have been used to assess the supply of municipal solid waste for energy production [21] and to examine the best locations, given economic and environmental considerations, for sitting bio-energy facilities [22,23].

Another study used a GIS-based modelling system to assess potential biomass supplies from energy crops at a regional

scale [24]. The modelling system was used to estimate potential switch grass costs and supplies. The sitting analysis of farm-based centralized anaerobic digester systems for distributed generation is another application using GIS [25]. In [25], a GIS model was studied for land-suitability assessment of potential energy systems featuring an anaerobic digester coupled with an energy generator [26]. Despite the widely agreed potential of bio-energy utilization, key problems regarding the use of biomass remain the limited availability in terms of time, owing to biomass seasonality, and the scattered geographical distribution over the territory that make the collection, transport and storage operations complex and expensive. These critical logistic aspects strongly affect the economic and energy performances of bio-energy conversion systems, introducing limitation on their suitability. Hu et al. (2013) [27] used GIS-based analysis to investigate the geospatial relationships between paddy rice farms and power plants to assess potential biomass for straw power generation in Taiwan. Also a sensitivity analysis of the biomass feedstock supply system was conducted for various cofiring scenarios.

IDENTIFICATION OF POTENTIAL SITES

GIS tool is very efficient tool for biomass estimation and data processing, and there are many advantages to use GIS for spatial analysis of biomass energy resources and supply systems in worldwide. GIS was used for identifying regions with high density of agricultural residues or idle croplands suitable for energy production, and to prepare the maps and cost-supply curves to present renewable energy potential sites in each region. GIS was also used to expand the depth of details for analysis of municipal solid waste as a potential power source and was recognized as a beneficial tool for renewable energy studies. GIS was used for environmental and economic models to characterize the land base, costs and potential supply of biomass for several regions. GIS also useful in assessment of ecological changes associated with biomass fuel production and consumption as it affects landscape patterns [17].

The complete Geospatial model with RS and GIS techniques has advantage in identification of biomass potential sites in large and inaccessible regions, where the conventional methods required huge man power, cost effective and time consuming. GIS can use as a site selection tool, which focused to identification of the optimal sites for energy production development based on the expected biomass yields or the allocation of biomass to existing power plants. GIS has not been used as a dynamic search engine for the selection of potential sites of power plant by using geographic distribution of biomass potential and expected electricity production cost [28].

GEOSPATIAL MODEL

Geospatial model will be developed for identification of biomass resources using satellite images by preparing various thematic maps such as, Land use and land cover map, forest map, crop map, waterbody and soil map etc. Other thematic maps like, boundary map, slope map were prepared from toposheets. Population map and filed data were used as reference data for analysis of all thematic maps using overlay analysis or spatial analysis tool, which existed in GIS software. The data base model was developed in GIS software, based on the information of earth surface layers and samples of chemical composition of biomass location and it will be helpful for further analysis and continuous assessment of biomass locations. After the analysis of data, the final map was generated, which gives the locations of biomass presented in the study area.

CONCLUSIONS

The Geospatial database management model highly helpful in identification, monitoring, assessment and analysis of biomass resources in a short time. The remote sensing techniques provide data of isolated regions for better identification of biomass resources. The various spectral and temporal satellite images improve the accuracy in identification biomass

resources. Geospatial model will become an efficient mapping software tool for identification, planning, project development, monitoring and assessment of biomass resources, which helps the researchers for identifying a region which has more potential of biomass energy resources.

REFERENCES

[1] S. N. Naik, et al., R & S Ener. Rev 14 (2014), 578
[2] Hall DO, Rosillo-Calle F, de Groot P: "Biomass energy lessons from case studies in developing countries". Energy Policy 1992; pp. 62–73
[3] McGowan F: "Controlling the greenhouse effect: the role of renewables", Energy Policy 1991, pp. 110-118
[4] Demirbas A: "Biomass resources for energy and chemical industry". Energy Edu Sci Technol 2000, pp. 21-45
[5] Demirbas A: "Combustion characteristics of different biomass fuels", Progress in Energy and Combustion Science, Vol. 30, No. 2, (2004), pp. 219-230
[6] R. Sims, et al., IEA Report (2008)
[7] Drake, J.B.; Knox, R.G.; Dubayah, R.O.; Clark, D.B.; Condit, R.; Blair, J.B.; Hofton, M. Above-ground biomass estimation in closed canopy neotropical forests using lidar remote sensing: Factors. Glob. Ecol. Biogeogr. 2003, 12, 147–159.
[8] Means, J.E.; Acker, S.A.; Fitt, B.J.; Renslow, M.; Emerson, L.; Hendrix, C.J. Predicting forest stand characteristics with airborne scanning lidar. Photogramm. Eng. Remote Sens. 2000, 66, 1367–1371
[9] Naesset, E. Predicting forest stand characteristics with airborne scanning laser using a practical two-stage procedure and field data. Remote Sens. Environ. 2002, 80, 88–99.
[10] Lillesand, M.T. and Kiefer, R. W. Remote Sensing and Image Interpretation, John Wiley and Sons, Newyork, 1994, 1-48.
[11] Neuenschwander, A.L., L A Magruder, Marcus Tyler, Landcover classification of small-footprint, full-waveform Lidar data. J. Appl. Remote Sens. 2009, 3(1), 033544
[12] Hill, T.C.; Williams, M.; Bloom, A.A.; Mitchard, E.T.A.; Ryan, C.M. Are inventory based and remotely sensed above-ground biomass estimates consistent? PLoS One 2013, 8, e74170
[13] Stilla, U.; Jutzi, B. Waveform analysis for small-footprint pulsed laser systems. In Topographic Laser Ranging and Scanning: Principles and Processing; Shan, J., Toth, C.K., Eds.; CRC Press: Boca Raton, FL, USA, 2009; pp. 215–234.
[14] Wagner, W.; Ullrich, A.; Ducic, V.; Melzer, T.; Studnicka, N. Gaussian decomposition and calibration of a novel small-footprint full-waveform digitising airborne laser scanner. ISPRS J. Photogramm. Remote Sens. 2006, 60, 100–112.
[15] Pirotti, F.; Guarnieri, A.; Vettore, A. Vegetation filtering of waveform terrestrial laser scanner data for DTM production. Appl. Geomat. 2013, 5, 311–322.
[16] Burrough P. A., and McDonnel R. A., (1998), "Principles of Geographical Information Systems," Oxford University Press, pp. 1-135.
[17] Charles E. Noon, et. al "GIS-based Biomass Resource Assessment with Bravo" (1996), Biomass and Bio-energy, Volume 10, Nos. 2-3, pp 101-109
[18] Ranney JW, et. al "Regional evaluation of woody biomass production for fuels in the southeast", Biotechnology and bioengineering symposium no. 10, New York: Wiley; 1980. pp 10-20
[19] Phillips V. D., et. al "Biomass systems model estimates of short-rotation hard wood production in Hawaii", Biomass and Bio-energy (1993); 5:421–9.
[20] Liu W., et. al "Estimating short-rotation Eucalyptus saligna production in Hawaii: an integrated yields and economic model" Bio-resource Technology 1993; 45:167–76.
[21] Tyson K. S., et. al "Future potential for MSW energy development" Biomass and Bio-energy, 1996; 10 (2–3): 111–24
[22] Dagnell SAP "Resource mapping and analysis of UK farm livestock manure" Proceedings of the second biomass conference of the Americas: energy, environment, agriculture, and industry, 1995, p.21–4
[23] Cole N., et .al "Resource mapping and analysis of potential sites for short rotation coppice in the UK—assessing the opportunities for biomass to energy technologies", Proceedings of the ninth European bio-energy conference: biomass for energy and environment, Oxford: Pergamon; 1996. p. 1811–6
[24] Graham R. L., "A Geographic Information System-based modeling system for evaluating the cost of delivered energy crop feedstock" Biomass and Bio-energy, 2000; 18: 309–29
[25] Ma J. G., "Siting analysis of farm-based centralized anaerobic digester systems for distributed generation using GIS" Biomass and Bioenergy 2005; 28: 591–600
[26] Marco Beccali, et. al "Assessment of bio-energy potential in Sicily: A GIS-based support methodology", Biomass & Bio-energy, 33 (2009) pp 79-87
[27] Ming-Che Hu, An-Lei Huang and Tzai-Hung Wen, GIS-based biomass resource utilization for rice straw cofiring in the Taiwanese power market, Energy, 55, 2013, pp. 354-360.
[28] Voivontas D., et. al "Assessment of biomass potential for power production: a GIS based method", Biomass & Bio-energy, 20 (2001) pp 101-112

5th International Engineering Symposium - IES 2016
March 2-4, 2016, Kumamoto University, Japan

Experimental Study of Filler Addition Effect on Thermal Conductivity of Rubber Composites

Masaaki Okuyama [1] and Toshio Tomimura [2]

1 *Associate Profesor, Department of Mechanical Systems Engineering, Yamagata University, Jounan, 4-3-16, Yonezawa, Yamagata 992-8510, Japan.*
e-mail: tg017@yz.yamagata-u.ac.jp
2 *Profesor, Department of Mechanical System Engineering, Kumamoto University, Kurokami, 2-39-1, Kumamoto 860-8555, Japan.*
email: tomi@mech.kumamoto-u.ac.jp

ABSTRACT: In this study, to improve the thermal conductivity of ethylene propylene diene rubber (EPDM), measurements of thermal conductivity of EPDM composites have been performed. As a result, it has been shown that the thermal conductivity of EPDM can be improved effectively by adding carbon nanofiber (CNF).

Keywords: *thermal conductivity, rubber, filler*

INTRODUCTION

Recently, in order to improve the thermal, electrical and mechanical properties of the polymeric materials, lots of studies have been conducted on the effects of the filler addition to the materials. Okuyama et al. (2007) measured the thermal and electrical conductivities of ethylene propylene diene rubber (EPDM) added with carbon nanofibers. Tomimura (2007) measured the thermal conductivity of the silicone grease added with carbon nanofiber (CNF), and further obtained an empirical equation between them. Wang et al. (2009) investigated the relation between the filler dispersion and the thermal conductivity of the epoxy resin added with CNF. As a result, shortened nanotubes were found to be easily dispersed into the resin, and consequently leading to an obvious improvement in its thermal conductivity. Sckilde et al. (2015) studied the carbon nanotube-epoxy composites, and showed that the thermal, electrical and mechanical properties increase with increasing CNT content. Kueseng et al. (2013) filled natural rubber and nitrile rubber blend with alignment carbon nanutubes. As a result, when the carbon naotube content was more than 4 phr, the increase in carbon nanotube agglomerates were observed.
In this study, to improve the thermal conductivity of EPDM, measurements of thermal conductivity of EPDM reinforced by filler have been performed.

EXPERIMENT

Measurement Principle of Thermal Conductivity

Fig. 1 shows a schematic view of the thermal conductivity measurement system.

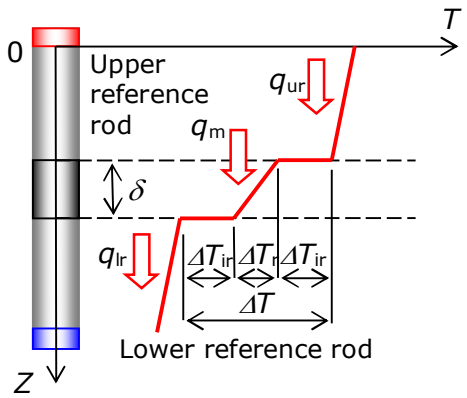

Fig. 1 Temperature distribution in reference rods and rubber

In this study, the conventional plate comparative method has been used to measure the thermal conductivity. As shown in the figure, the top surface of the upper reference rod is uniformly heated. On the other hand, the bottom surface of the lower reference rod is kept at a low temperature. And between them, a rubber with the thickness δ is placed. In order to form the one-dimensional temperature distribution as shown in the figure, the surroundings of the rods and the rubber are insulated. This temperature drop occurring between the upper and lower rods is composed of the following two factors; the first one is the temperature drop which is caused by the thermal contact resistance at the interface between the rod and the rubber. And the second one is the temperature drop which is attributed to the thermal resistance of rubber itself. In the present study, the temperature drop due to the thermal contact resistance is assumed negligible by introducing thin silicone grease layer at the contact interface. If the mean heat flux flowing through the rubber q_m is given by the arithmetic mean of the heat fluxes in the upper and lower reference rods q_{ur} and q_{lr}, then thermal conductivity of the rubber can be evaluated by the following equation.

$$\lambda_T = \frac{q_m}{(\Delta T / \delta)} \qquad (1)$$

Measurement Apparatus

Figure 2 shows a schematic of measuring apparatus. A copper cooling block is placed at the bottom surface of the lower brass reference rod. On the other hand, the upper brass reference rod is uniformly heated by the film heater of 40mm in diameter through a copper connecting truncated cone. And the rubber sheet is placed between the upper and lower reference rods.

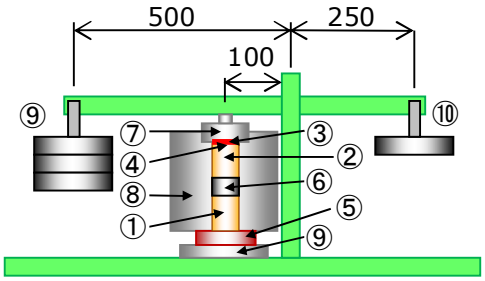

①Lower reference rod ②Upper reference rod ③Film heater ④Copper plate ⑤Cooling block ⑥Rubber ⑦Acrylic resin block ⑧Thermal insulation ⑨Weight ⑩Balancing weight

Fig. 2 Schematic of measuring apparatus

The test column (the upper and lower reference rods, and the rubber sheet) is covered with a styrene form wall of 65mm of thick, and on the film heater, an acrylic resin block of 20mm thick is placed for thermal insulation. The axial load F to the test column is applied by introducing a lever and hanging weight arrangement.

The reference rod is made of brass, and its diameter ($2r_0$) and length are 30mm and 45mm, respectively. In each reference rod, there are four holes of 0.55mm in diameter and 5mm in depth to measure its axial temperature distribution. The holes are located at 15, 22, 29 and 36mm from the contact surface with the rubber, and in there, the Type-T (copper-constantan) sheathed thermocouples of 0.5mm in diameter are inserted by applying a thermally conductive silver paste.

Concerning the surface properties of the contact surface of the upper and lower reference rod, the centreline average surface roughness measured with a stylus profile-meter was about 0.3 μm, though some weak waviness was observed. Here, the thermal conductivity of each reference rod, which is required to evaluate the heat flux flowing through each reference rod, was 113 W/(m· K) as the mean value of three measurements using the same rod of 90mm in length. In this study, the heat flow rate Q and the mean nominal contact pressure p_m ($=F/r_0^2$) applied to the test column were kept at 3.38-3.42 W and 0.0738 MPa, respectively.

Test Specimen

Table 1 lists the test specimens used in the present measurements. Five kinds of specimens in total (A) EPDM, (B) EPDM added with 5.6 wt.% CNF (C) EPDM added with 14.1 wt.% CNF, (D) EPDM added with 5.6 wt.% ZnO_2, (E) EPDM added with 14.1 wt.% ZnO_2 were examined. Here, "phr" means that "parts by weight per 100 parts by weight of rubber". In the table, the

thickness δ of the specimen was measured by the micro-meter.

Temperature measurement

Figure 3 shows the axial temperature distribution in the upper and lower reference rods at the time of thermal conductivity measurement of EPDM. In the figure, the vertical grey zone represents the rubber used in this measurement. Here, the temperature and the power supplied to the film heater were measured after the steady state conditions were attained.

RESULTS AND DISCUSSION

Figure 4 shows the SEM images of EPDM with carbon nanofibers. The contents of CNF are 5.6 wt.% in Fig. 4(a), and 14.1 wt.% in Fig. 4(b), respectively. The carbon nanofibers added in the rubber are aligned perpendicular to the heat flow direction. From these figures, it can be seen that CNF is uniformly dispersed in the rubber.

Figure 5 shows the relation between $\Delta T/q_m$ and the thickness δ of the rubber for each test specimen. In those figures, the closed circle is the measured data, and the solid line is the linear approximation line obtained from the data. From those figures, it can be seen that the deviation of the data from the linear approximation line is small in the case of (C) EPDM with CNT 14.1 wt.% and (D) EPDM with ZnO_2 5.6 wt.%. This would mean that relatively accurate measurements have been performed. On the other hand, in the case of (B) EPDM with 5.6 wt.% and (E) EPDM with ZnO_2 14.1 wt.%, fairly large deviation is observed. At this stage, the cause of the deviation has not been clarified yet, and that is our future issues.

Table 1 Test specimens

No.	Filler	Contents [phr]	Contents [wt.%]	δ [mm]
(A)	None	—	—	3*1)
(B)	CNF	20	5.6	1.026
				2.271
				2.964
(C)		50	14.1	0.95
				2.14
				3.11
(D)	ZnO_2	20	5.6	0.902
				2.248
				2.991
(E)		50	14.1	1.246
				2.145
				3.001

*1) : Nominal

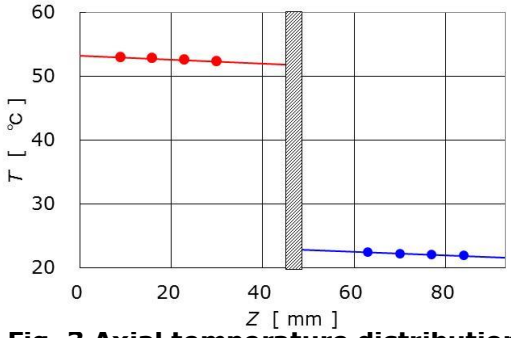

Fig. 3 Axial temperature distribution in reference rod [No. (A) EPDM]

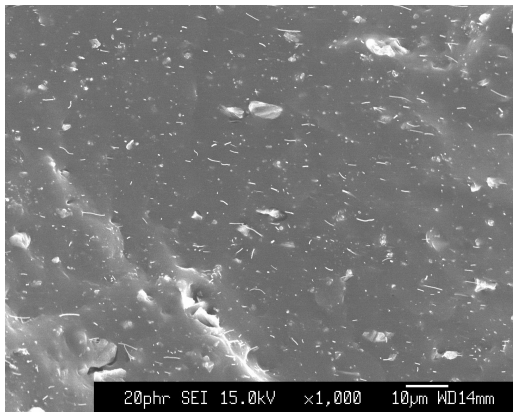

(a) No. (B) CNF 20 phr

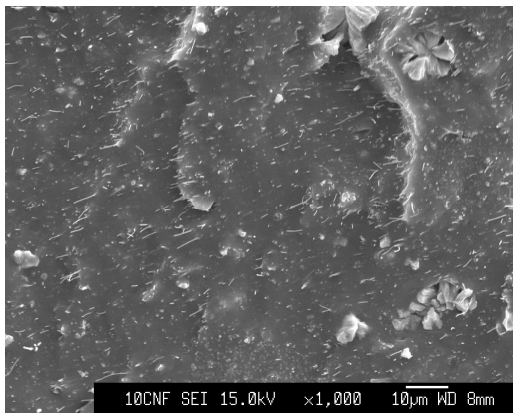

(b) No. (C) CNF 50 phr

Fig. 4 SEM images of rubber added with CNF

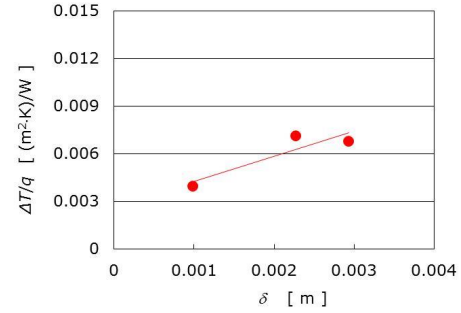

(a) No. (B) CNF 5.6 wt.%

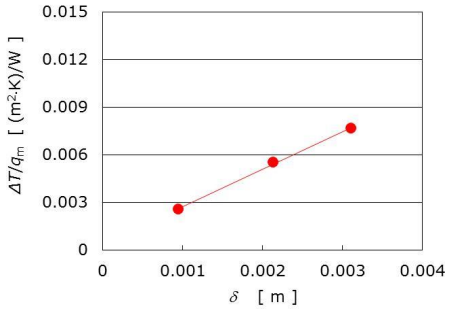

(b) No. (C) CNF 14.1 wt.%

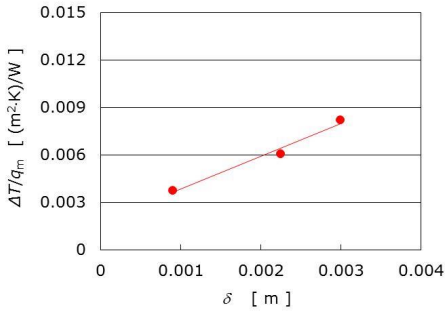

(c) No. (D) ZnO_2 5.6 wt.%

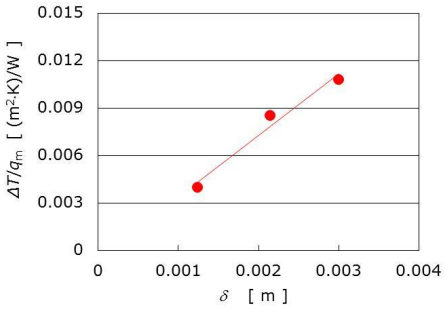

(d) No. (E) ZnO_2 14.1 wt.%

Fig. 5 Relation between $\Delta T/q_m$ and δ of rubbers

Table 2 Thermal conductivity of rubber composites

No.	Rubber composite	Thermal conductivity [W/(m²·K)]
(A)	Raw EPDM	0.35
(B)	EPDM+CNF 5.6 wt.%	0.64
(C)	EPDM+CNF 14.1 wt.%	0.42
(D)	EPDM+ZnO_2 5.6 wt.%	0.48
(E)	EPDM+ZnO_2 14.1 wt.%	0.30

The results on the thermal conductivity of each rubber composite evaluated based on Fig. 5 are listed in Table 2. From the table, it is clear that the CNF addition to EPDM is an effective way to improve its thermal conductivity.

CONCLUSIONS

The effect of filler addition on the thermal conductivity of EPDM has been studied experimentally, and the CNF addition has been shown effective to improve its thermal conductivity.

ACKNOWLEDGEMENTS

The authors would like to express our gratitude to Mr. Tomoyuki Kanaya at Miyasaka Rubber Co., Ltd. for providing EPDM and EPDM composites with CNF and ZnO_2.
This work was supported by Research project for utilizing advanced technologies in agriculture, forestry and fisheries, Project No. 18051.

REFERENCES

[1] Kueseng, P. et al. (2013), Anisotropic Studies of Multi-wall Carbon Nanotube (MWCNT)-filled Natural-Rubber (NR) and Nitrile Rubber (NBR) blends, Polyner Testing, Vol. 32, pp. 1229-1236.
[2] Okuyama, M. et al. (2007), Thermal and Electrical Conductivities of Rubber added with Carbon Nanofiber, Proc. of the Asian Thermophysical Properties Conf., Augst, NO.35.
[3] Shcilde, C. et al. (2015), Thermal, Mechanical and Electrical Properties of Highly Loaded CNT-epoxy Composites – A Model for the Electric Conductivity, Composites Science and Technology, Vol.107, pp.183-190.
[4] Tomimura, T. et al. (2007), Simple Measuring Method of Thermal Conductivity of Silicone Grease and Effect of Carbon Nanomateroals on Its Thermal conductivity, July, HT2007-32649.
[5] Wang, S. et al. (2009), Dispersion and Thermal Conductivity of Carbon Nanotube Composites, Carbon, Vol. 47 pp. 53-57.

ELECTRICAL, ELECTRONICS, COMPUTER ENGINEERING & RELATED FIELDS

5th International Engineering Symposium - IES 2016
March 2-4, 2016, Kumamoto University, Japan

Common mental disorders among People living with Human Immune-Virus/Acquired Immune Deficiency Syndrome (PLHA) in Dakshina Kannada District, Karnataka: A cross sectional study

Padmamohanan[1], Gururaj N.A.[2], Soumya Shetty[3]

[1]Associate Professor (Medical Sociology), [2]Assistant professor, [3] Biostatistician
Department of Community Medicine, Yenepoya Medical College, Yenepoya University, Mangalore - 575018, Karnataka. India
Corresponding Author: Dr. Padmamohanan, Email: padmamohanan@hotmail.com

ABSTRACT: Background: The relationship between HIV/AIDS and common mental disorders (CMD) has been scarcely investigated. This study set out to investigate the occurrence of CMD in People Living with HIV/AIDS in an ART centre in Mangalore.
Methods: Cross sectional analytical study was conducted among selected 225 subjects in the District ART centre of Mangalore. CMD was assessed through face to face interviews by trained clinical nurses using the Kessler 10 and General Health Questionnaire 12.
Results: 8.8% of the respondents were having severe psychological problems and 15.4% had severe mental disorder. The factors significantly associated with CMD included female sex, nuclear family type, marital status, religion, employment and CD4 cell count of 200 to 499 & above (cells/µL).Conclusion: CMD in this study was associated with socio-demographic factors and CD4 counts. The association of CMD and high risk sexual behaviour calls for the integration of HIV prevention in mental health care programs in high HIV prevalence settings.

***Keywords**: common mental disorders, People living with HIV/AIDS, Dakshina Kannada*

INTRODUCTION

The HIV/AIDS epidemic remains among the most significant challenges to public healthcare systems worldwide (Catalan, Collins, Mash, & Freeman, 2005). The negative impact of HIV infection includes co-morbidities in individuals, such as substance abuse, depression, and posttraumatic stress disorder (PTSD; Boarts JM. et al. 2006) and it profoundly impacts families and communities. Social stigma, marginalization, and discrimination of PLHA lead to further risk and vulnerability that results in poorer physical and mental health (Jenkins & Sarkar, 2007). Co-morbidity among PLHA has been linked to treatment outcomes and problems with medication compliance underscoring the importance of addressing psychological symptoms (Chander G. et al. 2006) There has been a paucity of research investigating mental health among PLHA in India. While psychiatric co-morbidity is known to have a strong association with HIV/AIDS (Chandra PS. et al. 2003; Treisman & Angelino, 2007), thus a research study is necessary to further understand the impact of mental disorders among PLHA. The study therefore aims to investigate the occurrence of CMD in People Living with HIV/AIDS in an ART centre in Mangalore.

METHODOLOGY

Study design, Setting and period

Institution based cross sectional study design was used. The study took place from June to September of 2013 at ART centre Mangalore Dakshina Kannada Karnataka. The sample required for this study was determined using the formula:

$$n = z^2_{\alpha} pq / \varepsilon^2 \quad (1)$$

Participants who were 18 years and above, tested HIV positive, currently receiving antiretroviral treatment and able to give interview selected by convenient sampling method. Data collection was done after informed consent was obtained. CMD was assessed through face to face interviews by trained clinical nurses using the pre-tested Kessler 10 and General Health Questionnaire 12. The number of respondents from ART centre is shown in Fig. 1.

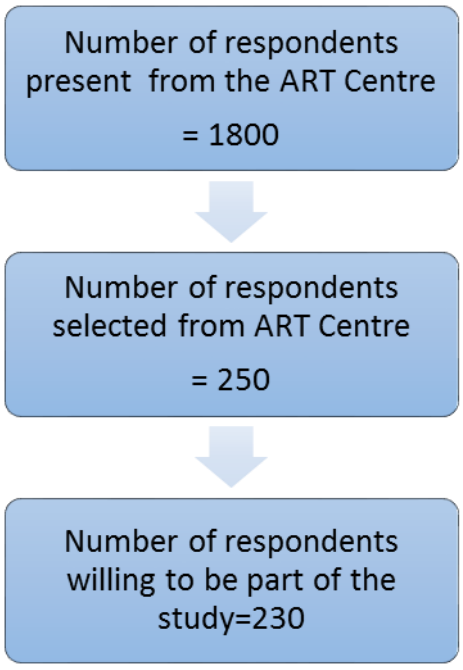

Fig. 1 Number of respondents from ART centre

Kessler 10 scale

The Kessler 10 scale is a psychological screening tool. It is widely recommended as a simple measure of psychological distress and as a means to monitor progress following treatment for common mental health disorders. Levels of disorder are mild, moderate and severe. The Kessler 10 scale consists of 10 five point Likert scale. (0=never, 1=rarely, 2=some of the time, 3=most of the time and 4=all of the time, Kessler RC. et al. (2002).

General Health Questionnaire12

The twelve question version of the General Health Questionnaire (GHQ 12) was used to measure psychological problems in this study. This is a standardized self-administered scale providing information about recent mental status designed by Goldberg (1972). The questionnaire comprises twelve questions about the general level of happiness, experience of depressive and anxiety symptoms and sleep disturbance over the last four weeks. The symptoms based on a four point response scale score. Not at all =0, same as usual=1, more than usual=2 and much more than usual =3. Goldberg D. et al. (1988). A pilot study was carried out among 25 HIV positive participants who were aged 18 years and above on ART treatment. Internal reliability The Cranach's alpha for this sample for GHQ-12 and Kessler 10 psychological distress scale was found to be 0.671 & 0.664 respectively.

Data analysis and Interpretation

The coded data was checked, cleaned and analyzed using SPSS version 19. Descriptive statistics were calculated for each variable. Mean and standard deviation were determined for all continuous variables including scores GHQ and Kessler scale. Proportions were determined for all categorical variables. P-value of less than 0.05 was considered statistically significant.

Ethical considerations

The University ethical committee approval was obtained. The written consent form was used to receive the willingness of the participants. Confidentiality was assured throughout the study.

RESULTS

230 subjects were identified for the study of this there were 225 positive responses received from the subjects with the response rate of 97.8%. The age of the respondents ranged from 18-67 years. The mean age of the participants was 41 years. From participants 56.8 were males and 43.1 were females. Majority 93.3% of the

respondents were from Hindu religion. One hundred and eighty two (80.8%) of the participants followed nuclear family type. Majority (56%) was primary educated and 61.3% were employed and had a source of income (Table 1). The mean score of GHQ 12 for stress level was 15% and the mean score of K10 for psychological distress was 24%.The distribution of respondents with respect to psychological distress status measured with the help of GHQ12 and mildly distressed to severe psychological problems to be 155 (69%).and Kessler10 scale showed mild mental disorder to severe mental disorder to be 179(80%) (Table 2). Factors associated with CMD were found to be gender, marital status, family type, religion, and most recent CD4 count (Kessler10) whereas the association of GHQ12 and other factors like gender, family type, employment and CD4 cell count were very significant. (Table 3). The results of univariate logistic regression and binary logistic regression the study indicates that female PLHA were more stressed 2.3 times more than males (P<0.01 OR=2.33, CI: 1.25-4.34).The odds of becoming stressed is 2.33times more among the PLHA living in nuclear or extended nuclear families than PLHA living in joint families.(P=0.03,OR=2.33, CI:1.067-5.1). The PLHA whose CD4 count>200(cells/μL) had 2.47 times more stress than PLHA who had a CD4 count<200(cells/μL). (P=0.01, OR=2.47, CI: 1.21-4.97).

Majority (84.8%) of the study participants were on WHO stage 1 category of HIV/AIDS clinical staging. 57.3% of them were having CD4 cell count between 200 to 499(cells/μL). One hundred and ninety one (84.1%) had >95% level of adherence to the ART treatment.

DISCUSSION

The proportion of psychiatric disorders showed an increase in the age group of 29-48 years (76.2%). and also among the married individuals the proportion of psychiatric disorders was significantly higher (64.4%) as compared to their unmarried, widowed and divorced counterparts (35.6%). This was in conformity to the findings by Ajay KT. (1999), who reported a high proportion of psychiatric morbidities among married individuals. The socio-demographic factors like gender, marital status, family type, religion occupation and most recent CD4 count of the PLHAs were found to be associated with psychological problems measured by K10. Whereas the psychological distress measured by GHQ 12 was associated with gender, family type,employment and most recent CD4 count. These were proved to be statistically significant. The results of univariate logistic regression and binary logistic regression the study indicates that female PLHAs were stressed 2.3 times more than male PLHAs. This was in conformity with a study by Patel V. (2007) for a complex variety of reasons; women are more vulnerable than men to HIV infection. Moreover women usually suffer from more depression than men. This makes a focus on the mental health of women particularly important. In a comparative study by Barua A. et al. (2007) in Karkala taluk of Udupi district, where psychiatric morbidity among the general population was found to be 63.8% and CMD among PLHAs in that study was very high. A study by John AJ. et al. (2008) also reported that major depression occurring among PLHAs was twice more as compared to general population.

CONCLUSION

In this study, the proportion of mental illnesses in adult population was determined to be high. The results of univariate logistic regression and binary logistic regression the study indicates that female PLHA were more stressed than male PLHAs. A statistical significant difference for psychiatric disorders was observed among the groups of socio-demographic correlates like nuclear family or extended nuclear family, the PLHA who had CD4 count > 200 cells have more stress than PLHA who had a CD4 count<200(cells/μL). Here the ART counselors should be sufficiently trained for periodically screening the PLHAs for CMD. There is an urgent need to provide early psychological intervention to PLHAs at the point of contact. These interventions can be done for targeted groups.

REFERENCES

[1] Ajay, KT, (2000), Psychiatric morbidity in a rural low socio-economic status population-An epidemiological field survey Kasturba Medical College MAHE.
[2] Barua, A et al., (2007), study on screening for psychiatric disorders in adult population. Indian j. community med., Vol.32, pp. 65-66.
[3] Boarts, JM et al., (2006), The differential impact of PTSD and depression on HIV disease markers and adherence to HAART in people living with HIV, AIDS and Behavior, Vol. 10, No. 3, pp. 253–261.
[4] Catalan, et al., (2005), Mental health and HIV/AIDS: Psychotherapeutic intervention in anti-retroviral (ARV), Therapy (for second level care). Mental Health and HIV/AIDS series. Geneva: WHO.
[5] Chander, G et al., (2006), Substance abuse and psychiatric disorders in HIV positive patients, Drugs, Vol. 66, No. 6, pp. 769-789.
[6] Chandra, PS et al. (2003), HIV risk behavior among psychiatric inpatients: Results from a hospital wide screening study in southern India, International Journal of STD and AIDS, Vol.14, pp.532-538.
[7] Goldberg, D et al., (1988), A users guide to the General Health Questionnaire, Available from; http://www.hwph.net/life_style_survey/_user_files/ mental/things/GHQ 12.
[8] Jenkins and Sarkar, (2007), Interventions for HIV prevention and support for vulnerable populations: focus on Asia and the Pacific, Bangkok.
[9] John, AJ et al., (2008), HIV/AIDS and psychiatry: Towards the establishment of a pilot program for detection and treatment of common mental disorders in people living with HIV/ AIDS in Cape Town, S. Afr. J. Psychiatr., Vol. 14, pp.122-4.
[10] Kessler, A C, et al., (2002), Short Screening Scales to monitor population prevalence and trends in non-specific psychological distress, Psychol. Med. Vol. 32, pp.959-74.
[11] Lazarus, R. and Freeman, M, (2009), Primary-Level Mental Health Care For Common Mental Disorder In Resource-Poor Settings: Models & Practice - A Literature Review. Sexual Violence Research Initiative, Medical Research Council, Pretoria, South Africa.
[12] Patel, V, (2007), Mental health in low and middle income countries. Br. Med. Bull., Vol. 81-82, No.1, pp. 81-96.
[13] Treisman, G, and Angelino, A, (2007), Interrelation between psychiatric disorders and the prevention and treatment of HIV infection. Psychiatric disorders and HIV infection, Clinical infectious diseases, Vol.45, No. 4.

Table 1 Distribution of study participants according to socio-demographic variables

Variables	Study Participants (n=225) Frequency (percentage)
Age (Yrs)	
18-28	11(4.9)
29-38	86(37.9)
39-48	87(38.3)
49-58	33(14.5)
>59 and above	8(3.5)
Gender	
Male	128(56.8)
Female	97(43.1)
Marital Status	
Single	31(13.7)
Married	145(64.4)
Divorced/Separated	7(3.1)
Widow /Widower	42(18.7)
Family Type	
Joint Family	33(14.7)
Nuclear/Extended Nuclear	192(85.3)
Religion	
Hindu	210(93.3)
Muslim	5(2.2)
Christian	10(4.4)
Education	
Illiterate	54(24)
Primary	126(56)
Secondary	37(16.4)
College/Above	10(4.4)
Occupation	
Professionals	7(3.1)
Skilled	23(10.2)
Unskilled	109(48.4)
Housewife	29(12.8)
Unemployed	57(25.1)
Employed/Source of Income	
Yes	138(61.3)
No	87(38.7)

Table 2 Distribution of participants according to psychological variables

Variables	Study Participants (n=225) Frequency (percentage)
Stress Level (GHQ 12 Scale)	
Normal	70(31.1)
Mildly Distressed	58(25.8)
Evidence of distress	77(34.2)
Severe psychological problems	20(8.9)
Psychological status (K-10 scale)	
Likely to be well	46(20.4)
Mild mental disorder	79(35.1)
Moderate mental disorder	65(28.9)
Severe mental disorder	35(15.6)

Table 3 Univariate and Multivariate (binomial logistic regression analysis) (Kessler 10 Psychological distress scale)

Variables	**Normal No %**	**mild No %**	**Moderate No %**	**Severe No %**	**p-value**
GENDER					
Male	32(25)	43(33.3)	30(23.3)	23(17.8)	
Female	15(15.3)	35(36.1)	35(35.7)	12(12.2)	0.068
Marital status					
Single	5 (16.1)	6 (19.4)	8 (25.8)		
Married	12 (38.7)	5 (16.1)	39 (26.9)	16 (11)	
divorced/separated	0 (0%)	2 (33.3%)	2 (33.3%)	3 (42.9)	0.011
widow/ widower	5 (13.1)	11 (28.9)	18 (42.9)	8 (19.0)	
FAMILY TYPE					
Joint family	7(21.2)	11(33.3)	8(24.2)	7(21.2)	
Nuclear Family/ Extended	39(20.3)	68(35.4)	57(31.3)	28(14.6)	0.038
Religion					
Hindu	40(19)	75(35.7)	63(30)	32(15.2)	
Muslim	3(60)	1(20)	0(0)	1(20)	0.001
Christian	5(50)	3(30)	1(10)	1(10s)	
Most recent CD4 (cells/µL).					
Less than 200	11(23.9)	18(39.13)	7(15.21)	10(21.7)	
200-499	30(23.7)	44(33.84)	37(28.4)	19(14.6)	
More than or equal to 500	7(14)	17(34)	20(40)	6(14.6)	0.013
General Health Questionnaire 12 Levels Of stress					
Gender					
Male	49 (70)	32 (55.2)	36 (46.8)	10 (50)	
Female	21 (30)	26 (44.8)	41 (53.2)	10 (50)	0.0251
Family type					
Joint family	16 (22.2)	0 (0)	15 (19.5)	2 (10)	0.05
Nuclear/extended nuclear family	54 (77.1)	58 (82.9)	62 (88.6)	18 (90)	

Table 3 continued.... Levels of psychological Distress (GHQ 12)

Variables	Normal No %	mild No %	Moderate No %	Severe No %	p-value
Employed/source of Income					
Yes	47(34)	43(31.2)	41(29.7)	7(5)	
No	25(28.7)	15(17.2)	36(41.8)	11(12.6)	0.031
Most recent CD4 cell (cells/μL)					
<200	23(31.9)	8(13.8)	12(15.5)	4(20)	
200-499	36(50)	36(62.1)	47(61)	11(55)	0.01
>500	11(15.7)	14(24.1)	18(23.4)	5(25)	

5th International Engineering Symposium - IES 2016
March 2-4, 2016, Kumamoto University, Japan

Iterative-Method for Nonlinear Ill-posed Operator Equations

Santhosh George

Profesor, Department of Mathematical and Computational Sciences, National Institute of Technology Karnataka, India-575 025, email : sgeorge@nitk.ac.in

ABSTRACT: We report on an iterative method which does not involve inversion of the operators for obtaining an approximate solution for the nonlinear ill-posed operator equation F(x) = y: The convergence analysis of the method is based on a suitably constructed majorizing sequence and the regularization parameter is chosen according to the balancing principle considered by Pereverzev and Schock (2005). The error estimate is derived under a general source condition and is of optimal order.

Keywords*: Iterative methods, ill-posed problem, majorizing sequence, balancing Principle.*

INTRODUCTION

This paper is devoted to the study of nonlinear ill-posed problem where

$$F(x) = y, \qquad (1)$$

where $F : D(F) \subseteq X \to Y$ is a nonlinear operator between the Hilbert spaces X and Y. We assume that F is a Fréchet-differentiable nonlinear operator acting between infinite dimensional Hilbert spaces X and Y. with corresponding inner products $\langle .,. \rangle$ and norms $\| . \|$ respectively. Further it is assumed that (1) has a solution $\hat{x}$, for exact data, i.e., $F(\hat{x}) = y$, but due to the nonlinearity of F this solution need not be unique. Further, it is assumed that $y^\delta \in Y$ is the available noisy data, for which we have the additional information that $\| y - y^\delta \| \le \delta$. It is known Tautenhahn and Jin(2003), that the unique solution x_α^δ of $F'(x)^*(F(x) - y^\delta) + \alpha(x - x_0) = 0$ is a good approximation to a solution $\hat{x}$ with minimal distance from x_0.

Ramlau (2003) considered the TIGRA method defined iteratively by,

$$x_{k+1}^\delta = x_k^\delta + \beta_k [F'(x_k^\delta)^*(y^\delta - F(x_k^\delta)) + \alpha_k (x_k^\delta - x_0)] \qquad (2)$$

where $x_0^\delta = x_0, \beta_k$ is a scaling parameter and α_k is a regularization parameter, which will change during the iteration and obtained a convergence rate estimate for the TIGRA algorithm under the following assumptions:

1. F is twice Fréchet differentiable with a continuous second derivative;
2. the first derivative is Lipschitz continuous:
   $\| F'(x_1) - F'(x_2) \| \le L \| x_1 - x_2 \|$,
3. there exists $w \in Y$ with $x_0 - \hat{x} = F'(\hat{x})w$, and
4. $\| w \| \le \rho$ and $L\rho \le 0.241$.

In this paper we consider a modified form of iteration (2). Precisely we consider the sequence $(x_{n,\alpha}^\delta)$ defined iteratively by

$$x_{n+1,\alpha}^\delta = x_{n,\alpha}^\delta - \gamma[c^2 F'(x_{n,\alpha}^\delta)^*(F(x_{n,\alpha}^\delta) - y^\delta) + \alpha(x_{n,\alpha}^\delta - x_0)], \qquad (3)$$

$x_{0,\alpha}^\delta := x_0$ where γ and c are scaling parameters and α is the regularization parameter. We prove that $x_{n,\alpha}^\delta$ converges to the unique solution $x_{c\alpha}^\delta$ of the equation

$$F'(x)^*(F(x) - y^\delta) + \frac{\alpha}{c^2}(x - x_0) = 0 \qquad (4)$$

and that $x_{c\alpha}^{\delta}$ is a good approximation for $\hat{x}$.

The organization of this paper is as follows. In section 2 we provide some preparatory results and section 3 deals with the convergence analysis of the proposed method. Error bounds under an a priori and under the balancing principle are given in section 4. Section 5 deals with the implementation of the method. Finally the paper ends with conclusion in section 6.

PREPARATORY RESULTS

Throughout this paper we assume that the operator F satisfies the following assumptions.

Assumption 1: There exists $r>0$ such that $B_r(x_0)\cup B_r(\hat{x})\subseteq D(F)$ and F is Fréchet differentiable at all $x\in B_r(x_0)\cup B_r(\hat{x})$.

Assumption 2:

(a) There exists a constant $k_0 > 0$ such that for every $x,u\in B_r(x_0)\cup B_r(\hat{x})$ and $v\in X$, there exists an element $\Phi(x,u,v)\in X$ satisfying
$[F'(x)-F'(u)]v = F'(u)\Phi(x,u,v)$, $\|\Phi(x,u,v)\|\le k_0\|v\|\,\|x-u\|$
for all $x,u\in B_r(x_0)\cup B_r(\hat{x})$ and $v\in X$.

(b) There exists a constant $k_1>0$, and for each $u,v\in B_r(x_0)\cup B_r(\hat{x})$ there exists a linear operator $R(u,v):Y\to X$ such that $F'(v)=F'(u)R(u,v)$, $\|R(u,v)\|\le k_1$.

(c) There exists a constant $k_2>0$ such that for every $(x,z,y)\in B_r(\hat{x})\times B_r(\hat{x})\times Y$, there exists $l(x,z,y)\in Y$ such that
$$(F'(x)^*-F'(z)^*)y = F'(z)^*l(x,z,y), \quad (5)$$
where $\|l(x,z,y)\|\le k_2\|x-z\|\,\|y\|$.

(d) $\|F'(x)\|\le\beta$ for all $x\in B_r(x_0)$

Note that Example 2.3 in Scherzer et al.(1997) is an example that satisfies the above Assumption, further observe that the condition (5) is less restrictive than the conditions (12)-(13) in Scherzer et al.(1993). The next assumption on source condition is based on a source function φ and a property of the source function φ. We will be using this assumption to obtain an error estimate for $\|\hat{x}-x_{\alpha}^{\delta}\|$.

Assumption 3: There exists a continuous, strictly monotonically increasing function $\varphi:(0,a]\to(0,\infty)$ with $a\ge\|F'(\hat{x})\|^2$ satisfying;

1. $\lim_{\lambda\to 0}\varphi(\lambda)=0$
2. $\sup_{\lambda\ge 0}\frac{\alpha\varphi(\lambda)}{\lambda+\alpha}\le c_{\varphi}\varphi(\alpha)$, $\forall\lambda\in(0,a]$.
3. there exists $v\in X$ such that $x_0-\hat{x}=\varphi(F'(\hat{x})^*F'(\hat{x}))v$

Remark 1:
The above assumption on source function φ, includes the logarithmic source condition considered in Kaltenbacher (2008).

Definition 1:
Let $q\in(0,1)$ and $\alpha>0$ be given parameters. We define parameters:
$$c<\min\{\sqrt{\frac{\alpha}{\beta^2}},1\},$$
$$0<\eta<\frac{(\sqrt{\alpha}-c\beta)^2}{c^2k_2}$$
and
$\gamma\in(\gamma_1,\gamma_2)$ where
$$\gamma_1 := (1-q)\frac{\alpha-c^2\beta^2-c^2k_2\eta-\sqrt{(\alpha-c^2\beta^2-c^2k_2\eta)^2-4k_2c^4\beta^2\eta}}{2k_2c^4\beta^2\eta}$$
and
$$\gamma_2 := \min\{\frac{1}{\alpha},(1-q)\frac{\alpha-c^2\beta^2-c^2k_2\eta+\sqrt{(\alpha-c^2\beta^2-c^2k_2\eta)^2-4k_2c^4\beta^2\eta}}{2k_2c^4\beta^2\eta}\}.$$

Remark 2:
Note that $\frac{(\sqrt{\alpha}-c\beta)^2}{c^2k_2}\le\frac{\alpha-c^2\beta^2}{c^2k_2}$ and hence $\gamma_1>0$. Further observe that the choice of our scaling parameter γ is less restrictive than the choice of scaling parameter β_k in Ranlau(2003) (see Lemma 4.4 in Ranlau(2003)).

The proof of the following Theorem is analogous to the proof of corresponding Theorems in Tautenhan and Jin(2003).

Theorem 1: (cf. Tautenhan and Jin(2003), Theorem 2.7) Let $x_{c\alpha}^{\delta}$ be the solution of the regularized problem (4) and $x_{c\alpha}$ be a solution (4) with y^{δ} replaced by the exact data y. Assume Assumption 2 with radius

$r = \frac{c\delta}{\sqrt{\alpha}} + 2\| x_0 - \hat{x}\|$. *If* $k_0\| x_0 - \hat{x}\| < 1$, then

$$\| x_{c\alpha}^{\delta} - x_{c\alpha}\| \le \frac{c\delta}{\sqrt{\alpha}\sqrt{1-k_0\| x_0-\hat{x}\|}}. \quad (6)$$

Theorem 2: (cf. Tautenhan and Jin(2003), Theorem 2.8) Let $x_{c\alpha}$ be a solution (4) with y^{δ} replaced by the exact data y. Assume Assumption 2 and Assumption 3 with radius

$$r \le \min\{\frac{c\delta}{\sqrt{\alpha}} + 2\| x_0 - \hat{x}\|, \frac{1-(1-c^2)k_1}{k_0/2 + ck_2}\},$$

then

$$\| x_{c\alpha} - \hat{x}\| \le \frac{c_{\varphi}\varphi(\alpha)\| v\|}{1-(k_0/2+ck_2)r-(1-c^2)k_1}.$$

CONVERGANCE ANALYSIS

During the convergence analysis we will be using the following Lemma on majorization, which is a reformulation of Lemma 1.3.12 in Argyros(2008).

Lemma 1: (cf Argyros(2008), Lemma 1.3.12) Let (t_n) be a majorizing sequence of (x_n) in X (i.e., $\| x_{n+1} - x_n\| \le t_{n+1} - t_n, \forall n \ge 0$). If $\lim_{n\to\infty} t_n = t^*$, then $x^* = \lim_{n\to\infty} x_n$ exists and $\| x^* - x_n\| \le t^* - t_n, \forall n \ge 0.$

Lemma 2: Let $q, \alpha, \beta, \delta, k_2, \eta,$ and γ be as in the Definition 1. Then the sequence $(t_n), n \ge 0$ defined iteratively by

$$t_0 = 0, t_1 = \gamma c^2 \beta\eta,$$
$$t_{n+1} = t_n + [(1-\gamma\alpha) + \gamma c^2 k_2(\beta t_n + \eta) + \gamma c^2\beta^2](t_n - t_{n-1}) \quad (7)$$

is monotonic increasing, bounded above by $\frac{\gamma c^2\beta\eta}{1-q}$ and converges to $t_* \le \frac{\gamma c^2\beta\eta}{1-q}$ such that $t_* - t_n \le \frac{q^n}{1-q}\gamma c^2\beta\eta.$

Theorem 3:

Let $x_{n,\alpha}^{\delta}$ be as in (3) and t_n as in (7). Then (t_n) is a majorizing sequence of the sequence $(x_{n,\alpha}^{\delta})$, $(x_{n,\alpha}^{\delta}) \in B_{t_*}(x_0)$ converges to $x_{c\alpha}^{\delta} \in \overline{B_{t_*}(x_0)} \subseteq B_r(x_0)$ such that $F'(x_{c\alpha}^{\delta})^*(F(x_{c\alpha}^{\delta}) - y^{\delta}) + \frac{\alpha}{c^2}(x_{c\alpha}^{\delta} - x_0) = 0.$

Further $\| x_{n,\alpha}^{\delta} - x_{\alpha}^{\delta}\| \le \frac{q^n}{1-q}\gamma c^2\beta\eta.$

Proof: Using induction one can prove that (t_n) is a majorizing sequence of the sequence $(x_{n,\alpha}^{\delta})$ and $(x_{n,\alpha}^{\delta}) \in B_r(x_0)$. So by Lemma 1, $(x_{n,\alpha}^{\delta}), n \ge 0$ is a Cauchy sequence and converges to some $x_{c\alpha}^{\delta} \in \overline{B_{t_*}(x_0)} \subseteq B_r(x_0).$ Further $\| x_{c\alpha}^{\delta} - x_n^{\delta}\| \le t_* - t_n \le \frac{q^n}{1-q}\gamma c^2\beta\eta.$ Now by letting $n \to \infty$ in (3) we obtain

$$F'(x_{c\alpha}^{\delta})^*(F(x_{c\alpha}^{\delta}) - y^{\delta}) + \frac{\alpha}{c^2}(x_{c\alpha}^{\delta} - x_0) = 0. \quad (8)$$

This completes the proof.

ERROR BOUNDS UNDER SOURCE CONDITIONS

Combining the estimates in Theorem 1, 2 and 3 we obtain the following.

Theorem 4: Let the assumptions in Theorem 1, 2 and 3 hold and let $x_{n,\alpha}^{\delta}$ be as in (3). Then

$$\| x_{n,\alpha}^{\delta} - \hat{x}\| \le \frac{q^n}{1-q}\gamma c^2\beta\eta + v\frac{c\delta}{\sqrt{\alpha}\sqrt{1-k_0\| x_0-\hat{x}\|}} + \frac{c_{\varphi}\varphi(\alpha)\| v\|}{1-(k_0/2+ck_2)r-(1-c^2)k_1}.$$

Further if $n_\delta := \min\{n : q^n < \frac{\delta}{\sqrt{\alpha}}\}$, then $\| x^\delta_{n_\delta,\alpha} - \hat{x}\| \le \tilde{C}(\frac{\delta}{\sqrt{\alpha}} + \varphi(\alpha))$ where

$$\tilde{C} := \max\{\frac{\gamma c\beta\eta}{1-q} + \frac{c}{\sqrt{1-k_0\|x_0-\hat{x}\|}}, \frac{c_\varphi\|v\|}{\sqrt{1-(k_0/2+ck_2)r-(1-c^2)k_1}}\}.$$

A priori choice of the parameter

Observe that the estimate $\frac{\delta}{\sqrt{\alpha}} + \varphi(\alpha)$ in Theorem 4 is of optimal order for the choice $\alpha := \alpha_\delta$ which satisfies $\frac{\delta}{\sqrt{\alpha}} = \varphi(\alpha)$. Now, using the function $\psi(\lambda) := \lambda\sqrt{\varphi^{-1}(\lambda)}, 0 < \lambda \le a$, we have $\delta = \sqrt{\alpha_\delta}\varphi(\alpha_\delta) = \psi(\varphi(\alpha_\delta))$ so that $\alpha_\delta = \varphi^{-1}[\psi^{-1}(\delta)]$. In view of the above observation, Theorem 4 leads to the following

Theorem 5

Let $\psi(\lambda) = \lambda\sqrt{\varphi^{-1}(\lambda)}, 0 < \lambda \le a$ and assumptions in Theorem 4 hold. For $\delta > 0$, let $\alpha_\delta = \varphi^{-1}[\psi^{-1}(\delta)]$ and let n_δ be as in Theorem 4. Then $\| x^\delta_{n_\delta,\alpha} - \hat{x}\| = O(\psi^{-1}(\delta))$.

Balancing Principle

Note that the a priori choice of the parameter could be achieved only in the ideal situation when the function φ is known. The point is that the best function φ measuring the rate of convergence in Theorem 4 is usually unknown. Therefore in practical applications different parameters $\alpha = \alpha_i$ are often selected from some finite set

$$D := \{\alpha_i : 0 < \alpha_0 < \alpha_1 < \cdots < \alpha_N\},$$

and corresponding elements $x^\delta_{n,\alpha_i}, i = 1,2,\cdots,N$ are studied on line. Let

$$n_i := \min\{i : q^n \le \frac{\delta}{\sqrt{\alpha_i}}\} \quad (9)$$

and let $x^\delta_{\alpha_i} := x^\delta_{n_i,\alpha_i}$. Then from Theorem 4, we have

$$\| x^\delta_{\alpha_i} - \hat{x}\| \le \tilde{C}(\frac{\delta}{\sqrt{\alpha_i}} + \varphi(\alpha_i)), \forall i = 1,2,\cdots N. \quad (10)$$

The main result of this section is the following theorem, proof of which is analogous to the proof of Theorem 4.4 in George(2010).

Theorem 5

Assume that there exists $i \in \{0,1,\cdots,N\}$ such that $\varphi(\alpha_i) \le \frac{\delta}{\sqrt{\alpha_i}}$. Let assumptions of Theorem 4 be satisfied and let

$$l := \max\{i : \varphi(\alpha_i) \le \frac{\delta}{\sqrt{\alpha_i}}\} < N,$$

$$k = \max\{i : \forall j = 1,2,\cdots,i\| x^\delta_{\alpha_i} - x^\delta_{\alpha_j}\| \le 4\tilde{C}\frac{\delta}{\sqrt{\alpha_j}}\}$$

where $\tilde{C}$ is as in Theorem 5. Then $l \le k$ and$\| x^\delta_{\alpha_k} - \hat{x}\| \le 6\tilde{C}\mu\psi^{-1}(\delta)$.

IMPLEMENTATION OF ADAPTIVE CHOISE RULE

In this section we provide an algorithm for implementing the method considered in this paper. For choosing the regularization parameter using the adaptive method we choose $\alpha_0 = \delta$ and $\mu > 1$ in D_N such that $\alpha_N \le 1$. Further we choose $\alpha_i = \mu^1\alpha_0$,

1. $c < \min\{\sqrt{\frac{\alpha_0}{\beta^2}}, 1\}$,
2. $q \in (0,1)$
3. $0 < \eta < \frac{(\sqrt{\alpha_0} - c\beta)^2}{c^2k_2}$
4. $\gamma \in (\gamma_1, \gamma_2)$ where

$$\gamma_1 := (1-q)\frac{\alpha_0 - c^2\beta^2 - c^2k_2\eta - \sqrt{(\alpha_0 - c^2\beta^2 - c^2k_2\eta)^2 - 4k_2c^4\beta^2\eta}}{2k_2c^4\beta^2\eta}$$

and

$$\gamma_2 := \min\{\frac{1}{\alpha_N}, (1-q)\frac{\alpha_N - c^2\beta^2 - c^2k_2\eta + \sqrt{(\alpha_N - c^2\beta^2 - c^2k_2\eta)^2 - 4k_2c^4\beta^2\eta}}{2k_2c^4\beta^2\eta}\}.$$

and

5. $n_i = \min\{i : q^n \le \frac{\delta}{\sqrt{\alpha_i}}\}$

Finally the adaptive algorithm associated with the choice of the parameter specified in Theorem 5 involves the following steps:

Algorithm

1. Set $i \leftarrow 0$.
2. Solve $x_i = x_{n_i,\alpha_i}^{\delta}$ by using the iteration (3).
3. If $\| x_i - x_j \| \geq 4\tilde{C}\sqrt{\frac{\delta}{\mu^j}}, j \leq i,$ then take $k = i-1$.
4. Set $i = i+1$ and return to step 2.

Example

Consider the equation

$$F(u) \equiv -\int\int_{\Omega} \frac{1}{[(x-x')^2+(y-y')^2+u^2(x',y')]^{1/2}} dx'dy' = f(x,y)$$

where $f(x,y) = \Delta g(x,y) + F(H)$

and $F : H'(\Omega) \subseteq L^2(\Omega) \rightarrow L^2(\Omega), \Omega = [0,m]\times[0,m].$

The derivative of the operator F at the point $u_0(x,y)$ is expressed by

$$F'(u_0)h = \int\int_D \frac{u_0(x',y')h(x',y')}{[(x-x')^2+(y-y')^2+(u_0(x',y'))^2]^{3/2}} dx'dy'.$$

Let us define the exact solution as

$$\hat{x}(x,y) = 5 - 2exp-[(x/10-3.5)^2(y/10-2.5)^2]$$
$$-3exp-[(x/10-5.5)^2(y/10-4.5)^2],$$

where $\hat{x}(x,y)$ is given on the domain $D = \{0 \leq x \leq m, 0 \leq y \leq m\}$.

Let $\Delta x = \Delta y = 1, M = m^2, \Delta = 0.25$ and $u_0 \equiv 5$. We have taken $f^{\delta} = F(\hat{x}(x,y)) + \delta$ in our computations. The exact and approximate solutions obtained are plotted in Figures 1 and 2, respectively for m=35 and δ =0.1.

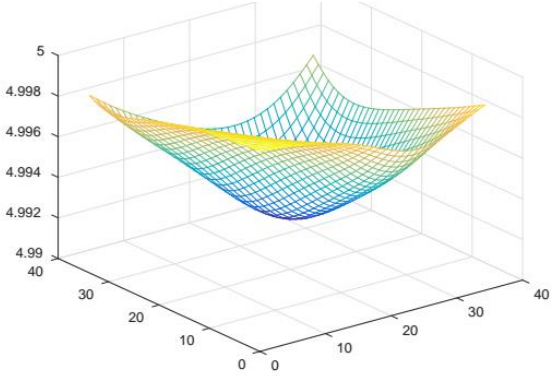

Fig 1: Exact solution for m=35

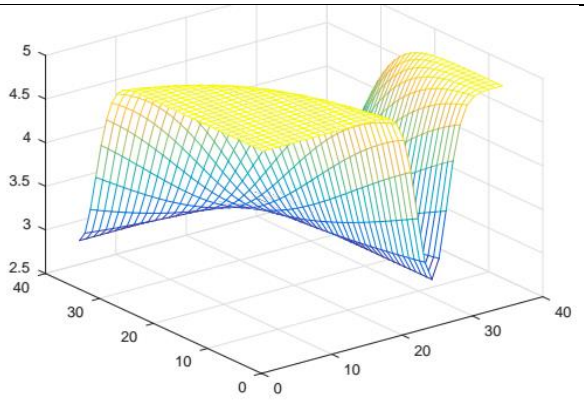

Fig 2: Approximate solution for m=35 and δ =0.1.

CONCLUSION

We have considered an iterative method which does not involve inversion of operator, for obtaining approximate solution for a nonlinear ill-posed operator equation $F(x) = y$ when the available data is y^{δ} in place of the exact data y. It is assumed that F is Fréchet differentiable in a neighborhood of the actual solution $\hat{x}$. The procedure involves finding the fixed point of the function $G(x) = x - \gamma[c^2F'(x)^*(F(x)-y^{\delta}) + \alpha(x-x_0)]$ in an iterative manner. For choosing the regularization parameter α we made use of the adaptive method suggested in [4] and for choosing the stopping index we made use of a majorizing sequence. The crucial assumption in the adopted procedure is the choice of the scaling parameter γ.

REFERENCES

[1] I.K.Argyros(2008), "Convergenve and Applications of Newton-type Iterations", Springer, New York.

[2] S.George(2010), On convergence of regularized modified Newton's method for nonlinear ill-posed problems, J.Inv.Ill-Posed Problems, 18, 133-146.

[3] B.Kaltenbacher(2008), A note on logarithmic convergence rates for nonlinear Tikhonov regularization, J.Inv.Ill-Posed Problems, 16, 79-88.

[4] S. Pereverzev and E. Schock(2005), On the adaptive selection of the parameter in regularization of ill-posed problems, SIAM.J.Numer.Anal., 43, 5, 2060-2076.

[5] R.Ramlau(2003), TIGRA-an iterative algorith for regularizing nonlinear ill-posed problems, Inverse Problems, 19, 433-465

[6] O.Scherzer, H.W.Engl and K.Kunisch(1993) , Optimal a posteriori parameter choice for Tikhonov regularization for solving nonlinear ill-

posed problems, SIAM J.NUMER.ANAL., Vol. 30, no.6, 1796-1838.
[7] U.Tautenhahn and Qi-nian Jin(2003), Tikhonov regularization and a posteriori rule for solving nonlinear ill-posed problems, Inverse Problems, 19,1-21.

5th International Engineering Symposium - IES 2016
March 2-4, 2016, Kumamoto University, Japan

A regularized shock coupled complex diffusion for enhancing blurred and speckled images

Jidesh P.

Assistant Professor, Department of Department of Mathematical and Computational Sciences, National Institute of Technology Karnataka, Surathkal, Mangalore 575025, India. e-mail: jidesh@nitk.ac.in, ppjidesh@gmail.com.

ABSTRACT: In this paper a method is proposed for enhancing images corrupted by data-dependent speckle noise (whose intensity is Gamma distributed) and spatially invariant linear sensor blur. Furthermore, the noise model is observed to be multiplicative in nature. This proposed strategy devises a nonlinear second-order diffusive-reactive model with an additional shock term for restoring and enhancing the corrupted images. The reactive term is derived based on the Maximum aposteriori (MAP) estimator, to adapt the filter to the noise distributions in the input data. Moreover, the piecewise-linear patch formation is drastically reduced and ramp-like edges are properly preserved, unlike the other second-order diffusion models. The reactive term (controlled by a scalar regularization parameter) helps deblurring images and the additional shock term plugged-in (controlled by a feature adaptive parameter) yields an impressive enhancement to the edges and finer details present in the images. The proposed model is suitable for restoring and enhancing ultrasound and Synthetic Aperture Radar (SAR) images which are commonly corrupted by speckles and sensor blurs. The experiments performed and demonstrated in this paper are justifying the above facts.

Keywords*: complex diffusion; image enhancement; deblurring; speckle reduction; regularization.*

INTRODUCTION

Image restoration and enhancement under data-correlated noise and spatially invariant blur is a matter of concern in many practical imaging modalities. Ultrasound and SAR images are commonly corrupted by the data-correlated multiplicative noise. Data-independent additive noise was analyzed quite extensively in the literature; refer (Weickert, 1997) and the references therein, for further details. Though there are few studies relating to the multiplicative speckle noise (see Aubert and Ajol (2008) and You and Acton (2002)), in general data-dependent multiplicative noise with different noise distributions (like Poisson, Gamma, Gaussian etc.) are not quite explored unlike data-independent noise distributions (see Aubert and Ajol (2008)). Rudin et al. (2003) proposed a variational model to handle the data-dependent noise. A data-dependent Gaussian distributed noise was considered in their work. Nevertheless, such a model lacks practical interest due to its limited application window.

Inspired by the renowned Perona and Malik (1990) model, some second-order noise-adaptive nonlinear diffusion methods are also proposed in the literature for speckled images, see Speckle Reducing Anisotropic Diffusion (SRAD) by Yu and Acton (2002), Improved SRAD by Sun et al. (2004), Oriented SRAD by Krissian et al. (2007) and speckle reducing self snakes model by Bini and Bhat (2014), and the references therein for the details. In these models the coefficient of diffusion (or Coefficient of Variation) is fine-tuned by integrating spatially adaptive Lee (1980) filter or Kuan (1985) Filter to handle speckles in images.

The other speckle reducing methods include level-set model by Li et al. (2010),

SUSAN controlled model by Yu et al. (2010), Non-linear Complex Diffusion (NCD) model proposed by Gilboa et al. (2004) and its improved versions proposed by Bernardes et al. (2010) (for OCT images) and Jidesh and Bini (2013). A shock-coupled despeckling filter was also recently proposed by Jidesh and Bini (2014). Nevertheless, most of these models eventually settle down to constant patches and also lack the capability to deblur and enhance images (without causing any theoretical instabilities) while despeckling them. All these facts motivate to propose an improved NCD model with deblurring and enhancing capabilities to despeckle images.

The remaining part of this paper is organized as follows. In Section 2 some of the well-known multiplicative denoising models are reviewed. In Section 3 a novel despeckling and deblurring model is proposed and its theoretical background is elaborated. Section 4 demonstrates the experimental results and discussions of the proposed model and a comparative study. Finally the paper is concluded in the last section.

MULTIPLICAATIVE MODELS FOR IMAGE DENOISING

Satellite and medical imaging systems commonly produce images degraded with multiplicative data-dependent noise, where the intensity of the noise is Gamma distributed and this forms speckles in captured images, see Aubert and Ajol (2008) and Jin and Yang (2011) for details. Since speckles are highly correlated with the input data the intensity of speckles is a function of the input image. This scenario makes the despeckling process tedious.

Variational framework is a well known tool for defining many energy minimizing problems. In variational formulation the uniqueness, existence and stability of the solution can be proved theoretically. In Aubert and Ajol (2008), the authors propose a variational model to handle data-dependent multiplicative noise. This model resembles to ultrasound and SAR imaging systems, where the noise amplitude follows Gamma distribution or the images are speckled. The evolution PDE for the model can be written as:

$$u_t = div\left(\frac{\nabla u}{|\nabla u|}\right) - \lambda\frac{(u-u_0)}{u^2}. \qquad (1)$$

Here λ is a regularization parameter and other symbols are already defined.

The above model is modified in the recent literature; see Huang et al. (2010) and Huang et al. (2010) for details. In Huang et al. (2010) the authors use a Weberized TV regularizer in place of TV regularizer for better restoration. Further in Huang et al. (2010), a functional which is invariably convex is being considered in the minimization problem. Here the fitting term is strictly convex unconditionally resulting in a unique solution.

The complex diffusion, which is generally encountered in quantum physics when dealing with time dependent Schrödinger wave equation, was adopted in image processing by Gilboa et al. (2004) in their work. An anisotropic complex diffusion described in this work can be written as:

$$u_t = \nabla.(c(Im(u))\nabla u), \qquad (2)$$

where $Im(u)$ denotes the imaginary component of complex image u and

$$c(Im(u)) = \frac{e^{i\theta}}{1+\left(\frac{Im(u)}{\kappa\theta}\right)^2}, \qquad (3)$$

where κ is a threshold parameter. Further it was shown by the authors that at the limiting case $lim_{\theta->0}(Im(u)/\theta) = t\Delta g_\sigma * u_0$, where $\Delta(g_\sigma * u_0)$ denotes the Gaussian convolved version of the Laplacian of the initial image. Since the coefficient of diffusion in this model is a function of Laplacian of the image, the ramp-like edges are preserved more naturally in the filtered output, unlike the other second-order nonlinear diffusion methods. However, this complex diffusion based model is not quite suited for data-dependent noise distributions. Many of the aforementioned diffusion methods including the complex diffusion perform diffusion based on the image gradient magnitude and give less care to the brightness of the image. Therefore the magnitude of diffusion does not depend on the image brightness values. Therefore

they are less suited for data-dependant noise distributions.

Though these despeckling models (discussed above) restore images from their distorted observations, they eventually settle down to piecewise constant images in the course of their evolution. In the following section a despeckling, deblurring and enhancing model that employs a piecewise planar approximation is being proposed. This model gives more natural look and feel to the restored images.

THE PROPOSED MODEL

This section proposes a complex diffusion driven PDE with a parameter controlled fidelity for restoring speckled and blurred images. The speckle noise amplitude is Gamma distributed and the blur is spatially invariant. This model is an extension of the model proposed by Jidesh and Bini (2013), where only the speckle noise degradation was considered. The degradation model assumed in this present study is:

$$u_0 = (k \otimes u)n, \tag{4}$$

where k is a spatially invariant blurring kernel, $\otimes$ is a linear convolution operation and n is speckle noise with Gamma distributed intensity values. The fidelity term in this model is similar to the one in Aubert and Ajol (2008). Bayesian Maximum aposteriori probability estimator is being used to derive the reactive (fidelity) term in order to tune the model to the input noise distributions. The proposed diffusion model takes the form:

$$u_t = \nabla.\big(c(Im(u))\nabla u\big) - \lambda\frac{(k*u-u_0)}{(k*u)^2} - \beta\frac{2}{\pi}(\arctan(G_\sigma * u_{\eta\eta})\,|\nabla u|, \tag{5}$$

where $c(.)$ is defined in Perona Malik (1990) and λ is a regularizing parameter which controls the diffusive and reactive behavior of the filter and β is a control parameter which controls the extent of shock at each iterations. The limiting case of the diffusion coefficient at smaller values of θ is assumed here. The diffusion coefficient is always considered to be positive in order to avoid the instability behavior of the filter for negative diffusion coefficient values. The reflective boundary condition (as already mentioned earlier) and the initial condition $u(x,y,0) = u_0(x,y)$ are assumed, where u_0 the initial (observed) image. Since a spatially invariant nature of the blurring function is assumed here, the blurring operation can be considered as a linear convolution with a finite impulse response. The space bounded blurring function is defined using a Gaussian function with a preset standard deviation σ ie. $k = \frac{1}{2\pi\sigma^2}e^{-(x^2+y^2)/2\sigma^2}$.

Complex diffusion can preserve ramp-like edges very effectively. Many gradient based diffusion coefficient functions lack the ability to detect the main features of ramps; namely its end points. In addition to this the gradient based functions have nearly uniform values across the whole smoothed ramp, eventually forcing the diffusion to slow down in those regions. Nevertheless Laplacian based diffusion functions are characterized by high magnitude values near the endpoints and low magnitude values elsewhere; therefore the noise over the ramp-edges gets suppressed considerably in the diffusion flow. The parameter controlled shock term helps in the enhancement of edges. Thus the proposed model is more effective in terms of noise reduction, ramp preservation, planar approximation, deblurring and enhancement compared to the other nonlinear second-order diffusion methods.

NUMERICAL IMPLEMENTATIONS

An explicit time marching method is being used for solving the PDE. The discretization for the regularization term is shown explicitly whereas it is trivial for the reactive (fidelity) term.

$$u^{n+1} = u^n + \Delta t\left(\begin{array}{l}\frac{\partial^-}{\partial x}\left(\frac{\partial^+ u}{\partial x}\times c(Im(u))\right)\\ +\frac{\partial^-}{\partial y}\left(\frac{\partial^+ u}{\partial y}\times c(Im(u))\right)\end{array}\right), \tag{6}$$

where $c(.)$ is defined in Perona and Malik (1990), u^n denotes the image at n^{th} iteration and the super scripts + and - denote the forward and backward

deference operators, respectively. The shock term (third term in (5)) is discretized using the upwind scheme; see Osher and Sethian (1988) for details. With the help of above discretizations one can finally descretize the gradient descent term in (5).

EXPEREMENTAL RESULTS

The efficiency of the proposed method is tested using a large number of test images (with different characteristics), however (for brevity) the results are demonstrated for only two different test images: Lena (a partially textured natural image) and an original ultrasound image (of a human liver). These test images are shown in their original from in Figure 1. The noise variance of the ultrasound image is not known. All the test images are blurred using a Gaussian kernel with a spread of 4 units. The images are tested with various noise densities and the proposed model is found to perform better in terms of noise reduction and details preservation as compared to the other methods considered in this work. A quantitative study is carried out using the statistical measures like Peak Signal to noise Ratio (PSNR) and Structural SIMilarity index (SSIM) (Wang et al. (2004)). For the real ultrasound image the noise variance is estimated from the uniform regions as done in Yu and Acton (2002). The response of the filters to various statistical measures is generalized by testing with 80 different images, under different experimental set-ups with various characteristics (like noise variance, noise distribution and spread of the blurring kernel etc.), however the results are shown for a selected set of images to maintain preciseness in explanation. The existing filters considered here for comparison (both visual and quantitative) are: Aubert and Ajol (2008) filter and total variation (TV) filter for multiplicative noise by Rudin et al. (2003) (RLO), SRAD and OSRAD.

Here it is recalled that a higher value for PSNR implies a better noise reduction/image restoration capability of the method under consideration. The PSNR of different methods (considered in this paper) for the test images at Gamma noise variance value 0.2 is provided in Table 1. It is observed that the PSNR values corresponding to the proposed method is higher than that of the other comparative methods.

Similarly, the structure preserving capability of a method is evaluated and compared using Structural Similarity Index (SSIM), it also compares the luminance and contrast features of the image under consideration, see Wang et al. (2004) for the details of formulation. Since SSIM gives a real value for each window considered in the image, Mean SSIM (MSSIM) is used as a consolidated measure of structural similarity. The range of output values of MSSIM lies in [0, 1] where 1 denotes a highest structural similarity. The MSSIM values evaluated for various methods are given in Table 2. The value given in the column corresponding to the proposed model is higher than the other entries. This implies a better structure, luminance and contrast preservation capability of the proposed model over the other ones.

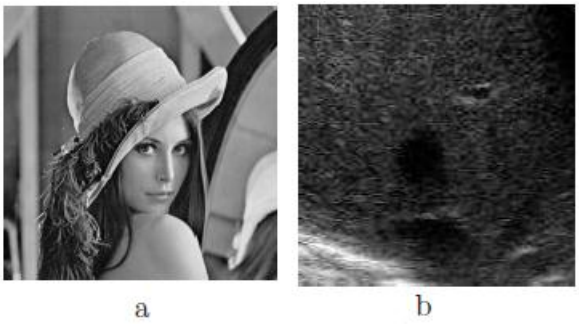

Fig 1: Original Test Images

The visual comparison of all the methods considered in this work (along with the one proposed in this paper) are shown in Figures 2 and 3. Though the performance is analyzed using a large number of test images (close to 80), the results are shown only for two different test images due to page constraints. From the results provided in these selected figures, one can confirm that the proposed method (shown in sub-figure (f) of the Figures 2 and 3) outperforms other methods in terms of visual appearance and the piecewise patch formation is not as evident as in the other nonlinear second-order methods considered in this work. This analysis is generalized in the

observations made about the other test image dataset (whose results are not shown in this paper) as well. Note that the results (outputs) of all these methods are shown at their optimal performance in terms of visual representation.

Table 1:PSNR (in dB) evaluated for various restoration methods for different images. (The Gamma noise variance of the input image Lena is: 0.2 and for the real noisy ultrasound image, additional noise of variance 0.2 is used).

Image name	Noisy	RLO	AA	SRAD	OSRAD	Proposed
Lena	23.3	24.4	25.6	26.1	26.9	27.9
Ultrasound (Liver)	24.2	27.1	28.2	28.6	28.9	29.6

CONCLUSIONS

In this paper a noise-adaptive despeckling and deblurring filter has been proposed. This second-order complex diffusion driven regularization filter restores and enhances images corrupted by speckle noise (whose intensity is Gamma distributed) and linear shift invariant blur. Ramp-like edges in images are preserved and visual artifact like *staircase* effect is reduced in this model. The experimental results shown in favor of the proposed model demonstrate the efficiency of the model to restore images in terms of visual and quantitative measures.

Table 2: MSSIM evaluated respectively for various restoration methods for different images, the gamma noise variance of the input image Lena is 0.2 and for ultrasound image, additional noise variance 0.2 is used

Image name	RLO	AA	SRAD	OSRAD	Proposed
Lena	0.62	0.71	0.75	0.76	0.79
Ultrasound (Liver)	0.62	0.71	0.74	0.75	0.77

Fig 2: Image (``Lena'') restored using various methods: (a) Noisy images with mean 1 and Gamma noise variance 0.3; (b) restored using AA method; (c) restored using RLO filter by Rudin et al. (d) SRAD method. (e) OSRAD method (f) restored using the proposed method.

REFERENCES

[1] Bernardes, R., Maduro, C., Serranho, P., Araujo, A., Barbeiro, S., and Cunha-Vaz, J. (2010), Improved adaptive complex diffusion despeckling filter, Optics Express, Vol. 18, No. 23, pp. 48–59

[2] Bini A. A. and Bhat M. S. (2014), Despeckling low SNR, low contrast ultrasound images via anisotropic level set diffusion, Multidimensional Systems and Signal Processing, Vol. 25, No. 1, pp. 41–65

[3] Gilboa, G., Sochen, N.A., Zeevi, Y.V. (2004), Image Enhancement and Denoising by Complex Diffusion Processes, IEEE Transaction on Pattern Analysis and Machine Intelligence, Vol. 26, pp. 1020–1036.

[4] Huang, L., Xiao, L., Wei, Z-H. (2010), Multiplicative Noise Removal via a Novel Variational Model, EURASIP Journal on Image and Video Processing, Vol. 2, No. 1, pp. 1–16.

[5] Huang, M., Ng, M.K., Wen,Y. (2009), A New Total Variation Method for Multiplicative Noise Removal, SIAM Journal of Imaging Sciences, Vol. 2, No. 1, pp 22–40.

[6] Jidesh P and Bini A.A. (2013), A Complex Diffusion Driven Approach for Removing Data-Dependent Multiplicative Noise, LNCS, Vol. 8251, pp. 284–289.

[7] Jidesh P and Bini A.A., (2014), Image Enhancement under Data-Dependent Multiplicative Gamma Noise, Applied Computational Intelligence and Soft Computing, Vol. 2014, pp. 1–8.

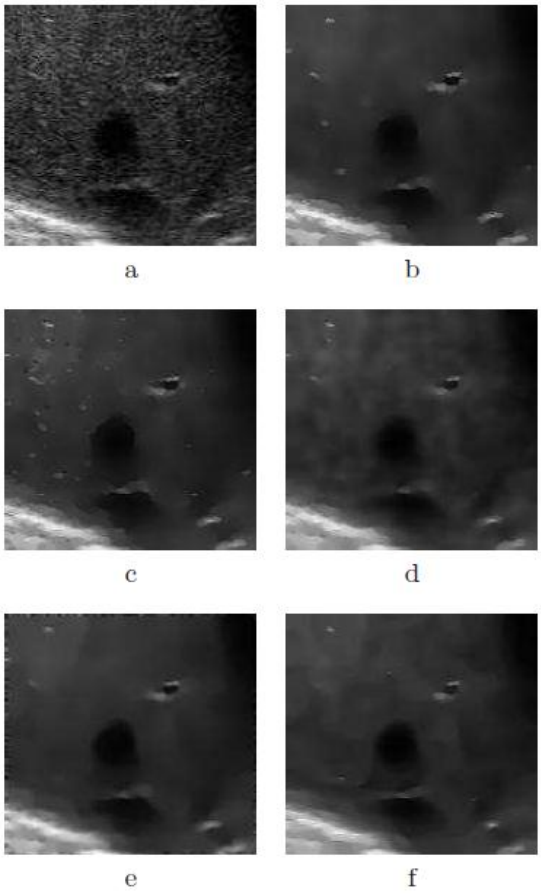

Fig 3: Image (Ultrasound image of a human liver) restored using various methods: (a): Noisy images with unknown mean and noise variance; (b) restored using AA method; (c) restored using RLO filter by Rudin et al.; (d) SRAD method. (e) OSRAD method; (f) restored using the proposed method.

[8] Jidesh P. (2014), A convex regularization model for image restoration, Computers and Electrical Engineering, Vol. 40, No. 8, pp. 66–78.

[9] Krissian, K., Westin, C.F., Kikinis, R., Vosburgh, K.G. (2007), Oriented speckle reducing anisotropic diffusion', IEEE Transactions on Image Processing, Vol. 16, No. 5, pp. 1412–1424.

[10] Kuan, D., Sawchuck, A., Strand, T. and Chavel, P. (1985), Adaptive noise smoothing filter for images with signal-dependent noise, IEEE Transactions on Pattern Analysis and Machine Intelligence, Vol. 7, No. 2, pp. 165–177.

[11] Lee, J. S. (1980), Digital image enhancement and noise filtering by using local statistics, IEEE Transactions on Pattern Analysis and Machine Intelligence, Vol. 2, No. 2, pp. 165–178.

[12] Li, H., Huang, B. and Huang, X. (2010), A level set filter for speckle reduction in SAR images, EURASIP Journal on Advances in Signal Processing, Vol. 20, No. 1, pp. 45–78.

[13] Osher S. and Sethian J. A. (1988), Fronts propagating with curvature dependent speed: algorithms based on Hamilton-Jacobi formulations, Journal of Computational Physics, Vol. 79, No. 1, pp. 12–49.

[14] Perona, P., Malik, J. (1990), Scale-space and edge detection using anisotropic diffusion, IEEE Transactions on Pattern Analysis and Machine Intelligence, Vol. 12, No. 7, pp. 629-639.

[15] Rudin, L.I., Lions, P.L., Osher, S. (2003), Multiplicative denoising and deblurring: theory and algorithms, in Geometric Level Set Methods in Imaging, Vision, and Graphics, Springer, Berlin, pp. 103–120.

[16] Rudin, L.I., Osher, S., Fehtami E (1992), Nonlinear total variation based noise removal algorithms, Physica. D., Vol. 68, No. 1, pp. 259–268.

[17] Setzer, S., Steidl, G., Teuber, T. (2010), Deblurring Poissonian Images by Split Bregman Techniques, Journal of Visual Communication and Image Representation, Vol. 21, No. 3, pp. 193–199.

[18] Sun, Q., Hossack J.A., Tang, J., Acton, S.T. (2004), Speckle reducing anisotropic diffusion for 3d ultrasound images, Computerized Medical Imaging and Graphics, Vol. 28, No. 8, pp. 461–470.

[19] Wang Z., Bovik A. C., Sheikh H. R. and Simoncelli E. P. (2004), Image Quality Assessment: From Error Visibility to Structural Similarity, IEEE Transaction on Image Processing, Vol. 13, No. 1, pp. 1–14.

[20] Weickert, J. (1997), A Review of Nonlinear Diffusion Filtering, Scale-Space, pp. 3–28.

[21] Yu, Y., Acton, S.T (2002), Speckle reducing anisotropic diffusion', IEEE Transactions on Image Processing., Vol. 11, No. 11, pp. 1260–1270.

[22] Yu, J., Tan, J., and Wang, Y. (2010), Ultrasound speckle reduction by a Susan-controlled anisotropic diffusion method. Pattern Recognition, Vol. 43, No. 9, pp. 3083–3092.

[23] Zhengmeng Jin and Xiaoping Yang (2011), A Variational Model to Remove the Multiplicative Noise in Ultrasound Images, Journal of Mathematical Imaging and Vision, Vol. 39, No. 1, pp. 62–74.

5th International Engineering Symposium - IES 2016
March 2-4, 2016, Kumamoto University, Japan

Real Time Scheduling in Contiki

V.Krishnapriya [1], Smriti Murali[2] and **K. Chandrasekaran[3]**

1 *Undergraduate Student, Department of Computer Science and Engineering, National Institute of Technology Karnataka, Surathkal, Mangalore 575025, India. email:vk22priya@gmail.com*
2 *Undergraduate Student, Department of Computer Science and Engineering, National Institute of Technology Karnataka, Surathkal, Mangalore 575025, India. email:m.smriti.95@gmail.com*
3 *Professor, Department of Computer Science and Engineering, National Institute of Technology Karnataka, Surathkal, Mangalore 575025, India. email: kchnitk@ieee.org*

ABSTRACT : The fast-paced nature of data in Internet of Things (IoT) applications demands that the operating systems be able to efficiently schedule tasks with no delays. Immediate processing of data implies there must not be any violation of hard deadlines. Contiki, an OS designed for IoT, does not however provide full support for real-time operations. The scheduler and timer modules of this OS are studied, and we compare the performances of the native scheduling algorithm and purely pre-emptive scheduling of tasks. Experiments are run on Cooja, a simulator provided for Contiki to run on desktop systems. We also take a look at the scheduling algorithms employed by other operating systems employed for IoT.

***Keywords**: Internet of Things, Contiki, scheduling, Cooja*

INTRODUCTION

The Internet of Things (IoT) is a term that refers to a network of inter-connected devices that are continuously communicating with each other. The ultimate aim of IoT is to create a global network of all objects – our cars, homes and everyday utilities – capable of communicating with each other and with human beings. From a technical perspective, these objects are basically embedded systems enabled with communicating capabilities. Developing a common underlying architecture and operating systems for all devices is, of course, a challenging task. Traditions OS like Linux and Windows cannot hope to scale across such diverse and constrained devices.

Wireless Sensor Networks (WSN) are one of the most important elements in realizing the vision of IoT. WSN are a network of miniature devices having the ability to sense, compute and communicate wirelessly in short distances (Gubbi, Jayavardhana, et al. 2013). Hence, WSNs can be seen as a building block of the IoT. These networks are characterized by memory, power, processing power and communication bandwidth.

Another important paradigm to consider in the context of IoT is real-time operations. The stream of data flowing through the network is real-time, i.e., it requires immediate processing. Any delay might as well render the data useless, and in the worst case, potentially harmful.

Operating systems aiming to work on IoT devices must therefore have real-time capabilities. This implies that the scheduling algorithms employed by these OS must ensure that no deadlines are broken – these are also called hard real-time operating systems. The most common design principles are :

•Event-driven scheduling – This algorithm switches between tasks only when there is an event of higher priority that needs to be processed. It's also called priority/preemptive scheduling.

•Time sharing scheduling – These algorithms switch between tasks based on a timer alert. These can be identified as round robin scheduling.

Scheduling in Contiki

We will now examine the scheduling mechanism employed in Conitki.

There are two main modes of execution – cooperative and preemptive. Cooperative code implies sequential execution of the tasks, one runs to completion before the other begins, and this is in the FIFO fashion. This cooperative execution is interrupted by timers or events to allow for execution in preemptive mode.

A process is called or run when another process posts an event to it. A synchronous event is delivered to the process immediately, whereas an asynchronous event is added to the event queue maintained by the kernel and then processed in that order.

This scheduling order is based on a new approach towards process handling called event-driven systems (Dunkels, A., Grönvall, B. and Voigt, T., 2004). In these systems, processes are implemented as event-handlers that run to completion. This approach saves memory by utilizing the same stack space, while also eliminating the need for concurrency and locking mechanisms.

Events are recognized by identifiers assigned to them – a few are listed below for reference :

PROCESS_EVENT_INIT – initiate new process

PROCESS_EVENT_EXIT – kill the process

In the next section, we will see the disadvantages of this event-driven mechanism and how pre-emption is achieved in Contiki.

Preemption in Contiki

Imagine a sensor network that requires the nodes to perform a computation on data that monopolizes the CPU time. The event-driven model does not allow for preemption – this leaves the other processes waiting till the computation is finished. As said before, this is not suitable for real-time data processing. To enable preemptive scheduling, Contiki allows for preemptive multi-threading. This is implemented as an application library on top of the kernel that can be optionally used, if required (Dunkels, A., Grönvall, B. and Voigt, T., 2004).

Another way in which Contiki supports preemption is through a polling mechanism. Polling breaks the sequential processing of the asynchronous event queue – similar to preemption due to a high priority process. When a particular process is polled, it tells the kernel that the process should be schedules as quickly as possible. Interrupts use this mechanism for events related to the hardware, such as checking for updates or new devices. Therefore in-between the asynchronous events, polling is done in order of priority. The following paragraph summarizes the scheduling mechanism :

First, the scheduler executes all the processes which have their polling flags set from the system's process list. When the list is exhausted, the scheduler moves to the event queue and dispatches the corresponding process. The event can be a single-process event or a broadcast event. If the event is for a single process, the corresponding process is dispatched and if it is a broadcast event, then each event is processed. The scheduler then goes back to the process list and repeats the cycle.

We now determine whether the multi-threading preemptive scheduling offers advantages over the inbuilt scheduler of Contiki. Before moving to the implementation details, the following section takes a brief look at the scheduling approach on other popular operating systems for the IoT.

Schedulers in IoT Operating Systems

Let us now look at scheduling techniques employed by other operating systems developed specifically for the IoT.

•TinyOS : Written in the nesC programming language, it employs the simplest FIFO scheduler with no real-time support. However, alternatives to this, such as the Earliest Deadline First algorithm, have also been implemented (Levis, Philip, et al. 2005). For preemption, it uses an event mechanism similar to that of Contiki.

•RIOT OS : This OS using a priority based preemptive scheduler, making it ideal for

real-time applications. Apart from this, it also implements tickless scheduling which prevents the timer from generating interrupts when the processor is idle, further conserving power. (Baccelli, Emmanuel, et al. 2012)

•FreeRTOS : This is a popular real-time operating system supporting tickless mode, that uses a priority based round-robin scheduling scheme. The scheduler can however be configured to run in cooperative mode.

Clearly, most of the operating systems developed are currently running on wireless sensors, making it necessary to support the cooperative execution mode. However, RIOT, which was developed with the Internet of Things in mind, provides full real-time support and should be seen as the way forward towards developing an OS devoted to the IoT. Real-time data which is extremely sensitive to delays is what most IoT applications are expected to generate, computationally extensive tasks will be few and mostly centrally computed by dedicated nodes.

Implementation Details

Contiki is written entirely in the C programming language. It can be run on desktop systems by using the Cooja simulator which runs as a virtual machine on VMware. The main purpose of our simulation was to compare the performance of Contiki in the preemptive and cooperative modes.

For this purpose, we took two processes, each involving a computation and ran them in the two modes mentioned above. For the cooperative mode, the first process ran and then send and event to start the second process, resulting in a sequential execution. Pre-emption was achieved by utilizing the multi-thread library provided by Contiki, each process running as a thread. The progress of the process at each step of the computation along with the corresponding time stamp was recorded and graphs for plotted for the same. The graph for cooperative mode can be seen in Figure 1, and Figure 2 is the result obtained for preemptive multithreading.

In this experiment we have chosen Sky mote due to its wide usage in IoT applications.

Results and Analysis

The analysis reveals very interesting results that tell us the reasons behind Contiki's OS design.

In the cooperative mode, the process completion times are very small – each process is completed in a short duration. There is a difference between the completion time of the first and begin time of the second process. This is the time needed for event delivery and process initialization. This approach however, as discussed, fails when process is a real-time event that needs immediate processing and process one is computation intensive.

Figure 2 clearly shows that both the processes are concurrently executing. However, there is a sharp increase in the execution times when compared to the cooperative mode. Clearly, this depends on setting an appropriate value for the interrupt timer; nevertheless, there are time costs due to the frequent context switching. While this approach is suitable if all the data coming in real-time, if process 2 is the only real-time event then constantly interrupting it is not desirable.

This then shows us the best approach for all situations, especially in the current situation when the data is a mixture of real-time and computation, polling. Every real-time task should be polled, and thus called as soon as possible. Given the three scheduling approaches in Contiki, this can be seen as the best approach, though it will not work very well for pure real-time data.

Conclusions

The following conclusions were drawn after the study:

- Of the cooperative, preemptive and polling options for scheduling processes, the one that provided the best results is polling. This may not, however, apply for IoT applications of the future that demand immediate processing.
- For such purposes, the multi-threading library provided a preemptive mode, however this is an external library and hence incurs extra cost.

- Thus, while well suited for the WSN applications on which it is currently deployed, Contiki does not provide suitable real-time scheduling options as part of the core OS features.

Acknowledgements

The Ministry of Education, Government of Japan provided financial support to carry out this research, and we are very grateful for their encouragement. We would also like to thank Prof Katta, Dean(Academic) NITK, Prof Torii, Kumamoto University and the administration of NITK and TEQIP, Government of India for providing us with this opportunity and furthering our passion for research.

References

[1] Baccelli, Emmanuel, et al. "RIOT: One OS to Rule Them All in the IoT." (2012).
[2] Baccelli, Emmanuel, et al. "RIOT OS: Towards an OS for the Internet of Things." Computer Communications Workshops (INFOCOM WKSHPS), 2013 IEEE Conference on. IEEE, 2013.
[3] Dunkels, Adam, Björn Grönvall, and Thiemo Voigt. "Contiki-a lightweight and flexible operating system for tiny networked sensors." Local Computer Networks, 2004. 29th Annual IEEE International Conference on. IEEE, 2004.
[4] Dwivedi, A. K., M. K. Tiwari, and O. P. Vyas. "Operating Systems for Tiny Networked Sensors: A Survey." International Journal of Recent Trends in Engineering 1.2 (2009): 152-157.
[5] Gubbi, Jayavardhana, et al. "Internet of Things (IoT): A vision, architectural elements, and future directions." Future Generation Computer Systems 29.7 (2013): 1645-1660.
[6]Levis, Philip, et al. "Tinyos: An operating system for sensor networks." Ambient intelligence. Springer Berlin Heidelberg, 2005. 115-148.
[7] Österlind, Frederik, et al. "Simulation with COOJA." Obtained from http://www. sics. se/~ fros/osterlind06crosslevel. pdf (last accessed on September 21, 2011).
[8] Tabuada, Paulo. "Event-triggered real-time scheduling of stabilizing control tasks." Automatic Control, IEEE Transactions on 52.9 (2007): 1680-1685.

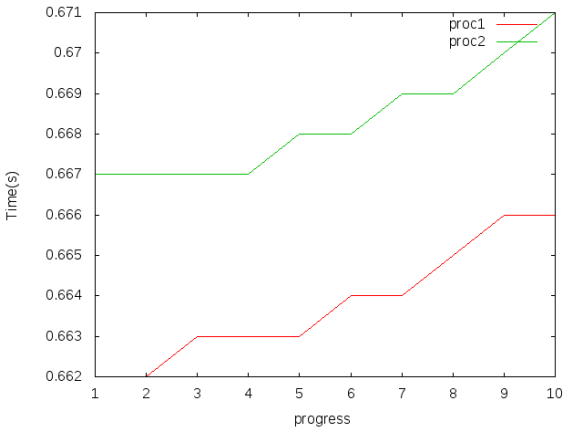

Figure 1: Graph showing the execution times along with process progress in cooperative mode.

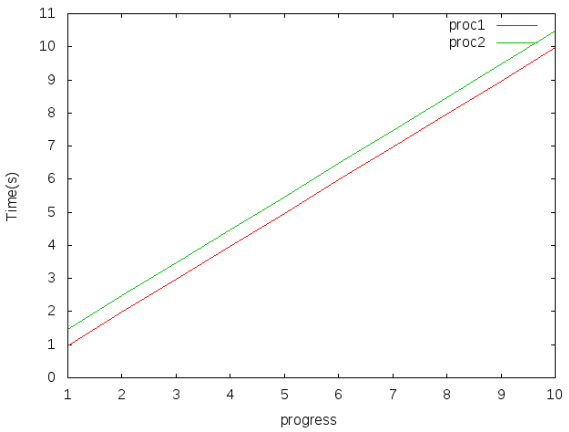

Figure 2: Graph showing the execution times along with process progress in multi-threading preemptive mode.

5th International Engineering Symposium - IES 2016
March 2-4, 2016, Kumamoto University, Japan

Contiki as RTOS
A look at Contiki's Flash File System – Coffee

Smriti Murali [1], V. Krishnapriya [2] and **K. Chandrasekaran[3]**

1 *Undergraduate Student, Department of Computer Science and Engineering National Institute of Technology Karnataka, Surathkal, Mangalore 575025, India. email:m.smriti.95@gmail.com*
2 *Undergraduate Student, Department of Computer Science and Engineering National Institute of Technology Karnataka, Surathkal, Mangalore 575025, India. email:vk22priya@gmail.com*
3 *Professor, Department of Computer Science and Engineering, National Institute of Technology Karnataka, Surathkal, Mangalore 575025, India. email: kchnitk@ieee.org*

ABSTRACT: The success of IoT (Internet of Things) depends upon the inclusion of many cross platform heterogeneous devices which have severe memory, energy, processing power and communication bandwidth constraints. A real-time application is expected to process data instantly without buffering delays or jitter. Contiki, an open source OS, provides only partial support for such operations. In this paper, we examine how Coffee is better than CFS-POSFIX for real-time operations and validate it by running a simulation on Cooja. We further explore Coffee's prominent features such as garbage collection, wear levelling, etc. We suggest improvements to reduce the unpredictable delays caused by long tasks like file extension and garbage collection. We then examine how latencies in file operations can be reduced to enhance its real time performance.

Keywords*: Internet of Things, Contiki, RTOS, File System, Coffee, Cooja*

INTRODUCTION

File systems in Contiki are implemented as a part of the Contiki File System (CFS) interface. Coffee (Flash file system) and CFS-POSIX provide full functionality. CFS-POSIX is used where Contiki platforms run in native mode that is without internal memory in sensor nodes. Coffee, on the other hand is aimed at sensor nodes which have local storage such as flash memory or EEPROM. It is written in C and is designed exclusively for flash memories and EEPROM, taking into consideration their peculiar characteristics. The prominent features of Coffee are garbage collection, fault recovery and wear levelling which make coffee efficient and reliable. In its default setup, it requires 5kb ROM for the code, and 0.5kb RAM. (Tsiftes, Nicolas, et al, 2009).The implementation of the Coffee file system is not specific to Contiki but can be implemented on other systems and flash devices as well.

Necessity Of Coffee

Coffee in implemented primarily on wireless sensor network (WSN). Nodes must either transmit data collected or store data on devices such as the flash memory chips which are located outside the microcontroller. These nodes are battery powered and operate autonomously for long periods of time. They have around 4 KB of RAM. In such sensors, power and memory are scarce.

The modes in which the sensors typically operate are

- Low power mode or sleep mode .Contiki makes use of sleepy routers for power efficiency.
- Processing the data, since many a times processed data is transmitted instead of raw sensor data

- Transmission of data across the network.

Of the three modes, transmission of data outside a node which requires radio communication is the most energy intensive as transmitting one bit consumes about as much power as executing 800-1000 instructions (Karlof, Chris, Naveen Sastry, and David Wagner, 2004.). Hence, in many situations it is more efficient to store data in the node and send it in batches than to send it as and when it is collected. Some sensor nodes have to store a large quantity of data, like images and videos which require a file system with has a fast and less expensive append operation. Thus we need a file system which is reliable and operates autonomously and reliably on flash memory. Coffee is a suitable file system for sensor nodes given the above stated concerns.

Properties And Limitations Of Flash Memory

Flash memory poses many challenges to the effective implementation of file systems. However, since flash memory is light weight, consumes very less power, and is resistant to shock, it is widely used in sensor nodes. It is a non-volatile memory IC which can hold data without power being supplied. Its contents are electrically erasable and rewritable. Flash memory is different from magnetic disks since its content cannot be overwritten easily since a sector must be erased before new data is stored. Apart from this there are memory constraints on the flash memory in sensor node. It is not feasible to have metadata or large buffer caches in RAM. Another major limitation is that there is a limit on the number of erase operations a memory cell can perform (order of 100 000) beyond which there is a high likelihood of data getting corrupted.

Benefits Of Coffee

In Coffee, every open file uses a small and constant memory footprint O (1) (Tsiftes, Nicolas, et al., 2009). It can thus be used for a system having many small files as well as one having a small number of large files. The performance overhead of Coffee is low. The throughput is at least 92% of the achievable direct flash driver throughput (Tsiftes, Nicolas, et al., 2009). These files have the layout of an extent, and could be coupled with a micro log. Every ordinary file has a header as well as a data area. Each micro log file substitutes a log index table and a log entry table with the data area. Micro logs are handled transparently by Coffee. The basic idea behind a log-structured file system is to improve write performance by buffering a sequence of file changes in the file cache and then writing all the changes to disk sequentially in a single disk write operation. Thus a large amount of data is collected in a file cache in Main Memory, and then the data is written to disk in large Input /Output operation. Coffee uses micro logs to modify data on storage devices since in place updates are expensive. Coffee uses sequential page structures for its files. Append-only files are stored in the simplest way as contiguous group of pages. Coffee uses first fit page allocation to assign pages. A sequential structure of certain size is reserved when a file is opened for the first time, if not; it is allocated a default size. When a file has a strict limit on its size, we cannot write beyond this limit. CFS_COFFEE_IO_FIRM_SIZE is used to instruct Coffee not to attempt to extend the file when there is an attempt to write past the reserved file size. After a file is modified, Coffee creates an accompanying micro log structure and links it with the file (Dunkels, Adam, Bjorn Gronvall, and Thiemo Voigt., 1989).When file data is modified for the first time, a micro log is created for the file. It stores a table of modifications whose parameters, the log size and the log entry size, can be modified using cfs_coffee_configure_log function. Thus we can fine-tune their micro logs according to the expected access pattern of a file to increase the performance significantly.

Flash storage algorithms can be implemented on top of Coffee using CFS_COFFEE_IO_FLASH_AWARE defined in cfs-coffee.h which makes sure Coffee does not invoke its own micro logs when file modifications occur.

Garbage Collection

The garbage collector reclaims obsolete pages when a file reservation request cannot be satisfied and is triggered only when a new file is created. There are two types of garbage collector Greedy and Reluctant. The greedy garbage collector erases as many sectors as it can when invoked, the reluctant garbage collector on the other hand erases only one sector each time it is invoked. A sector can be erased by the garbage collector only if it has only free and obsolete pages present. The garbage collection gets the status of each sector and stores it in a 'stats' structure. Page statistics from each sector determine whether a given sector is to be erased or not. If it contains at least one obsolete page and not a single active page, it is erased, not just the least recently written sector .This ensures uniformity in the flash memory erasures and supports wear levelling.

Wear Levelling

As mentioned earlier, flash memory is prone to wear and may not last for more than 100,000 erasures. With each erasure, the chances of memory corruption also increase. Sensor nodes have a lifetime of about 10 years, to ensure we don't cross the threshold in the given lifespan; we have to optimise the erasures. Wear levelling is used to erase all sectors uniformly so that all sectors are evenly worn out. In usual logging of sensor data, chances of corruption are generally low. However, in a traffic-intensive network when data is written and erased at a very high rate, wear levelling is important to ensure the data does not get corrupted. Wear levelling ensures all sectors are uniformly erased so that all of them are evenly worn out. The garbage collection policy supports wear levelling by delaying erasing as it collects garbage memory only when no space is available to allot for a new file. Page allocations are also rotated over the full flash memory to a high degree, but sectors having old files are exempted from garbage collection until a background process concatenates old files from different sectors into one file. We can prevent the OS from erasing sectors immediately after removing a file using the macro
COFFEE_EXTENDED_WEAR_LEVELLING
and thereby ensure wear levelling; this however results in a more tedious garbage procedure.

Real Time performance

As we have seen, Contiki does not provide full support for real time operations. One of the major reasons for this is the Coffee file system. By using a ring file system, we can make Coffee a real time file system and improve Contiki's over-all real time performance. Coffee file system though versatile supports only limited random access capabilities. In coffee, when a file is created, its size needs to be reserved beforehand. It is effective when the file size and file access patterns are known, as the log size and structure can be modified accordingly. It is however inefficient if these details are not known. If we have to write more data than what has been reserved for the file, the file has to be extended by allotting bigger file. The contents are copied from the old file to the bigger file. This consumes a lot of time and can cause a hindrance when we use coffee in real time. Also a page reservation request cannot be granted, the garbage collector which performs a lengthy operation must be invoked. Hence, a real time file system should separate tasks that have small and known runtime such as normal read- write operations from task with longer run times such as extending a file and performing garbage collection. Advance warning must be given that long operations are in progress. And we must enable the file system to write to files while these long operations are in progress. These maintenance operations can be scheduled. For instance we can choose between greedy and reluctant according to the real time demands.

EXPERIMENTAL RESULTS AND ANALYSIS

We aim to prove the above claims and show how coffee can efficiently reduce the power consumed in radio transmission. We hence propose to use only the coffee file system for real time applications. We have implemented the above ideas by running

simulations on the Cooja simulator provided for Contiki.

The procedure followed is as follows:

- In this experiment we have chosen Sky mote due to its wide usage in IoT applications.
- We create two motes of the type Sky Mote and load the coffee file system for one, and the default CFS for the other mote.
- We then simulate communication between the motes to measure the effect of change in file system on the radio power consumed by each mote.

CONCLUSIONS

The following conclusions are deduced from this study:

- In this paper, we see that Contiki is suited for applications developed for the Internet of Things, and it's limitations as a real-time operating system.
- We also critically examined the Contiki file System, and how the Coffee file system complements the inherent flash properties of sensor networks.
- In the simulations, from Figure 1 and Figure 2 we can clearly see that the Coffee file system surpasses the CFS by a noticeable margin in terms of efficiency and speed. For a given running time, the transmission time of the Coffee file system is less than CFS by almost 0.4% on an average. For a RTOS which runs for years, this is a major difference.
- We thus conclude in terms of file system capabilities as well as radio transmission and power efficiency, coffee outweighs the default CFS file system. Thus we can focus our further study exclusively on the coffee file system.

ACKNOWLEDGEMENTS

We would like to thank the Ministry of Education, Government of Japan for providing financial support to carry out this research. We are grateful to Prof Katta, Dean (Academic) NITK, Prof Torii, Kumamoto University and the administration of NITK and TEQIP for their encouragement and support.

REFERENCES

[1]Adam Dunkels, BjÃ¶rnGrÃ¶nvall, and Thiemo Voigt. Contiki - a lightweight and flexible operating system for tiny networked sensors. In Proceedings of the First IEEE Workshop on Embedded Networked Sensors (Emnets-I), Tampa, Florida, USA, November 2004.
[2]Dunkels, Adam, Bjorn Gronvall, and Thiemo Voigt. "Contiki-a lightweight and flexible operating system for tiny networked sensors." Local Computer Networks, 2004. 29th Annual IEEE International Conference on. IEEE, 2004.M. Young, The Technical Writer's Handbook. Mill Valley, CA: University Science, 1989.
[3] Karlof, Chris, Naveen Sastry, and David Wagner. "TinySec: a link layer security architecture for wireless sensor networks." Proceedings of the 2nd international conference on Embedded networked sensor systems. ACM, 2004.
[4] Kawaguchi, Atsuo, Shingo Nishioka, and Hiroshi Motoda. "A Flash-Memory Based File System." USENIX. 1995.
[5]Tsiftes, Nicolas, et al. "Enabling large-scale storage in sensor networks with the coffee file system." Proceedings of the 2009 International Conference on Information Processing in Sensor Networks. IEEE Computer Society, 2009.

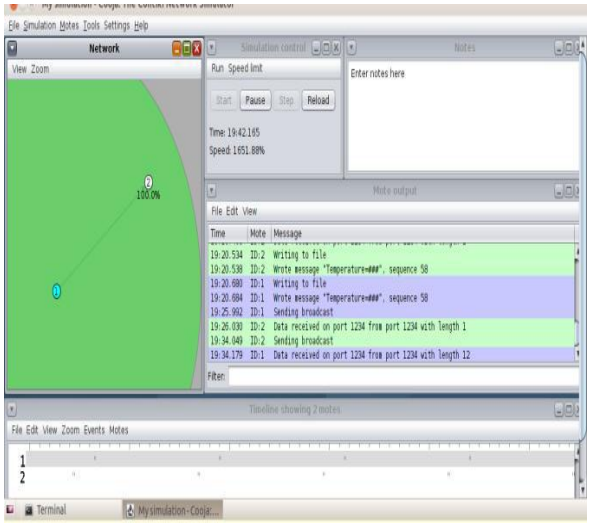

Fig.1 Simulation screenshot

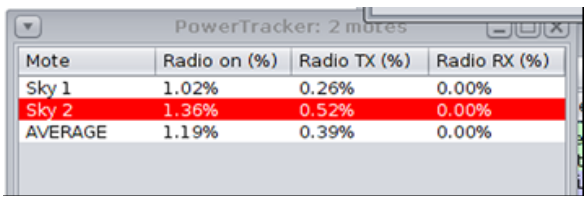

Fig.1 Power tracking in different file systems

5th International Engineering Symposium - IES 2016
March 2-4, 2016, Kumamoto University, Japan

Parallelization of Query Execution in a Database System

Pravalika A[1], Vaishakh K[1], Abhishek D V[1] *and* **Geetha V[2]**

1 *UG Students, Department of Information Technology, National Institute of Technology Karnataka, Surathkal, Mangalore 575025, India.email:avvarupravalika@gmail.com email:kvaishakhnambiar@gmail.com email:dv.abhishek@gmail.com*
2 *Assistant Professor, Department of Information Technology, National Institute of Technology Karnataka, Surathkal, Mangalore 575025, India.email:geethav.nitk@gmail.com*

ABSTRACT: Parallelization is the simultaneous use of resources to improve the performance while solving a computational problem. Most of the applications today involve handling Big Data. Update and retrieval are two kinds of operations performed on database files. Update operations change the data values on insertion, deletion, or updating while retrieval operations do not alter the data but retrieve them after optional conditional filtering. In both types of operations, selection of relevant data plays an important a role. Selecting records sequentially is a time consuming operation and the system resources are not utilised effectively. Parallelising query execution results in effective utilisation of system resources and also reduces the execution time. Thus giving a better performance especially on huge data sets.

Keywords*: Parallelization, Optimisation, OpenMP, Scheduling.*

INTRODUCTION

Query optimisation involves coming up with the best execution plan for a given SQL statement. This execution plan should have the lowest cost. This cost estimates the runtime cost of evaluating the query in terms of the number of I/Ooperations required, CPU path length, amount of disk buffer space, disk storage service time, and interconnect usage between units of parallelism. There are various optimisation techniques which are implemented at different stages of query execution. In this work, we aim at improving the performance once the database file is loaded into the main memory. Through our work, we would suggest to include this technique in the execution plan of a given SQL statement.

WORK

We have mainly focussed on parallelising the SELECT, UPDATE and DELETE queries. Select queries usually occur with conditional filtering, ordering or grouping of records. Update and Delete also involves conditional filtering followed by updating or deletion of filtered records. We have come up with parallel execution plans for different types of such queries.

Getting relevant records from a table

The section of the table present in the memory is partitioned horizontally and each part is assigned to a new thread. Each thread applies the filtering conditions on the tuples assigned to it to obtain the relevant records in parallel. We maintain an array which stores the surrogate key index of each of these relevant records. These indexes will grant access to the records in constant time i.e O(1).

Select without any filtering
The data in the memory is distributed among the considered threads so that these threads can process the data concurrently.

Select with a conditional filtering
This is nothing but getting relevant records from the table as mentioned above.

Select with ordering
In this case, the result needs to be sorted based on a specific column. Once the relevant records are obtained, the array containing the index of relevant records is sorted based on the specified column. Quick sort algorithm is used to perform sorting in parallel as it does in place sorting. Also we reorder index array instead of reordering the records while sorting as it is more efficient.

Select with groupby and aggregate function
When the output needs to be grouped by a certain column, we first obtain the relevant records in parallel by applying conditional filtering. After obtaining the relevant records, the records are ordered by that column by performing a parallel sort as mentioned previously. After which the beginning and end of each group is found out sequentially and then for each of those groups, the count or the aggregate functions (SUM, MIN, MAX, AVG) are computed in parallel.

Select with aggregate
Aggregate without any sort of filtering conditions on it, follows a different procedure. The data is divided into sections and each section of data is assigned to a thread to perform the aggregate function on that data section. After all the threads calculate the partial output, they send it to the master thread for further processing. The master thread further applies the aggregate function on the partial output calculated by each thread to obtain the final output. If the input query has a conditional filteringthen the relevant records are first obtained then aggregate functions are applied to this data as mentioned above.

Update
Update query also involves getting relevant records in parallel. Once this is done, we update these records to the new values specified in the query in parallel.

Delete/Insert
Delete query involves deleting records from the table. Deleting a record implies a logical delete from the table and it doesn't assure a physical delete from the memory. The relevant records can be obtained with or without conditional filtering. When records need to deleted based on a condition then, relevant records to be deleted are obtained in parallel in the same manner as select with a conditional filtering as mentioned previously. On obtaining the relevant records, the master thread assigns a section of records to each of its child threads to delete those records simultaneously.
Deleting a record doesn't necessarily delete it form the memory, and the records in this memory shouldn't be used for future query operations. Hence management of this memory is an important issue. To tackle this issue and to have an optimal trade between space and time, we have maintained a queue of fixed size that holds the indexes of the dead records. The indexes of the dead records are added to this queue till the queue is full. Once the queue is full,those records whose indexes are stored in the queue are deletedphysically and reordering is done. We then flush the contents of the queue. Reordering is a costly and a time consuming process as itinvolves deleting dead records from the memory and creating newindexes for the existing records. Reordering prevents storing andprocessing of dead records so reduces the execution timenoticeably. So, only when the queue is full, reordering operation isexecuted in the query plan.
When an insert happens, if the queue isn't empty, then the new record is inserted in the place of the record whose index is dequeued from the queue. If the queue is empty, then record is inserted after the last record in the table.

Queries involving JOIN

We can have SELECT, UPDATE and DELETE queries involving multiple tables that require a JOIN. Instead of doing a cross product which consumes lot of memory and time, our system first fetches the relevant records from the tables involved in parallel. We then sort in parallel the array containing indexes based on the column over which it has to be joined. Later we find the match for each of these record in parallel to create a new table.

Scheduling Algorithms

We have compared between three scheduling algorithm to analyse which would achieve maximum load balancing and maintain data locality with the least dispatch overhead. In static even scheduling the loop iterations are divided into N chunks and each chunk is assigned to a processor statically. In dynamic scheduling a chuck of the loop iteration is dispatched to an idle thread at the runtime. Guided scheduling is similar to dynamic scheduling but here the chunk sizes keep shrinking till it reaches a predefined value.

IMPLEMENTATION AND RESULTS

We have implemented parallel querying on an inventory database consisting of two tables.The tables are item table and transaction table. Item table consists of *item_code, item_name, item_price, item_type, item_quantity and item_reorder_level*. Transaction table consists of *transaction_id, item_code, transaction_quantity, total_price and transaction_date*. The whole database system has been implemented in C. OpenMP has been used for the parallel execution. It uses the fork-join model of parallel execution where the master thread creates a team of threads and the parallel region construct is executed in parallel among the member threads. When the member threads complete executing the parallel region construct, they synchronize and terminate, leaving only the master thread. Load balancing has been achieved by assigning tasks to threads using static, dynamic, guided scheduling.A noticeable increase in the performance has been observed on parallel execution of queries. Here we analyse the improvement based on the number of threads among which tasks have been scheduled and the number of tuples on which the query occurs. We shall quantitatively represent the betterment of the execution using speedup and efficiency. Speedup is a measure for the improvement in performance between two systems working on the same problem. If T_{serial} is the time taken for sequential execution and T_{parallel} is time taken for parallel execution , then speedup is given by

$$S = \frac{T\text{serial}}{T\text{parallel}} \qquad (1)$$

Efficiency is ratio of speedup to the number of processors(or threads) executing concurrently. It is a value between 0 and 1.

$$\eta = \frac{S}{p} \qquad (2)$$

When an update query was taken for example:

"UPDATE *item*
SET *item_price* = 50 WHERE *item_code* IN (SELECT *item_code* FROM *transaction* WHERE *transaction_id* > 5);"

The sequential time taken for the execution of query is 212.159s while parallel execution with 8 threads is 170.050s. The speedup is 1.185 and the efficiency is 0.148. The values are shown in Table 1.

When a select query with filtering is taken as an example:

"SELECT *item_name, transaction_id* FROM *item*, *transaction* WHERE *item.item_code*> 20 AND *transaction_id*> 30 AND *item.item_code = transaction.item_code*;"

The sequential execution time for this query is 4.437s while the execution time when executed in parallel is 2.314. The speedup observed here is 1.917 while the efficiency has been increased by 0.119. The result is shown in Fig.1

We have analysed different scheduling techniques for a query when the data size is 50000 and the chunk size is 8.Fig.3 is the graph obtained for the same.

It is clear from the graph that dynamic scheduling achieves the maximum load balancing followed by static scheduling. This is because threads are less idle in this scheduling as master thread

assignschunk to that thread which finishes the work faster and is idle.
We have observed that queries involving a join have a better performance gain as we have parallelised retrieval of relevant records from the item and transaction table. UPDATE, SELECT and queries involving aggregate have also given a good performance.

CONCLUSION

Parallelisation of query execution improves the performance of the database system especially on huge databases. It ensures effective utilisation of resources and rendering of results to the user at a faster pace. On analysing the results obtained, we have observed the optimisations mentioned in the paper are most effective on a large dataset. Also these parallelisation techniquesare most effective in queries involving multiple relations. Further it has beenobserved that parallel execution proves to be effective when there is sufficient memory to support additional memory-intensive processes such as sorts, hashing, and I/O buffers. We would want to further extend this parallelisation to distributed memory systems, Symmetric multiprocessors (SMP)and massively parallel systems (multiple CPU's) to increase the portability of our system.

REFERENCES

[1]David J. DeWitt and Jim Gray, Parallel Database Systems: The Future of Database Processing or a Passing Fad?, Microsoft Research, November 1991.
[2]Oracle, Parallel Execution of SQL Statements, Oracle, accessed October 8, 2015, http://docs.oracle.com/cd/B10500_01/server.920/a96524/c20paral.htm
[3]Peter S. Pacheco, An Introduction to Parallel Programming,1st Edition,Morgan Kaufmann Publishers, Burlington, USA, 2011.

Table 1

Data Size	Sequential	2 threads	4 threads	8 threads	16 threads
200	0.000272	0.001637	0.000445	0.000954	0.000786
20000	0.632578	0.338704	0.328626	0.353855	0.351529
200000	104.389779	79.843712	47.961750	51.862663	53.505413

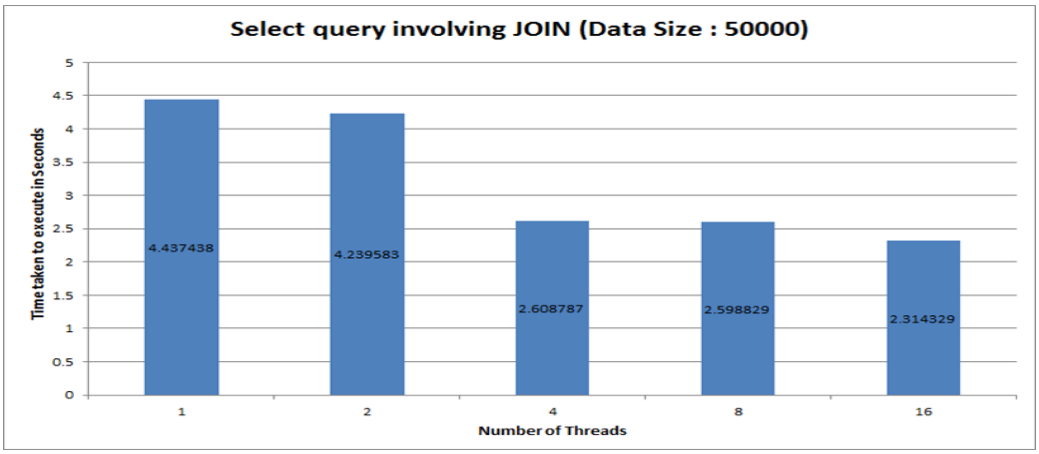

Fig.1 SELECT Query involving JOIN

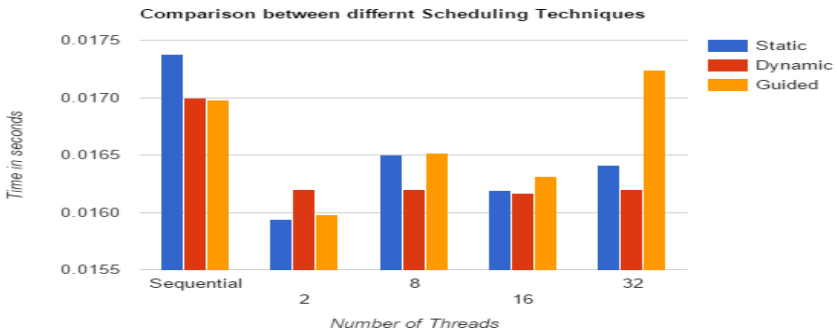

Fig.2 Comparison between different Scheduling Techniques

5th International Engineering Symposium - IES 2016
March 2-4, 2016, Kumamoto University, Japan

Medical diagnostics and cure prediction

Deepthi M Hegde

Undergraduate Student, Department of Information Technology, National Institute of Technology Karnataka, Surathkal, Mangalore 575025, India.
e-mail:deepthimhegde@gmail.com

ABSTRACT: The growing demand for digitization and automation of healthcare in recent years has motivated extensive research in the field. Numerous probabilistic and set theoretic approaches have been developed on clinical data that exhibit acceptable levels of accuracy. However, complex and hybrid data models have seldom been explored. This paper proposes a Pipeline Model to develop a system that diagnoses the disease based on the symptoms of the patient and suggests a cure accordingly. Supervised learning techniques are used for disease diagnosis and fuzzy matching of patient parameters is used to predict the cure for the diagnosed disease. The model simulates a human doctor.

***Keywords**: healthcare, clinical data, pipeline model*

INTRODUCTION

The advent of the digital age has revolutionised the scope and reach of technology. A number of online healthcare platforms have brought home the technology that avails medical attention to every remote corner of the world. This has led to a tremendous increase in online clinical data which can be tapped to extract valuable predictive results. Knowledge acquisition from experts plays a key role in medical expert systems. In order to automate this process, many inductive learning methods, such as induction of decision trees (Breiman, et al. 1984; Quinlan 1993) rule induction methods (Michalski 1983; Michalski, et al. 1986; Quinlan 1993) and rough set theory (Pawlak 1991; Ziarko 1993), are introduced and applied to extract knowledge from databases, which shows that these methods are appropriate. Matsumura et al. proposed a diagnostic model, which consists of three reasoning processes, and developed an expert system, called RHINOS (Rule-based Headache and facial pain INformation Organizing System) (Matsumura, et al. 1986).

This paper discusses a pipeline model called RoboDoc, that simulates the procedure carried out by a human doctor on a patient right from making an initial diagnosis to prescribing a suitable treatment. First, based on the symptoms as seen by the patient a broad classification of the disease is made. Further, based on the class of disease the symptoms belong to, observations and test results are fed as features for the learning model. As we move down the pipeline, more data is collected and links are made between symptoms and diagnosis. The class of predicted disease becomes narrower and results in a specific disease. This diagnosis is mapped with the previous records of patients with the same diagnosis and closest characteristics (same age, sex etc.) and symptoms with the patient under consideration to obtain the cure. This can also be personally modelled to replicate a doctor or a hospital by selectively learning on how a doctor or a hospital treats diseases. The stages in the pipeline are as shown in Fig. 1.

METHODOLOGY

The pipeline consists of 2 parts:

1. Diagnosis
2. Cure prediction

***Diagnosis**:*

Stage 1:

Classes of diseases and their symptoms are built as knowledge graphs from the data obtained from the website

http://www.medicinenet.com. Tumour and its symptoms are depicted in Fig. 2. Distinguishing symptoms are symptoms that are necessary and sufficient to identify the class of disease that a set of symptoms belong to. Distinguishing symptoms are identified for each of the disease classes through medical expertise and are considered to be unique. Examples of disease classes are- heart disease, liver disorder, stomach disease, tumour etc. The symptoms of the patient are compared with these distinguishing symptoms of each class and a match is obtained.

Stage 2:

Depending on the class identified in stage 1, the observations specific to the identified class of diseases are extracted and fed to an SVM (Support Vector Machine) classifier which narrows down the prediction to a specific disease in the class. For example, if the output of stage 1 is "tumour", the output of stage 2 could be "brain tumour".

Stage 3:

This stage uses Logistic Regression or SVM to go one level further down in predicting the type or level of disorder of the disease.

Cure prediction:

List of treatments for the diseases are obtained from the website http://www.medicinenet.com.

The patient with the closest match of symptoms and characteristics (like age, sex etc.) is mapped to the patient at hand and the treatment that was given to the matched patient is advised for the patient under consideration. Fuzzy matching technique is used for comparison and percentage of match.

Depending on the disease, the diagnosis may go through any number of pipeline stages.

IMPLEMENTATION

Diagnosis:

Stage 1: Diagnosis and treatment of tumour was considered. Swelling and presence of lumps in the body is taken as the distinguishing symptom for tumour.

Stage 2: A subset of primary-tumour dataset from UCI repository was chosen to classify the tumour. The dataset consisted of 339 instances and 16 attributes. The classes consisted of lung, head & neck, thyroid, stomach, pancreas, gall bladder, kidney, ovary, corpus uteri and breast tumour. This was trained using SVM (Support Vector Machine) classifier and tested.

Stage 3: A subset of Wisconsin breast cancer dataset was used to detect whether the tumour was malignant or benign. The dataset consisted of 520 instances and 11 attributes.

UCI lung cancer dataset was used to classify lung tumour as malignant or benign. The dataset consisted of 32 instances having 57 attributes each.

Cure prediction:

The patient's symptoms and characteristics were fuzzy matched with the records of patients in the database. A threshold of 80% was defined for each match. The treatment given to the patient with the highest percentage of symptoms and characteristics match was advised for the patient under consideration. For simulating a single doctor, a match was made against only those patients that the doctor has treated previously.

RESULTS

SVM on tumor dataset gave results with an accuracy of 51.85% and 68% precision.

SVM on breast tumor gave results with an accuracy of 68.43% and 66% precision.

SVM on lung tumor gave results with an accuracy of 71.42% and 100% precision.

CONCLUSIONS

In this paper, the conception and implementation of RoboDoc, a pipeline method for diagnosing and predicting cure for diseases is discussed which simulates the real-time diagnosis and treatment carried out by human doctors on ailing patients. This model replicates the process carried out by a human doctor with considerable efficiency.

ACKNOWLEDGEMENTS

The Ministry of Education, Government of Japan provided financial support to carry out this research and we are very grateful for their encouragement. We would also like to thank Prof. Katta, Dean (academic)

NITK and Prof. Torii, Kumamoto University, the administration of NITK and TEQIP for giving us this opportunity and for their support.

FUTURE WORK

The model considers only single disease cases. Complicated and multiple disease cases need more processing in order to identify multiple classes and to make predictions. The future symptoms that the patient might encounter can be predicted with the help of knowledge graphs.

REFERENCES

[1] Breiman, L., F'reidman, J., Olshen, R., and Stone, C. (1984). Classification And Regression frees. Belmont, CA: Wadsworth International Group.
[2] Matsumura, Y., et al. (1986). Consultation system for diagnoses of headache and facial pain: RHINOS. Medical Informatics, 11, 145-157
[3] Michalski, R. S., Mozetic, I., Hong, J., and Lavrac, N. (1986). The Multi-Purpose Incremental Learning System A&15 and its Testing Application to Three Medical Domains. Proceedings of the fifth National Conference on Artificial Intelligence, 1041-1045, AAAI Press, Palo Alto.
[4] Pawlak, Z. (1991). Rough Sets. Kluwer Academic Publishers, Dordrecht.
[5] Quinlan, J.R. (1993). C4.5 - Programs for Machine Learning, Morgan Kaufmann, CA.
[6] Ziarko, W. (1993). Variable Precision Rough Set Model. Journal of Computer and System Sciences, 46, 39-59.

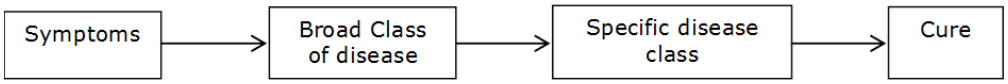

Fig. 1. Pipeline Architecture

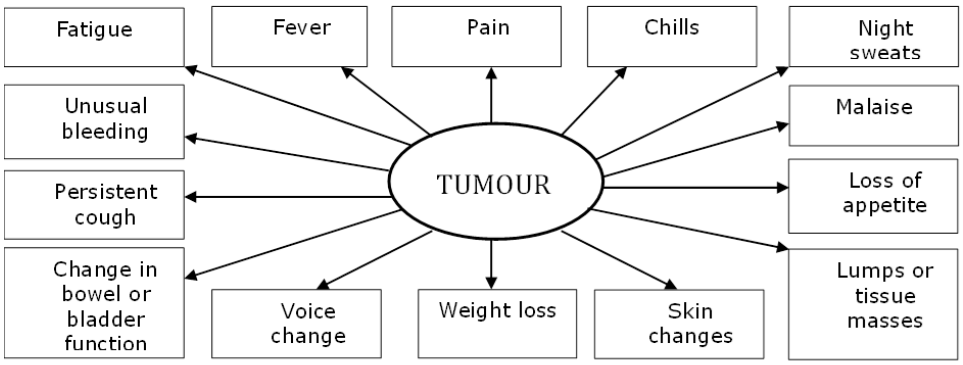

Fig. 2. Symptoms of tumour

5th International Engineering Symposium - IES 2016
March 2-4, 2016, Kumamoto University, Japan

Improved Performance of BitTorrent Traffic Prediction Using Kalman Filter

Hari Sankar S[1], Pranav Channakeshava[2] and **Pathipati Srihari[3]**

1,2 Undergraduate, Department of Electronics and Communication Engineering, National Institute of Technology Karnataka, Surathkal, Mangalore 575025, India.
Email: harisankarhss@gmail.com[1], pranav_channakeshava@ieee.org[2]
3 Assistant Professor, Department of Electronics and Communication Engineering, National Institute of Technology Karnataka, Surathkal, Mangalore 575025, India.
Email: srihari.js@gmail.com

ABSTRACT: Supervising internet traffic is essential for any Internet Service Provider (ISP) to dynamically allocate bandwidth in an optimized manner. BitTorrent is a well-known peer-to-peer file-sharing protocol for bulky file transfer. Its extensive bandwidth consumption affects the Quality of Service (QoS) and causes latency to other applications. There is a strong requirement to predict the BitTorrent traffic to improve the QoS. In this paper, we propose a Kalman filter (KF) based method to predict the network traffic for various traffic data sets. The observed performance of KF is superior in terms of both Mean Square Error (MSE) and total computation time, when compared to Auto Regressive Moving Average (ARMA) model.

***Keywords**: BitTorrent, Kalman filter, MSE, ARMA, prediction*

INTRODUCTION

BitTorrent has emerged as a widely popular peer-to-peer (P2P) content distribution protocol over the Internet. It offers scalability and effective utilisation of bandwidth through swarming file delivery, which makes it very attractive for large file transfers. As opposed to the traditional client-side paradigm, BitTorrent uses a node in the network to share its content to its peers by acting as a source. Its "rarest first" approach for transfer of blocks of data emphasises on fast and efficient content distribution by organizing peers which share the same file, into a P2P network.

As P2P systems support important and reliable services like bulky data sharing, video streaming and Voice-over-IP, they have been reported to generate around 70% of internet traffic globally [11]. Their popularity has led to financial benefits for Internet Service Providers (ISPs), as users tend to upgrade to broadband for better performance. Given the high bandwidth utilization by the BitTorrent protocol, several issues of traffic engineering challenges have been continuously raised. The protocol's decisions are based on the application layer routing and are independent of the network topology, which causes an increase in the cross-ISP traffic [3]. As it generates a high volume of packet transaction, it causes users, who are not using the BitTorrent protocol, to experience packet loss if they are connected to the same LAN as that used by the BitTorrent users. This has led to ISPs limiting a user's P2P traffic to ensure fairness among all users of the network.

A lot of research has been done in the past, on looking into how this issue can be solved through ISPs analysing the traffic patterns, so that they can plan a throttling mechanism to ensure that all users get similar network resources. Hoong et al. (2012) proposed a prediction model using the Auto Regressive Moving Average (ARMA) time series model. In this paper, we propose an improved model for predicting the BitTorrent traffic based on Kalman Filtering which gives better accuracy, as measured by the mean square error and is also faster in terms of

the computation time. We compare the results of the ARMA prediction with that of the KF predictor to analyse their performance for seasonal BitTorrent network traffic data.

BASICS

BitTorrent Protocol

BitTorrent adopts a swarming approach through a set of peers, who can upload or download data from each other simultaneously. The protocol organizes the peers into a 'Torrent' network that has interactions among the peers and occasionally with the server for locating new peers. The peers are classified as a downloader or a seed, where downloaders are the peers who possess a part of the file while the seeds are the peers having the complete file. The seeds stay online in the network in order to share their data content while the downloaders obtain the parts of the file, which they do not have. The downloaders can subsequently become the seeds once they have the complete file.

In order to allow the client to arrange the pieces that are downloaded non-sequentially, each part of the file is hashed by a cryptographic torrent descriptor. As a result, the protocol allows for sudden halts in the download process at any instance without losing the already downloaded data. This also allows the client to search for the readily available pieces and initiate their download immediately rather than wait for sequential pieces that may not be available. These advantages play a crucial role in reducing the file transfer time.

The peer selection mechanism used by BitTorrent consists of the tit-for-tat, anti-snubbing, optimistic unchoking and upload-only strategies. These ensure that the download performance of the peers, who act as seeds in the network, is better than that of peers who act as free riders and do not contribute to the sharing [9].

Auto Regressive Moving Average

Auto Regressive Moving Average (ARMA) is a time series stochastic model consisting of the Auto Regressive (AR) part which sums the previous observations, and the Moving Average (MA) part which consists of the sum of previous error terms. The model is represented by Eq. 1.

$$X_t = \sum_{i=1}^{p} \theta_i X_{t-1} + \sum_{i=1}^{q} \emptyset_i \varepsilon_{t-1} + \varepsilon_t \qquad (1)$$

The first term in Eq. 1 refers to AR process and second term to MA process with their respective parameters θ_i and $\emptyset_i$. The terms are summed with Gaussian white noise ε_t. The parameters have to be determined to characterize a model. The p and q parameters characterise the AR and MA components of ARMA respectively. Different orders of ARMA are used to describe stationary time series and prediction based on the causal data.

Kalman Filter

Kalman filtering (KF) is an established technique proposed by Kalman (1960). It is often used in estimation theory as an optimal predictor of the parameters of the state equations. The filter is fed the differences between the actual and predicted state variables as input. It minimizes the MSE and produces an estimate for the next time instance. The recursive equations process the newly observed data and estimate the state vector with the given information about previous data samples at time t.

KF assumes a linear stochastic equation for the estimated value x_k , which is a linear combination of its previous values plus the control signal u_k and a process noise w_k, which is Gaussian. The measurement value z_k is expressed as a linear combination of the signal value and the measurement noise.

$$x_k = Ax_{k-1} + Bu_k + w_k \qquad (2)$$

$$z_k = Hx_k + v_k \qquad (3)$$

KF uses a prediction step which is given by the following time update equations:

$$\hat{x}_k = A\hat{x}_{k-1} + Bu_k \qquad (4)$$

$$P_k = AP_{k-1}A^T + Q \qquad (5)$$

The equations project the next state and the error covariance. The prior estimate $\hat{x}_k$ gives the rough estimate before the measurement update correction. The prior error covariance is P_k. The prior values are used in the following measurement update equations.

$$K_k = P_k H^T (H P_k H^T + R)^{-1} \quad (6)$$
$$\hat{x}_k = \hat{x}_k + K_k (z_k - H\hat{x}_k) \quad (7)$$
$$P_k = (I - K_k H) P_k \quad (8)$$

These equations estimate x at time k by evaluating $\hat{x}_k$. Also, computing the error covariance P_k is necessary for the future estimate, together with $\hat{x}_k$. Once the correction is done for the measurement update, the next prediction is estimated using the time update equations and this process is iterated.

KF prediction is recursive where it processes a data sample at a time instead of all the previous samples. The previous data is represented in X_n and therefore, there is no need to store the data. The Kalman gain factor K_k considers the previous estimates while predicting the future values.

IMPLEMENTATION

We base our study on the BitTorrent data collected using Wireshark, which is a network protocol analyser. A BitTorrent application was utilized to start the P2P communication and 5 sets of data packets were gathered during various times of the day. Network traffic was filtered for only TCP and UDP packets. We then convert the time series into CSV format and analyse it using MATLAB. We difference the time series to obtain the number of packets per second (frequency). Log transformation was applied to enhance the minute variations. We then perform a box centering using a rectangular window of size 10 and 50% overlap, to get a stationary time series.

We use the data sets for the prediction models. We compare the performance of the Kalman prediction with the ARMA model, by computing the Mean Squared Error (MSE) and the computation time. For the ARMA (p,q) model, different values of p and q were estimated and tried on all the 5 data sets. MSE is calculated based on the difference between the predicted data and actual data. The scaled stationary time series is also used for the Kalman predictor, to obtain its prediction accuracy. We assume a Gaussian random noise of variance 0.01.

RESULTS AND DISCUSSION

The prediction has been tested for 5 different data sets. For ARMA, we observe that ARMA (2, 1) predicts with the least MSE although ARMA (3, 0) is a close competitor. By adopting Kalman prediction, we find the prediction to be much improved. Figure 1 shows the superimposition of ARMA (2, 1) and KF for time series A which is validated against the actual bit torrent data. The comparison of MSE of KF prediction and different ARMA models for 5 data sets is shown in Table 1.

We have collected seasonal BitTorrent data and the MA parameter q is significant for the data since we assign same weights to all the observations irrespective of the peaks and valleys in the plot. ARMA (2, 1) proves to be better for predicting seasonal traffic patterns while ARMA (3, 0) is suitable for cyclic patterns which can be studied at a later stage. Variation in seasonal patterns allows us to estimate the pattern accurately only to a certain extent. This variation can be better estimated through the time update iterations of the Kalman filter and as such, a lower MSE is observed.

As seen from Table 1, it is clear that KF based method reduces the MSE by a factor of 5, and as such provides a more accurate model for predicting BitTorrent traffic. Table 2 compares the computation time required by the ARMA model and KF predictor as measured on MATLAB 2015a on a Windows 8 platform with 8GB RAM. It is evident that KF is much faster than ARMA estimation in terms of its speed of computation.

CONCLUSIONS

Given BitTorrent's popularity for large file transfer over the Internet, its use has been increasing significantly over the last decade. Though it represents an efficient mechanism for fast data transfer, its high bandwidth usage causing unequal resource distribution amongst network users has been an issue for ISPs, leading to restrictions placed on such transfers. One possible way to address this issue is through predictive measures by ISPs to ensure an equitable distribution.

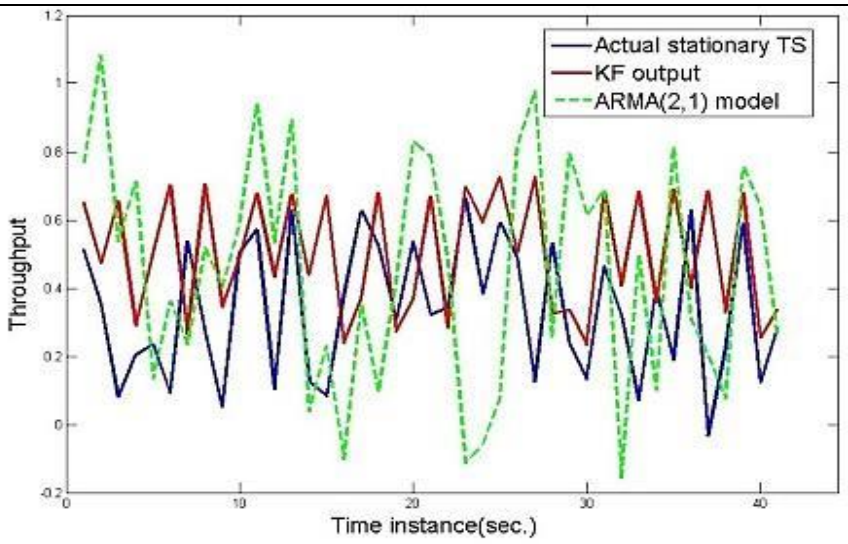

Fig.1 BitTorrent Prediction using Kalman Filter predictor and ARMA (2,1)

We propose the Kalman Filter based predictor as an effective model to estimate bandwidth requirements for BitTorrent traffic data. The technique proves to be a more accurate model as it achieves lower MSE when compared to previously proposed ARMA model by Hoong et al. (2012). Our prediction technique produces better estimates and is also superior in terms of its computation speed when compared to ARMA.

Thus, the prediction model can be used by ISPs to better understand BitTorrent traffic data, which will enable them to effectively allocate network resources in a more equitable manner amongst its users.

REFERENCES

[1] A. R. Bharambe et al. (2006) "Analyzing and Improving BitTorrent Network's Performance Mechanism", In the proceeding of the 25th IEEE International Conference on Computer Communications, pp. 1-12.
[2] Bar-Shalom et al. (1993), Estimation and Tracking: Principles, Techniques and Software, Artech House Boston
[3] David R. Choffnes et al. (2008) Taming the torrent: a practical approach to reducing cross-isp traffic in peer-to-peer systems. SIGCOMM Comput. Commun
[4] DongyuQiu et al. (2004), "Modeling and Performance Analysis of BitTorrent-Like Peer-to-PeerNetworks", In the Proceedings of the conference on Applications, technologies, architectures, and protocols for computer communications
[5] Huang, S. J., Shih, K. R. (2003). Short-term load forecasting via ARMA model identification including non-Gaussian process considerations. Power Systems, IEEE Transactions on, 18(2), 673-679.
[6] Hoong, P K et al. (2012), Bittorrent Network Traffic Forecasting With ARMA, International Journal of Computer Networks & Communications (IJCNC) Vol.4, No.4, July 2012
[7] Kalman R.E. (1960), A new approach to linear filtering and prediction problems, Trans. ASME J. Basic Engrg., ser. D, 82, 35—45
[8] Kalman R.E. et al. (1961), New results in linear filtering and prediction problems, Trans. ASME J. Basic Engrg., ser. D, 83, 95--108.
[9] Kunjie Xu (2013), Performance Modeling of BitTorrent Peer-to-Peer File Sharing Networks, Graduate Telecommunications and Networking Report, University of Pittsburgh
[10] "BitTorrent", http://bittorrent.com
[11] IPOQUE. Internet Study 2007: Data about P2P, VoIP, Skype, file hosters like RapidShare and streaming services like YouTube, November 2007. *http://www.ipoque.com/media/internet_studies/internet_study_2007*

Table 1 Comparison of MSE

SET	ARMA (2,0)	ARMA (2,1)	ARMA (2,2)	ARMA (3,0)	ARMA (3,1)	KF
A	0.10	0.089	0.091	0.092	0.093	0.024
B	0.095	0.090	0.094	0.094	0.12	0.035
C	0.096	0.092	0.095	0.095	0.12	0.029
D	0.098	0.088	0.098	0.090	0.12	0.026
E	0.099	0.089	0.097	0.094	0.10	0.032

Table 2 Comparison of Computation Time (sec)

SET	ARMA (2,0)	ARMA (2,1)	ARMA (2,2)	ARMA (3,0)	ARMA (3,1)	KF
A	20	25	26	27	29	0.54
B	18	24	25	25	24	0.53
C	15	24	24	25	22	0.50
D	12	23	24	23	21	0.49
E	12	20	21	21	20	0.48

Compound Word Generator for Sanskrit based on Sandhi Rules given by Panini(Paninian Grammar)

Vaishakh K[1], Pravalika A[1], Abhishek D V[1], Sowmya Kamath S[2] *and* **Prakash P[3]**

1 *UG Students, Department of Information Technology, National Institute of Technology Karnataka, Surathkal, Mangalore 575025, India.*
email:kvaishakhnambiar@gmail.com
email:avvarupravalika@gmail.com
email:dv.abhishek@gmail.com
2 *Assistant Professor, Department of Information Technology, National Institute of Technology Karnataka, Surathkal, Mangalore 575025, India.*
email:sowmyakamath@nitk.ac.in
3 *Assistant Lecturer, Department of Information Technology, National Institute of Technology Karnataka, Surathkal, Mangalore 575025, India.*
email:athi4prakash@gmail.com

ABSTRACT: Sanskrit is one of the oldest languages of the world. It is a very structured language and has context free grammar. Compound words are very common in Sanskrit. Sandhi(joining or compound word generation) is a phonological process that occurs at the morpheme or word boundaries based on Paninian Grammar. Panini in his work "Ashtadhyayi" has given the rules for various Sandhi in terms of the 14 Maheshwara Sutras. Our system is built based on these rules. This generator incorporates all the Svara, Vyanjana and Visarga Sandhi. Sandhi is of high importance in Natural Language Processing(NLP) perspective. This system can be integrated with a Sanskrit Machine Translation(MT) system, Search Engine where analysis of compound words is required.

Keywords*: Sandhi, Natural Language Processing, Morpheme.*

INTRODUCTION

"Compound Word Generation" involves combination of more than one word into a single word which conveys the same meaning as that of the collection of component words together. Sanskrit language is rich in compound formation. Almost every fifth word in any Sanskrit text is a compound. Panini in his work "Ashtadhyayi" has given a lot of rules which deal with the semantic conditions and grammatical processes involved in the compound formation. Compound formation can be of various types.

In this paper, we present a Compound Word Generator for Sanskrit,that is based on the Sandhi rules given by Panini, in his 4th century BC work "Ashtadhyayi". We first studied the Sandhi rules and designed the proposed system to accept and analyse two given morphemes to determine the most appropriate Sandhi, and then generate a compound word. We have included all the Svara, Vyanjana and Visarga Sandhi and have also taken care of the exception cases which depend on factors like the morphology of the word. The designed system can be integrated with a Machine Translation (MT) system, a Search Engine for Sanskrit or any other applications which involves linguistic computation of compound words.

SANSKRIT LANGUAGE

Sanskrit is an Indian classical languagewith an ancient history. The word Sanskrit itself means 'well formed' or 'refined'. Sanskrit language is very structured and is supposed to have a context-free grammar. The phonology and morphology of Sanskrit make it very special when compared to other classical and modern languages. It is to be noted,

that over the years, there has never been any change in the science that defines the Sanskrit grammar.

In Sanskrit, a word is formed from a root word called 'dhatu' in a precise grammatical order. Any number of desired words could be formed through root words and the prefix and suffix system as explained by Panini in his work "Ashtadhyayi". One could form 90 forms of each verb and 21 forms of each noun/pronoun, thus enabling their usage in any situation and multiple contexts. The sound of each of the vowels and consonants are fixed and precise and thus never alter. The words in Sanskrit language always have had the same pronunciation as they have today. It is said that Panini conceived fourteen sounds from Lord Shiva's musical instrument called the damru, and described the grammar for Sanskrit in his work "Ashtadhyayi". These 14 sounds form the Maheshwara Sutras, and are shown in Fig.1

SANDHI FORMATION

Every language has a set of sounds that makes up the words and sentences. The sounds are quite easy to pronounce, especially for native speakers. Even though the sounds might be easy to pronounce when they are separate, some of them can become quite difficult when they are put together, especially when speaking quickly. So to simplify pronunciation, euphonic changes are made. This is referred to as Sandhi in Sanskrit.

The word "Sandhi" means junction or combination. It refers to the combination of two sounds that occur next to each other. A Sandhi rule can be expressed as a triple (x, y, z) where x is the last sound of the first primitive, y is the first sound of the second primitive and z is the letter sequence resulting from the euphonic combination of x and y.

Generation of compound word based on Sandhi rules depends on the following:

1) Sequence of phonemes
2) Morphology of the words
3) Meaning of the words
4) Ontological category of the words

Sandhi can be broadly classified into 3 categories.

1) Svara Sandhi (Vowel)

The basic principle of Svara Sandhi is that two vowels cannot be next to each other. If the last sound of the first word and the first sound of the second word are vowels, then Svara Sandhi can happen.Svara Sandhi is basically of two types. Namely,combination of similar vowels and combination of dissimilar vowels. The former one results in a corresponding long vowel while the latter one resultsin a letter sequence which depends on the first vowel.

Examples: xeva + AlayaH = xevAlayaH
iwi + Aha = iwyAha

In certain cases the morphology of the words effects the Sandhi formation. If a preposition ending with 'a' is followed by a vowel then the compound word generated will not follow the usual rule. When the first word is a dual ending with 'I', 'U' or 'E' is followed by a dissimilar vowel there is no Sandhi happening.

Examples: pra + ejawe = prejawe
harI + ewO = harI ewO

2) Vyanjana Sandhi (Consonant)

There are two possibilities namely consonant+vowel,consonant+consonant. Vyanjana Sandhi usually involves replacing one consonant by another. The consonant must be changed so that it matches the following consonant. The matching of the consonant can be based on voicing alone or both voicing and place of articulation. So there should be a proper analysis on the class to which the sound belongs to.

Examples: waw + ca = wacca
Rat + mAsAH = RaNmAsAH

3) Visarga Sandhi

If the first word ends with a Visarga, then Visarga Sandhi can happen.Depending on the letter that follows the Visarga, the Visarga can be substituted by 'S', 'R', 's', 'o', 'r'. There are also cases when the Visarga is just dropped.

Examples: rAmaH + ca = rAmaSca
saH + iccawi = sa iccawi

IMPLEMENTATION DETAILS

We have used WX notation for the input and output. WX notation is a transliteration scheme for representing Indian languages in ASCII. It is widely used among the Natural Language Processing community in India. Fig.2, Fig.3 and Fig.4 depict the WX notation of Sanskrit letters.Algorithm 1 illustrates the workflow of the proposed system.

Algorithm 1

1. Input two morphemes represented in WX notation.
2. Check the last letter of the first word and first letter of the second word to determine the type of Sandhi.
    1. If both are vowels then, Svara Sandhi.
    2. If the first word ends with a Visarga then, Visarga Sandhi.
    3. If there is a consonant at the end of first word or at the beginning of second word then, Vyanjana Sandhi
3. Determine the exact Sandhi rule based on the words.
4. Output the compound word in WX notation along with the Sandhi name.

Once we determine the category of the Sandhi, we analyse the two letters to determine the exact Sandhi. Before generating the compound, we see if it comes under the exception cases based on the morphology of the words. The morphology of the word tells about its root word, gender, number, POS etc. If it follows an exception case, then the word is generated based on this exception. If not, the word is generated based on the standard rule to which the present words belong to.

The proposed system is implemented such that the number of comparisons required in determining the Sandhi is minimal and redundant computations are avoided. In addition, the order in which the Sandhi is checked for is based on the probability of occurrence of theindividual Sandhi. We have looked into a set of Sanskrit texts and have consulted linguists to determine this order. Fig.5 shows the architecture of our proposed system.

RESULTS

We have tested our system for a set of words. The choice of these words was based on how often such words occur in any Sanskrit text. Table 1 describes the accuracy of our system.

- Since we have implemented all the Sandhi rules and included most of the exception cases, our system has a good accuracy.
- Our system is also efficient because we have ordered the checking for Sandhi based on a probabilistic model.

CONCLUSION

In this work, we have proposed a system that can generate compound word based on Sandhi rules given by Panini. All the three Sandhi of Sanskrit language – Svara, Vyanjana and Visarga have been studied and have built a system based on these rules. Further the system handles exception cases thus improving the accuracy. As many Dravidian languages are based on Sanskrit, the proposed system can be employed for those languages also.As a part of future work, we would like to integrate our system with a Sanskrit morphological analyser. This will help in validating the input and will also improve the accuracy.

REFERENCES

[1]Bharati, A., Chaitanya, V., Sangal, R., & Ramakrishnamacharyulu, K. V. (1995). Natural language processing: a Paninian perspective (pp. 65-106). New Delhi: Prentice-Hall of India.

[2]Kale M R, A Higher Sanskrit Grammar, Motilal Banarsidass, Delhi, 1961, pp. 1-32.

[3]KleenankandyJeena, Implementation of Sandhi-rule Based Compound Word Generator for Malayalam,Advances in Computing and Communications (ICACC), 2014, pp. 134-137.

[4]S. Aparna and M. Ingle, Morphological parsing of Sandhi based words in Sanskrit text, Language in India, Volume 4, December 2004.

[5]Vasu, Śrīśa Chandra, ed. The Ashtādhyāyī of Pānini. Vol. 2. Motilal Banarsidass Publ., 1962.

१. अ इ उ ण् ।
२. ऋ ऌ क् ।
३. ए ओ ङ् ।
४. ऐ औ च् ।
५. ह य व र ट् ।
६. ल ण् ।
७. ञ म ङ ण न म् ।
८. झ भ ञ् ।
९. घ ढ ध ष् ।
१०. ज ब ग ड द श् ।
११. ख फ छ ठ थ च ट त व् ।
१२. क प य् ।
१३. श ष स र् ।
१४. ह ल् ।

Fig.1 14 Maheshwara Sutras

अ	आ	इ	ई	उ	ऊ	ए	ऐ	ओ	औ	ऋ	ॠ	ऌ
a	A	i	I	u	U	e	E	o	O	q	Q	L

Fig.2 Svaras in WX notation

अं	अः
M	H

Fig.3 Anusvara and Visarga in WX notation

क्	ख्	ग्	घ्	ङ्	Velar
k	K	g	G	f	
च्	छ्	ज्	झ्	ञ्	Palatal
c	C	j	J	F	
ट्	ठ्	ड्	ढ्	ण्	Retroflex
t	T	d	D	N	
त्	थ्	द्	ध्	न्	Dental
w	W	x	X	n	
प्	फ्	ब्	भ्	म्	Labial
p	P	b	B	m	
य्	र्	ल्	व्		Semi-vowel
y	r	l	v		
श्	ष्	स्	ह्		Fricative
S	R	s	h		

Fig.4 Vyanjanas in WX notation

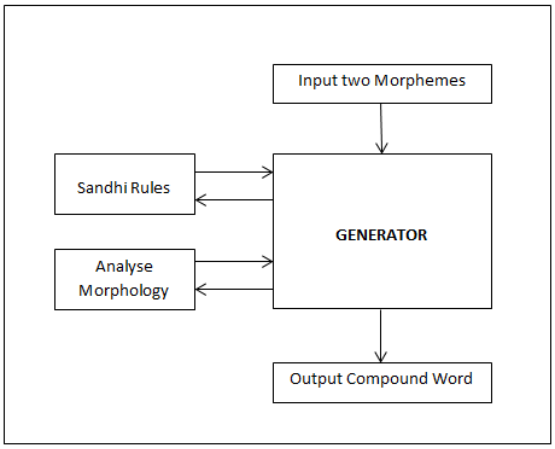

Fig.5 System Architecture

Table 1 Results

Sandhi	Number of words tested	Number of correct results	Accuracy (%)
Svara	100	95	95%
Vyanjana	100	95	95%
Visarga	100	97	97%
Total	300	287	95.6%

PERFORMANCE AND EFFICIENCY OF INDIAN BANKS: A DATA ENVELOPMENT APPROACH (DEA).

Shubham Bhutada [1] and Suprabha K R [2]

1 *UG Student, Department of Civil Engineering, National Institute of Technology Karnataka, Surathkal, Mangalore, 575025, India. e-mail:shubhamb2803@gmail.com*
2 *Assistant Professor, School of Management, National Institute of Technology Karnataka, Surathkal, Mangalore 575025, India. email:suprabha.kr@gmail.com*

ABSTRACT: Banks use public money and their performance is directly related to development of the country. In the present scenario banks are operating in a very competitive and uncertain environment. Therefore a need was felt to compare the public sector banks and their private and foreign counterparts on their productivity and technical efficiency using Data Envelopment Analysis (DEA) Approach. This paper evaluates the extent of pure technical and scale efficiencies in Indian public and private sector banking industry using cross-sectional data for 34 banks in the year 2012-13. To realize the research objectives, a two-stage DEA framework was applied in which the estimates of pure technical and scale efficiencies for individual PSBs were obtained by CCR and BCC models by Max DEA version 5 software. The results showed that only 11 banks were efficient and defined the *efficiency frontier.* Out of these efficient banks, 4 were PSBs and the remaining 7 were from the private sector.

Keywords*: DEA, Technical Efficiency, Productivity, Efficiency Frontier, Performance.*

INTRODUCTION

Economic growth of a country depends on the efficiency and effectiveness of the financial system prevailing in it, where commercial banks plays a major role by supplying the surplus to the needy people. Liberalization, privatization and globalization changed the traditional Indian banking to advanced economic activity. Since 2000, Indian banking sector has undergone drastic changes and development. New entrants have created the concept of competition hence new financial inventions and technology has changed the phase of Indian banking sector. In order to survive in modern competition each and every bank became target oriented through changing rigid terms and conditions to flexible practices. Banks are using public money and their performance is directly related to development of the country. In present scenario banks are operating in uncertain business environment so it is important to determine and evaluate the technical efficiency of these banks. Therefore, a need was felt to compare the public sector banks and their private and foreign counterparts on productivity and efficiency parameters using Data Envelopment Analysis (DEA) Approach.

PRODUCTIVITY AND EFFICIENCY OF BANKS

Efficiency of the banking sector has been a major concern since 1970s. Most of the earlier studies are based on the comparison of the financial and operational performance. While a few studies concentrate on the efficiency of only public sector banks, others look at the relationship between ownership and efficiency. The present study was undertaken to compare the efficiency of public and private sector banks operating in India, to identify the critical factors affecting the efficiency of banks, and to analyze the gap between efficient and inefficient banks. The study has employed the DEA model to analyze the efficiency of banks, and to identify critical factors affecting the efficiency of banks.

DATA AND METHODOLOGY

The study is carried out across 19 public sector banks and 15 private sector banks for the period 2012-2013. Further, the study confines itself to 19 nationalized banks and excludes State Bank of India (SBI) & it's associates as the latter is constituted under separate legislation i.e. SBI Act 1955. Data Envelopment analysis (DEA) is used in this study. Max DEA version 5 software is used here for analysing the efficiencies of banks using DEA. DEA was initially developed by Charnes et al. (1978) as a linear programming algorithm with the intention of examining the efficiency of non-profit organizations in the public sector. The DEA technique defines an efficiency measure of a production unit by its position relative to the frontier of the best performance established mathematically by the ratio of weighted sum of outputs to weighted sum of inputs. This ratio is normalized according to best practical peers and efficiency is calculated to be between 0 and 1, as 1 representing efficient unit.

A measure of technical efficiency under the assumption of constant returns-to-scale (CRS) is known as a measure overall technical efficiency (OTE). The research applied DEA technique based on CCR (named after Charnes et al., 1978) and BCC (named after Banker et al., 1984) models to obtain efficiency measures under CRS (constant return on scale) and VRS (variable return on scale) assumptions. The TE and PTE were determined by CCR (CRS) model and BCC (VRS) model, respectively.

The OTE measure helps to determine inefficiency due to the input/output configuration as well as the size of operations. The efficiency measure corresponding to VRS assumption represents pure technical efficiency (PTE) which measures inefficiencies due to only managerial underperformance. A measure of scale efficiency (SE) can be obtained by comparing TE measures derived under the assumptions of constant returns-to-scale (CRS) and variable returns-to-scale (VRS).
The CCR mathematical model is defined by equation 1
The BCC mathematical model is defined by equation 2.The BCC model allows a calculation of PTE that is measured without the SE.

1) The CCR model

$$\textbf{Max}=\sum_{r=1}^{s} u_r y_{r0} \Big/ \sum_{i=1}^{m} v_i x_{i0}.$$

$$\textbf{S.t max}=\frac{\sum_{r=1}^{s} u_r y_{rj}}{\sum_{i=1}^{m} v_i x_{ij}} \leq 1$$

$$j = 1, \ldots . n \quad -(1)$$

$$u_r, v_i \geq \varepsilon; \quad r=1 \ldots s, i=1 \ldots m$$

2) The BCC model

$$\textbf{Max}=\sum_{r=1}^{s} u_r y_{r0} + u_0 \Big/ \sum_{i=1}^{m} v_i x_{i0}.$$

$$\textbf{S.t max}=\sum_{r=1}^{s} u_r y_{rj} + u_0 - \sum_{i=1}^{m} v_i x_{ij} \leq 1$$

$$j = 1, \ldots . n \quad -(2)$$

$$u_r, v_i \geq \varepsilon; \quad r=1 \ldots s, i=1 \ldots m$$

Simply, Efficiency means the ability of a firm in transforming its inputs into outputs in the best possible manner. In the present study, each bank is considered as a decision making unit (DMU). Efficiency measurement by DEA requires the specification of inputs and outputs. There has been a constant debate on the choice of inputs and outputs of a bank for measuring the efficiency of the banks. The choice of inputs and output by and large depends on how the financial institutions are viewed in terms of business. The specification can be done either through using production approach or through intermediation approach, and the banking literature has been dominated by these two approaches (Neal, 2004).

This study employs intermediation approach for selecting input and output variables for computing the various efficiency scores for individual public and private sector banks.

Since many researchers like Avkiran (2006), Casu and Molineux (1999), and Colwell and Davis (1992) treat it as superior to production approach. This study uses three inputs and four outputs for measuring cost efficiency. Amount of deposits, interest expenses and operating expenses are the inputs used in this study. On the other hand, investment, loans and advances, interest income and other

income are considered as the outputs. The data are secondary arise from the balance sheets submitted to the Reserve Bank of India for 2012-2013 by the commercial banks.

RESULT AND DISCUSSION.

The DEA model has been run for all banks both public and private sector so considered in study, for computing the technical efficiency under CCR model and pure technical and scale efficiency by BCC model. Of the 19 PSBs, 4 banks were found to be technically efficient since they had OTE score of 1. These banks together define the best practice or efficient frontier and, thus, form the reference set for inefficient banks. Table 2 depicts the efficiency score of public sector banks and table 3 narrates the efficiency score of private sector banks.

In DEA terminology, these banks are called peers and set an example of good operating practices for inefficient banks to emulate. The efficient banks among Indian public sector banks are Bank of Baroda, Bank of India, Syndicate Bank and UCO Bank. The remaining 15 banks have OTE score less than 1 which are deemed to be technically inefficient. OTE score of inefficient score range from 0.92241 of Vijaya Bank to 0.996718 of Punjab National Bank. This finding implies that Vijaya Bank and Punjab National Bank can potentially reduce their current input levels by 7.7 percent and 0.32 percent, respectively while leaving their output levels unchanged. This interpretation of OTE scores can be extended for other inefficient banks in the sample. On the whole, we observed that OTE levels ranged from 1.2 percent to 9.5 percent among inefficient PSBs. 7 out of 15 private sector banks had an OTE of 1. Axis Bank, HDFC Bank, ICICI Bank, Jammu & Kashmir Bank, Kotak Mahindra Bank, Tamilnad Mercantile Bank and Yes Bank are efficient among the private sector banks. The remaining 8 private sector banks are deemed to be technically inefficient.

OWNERSHIP AND EFFICIENCY DIFFERENCES

Six public sector and seven private sector banks were 'locally efficient' as they had a PTE of 1. In DEA literature, the banks attaining OTE and PTE scores equal to 1 are known as 'globally efficient' and 'locally efficient' banks, respectively. In addition, 2 banks namely Punjab National Bank and Canara Bank attained the PTE score equal to 1 and lie on the efficient frontier under VRS assumption. The banks which are efficient under VRS assumption but have been found to be inefficient under CRS case, it can be stated that the OTIE in these banks is not caused by poor input utilization (i.e., managerial inefficiency) rather caused by the operations of the banks with inappropriate scale size. Of the rest of the banks whose OTE is less than one, all are having PTE score less than SE score. This indicates that the inefficiency in resource utilization (i.e., OTIE) is primarily attributed to the managerial inefficiency rather than to the scale inefficiency.

Table 1 provides the descriptive statistics of OTE, PTE and SE scores for both public and private sector banks. It has been observed that mean OTE for 19 PSBs is equal to 0.967, whereas the same for 15 private sector banks is 0.964. This indicates that the private sector banks, on an average, are more or less equally efficient in utilizing inputs like the public sector banks. Further, the variation in OTE has been observed to be almost same in both segments of Indian domestic banking industry. The of the table further states that, on an average, the extent of managerial efficiency as reflected by PTE score, is more in private sector banks relative to public sector banks. This is obvious from the fact that the values of mean PTE have been observed to be 0.9743 and 0.9692 for public and private sector banks, respectively. The results further provide that, on an average, both public and private sector banks have almost identical levels of scale efficiency.

CONCLUSION

This paper evaluates the extent of technical, pure technical, and scale efficiencies in Indian public and private sector banking industry using cross-sectional data for 34 banks in the year 2012-13.

- To realize the research objectives, a two-stage DEA framework has been applied in

which the estimates of technical, pure technical, and scale efficiencies for individual PSBs have been obtained by CCR and BCC models.

- DEA technique is used to evaluate the efficiency scores and it is observed that only 11 out of 34 selected banks are efficient. These 11 banks define the *efficiency frontier.*
- Out of these efficient banks, 4 banks are from the public sector and the remaining seven are from the private sector.
- The present study is carried out for one year i.e. 2011-2012. The results may differ if longer period of time is taken. Also the study considered three input variables and four output variables, however there are many other input and output variables that can be used for evaluating the efficiency.

REFERENCES

1) Angadi VB, (1987), integrated approach to study banks' profitability, Prajnam 16 (4).
2) Rangrajan, C. and Mempilly, P. (1972). Economies of scale in Indian banking in Technical studies for banking commission report. Reserve Bank of India, Mumbai.
3) Rajeev.Meenakshi.(2004):"Liberalization and Productive Efficiency of Indian Commercial Banks: A Stochastic Frontier Analysis".
4) Subramanian G, (1993), Productivity growth in Indian Public Sector banks, Journal of quantitative Economics, 9.
5) Swamy, S. B. and Subramanian G. (1983),Comparative performance of public sector banks in India, Prajnam, 22(2).
6) Tyagarajan (1975), Expansion of commercial banking: An Assessment Economic and Political Weekly, 10.

TABLES

Statistics	Public Sector Banks (PUSB)	Private Sector Banks (PVSB)
Overall Technical Efficiency		
No. of Banks	19	15
Mean	0. 9670	.9641
Median	0. .9671	.9639
Standard Deviation	.03239	.03858
Q1	.9390	.9357
Q3	1.00	1.00
Minimum	.90	.90
Maximum	1.00	1.00
Pure Technical Efficiency		
No. of Banks	19	15
Mean	.9743	.9692
Median	.9865	.9735

Tables 1
Descriptive statistics of OTE, PTE AND SE Score

Statistics	PUSB	PVSB
Standard Deviation	.02607	.03399
Q1	.9547	.9420
Q3	1.000	1.00
Minimum	.92	.91
Maximum	1.00	1.00
Scale Efficiency		
No. of Banks	19	15
Mean	.9948	.9946
Median	.9987	.9979
Standard Deviation	.01614	.00984
Q1	.9970	.9935
Q3	1.0000	1.0000
Minimum	.93	.96
Maximum	1.00	1.00

Table 2

Efficiency Score of Public Sector Banks

S. NO	DMU NAME	OTE Score	OTIE (%)	PTE Score	PTIE (%)	SE Score	SIE (%)	RTS
1	Allahabad Bank	0.949843	5.0157	0.949886	5.0114	0.999955	0.0045	IRS
2	Andhra Bank	0.992455	0. 7545	0.993813	0.6187	0.998634	0.137	IRS
3	Bank of Baroda	1	0	1	0	1	0	CRS
4	Bank of India	1	0	1	0	1	0	CRS
5	Bank of Maharashtra	0.985509	1.4491	0.988468	1.1532	0.997007	0.299	IRS
6	Canara Bank	0.928536	7.1464	1	0	0.928536	7.146	DRS
7	Central Bank of India	0.928347	7.1653	0.928858	7.1142	0.999449	0.055	IRS
8	Corporation Bank	0.985094	1.4906	0.986475	1.3525	0.9986	0.14	IRS
9	Dena Bank	0.97025	2.975	0.972574	2.7426	0.997611	0.239	IRS
10	Indian Bank	0.960321	3.9679	0.961243	3.8757	0.999041	0.096	IRS
11	Indian Overseas Bank	0.958726	4.1274	0.958887	4.1113	0.999832	0.017	IRS
12	Oriental Bank of Commerce	0.961781	3.8219	0.968149	3.1851	0.993422	0.658	DRS
13	Punjab and Sind Bank	0.933673	6.6327	0.936881	6.3119	0.996576	0.342	IRS
14	Punjab National Bank	0.996718	0.3282	1	0	0.996718	0.328	DRS
15	Syndicate Bank	1	0	1	0	1	0	CRS
16	UCO Bank	1	0	1	0	1	0	CRS
17	Union Bank of India	0.987347	1.2653	0.987367	1.2633	0.99998	0.002	DRS
18	United Bank of India	0.953454	4.6546	0.954743	4.5257	0.99865	0.135	IRS
19	Vijaya Bank	0.92241	7.759	0.924502	7.5498	0.997737	0.226	IRS

Table 3

Efficiency Score of Private Sector Banks

S.NO	DMU NAME	OTE Score	OTIE (%)	PTE Score	PTIE (%)	SE Score	SIE (%)	RTS
1	Axis Bank	1	0	1	0	1	0	CRS
2	City Union Bank	0.960406	3.9594	0.973521	2.6479	0.986529	1.3471	IRS
3	Federal Bank	0.963855	3.6145	0.968183	3.1817	0.99553	0.447	IRS
4	HDFC Bank	1	0	1	0	1	0	CRS
5	ICICI Bank	1	0	1	0	1	0	CRS
6	IndusInd Bank	0.940056	5.9944	0.942035	5.7965	0.997899	0.2101	DRS
7	ING Vysya Bank	0.904738	9.5262	0.907193	9.2807	0.997294	0.2706	IRS
8	Jammu & Kashmir Bank	1	0	1	0	1	0	CRS
9	Karnataka Bank	0.907671	9.2329	0.913647	8.6353	0.993459	0.6541	IRS
10	Karur Vysya Bank	0.935653	6.4347	0.941741	5.8259	0.993536	0.6464	IRS
11	Kotak Mahindra Bank	1	0	1	0	1	0	CRS
12	Lakshmi Vilas Bank	0.907222	9.2778	0.943052	5.6948	0.962006	3.7994	IRS
13	South Indian Bank	0.942442	5.7558	0.948962	5.1038	0.993129	0.6871	IRS
14	Tamilnad Mercantile Bank	1	0	1	0	1	0	CRS
15	Yes Bank	1	0	1	0	1	0	CRS

Where,

OTE= Overall Technical Efficiency.
OTIE=Overall Technical Inefficiency= (1-OTE).
PTE= Pure Technical Efficiency.
PTIE=Pure Technical Inefficiency= (1-PTE).
SE= Scale efficiency.
SIE=Scale inefficiency= (1-SE).
RTS=returns-to-scale.
IRS= increasing returns-to-scale.
CRS=constant returns-to-scale.
DRS=decreasing returns-to-scale.

5th International Engineering Symposium - IES 2016
March 2-4, 2016, Kumamoto University, Japan

Tikhonov regularization for Statistical data tomography

Akio Tanaka[1]

1 Researcher, Department of Faculty of Engineering, Kumamoto University , Kurokami, 2-39-1, Kumamoto 860-8555, Japan. e-mail:a-tanaka@kumamoti-u.ac.jp

ABSTRACT: This study was conducted to develop a tomography method, a non-invasive statistical inner structure imaging technique, for statistical data tables. This study proposed the new Tikhonov regularization method for statistical data tomography. The method is designated by the author as Matrix Compression Method (MC Method). This method is useful not only for statistical data but also for underdetermined systems.

***Keywords**:* Tikhonov regularization*, S*tatistical data*,* Matrix Compression Method

1. INTRODUCTION

This study was conducted to develop a tomography method, a non-invasive statistical inner structure imaging technique, for statistical data tables.
Many nationwide and regularly administered surveys are used in Japan. The data obtained from them are useful for planning environmental and energy policies. However, environmental issues are becoming more complicated year by year. More detailed environmental information must be obtained. Although users might want to break down of individual statistical data, as a rule, individual data are undisclosed. The individual data entail numerous risks such as response error, typing errors, and biased samples.

Therefore this study was undertaken to apply computer tomography for statistical data and to assess the accuracy of the method. The technology is expected to be a useful method to elucidate the structures underlying many social problems.

2. APPLICATION OF COMPUTER TOMOGRAPHY METHOD TO STATISTICAL DATA

2.1 TIKHONOV REGULARIZATION AND STATISTICAL COMPUTER TOMOGRAPHY

Vector **b** is observation model data that constitute a multi-cross-tabulation table of observation data. Vector **x** is the system model of **b**. These relations are expressed as shown below.

$$\mathbf{Ax}=\mathbf{b}, \qquad \mathbf{A}\in\mathbf{R}^{m\times n} \tag{1}$$

According to the theory of inverse radon transformation, using a sufficient dataset of line integration data, called a sinogram, we can uniquely determine **x** even if we do not know **b**[1)] . The method is used widely in radiology, archaeology, biology, material science, and other sciences. It is based on a mathematical procedure called tomographic reconstruction. However, mostly eq. (1) is a linear discrete ill-posed problem because of multicollinearities, uncertainties, and singular values in social phenomena.
Tikhonov regularization, named after Andrey Tikhonov, is the most commonly used method of regularizing it. This approach is a method that identifies the minimized vector $\mathbf{x}_\lambda$ of a functional as the approximate solution of the regularization parameter of eq. (2)[2)] .

$$\begin{aligned} F_\lambda(\mathbf{x}) &= \left\|\mathbf{Ax}-\mathbf{b}\right\|_2^{\,2}+\lambda\left\|\mathbf{x}\right\|_2^{\,2} \\ &= \left\|\mathbf{Ax}-\mathbf{b}\right\|_2^{\,2}+\mathbf{T}^2 \end{aligned} \tag{2}$$

Therein, $\left\|\bullet\right\|$ stands for a norm, λ

denotes a regularization parameter, and **T** signifies the Tikhonov regularization vector (a "regularization term"). The method provides prior information that the output value changes smoothly as the variable value changes. Consequently, one can expect to obtain stable solutions. Many solution algorithms exist for the regularization term.

For this study, computed tomography was applied to statistical data. It can be regarded as statistical computer tomography (SCT).

An important shortcoming is that there are insufficient sinogram data. Therefore, the author developed a new regularization algorithm for SCT.

2.2 Estimation of regulation parameters using Matrix Compression Method

Reports of previous studies described a regularization method for SCT[3]. It is a combined method of Bayes' theorem with a genetic algorithm. Problems of the algorithm include its very large number of calculations and the non-uniqueness of solutions.

Therefore, the author proposes a new regulation algorithm: matrix compression (MC) method.

Y is a multi-cross-tabulation table of the observation model. **S** is a sinogram vector as aggregated statistical data **Y**. **X** is a system model for **Y**.

The following process is the cross-section table procedure presented as an example:

1) Estimate a vector component $x_{ij}(\in \mathbf{X})$ using Bayesian inference with $s(\in \mathbf{S})$.

The relations can be described as shown in eqs. (4) and (5)

$$s_1 = \sum_l y_{il} = x_{ij} + \sum_{l \neq j} x_{il} + \mathbb{t}_1 \quad (4)$$

$$s_2 = \sum_k y_{kj} = x_{ij} + \sum_{k \neq i} x_{kj} + \mathbb{t}_2 \quad (5)$$

Table 1 Compressed cross-section table

x_{ij}	Σx_{il}	s_1
Σx_{kl}	-	-
s_2	-	-

- : Leave out of consideration

Table 1 is a compressed cross-section table from the original one to a 2×2 one.

2) Calculate solution $\mathbb{t}_1$–$\mathbb{t}_3$ under the following conditions from eqs. (4) and (5).

- $\mathbb{t}_1$ depends exclusively on x_{ij}.
- $\mathbb{t}_2$ depends exclusively on x_{ij}.
- $\mathbb{t}_3$ is a solution of a system of eqs. (4) and (5).*

* We use singular value decomposition method for calculations because it is an underdetermined system.

Continuously, calculate $\Delta\mathbb{t}$ from eqs.(6)

$$\Delta\mathbb{t} = (\mathbb{t}_1 + \mathbb{t}_2 + \mathbb{t}_3)/3 \quad (6)$$

3) Choose t_{ij} as shown below.

$$t_{ij} = \begin{cases} 0, & \left(\left|\sum \mathbb{t}_i\right| = \sum |\mathbb{t}_i| \text{ and } |\Delta\mathbb{t}| \geq \alpha\ x_{ij}\right) \\ \Delta\mathbb{t}, & (\text{other wise}) \end{cases} \quad (7)$$

where α is regularization acceptability coefficient and a hyperparameter.

3. Numerical experiment

This section describes testing of the accuracy of the regularization method by MC method using a numerical experiment.

3.1 Artificial data

Next we conduct numerical experiments using artificial dataset **y'**, which is the data vector of a family's yearly electric bills.

$$y' = x'_{df} + t_{df} + \mathcal{N} \quad (8)$$

In that equation, the following notation is used.

$$x'_{df} = k_d k_f y' \quad (9)$$

$$\mathcal{N} = N(0, 0.05 \times y') \quad (10)$$

These datasets have high correlation with district ñdò and family size ñyô. Multicollinearity t_{df} is assumed to exist between the two variables and observation error $\mathcal{N}$.

Table 2 shows a cross-tabulation table by attributes from the sample number of **y'**. The sample size is 5 million households. The sample attribute is close to the national average. Table 3 presents a cross-tabulation table of the electric bill by the attribute of **y'**.

Table 2 Number of samples

Family size	Area 1	Area 2	Area 3	Area 4
2	176,730	207,412	1,200,063	355,044
3	85,466	138,778	771,518	204,840
4	66,484	109,101	643,062	164,057
5	16,902	54,723	200,195	66,791

Total :5,000,000

Table 3 Average electric bill (Observed value)

Family size	Area 1	Area 2	Area 3	Area 4
2	86,483	113,472	112,670	101,040
3	116,512	132,729	135,025	118,186
4	123,049	144,596	143,574	128,753
5	134,329	163,000	151,944	136,350

3.2 COMPARISON OF THE BESSELIAN INFERENCE METHOD TO MC METHOD

Table 4 presents the estimated average electric bill by the attribute of **y'** using Bayesian method. The mean square error ratio is 11.6. Table 5 showed the estimated average electric bill by the attribute of **y'** using Bayes' theorem with a genetic algorithm. The mean square error ratio is 8.9. Table 6 shows the estimated average electric bill by the attribute of **y'** using MC method. The α is 0.03. The mean square error ratio is 5.1.

MC method solution is superior by 6.5 points to that obtained using Bayesian method.

Table 4 Results obtained using Bayesian method

Family size	Area 1	Area 2	Area 3	Area 4
2	89,897 (3.9%)	113,745 (0.2%)	111,975 (-0.6%)	99,410 (-1.6%)
3	108,442 (-6.9%)	137,210 (3.4%)	135,075 (0.0%)	119,917 (1.5%)
4	116,129 (-5.6%)	146,936 (1.6%)	144,650 (0.7%)	128,418 (-0.3%)
5	124,393 (-7.4%)	157,393 (-3.4%)	154,944 (2.0%)	137,557 (0.9%)

The mean square error ratio= 11.6.
( ): Error ratio

Table 5 Results obtained using Bayes' theorem with a genetic algorithm.

Family size	Area 1	Area 2	Area 3	Area 4
2	89,152 (3.1%)	113,890 (0.4%)	113,081 (0.4%)	96,937 (-4.1%)
3	109,044 (-6.4%)	135,299 (1.9%)	131,072 (-2.9%)	120,970 (2.4%)
4	119,112 (-3.2%)	145,175 (0.4%)	143,621 (0.0%)	128,486 (-0.2%)
5	125,977 (-6.2%)	159,161 (-2.4%)	151,544 (-0.3%)	134,427 (-1.4%)

The mean square error ratio= 8.9
( ): Error ratio

Table 6 Results obtained using MC method

Family size	Area 1	Area 2	Area 3	Area 4
2	89,897 (3.9%)	113,116 (-0.3%)	112,155 (-0.5%)	101,270 (0.2%)
3	110,299 (-5.3%)	134,708 (1.5%)	134,536 (-0.4%)	119,746 (1.3%)
4	117,776 (-4.3%)	143,532 (-0.7%)	143,900 (0.2%)	127,944 (-0.6%)
5	134,464 (0.1%)	157,393 (-3.4%)	153,849 (1.3%)	137,553 (0.9%)

The mean square error ratio= 5.1
( ): Error ratio

4. CONCLUSIONS

This paper proposed the new Tikhonov regularization method for statistical data tomography.

The method is designated by the author as Matrix Compression Method (MC Method).

The new regulation procedure is the following:

1. Estimate system model **X** and observation model **Y** using sinogram **S**, which is a line integral of **Y** and Bayesian theory.
2. Make a compressed cross-section

table from **X**

3. Calculate the solution using a compressed cross-section table by an algebraic solution.

This method is useful not only for statistical data but also for underdetermined systems.

ACKNOWLEDGEMENTS

I would like to thank for Professor Nobuki Murayama, Kazuhisa Iki, Osamu Ishihara and Hajime MIyauchi, Graduate school of Science and Technology, Kumamoto University, Japan, for providing some helpful comments.

REFFERENCES

[1] Shinohara, H and Sakaguchi , K and Hashimoto, T(2007）, Introduction of Image reconstruction technology by EXCEL (In Japanese), Iryo Kagaku-sya

[2]Nakata, S et.al. (2000), Image Reconstruction by Regulation Method Using QR Factorization (In Japanese) , Institute of Electronics, Information, and Communication Engineers, Vol.J83-D-II, No.9, pp.1888-1894

[3] Tanaka, A et.al.（2006）, Analyzing Residential Energy Consumption, Household Attribute and Regional Factors - Maximum Likelihood Estimation of Unknown Data Using Genetic Algorithm -, IEEJ Energy Journal, July 2006,pp 1-28